

Mineral Resource Reviews

Daniel Müller
David I. Groves

Potassic Igneous Rocks and Associated Gold-Copper Mineralization

Fourth Edition



 Springer

Mineral Resource Reviews

Series editor

John Slack, Reston, VA, USA

More information about this series at <http://www.springer.com/series/11683>

Daniel Müller · David I. Groves

Potassic Igneous Rocks and Associated Gold-Copper Mineralization

Fourth Edition



 Springer

Daniel Müller
Eschborn
Germany

David I. Groves
Department of Geology and Geophysics
Centre for Exploration Targeting
University of Western Australia
Crawley, WA
Australia

ISSN 2365-0559

ISSN 2365-0567 (electronic)

Mineral Resource Reviews

ISBN 978-3-319-23050-4

ISBN 978-3-319-23051-1 (eBook)

DOI 10.1007/978-3-319-23051-1

Library of Congress Control Number: 2015947403

Springer Cham Heidelberg New York Dordrecht London

© Springer International Publishing Switzerland 1995, 1997, 2000, 2016

This work is subject to copyright. All rights are reserved by the Publisher, whether the whole or part of the material is concerned, specifically the rights of translation, reprinting, reuse of illustrations, recitation, broadcasting, reproduction on microfilms or in any other physical way, and transmission or information storage and retrieval, electronic adaptation, computer software, or by similar or dissimilar methodology now known or hereafter developed.

The use of general descriptive names, registered names, trademarks, service marks, etc. in this publication does not imply, even in the absence of a specific statement, that such names are exempt from the relevant protective laws and regulations and therefore free for general use.

The publisher, the authors and the editors are safe to assume that the advice and information in this book are believed to be true and accurate at the date of publication. Neither the publisher nor the authors or the editors give a warranty, express or implied, with respect to the material contained herein or for any errors or omissions that may have been made.

Printed on acid-free paper

Springer International Publishing AG Switzerland is part of Springer Science+Business Media
(www.springer.com)

Preface

In recent years, there has been increasing interest from geoscientists in potassic igneous rocks. Academic geoscientists have been interested in their petrogenesis and their potential value in defining the tectonic setting of the terranes into which they were intruded, and exploration geoscientists have become increasingly interested in the growing acceptance of an association of these rocks with major epithermal gold and porphyry gold-copper deposits. In recent years, there has also been growing recognition of an association of such rocks with iron oxide copper-gold (IOCG) deposits, intrusion-related gold deposits (IRGDs), and possibly even Carlin-type gold deposits. Despite this current interest, there is no comprehensive textbook that deals with these aspects of potassic igneous rocks.

This book redresses this situation by elucidating the characteristic features of potassic (high-K) igneous rocks, erecting a hierarchical scheme that allows interpretation of their tectonic setting using whole-rock geochemistry, and investigating their associations with a wide variety of both arc-related and non-arc gold and copper-gold deposits, worldwide. About half of the book is based on a Ph.D. thesis by Dr. Daniel Müller which was produced at the Centre for Strategic Mineral Deposits (former ARC Key Centre) within the Department of Geology and Geophysics at the University of Western Australia under the supervision of Prof. David Groves, the late Dr. Nick Rock, the late Prof. Eugen Stumpfl, Dr. Wayne Taylor, and Dr. Brendan Griffin. The remainder of the book was compiled from the literature using the collective experience of the two authors. The book is dedicated to the memory of Nick Rock and Eugen Stumpfl who initiated the research project on which it is based but died before its completion.

Earlier editions of this book have encouraged more focus on the relationship between high-K magmatism and hydrothermal gold and gold-copper mineralization worldwide, which is reflected in numerous new case studies and research papers that have been published since our Third Edition in 2000. This new updated and enlarged Fourth Edition incorporates new data and references from Africa, Australia, Brazil, China, Greece, Iran, Mongolia, North America, Russia, and Turkey, including new maps and sections and

new plates of high-grade gold-copper ore from major deposits hosted by potassic igneous rocks. Not only the new edition does incorporate the latest literature on the topic, but it also provides practical suggestions for the target generation teams of mining companies exploring for world-class gold and/or copper deposits in modern and ancient arc and non-arc terranes.

Sincere thanks are due to our colleagues and friends at the former Key Centre (currently evolved into The Centre for Exploration Targeting at the University of Western Australia) for providing a stimulating environment in which to do the research and to write the first drafts of the book. Gratitude is also expressed to former colleagues at Placer Dome Exploration Inc. in Santiago; North Limited in Parkes; Kanowna Belle Gold Mines in Kalgoorlie; PT North Mining Indonesia in Jakarta; TU Bergakademie in Freiberg; ETH in Zürich; Ivanhoe Mines in Hohhot; Citadel Resource Group in Jeddah; Coventry Resources in Toronto; and BHP Billiton in Perth, Singapore, and Santiago, for encouraging the completion and revision, respectively, of all four editions of the book. The late Prof. Eugen Stumpfl is also sincerely thanked for his hospitality and assistance in the early stages of the research recorded in the book. Col Steel is also thanked for his excellent drafting of the more complex maps displayed in the book. Dr. Annett Büttner, Dörthe Mennecke-Bühler, and the late Dr. Wolfgang Engel of Springer-Verlag are thanked for their continued enthusiastic support and encouragement of the project.

The following colleagues also provided support, contributed ideas, shared authorship on papers, and/or provided unpublished information:

Anita-Kim Appleby, Antonio Arribas, Chris Ballhaus, Graham Begg, Frank Bierlein, Phil Blevin, Eric Bloem, Renato Bobis, Geoff Booth, David Bowes, Selina Brown, Josh Bryant, Bob Burke, Mari Carrizo, Megan Clark, Hilko Dalstra, Alan Edgar, Sergio Espinosa, Michael Farrand, Fine Fiedler, Peter Forrestal, Richard Förster, Leander Franz, Ron Frost, Michael Gareau, Simon Gatehouse, Silke Gawlick, Musie Gebre-Mariam, Rich Goldfarb, Sue Golding, Eliseo Gonzalez-Urien, Roland Gorbatshev, Torsten Graupner, Lalou Gwalani, Greg Hall, Adolf Helke, Chris Heinrich, Paul Heithersay, Bruce Hooper, Steve Hunt, Paul Ivascanu, Abraham Janse, Rod Jones, Roger Jones, Klaus Kaminski, Michael Kande, Imants Kavalieris, Bat-Erdene Khashgerel, Doug Kirwin, Tilo Kroll, Jeffrey Keith, Megan Kenny, David Keough, Rob Kerrich, Kalin Kouzmanov, Marianne Landtwing, Ken Lawrie, Bernd Lehmann, Li Yuan, Don Lindsley, Liu Huairan, Bob Love, John Mair, George MacDonald, Mannie Mehu, Neal McNaughton, Ian Miles, Claudio Milliotti, Aberra Mogessie, Brian Morris, Gregg Morrison, Peter Neumayr, Juhani Ojala, Julian Pearce, Sven Petersen, Irena Peytcheva, Joe Piekenbrock, Albrecht von Quadt, David Quick, David Radclyffe, Rob Ramsay, Steve Rose, Hector Salgado, Wolfram Schuh, Thomas Seifert, Dave Selley, Steve Sheppard, Richard Sillitoe, Serguei Soloviev, Henning Sørensen,

Hernan Soza, Jon Standing, Craig Stegman, Joe Stolz, Firman Sumarwan, Shen-Su Sun, William Threlkeld, Spencer Titley, Linda Tompkins, Takeshi Uemoto, Ignacio Ugalde, Theo van Leeuwen, Stefan Uhlig, Gianpiero Venturelli, Marcial Vergara, Richard and Noreen Vielreicher, Mike Wheatley, Noel White, Paul Warren, Rohan Wolfe, Doone Wyborn, Derek Wyman, and Zhang Andi.

Eschborn
Perth

Daniel Müller
David I. Groves

Contents

1	Introduction	1
1.1	Preamble: Potassic Igneous Rocks and Their Importance.	1
1.2	Scope of Book	3
	References.	3
2	Definitions and Nomenclature	9
2.1	Historical Perspective of Potassic Igneous Rocks	9
2.2	Potassic Igneous Rocks as an Umbrella Term.	10
2.3	Shoshonites	10
2.4	Shoshonitic and Alkaline Lamprophyres	11
2.5	Ultrapotassic Rocks.	11
2.5.1	Introduction	11
2.5.2	Lamproites.	12
2.5.3	Kamafugites.	12
2.5.4	Orogenic Ultrapotassic Rocks.	13
2.6	Group II Kimberlites	13
2.7	Potassic Igneous Rocks as Considered in This Book	14
2.8	Field Recognition of Potassic Igneous Rocks	14
	References.	15
3	Tectonic Settings of Potassic Igneous Rocks	19
3.1	Introduction	19
3.2	Tectonic Settings of Potassic Igneous Rocks	19
3.2.1	Continental Arc	19
3.2.2	Postcollisional Arc	19
3.2.3	Oceanic (Island) Arc	20
3.2.4	Within-Plate	22
3.2.5	Problems with Tectonic Classification	23
3.3	History of Discrimination of Tectonic Setting by Geochemical Means	24
3.4	Erection of Databases SHOSH1 and SHOSH2	28
3.5	Discrimination of Tectonic Setting by Multivariate Statistical Methods	33

3.6	Discrimination via Simple Geochemical Diagrams	35
3.7	Theoretical Basis for Discrimination Between Potassic Igneous Rocks in Different Tectonic Settings	36
3.8	Conclusions	43
	References.	43
4	Selected Type-Localities of Potassic Igneous Rocks from the Five Tectonic Settings	53
4.1	Roman Province (Italy): Example from a Continental Arc Setting	53
4.1.1	Introduction	53
4.1.2	Regional Geology	53
4.1.3	Mineralogy and Petrography of the Potassic Igneous Rocks	54
4.1.4	Geochemistry of the Potassic Igneous Rocks	54
4.2	Kreuzeck Mountains, Eastern Alps (Austria): Example from a Postcollisional Arc Setting	56
4.2.1	Introduction	56
4.2.2	Regional Geology	56
4.2.3	Mineralogy and Petrography of the Lamprophyres	58
4.2.4	Geochemistry of the Lamprophyres.	59
4.3	Northern Mariana Arc (West Pacific): Example from an Initial Oceanic Arc Setting.	65
4.3.1	Introduction	65
4.3.2	Regional Geology	65
4.3.3	Mineralogy and Petrography of the Potassic Igneous Rocks	67
4.3.4	Geochemistry of the Potassic Igneous Rocks	67
4.4	Vanuatu (Southwest Pacific): Example from a Late Oceanic Arc Setting	67
4.4.1	Introduction	67
4.4.2	Regional Geology	67
4.4.3	Mineralogy and Petrography of the Potassic Igneous Rocks	69
4.4.4	Geochemistry of the Potassic Igneous Rocks	69
4.5	African Rift Valley (Rwanda, Uganda, Democratic Republic of Congo): Example from a Within-Plate Setting.	70
4.5.1	Introduction	70
4.5.2	Regional Geology	71
4.5.3	Mineralogy and Petrography of the Potassic Igneous Rocks	71
4.5.4	Geochemistry of the Potassic Igneous Rocks	72
	References.	73

5	Primary Enrichment of Precious Metals in Potassic Igneous Rocks	77
5.1	Introduction	77
5.2	Theoretical Discussion	77
5.3	Case Study: Potassic Alkaline Lamprophyres with Elevated Gold Concentrations from the Karinya Syncline, South Australia	80
5.3.1	Introduction	80
5.3.2	Regional Geology and Tectonic Setting	81
5.3.3	Mineralization in the Vicinity of the Lamprophyres	82
5.3.4	Nature of the Lamprophyres	83
5.3.5	Petrology and Geochemistry of the Lamprophyres	84
5.3.6	Precious Metal Abundance and Significance	88
5.4	Comparison of Precious Metal Abundances for Lamprophyres from the Karinya Syncline and Kreuzeck Mountains	90
	References	93
6	Direct Associations Between Potassic Igneous Rocks and Gold-Copper Deposits in Volcanic Arcs	97
6.1	Direct Associations in Specific Tectonic Settings: Introduction	97
6.2	Erection of Database GOLD1	103
6.3	Late Oceanic Arc Associations	105
6.3.1	Ladolam Gold Deposit, Lihir Island, Papua New Guinea	105
6.3.2	Emperor Gold Deposit, Viti Levu, Fiji	113
6.3.3	Dinkidi Copper-Gold Deposit, Didipio, Philippines	116
6.3.4	Northparkes (Goonumbla) Copper-Gold Deposit, New South Wales, Australia	121
6.3.5	Cadia Ridgeway Copper-Gold Deposit, New South Wales, Australia	127
6.3.6	Hugo Dummett (Oyu Tolgoi) Copper-Gold Deposit, Mongolia	130
6.3.7	Peschanka Copper-Gold Deposit, Siberia, Russia	136
6.4	Continental Arc Associations	142
6.4.1	Bajo de La Alumbrera Copper-Gold Deposit, Catamarca Province, Argentina	142
6.4.2	Bingham Copper-Molybdenum Deposit, Utah, USA	146
6.4.3	El Indio Gold Deposit, Chile	151
6.4.4	Cripple Creek Gold Deposit, Colorado, USA	158
6.4.5	Skouries Copper-Gold Deposit, Chalkidiki, Greece	162

6.5	Postcollisional Arc Associations	166
6.5.1	Grasberg Copper-Gold Deposit, Irian Jaya, Indonesia	166
6.5.2	Misima Gold Deposit, Misima Island, Papua New Guinea	171
6.5.3	Porgera Gold Deposit, Papua New Guinea	174
6.6	Synthesis of Direct Genetic Associations	178
	References.	180
7	Direct Associations Between Potassic Igneous Rocks and Copper-Gold Deposits on Craton Margins.	191
7.1	Introduction	191
7.2	Iron-Oxide Copper-Gold (IOCG) Deposits and Potassic Igneous Rocks	193
7.2.1	Introduction	193
7.2.2	Olympic Dam Cu-Au-U-REE Deposit, South Australia.	194
7.3	Intrusion-Related Gold Deposits (IRGD) and Potassic Igneous Rocks	197
7.3.1	Introduction	197
7.3.2	Fort Knox Gold Deposit, Alaska, USA	197
	References.	200
8	Indirect Associations Between Lamprophyres and Gold-Copper Deposits	203
8.1	Introduction	203
8.2	Shoshonitic Lamprophyres with Elevated Gold Concentrations from the Goodall Gold Deposit, Northern Territory, Australia (Proterozoic)	204
8.2.1	Introduction	204
8.2.2	Regional Geology	204
8.2.3	Nature of Orogenic Gold Mineralization	205
8.2.4	Mineralogy of the Lamprophyres	205
8.2.5	Geochemistry of the Lamprophyres.	207
8.2.6	Direct or Indirect Link Between Potassic Lamprophyres and Mineralization	207
8.3	Shoshonitic Lamprophyres from the Tom's Gully Gold Deposit, Northern Territory, Australia (Proterozoic)	209
8.3.1	Introduction	209
8.3.2	Regional Geology	210
8.3.3	Nature of Orogenic Gold Mineralization	211
8.3.4	Petrology and Geochemistry of the Lamprophyres	212
8.3.5	Indirect Link Between Lamprophyres and Gold Mineralization	212

8.4	Shoshonitic Lamprophyres from the Eastern Goldfields, Yilgarn Block, Western Australia (Archaean)	212
8.4.1	Introduction	212
8.4.2	Regional Geology	213
8.4.3	Nature of Orogenic Gold Mineralization	215
8.4.4	Lamprophyres and Their Association with Mineralization	215
8.4.5	Petrology and Geochemistry of the Lamprophyres	216
8.5	Shoshonitic Lamprophyres from the Superior Province, Canada (Archean)	216
8.5.1	Introduction	216
8.5.2	Regional Geology	216
8.5.3	Nature of Orogenic Gold Mineralization	217
8.5.4	Lamprophyres and Their Association with Mineralization	218
8.5.5	Petrology and Geochemistry of the Lamprophyres	219
8.6	Indirect Link Between Lamprophyres and Archaean Gold Mineralization	220
8.7	Synthesis of Indirect Associations	222
	References.	223
9	Halogen Contents of Mineralized Versus Unmineralized Potassic Igneous Rocks.	227
9.1	Introduction	227
9.2	Erection of Database MICA1	228
9.3	Discussion	229
9.3.1	Behaviour of Halogens in Magmatic Hydrothermal Systems.	229
9.3.2	Halogen Contents of Mica in Potassic Igneous Rocks	231
9.3.3	Significance of Halogen Data	236
	References.	241
10	Implications for Mineral Exploration in Arc Environments	247
10.1	Introduction	247
10.2	Target Generation	247
10.2.1	Composition of Host Rocks	247
10.2.2	Tectonic Setting	248
10.3	Prospect Evaluation.	249
10.3.1	Favourable Tectonic Elements on the Prospect Scale	249
10.3.2	High Oxygen Fugacities (fO ₂) of the Magmas	249
10.3.3	Elevated Halogen Contents of the Magmas	252
	References.	252

11 Characteristics of Some Gold-Copper Deposits	
Associated with Potassic Igneous Rocks	257
11.1 Abbreviations	257
11.2 Tables of Deposit Characteristics	257
References	290
Subject Index	297

Abbreviations

HFSE	High-field-strength elements (e.g. Ti, Y, Zr, Nb, Hf, Ta). These elements are characterized by small ionic <i>radii</i> and high atomic charges. They are normally accommodated into the lattice sites of titanites and apatites. Subduction-derived potassic igneous rocks have very low abundances of high-field-strength elements, while those generated in within-plate tectonic settings have high concentrations. Generally, high abundances of high-field-strength elements are considered to reflect deep asthenospheric magma sources.
LILE	Large-ion lithophile elements (e.g. K, Rb, Sr, Cs, Ba). These elements are characterized by large ionic <i>radii</i> and low atomic charges. They are not readily accommodated into the lattice of upper mantle minerals and are mantle incompatible. Large-ion lithophile elements are strongly partitioned into the first melt increments during small degrees of partial melting. They are commonly located in hydrous minerals such as biotites, phlogopites, and amphiboles. Potassic igneous rocks are enriched in large-ion lithophile elements.
LOI	Loss on ignition. This is the proportion of mass lost (as volatiles) when rock powder is heated at about 1100 °C in a furnace for an hour or more. It usually corresponds to the total content of H ₂ O, CO ₂ , and S.
LREE	Light rare earth elements (e.g. La, Ce, Nd). They are part of the lanthanides (atomic numbers 57–71), commonly equated by petrologists with the rare earth elements. The light rare earth elements represent those lanthanides with the lower atomic numbers and the larger atomic <i>radii</i> due to the ‘lanthanide contraction’ with increasing atomic numbers. They are mantle incompatible and are preferentially enriched in the first melt increments during low degrees of partial melting. Light rare earth element abundances tend to increase during the process of differentiation. They are normally accommodated into the lattice sites of clinopyroxenes and apatites. Potassic igneous rocks are enriched in light rare earth elements.
mg#	Molecular Mg/(Mg+Fe ²⁺). Unless otherwise indicated, this value is calculated in this book with molecular Fe ²⁺ /(Fe ²⁺ +Fe ³⁺) set at 0.15, a common ratio in potassic igneous rocks.

MORB	Mid-ocean ridge basalt. These basalts occur at the spreading centres of the mid-ocean ridges. They are derived from partial melting of a depleted mantle source, and their geochemical composition is tholeiitic with low concentrations in mantle-incompatible trace elements.
OIB	Oceanic island basalt. These basalts are generally regarded as being derived from chemically anomalous mantle sources and to represent hot spot magmatism where deep asthenospheric mantle plumes impinge on the surface of oceanic crust. Their geochemistry is alkaline with characteristic enrichments in mantle-incompatible elements such as potassium. Examples where oceanic island basalts occur are Tristan da Cunha and Gough Island in the South Atlantic.
PGE	Platinum-group elements (e.g. Pt, Pd). The group of precious metallic elements comprising ruthenium, rhodium, palladium, osmium, iridium, and platinum.
Enriched	The terms 'enriched' and 'depleted' refer qualitatively to the gain and loss of mantle-incompatible elements, respectively.
Primitive	The term 'primitive' is used to reflect the amount of basaltic component present in a mantle-derived melt (based on their respective mg#, as well as MgO, Al ₂ O ₃ , and CaO contents).
Refractory	The term 'refractory' refers to mantle minerals and/or mantle-compatible elements which remain in the mantle peridotite during the onset of small degrees of partial melting (e.g. garnets and compatible elements such as Cr, Ni, V, and HREE).

Notes Regarding Tables of Geochemical Data

Major elements are listed in order of decreasing valency from SiO₂ to K₂O, followed by P₂O₅, LOI, SrO, BaO, Cl, and F where data are available and the abundance is sufficient for the element to be considered a major, rather than trace, element.

Trace elements are listed in order of increasing atomic number.

Where data are available, *precious metals* have been separated and listed in order of increasing atomic number.

List of Figures

Fig. 1.1	Location of the largest gold-rich porphyry and epithermal gold deposits of the circum-pacific region. Deposits with approximate tonnes of contained gold given in <i>brackets</i> are those associated with high-K igneous rocks. Adapted from Sillitoe (1997)	3
Fig. 3.1	Global distribution of Cenozoic potassic igneous rock suites used to erect the series of discriminatory diagrams. Data from many additional pre-Cenozoic rock suites were compiled in unfiltered database SHOSH1, but are not shown because their tectonic settings are uncertain. See Table 3.1 for data sources. 1 Aegean Islands, 2 Aeolian Islands, 3 Chile, 4 Peru, 5 Costa Rica, 6 Mexico, 7 New Mexico, 8 Roman Province, 9 Eastern Alps, 10 Western Alps, 11 Iran, 12 Papua New Guinea, 13 Roumania, 14 Mariana Islands, 15 Fiji, 16 Kuril Islands, 17 Vanuatu, 18 Sunda Arc, 19 Borneo, 20 Gough Island, 21 Arizona, 22 Colorado, 23 California, 24 Wyoming, 25 New South Wales, 26 Tristan da Cunha. From Müller et al. (1992a).	20
Fig. 3.2	Schematic overview of potassic igneous rocks from different tectonic settings. <i>CAP</i> continental arc; <i>PAP</i> postcollisional arc; <i>LOP</i> late oceanic arc; <i>WIP</i> within-plate setting; <i>MORB</i> mid-ocean ridge basalt; <i>OIB</i> oceanic island basalt. Modified after Mitchell and Garson (1981).	23
Fig. 3.3	Non-validity of two popular geochemical discrimination diagrams (Pearce and Cann 1973) when applied to potassic igneous rocks. Data from SHOSH2. In (a), fields A + B = low-K tholeiites (LKT), B + C = calc-alkaline basalts, B + D = ocean-floor basalt. In (b), <i>WPB</i> within-plate basalts, <i>LKT</i> low-K tholeiites, <i>OFB</i> ocean-floor basalts, <i>CAB</i> calc-alkaline basalts. From Müller et al. (1992a)	25

- Fig. 3.4 Confirmation of shoshonitic affinities of rocks used in this study. Diagram from Pearce (1982), data from SHOSH2. Note that only a minority of samples in SHOSH2 have determinations for Ta, Yb, Ce and/or Th and can thus be plotted on this diagram. From Müller et al. (1992a) 26
- Fig. 3.5 Representative chondrite-normalized spidergram patterns for potassic igneous rocks from the five tectonic settings recognized in this study. Element order and normalizing factors after Thompson (1982). **a** Continental arc settings. **b** Postcollisional arc settings. **c** Initial oceanic arc settings. **d** Late oceanic arc settings. **e** Within-plate settings. Sources are listed in references. From Müller et al. (1992a) 27
- Fig. 3.6 Established classification diagrams illustrating the range of compositions in the filtered database SHOSH2. **a** TAS diagram recommended by the IUGS Subcommission on Igneous Rock Systematics (Le Maitre 1989). **b** K_2O-SiO_2 diagram (Peccerillo and Taylor 1976a) now widely adopted in the literature; this differs in essence from the equivalent IUGS diagram only in the absence of the top three fields. Analyses have been recalculated to 100 % free of volatiles before plotting as wt% in both diagrams. From Müller et al. (1992a) 29
- Fig. 3.7 Suggested flow-chart for separating unknown samples of potassic igneous rocks into the five investigated tectonic settings. In order to achieve a maximum discrimination effect, the following scheme is recommended: 1 Plot unknown samples on Fig. 3.9a, e and/or f to separate within-plate potassic igneous rocks. 2 Plot non-within-plate samples on Fig. 3.9b or 3.10a to separate oceanic arc rocks. 3 Plot oceanic arc potassic igneous rocks on Figs. 3.9c and/or 3.10b to separate those from initial and late settings. 4 Plot remaining samples on Figs. 3.9d and/or 3.10c to discriminate between continental and postcollisional arc potassic igneous rocks. From Müller et al. (1992a) 32
- Fig. 3.8 Discrimination diagrams for potassic igneous rocks from different tectonic settings, based on multigroup linear discriminant analysis using: **a** major-elements, **b** immobile elements only. The X and Y axes respectively plot the first two of the discriminant functions (canonical vectors or factors) which contribute most to the multi-

	dimensional group separation. Standardized versions of the weights (canonical coefficients) used to calculate these discriminant functions are given in the first two columns of Table 3.3, respectively. From Müller et al. (1992a)	35
Fig. 3.9	Hierarchical set of discrimination diagrams for potassic igneous rocks from different tectonic settings, based on simple ratios of “immobile” elements revealed by discriminant analysis (Table 3.3) as contributing most effectively to group separation. As illustrated further in Figs. 3.7 and 3.9a should be used first to extract within-plate potassic igneous rocks (Fig. 3.9e and/or f are alternatives); Fig. 3.9b should then be used to separate oceanic arc from continental and postcollisional arc settings, with the former distinguished as initial or late using Fig. 3.9c, and the latter using Fig. 3.9d. From Müller et al. (1992a).	37
Fig. 3.10	Discrimination diagrams for potassic igneous rocks from different tectonic settings, partly based on the more exotic trace elements. Numbers of points are much less than on Fig. 3.9 owing to missing data. Figure 3.10a complements Fig. 3.9b in separating continental and postcollisional arcs from oceanic arcs; Fig. 3.10b complements Fig. 3.9c in separating initial and late oceanic arcs; Fig. 3.10c complements Fig. 3.9d in separating continental and postcollisional arcs. The ratio $\text{TiO}_2/100$ in Fig. 3.10a and the ratios $\text{TiO}_2/10$ and $\text{P}_2\text{O}_5/10$ in Fig. 3.10b are calculated in ppm. From Müller et al. (1992a).	38
Fig. 3.11	Schematic cross section showing the main components of a continental arc and distribution of elements (see also Müller et al. 1992a)	41
Fig. 4.1	Geological overview of the Roman Province, Central Italy. Geological provinces: Tuscan; Roman; Campanian. Modified after Holm et al. (1982) and van Bergen et al. (1983).	54
Fig. 4.2	Geological overview of the Eastern Alps, Austria, showing the location of the Kreuzeck Mountains. Modified after Reimann and Stumpfl (1985)	56
Fig. 4.3	Geographic map of the Kreuzeck Mountains, Austria, showing major mining areas and the location of shoshonitic and alkaline lamprophyres. Modified after Müller et al. (1992a)	57

Fig. 4.4	Photomicrographs (crossed nicols) of typical lamprophyre samples from the Kreuzeck Mountains, Austria. The field of view (FOV) is given in square brackets. a Porphyritic texture of tschermakite-bearing shoshonitic lamprophyre (119050) [FOV 3.5 mm]; the tschermakite phenocrysts show multiple zoning with Fe-rich rims and Mg-rich cores. b Porphyritic texture of phlogopite-bearing alkaline lamprophyre (119040) [FOV 2.0 mm]; the phlogopite phenocryst is zoned with dark brown Fe-rich rim and pale Mg-rich core. c Zoned tschermakite with Fe-rich rim and Mg-rich core (119051) [FOV 2.0 mm]. Sample numbers refer to specimens held in the Museum of the Department of Geology and Geophysics, The University of Western Australia	59
Fig. 4.5	($\text{Na}_2\text{O} + \text{K}_2\text{O}$) versus SiO_2 (TAS) plot of dykes in the Kreuzeck Mountains, Austria, from this study and Deutsch (1980, 1986). The dykes are clearly divided into two groups: a SiO_2 -rich calc-alkaline to shoshonitic group and a less SiO_2 -rich alkaline group. Modified from Müller et al. (1992a).	62
Fig. 4.6	Ba/Rb versus TiO_2 plot showing the four geochemical groups of investigated dykes. From Müller et al. (1992a)	65
Fig. 4.7	Geographic overview of the Mariana Island Arc, West Pacific. Modified after Stern (1979) and Bloomer et al. (1989)	66
Fig. 4.8	Geographic overview of Vanuatu, Southwest Pacific. Modified after Gorton (1977)	69
Fig. 4.9	Geological overview of the Virunga Volcanic Province, African Rift Valley, Uganda. Modified after De Mulder et al. (1986)	71
Fig. 5.1	Geological overview of the southern part of the Adelaide Geosyncline, South Australia, showing the study area, which includes the Karinya Syncline. Modified after Müller et al. (1993)	81
Fig. 5.2	Geological overview of the investigated area within the Karinya Syncline, South Australia. The map shows lamprophyre localities and two former base-metal mines in the area; <i>circles</i> represent samples from petrographic group 1 and <i>squares</i> represent those from petrographic group 2. The <i>rose diagram</i> shows the different strike directions of the two distinctive petrographic groups. Modified after Müller et al. (1993)	82

Fig. 5.3	Photomicrographs (crossed nicols) of typical lamprophyre samples from the Karinya Syncline, South Australia. a Two generations of mica phenocrysts with varying size (119068) [FOV 4.0 mm]. b Flow textures displayed by phlogopite phenocrysts (119072) [FOV 2.0 mm]. c Battlement structures in phlogopite phenocryst (119068) [FOV 2.0 mm]. d Zoned phlogopite (119079) [FOV 3.0 mm]. Sample numbers refer to specimens held in the Museum of the Department of Geology and Geophysics, The University of Western Australia. From Müller et al. (1993)	84
Fig. 5.4	a Al-Mg-Fe triangular plot showing 47 representative mica analyses from the Karinya Syncline, South Australia. b Fe ₂ O ₃ versus orthoclase biaxial plot showing 21 representative K-feldspar analyses for lamprophyres from the Karinya Syncline, South Australia. The orthoclase component of the investigated feldspar phases is given in %. Data from Müller et al. (1993). Modified from Sheppard and Taylor (1992)	87
Fig. 5.5	K ₂ O versus SiO ₂ plot (after Peccerillo and Taylor 1976) showing the potassic or ultrapotassic chemistry of the lamprophyres from the Karinya Syncline, South Australia. * = ultrapotassic, as defined by Foley et al. (1987); CAB = calc-alkaline basalts. From Müller et al. (1993)	90
Fig. 5.6	Discrimination diagrams for potassic igneous rocks (see Chap. 3) indicating a within-plate tectonic setting for the investigated lamprophyres. a TiO ₂ versus Al ₂ O ₃ plot. b Y versus Zr plot. c Zr/Al ₂ O ₃ versus TiO ₂ /Al ₂ O ₃ plot. From Müller et al. (1993)	91
Fig. 5.7	Abundances of chalcophile elements in lamprophyres from the Karinya Syncline, South Australia, relative to primitive mantle. Normalizing factors after Brüggmann et al. (1987).	91
Fig. 5.8	Plot of Cu versus Au for lamprophyres from the Kreuzeck Mountains, Austria.	92
Fig. 5.9	Abundances of chalcophile elements in dykes from the Kreuzeck Mountains, Austria, relative to the primitive mantle. Normalizing values after Brüggmann et al. (1987). a Dykes from the northern and southern parts of the area. b Dykes from the central part of the area where most former gold mines are located	92

Fig. 6.1	Overview in terms of gross tectonic setting of some major gold and base-metal deposits hosted by potassic igneous rocks in the Southwest Pacific area. Modified after Müller and Groves (1993). See Fig. 1.1 for a more complete overview of the entire Pacific Rim.	98
Fig. 6.2	K ₂ O versus SiO ₂ plot (after Peccerillo and Taylor 1976a) showing data from database GOLD1. CAB = calc-alkaline basalts. Adapted from Müller and Groves (1993).	104
Fig. 6.3	TiO ₂ versus Al ₂ O ₃ diagram (see Chap. 3) showing discriminant fields and the position of shoshonitic and potassic igneous rocks associated with gold-copper mineralization. Mount Bundey is the intrusion adjacent to the Tom's Gully gold deposit, Northern Territory, Australia. Adapted from Müller and Groves (1993).	104
Fig. 6.4	Y versus Zr diagram (see Chap. 3) showing discriminant fields and the position of shoshonitic and potassic igneous rocks associated with gold-copper mineralization. Adapted from Müller and Groves (1993)	105
Fig. 6.5	(TiO ₂ /100)-La-(Hfx10) triangular diagram (see Chap. 3) discriminating between samples from oceanic arcs (<i>black symbols</i>) and those from continental or postcollisional arc settings (<i>white symbols</i>). The symbols are the same as in Figs. 6.2, 6.3 and 6.4. Adapted from Müller and Groves (1993).	106
Fig. 6.6	Samples from oceanic arcs (Lihir Island, Viti Levu, Goonumbla) plotted on the (TiO ₂ /10)-(Lax10)-(P ₂ O ₅ /10) triangular diagram (see Chap. 3) suggesting their genesis in a late oceanic arc. From Müller and Groves (1993).	106
Fig. 6.7	Structural map of the New Britain arc-trench complex, showing major structures and the locations of Lihir Island and Conical Seamount, respectively. Edison and TUBAF seamounts, which are close together, are located about 20 km southwest of Lihir Island (not shown). Modified after Lindley (1988)	107
Fig. 6.8	Alteration map of the Ladolam gold deposit, Lihir Island, Papua New Guinea. Modified after Dimock et al. (1993)	108
Fig. 6.9	Representative ore samples from the Ladolam gold deposit, Lihir Island, Papua New Guinea (photos taken by D. Müller): a hydrothermal breccia containing large clast of silicified and potassic altered monzodiorite with disseminated	

	pyrite ± chalcopyrite and cut by pyrite ± quartz stockwork veining (early-stage porphyry-style mineralization) [FOV 4 × 8 cm]; b bulk ore of strongly mineralized and poorly sorted heterolithic hydrothermal breccia containing approximately 20 vol.% of fine-grained auriferous pyrite in the matrix (transitional style) [FOV 4 × 8 cm]; c hydrothermal breccia cut by <i>blue</i> quartz-chalcedony-illite-adularia-pyrite vein (late-stage low-sulphidation epithermal style) [FOV 3 × 12 cm]	110
Fig. 6.10	MgO versus Al ₂ O ₃ biaxial diagram showing one single fractionation trend for the potassic igneous rocks from Lihir Island and Conical Seamount. Adapted from Müller et al. (2003).	113
Fig. 6.11	Geological overview of the Emperor gold deposit, Fiji. Modified after Setterfield et al. (1991)	114
Fig. 6.12	Geological overview of the Dinkidi copper-gold deposit, Didipio, Philippines. Modified after Haggman (1997b) and Wolfe et al. (1998)	117
Fig. 6.13	Geological overview of the Northparkes copper-gold deposits, Goonumbla igneous complex, New South Wales, Australia. Modified after Heithersay et al. (1990).	122
Fig. 6.14	Representative ore samples from the Northparkes copper-gold deposits, E48 orebody, Goonumbla igneous complex, New South Wales, Australia (photos taken by C. Stegman): a potassic altered quartz-monzonite porphyry cut by intense quartz-bornite (A-type) stockwork veining; note the cross-cutting late-stage S-type vein [FOV 5 × 12 cm]. b Quartz-monzonite porphyry cut by intense quartz-bornite-chalcopyrite (A-type) stockwork veining, locally with hydrothermal orthoclase flooding; note that the original potassic alteration is overprinted by a late-stage pervasive sericite alteration [FOV 5 × 12 cm]	125
Fig. 6.15	Geological overview of the Cadia copper-gold deposits, Cadia igneous complex, New South Wales, Australia. Modified after Holliday et al. (2002)	128
Fig. 6.16	Representative ore from the Cadia Ridgeway copper-gold deposit, Cadia igneous complex, New South Wales, Australia (photo taken by M. Foster). Potassic altered quartz-monzonite porphyry cut by quartz-bornite-chalcopyrite (A-type) stockwork veining [FOV 8 × 15 cm].	129

Fig. 6.17	Location of the Oyu Tolgoi porphyry copper-gold district including the Hugo Dummett, Central, South West, South, and Heruga copper-gold deposits and the Ulan Khud prospect, Mongolia. Adapted from Kashgerel et al. (2008)	133
Fig. 6.18	High-grade ore samples from the Qv90 zone, Hugo Dummett copper-gold deposit, Mongolia (photos taken by B.E. Khashgerel): a intense quartz-bornite mineralization from the Qv90 high-grade zone [FOV 6 × 10 cm]. b Intense quartz-bornite ± chalcopyrite mineralization from the Qv90 zone; note that bornite impregnates quartz, filling spaces and fractures within the Qv90 zone [FOV 6 × 12 cm].	135
Fig. 6.19	Geological overview of the Peschanka copper-gold deposit, Siberia, Russia. Adapted from Nokleberg et al. (2005) and Chitalin et al. (2012)	139
Fig. 6.20	Representative ore samples from the Peschanka copper-gold deposit, Siberia, Russia (photos taken by A. Chitalin): a potassic altered quartz-monzonite porphyry cut by sheeted quartz-bornite-chalcopyrite veining [FOV 4 × 10 cm]. b Potassic altered quartz-monzonite porphyry cut by quartz-molybdenite veins [FOV 4 × 8 cm]. c Drill core box (HQ size) with potassic altered quartz-monzonite porphyry cut by intense quartz-bornite (A- and B-type) stockwork veining from Peschanka	140
Fig. 6.21	Geographic overview of the major copper-gold deposits of the Chilean and Argentinian Andes that are hosted by high-K calc-alkaline rocks. Modified after Vila and Sillitoe (1991).	143
Fig. 6.22	Geological overview of the Catamarca Province, northwest Argentina, showing the location of the Bajo de la Alumbrera copper-gold deposit. Modified after Allmendinger et al. (1983), Allmendinger (1986), and Strecker et al. (1989)	144
Fig. 6.23	(Zrx3)-(Nbx50)-(Ce/P2O5) triangular diagram (see Chap. 3) showing only samples from continental and postcollisional arcs. Samples from the latter tectonic setting show some overlap due to P mobilization in altered Archaean shoshonitic lamprophyres. Adapted from Müller and Groves (1993).	148
Fig. 6.24	Simplified geologic map of the eastern Oquirrh Mountains in relation to Bingham intrusive	

	units, Utah, USA. The location of the Bingham copper-gold deposit is outlined in <i>black</i> . Modified after Maughan et al. (2002)	149
Fig. 6.25	Geological overview of the high Andes of north-central Chile showing the locations of the El Indio and Tambo gold deposits. Modified after Siddeley and Araneda (1986)	153
Fig. 6.26	Simplified geologic map of the El Indio-Pascua belt showing the locations of the El Indio and Tambo gold deposits, Chile. Modified after Siddeley and Araneda (1986)	155
Fig. 6.27	Simplified map illustrating locations of major gold deposits hosted by high-K alkaline rocks in Colorado and New Mexico, their relative ages and their distribution to Laramide or Tertiary igneous rocks; the locations of the Colorado Mineral belt and the Rio Grande rift are also shown. Modified after Kelley and Ludington (2002)	158
Fig. 6.28	Simplified geologic map of northeast Chalkidiki Peninsula, Greece, showing the location of the Skouries copper-gold deposit. Modified after Frei (1995) and Kroll et al. (2002)	163
Fig. 6.29	Representative ore samples from the Skouries copper-gold deposit, Chalkidiki, Greece (photos taken by T. Kroll): a late-stage monzonite porphyry cut by hydrothermal orthoclase veinlet [FOV 4 × 6 cm]. b Pink monzonite porphyry with large, up to 4 cm, K-feldspar phenocrysts [FOV 4 × 16 cm]. c Main monzonite porphyry with quartz-chalcopyrite vein containing large, up to 1 cm, crystals of hydrothermal biotite [FOV 4 × 6 cm]. d Main monzonite porphyry intersected by hydrothermal orthoclase veinlet and cross-cutting quartz veinlets [FOV 4 × 17 cm]. e Main monzonite porphyry cut by A-type quartz-chalcopyrite-bornite veins which intersect an earlier black biotite-magnetite veinlet [FOV 4 × 6 cm]. f Main mineral porphyry cut by B-type quartz-chalcopyrite-biotite vein; note that the original potassic alteration assemblage is overprinted by a late-stage pervasive sericite alteration [FOV 4 × 6 cm]	165
Fig. 6.30	Geological overview of the Grasberg copper-gold deposit, Irian Jaya, Indonesia. Modified after MacDonald and Arnold (1994)	168
Fig. 6.31	Representative high-grade ore samples from the Grasberg copper-gold deposit, Irian Jaya, Indonesia (photos taken by F. Sumarwan and	

P. Warren): **a** potassic altered monzodiorite porphyry with intense disseminated chalcopyrite mineralization and cut by (S-type) chalcopyrite-bornite veinlets [FOV 5 × 12 cm]. **b** Potassic altered monzodiorite porphyry with intense disseminated chalcopyrite ± bornite mineralization and cut by (S-type) chalcopyrite-bornite veinlets [FOV 4 × 8 cm]. **c** Potassic altered monzodiorite porphyry with intense disseminated chalcopyrite-bornite mineralization and cut by (S-type) bornite-chalcopyrite veinlets; note the *brown patches* of hydrothermal biotite alteration intergrown with fine-grained chalcopyrite [FOV 5 × 11 cm] 170

Fig. 6.32 Geological overview of Misima Island, Louisiade Archipelago, Papua New Guinea, showing gold-silver mineralization. Modified after Appleby et al. (1995) 173

Fig. 6.33 Geological cross-section (SW-NE) of Misima Island, Louisiade Archipelago, Papua New Guinea. Modified after Appleby et al. (1995) 174

Fig. 6.34 Geological overview of the Porgera and Mount Kare (see Sect. 11.2.19) gold deposits, Enga Province, Papua New Guinea. Modified after Richards and Kerrich (1993) 176

Fig. 7.1 Geographical distribution of IOCG and IRGD shown relative to the position of Archaean and Proterozoic cratons. Modified after Groves et al. (2010) 192

Fig. 7.2 Magmatic-hydrothermal model for IOCG deposits associated with high-K alkaline magmatism derived from metasomatized lithosphere on craton margins. *SCLM* = Subcontinental lithospheric mantle. Modified after Groves and Santosh (2015) 192

Fig. 7.3 Regional geologic map of the Gawler Craton, South Australia. The Olympic Dam copper-gold-uranium-REE deposit lies in the northeast of the craton beneath the sedimentary units of the Stuart Shelf. Modified after Johnson and McCulloch (1995) 194

Fig. 7.4 Simplified geologic map of the Olympic Dam copper-gold-uranium-REE deposit, South Australia, at the main development level of the mine. The position of the Whenan Shaft is shown. Note the lithological zonation from the host monzogranite at the margins to progressively more hematite-rich lithologies in the centre

	of the breccia complex. Modified after Johnson and McCulloch (1995)	196
Fig. 7.5	Simplified geologic map of the Fort Knox gold deposit, Alaska, USA, showing the dominant northeast-oriented regional structural trend. Modified after Quandt et al. (2008)	198
Fig. 7.6	Geological cross-section (N-S) of the Fort Knox gold deposit, Alaska, USA, showing the composite monzogranite stock that hosts the mineralization. At least three intrusive phases ranging from coarse- to fine-grained may be distinguished. The late-stage shear zones containing high-grade gold mineralization (up to 1.0 oz/t) are also shown. Adapted from Bakke et al. (2000)	199
Fig. 8.1	Geological overview of the Pine Creek Geosyncline, Northern Territory, Australia, showing the Goodall and Tom's Gully gold deposits. The Mount Bonnie Formation, Gerowie Tuff, and Koolpin Formation comprise the South Alligator Group. Modified after Stuart-Smith et al. (1986)	205
Fig. 8.2	Application of geochemical discrimination diagrams based on immobile trace elements (after Pearce 1982) in order to illustrate the shoshonitic character of the highly altered lamprophyres from Goodall, Northern Territory. a (Ce/Yb) versus (Ta/Yb) plot. b (Th/Yb) versus (Ta/Yb) plot. Data for the Goodall lamprophyres are from Müller (1993) and those for lamprophyres from the Mount Bunday area, about 40 km northeast, are from Sheppard and Taylor (1992)	210
Fig. 8.3	Abundances of chalcophile elements in lamprophyres from the Goodall gold deposit, Northern Territory, relative to the primitive mantle. Normalizing factors after Brüggemann et al. (1987). Data from Müller (1993).	211
Fig. 8.4	Geological overview of the Yilgarn Craton, Western Australia, showing the Eastern Goldfields Province and the Kambalda, Mount Morgans and Wiluna gold deposits, which are spatially associated with shoshonitic lamprophyres. After Gee et al. (1981)	214
Fig. 8.5	Abundances of chalcophile elements in lamprophyres from the Yilgarn Craton relative to the primitive mantle. a Data for lamprophyres distal to gold deposits. b Data for lamprophyres from	

	the vicinity of gold deposits. Normalizing factors after Brüggmann et al. (1987). Data from Taylor et al. (1994)	218
Fig. 8.6	Geological overview of the Kirkland Lake area, Superior Province, Canada. Modified after Rowins et al. (1993).	220
Fig. 8.7	Abundances of chalcophile elements in lamprophyres from the Superior Province relative to the primitive mantle. All data are from lamprophyres distal to gold deposits. Normalizing factors after Brüggmann et al. (1987). Data from Wyman and Kerrich (1989a).	222
Fig. 9.1	Chlorine and F compositions of mica phenocrysts from potassic igneous rocks from barren and mineralized environments (data sources are listed in Table 9.1). Adapted from Müller and Groves (1993).	232

List of Tables

Table 3.1	Data sources for potassic igneous rocks in filtered database SHOSH2	21
Table 3.2	Numbers of sodic, potassic, and ultrapotassic rock analyses included in final filtered database SHOSH2	31
Table 3.3	Geochemical differences between potassic igneous rocks in five tectonic settings, revealed by multigroup discriminant analysis	34
Table 4.1	Representative whole-rock major- and trace-element geochemistry of potassic igneous rocks from the Roman Province, Central Italy.	55
Table 4.2	Microprobe (energy-dispersive spectra—EDS) analyses of selected phenocrysts from lamprophyres and basaltic dykes from the Kreuzeck Mountains, Eastern Alps, Austria	60
Table 4.3	Representative whole-rock major- and trace-element geochemistry of investigated lamprophyres from the Kreuzeck Mountains, Austria. Major elements are in wt%, trace elements are in ppm, and precious metals are in ppb	63
Table 4.4	Whole-rock K-Ar dating on lamprophyres and basaltic dykes from the Kreuzeck Mountains, Austria	65
Table 4.5	Representative whole-rock major- and trace-element geochemistry of potassic igneous rocks from the Mariana Island arc, West Pacific.	68
Table 4.6	Representative whole-rock major- and trace-element geochemistry of potassic igneous rocks from Vanuatu, Southwest Pacific	70
Table 4.7	Representative whole-rock major- and trace-element geochemistry of potassic igneous rocks from the Virunga volcanic field, Uganda.	72
Table 5.1	Compilation of precious metal abundances in potassic igneous rocks	78
Table 5.2	Whole-rock K-Ar dating on lamprophyres from the Karinya Syncline, South Australia	83

Table 5.3	Microprobe (wavelength dispersive spectrum—WDS) analyses of mica phenocrysts from lamprophyres from the Karinya Syncline, South Australia	85
Table 5.4	Selected major-element analyses (in wt%) of lamprophyres from the Karinya Syncline, South Australia.	88
Table 5.5	Selected trace-element analyses of lamprophyres from the Karinya Syncline, South Australia	89
Table 5.6	Correlation matrix for precious metals (Au, Pd, Pt), Cu, and gold pathfinder elements (As, Sb, W) of lamprophyres from the Karinya Syncline, South Australia.	92
Table 5.7	Correlation matrix for precious metals (Au, Pd, Pt), Cu, and gold pathfinder elements (As, Sb, W) of dykes from the Kreuzeck Mountains, Austria	93
Table 6.1	Some representative major and base-metal deposits associated with potassic igneous rocks through time . .	99
Table 6.2	Whole-rock data sources for samples in database GOLD1	103
Table 6.3	Major- and trace-element analyses of potassic igneous rocks from Lihir Island and Conical Seamount, New Ireland Province, Papua New Guinea.	112
Table 6.4	Major- and trace-element analyses of shoshonitic rocks from the Emperor gold deposit, Fiji	116
Table 6.5	Major- and trace-element analyses of potassic igneous rocks from the Dinkidi copper-gold deposit, Didipio, Philippines	120
Table 6.6	Major- and trace-element analyses of shoshonitic rocks from the Northparkes copper-gold deposits, Goonumbla igneous complex, New South Wales, Australia	126
Table 6.7	Major- and trace-element analyses of shoshonitic rocks from the Cadia copper-gold deposits, New South Wales, Australia.	131
Table 6.8	Major- and trace-element analyses of potassic igneous rocks from the Oyu Tolgoi copper-gold deposits, Mongolia	137
Table 6.9	Major-element analyses (in wt%) of potassic igneous rocks from the Peschanka copper-gold deposit, Siberia, Russia	141
Table 6.10	Major- and trace-element analyses of dacitic rocks from the Bajo de la Alumbrera copper-gold deposit, Catamarca Province, Argentina.	147
Table 6.11	Major- and trace-element analyses of potassic igneous rocks from the Bingham copper-gold deposit, Utah, USA.	152
Table 6.12	Major- and trace-element analyses of potassic igneous rocks from the El Indio gold deposit, Chile.	157

Table 6.13	Major- and trace-element analyses of potassic igneous rocks from the Cripple Creek gold deposit, Colorado, USA	161
Table 6.14	Major- and trace-element analyses of shoshonitic rocks from the Skouries copper-gold deposit, Chalkidiki, Greece	167
Table 6.15	Major- and trace-element analyses of potassic igneous rocks from the Grasberg copper-gold deposit, Irian Jaya, Indonesia	172
Table 6.16	Major- and trace-element analyses of potassic igneous rocks from the Misima gold deposit, Louisiade Archipelago, Papua New Guinea	175
Table 6.17	Major- and trace-element analyses of potassic igneous rocks from the Porgera gold deposit, Enga Province, Papua New Guinea	179
Table 8.1	Microprobe (WDS) analyses of mica phenocrysts from lamprophyres at Goodall gold deposit, Northern Territory, Australia	206
Table 8.2	Major- and trace-element analyses of lamprophyres from Goodall gold deposit, Northern Territory, Australia	208
Table 8.3	Correlation matrix for precious metals (Au, Pd, Pt), Cu, and gold pathfinder elements (As, Sb, W) of lamprophyres from the Goodall gold deposit, Australia	211
Table 8.4	Major- and trace-element analyses of lamprophyres from the Mount Bundey district, Northern Territory, Australia	213
Table 8.5	Major- and trace-element analyses of lamprophyres from the Eastern Goldfields Province, Yilgarn Craton, Western Australia	217
Table 8.6	Correlation matrix for precious metals (Au, Pd, Pt), Cu, and gold pathfinder elements (As, Sb, W) of lamprophyres from the Yilgarn Craton, Western Australia	219
Table 8.7	Major- and trace-element analyses of lamprophyres from the Superior Province, Canada	221
Table 8.8	Correlation matrix for precious metals (Au, Pd, Pt), Cu, and gold pathfinder elements (As, Sb, W) of lamprophyres from the Superior Province, Canada	222
Table 9.1	Data sources of mica compositions from database MICA1	229
Table 9.2	Microprobe (WDS) analyses of mica phenocrysts from potassic igneous rocks from the Ladolam gold deposit, Lihir Island, and Conical Seamount, Papua New Guinea	233

Table 9.3	Microprobe (WDS) analyses of mica phenocrysts from potassic igneous rocks from the Porgera gold deposit, Papua New Guinea	235
Table 9.4	Microprobe (WDS) analyses of mica phenocrysts from potassic igneous rocks from the Grasberg copper-gold deposit, Irian Jaya, Indonesia	237
Table 9.5	Microprobe (WDS) analyses of mica phenocrysts from shoshonitic rocks from the Northparkes copper-gold deposit E26 N, Goonumbla igneous complex, New South Wales, Australia.	238
Table 9.6	Microprobe (WDS) analyses of mica phenocrysts from shoshonitic lamprophyres from the Kambalda gold province and from Mount Morgans gold deposit, Yilgarn Craton, Western Australia.	239
Table 9.7	Microprobe (WDS) analyses of mica phenocrysts from shoshonitic lamprophyres from the Kirkland Lake gold district, Superior Province, Canada.	240
Table 11.1	Andacollo, Chile.	258
Table 11.2	Axi, Xinjiang Province, China	259
Table 11.3	Bajo de la Alumbreira, Catamarca Province, Argentina.	260
Table 11.4	Bingham, Utah, USA	261
Table 11.5	Buchim, Macedonia	262
Table 11.6	Cadia, New South Wales, Australia.	263
Table 11.7	Choquelimpie, Chile	264
Table 11.8	Cripple Creek, Colorado, USA	265
Table 11.9	Dinkidi, Didipio, Philippines	266
Table 11.10	El Indio, Chile	267
Table 11.11	Emperor, Viti Levu, Fiji	268
Table 11.12	Northparkes (Goonumbla), New South Wales, Australia	269
Table 11.13	Grasberg, Indonesia.	270
Table 11.14	Guilaizhuang, China	271
Table 11.15	Kirkland Lake Mining District, Superior Province, Canada	272
Table 11.16	Ladolam, Lihir Island, Papua New Guinea.	273
Table 11.17	Maricunga Belt Mining District, Chile.	274
Table 11.18	Misima, Misima Island, Papua New Guinea.	275
Table 11.19	Mount Kare, Enga Province, Papua New Guinea	276
Table 11.20	Mount Morgans, Eastern Goldfields, Western Australia	277
Table 11.21	Ok Tedi, Papua New Guinea	278
Table 11.22	Oyu Tolgoi, Mongolia.	279
Table 11.23	Peschanka, Russia.	280
Table 11.24	Porgera, Enga Province, Papua New Guinea.	281
Table 11.25	Qulong, Tibet Province, China	282
Table 11.26	Skouries, Chalkidiki Province, Greece.	283
Table 11.27	Summitville, Colorado, USA	284
Table 11.28	Touzar, Iran	285

Table 11.29 Twin Buttes, Arizona, USA	286
Table 11.30 Wiluna, Eastern Goldfields, Western Australia	287
Table 11.31 Woodlark Island, Papua New Guinea	288
Table 11.32 Yao'an, Yunnan Province, China	289

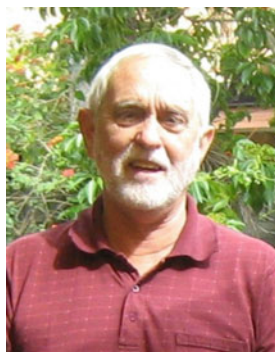
About the Authors



Daniel Müller (born 1962) studied geology and mineralogy at the Johannes Gutenberg University of Mainz, Germany, after serving 3 years as first lieutenant at German Air Force. He obtained a Ph.D. at the Key Centre for Strategic Mineral Deposits, University of Western Australia, Perth, Australia, and completed his Habilitations Degree at the Institute for Mineralogy, TU Bergakademie, Freiberg, Germany. Daniel is an experienced geologist with over 20 years exploring for base and precious metal deposits with international mining companies such as Placer Dome, North Limited, Ivanhoe Mines, Citadel Resource Group, Coventry Resources and BHP Billiton in Africa, Asia, Australia, Europe, North and South America, and the Middle East. He is currently working as a geological consultant in Asia and Eastern Europe.

Dr. Daniel Müller
Schwabenweg 17
65760 Eschborn
Germany

e-mail: danielmuller33@yahoo.com



David I. Groves (born 1942) received a B.Sc. Honours (1st class) and Ph.D. from the University of Tasmania. He joined the University of Western Australia (UWA) in 1972 as lecturer and became full professor and founder and director of the Key Centre for Strategic Mineral Deposits (later Centre for Global Metallogeny) in 1987. Throughout his career, he has supervised over 250 graduates for B.Sc. Honours, M.Sc., or Ph.D. degrees and authored or co-authored around 500 publications in Economic Geology. He has been president of the Geological Society of Australia, SEG and SGA, and has been awarded 11 medals for his research, including both the Gold Medals of SEG and SGA for lifetime contributions to Economic

Geology and the Geological Association of Canada Medal. He is a fellow of the Australian Academy of Sciences. Before retirement from UWA as emeritus professor, he organized the foundation of the now-successful Centre for Exploration Targeting at UWA. Since retirement, he has been awarded an honorary D.Sc. from UWA and consulted to the gold exploration industry and investment groups on all continents. He has also presented workshops on geological aspects of the business of exploration in Canada and the UK to brokers and investors. Recently, he has become a novelist, with his most recent book *The Digital Apocalypse*.

Prof. Dr. David I. Groves
Emeritus Professor of Economic Geology
Centre for Exploration Targeting
Department of Geology and Geophysics
The University of Western Australia
Crawley, W.A. 6009, Australia
e-mail: di_groves@hotmail.com

1.1 Preamble: Potassic Igneous Rocks and Their Importance

Potassic igneous rocks occur in many different tectonic settings (e.g. Rock 1991; Foley and Peccerillo 1992; Rios et al. 2007; Costa et al. 2011; Torabi 2011; Yang et al. 2012; Orozco-Garza et al. 2013; Hari et al. 2014; Nabatian et al. 2014; Rao et al. 2014; Ding et al. 2015; Liu et al. 2015a), and include a variety of compositions ranging from shoshonites associated with calc-alkaline volcanic rocks to ultrapotassic leucitites (Foley and Peccerillo 1992; Peccerillo 1992; Campbell et al. 2014; Soloviev 2014a). They are of increasing economic interest due to their association with mineralization, and are of tectonic significance because of their potential value in reconstructing the tectonic setting of ancient terranes.

On the *economic* front, potassic igneous rocks are now established as being closely related to certain types of gold and base metal deposits (e.g. Mitchell and Garson 1981; Mutschler et al. 1985; Heithersay et al. 1990; Kavalieris and Gonzalez 1990; Richards et al. 1991; Setterfield 1991; Mutschler and Mooney 1993; Müller and Groves 1993; Sillitoe 1997, 2002; Müller et al. 2001; Maughan et al. 2002; Kroll et al. 2002; Müller 2002; Zhenhua et al. 2003; Mikulski 2005, 2007; Chitalin et al. 2012; Lehmann et al. 2013; Bissig and Cooke 2014; Soloviev 2014a, b; Fu et al. 2015; Jamali and Mehrabi 2015; Liu et al. 2015b; Soloviev 2015). Some may even be intrinsically

enriched in Au and platinum-group elements (PGE) (Wyborn 1988; Müller et al. 1992a, 1993; McDonald et al. 1995). Some of the world's largest volcanic- and intrusion-hosted gold and copper-gold deposits are intimately related to potassic igneous rocks. For example, the world-class epithermal gold deposits at Axa, Xinjiang Province, China (Yang et al. 2009; Chen et al. 2012; Zhao et al. 2014a), Ladolam and Porgera, Papua New Guinea (Moyle et al. 1990; Richards 1990a, b; Carman 1994; White et al. 1995; Müller et al. 2002a, b), Baguio, Philippines (Cooke et al. 1996), Cripple Creek, Colorado (Thompson 1992; Kelley and Ludington 2002), and Emperor, Fiji (Anderson and Eaton 1990; Setterfield 1991) are all hosted in high-K calc-alkaline or alkaline rocks. Similarly, there are equivalent host plutons associated with the porphyry copper-gold deposits at Bingham, Utah (Keith et al. 1997; Maughan et al. 2002), Bajo de la Alumbrera, Argentina (Guilbert 1995; Müller and Forrestal 1998; Ulrich and Heinrich 2002), Cadia and Northparkes, NSW, Australia (Heithersay et al. 1990; Müller et al. 1994; Holliday et al. 2002), Grasberg, Indonesia (Hickson 1991; McMahon 1994; Pollard et al. 2005), Ok Tedi, Papua New Guinea (Rush and Seegers 1990), Oyu Tolgoi, Mongolia (Kashgerel et al. 2006, 2008; Wainwright et al. 2011), Peschanka, Siberia (Chitalin et al. 2012; Soloviev 2014a), Skouries, Greece (Tobey et al. 1998; Kroll et al. 2002), and Yao'an, China (Bi et al. 2004; Hu et al. 2004; Lu et al. 2013a, b). Although emphasized in previous

editions of this book, this association had not been stressed in prior reviews on porphyry and epithermal styles of mineralization. However, Sillitoe (1997), in a review of world-class gold-rich porphyry and epithermal deposits in the circum-Pacific region, emphasizes the association of many of these giant deposits with potassic igneous rocks: their location and approximate gold content is shown in Fig. 1.1. Sillitoe (1997, 2002) points out that, even excluding those deposits associated with potassic igneous rocks of other magmatic associations (e.g. high-K calc-alkaline suites), about 20 % of the large gold deposits are associated with shoshonitic and alkaline rocks, with such rocks unlikely to exceed 3 % by volume of circum-Pacific igneous rocks. Sillitoe (1997, 2002) lists the association between gold deposits and potassic igneous rocks as one of only four criteria favourable for *both* world-class porphyry and epithermal gold-rich deposits in the circum-Pacific region, and attributes this association to the partial melting of stalled lithospheric slabs in the mantle, immediately following collision or arc migration, as a preferred mechanism to promote oxidation of mantle sulphides and the release of gold.

In addition, less important examples from an economic viewpoint include the Lamaque stockwork at Val d'Or, Quebec, Canada (Burrows and Spooner 1991), the porphyry copper-gold mineralization associated with shoshonitic rocks in British Columbia, Canada (Barrie 1993; Kirkham and Margolis 1995; Kirkham and Sinclair 1996), the porphyry copper \pm gold mineralization at Mirkuh Ali Mirza (Maghsoudi et al. 2014) and Khopik (Shafaroudi et al. 2015), Iran, the Jinjushan epithermal gold deposit, Lower Yangtze region, China (Zhou et al. 1996), and Prospector Mountain, Yukon, Canada (Glasmacher and Günther 1991). Subduction-related cobalt-nickel mineralization in northeast Scotland, formed during an arc-continent collision during the Grampian Orogeny, is also associated with potassic igneous rocks (Dunham 1974; Mitchell and McKerrow 1975).

A number of other gold and Cu-Au deposits that occur on craton margins are also associated with potassic igneous rocks that are directly related to melting of metasomatized lithosphere in within-plate plume-related settings. These include numerous world-class iron-oxide copper-gold (IOCG) deposits, including the giant Olympic Dam deposit on the Gawler Craton of South Australia and a cluster of giants in the Carajas region on the Amazon Craton of Brazil (Groves et al. 2010). Intrusion-related gold deposits (IRGD), including the giant Fort Knox deposit of Alaska, have a similar setting and genesis (Goldfarb et al. 2005; Groves et al. 2010; Mair et al. 2011). The giant Carlin gold district of Nevada has recently been connected to high potassic magmatism (Muntean et al. 2011), although the association may be less direct than for the other deposit types (e.g. Groves and Santosh 2015).

Potassic igneous rocks are thus becoming important exploration targets in their own right (cf. Chap. 10).

On the *tectonic* front, potassic igneous rocks have been recognized as an important and integral component of magmatism at destructive continental margins (e.g. Hatherton and Dickinson 1969; Morrison 1980; Saunders et al. 1980; Carr 1998; Yang et al. 2012; Abbasi et al. 2014). Although there are exceptions (Arculus and Johnson 1978), arc-related potassic igneous rocks are generally younger, stratigraphically higher, and erupted further from the suture than less potassic rocks, implying that they form at greater depth in a Benioff Zone. This has led to the use of potassic igneous rocks to attribute arc-like tectonic affinities to ancient terranes (Brooks et al. 1982; Barley et al. 1989; Wyman and Kerrich 1989a, b; Wyborn 1992).

It is becoming important, whether in improving exploration models for ancient mineral deposits, or in reconstructing ancient terranes, to be able to distinguish the tectonic settings in which ancient potassic igneous rocks were generated.

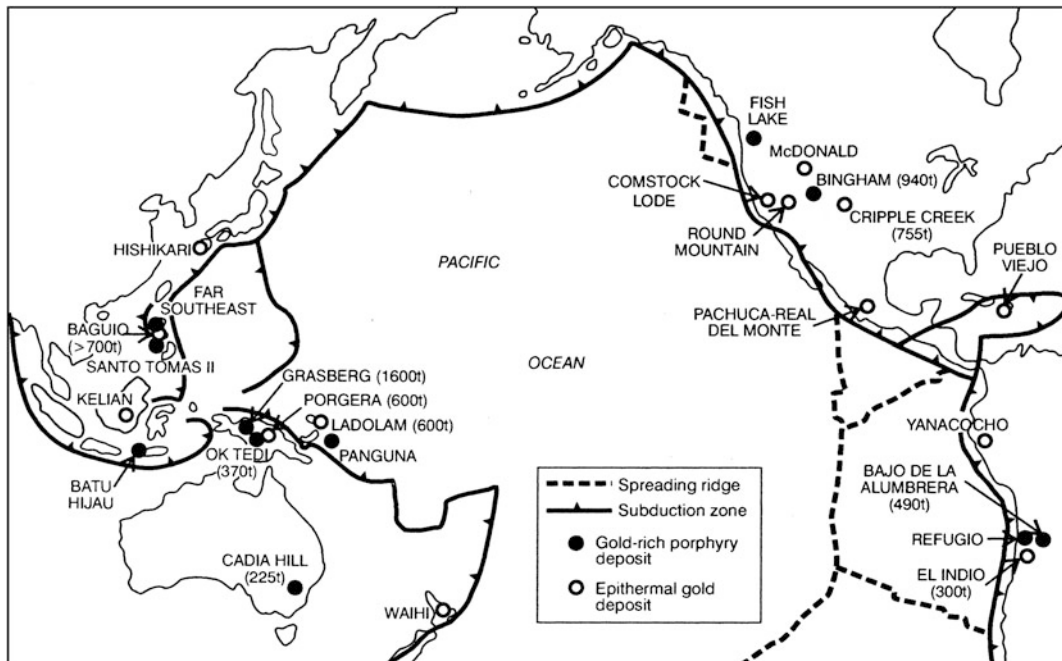


Fig. 1.1 Location of the largest gold-rich porphyry and epithermal gold deposits of the circum-pacific region. Deposits with approximate tonnes of contained gold given

in brackets are those associated with high-K igneous rocks. Adapted from Sillitoe (1997)

1.2 Scope of Book

As part of the “*Drosophila* of igneous petrology” (Barker 1983, p. 297), potassic igneous rocks have gained much attention among petrologists worldwide, mainly due to their distinct geochemistry, and many geoscientists still consider them as petrological curiosities with an obscure petrogenesis. In the past, a plethora of genetic hypotheses and a large number of local names for potassic igneous rocks from different localities have been created (see reviews by Sørensen 1974; Peccerillo 1992). This has produced some confusion in the literature.

This book reviews the geochemical and petrological characteristics of the potassic igneous rock clan, and investigates the different tectonic settings in which these rocks occur. The authors seek to provide an overview and a classification of those rocks, and to elucidate the geochemical differences between barren and mineralized potassic igneous complexes. As discussed above,

many epithermal gold and porphyry copper-gold deposits are hosted by potassic igneous rocks and there is increasing evidence that IOCG deposits and IRGDs are related to high-K magmatism. Therefore, this book is not only relevant to the academic petrologist working on alkaline rocks, but also to the exploration geologist prospecting for hydrothermal gold, gold-copper and copper deposits in modern and ancient terranes.

References

- Abbasi S, Tabatabaei Manesh SM, Karimi S, Parfenova OV (2014) Relative contributions of crust and mantle to generation of Oligocene-Miocene medium-K calc-alkaline I-type granitoids in a subduction setting—a case study from the Nabar pluton, Central Iran. *Petrology* 22:310–328
- Anderson WB, Eaton PC (1990) Gold mineralization at the Emperor mine, Vatukoula, Fiji. In: Hedenquist JW, White NC, Siddeley G (eds) Epithermal gold mineralization of the Circum-Pacific; geology, geochemistry, origin and exploration, II; *J Geochem Explor* 36:267–296

- Arculus RJ, Johnson RW (1978) Criticism of generalized models for the magmatic evolution of arc-trench systems. *Earth Planet Sci Lett* 39:118–126
- Barker DS (1983) *Igneous Rocks*. Prentice Hall, Englewood Cliffs, NJ, p 417
- Barley ME, Eisenlohr BN, Groves DI, Perring CS, Vearncombe JR (1989) Late Archaean convergent margin tectonics and gold mineralization: a new look at the Norseman-Wiluna Belt, Western Australia. *Geology* 17:826–829
- Barrie CT (1993) Petrochemistry of shoshonitic rocks associated with porphyry copper-gold deposits of central Quesnellia, British Columbia, Canada. *J Geochem Explor* 48:225–258
- Bi X, Hu R, Cornell DH (2004) The alkaline porphyry associated Yao'an gold deposit, Yunnan, China: rare earth element and stable isotope evidence for magmatic-hydrothermal ore formation. *Miner Deposita* 39:21–30
- Bissig T, Cooke DR (2014) Introduction to the special issue devoted to alkali porphyry Cu-Au and epithermal Au deposits. *Econ Geol* 109:819–825
- Brooks C, Ludden J, Pigeon Y, Hubregtse JJMW (1982) Volcanism of shoshonite to high-K andesite affinity in an Archaean arc environment, Oxford Lake, Manitoba. *Can J Earth Sci* 19:55–67
- Burrows DR, Spooner ETC (1991) The Lamaque Archaean stockwork Au system, Val d'Or, Quebec: relationship to a 20 Ma, calc-alkaline, intrusive sequence. *GAC-MAC Program Abstr* 16:17
- Campbell IH, Stepanov AS, Liang HY, Allen CM, Norman MD, Zhang YQ, Xie YW (2014) The origin of shoshonites: new insights from the Tertiary high-potassium intrusions of eastern Tibet. *Contrib Miner Petrol* 167:983–1005
- Carman GD (1994) Genesis of the Ladolam gold deposit, Lihir Island, Papua New Guinea. Unpl. Ph.D. thesis, Monash University, Melbourne
- Carr PF (1998) Subduction-related Late Permian shoshonites of the Sydney Basin, Australia. *Mineral Petrol* 63:49–71
- Chen YJ, Pirajno F, Wu G, Qi JP, Xiong XL (2012) Epithermal deposits in North Xinjiang, NW China. *Int J Earth Sci* 101:889–917
- Chitalin AF, Fomichev E, Usenko V, Agapitov D, Shtengelov A (2012) Structural model of the Peschanka porphyry Cu-Au-Mo deposit, western Chukotka, Russia. In: Vearncombe J (ed) *Structural geology and resources—2012*. Australian Institute of Geosciences Symposium, Kalgoorlie, 26–28 Sept 2012, pp 21–27
- Cooke DR, McPhail DC, Bloom MS (1996) Epithermal gold mineralization, Acupan, Baguio district, Philippines: geology, mineralization, alteration, and the thermochemical environment of ore deposition. *Econ Geol* 91:243–272
- Costa FG, Oliveira EP, McNaughton NJ (2011) The Fazenda Gavião granodiorite and associated potassic plutons as evidence for Paleoproterozoic arc-continent collision in the Rio Itapicuru greenstone belt, Brazil. *J S Am Earth Sci* 32:127–141
- Ding H, Zhang Z, Dong X, Yan R, Lin Y, Jiang H (2015) Cambrian ultrapotassic rhyolites from the Lhasa terrane, south Tibet: evidence for Andean-type magmatism along the northern active margin of Gondwana. *Gondwana Res* 27:1616–1629
- Dunham KC (1974) Geological setting of the useful minerals in Britain. *Proc Roy Soc A* 339:273–288
- Foley SF, Peccerillo A (1992) Potassic and ultrapotassic magmas and their origin. *Lithos* 28:181–185
- Fu Y, Sun X, Lin H, Zhou H, Li X, Ouyang X, Jiang L, Shi G, Liang Y (2015) Geochronology of the giant Beiya gold-polymetallic deposit in Yunnan Province, Southwest China, and its relationship with the petrogenesis of alkaline porphyry. *Ore Geol Rev* 71:138–149
- Glasmacher U, Günther F (1991) Gold-bearing sulphide veins in shoshonites formed by high-T, high-Cl alkaline fluids, Prospector Mountain, Yukon Territory. *GAC/MAC Program Abstr* 16:A46
- Goldfarb RJ, Baker T, Dubè B, Groves DI, Hart CJR, Gosselin P (2005) Distribution, character, and genesis of gold deposits in metamorphic terranes. *Econ Geol* 100:407–450
- Groves DI, Santosh M (2015) Province-scale commonalities of some world-class gold deposits: implications for mineral exploration. *Geosci Front* 6:389–399
- Groves DI, Bierlein FP, Meinert LD, Hitzman MW (2010) Iron oxide copper-gold (IOCG) deposits through earth history: implications for origin, lithospheric setting, and distinction from other epigenetic iron oxide deposits. *Econ Geol* 105:641–654
- Guilbert JM (1995) Geology, alteration, mineralization, and genesis of the Bajo de la Alumbrera porphyry copper-gold deposit, Catamarca Province, Argentina. In: Pierce FW, Bolm JG (eds) *Porphyry copper deposits of the American Cordillera*, vol 20. Arizona Geological Society Digest, pp 646–656
- Hari KR, Rao NVC, Swarnkar V, Hou G (2014) Alkali feldspar syenites with shoshonitic affinities from Chhotaudepur area: implication for mantle metasomatism in the Deccan large igneous province. *Geosci Front* 5:261–276
- Hatherton T, Dickinson WR (1969) The relationship between andesite volcanism and seismicity in Indonesia, the Lesser Antilles and other island arcs. *J Geophys Res* 74:5301–5310
- Heithersay PS, O'Neill WJ, van der Helder P, Moore CR, Harbon PG (1990) Goonumbla porphyry copper district—Endeavour 26 North, Endeavour 22 and Endeavour 27 copper-gold deposits. In: Hughes FE (ed) *Geology of the mineral resources of Australia and Papua New Guinea*, vol 14. Australasian Institute of Mining and Metallurgy, Parkville, Monograph, pp 1385–1398
- Hickson RJ (1991) Grasberg open-pit: Ertsberg's big brother comes onstream in Indonesia. *Min Eng* 43:385–391
- Holliday JR, Wilson AJ, Blevin PL, Tedder IJ, Dunham PD, Pfitzner M (2002) Porphyry gold-copper mineralization in the Cadia district, eastern Lachlan

- Fold Belt, New South Wales, and its relationship to shoshonitic magmatism. *Miner Deposita* 37:100–116
- Hu RZ, Burnard PG, Bi XW, Zhou MF, Pen JT, Su WC, Wu KX (2004) Helium and argon isotope geochemistry of alkaline intrusion-associated gold and copper deposits along the Red River–Jinshajiang fault belt, SW China. *Chem Geol* 203:305–317
- Jamali H, Mehrabi B (2015) Relationships between arc maturity and Cu–Mo–Au porphyry and related epithermal mineralization at the Cenozoic Arasbaran magmatic belt. *Ore Geol Rev* 65:487–501
- Kashgerel BE, Rye RO, Hedenquist JW, Kavalieris I (2006) Geology and reconnaissance stable isotope study of the Oyu Tolgoi porphyry Cu–Au system, South Gobi, Mongolia. *Econ Geol* 101:503–522
- Kashgerel BE, Kavalieris I, Hayashi KI (2008) Mineralogy, textures, and whole-rock geochemistry of advanced argillic alteration: Hugo Dummett porphyry Cu–Au deposit, Oyu Tolgoi mineral district, Mongolia. *Miner Deposita* 43:913–932
- Kavalieris I, Gonzalez JM (1990) Geology and mineralization of the Pao Prospect: a high sulphidation epithermal gold system hosted in alkaline volcanic, North Luzon, Philippines. In: Pacific Rim congress 90, 6–12 May 1990, Gold Coast, Queensland, Proceedings Australasian Institute of Mining and Metallurgy, Parkville, pp 413–418
- Keith JD, Whitney JA, Hattori K, Ballantyne GH, Christiansen EH, Barr DL, Cannan TM, Hook CJ (1997) The role of magmatic sulphides and mafic alkaline magmas in the Bingham and Tintic mining districts, Utah. *J Petrol* 38:1679–1690
- Kelley KD, Ludington S (2002) Cripple Creek and other alkaline-related gold deposits in the southern Rocky Mountains, USA: influence of regional tectonics. *Miner Deposita* 37:38–60
- Kirkham RV, Margolis J (1995) Overview of the Sulphurets area, NW-British Columbia. In: Schroeter TG (ed) Porphyry deposits of the NW-Cordillera of North America, vol 46. Canadian Institute of Mining, Metallurgy and Petroleum Special Publication, Montreal, pp 473–483
- Kirkham RV, Sinclair WD (1996) Porphyry copper, gold, molybdenum, tungsten, tin, silver. In: Eckstrand OR, Sinclair WD, Thorpe RI (eds) Geology of Canadian mineral deposit types, vol 8. Geological Survey of Canada, Ottawa, pp 405–430
- Kroll T, Müller D, Seifert T, Herzig PM, Schneider A (2002) Petrology and geochemistry of the shoshonite-hosted Skouries porphyry Cu–Au deposit, Chalkidiki, Greece. *Miner Deposita* 37:137–144
- Lehmann St, Barcikowski J, von Quadt A, Gallhofer D, Peytcheva I, Heinrich CA, Serafimovski T (2013) Geochronology, geochemistry and isotope tracing of the Oligocene magmatism of the Buchim–Damjan–Borov Dol ore district: implications for timing, duration and source of the magmatism. *Lithos* 181:216–233
- Liu Z, Jiang Y, Jia R, Zhao P, Zhou Q (2015a) Origin of Late-Triassic high-K calc-alkaline granitoids and their potassic microgranular enclaves from the western Tibet Plateau, northwest China: implications for Paleo-Tethys evolution. *Gondwana Res* 27:326–341
- Liu B, Liu H, Zhang C, Mao Z, Zhou Y, Huang H, He Z, Su G (2015b) Geochemistry and geochronology of porphyries from the Beiya gold-polymetallic orefield, western Yunnan, China. *Ore Geol Rev* 69:360–379
- Lu YJ, Kerrich R, McCuaig TC, Li ZX, Hart CJR, Cawood PA, Hou ZQ, Bagas L, Cliff J, Belousova EA, Tang S (2013a) Geochemical, Sr–Nd–Pb, and zircon Hf–O isotopic compositions of Eocene–Oligocene shoshonitic and potassic adakite-like felsic intrusions in western Yunnan, SW China: petrogenesis and tectonic implications. *J Petrol* 54:1309–1348
- Lu YJ, Kerrich R, Kemp AIS, McCuaig TC, Hou ZQ, Hart CJR, Li ZX, Cawood PA, Bagas L, Yang ZM, Cliff J, Belousova EA, Jourdan F, Evans NJ (2013b) Intracontinental Eocene–Oligocene porphyry Cu mineral systems of Yunnan, western Yangtze Craton, China: compositional characteristics, sources, and implications for continental collision metallogeny. *Econ Geol* 108:1541–1576
- Maghsoudi A, Yazdi M, Mehrpartou M, Vosoughi M, Younesi S (2014) Porphyry Cu–Au mineralization in the Mirkuh Ali Mirza magmatic complex, NW Iran. *J Asian Earth Sci* 79:932–941
- Mair JL, Farmer GL, Groves DI, Hart CJR, Goldfarb RJ (2011) Petrogenesis of postcollisional magmatism at Scheelite Dome, Yukon, Canada: evidence for a lithospheric mantle source for magmas associated with intrusion-related gold systems. *Econ Geol* 106:451–480
- Maughan DT, Keith JD, Christiansen EH, Pulsipher T, Hattori K, Evans NJ (2002) Contributions from mafic alkaline magmas to the Bingham porphyry Cu–Au–Mo deposit, Utah, USA. *Miner Deposita* 37:14–37
- McDonald I, de Wit MJ, Smith CB, Bizzi LA, Viljoen KS (1995) The geochemistry of the platinum-group elements in Brazilian and southern African kimberlites. *Geochim Cosmochim Acta* 59:2883–2903
- McMahon T (1994) Pliocene intrusions in the Gunung Bijih (Ertsberg) Mining District, Irian Jaya, Indonesia: major and trace element chemistry. *Int Geol Rev* 36:925–946
- Mikulski SZ (2005) Geological, mineralogical and geochemical characteristics of the Radzimowice Au–As–Cu deposit from the Kaczawa Mountains (Western Sudetes, Poland): an example of the transition of porphyry and epithermal style. *Miner Deposita* 39:904–920
- Mikulski SZ (2007) The late Variscan gold mineralization in the Kaczawa Mountains, Western Sudetes. *Pol Geol Inst Spec Pap* 22:1–162
- Mitchell AHG, Garson MS (1981) Mineral deposits and global tectonic setting. Academic Press, London, p 421
- Mitchell AHG, McKerrow WS (1975) Analogous evolution of the Burma orogen and the Scottish Caledonides. *Bull Geol Soc Am* 86:305–315
- Morrison GW (1980) Characteristics and tectonic setting of the shoshonite rock association. *Lithos* 13:97–108
- Moyle AJ, Doyle BJ, Hoogvliet H, Ware AR (1990) Ladolam gold deposit, Lihir Island. In: Hughes FE (ed) Geology of the mineral resources of Australia and Papua New Guinea, vol 14. Australasian Institute of

- Mining and Metallurgy, Parkville, Monograph, pp 1793–1805
- Müller D (2002) Preface—gold-copper mineralization in alkaline rocks. *Miner Deposita* 37:1–3
- Müller D, Forrestal P (1998) The shoshonite porphyry Cu-Au association at Bajo de la Alumbrera, Catamarca Province, Argentina. *Mineral Petrol* 64:47–64
- Müller D, Groves DI (1993) Direct and indirect associations between potassic igneous rocks, shoshonites and gold-copper deposits. *Ore Geol Rev* 8:383–406
- Müller D, Stumpfl EF, Taylor WR (1992) Shoshonitic and alkaline lamprophyres with elevated Au and PGE concentrations from the Kreuzeck Mountains, Eastern Alps, Austria. *Mineral Petrol* 46:23–42
- Müller D, Morris BJ, Farrand MG (1993) Potassic alkaline lamprophyres with affinities to lamproites from the Karinya Syncline, South Australia. *Lithos* 30:123–137
- Müller D, Heithersay PS, Groves DI (1994) The shoshonite porphyry Cu-Au association in the Goonumbra district, N.S.W. Australia. *Mineral Petrol* 51:299–321
- Müller D, Franz L, Herzig PM, Hunt S (2001) Potassic igneous rocks from the vicinity of epithermal gold mineralization, Lihir Island, Papua New Guinea. *Lithos* 57:163–186
- Müller D, Kaminski K, Uhlig S, Graupner T, Herzig PM, Hunt S (2002a) The transition from porphyry- to epithermal-style gold mineralization at Ladolam, Lihir Island, Papua New Guinea: a reconnaissance study. *Miner Deposita* 37:61–74
- Müller D, Herzig PM, Scholten JC, Hunt S (2002b) Ladolam gold deposit, Lihir Island, Papua New Guinea: gold mineralization hosted by alkaline rocks. *Econ Geol Spec Publ* 9:367–382
- Muntean JL, Cline JS, Simon AC, Longo AA (2011) Magmatic-hydrothermal origin of Nevada's Carlin-type gold deposits. *Nat Geosci* 4:122–127
- Mutschler FE, Mooney TC (1993) Precious-metal deposits related to alkalic igneous rocks: provisional classification, grade-tonnage data and exploration frontiers. In: Kirkham RV, Sinclair WD, Thorpe RI, Duke JM (eds) *Mineral deposit modeling*, vol 40. Geological Association of Canada, Toronto, Special Paper, pp 479–520
- Mutschler FE, Griffin ME, Scott-Stevens D, Shannon SS (1985) Precious-metal deposits related to alkaline rocks in the North American Cordillera—an interpretative view. *Trans Geol Soc S Afr* 88:355–377
- Nabatian G, Ghaderi M, Neubauer F, Honarmand M, Xiaoming Liu, Dong Y, Jiang SY, von Quadt A, Bernroider M (2014) Petrogenesis of Tarom high-potassic granitoids in the Alborz-Azarbaijan belt, Iran: geochemical, U-Pb zircon and Sr-Nd-Pb isotopic constraints. *Lithos* 187:324–345
- Orozco-Garza A, Dostal J, Keppie JD, Paz-Moreno FA (2013) Mid-Tertiary (25–21 Ma) lamprophyres in NW Mexico derived from subduction-modified subcontinental lithospheric mantle in an extensional backarc environment following steepening of the Benioff zone. *Tectonophysics* 590:59–71
- Peccerillo A (1992) Potassic and ultrapotassic rocks: compositional characteristics, petrogenesis, and geologic significance. *IUGS Episodes* 15:243–251
- Pollard PJ, Taylor RG, Peters L (2005) Ages of intrusion, alteration, and mineralization at the Grasberg Cu-Au deposit, Papua, Indonesia. *Econ Geol* 100:1005–1020
- Rao NVC, Srivastava RK, Sinha AK, Ravikant V (2014) Petrogenesis of Kerguelen mantle plume-linked Early Cretaceous ultrapotassic intrusive rocks from the Gondwana sedimentary basins, Damodar Valley, Eastern India. *Earth Sci Rev* 136:96–120
- Richards JP (1990a) The Porgera gold deposit, Papua New Guinea: geology, geochemistry and geochronology. Unpl. Ph.D. thesis, The Australian National University, Canberra
- Richards JP (1990b) Petrology and geochemistry of alkaline intrusive at the Porgera gold deposit, Papua New Guinea. *J Geochem Explor* 35:141–199
- Richards JP, McCulloch MT, Chappell BW, Kerrich R (1991) Sources of metals in the Porgera gold deposit, Papua New Guinea: evidence from alteration, isotope, and noble metal geochemistry. *Geochim Cosmochim Acta* 55:565–580
- Rios DC, Conceição H, Davis DW, Plá Cid J, Rosa MLS, Macambira MJB, McReath I, Marinho MM, Davis WJ (2007) Paleoproterozoic potassic-ultrapotassic magmatism: Morro do Afonso Syenite Pluton, Bahia, Brazil. *Precambr Res* 154:1–30
- Rock NMS (1991) *Lamprophyres*. Blackie, Glasgow, p 285
- Rush PM, Seegers HJ (1990) Ok Tedi copper-gold deposit. In: Hughes FE (ed) *Geology of the mineral deposits of Australia and Papua New Guinea*, vol 14. Australasian Institute of Mining and Metallurgy, Parkville, Monograph, pp 1747–1754
- Saunders AD, Tarney J, Weaver SD (1980) Transverse geochemical variations across the Antarctic peninsula: implications for the genesis of calc-alkaline magmas. *Earth Planet Sci Lett* 46:344–360
- Setterfield TN (1991) Evolution of the Tavua caldera and associated hydrothermal systems, Fiji. Unpl. Ph.D. thesis, University of Cambridge, Cambridge
- Shafaroudi AM, Karimpour MH, Stern CR (2015) The Khopik porphyry copper prospect, Lut Block, Eastern Iran: geology, alteration and mineralization, fluid inclusion, and oxygen isotope studies. *Ore Geol Rev* 65:522–544
- Sillitoe RH (1997) Characteristics and controls of the largest porphyry copper-gold and epithermal gold deposits in the circum-Pacific region. *Aust J Earth Sci* 44:373–388
- Sillitoe RH (2002) Some metallogenic features of gold and copper deposits related to alkaline rocks and consequences for exploration. *Miner Deposita* 37:4–13
- Soloviev SG (2014a) The metallogeny of shoshonitic magmatism, vol I. Scientific World Publications, Moscow, pp 1–528 (in Russian)
- Soloviev SG (2014b) The metallogeny of shoshonitic magmatism, vol II. Scientific World Publications, Moscow, pp 1–472 (in Russian)

- Soloviev SG (2015) Geology, mineralization, and fluid inclusion characteristics of the Kumbel oxidized W-Cu-Mo skarn and Au-W stockwork deposit in Kyrgyzstan, Tien Shan. *Miner Deposita* 50:187–220
- Sørensen H (1974) Origin of the alkaline rocks: a summary and retrospect. In: Sørensen H (ed) *The Alkaline Rocks, Petrogenesis*. John Wiley and Sons, London, pp 535–539
- Thompson TB (1992) Mineral deposits of the Cripple Creek district, Colorado. *Min Eng* 44:135–138
- Tobey E, Schneider A, Alegria A, Olcay L, Perantonis G, Quiroga J (1998) Skouries porphyry copper-gold deposit, Chalkidiki, Greece. In: Porter TM (ed) *Porphyry and hydrothermal Cu-Au deposits. A global perspective*. Australian Mineral Foundation Conference Proceedings, Glenside, South Australia, pp 159–168
- Torabi G (2011) Middle Eocene volcanic shoshonites from the western margin of the Central-East Iranian microcontinent (CEIM), a mark of previously subducted CEIM-confining oceanic crust. *Petrology* 19:675–689
- Ulrich T, Heinrich CA (2002) Geology and alteration geochemistry of the porphyry Cu-Au deposit at Bajo de la Alumbrera, Argentina. *Econ Geol* 97:1865–1888
- Wainwright AJ, Tosdal RM, Wooden JL, Mazdab FK, Friedman RM (2011) U-Pb (zircon) and geochemical constraints on the age, origin, and evolution of Paleozoic arc magmas in the Oyu Tolgoi porphyry Cu-Au district, southern Mongolia. *Gondwana Res* 19:764–787
- White NC, Leake MJ, McCaughey SN, Parris BW (1995) Epithermal gold deposits of the Southwest Pacific. *J Geochem Explor* 54:87–136
- Wyborn D (1988) Ordovician magmatism, Au mineralization and an integrated tectonic model for the Ordovician and Silurian history of the Lachlan Fold Belt, NSW. *Austr Bur Mineral Res Canberra BMR Res Newslett* 8:13–14
- Wyborn D (1992) The tectonic significance of Ordovician magmatism in the eastern Lachlan Fold Belt. *Tectonophysics* 214:177–192
- Wyman D, Kerrich R (1989a) Archaean shoshonitic lamprophyres associated with Superior Province gold deposits: distribution, tectonic setting, noble metal abundances and significance for gold mineralization. In: Keays RR, Ramsay WRH, Groves DI (eds) *The geology of gold deposits: the perspective in 1988*, vol 6. *Economic Geology Monograph*, pp 651–667
- Wyman D, Kerrich R (1989b) Archaean lamprophyre dykes of the Superior Province, Canada: distribution, petrology and geochemical characteristics. *J Geophys Res* 94:4667–4696
- Yang F, Mao J, Bierlein FP, Pirajno F, Zhao C, Ye H, Liu F (2009) A review of the geological characteristics and geodynamic mechanisms of Late Paleozoic epithermal gold deposits in North Xinjiang, China. *Ore Geol Rev* 35:217–234
- Yang WB, Niu HC, Shan Q, Luo Y, Sun WD, Li CY, Li NB, Yu XY (2012) Late Paleozoic calc-alkaline to shoshonitic magmatism and its geodynamic implications, Yuximolegai area, western Tianshan, Xinjiang. *Gondwana Res* 22:325–340
- Zhao X, Xue C, Symons DTA, Zhang Z, Wang H (2014) Microgranular enclaves in island-arc andesites: a possible link between known epithermal Au and potential porphyry Cu-Au deposits in the Tulasu ore cluster, western Tianshan, Xinjiang, China. *J Asian Earth Sci* 85:210–223
- Zhenhua Z, Xiaolin X, Qiang W, Zhiwei B, Yuquan Z, Yingwen X, Shuangkui R (2003) Alkali-rich igneous rocks and related Au and Cu large and superlarge deposits in China. *Sci China Ser D Earth Sci* 46:1–13
- Zhou JC, Zhou JP, Liu J, Zhao TP, Chen W (1996) Copper (gold) and non-metal deposits hosted in Mesozoic shoshonite and K-rich calc-alkaline series from Lishui in the Lower Yangtze region, China. *J Geochem Explor* 57:273–283

2.1 Historical Perspective of Potassic Igneous Rocks

Potassic igneous rocks were originally recognized in the late 19th century by Iddings (1895), who described some orthoclase-bearing basalts from the Yellowstone Park, Wyoming, and coined the term “shoshonite”. In the last century, petrologists generated many names for potassic igneous rocks which were either based on their mineralogy or, more commonly, based on the locality of their occurrence. The practice was to name a new rock after a place where it occurred—the type locality. These different names for essentially similar rocks from different localities led to great confusion (Sørensen 1974; De Wit 1989; Rock 1991; Peccerillo 1992).

The first attempts to explain the petrogenesis of potassic magmatism date back to the beginning of the 20th century when Daly (1910) explained potassic melts as products of the assimilation of carbonate sediments by uprising basaltic magmas. Rittmann (1933) adopted this hypothesis in order to explain the potassic magmatism of the Vesuvius volcano and the *Mediterranean Series*, as potassic igneous rocks were named at that time (Peccerillo 1992), with the assimilation of carbonates by evolved trachytic magmas. This model was widely accepted until the 1960s, although it was unable to explain the potassic magmatism in the East African Rift (e.g. Foley et al. 2011), where carbonates are absent. However, Savelli (1967) was able to demonstrate that potassic magmas have much

higher abundances of large-ion lithophile elements (LILE) and mantle-compatible elements, such as Cr, Ni, and V, than do both carbonates and basalts. Therefore, the *assimilation model* appeared rather unlikely and alternative explanations were developed. One of these was the *zone-refining model* proposed by Harris (1957). This model was adapted from the steel industry, where the process of zone-refining was used to purify metal bars. Harris (1957) suggested that a mantle plume would rise adiabatically by melting the roof rocks at its top and by crystallizing minerals at its base. This process would allow the rising melt to incorporate all the mantle-incompatible impurities such as LILE and light rare-earth elements (LREE). As a result, the migrating melt would become progressively enriched in these elements and gain a potassic composition. Another model to explain potassic magmatism was based on observations from trace-element modeling (Kay and Gast 1973), which implied that the enrichments in LILE and LREE in potassic igneous rocks were an effect of very low degrees of partial melting (i.e. melt increments of <1 vol.%) of a garnet-peridotite in the upper mantle.

However, the advent of the *concept of mantle metasomatism* (e.g. Menzies and Hawkesworth 1987) represented a major breakthrough in understanding of the petrogenesis of potassic igneous rocks (Peccerillo 1992). Direct evidence for heterogeneous mantle compositions on a small scale was provided by the petrographic studies of mantle xenoliths from deep-seated kimberlite and trachybasalt eruptions (e.g. Harte

and Hawkesworth 1989; Grègoire et al. 2000; Franz et al. 2002; Franz and Romer 2010) which revealed the presence of LILE-bearing hydrous minerals such as phlogopite and apatite within the peridotites of the upper mantle. These minerals, which may occur either in veins or dispersed within the mantle peridotite (Bailey 1982; Franz et al. 2002), are believed to have been metasomatically introduced by volatile- and LILE-enriched fluids and/or LILE- and LREE-enriched alkalic melts (see Chap. 3). The nature and origin of these metasomatizing agents are still under debate (Peccerillo 1992; Till et al. 2012; Li et al. 2013; Lu et al. 2013; Liu et al. 2014).

Interest in the petrogenesis of potassic magmas has, for many years, been aimed at describing specific occurrences and explaining the differences between these and normal basalts (Foley and Peccerillo 1992). Potassic igneous rocks have features in common with both the alkaline and calc-alkaline rock associations, but also have geochemical characteristics that distinguish them from the other rock associations and, therefore, they must be considered a distinct rock association (Morrison 1980; Campbell et al. 2014).

In the first comprehensive study of potassic igneous rocks from different localities, undertaken by Sahama (1974), only ultrapotassic rocks were considered and these were divided into kamafugitic and orenditic types. However, the peralkaline orenditic ultrapotassic igneous rocks and the kamafugites, which are represented by groups I and II in Foley et al. (1987), are not considered further in this study (see definitions in Sects. 2.5.2 and 2.5.3). Modern studies of shoshonites and potassic igneous rocks (e.g. Morrison 1980; Lu et al. 2013; Liu et al. 2014) re-established their importance as a distinctive group among the spectrum of igneous rocks. High-K rocks such as shoshonites have been formally incorporated in numerous classification schemes (Peccerillo and Taylor 1976), including that recommended by the IUGS Subcommittee (Le Maitre 1989).

2.2 Potassic Igneous Rocks as an Umbrella Term

The *potassic igneous rocks*, as considered here, comprise volcanic, hypabyssal and plutonic rocks. Petrographically, potassic igneous rocks range from trachybasalts and trachyandesites to trachytes, which normally have porphyritic textures with phenocrysts of plagioclase, K-feldspar, clinopyroxene, olivine, amphiboles, biotite and/or phlogopite, and minor apatite microphenocrysts. The term “potassic igneous rocks” is used in this book as an umbrella term to describe those rocks which are silica-saturated and more K-rich than typical igneous rocks (i.e. $K > Na$). The term includes subduction-related high-K calc-alkaline rocks and shoshonites, high-K rocks from within-plate tectonic settings, hypabyssal high-K rocks such as shoshonitic and alkaline lamprophyres (cf. Rock 1991), and the orogenic ultrapotassic rocks (group III of Foley et al. 1987), which are defined in Sect. 2.5. For a detailed review of the silica-deficient alkaline rocks, which are characterized by feldspathoids such as leucite and nepheline, and commonly occur in rift-related within-plate tectonic settings, the reader is referred to the recent work of Gupta (2014).

2.3 Shoshonites

Shoshonites (sensu stricto) are potassic igneous rocks which occur in subduction-related tectonic settings (Morrison 1980; Torabi 2011; Lu et al. 2013; Campbell et al. 2014; Soloviev 2014). They are commonly formed during the late stage of arc-evolution, being erupted after the low-K tholeiites and calc-alkaline rock series. Although there are a few exceptions, they are commonly most distant from the trench and are erupted above the deepest parts of the Benioff Zone. The shoshonite association is geochemically defined by high total alkalis ($K_2O + Na_2O > 5$ wt%), high K_2O/Na_2O ratios (>0.6 at 50 wt% SiO_2 , >1.0

at 55 wt% SiO₂), low TiO₂ (<1.3 wt%), high but variable Al₂O₃ (14–19 wt%), and a strong enrichment in LILE and LREE (e.g. Morrison 1980). Trachybasalts and basaltic andesites predominate in the shoshonite association. Shoshonites have porphyritic textures with phenocrysts of plagioclase, clinopyroxene, olivine, phlogopite and/or amphiboles in a very fine-grained, commonly glassy, groundmass consisting mainly of K-feldspar (sanidine), plagioclase, and clinopyroxene (Morrison 1980).

2.4 Shoshonitic and Alkaline Lamprophyres

Lamprophyres (Greek *lampros*, *porphyros*: glistening porphyry) form an extremely heterogeneous group of predominantly hypabyssal alkaline igneous rocks which occur in a wide variety of geological settings throughout the world (Rock 1991). In many localities, lamprophyres are associated with granitic, shoshonitic, syenitic, or carbonatitic magmatism (Rock 1991; Rowins et al. 1993; Maughan et al. 2002; Orozco-Garza et al. 2013; Chen et al. 2014; Karsli et al. 2014; Štemprok et al. 2014; Lu et al. 2015). Several contradictory classifications for lamprophyres have been used over the past century. However, lamprophyres have been comprehensively defined by Rock (1987, 1991) as hypabyssal, melanocratic igneous rocks with porphyritic textures carrying only mafic phenocrysts, essentially phlogopite-biotite and/or amphibole with minor olivine. Phlogopite or biotite phenocrysts are commonly zoned, with dark brown Fe-rich rims and pale yellow Mg-rich cores (Rock et al. 1988; Müller et al. 1992, 1993). Felsic minerals are generally restricted to the groundmass (cf. Rock 1987). However, quartz xenocrysts are common due to the volatile-driven rapid uprising of lamprophyric magmas (Rock 1991). Lamprophyres are also characterized by battlemented phlogopites and globular structures, which are due to the segregation of late-stage melts, commonly with evolved syenitic compositions, into vugs within

the crystal mush (Foley 1984; Rock 1991). The rocks occur as dykes, sills, plugs, stocks, or vents and associated intrusive or explosion breccias.

Geochemically, lamprophyric magmas have primitive compositions, as shown by high mg# [where mg# = molecular Mg/(Mg + Fe²⁺), with molecular Fe²⁺/(Fe²⁺ + Fe³⁺) set at 0.15, a common ratio in potassic igneous rocks] and high Cr, Ni, and V contents. They are typically enriched in LILE, LREE, and volatiles such as CO₂, H₂O, F, and Cl (Rock 1987; Rock et al. 1990), which are sited in the lattice of hydrous minerals such as amphiboles or micas, or hosted by primary carbonates, zeolites, epidotes, fluorites, or sulphates (Rock et al. 1988).

The lamprophyre clan comprises shoshonitic (calc-alkaline), alkaline, and ultramafic lamprophyres, as well as lamproites and kimberlites (Rock 1991). Only the first two varieties, shoshonitic and alkaline lamprophyres with high K₂O (>1 wt%) and SiO₂ contents (>40 wt%), are considered in this study. *Shoshonitic lamprophyres* with groundmass plagioclase > K-feldspar are further divided into the amphibole-bearing spessartites and mica-bearing kersantites, whereas those with K-feldspar > plagioclase are divided into the amphibole-bearing vogesites and mica-bearing minettes (Rock 1977). *Alkaline lamprophyres* are normally characterized by biotite or phlogopite phenocrysts in a groundmass with K-feldspar > plagioclase (e.g. Müller et al. 1992, 1993). Many alkaline lamprophyres would be classified as volatile-rich alkali basalts or basanites when plotted on the Na₂O + K₂O versus SiO₂ diagram (Rock 1991) which is recommended by the IUGS Subcommittee on Igneous Rocks Systematics (cf. Le Maitre 1989).

2.5 Ultrapotassic Rocks

2.5.1 Introduction

Ultrapotassic rocks are defined by using the chemical screens K₂O >3 wt%, MgO >3 wt%, and K₂O/Na₂O >2 for whole-rock analyses

(Foley et al. 1987). They can be further divided into four groups:

- Group I (e.g. the Gausberg lamproites, Antarctica), characterized by low CaO (<8 wt%), Al_2O_3 <12 wt%, Na_2O <2 wt%, and high mg# (~60–85).
- Group II (e.g. the kamafugites of the Toro-Ankole region, East African Rift), characterized by very low SiO_2 (<40 wt%) and high CaO (>10 wt%).
- Group III (e.g. the orogenic ultrapotassic rocks of the Roman Province), which occur in orogenic areas and have high CaO (>5 wt%), high Al_2O_3 (>12 wt%), and low mg# (~40–65).
- Group IV showing transitional chemical characteristics between groups I and III (Foley et al. 1987).

2.5.2 Lamproites

Lamproites commonly occur as volumetrically small vents, pipes, or dykes, and form a group within the potassic igneous rock clan which shares certain petrogenetic aspects with the alkali basalts, kimberlites, and lamprophyres (Bergman 1987). Lamproites have achieved increased economic importance since the discovery of the diamond-bearing Argyle lamproite pipe, Western Australia (Rock 1991; Lugué et al. 2009). Their occurrence is restricted to within-plate tectonic settings (Mitchell 1986; Mitchell and Bergman 1991).

Lamproites are derived by small degrees of partial melting of a phlogopite-harzburgite mantle source under reducing conditions, and two varieties, olivine lamproite and leucite lamproite, may be distinguished (Edgar and Mitchell 1997). Lamproites are normally characterized (Prider 1960; Mitchell and Bergman 1991; Peccerillo 1992) by the presence of rare minerals such as titanian phlogopite, potassic richterite, leucite, jeppeite, sanidine, aluminium-poor diopside, potassic titanites (e.g. priderite), potassic zirconian silicates (e.g. wadeite), shcherbakovite, and armalcolite (cf. Contini et al. 1993). Lamproites

characteristically do not contain plagioclase, nepheline, or melilite (Bergman 1987). Geochemically, lamproites have high $\text{K}_2\text{O}/\text{Al}_2\text{O}_3$ ratios (>0.6; Foley et al. 1987), moderately high CaO (>4 wt%) and very low Al_2O_3 contents (<12 wt%; Mitchell and Bergman 1991). Most lamproites are peralkaline and have $(\text{Na} + \text{K})/\text{Al}$ ratios >1 (Mitchell and Bergman 1991). Additionally, they are characterized by high concentrations of mantle-compatible elements (e.g. ~150 ppm V, ~400 ppm Cr, ~250 ppm Ni), high LILE (e.g. ~6000 ppm Ba, ~2000 ppm Sr), and high LREE (e.g. ~250 ppm La, ~400 ppm Ce; Mitchell and Bergman 1991).

In the previous literature, there has been some debate about whether to consider lamproites as a distinctive petrogenetic group, as proposed by Bergman (1987) and Mitchell and Bergman (1991), or to include them into the lamprophyre clan as suggested by Rock (1991). In hand specimen, lamproites appear very similar to rocks of the lamprophyre clan (e.g. the shoshonitic lamprophyre varieties kersantite and minette, and most alkaline lamprophyres; Müller et al. 1992, 1993) due to their porphyritic textures with abundant ferromagnesian phenocrysts such as phlogopite and lack of leucocratic phenocrysts. However, based on mineralogical and geochemical considerations, they are quite different. In contrast to lamprophyres, lamproites may contain alkali amphiboles such as riebeckite or richterite, but they lack plagioclase, a major component of many lamprophyres, at least in their groundmass. Lamproites also have much lower SiO_2 (<40 wt%) and Al_2O_3 (<12 wt%) contents than shoshonitic or alkaline lamprophyres (commonly >45 and >14 wt%, respectively; Rock 1991). Based on their exotic mineralogy, their distinct geochemistry, and their very rare occurrence in nature, lamproites are not further considered in this book.

2.5.3 Kamafugites

Kamafugites are mafic kalsilite-bearing lavas, and they represent the rarest examples of the magmatic rocks (Mitchell and Bergman 1991).

Kamafugites may occur as dykes or lavas which are restricted to within-plate settings. Important type-localities are the igneous rocks (e.g. katungites, mafurites, ugandites) from the Toro Ankole region, Uganda (Holmes 1950; Barton 1979; Foley et al. 2011), and those from Cupello and San Venanzo, Italy (Mittempergher 1965; Gallo et al. 1984). The term “kamafugite” (*katungite-mafurite-ugandite*) was introduced by Sahama (1974), and subsequently has been established in the modern literature (cf. Foley et al. 1987).

Mineralogically, kamafugites are characterized by the presence of olivine phenocrysts in a groundmass consisting of phlogopite, clinopyroxene, leucite, melilite, perovskite, and kalsilite, the latter reflecting their very low SiO₂ contents (Gallo et al. 1984; Foley et al. 1987, 2011). Kamafugites are petrographically distinguished from lamproites by the presence of kalsilite and melilite, and absence of sanidine (Mitchell and Bergman 1991). Apatite and perovskite normally represent only minor phases (Gallo et al. 1984). Kamafugites are geochemically distinct with extremely low SiO₂ (<45 wt%), very low Al₂O₃ (<12 wt%), low Na₂O (<1.38 wt%), and very high CaO contents (>8 wt%), as discussed by Gallo et al. (1984) and Foley et al. (1987). Their characteristically high concentrations of LREE (e.g. up to 470 ppm Ce) and high field-strength elements (HFSE) (e.g. up to 44 ppm Y and up to 680 ppm Zr; Gallo et al. 1984) are consistent with their restricted occurrence in within-plate tectonic settings.

2.5.4 Orogenic Ultrapotassic Rocks

The group of *orogenic ultrapotassic rocks* is equivalent (Foley et al. 1987) to the highly potassic igneous rocks from the Roman Magmatic Province, Italy (e.g. Holm et al. 1982; Rogers et al. 1985; Boari et al. 2009; and see Chap. 4).

Geochemically, orogenic ultrapotassic rocks are characterized by relatively low K₂O/Al₂O₃ ratios (<0.5) when compared with the extreme K₂O-enrichments of lamproites and kamafugites (K₂O/Al₂O₃ >0.6). They may occur either as dykes (e.g. Müller et al. 1993) or as lavas (e.g. Cundari 1973; Boari et al. 2009). Orogenic ultrapotassic rocks from the Roman Province typically have high Al₂O₃ contents (>12 wt%; Civetta et al. 1981; Holm et al. 1982; Rogers et al. 1985; Boari et al. 2009).

2.6 Group II Kimberlites

Kimberlites are rare, volatile-rich, ultrabasic, potassic igneous rocks occupying small vents, sills, and dykes (Dawson 1987). Kimberlites have been divided by Smith et al. (1985) into two distinct varieties termed Group I and Group II kimberlites. Group I is also known as mica-poor and Group II as mica-rich kimberlites (Dawson 1987). Petrographically, Group I kimberlites are characterized by the presence of olivine, phlogopite, apatite, monticellite, calcite, serpentine, and minor magnesian ilmenite (Mitchell 1989). Groundmass spinels and perovskite are abundant (Mitchell 1989). Group II kimberlites, which have been only recognized in Russia, South Africa and Swaziland to date, are dominated by phlogopite, and minor diopside and apatite phenocrysts (Mitchell 1989; Priyatkina et al. 2014). Their groundmass is mainly phlogopite, diopside, and leucite, whereas monticellite and magnesian ilmenite are absent (Skinner 1989). Group II kimberlites are rarely accompanied by other potassic intrusions such as lamprophyres (Dawson 1987). Both groups are geochemically different, with higher concentrations of P, Rb, Ba, and LREE, and lower concentrations of Ti and Nb in Group II kimberlites (Smith et al. 1985; Skinner 1989). Importantly, Group II

kimberlites are highly potassic, with K_2O contents of about 3 wt% (cf. Mitchell 1989).

2.7 Potassic Igneous Rocks as Considered in This Book

Potassic igneous rocks, as considered in this book, are defined by molar K_2O/Na_2O ratios of about or slightly higher than unity (cf. Peccerillo 1992). While potassic igneous rocks from within-plate settings tend to occur as isolated geological bodies, those from subduction-related tectonic settings normally occur as the end-members of a continuous igneous-rock spectrum that might range from boninites and tholeiites to high-K calc-alkaline rocks and shoshonites during arc evolution (see Chap. 3). In these settings, the authors also consider rocks with molar K_2O/Na_2O ratios <1 , if the whole-rock compositions are $K_2O >1$ wt% at about 50 wt% SiO_2 (e.g. the basalts from the Mariana Arc: see discussion in Chaps. 3 and 4).

This book does not consider Group II kimberlites, due to their very distinctive geochemistry with low SiO_2 (~ 36 wt%) and very high MgO contents (~ 30 wt%), their exotic mineralogy, and their rare occurrence in nature (cf. Mitchell 1989; Priyatkina et al. 2014). The book also excludes lamproites and kamafugites (Groups I and II of Foley et al. 1987), because of their limited occurrence in nature and their exotic mineralogy (e.g. rare minerals including richterite, melilite, perovskite, and priderite occur as well as leucite and/or kalsilite). They tend to be isolated and are normally not associated with other high-K rocks. Lamproites and kamafugites occur typically in mobile belts at craton margins (lamproites) or in rift valleys (kamafugites), but not in orogenic areas, and they are not associated with gold or base-metal mineralization (Mitchell and Bergman 1991; Foley et al. 1987, 2011). It is considered, therefore, that eliminating lamproites and kamafugites from the potassic igneous rock database SHOSH2 (database discussed in Chap. 3) not only has a sound basis, but also allows the discrimination to concentrate on finer

chemical differences among the remaining *orogenic* potassic igneous rocks (including Groups III and IV ultrapotassic rocks), which are of more interest here. This decision does leave some leucite-bearing rocks in SHOSH2, such as those of the Roman Province, Italy, and the leucitites of New South Wales, Australia. Lamproites and kamafugites were eliminated on a province-by-province basis, but the criteria are equivalent to such chemical screens as $CaO/Al_2O_3 < 1.3$, $CaO < (SiO_2 - 30)$, $CaO > (21 - SiO_2)$, and $CaO > [22 - (1.25 \times Al_2O_3)]$, based on Figs. 1 and 3 of Foley et al. (1987).

2.8 Field Recognition of Potassic Igneous Rocks

There is no golden rule for the recognition of potassic igneous rocks in the field because the characteristics vary from more mafic to more felsic varieties, and from plutonic to volcanic settings.

Volcanic and hypabyssal high-K rocks are generally characterized by porphyritic textures with phenocrysts of clinopyroxene, amphibole, biotite, phlogopite, and apatite in a fine-grained groundmass which is dominated by K-feldspar and plagioclase. Extrusive shoshonitic igneous rocks are commonly dominated by plagioclase and clinopyroxene phenocrysts which are accompanied by amphibole, biotite, phlogopite, and apatite phenocrysts. However, the volatile-rich hydrous phenocrysts such as amphibole, biotite, phlogopite, and apatite are mainly developed in lamprophyres, which crystallize at shallow levels in the crust under low confining pressures of the overlying rocks.

Plutonic high-K rocks are characterized by holocrystalline equigranular, and more rarely, sparsely porphyritic textures comprising larger crystals of plagioclase, amphibole, biotite, and phlogopite in a medium-grained groundmass of K-feldspar and plagioclase. Typical examples are the potassic quartz-monzodiorites and/or quartz-monzonites which host the world-class porphyry copper-gold deposits of Cadia (Fig. 6.16) and

Northparkes, Australia (Fig. 6.14), Skouries, Greece (Fig. 6.29), and Peschanka, Siberia (Fig. 6.20).

Potassic igneous rocks are commonly dark grey (e.g. at Bajo de la Alumbrera, Argentina, and Bingham, Utah). However, they can be pink due to the presence of Fe in the orthoclase structure (e.g. at Skouries, Greece; Fig. 6.29). In rare cases, mineralized high-K intrusions are overprinted by an intense pervasive hematite-sericite alteration (i.e. “hematite-dusting”), resulting in brick-red colours (e.g. at Cadia, Northparkes, and Peschanka; Figs. 6.14, 6.16 and 6.20).

References

- Bailey DK (1982) Mantle metasomatism—continuing chemical change within the earth. *Nature* 296:525–530
- Barton M (1979) A comparative study of some minerals occurring in the potassium-rich alkaline rocks of the Leucite Hills, Wyoming, the Vico volcano, western Italy, and the Toro Ankole region, Uganda. *Neues Jahrbuch Mineralogische Abhandlungen* 137:113–134
- Bergman SC (1987) Lamproites and other potassium-rich igneous rocks: a review of their occurrence, mineralogy and geochemistry. In: Fitton JG, Upton BGJ (eds) *Alkaline igneous rocks*, vol 30. Geological Society, London, Geological Society Special Publication, pp 103–190
- Boari E, Avanzinelli R, Melluso L, Giordano G, Mattei M, De Benedetti AA, Morra V, Conticelli S (2009) Isotope geochemistry (Sr-Nd-Pb) and petrogenesis of leucite-bearing volcanic rocks from “Colli Albani” Volcano, Roman Magmatic Province, Central Italy: inferences on volcano evolution and magma genesis. *Bull Volc* 71:977–1005
- Campbell IH, Stepanov AS, Liang HY, Allen CM, Norman MD, Zhang YQ, Xie YW (2014) The origin of shoshonites: new insights from the tertiary high-potassium intrusions of eastern Tibet. *Contrib Miner Petrol* 167:983–1005
- Chen Y, Yao S, Pan Y (2014) Geochemistry of lamprophyres at the Daping gold deposit, Yunnan Province, China: constraints on the timing of gold mineralization and evidence for mantle convection in the eastern Tibetan Plateau. *J Asian Earth Sci* 93:129–145
- Civetta L, Innocenti F, Manetti P, Peccerillo A, Poli G (1981) Geochemical characteristics of potassic volcanic from Mts. Ernici, southern Latium, Italy. *Contrib Miner Petrol* 78:37–47
- Contini S, Venturelli G, Toscani L, Capedri S, Barbieri M (1993) Cr-Zr-arnalcolite-bearing lamproites of Canarix, SE Spain. *Miner Mag* 57:203–216
- Cundari A (1973) Petrology of the leucite-bearing lavas in New South Wales. *J Geol Soc Aust* 20:465–492
- Daly RA (1910) Origin of the alkaline rocks. *Bull Geol Soc Am* 21:87–115
- Dawson JB (1987) The kimberlite clan: relationship with olivine and leucite lamproites, and inferences for upper-mantle metasomatism. In: Fitton JG, Upton BGJ (eds) *Alkaline igneous rocks*, vol 30. Geological Society Special Publication, pp 95–101
- De Wit MJ (1989) Book review: alkaline igneous rocks. *Lithos* 24:81–82
- Edgar AD, Mitchell RH (1997) Ultra high pressure-temperature melting experiments on an SiO₂-rich lamproite from Smoky Butte, Montana: derivation of siliceous lamproite magmas from enriched sources deep in the continental mantle. *J Petrol* 38:457–477
- Foley SF (1984) Liquid immiscibility and melt segregation in alkaline lamprophyres from Labrador. *Lithos* 17:127–137
- Foley SF, Peccerillo A (1992) Potassic and ultrapotassic magmas and their origin. *Lithos* 28:181–185
- Foley SF, Venturelli G, Green DH, Toscani L (1987) The ultrapotassic rocks: characteristics, classification, and constraints for petrogenetic models. *Earth Sci Rev* 24:81–134
- Foley SF, Jacob DE, O’Neill HSC (2011) Trace element variations in olivine phenocrysts from Ugandan potassic rocks as clues to the chemical characteristics of parental magmas. *Contrib Miner Petrol* 162:1–20
- Franz L, Romer RL (2010) Different styles of metasomatic veining in ultramafic xenoliths from the TUBAF seamount (Bismarck microplate, Papua New Guinea). *Lithos* 114:30–53
- Franz L, Becker KP, Kramer W, Herzig PM (2002) Metasomatic mantle xenoliths from the Bismarck microplate (Papua New Guinea)—thermal evolution, geochemistry and extent of slab-induced metasomatism. *J Petrol* 43:315–343
- Gallo F, Giammetti F, Venturelli G, Vernia L (1984) The kamafugitic rocks of San Venanzo and Cuppaello, Central Italy. *Neues Jahrbuch Mineralogische Monatshefte* 5:198–210
- Gregoire M, Moine BN, O’Reilly SY, Cottin JY, Giret A (2000) Trace element residence and partitioning in mantle xenoliths matasomatized by highly alkaline, silicate- and carbonate-rich melts (Kerguelen Islands, Indian Ocean). *J Petrol* 41:477–509
- Gupta AK (2014) Origin of potassium-rich silica deficient igneous rocks. Springer, Heidelberg, p 536
- Harris PG (1957) Zone refining and the origin of potassic basalts. *Geochim Cosmochim Acta* 12:195–208
- Harte B, Hawkesworth CJ (1989) Mantle domains and mantle xenoliths. In: Ross J, Jaques AL, Ferguson J, Green DH, O’Reilly SY, Danchin RV, Janse AJA

- (eds) Kimberlites and related rocks, vol 14. Geological Society of Australia Special Publication, pp 649–686
- Holm PM, Lou S, Nielsen A (1982) The geochemistry and petrogenesis of the lavas of the Vulsinian district, Roman Province, Central Italy. *Contrib Miner Petrol* 80:367–378
- Holmes A (1950) Petrogenesis of katungite and its associates. *Am Miner* 35:772–792
- Iddings JP (1895) Absarokite-shoshonite-banakite series. *J Geol* 3:935–959
- Karsli O, Dokuz A, Kaliwoda M, Uysal I, Aydin F, Kandemir R, Fehr K-T (2014) Geochemical fingerprints of Late Triassic calc-alkaline lamprophyres from the eastern Pontides, NE Turkey: a key to understanding lamprophyre formation in a subduction-related environment. *Lithos* 197:181–197
- Kay RW, Gast PW (1973) The rare earth content and origin of alkali-rich basalts. *J Geol* 81:653–682
- Le Maitre RW (ed) (1989) A classification of igneous rocks and glossary of terms: recommendations of the International Union of Geological Sciences Subcommittee on the systematics of igneous rocks. Blackwell Scientific Publications, Oxford, p 193
- Li XH, Li ZX, Li WX, Wang XC, Gao Y (2013) Revisiting the “C-type adakites” of the lower Yangtze River belt, central eastern China: in-situ zircon Hf-O isotope and geochemical constraints. *Chem Geol* 345:1–15
- Liu D, Zhao Z, Zhu DC, Niu Y, DePaolo DJ, Harrison TM, Mo X, Dong G, Zhou S, Sun C, Zhang Z, Liu J (2014) Postcollisional potassic and ultrapotassic rocks in southern Tibet: mantle and crustal origins in response to India-Asia collision and convergence. *Geochim Cosmochim Acta* 143:207–231
- Lu YJ, Kerrich R, McCuaig TC, Li ZX, Hart CJR, Cawood PA, Hou ZQ, Bagas L, Cliff J, Belousova EA, Tang S (2013) Geochemical, Sr-Nd-Pb, and zircon Hf-O isotopic compositions of Eocene-Oligocene shoshonitic and potassic adakite-like felsic intrusions in western Yunnan, SW China: petrogenesis and tectonic implications. *J Petrol* 54:1309–1348
- Lu YJ, McCuaig TC, Li ZX, Jourdan F, Hart CJR, Hou ZQ, Tang S (2015) Paleogene post-collisional lamprophyres in western Yunnan, western Yangtze Craton: mantle source and tectonic implications. *Lithos* (in press)
- Luguet A, Jaques AL, Pearson DG, Smith CB, Bulanova GP, Roffey SL, Rayner MJ, Lorand JP (2009) An integrated petrological, geochemical and Re-Os isotope study of peridotite xenoliths from the Argyle lamproite, western Australia, and implications for cratonic diamond occurrences. *Lithos* 112:1096–1108
- Maughan DT, Keith JD, Christiansen EH, Pulsipher T, Hattori K, Evans NJ (2002) Contributions from mafic alkaline magmas to the Bingham porphyry Cu-Au-Mo deposit, Utah, USA. *Mineral Deposita* 37:14–37
- Menzies MA, Hawkesworth CJ (eds) (1987) *Mantle metasomatism*. Academic Press, London, p 472
- Mitchell RH (1986) *Kimberlites: mineralogy, geochemistry, and petrology*. Plenum Press, New York, p 442
- Mitchell RH (1989) Aspects of the petrology of kimberlites and lamproites: some definitions and distinctions. In: Ross J, Jaques AL, Ferguson J, Green DH, O’Reilly SY, Danchin RV, Janse AJA (eds) *Kimberlites and related rocks*, vol 14. Geological Society of Australia Special Publication, pp 7–45
- Mitchell RH, Bergman SC (1991) *Petrology of lamproites*. Plenum Press, New York, p 447
- Mittempergher M (1965) Volcanism and petrogenesis in the San Venanzo area, Italy. *Bull Volc* 28:1–12
- Morrison GW (1980) Characteristics and tectonic setting of the shoshonite rock association. *Lithos* 13:97–108
- Müller D, Stumpfl EF, Taylor WR (1992) Shoshonitic and alkaline lamprophyres with elevated Au and PGE concentrations from the Kreuzeck Mountains, Eastern Alps, Austria. *Miner Petrol* 46:23–42
- Müller D, Morris BJ, Farrand MG (1993) Potassic alkaline lamprophyres with affinities to lamproites from the Karinya Syncline, South Australia. *Lithos* 30:123–137
- Orozco-Garza A, Dostal J, Keppie JD, Paz-Moreno FA (2013) Mid-tertiary (25–21 Ma) lamprophyres in NW Mexico derived from subduction-modified subcontinental lithospheric mantle in an extensional backarc environment following steepening of the Benioff zone. *Tectonophysics* 590:59–71
- Peccerillo A (1992) Potassic and ultrapotassic rocks: compositional characteristics, petrogenesis, and geologic significance. *IUGS Episodes* 15:243–251
- Peccerillo A, Taylor SR (1976) Geochemistry of Eocene calc-alkaline volcanic rocks from the Kastamonu area, northern Turkey. *Contrib Miner Petrol* 58:63–81
- Prider RT (1960) The leucite lamproites of the Fitzroy Basin, western Australia. *J Geol Soc Aust* 6:71–118
- Priyatkina N, Khudoley AK, Ustinov VN, Kullerud K (2014) 1.92 Ga kimberlitic rocks from Kimozero, NW Russia: their geochemistry, tectonic setting and unusual field occurrence. *Precamb Res* 249:162–179
- Rittmann A (1933) Die geologisch bedingte Evolution und Differentiation des Somma-Vesuv Magmas. *Zeitschrift für Vulkanologie* 15:8–94
- Rock NMS (1977) The nature and origin of lamprophyres: some definitions, distinctions and derivations. *Earth Sci Rev* 13:123–169
- Rock NMS (1987) The nature and origin of lamprophyres: an overview. In: Fitton JG, Upton BGJ (eds) *Alkaline igneous rocks*, vol 30. Geological Society of London Special Publication, pp 191–226
- Rock NMS (1991) *Lamprophyres*. Blackie, Glasgow, p 285
- Rock NMS, Hallberg JA, Groves DI, Mather PJ (1988) Archaean lamprophyres in the goldfields of the Yilgarn block, western Australia: new indications of their widespread distribution and significance. In: Ho SE, Groves DI (eds) *Advances in understanding Precambrian gold deposits volume II*, vol 12. Geology Department and University Extension, The University of Western Australia Publication, pp 245–275
- Rock NMS, Taylor WR, Perring CS (1990) Lamprophyres—what are lamprophyres? In: Ho SE, Groves DI, Bennett JM (eds) *Gold deposits of the Archaean Yilgarn block, Western Australia: nature, genesis and exploration guides*, vol 20. Geology Department and

- University Extension, The University of Western Australia Publication, pp 128–135
- Rogers NW, Hawkesworth CJ, Parker RJ, Marsh JS (1985) The geochemistry of potassic lavas from Vulcini, Central Italy, and implications for mantle enrichment processes beneath the Roman Region. *Contrib Miner Petrol* 90:244–257
- Rowins SM, Cameron EM, Lalonde AE, Ernst RE (1993) Petrogenesis of the late Archaean syenitic Murdoch Creek pluton, Kirkland Lake, Ontario: evidence for an extensional tectonic setting. *Can Miner* 31:219–244
- Sahama AG (1974) Potassium-rich alkaline rocks. In: Sørensen H (ed) *The alkaline rocks*. Wiley, New York, pp 96–109
- Savelli C (1967) The problem of rock assimilation by Somma-Vesuvius magma: I. composition of Somma and Vesuvius lavas. *Contrib Miner Petrol* 16:328–353
- Skinner EMW (1989) Contrasting group 2 and group 1 kimberlite petrology: towards a genetic model for kimberlites. In: Ross J, Jaques AL, Ferguson J, Green DH, O'Reilly SY, Danchin RV, Janse AJA (eds) *Kimberlites and Related Rocks*, vol 14. Geological Society of Australia, Sydney, Special Publication, pp 528–544
- Smith CB, Gurney JJ, Skinner EMW, Clement CR, Ebrahim N (1985) Geochemical character of southern African kimberlites: a new approach based upon isotopic constraints. *Trans Geol Soc South Afr* 88:267–280
- Soloviev SG (2014) *The metallogeny of shoshonitic magmatism*, vol I. Scientific World Publications, Moscow, pp 1–528 (in Russian)
- Sørensen H (1974) Origin of the alkaline rocks: a summary and retrospect. In: Sørensen H (ed) *The alkaline rocks, petrogenesis*. Wiley, London, pp 535–539
- Štemprok M, Dolejš D, Holub F (2014) Late Variscan calc-alkaline lamprophyres in the Krupka ore district, Eastern Krušné hory/Erzgebirge: their relationship to Sn-W mineralization. *J Geosci* 59:41–68
- Till CB, Grove TL, Withers AC (2012) The beginnings of hydrous mantle wedge melting. *Contrib Miner Petrol* 163:669–688
- Torabi G (2011) Middle Eocene volcanic shoshonites from the western margin of the Central-East Iranian microcontinent (CEIM), a mark of previously subducted CEIM-confining oceanic crust. *Petrology* 19:675–689

3.1 Introduction

Modern potassic igneous rocks occur in a wide range of tectonic environments, from continental to oceanic and within-plate settings, some of which are not apparently associated with subduction (Joplin 1968; Morrison 1980; Müller et al. 1992a; Müller 2002; Li et al. 2013; Rao et al. 2014; Soloviev 2014a, b; Jamali and Mehrabi 2015; Liu et al. 2015). It is therefore important, whether for improving exploration models for ancient mineral deposits or reconstructing ancient terranes, to be able to distinguish the tectonic settings in which ancient potassic igneous rocks were generated. The following chapter seeks to provide such a distinction.

3.2 Tectonic Settings of Potassic Igneous Rocks

Young (<60 Ma) potassic igneous rocks have been recognized throughout the world in five principal tectonic settings (Fig. 3.1 and Table 3.1), of which two are closely related (Müller et al. 1992a). A schematic overview of the different tectonic settings in which potassic igneous rocks are recorded is shown in Fig. 3.2.

3.2.1 Continental Arc

Continental arc potassic igneous rocks are well represented in the Andean volcanic belt (e.g.

Venturelli et al. 1978; Kontak et al. 1986) and in the Aeolian Islands in the Mediterranean (Ellam et al. 1989). Such settings are associated with reorganization of plate boundaries due to oblique plate convergence, and are normally characterized by relatively flat subduction and broad Benioff Zones. The nature and distribution of magmatic activity in the overriding plate is a function of the convergence rate, the age of the subducted lithosphere, and the presence of features such as seamount chains or aseismic ridges (Wilson 1989; Kay and Mpodozis 2001; Kay et al. 2005).

3.2.2 Postcollisional Arc

Postcollisional arc potassic igneous rocks are exemplified by the Eastern and Western Alps (e.g. Venturelli et al. 1984; Müller et al. 1992a), where the continental plates collided during the Eocene and subduction has long since ceased. High-K rocks derived in a postcollisional arc setting are also documented in southern Tibet (e.g. Guo et al. 2013), and Yunnan province in China (e.g. Lu et al. 2013a, b). This setting represents the most complex case of subduction-related magmatism, in which the suture zone forms an area of crustal thickening, characterized by complex magmatic activity and tectonic uplift (Wilson 1989; Lu et al. 2013b; Chen et al. 2015; Jiang et al. 2015). After collision, potassic igneous rocks may be emplaced as dykes, commonly followed by alkaline volcanism where extensional tectonic regimes develop

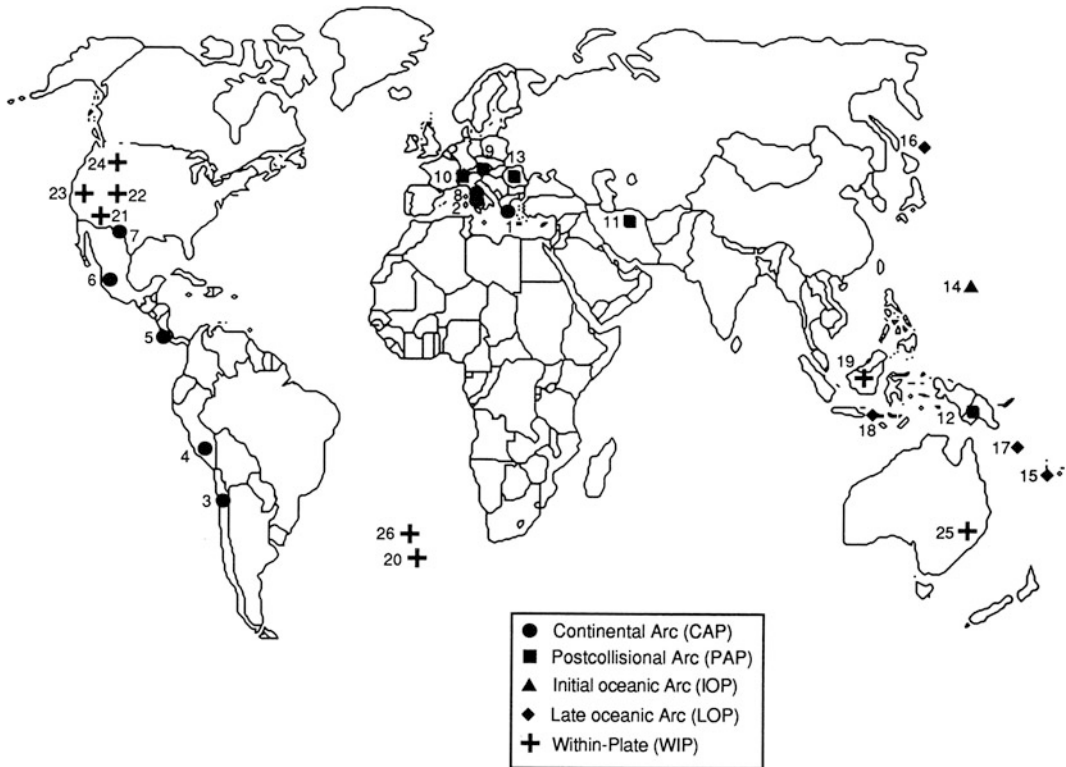


Fig. 3.1 Global distribution of Cenozoic potassic igneous rock suites used to erect the series of discriminatory diagrams. Data from many additional pre-Cenozoic rock suites were compiled in unfiltered database SHOSH1, but are not shown because their tectonic settings are uncertain. See Table 3.1 for data sources. 1 Aegean Islands, 2 Aeolian Islands, 3 Chile, 4 Peru, 5 Costa Rica, 6

Mexico, 7 New Mexico, 8 Roman Province, 9 Eastern Alps, 10 Western Alps, 11 Iran, 12 Papua New Guinea, 13 Roumania, 14 Mariana Islands, 15 Fiji, 16 Kuril Islands, 17 Vanuatu, 18 Sunda Arc, 19 Borneo, 20 Gough Island, 21 Arizona, 22 Colorado, 23 California, 24 Wyoming, 25 New South Wales, 26 Tristan da Cunha. From Müller et al. (1992a)

as a consequence of uplift (Wilson 1989; Müller et al. 1992a).

3.2.3 Oceanic (Island) Arc

Oceanic (island) arc potassic igneous rocks are generated at the site of subduction of one oceanic lithospheric plate beneath another. Oceanic arc settings normally show steep subduction and, compared to continental arc settings, relatively short distances between volcanic arc and subduction trench where projected to surface. High-K rocks from this setting can be subdivided into two types: *initial* and *late* oceanic arc potassic igneous rocks.

Initial Oceanic Arc Potassic Igneous Rocks

Initial oceanic arc settings are exemplified by unusual potassic igneous rocks (including shoshonites) from the northern Mariana Arc (Stern et al. 1988; Bloomer et al. 1989; Lin et al. 1989). Whereas the initial and fore-arc melts in most island arcs have boninitic or low-K tholeiitic affinities, and potassic igneous rocks occur only in the mature, back-arc stages of arc evolution, the Mariana potassic igneous rocks occur along the magmatic front, and may represent the reconstruction of the arc following an episode of back-arc rifting (Stern et al. 1988). More recent work (Till et al. 2012) explains the unique compositions of the potassic igneous rocks in the

Table 3.1 Data sources for potassic igneous rocks in filtered database SHOSH2

1. Continental arcs	2. Postcollisional arcs	3a. Oceanic arcs (initial)	3b. Oceanic arcs (late)	4. Within-plate settings
<i>Aegean Islands, Greece^a</i>	<i>Alps (Eastern)</i>	<i>Mariana Islands^a</i>	<i>Fiji^a</i>	<i>Borneo</i>
Pe-Piper (1980) 4/8	Deutsch (1984) 5/5	Bloomer et al. (1989) ^b 2/7	Gill and Whelan (1989) 1/9	Bergman et al. (1988) 6/11
	Müller et al. (1992b) 8/11	Dixon and Batiza (1979) 6/10		
<i>Aeolian Islands, Italy</i>		Garcia et al. (1979) 1/6	<i>Kuril Islands</i>	<i>Gough Island, Atlantic</i>
Ellam et al. (1989) 7/22	<i>Alps (Western)^a</i>	Lin et al. (1989) ^c 2/7	Bailey et al. (1989) 3/4	Le Maitre (1962) 4/13
Keller (1974) 3/9	Beccaluva et al. (1983) 6/6	Meijer and Reagan (1981) 14/14		Le Roex (1985) 7/19
	Dal Piaz et al. (1979) 2/13	Stern (1979) 2/3	<i>Sunda Arc</i>	Weaver et al. (1987) 2/4
<i>Andes, Chile</i>	Venturelli et al. (1984) 5/7	Taylor et al. (1969) 1/2	Foden (1979) 12/121	
Deruelle (1982) 1/5			J.D. Foden (unpl. data) 5/97	<i>North American Cordillera^a</i>
Thorpe et al. (1976) 3/4	<i>Iran (Northeast)</i>		Foden and Varne (1980) 6/10	Arizona
	Spies et al. (1984) 4/6		Hutchison and Jezek (1978) 6/19	Nicholls (1969) 2/2
<i>Andes, Peru^a</i>			Wheller (1986) 29/122	Roden (1981) 2/2
Kontak et al. (1986) 4/4	<i>Papua New Guinea</i>		Whitford (1975) 12/160	Roden and Smith (1979) 1/2
	BMR ^d (unpl. data) 83/166		Whitford and Jezek (1979) 2/8	Rogers et al. (1982) 5/5
<i>North American Cordillera^a</i>	De Paolo and Johnson (1979) 1/8		Whitford et al. (1979) 2/13	Colorado
Costa Rica	Jakes and Smith (1970) 13/24			Alibert et al. (1986) 1/1
Reagan and Gill (1989) 4/4	Jaques (1976) 3/17		<i>Vanuatu^a</i>	Leat et al. (1988) 6/6
Mexico	McKenzie and Chappell (1972) 3/10		Gorton (1977) 10/12	Thompson et al. (1984) 4/5
Allan and Carmichael (1984) 3/3	J.P. Richards (unpl. data) 16/30			California, Sierra Nevada
Carmichael (pers. comm.) 2/2	Smith (1972) 2/29			Dodge and Moore (1981) 18/19
Luhr and Kyser (1989) 1/1	Sombroek (1985) 19/47			Van Kooten (1980) 13/13
Luhr et al. (1989) 7/8				Wyoming
New Mexico, Rio Grande	<i>Roumania</i>			Barton and van Bergen (1981) ^b 1/5

(continued)

Table 3.1 (continued)

1. Continental arcs	2. Postcollisional arcs	3a. Oceanic arcs (initial)	3b. Oceanic arcs (late)	4. Within-plate settings
Duncker et al. (1991) 2/8	Peccerillo and Taylor (1976b) ^c 4/4			Gest and McBirney (1979) 2/5
				Nicholls and Carmichael (1969) 1/4
<i>Roman Province</i> ^a				
Appleton (1972) 2/12				<i>New South Wales, Australia</i>
Civetta et al. (1981) 6/6				Cundari (1973) 32/37
Cox et al. (1976) 2/4				
Cundari (1979) 6/14				<i>Tristan da Cunha, Atlantic</i> ^a
Cundari and Mattias (1974) 5/17				Weaver et al. (1987) 2/4
Fornaseri et al. (1963) 7/37				
Ghiara and Lirer (1976) 2/6				
Holm et al. (1982) 2/6				
Poli et al. (1984) 4/4				
Rogers et al. (1985) 7/8				
Savelli (1967) 5/19				
Thompson (1977) 1/2				
Van Bergen et al. (1983) 8/8				

3/6 = 3 analyses were retained in filtered database SHOSH2 from 6 analyses in unfiltered database SHOSH1 and original reference From Müller et al. (1992a)

^aAdditional references were incorporated in SHOSH1, but all analyses were filtered out for SHOSH2

^bOnly major elements

^cOnly trace elements

^dBureau of Mineral Resources, Geology and Geophysics, Australia (now Australian Geological Survey Organisation), PETCHEM database

northern Mariana Arc as the product of chlorite dehydration melting in a relatively cool subduction zone (see Sect. 4.3).

and/or calc-alkaline rocks and farthest from the trench, in the classic volcanic sequence referred to above.

Late Oceanic Arc Potassic Igneous Rocks

Late oceanic arc settings are well represented in Fiji (Gill 1970), the New Hebrides (Gorton 1977; Marcelot et al. 1983), and Lihir Island, Papua New Guinea (Wallace et al. 1983; Müller et al. 2001) in the western Pacific. Here, potassic igneous rocks form the *youngest* volcanic products; they were erupted after lower K-tholeiitic

3.2.4 Within-Plate

Within-plate potassic igneous rocks are not related to any form of subduction. They are particularly well represented in the North American Cordillera (Fig. 3.1 and Table 3.1). They may be associated with hot-spot activity or with extensional (particularly rift) tectonics (e.g. in the western branch of

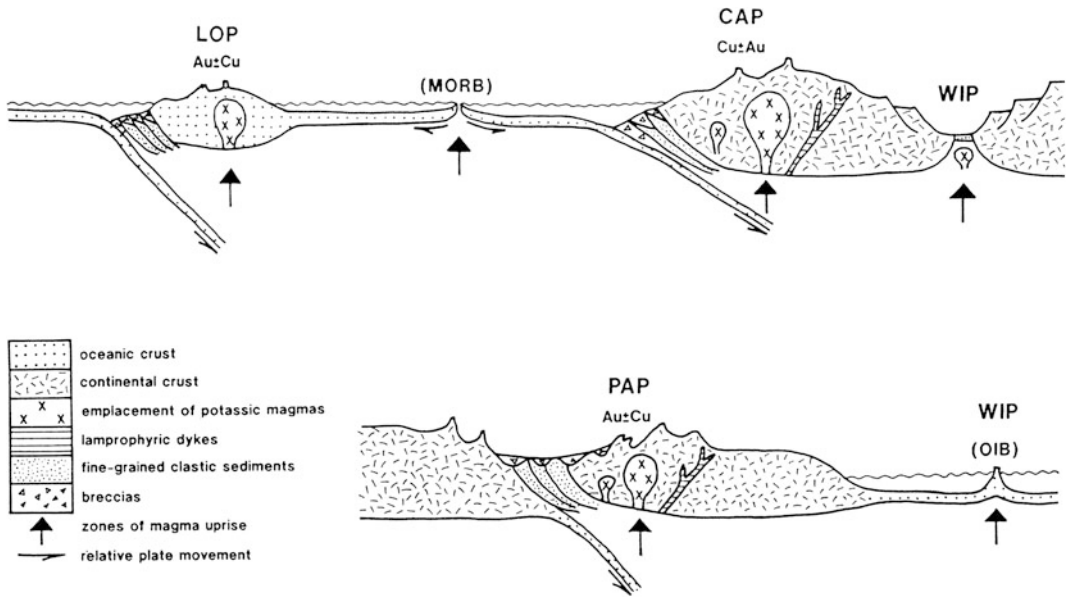


Fig. 3.2 Schematic overview of potassic igneous rocks from different tectonic settings. *CAP* continental arc; *PAP* postcollisional arc; *LOP* late oceanic arc; *WIP*

within-plate setting; *MORB* mid-ocean ridge basalt; *OIB* oceanic island basalt. Modified after Mitchell and Garson (1981)

the East African Rift), and the magmas from which they crystallize are commonly generated at greater depths than those of the other four categories (Foley et al. 1987, 2011).

3.2.5 Problems with Tectonic Classification

In areas of plate tectonic complexity, there may be ambiguity about the classification even of young potassic igneous rocks into one of these five settings. In the western Sunda Arc of Indonesia (Curry et al. 1977), for example, not only does the crustal seismic-velocity structure change from continental to oceanic moving east from Sumatra into Java, but the subduction angle and traceable depth of subduction also change from oblique, shallow, and <200 km in Sumatra to orthogonal, steep, and >600 km in Java. Reflecting these changes, potassic igneous rocks occur on the back-arc side of Java and islands further east (Whitford et al. 1979), and are hence attributed to a late oceanic arc setting. In Sumatra, however,

they are relatively early, occur on the fore-arc side (Rock et al. 1982), and are better attributed to an initial oceanic arc setting.

Other difficulties arise in continental-scale igneous provinces such as the Cenozoic of the North American Cordillera. Although potassic igneous rocks in young volcanic suites along the western seaboard (e.g. Crater Lake, Oregon; Bacon 1990) are unequivocally continental arc, and potassic igneous rocks from states well inland (e.g. North Dakota; Kirchner 1979) are within-plate by definition, many potassic igneous rocks from intervening states (e.g. Colorado, Wyoming; Gest and McBirney 1979; Leat et al. 1988) could be of either affinity. Following most previous authors, within-plate affinities are assumed where there is a clear association with rifting (e.g. Sierra Nevada lavas, California; Van Kooten 1980), or where the depth of magma generation is too great for subduction affinities (e.g. Navajo Province, New Mexico; Rock 1991).

A further set of ambiguities arises from differing opinions in the literature. For example,

Cundari (1979) uniquely assumes a within-plate setting for the Sabatini lavas of Italy, whereas all other authors concerned with Roman Province potassic igneous rocks assume a continental arc setting (e.g. Civetta et al. 1981; Peccerillo 1985; Beccaluva et al. 1991).

3.3 History of Discrimination of Tectonic Setting by Geochemical Means

First put forward to distinguish the tectonic setting of ancient basalts (e.g. Pearce and Cann 1973), geochemical discrimination diagrams were used widely in the late 1970s and early 1980s. Equivalent diagrams were introduced to classify granites (*sensu lato*) tectonically (e.g. Pitcher 1983; Pearce et al. 1984), and the method was also extended to the petrological classification of altered and/or metamorphosed igneous rocks (e.g. Floyd and Winchester 1975). As with many other geological methods, a period of criticism and reappraisal followed (e.g. Smith and Smith 1976; Morrison 1978), but these drawbacks have proved insufficient to seriously limit the use of the method. Geochemical discrimination diagrams, although initially empirical, subsequently received a formal basis from statistical analysis and theoretical arguments (e.g. Pearce 1976).

The principle behind the successful use of these diagrams is the delineation of trace-element differences between modern rocks in different known settings, based on a comprehensive database; these differences are then depicted in diagrams which can be used to assign older samples from equivocal tectonic settings. The assumed relatively immobile HFSE (namely Ti, Y, Zr, Nb, Hf, Ta), REE, as well as the elements Th and P, are generally considered to be most suitable for use in these diagrams, although some studies have suggested that Th (Wood et al. 1979; Villemant et al. 1993) and REE (Hellman et al. 1979; Allen and Seyfried 2005; Tropper et al. 2011) may be mobile under certain conditions, and most of these

elements may be somewhat mobile in highly altered, mineralized wallrocks.

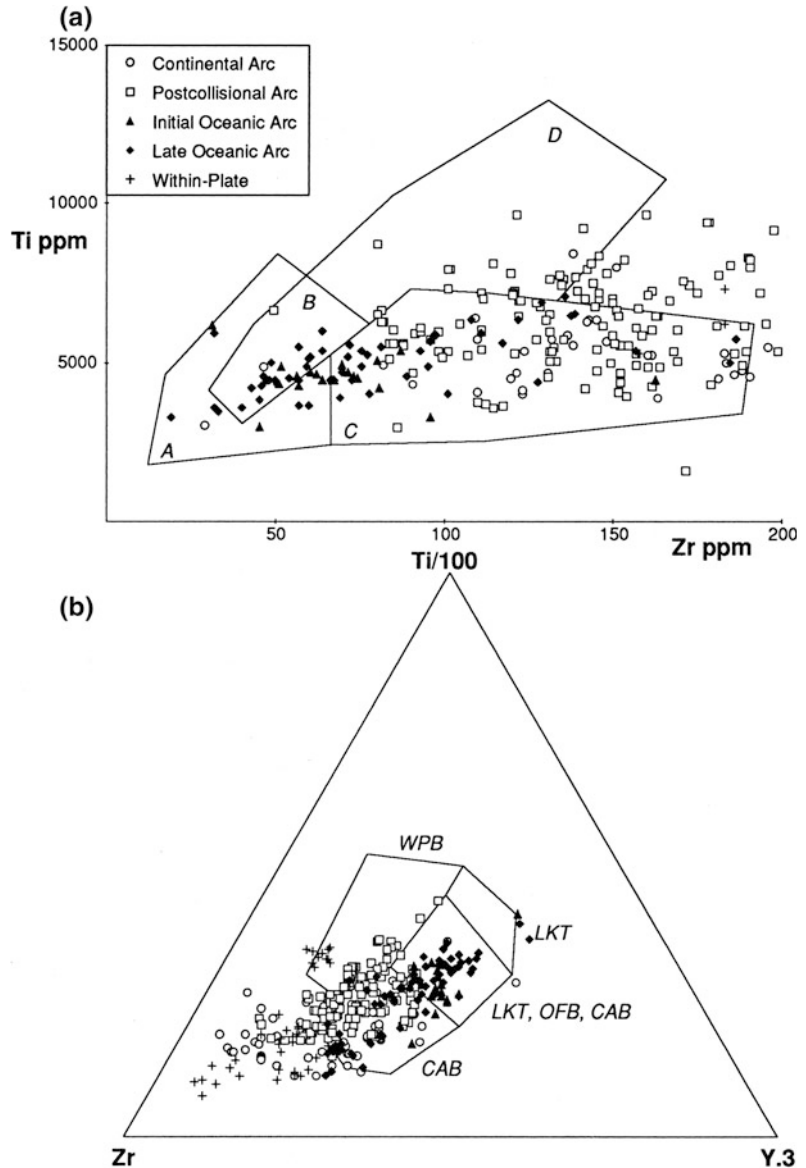
Previous discrimination diagrams, which have been developed for basalts and granitic rocks, are not suitable for discriminating the tectonic setting of potassic igneous rocks. For example:

- Ti–Zr and Ti–Zr–Y diagrams of Pearce and Cann (1973): Potassic igneous rocks extend to compositions well outside the defined fields on these diagrams and, in particular, within-plate potassic igneous rocks normally show much higher Zr concentrations than indicated by the defined within-plate field for other igneous rocks (Fig. 3.3).
- Ti–Zr–Sr diagram of Pearce and Cann (1973): This diagram cannot separate within-plate from subduction-related potassic igneous rocks. Most potassic igneous rocks plot misleadingly in the calc-alkaline field, and those from postcollisional settings plot erroneously into the ocean-floor basalt field. The discrimination is also subject to the severe limitation of Sr mobility for hydrothermally altered rocks.
- Zr/Y versus Zr diagram of Pearce and Norry (1979): Subduction-related potassic igneous rocks from continental arcs and from intra-oceanic tectonic settings plot erroneously within the mid-ocean ridge basalt (MORB) and within-plate basalt fields on this diagram.
- Hf/3–Th–Ta diagram of Wood et al. (1979): Nearly all potassic igneous rocks, even those from known within-plate tectonic settings, plot misleadingly into the subduction-related field on this diagram.

The few previously developed diagrams that actually accommodate potassic igneous rocks (Pearce 1982), only allow them to be identified petrologically; the diagrams do not discriminate the tectonic settings of the rocks (see Fig. 3.4).

Another common plot for comparing geochemical patterns is the spidergram (Thompson 1982), but spidergrams do not effectively separate potassic igneous rocks from different tectonic settings (Fig. 3.5). For example, although

Fig. 3.3 Non-validity of two popular geochemical discrimination diagrams (Pearce and Cann 1973) when applied to potassic igneous rocks. Data from SHOSH2. In (a), fields A + B = low-K tholeiites (LKT), B + C = calc-alkaline basalts, B + D = ocean-floor basalt. In (b), *WPB* within-plate basalts, *LKT* low-K tholeiites, *OFB* ocean-floor basalts, *CAB* calc-alkaline basalts. From Müller et al. (1992a)



arc-related potassic igneous rocks (Fig. 3.5a–d) show relatively high values of K, Rb, Cs, Ba, and Pb (Sun and McDonough 1989) and the supposedly diagnostic (negative) Ti–Nb–Ta (TNT) anomalies (Saunders et al. 1980; Briquieu et al. 1984; Foley and Wheller 1990), these features are also shown by some within-plate potassic igneous rocks (e.g. the potassic lamprophyres from Borneo; Bergman et al. 1988; see Fig. 3.5e). There is no simple relationship between TNT anomalies in spidergram patterns

and subduction-related processes of magma generation, because potassic igneous rocks without those anomalies can also occur in subduction settings (Rock 1991).

Many workers have tried to explain the negative anomalies of the HFSE Ti, Nb, and Ta, in terms of their retention in the subducted oceanic slab during the dehydration process (Pearce and Peate 1995; Rudnick and Fountain 1995; Tiepolo et al. 2000; Kalfoun et al. 2002). This is because these elements are thought to have low

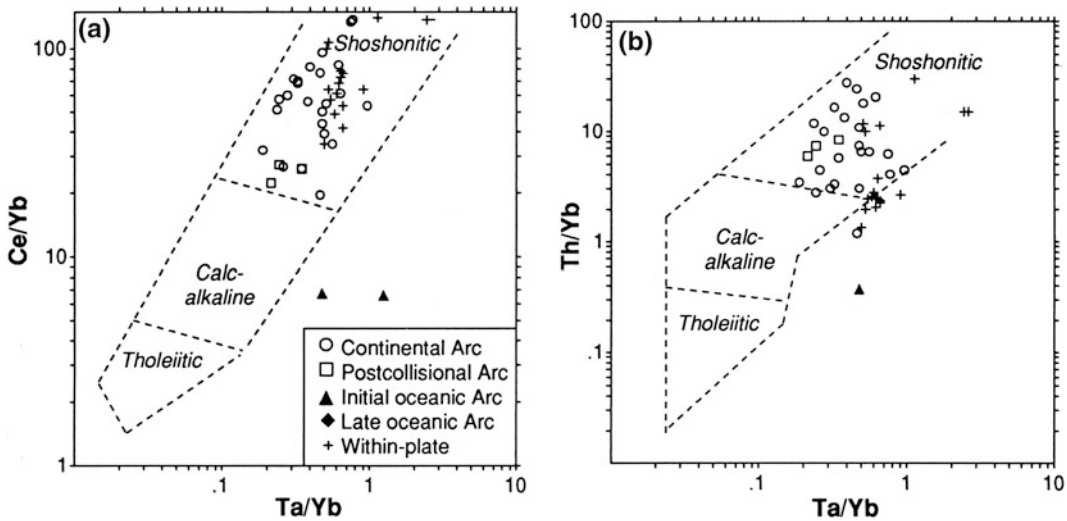


Fig. 3.4 Confirmation of shoshonitic affinities of rocks used in this study. Diagram from Pearce (1982), data from SHOSH2. Note that only a minority of samples in

SHOSH2 have determinations for Ta, Yb, Ce and/or Th and can thus be plotted on this diagram. From Müller et al. (1992a)

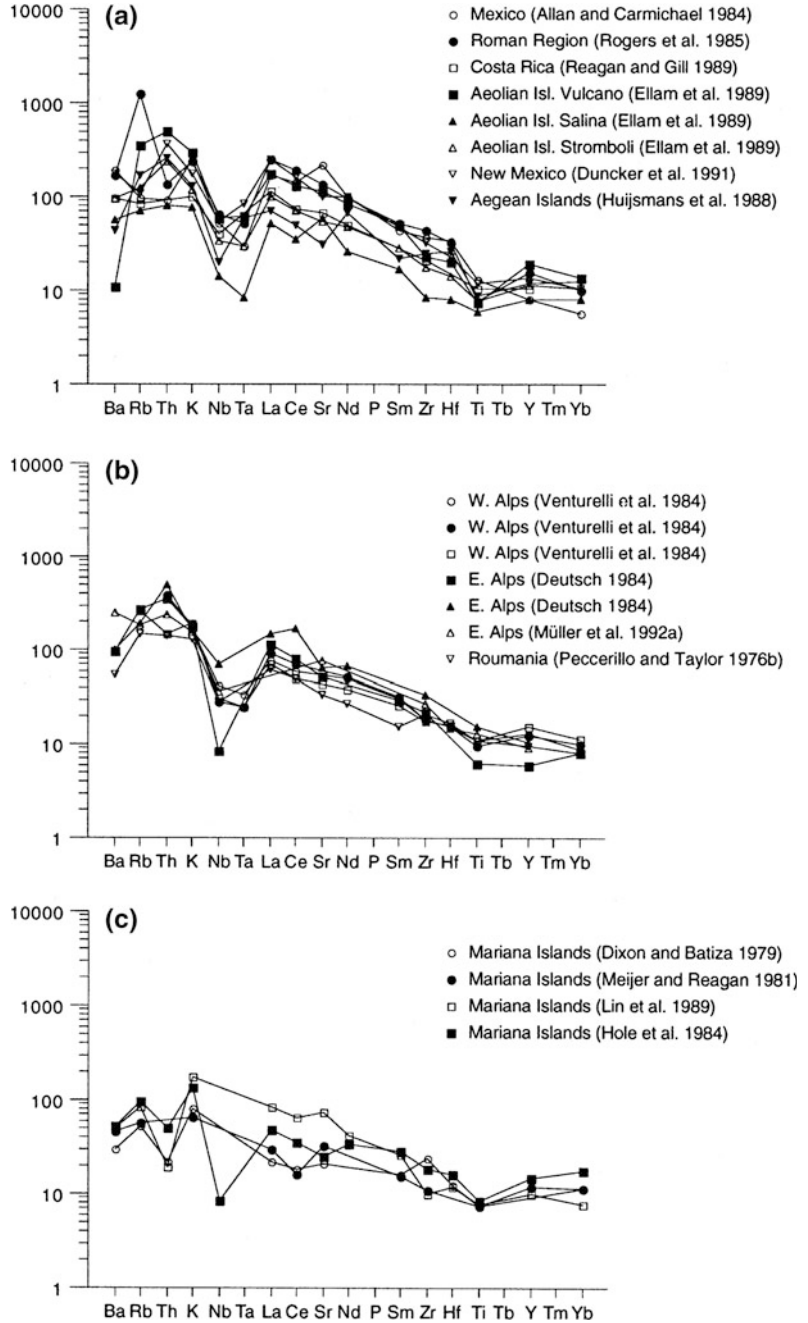
solubilities in the metasomatic fluids that transport mantle-incompatible elements from the subducted slab into the overlying mantle wedge (e.g. Saunders et al. 1991). It has been suggested also that these elements were retained in the mantle wedge in minerals such as rutile, ilmenite, and titanite during partial melting (Foley and Wheller 1990; Kalfoun et al. 2002). However, more recent studies attempt to explain the Ti depletion of arc magmas as a result of the higher oxygen fugacities (fO_2) in subduction zones (Lange et al. 1993; Toplis and Carroll 1995; Dalpè and Baker 2000). At high fO_2 and during small degrees of partial melting of upper mantle material, the HFSE, such as Ti, are preferentially retained in refractory rutile phases. Experimental studies by Colasanti et al. (2011) suggest that, with decreasing fO_2 , hydrogen may substitute into rutile as hydroxyl (OH^-), thus increasing its solubility. Generally, higher temperatures are required to melt Ti-bearing phases when fO_2 is higher, thus producing Ti depletion in the potassic melts derived from subduction zones (Edwards et al. 1994). Other studies suggest that the HFSE depletions in arc magmas are caused by the precipitation of HFSE-bearing phases as the melt migrates upwards through the mantle

wedge, while simultaneously dissolving phases with relatively low HFSE abundances (Kelemen et al. 1990; Woodhead et al. 1993).

More recently, the results of Ionov and Hofmann (1995) suggest that amphibole is an important host mineral for Nb and Ta in the upper mantle, and may control the development of negative Nb–Ta anomalies in arc magmas (Tiepolo et al. 2000). Ionov and Hofmann (1995) postulated a model in which fluids, generated by dehydration of the subducted oceanic slab, ascend through the mantle wedge and precipitate amphiboles. Niobium and Ta are transferred with these fluids into the mantle wedge, where these elements are partitioned into crystallizing amphibole, thus inducing low Nb and Ta concentrations in the residual fluid. As the residual fluids migrate further, they may induce partial melting in high-temperature regions of the mantle wedge, thus producing melts with negative Nb and Ta anomalies (Ionov and Hofmann 1995).

In view of the discussions above, the use of geochemical discrimination diagrams in isolation from other lines of evidence for tectonic setting is never recommended. Wherever possible, geochemistry should be combined with other geoscientific information, and attempts to combine

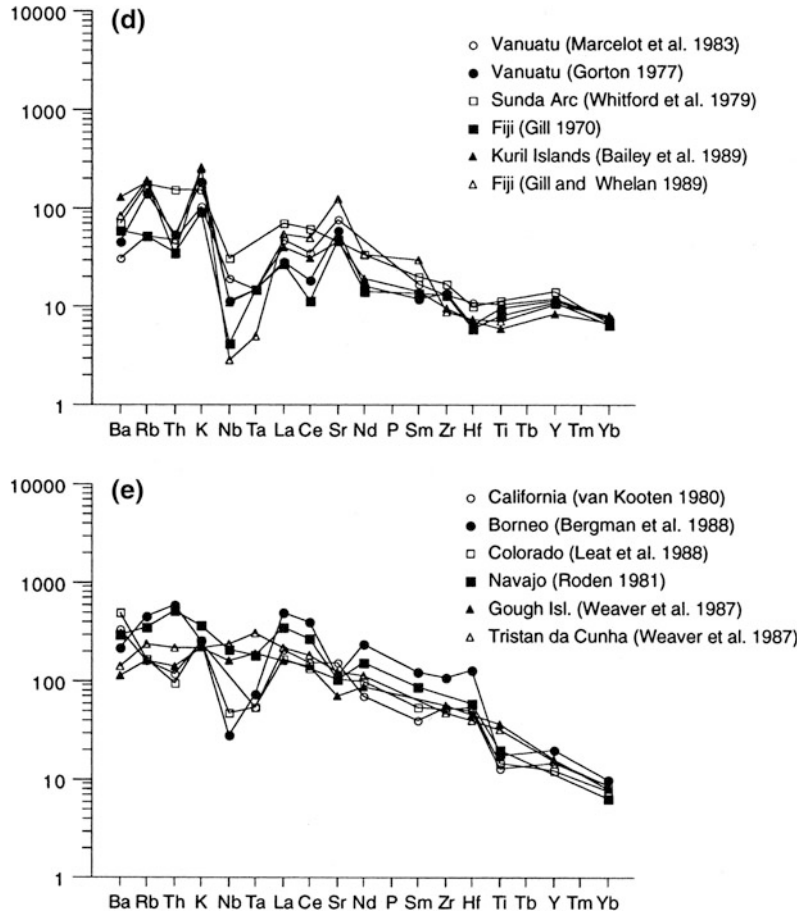
Fig. 3.5 Representative chondrite-normalized spidergram patterns for potassic igneous rocks from the five tectonic settings recognized in this study. Element order and normalizing factors after Thompson (1982).
a Continental arc settings. **b** Postcollisional arc settings. **c** Initial oceanic arc settings. **d** Late oceanic arc settings. **e** Within-plate settings. Sources are listed in references. From Müller et al. (1992a)



all these lines of evidence into an expert-system should be made (Pearce 1987). However, understanding of potassic igneous rocks is at present insufficiently advanced for such a sophisticated approach. The pilot study presented

here, therefore, attempts to show that potassic igneous rocks from different tectonic settings are geochemically distinct, and then uses this to erect discrimination diagrams for the tectonic settings of older potassic igneous rocks.

Fig. 3.5 (continued)



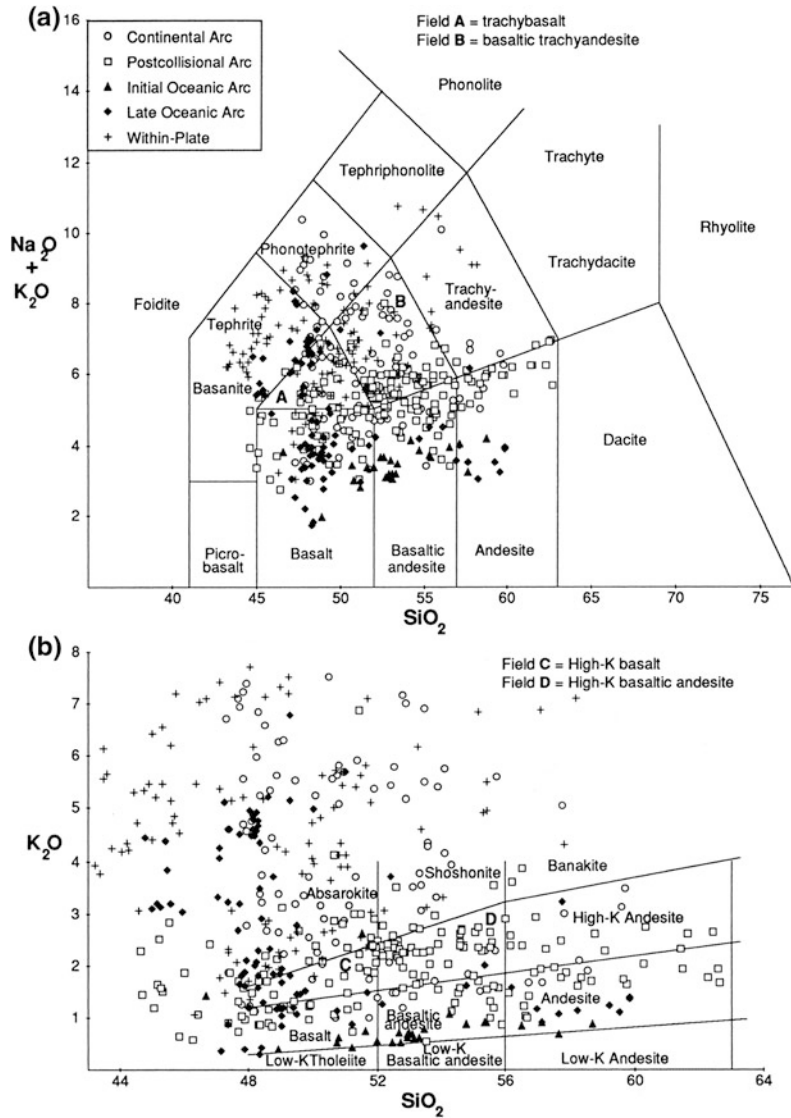
3.4 Erection of Databases SHOSH1 and SHOSH2

There are many possible options to balance the breadth of the database used against the precision of discrimination actually achieved. For example, at one extreme, it might be possible to discriminate the tectonic setting of *all* igneous rocks irrespective of their compositions; this would be comprehensive in its scope, but limited in its discriminatory power. At the other extreme, it might be possible to restrict attention to a very narrow range of compositions (e.g. rocks within the shoshonite field on Fig. 3.6b); this would no doubt achieve much better discrimination, but would be very limited in its scope. In general, the

more diffuse (less internally coherent) the database, the lower its discriminatory power.

There is also a multitude of options for screening an initial database. Many authors have used chemical screens: for example, Pearce and Cann (1973) restrict attention to analyses with total (MgO + CaO) contents between 12 and 20 wt%, and Pearce and Norry (1979) use those analyses with total alkalis below 20 wt%. However, such screens are always arbitrary and artificially imposed. It is considered preferable here to embrace the entire natural compositional range of an igneous suite as far as possible. The major exception, where the argument for screening is irrefutable, is in isolating chemical differences that are due to tectonic setting (that is, reflect the nature of the source region and magma

Fig. 3.6 Established classification diagrams illustrating the range of compositions in the filtered database SHOSH2. **a** TAS diagram recommended by the IUGS Subcommittee on Igneous Rock Systematics (Le Maitre 1989). **b** K_2O-SiO_2 diagram (Peccerillo and Taylor 1976a) now widely adopted in the literature; this differs in essence from the equivalent IUGS diagram only in the absence of the top three fields. Analyses have been recalculated to 100 % free of volatiles before plotting as wt% in both diagrams. From Müller et al. (1992a)



generation processes within it), from those that reflect the subsequent history of the magma (magmatic differentiation or accumulation, secondary alteration or weathering, etc.). This usually requires restricting the rocks within a database to fresh and primitive samples.

This book attempts a compromise in both the breadth of the database used and in its screening so that it is sufficiently broad in scope but still provides critical discriminatory power. Over 100 published references containing relevant data were first identified by combining traditional

(manual) and computerized literature search, using keywords such as “shoshonitic”, “K-rich”, and “potassic”. Bibliographic indexes searched include *Mineralogical Abstracts*, *Geological Abstracts* and the CD-ROM version of *GeoRef*. Some large existing source databases such as IGBA, LAMPDA (Rock 1991), the ultrapotassic rocks database of Foley et al. (1987), and PET-CHEM (Australian Bureau of Mineral Resources) were also searched. Data from all these sources were supplemented by 50 new high-precision analyses of potassic igneous rocks from

Australia and Papua New Guinea for a comprehensive suite of up to 35 major and trace elements. Methods outlined by Rock (1988, 1991) for the compilation of petrological databases were used to validate and check the quality of the data, to classify them consistently, and to eliminate duplicates. Altogether, this yielded an initial global database (SHOSH1) comprising 2222 analyses of potassic igneous rocks for up to 11 major and 24 trace elements, all classified according to igneous province, occurrence (i.e. suite or volcano), age, and tectonic setting. Author's published descriptions and classifications of these features were adhered to, except in cases of significant inconsistency. SHOSH1 includes many relatively K-poor (calc-alkaline) compositions coeval with potassic igneous rocks, but is not intended to cover the whole spectrum of orogenic volcanic rocks from low-K to high-K.

SHOSH1 was then carefully filtered and checked as follows to generate a final working database (SHOSH2) of 497 analyses (for the same range of 35 elements):

1. **Age:** All pre-Cenozoic analyses were eliminated.
2. **Alteration:** All analyses with >5 wt% loss-on-ignition (LOI) were eliminated. This limit was not entirely arbitrary, but marked a natural break in the rocks in SHOSH1 between apparently fresh and more weathered or altered samples.
3. **Primitive Chemistry:** To eliminate evolved and cumulate samples, as mentioned above, all analyses with mg# outside the range 0.5–0.8 were filtered out.
4. **Potassic versus Ultrapotassic:** A more complex and subjective decision involved whether to retain ultrapotassic as well as potassic rocks. Ultrapotassic rocks commonly contain leucite, whereas potassic rocks, such as shoshonites, normally do not. Fortunately, an exhaustive global survey of these already exists (see Foley et al. 1987), and their definitions are outlined in Chap. 2. Although orogenic ultrapotassic rocks are considered in this study, the ultrapotassic lamproites and

kamafugites have been excluded, as discussed in Chap. 2.

5. **Outliers:** Outlying compositions not only reduce the internal coherence of a database (and hence reduce the potential efficiency of discrimination), but are quite likely to be samples which are altered, weathered, or otherwise unrepresentative. The analyses which remained after stages 1–4 were therefore plotted on various standard classification diagrams (e.g. Figs. 3.4 and 3.6), in order to eliminate gross outliers. For example, two analyses lying in the trachyte and dacite fields on Fig. 3.6a and b were eliminated, not only on grounds of internal self-consistency, but also because Hf and Zr, which were expected to be useful discriminants in this study, may be lost via zircon fractionation from rocks with >68 wt% SiO₂ (Pearce et al. 1984). Three analyses in the foidite field were also eliminated.
6. **Classification:** To ensure logical coherence, it was checked that the final contents of SHOSH2 were substantially potassic (Table 3.2), and that the minority of samples analyzed for the appropriate elements plotted predominantly in the shoshonitic fields on Fig. 3.4.

The overall major-element spectrum of the analyses in SHOSH2, and the range of compositions to which the diagrams developed in the following sections therefore apply, are given at the top of Fig. 3.7. The global distribution and numbers of analyses from various suites are quoted in Table 3.1.

Although the above compilation and screening procedures are claimed to have been as careful and as scientifically thorough as the current literature permits, the resultant databases SHOSH1 and SHOSH2 are still recognized as suffering from a number of drawbacks, including the following:

- **Homogeneity:** Different published papers quote data for completely different sets of trace elements, and some include only major or only trace elements. Hence, both SHOSH1 and

Table 3.2 Numbers of sodic, potassic, and ultrapotassic rock analyses included in final filtered database SHOSH2

Tectonic setting	Sodic ^a	Potassic ^a	Unassigned ^a	Ultrapotassic ^b	Total ^c
Continental arc	0	60	36	42	96
Postcollisional arc	0	17	153	2	170
Initial oceanic arc	0	1	25	0	26
Late oceanic arc	0	47	42	20	89
Within plate	0	85	26	54	111
Totals	0	209	285	118	492

From Müller et al. (1992a)

^aGeneral definition of IUGS (Le Maitre 1989): “sodic” means $(\text{Na}_2\text{O} - 4.0 \text{ wt}\%) > \text{K}_2\text{O}$, “potassic” means $\text{Na}_2\text{O} < \text{K}_2\text{O}$; otherwise unassigned

^bDefinition of Foley et al. (1987): $\text{K}_2\text{O} > 3.0 \text{ wt}\%$, $\text{MgO} > 3.0 \text{ wt}\%$, and $\text{K}_2\text{O}/\text{Na}_2\text{O} > 2$

^cSum of sodic, potassic and unassigned analyses; five analyses of the 497 in SHOSH2 do not have values for Na_2O

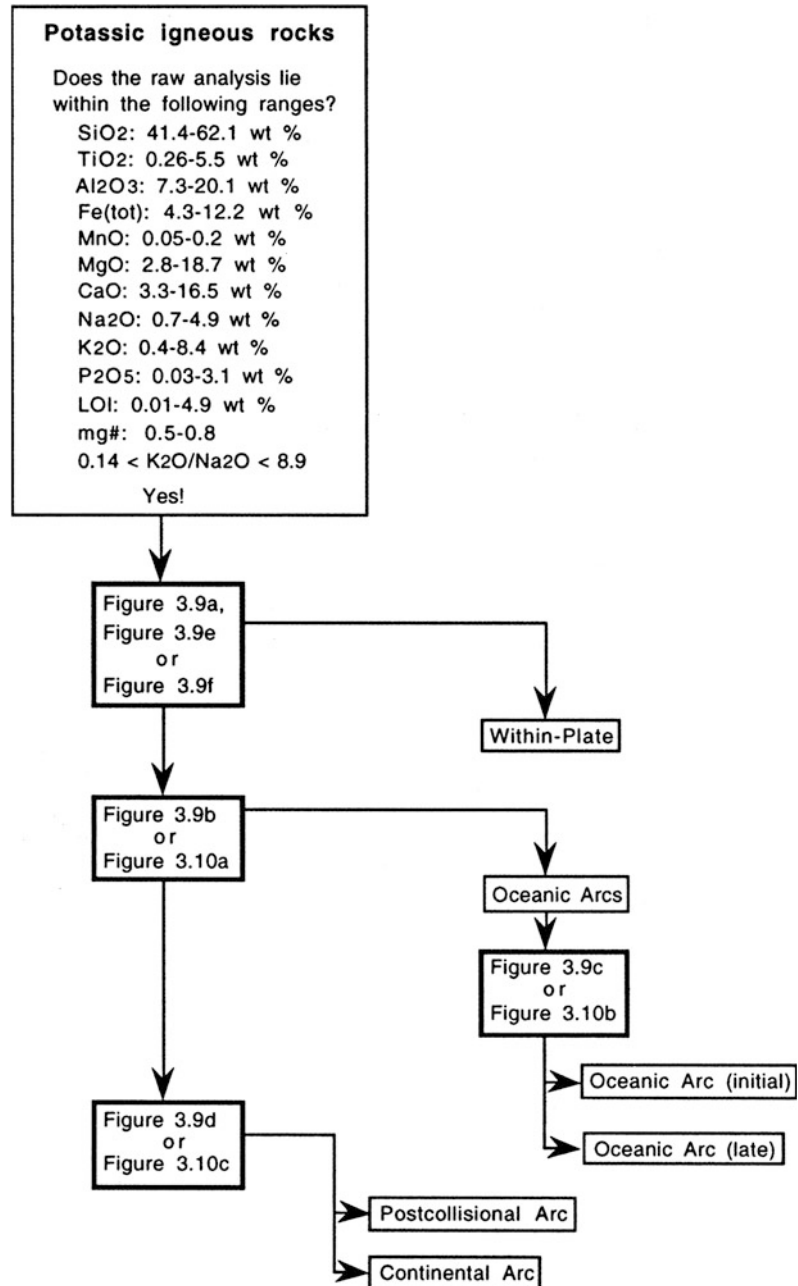
SHOSH2 are unavoidably replete with missing data for the full set of 35 elements compiled. Some elements such as Mo, Sb, Sn, and Cs were not compiled at all, because data were so few. Some published papers also fail to distinguish clearly between data which are “not analyzed” (missing) or “not detected”, both being variously indicated by “nd” or “zero” in tables. It has been consistently assumed that these indicate the absence of data.

- *Analytical Differences*: It is impossible to make any allowance in a compilation such as this for the differing precision and accuracy of the wide range of analytical methods used in the literature (XRF, ICP-MS, INAA, AAS, etc.), and particularly the lower precision of earlier data produced before the advent of the flame photometer. Although this is unlikely to be a problem for major elements, where at least the internal check of 100 wt% analytical totals is available, it is more of a problem for trace elements, on which tectonic setting discrimination for ancient potassic igneous rocks must substantially depend.
- *Potassic Alteration*: Potassic alteration is a widely recognized phenomenon in mineralized igneous systems, including porphyry copper and orogenic gold deposits. For certain gold-associated potassic igneous rocks compiled in SHOSH1, it can be shown that some high K_2O values are not primary, but alteration-induced (e.g. Porgera; Rock and

Finlayson 1990). Although screening steps 2, 3, and 5 above are likely to have minimized this problem, there are simply insufficient descriptive (e.g. petrographic) data in most source references to determine the extent of hydrothermal alteration (and weathering) in individual samples incorporated into SHOSH1. Consequently, SHOSH2 may contain some analyses whose high K contents are at least partly due to secondary processes rather than primary enrichment.

- *Initial Oceanic Arc Setting*: Further difficulties are presented by the initial oceanic arc setting and whether it should be included at all. There is only one example of this suite (the Mariana Arc), which raises questions about its representativeness. Moreover, most available analyses from this one suite were eliminated by the above screening procedures, whereupon remaining data in SHOSH2 then included only one potassic rock (Table 3.2) and plotted outside the shoshonite field on Fig. 3.4. It was eventually decided to retain the setting on the grounds that the unscreened data-set in SHOSH1 shows clear potassic affinities—one of 51 analyses lies in the absarokite and three in the TAS high-K basaltic andesite field on Fig. 3.6b, and all five analyses in the trachyandesite field on Fig. 3.6a are potassic. Nevertheless, the efficiency of discrimination for this particular setting is recognized as being limited.

Fig. 3.7 Suggested flow-chart for separating unknown samples of potassic igneous rocks into the five investigated tectonic settings. In order to achieve a maximum discrimination effect, the following scheme is recommended: 1 Plot unknown samples on Fig. 3.9a, e and/or f to separate within-plate potassic igneous rocks. 2 Plot non-within-plate samples on Fig. 3.9b or 3.10a to separate oceanic arc rocks. 3 Plot oceanic arc potassic igneous rocks on Figs. 3.9c and/or 3.10b to separate those from initial and late settings. 4 Plot remaining samples on Figs. 3.9d and/or 3.10c to discriminate between continental and postcollisional arc potassic igneous rocks. From Müller et al. (1992a)



The ideal approach to the present problem would be to generate a more self-consistent database. This would comprise *new* data for fresh samples chosen carefully and at first hand, from intimate geological and petrographical knowledge of all the studied suites of rocks, and analyzed for exactly the same set of critical elements by the

same laboratory and analytical techniques. Unfortunately, to generate such a database of the size of SHOSH1 (2222 analyses) is not a short-term option. The present work can therefore only be regarded as a pilot study, pending the availability of a database which approaches this ideal.

3.5 Discrimination of Tectonic Setting by Multivariate Statistical Methods

Multigroup linear discriminant analysis is the statistical method that optimizes separation between several groups of multivariate data. Le Maitre (1982) and Rock (1988) provide details of the method in a geological and specifically petrological context, and Pearce (1976) gives a particularly relevant application in separating basalts from different tectonic settings. Multigroup linear discriminant analysis does so by maximizing the ratio of between-groups to within-group variances. The raw data are first recast into a set of *discriminant functions*, namely linear weighted combinations of the measured major and/or trace element variables. There are $N - 1$ discriminant functions for N groups of data, and for viability there should be at least $N \times M$ rock analyses (samples) in the database, where M is the number of variables (major and trace elements) to be used in the discriminant functions. Attempting to discriminate five tectonic settings, will, therefore, lead to four discriminant functions, and the total of 497 potassic igneous rock samples in SHOSH2 is sufficient to allow any combination of the up to 35 measured major and trace elements to be used as discriminating variables. Figure 3.6 shows two established classification diagrams illustrating the range of compositions in the filtered database SHOSH2.

The main problem in applying multigroup linear discriminant analysis to SHOSH2 arises from the missing data referred to in Sect. 3.4. Multigroup linear discriminant analysis requires a complete and consistent data-matrix: that is, with a measured value in every sample for every element to be incorporated in the discriminant functions. To generate such a data-matrix from SHOSH2, samples or elements with missing values must be eliminated, and obviously there is no unique solution to this process. Table 3.3 therefore presents the results of two end-member runs of multigroup linear discriminant analysis; one using major elements, for which 486 of the

497 incorporated potassic volcanic rocks have been analyzed (Table 3.3a); and one based on the optimum (i.e. largest possible) combination of samples and immobile elements (Table 3.3b).

Initial results showed that multigroup linear discriminant analysis can distinguish potassic igneous rocks from different tectonic settings, but with varying degrees of efficiency. Careful examination then identified several complete sets of analyses which were consistently misclassified. One of these was Cundari's (1979) analyses for the Sabatini lavas, assigned by him as within-plate; these were all classified by the multigroup linear discriminant analysis as continental arc, the setting assumed by all other authors (e.g. Civetta et al. 1981) concerned with the Roman potassic igneous rocks, and their assignment was therefore adjusted in SHOSH2. Other datasets which split between two or more tectonic settings were predictably those for which ambiguities were already known to apply, for example:

- Potassic volcanic rocks of Sierra Nevada (California) and parts of Wyoming were split between the within-plate and continental arc settings, either of which are perfectly admissible interpretations for their tectonic setting (Van Kooten 1980; Dodge and Moore 1981; Wakabayashi and Sawyer 2001).
- Potassic igneous rocks from Chile and Peru were misclassified as postcollisional, possibly because they are sited away from the trench and may have ascended through thick continental crust (Thorpe et al. 1976; Dostal et al. 1977a, b; Kontak et al. 1986).
- Potassic igneous rocks from Costa Rica were also misclassified as postcollisional, but were already known to be geochemically anomalous (Reagan and Gill 1989).

All these observations, far from undermining the basis of the treatment, are therefore considered to confirm very clearly that the multigroup linear discriminant analysis defines real compositional differences.

Table 3.3 Geochemical differences between potassic igneous rocks in five tectonic settings, revealed by multigroup discriminant analysis*(a) Based on major elements (486 samples divided among five tectonic settings)^a**Dependent variable canonical coefficients (standardized by within-group pooled standard deviations)*

Discriminant function	1	2	3	4
TiO ₂	0.772	0.061	0.237	0.788
Al ₂ O ₃	0.092	0.050	0.804	0.352
Fe ₂ O ₃	-0.407	-0.211	-0.943	-0.394
MgO	0.511	0.136	0.904	-0.756
CaO	-0.270	-0.558	0.248	0.084
Na ₂ O	0.061	0.293	0.230	-0.916
K ₂ O	0.298	-0.654	0.690	-0.685
P ₂ O ₅	0.270	0.235	-0.373	0.209

Prediction success: observed settings (rows) by predicted settings (columns)^b

		Predicted					Observed totals
		CAP	PAP	IOP	LOP	WIP	
Observed	CAP	52	19	6	8	11	96
	PAP	1	154	6	7	1	169
	IOP	0	0	21	0	0	21
	LOP	11	2	15	61	0	89
	WIP	8	13	2	0	88	111
Predicted totals		72	188	50	76	100	486

*(b) Based on maximum samples for immobile elements (150 samples divided among four tectonic settings)^c**Dependent variable canonical coefficients (standardized by within-group pooled standard deviations)*

Discriminant function	1	2	3
TiO ₂	-0.670	0.598	-0.656
P ₂ O ₅	0.409	0.406	0.057
Y	0.074	0.528	0.677
Zr	-0.779	-0.755	0.201
Nb	-0.181	-0.093	0.682
Ce	0.125	-0.543	-0.209

Prediction success: observed settings (rows) by predicted settings (columns)^b

		Predicted				Observed totals
		CAP	PAP	LOP	WIP	
Observed	CAP	18	7	10	4	39
	PAP	6	31	4	0	41
	LOP	0	23	26	0	49
	WIP	7	1	0	13	21
Predicted totals		31	62	40	17	150

CAP continental arcs, PAP postcollisional arcs, IOP initial oceanic arcs, LOP late oceanic arcs, WIP within-plate settings

^aBoth SiO₂ and LOI are omitted from this table to minimize the closure problem (Le Maitre 1982; Rock 1988). A check was also made to ensure that inclusion of SiO₂ did not significantly affect the classification efficiency^bIn prediction success tables, bold figures indicate analyses that are correctly assigned to their tectonic setting by the discriminant functions; e.g. in Table (b), 18 of 39 CAP analyses are correctly assigned by their chemistry whereas 10 are misassigned to the LOP setting^cThis table is a compromise between excessively limiting the number of samples and elements incorporated into the multigroup discriminant analysis; other important immobile elements (Hf, Ta, Th) were excluded outright because data were insufficient. Only four tectonic settings can be distinguished because no potassic igneous rocks from IOP settings (i.e. Mariana Islands) have been analyzed for the required element combination

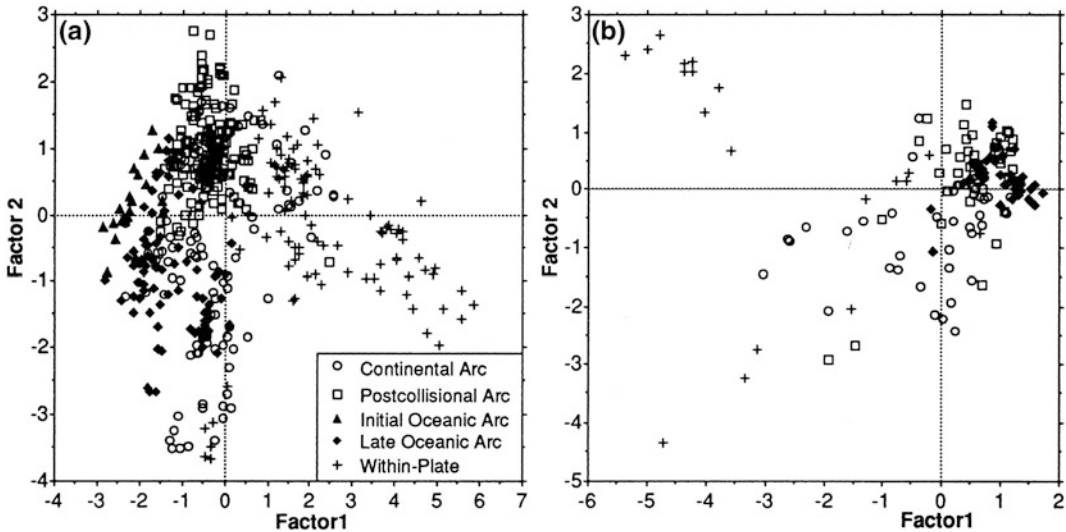


Fig. 3.8 Discrimination diagrams for potassic igneous rocks from different tectonic settings, based on multigroup linear discriminant analysis using: **a** major-elements, **b** immobile elements only. The X and Y axes respectively plot the first two of the discriminant functions (canonical

vectors or factors) which contribute most to the multidimensional group separation. Standardized versions of the weights (canonical coefficients) used to calculate these discriminant functions are given in the first two columns of Table 3.3, respectively. From Müller et al. (1992a)

The final results of the multigroup linear discriminant analysis, after reassignment of these initially misclassified analyses, are summarized in Table 3.3a and Fig. 3.8. In summary, 54 % of continental arc, 100 % of initial oceanic arc, 67 % of late oceanic arc, 91 % of postcollisional arc, and 79 % of within-plate potassic igneous rocks can be correctly attributed to their tectonic setting from their major-element chemistry alone. In more detail, the minimal misclassifications of initial oceanic arc samples indicates that these are very distinctive compositions, probably due to their origin by chlorite dehydration melting in a relatively cool subduction zone as suggested by Till et al. (2012), and as evident from Fig. 3.6b. Conversely, the relatively large misclassification of continental arc with respect to postcollisional arc samples indicates that the two groups are geochemically similar. In Table 3.3b, the percentages of correctly classified analyses are predictably lower, because fewer variables have been employed on an unavoidably smaller data-set, but the pattern is similar. Table 3.3a is of interest in pinpointing geochemical differences attributable to a tectonic setting in young potassic

igneous rocks not affected by potassic alteration, and hence when seeking genetic explanations. Table 3.3b is likely to be applicable to ancient potassic igneous rocks, where alteration and metamorphism effects are more likely, because it relies on immobile elements alone.

3.6 Discrimination via Simple Geochemical Diagrams

Since Fig. 3.8 and Table 3.3 represent the best possible separation between the five groups that can be achieved on a two-dimensional diagram or by multivariate calculation, it is clear that no *single* graphical or mathematical treatment is likely to be adequate to assign an individual potassic igneous rock analysis to its tectonic setting. Any multigroup linear discriminant treatment which includes all five settings will inevitably dissipate much of its power separating settings which are most distinctive, in turn leaving relatively little discriminatory power to separate the remainder. A *hierarchical* discrimination scheme is therefore

appropriate, in which the most distinctive settings are successfully stripped out, allowing each new discriminatory criterion in turn to target those subtle distinctions to which it is most suited. Since multigroup linear discriminant analysis is a relatively complex mathematical technique, and because its requirement of a full data-matrix is commonly impossible to meet (wherever literature data are involved), a hierarchical set of diagrams based on more conventional bivariate and triangular plots, rather than multivariate plots, was developed (Müller et al. 1992a).

The scheme is based as much as possible on immobile element *ratios*, including triangular plots, rather than absolute values, since such ratios are not only less affected by inter-laboratory variations, and easier to measure accurately, but are also theoretically unaffected by simple dilution or concentration affects such as the addition or removal of $\text{CO}_2 \pm \text{H}_2\text{O}$ during weathering, metamorphism and/or hydrothermal alteration. Most of the elements used in the developed diagrams are mantle-incompatible as well as immobile, so that their ratios are also little affected by fractionation or accumulation of major rock-forming minerals, and hence reflect primary source differences, such as those due to tectonic setting.

A first set of diagrams (Fig. 3.9) was based on the multigroup linear discriminant analysis itself, by using ratios of elements that have the highest absolute but opposite canonical coefficients in Table 3.3. Adequate separation could not be achieved in some cases using simple ratios of immobile elements alone, but improved markedly when Al_2O_3 was used as a normalizing factor; since Al_2O_3 is the least mobile of the major elements, this result is considered to be reasonably satisfactory. Simple ratio diagrams (e.g. Fig. 3.9) can never achieve the same separation efficiency as Fig. 3.8 (or Table 3.3), because they necessarily use less of the total multivariate information in the data, yet they are more accessible for routine use. A second set of diagrams (Fig. 3.10) was devised more-or-less empirically, to take account of the more exotic trace elements, notably La, Ce, and Hf, which are only available for a minority of analyses in the database SHOSH2.

Together, these analyses lead to the hierarchical scheme outlined in Fig. 3.7. In the first step, within-plate potassic igneous rocks can be separated from the four arc-related settings, by plotting data on Fig. 3.9a, e, or f, respectively; samples with TiO_2 contents above 1.5 wt%, Zr above 350 ppm, or Hf above 10 ppm can be considered with particular confidence as within-plate types (cf. Müller et al. 1992a). More recent work confirms the distinctly elevated HFSE concentrations of potassic igneous rocks derived in within-plate settings (Churikova et al. 2001; Kontinen et al. 2013; Rao et al. 2014). In the second step, remaining samples should be plotted on Fig. 3.10a, which discriminates oceanic arc from continental and postcollisional arc settings with almost 100 % efficiency, based on the lower La and Hf contents of the former. Depending on the result in this step, remaining samples are plotted in the third and final step on either of Fig. 3.9c or 3.10b, which separate initial from late oceanic arc potassic igneous rocks based essentially on the lower La content of the former; or on Fig. 3.9d or 3.10c, which separate continental from postcollisional potassic igneous rocks based on slightly lower Ce/P ratios in the latter. However, since both the final settings involve destruction of oceanic crust in a subduction setting, they not unexpectedly generate potassic igneous rocks of similar composition, and therefore overlaps are unavoidable.

3.7 Theoretical Basis for Discrimination Between Potassic Igneous Rocks in Different Tectonic Settings

The discussion attempts to provide a theoretical foundation for the empirical observations in previous sections. It examines those factors which can, in principle, be expected to induce differences between potassic igneous rocks erupted in different tectonic settings, and shows how the geochemical differences outlined above can be derived. As genetic processes in arc and

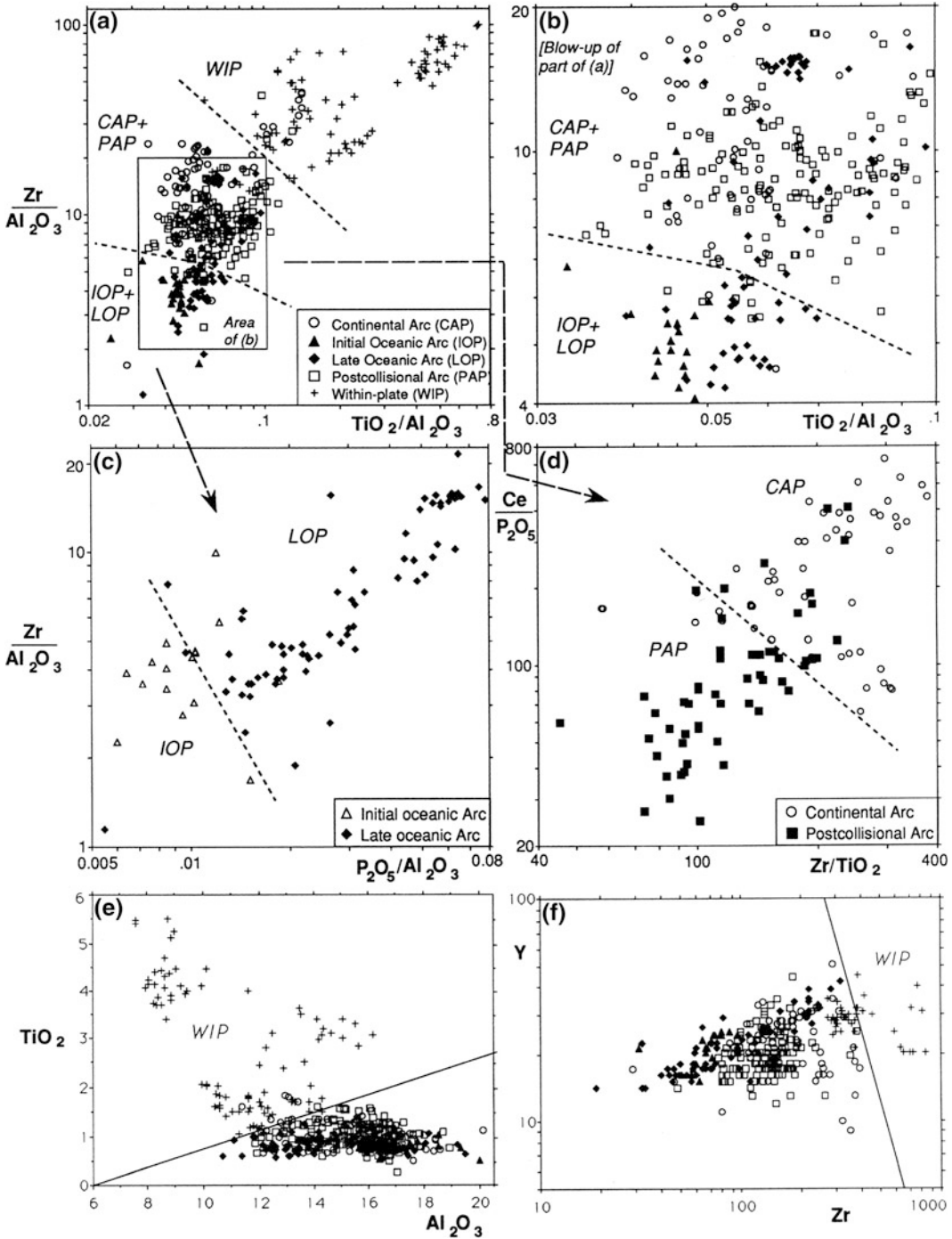


Fig. 3.9 Hierarchical set of discrimination diagrams for potassic igneous rocks from different tectonic settings, based on simple ratios of “immobile” elements revealed by discriminant analysis (Table 3.3) as contributing most effectively to group separation. As illustrated further in Figs. 3.7 and 3.9a should be used first to extract

within-plate potassic igneous rocks (Fig. 3.9e and/or f are alternatives); Fig. 3.9b should then be used to separate oceanic arc from continental and postcollisional arc settings, with the former distinguished as initial or late using Fig. 3.9c, and the latter using Fig. 3.9d. From Müller et al. (1992a)

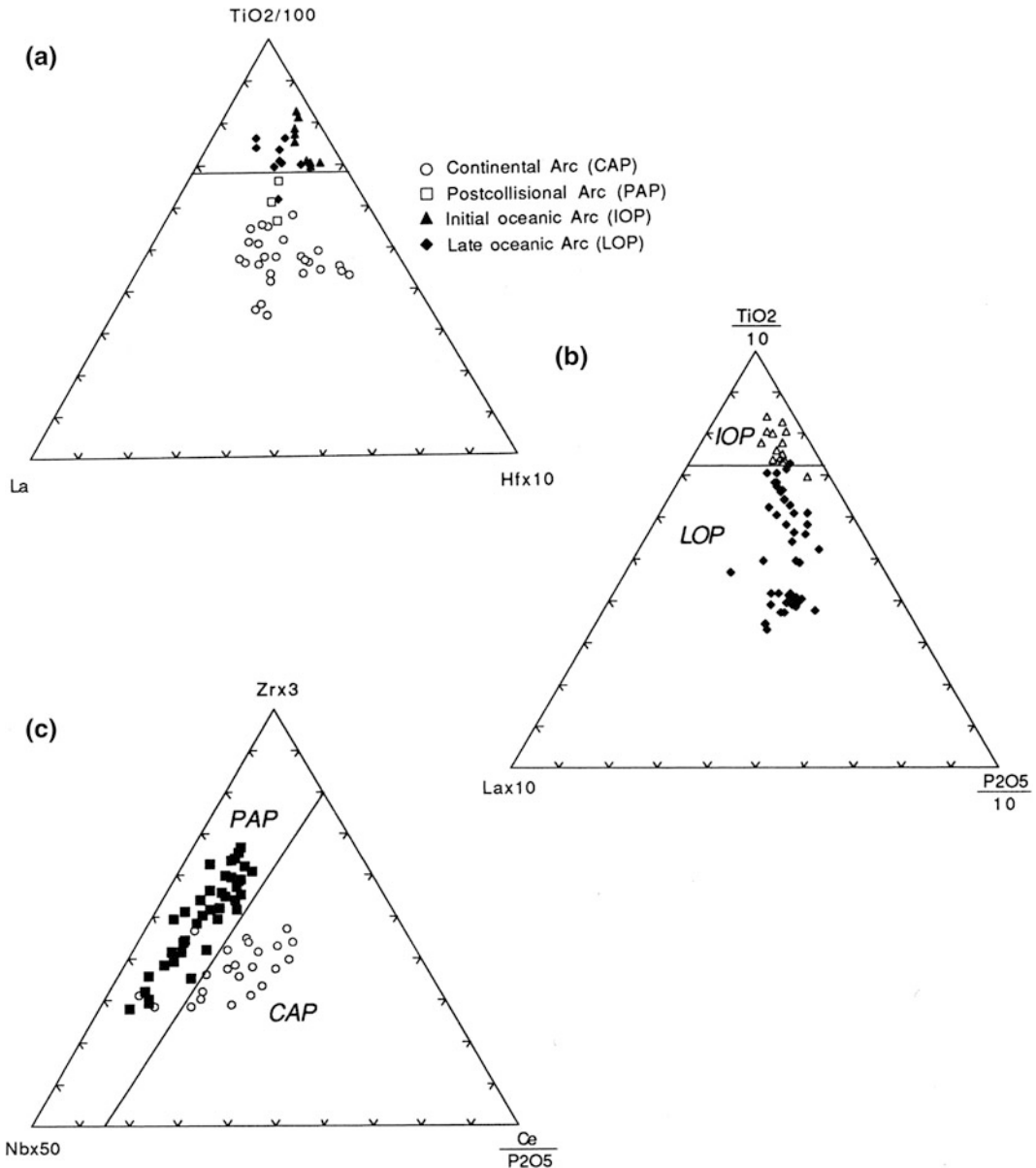


Fig. 3.10 Discrimination diagrams for potassic igneous rocks from different tectonic settings, partly based on the more exotic trace elements. Numbers of points are much less than on Fig. 3.9 owing to missing data. Figure 3.10a complements Fig. 3.9b in separating continental and postcollisional arcs from oceanic arcs; Fig. 3.10b

complements Fig. 3.9c in separating initial and late oceanic arcs; Fig. 3.10c complements Fig. 3.9d in separating continental and postcollisional arcs. The ratio $TiO_2/100$ in Fig. 3.10a and the ratios $TiO_2/10$ and $P_2O_5/10$ in Fig. 3.10b are calculated in ppm. From Müller et al. (1992a)

within-plate settings are so distinct, arc potassic igneous rocks are discussed first.

Despite the amount of literature published about high-K rocks, the petrogenetic processes

producing the various types of potassic igneous rocks are still debated (Peccerillo 1992; Miller et al. 1999; Srivastava et al. 2009; Guo et al. 2013; Lu et al. 2013a; Tan et al. 2013a; Bucholz

et al. 2014; Liu et al. 2014; Wang et al. 2014; Aghazadeh et al. 2015). However, there is a general consensus that potassic magmas cannot be derived by partial melting of normal mantle peridotite, but require heterogeneous mantle sources which have been metasomatically enriched in LILE and LREE (Edgar 1987; Foley and Peccerillo 1992; Guo et al. 2013; Kuritani et al. 2013; Tan et al. 2013b; Bucholz et al. 2014; Aghazadeh et al. 2015; Yang et al. 2015).

Potassic igneous rocks are commonly enriched in LILE, LREE, volatiles such as H₂O, and halogens, particularly Cl and F (Aoki et al. 1981; Bailey and Hampton 1990; Foley 1992, 1994; Zhang et al. 1995; Müller et al. 2001; Guo et al. 2006; Chevychelov et al. 2008; Zajacz et al. 2010; Melluso et al. 2012; Yang et al. 2015). However, average estimated maximum H₂O contents of typical mantle material, such as garnet-lherzolite or eclogite, are generally <1.2 wt% (Leech 2001) and single-stage partial melting of such rocks would not produce the volatile-rich and fertile melts with sufficient H₂O contents capable to produce porphyry copper-gold mineralization (i.e. up to 9 wt% H₂O; Lu et al. 2013a). Therefore, significant exogenous water (>3 wt%) must be added to the mantle source in order to produce the hydrous melts required (Yang et al. 2015). The exogenous water, as well as the LILE, LREE and halogens, are mainly incorporated in hydrous phenocrysts such as phlogopite and/or amphibole (Aoki et al. 1981; Fuge et al. 1986; Richter et al. 2002; Yang and Lentz 2005; Sarjoughian et al. 2014; Teiber et al. 2015). As a result, portions of the Earth's upper mantle rich in phlogopite ± clinopyroxene are considered to be important in the genesis of potassic melts (Edgar and Arima 1985; Foley 1992; Till et al. 2012; Guo et al. 2013; Lu et al. 2013a). Meen (1987) considers that potassic igneous rocks form by low degrees of partial melting, under hydrous conditions in a low heat-flow environment, of upper mantle lherzolite that has been metasomatically enriched in such elements as LILE and LREE. In arc settings, the partial melting may be achieved by modification of mantle geotherms in proximity to the cold subducted slab (Taylor et al. 1994), while the metasomatic enrichment may be

achieved by overprinting and veining of the mantle wedge by either volatile- and LILE-enriched *fluids* (Saunders et al. 1980, 1991; Grove et al. 2002; Till et al. 2012) and/or by actual alkali, low-temperature, LILE- and LREE-enriched partial *melts* (i.e. adakites) derived during dehydration of the subducted oceanic slab (Pearce 1983; Bailey et al. 1989; Sun and McDonough 1989; Zhang et al. 1995; Sajona et al. 2000; Vigouroux et al. 2008; Campbell et al. 2014; Wang et al. 2014). It is still debated whether these metasomatizing fluids or melts are derived from subducted sediments (Rogers and Setterfield 1994; Prelevic et al. 2010; Mallik et al. 2015) or from altered oceanic crust (Nowell et al. 2004; Gaffney et al. 2007). Dehydration of the serpentinized subducted oceanic slab might supply sufficient free H₂O to trigger partial melting at the H₂O-saturated solidus in the mantle wedge (Till et al. 2012). Nevertheless, identification of the metasomatic material from the various derivations is quite difficult (Prelevic et al. 2010; Kuritani et al. 2013). However, metasomatic phlogopite veins documented in ultramafic mantle xenoliths from grab samples of submarine seamount trachybasalts in the Bismarck Sea, Papua New Guinea, provide a direct witness of these enriched mantle sources (Franz et al. 2002; Franz and Romer 2010). Detailed studies of altered mantle xenoliths (Bailey 1982; Menzies and Hawkesworth 1987; Gregoire et al. 2000; Franz et al. 2002; Franz and Romer 2010) reveal that the metasomatically introduced volatiles, LILE, and LREE are preferentially sited in hydrous minerals such as phlogopite, amphibole, and apatite which are concentrated either in vein networks or dispersed throughout the upper mantle peridotite (Peccerillo 1992; Ionov and Hofmann 1995; Gregoire et al. 2000; Franz et al. 2002; Franz and Romer 2010; Aghazadeh et al. 2015). These minerals have lower melting temperatures than the surrounding mantle peridotite, and hence partial melting may preferentially affect these metasomatic hydrous veins, thus generating potassic magmas (Prelevic et al. 2005; Tommasini et al. 2011; Aghazadeh et al. 2015).

Once partial melting has been initiated, the interplay of two further factors is then generally

considered to influence the chemistry of *all* subduction-related melts actually produced:

- Differing rates and/or angles of the subduction process (Saunders et al. 1980; Rock et al. 1982; Kay and Abbruzzi 1996; Kay et al. 1987, 2005; Stern et al. 2011).
- Differing relative inputs from at least three identified source components (Wheller et al. 1986; Vigouroux et al. 2008; Till et al. 2012; Lu et al. 2013a; Aghazadeh et al. 2015):
 1. *Subducted oceanic crust*, characterized by high LILE/LREE ratios (e.g. high Sr/Nd and Rb/Nd) and high LILE/HFSE ratios (e.g. high Ba/Nb and Th/Ta) (Class et al. 2000; Shen et al. 2008).
 2. *Subducted marine sediment*, characterized by low Sr/Nd (<7), Ce/Pb (<5), Ba/La (<50), and Nb/La ratios (<0.5), but high Th/Ta (>100), Th/La (>1.5), Th/Yb (>100), and Ba/Nb ratios (>130) (Rogers et al. 1985; Miller et al. 1999; Woodhead et al. 2001; Liu et al. 2014; Mallik et al. 2015), high Pb, Ba, and La contents (Sun and McDonough 1989; Wang et al. 2014), and by negative Eu anomalies in chondrite-normalized REE spidergram plots (McLennan and Taylor 1981; Guo et al. 2013; Liu et al. 2014) that are unrelated to plagioclase fractionation (Miller et al. 1999).
 3. The *overlying mantle wedge*, characterized by low Rb (<50 ppm) and especially Pb contents (Ellam and Hawkesworth 1988; Bucholz et al. 2014).

Melts may be further influenced by the nature of the crust through which they must pass before eruption, if any contamination or assimilation takes place. There is also the classic increase in K in arc-related suites with increasing distance from the subduction trench, the cause of which remains controversial. This may be accompanied by sympathetic increases in Th, Ta, and Nb (cf. Brown et al. 1984), attributed by some to the derivation of liquids from heterogeneous mantle which changes characteristics from subduction-related to within-plate type away from the trench.

A schematic cross-section showing the distribution of the elements in a subduction zone (continental arc) is illustrated in Fig. 3.11.

On this basis, it is possible to account for some of the recorded differences among the four arc settings discussed above. As indicated in Figs. 3.9 and 3.10, continental and postcollisional arc potassic igneous rocks are enriched in Zr, Hf, Nb, and LREE; they also have higher Sr and Ba contents, higher K/Na, Nb/Y (>0.55), and higher LREE/HREE ratios than oceanic arc potassic igneous rocks (cf. Fig. 3.6). This might be explained by a greater role for the alkali *melt*-induced metasomatism of the mantle wedge, which is believed to yield stronger enrichments in these particular elements than *fluid*-induced metasomatism (Bailey et al. 1989; Zhang et al. 1995; Sajona et al. 2000; Ishimaru et al. 2007; Wang et al. 2014). Partial *melts* derived from subducted sediments are characterized by relatively high LREE contents (Guo et al. 2013). Such an augmented role might also further explain the progressive transition of potassic igneous rocks to more strongly alkaline (i.e. adakitic) magmatism in some postcollisional arc settings (Oyhantçabal et al. 2007; Chen et al. 2015; see Sect. 4.2). Chen et al. (2015) suggest that high-K rocks from postcollisional arcs are associated with underplating of subduction-modified basaltic material beneath the lower crust, resulting in the transformation into amphibolites and eclogites. Partial melting of this thickened lower crust produces the typical adakitic magma compositions that characterize potassic igneous rocks from postcollisional arc settings (Chen et al. 2015). By contrast, high-K magmas derived in continental arcs are formed by partial melting, assimilation, storage, and homogenization (MASH) processes (Hou et al. 2009, 2011; Chen et al. 2015). The passage of continental and postcollisional potassic igneous rocks through thick continental crust, as opposed to relatively thin depleted MORB in the case of oceanic arc potassic igneous rocks, could also account, in part, for their higher LILE and LREE contents (Müller and Groves 1993). However, enrichments in LREE can also be explained by metasomatic fluids enriched in volatiles such as chloride, with chloride complexes preferentially

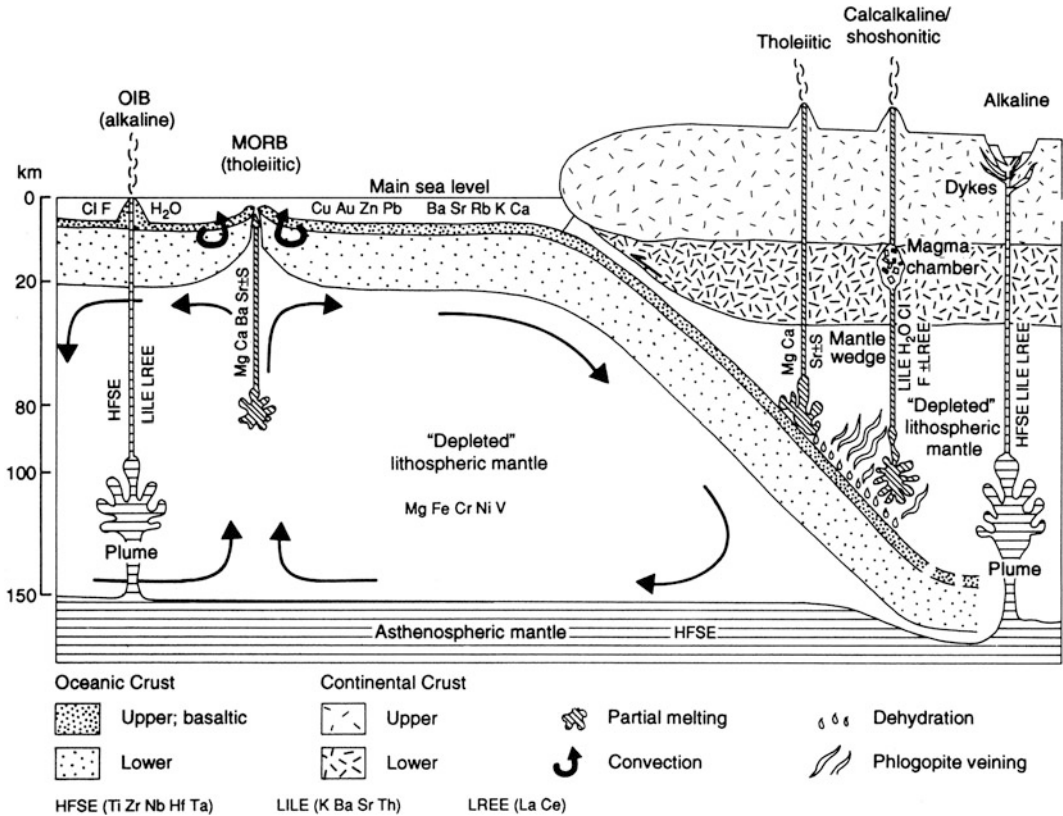


Fig. 3.11 Schematic cross section showing the main components of a continental arc and distribution of elements (see also Müller et al. 1992a)

transporting the LREE (Campbell et al. 1998; Pan and Fleet 2002; Pourtier et al. 2010; Tropper et al. 2011).

Continental arc potassic igneous rocks have slightly higher LILE (e.g. Rb, Sr, Ba) and Ce, but lower Nb and P contents, than postcollisional arc potassic igneous rocks: see positive Sr anomalies of the former on Fig. 3.5a. These differences are not easy to explain, but may result from the above-mentioned progressive transition to more alkaline magmatism in some postcollisional arcs (cf. Coulon et al. 2002; Oyhantçabal et al. 2007).

Oceanic (island) arc potassic igneous rocks generally have the lowest concentrations of LILE (i.e. <310 ppm Rb, <1500 ppm Sr, <1500 ppm Ba), LREE (e.g. <115 ppm La, <150 ppm Ce), and HFSE (e.g. <300 ppm Zr, <20 ppm Nb, <5 ppm Hf). They also commonly have higher Ba/Th (>110), Ba/La (>50), Sr/Th (>70), and U/Th (>0.2)

ratios than potassic igneous rocks from continental or postcollisional arc-settings (Woodhead et al. 2001; Guo et al. 2013; Liu et al. 2014). This may be explained via a mainly fluid-derived metasomatic enrichment of the underlying mantle wedge in oceanic arc settings (Briqueu et al. 1984; Bailey et al. 1989; Ishimaru et al. 2007). Aqueous fluids derived from the subducted oceanic slab carry very little REE, Th and HFSE, but introduce significant amounts of LILE into the mantle wedge (Guo et al. 2013). A fluid-dominated metasomatic enrichment does not significantly increase LREE and HFSE concentrations of mantle material because these elements are not mobilized due to their retention in insoluble phases in the subducted plate (Briqueu et al. 1984; Bailey et al. 1989; Ishimaru et al. 2007). The HFSE are insoluble in subduction-derived fluids (Woodhead et al. 1993), but can be transported in melts derived from

subducting sediment (Class et al. 2000; Shen et al. 2008). The relatively low LILE concentrations of the rocks may reflect their origin in an environment where oceanic crust, derived from a depleted mantle, has been subducted beneath the oceanic crust of another plate. During uprise, the melts produced in this setting must pass through a relatively thin oceanic crust consisting of depleted MORB. This could explain their very low concentrations of LILE compared to magmas from within-plate settings, where the melts have to pass through a relatively thick continental crust during their ascent. The probability of crustal assimilation for within-plate related potassic igneous rocks, and a resulting enrichment in LILE, is therefore much higher. Oceanic (island) arc potassic igneous rocks can be further subdivided into two subgroups (*initial* and *late*) based on their geochemistry. Those derived in *initial* oceanic arc settings are defined by unique geochemical compositions with very low LREE contents (<42 ppm La, <33 ppm Ce), and very low P_2O_5/Al_2O_3 ratios (<0.01). Their unique geochemistry is explained as the product of chlorite dehydration melting in a cool subduction zone (Till et al. 2012). Chlorite can form when water is released during the dehydration of serpentine and amphibole in the subducting oceanic crust (Grove et al. 2006; Iwamori 2007) and/or from the dehydration of subducted sediments in the mantle wedge nose at <80 km depth (Till et al. 2012). In a cool subduction zone like the northern Marianas, no free H_2O is available to trigger melting until chlorite breakdown in the lowermost mantle wedge and the dominant form of melting at sub-arc depths is likely to be chlorite dehydration melting (Till et al. 2012).

For within-plate settings, the partial melting required to generate potassic igneous rocks may be caused by processes such as pressure-release during intraplate rifting (Nelson et al. 1986; Leat et al. 1988), or by asthenospheric upwelling associated with lithospheric thinning. The required metasomatic enrichment of the source, in turn, may be induced by the local invasion of regions within the subcontinental mantle by

incompatible-element-enriched mantle-plumes. The plumes are probably derived from sources near the 650-km seismic discontinuity or near the core-mantle boundary (Ringwood 1990), and have heads that can be as large as 400 km² (Halliday et al. 1990; Montelli et al. 2004). Alternatively, the enrichment may reflect pre-existing, long-term, intrinsic heterogeneities within the upper mantle and bear no relation to the actual melting event (Schiano et al. 1997; Kogiso et al. 2004). At any rate, small degrees of partial melting of phlogopite-bearing mantle peridotite, at depths below the level of amphibole stability and in the presence of CO_2 , are believed to generate potassic melts (Nelson et al. 1986; Prelevic et al. 2005; Tommasini et al. 2011; Guo et al. 2013; Hudgins et al. 2015). The fact that within-plate potassic igneous rocks show the highest HFSE contents (up to 5.50 wt% TiO_2 , 840 ppm Zr, 74 ppm Nb, 30 ppm Hf) of the investigated settings (cf. Müller et al. 1992a) and very high Nb/Y (up to 3) and Nb/U ratios (up to 47), may reflect this assumed greater role for CO_2 , which mobilizes many HFSE (Pearce and Norry 1979; Piercey 2009; Guo et al. 2013). Within-plate potassic igneous rocks are also characterized by the highest LILE (i.e. up to 640 ppm Rb, 4600 ppm Sr, 9000 ppm Ba) and LREE contents (e.g. up to 230 ppm La, 390 ppm Ce) of all investigated settings, but geochemical explanations for this are obscure (e.g. Foley et al. 1987, 2011).

In areas where the composition of potassic igneous rocks results from mixing processes between melts from both asthenospheric (characterized by within-plate geochemistry) and lithospheric (subduction-modified) mantle sources (e.g. Wyoming Province; see McDonald et al. 1992; Gibson et al. 1993), the geochemical discrimination of the tectonic setting becomes problematical. In those areas, some asthenosphere-derived magma plumes might have been contaminated by pockets of subduction-metasomatized lithosphere during ascent, whereas others remained relatively uncontaminated (Gibson et al. 1993).

3.8 Conclusions

- Young potassic igneous rocks, from the five main tectonic settings in which they occur, have somewhat different major- and trace-element compositions.
- Potassic igneous rocks from within-plate settings—such as the western USA—are very distinctive, due to very high concentrations of LILE (e.g. Rb, Sr, Ba), LREE (e.g. La, Ce, Sm) and HFSE (notably Ti, Zr, Nb, Hf).
- Potassic igneous rocks from oceanic (island) arc settings have the lowest concentrations of LILE, LREE and HFSE of such rocks from all investigated settings, and those from initial and late oceanic arc settings can be discriminated by the higher P, Zr, Nb, and La concentrations of the latter.
- Potassic igneous rocks from continental and postcollisional settings show the most subtle differences, but can still be distinguished by the slightly higher Sr, Zr, and Ce concentrations of the former.
- The above-mentioned differences extend to immobile elements, so it is possible, in principle, to identify the tectonic setting of older potassic igneous rocks from their geochemistry, even where direct geological evidence is equivocal. This is best done in a hierarchical set of diagrams, or by formal stepwise discriminant analysis, which successively strips off the most distinctive compositions in order to progressively discriminate more subtle differences.
- Potassic igneous rocks in certain continental, postcollisional, and late oceanic arc settings are associated with world-class deposits of gold and/or base metals (Chaps. 6 and 7), and hence these new discrimination methods may be useful in exploration as well as in tectonic and petrogenetic studies (cf. De Min et al. 2007; Dawod et al. 2010; Costa et al. 2011; Torabi 2011; Aliani et al. 2013; Torabi et al. 2014; Orozco-Garza et al. 2013; Abbasi et al. 2014; Rao et al. 2014; Ghasemi and Rezaei-Kahkhaei 2015; Jiang et al. 2015; Liu et al. 2015). By identifying those older potassic igneous rocks which have the most

favourable tectonic settings, it may be possible to identify, more efficiently, those terranes which have enhanced economic potential for specific styles of mineralization associated with high-K igneous rocks (cf. Maughan et al. 2002; Bagheri et al. 2007; Mikulski 2007; Farahkhan et al. 2010; Betsi and Lentz 2011; Soloviev and Krivoschekov 2011; Lehmann et al. 2013; Soloviev et al. 2013; Eyuboglu et al. 2014; Soloviev 2014a, b, 2015; Jamali and Mehrabi 2015). This is further discussed in Chap. 6.

References

- Abbasi S, Tabatabaei Manesh SM, Karimi S, Parfenova OV (2014) Relative contributions of crust and mantle to generation of Oligocene–Miocene medium-K calc-alkaline I-type granitoids in a subduction setting—A case study from the Nabar pluton, Central Iran. *Petrology* 22:310–328
- Aghazadeh M, Prelevic D, Badrzadeh Z, Braschi E, van den Bogaard P, Conticelli S (2015) Geochemistry Sr–Nd–Pb isotopes and geochronology of amphibole- and mica-bearing lamprophyres in northwestern Iran: implications for mantle wedge heterogeneity in a paleo-subduction zone. *Lithos* 217:352–369
- Aliani F, Dadfar S, Maanijou M, Miri M (2013) Geochemistry and tectonomagmatic setting of the intrusive rocks in the Hezarkhani area (Northeast Sonqor, West Iran). *Middle-East J Sci Res* 13:1245–1253
- Alibert C, Michard A, Albarede F (1986) Isotope and trace element geochemistry of Colorado plateau volcanics. *Geochimica et Cosmochimica Acta* 50:2735–2750
- Allan JF, Carmichael ISE (1984) Lamprophyric lavas in the Colima graben, SW Mexico. *Contrib Miner Petrol* 88:203–216
- Allen DE, Seyfried WE (2005) REE controls in ultramafic hosted MOR hydrothermal systems: an experimental study at elevated temperature and pressure. *Geochim Cosmochim Acta* 69:675–683
- Aoki K, Ishiwaka K, Kanisawa S (1981) Fluorine geochemistry of basaltic rocks from continental and oceanic regions and petrogenetic application. *Contrib Miner Petrol* 76:53–59
- Appleton JD (1972) Petrogenesis of potassium-rich lavas from the Roccamonfina volcano, Roman Region, Italy. *J Petrol* 13:425–456
- Bacon CA (1990) Calc-alkaline, shoshonitic and primitive tholeiitic lavas from monogenetic volcanoes near Crater Lake, Oregon. *J Petrol* 31:135–166

- Bagheri H, Moore F, Alderton DHM (2007) Copper–Ni–Co–As (U) mineralization in the Anarak area of central Iran. *J Asian Earth Sci* 29:651–665
- Bailey DK (1982) Mantle metasomatism—Continuing chemical change within the Earth. *Nature* 296:525–530
- Bailey DK, Hampton CM (1990) Volatiles in alkaline magmatism. *Lithos* 26:157–165
- Bailey JC, Frolova TI, Burikova IA (1989) Mineralogy, geochemistry and petrogenesis of Kurile island-arc basalts. *Contrib Miner Petrol* 102:265–280
- Barton M, van Bergen MJ (1981) Green clinopyroxenes and associated phases in a potassium-rich lava from the Leucite Hills, Wyoming. *Contrib Miner Petrol* 77:101–114
- Beccaluva L, Bigioggero LB, Chiesa S, Colombo A, Fanti G, Gatto GO, Gregnanin A, Montrasio A, Piccirillo EM, Tunesi A (1983) Postcollisional orogenic dyke magmatism in the Alps. *Mem Soc Geol Italy* 26:341–359
- Beccaluva L, Di Girolamo P, Serri G (1991) Petrogenesis and tectonic setting of the Roman Volcanic Province, Italy. *Lithos* 26:191–221
- Bergman SC, Dunn DP, Krol LG (1988) Rock and mineral chemistry of the Linhaisai minette and the origin of Borneo diamonds, Central Kalimantan, Indonesia. *Can Mineral* 26:23–44
- Betsi TB, Lentz D (2011) Petrochemistry of subvolcanic dyke swarms associated with the Golden Revenue Au–Cu and the Stoddart Mo–Cu ± W mineralizations (Dawson Range, Yukon Territory, Canada) and implications for ore genesis. *Ore Geol Rev* 39:134–163
- Bloomer SH, Stern RJ, Fisk E, Geschwind CH (1989) Shoshonitic volcanism in the northern Marianas arc. 1. Mineralogic and major and trace element characteristics. *J Geophys Res* 94:4469–4496
- Briqueu L, Bougault H, Joron JL (1984) Quantification of Nb, Ta, Ti and V anomalies in magmas associated with subduction zones: petrogenetic implications. *Earth Planet Sci Lett* 68:297–308
- Brown GC, Thorpe RS, Webb PC (1984) The geochemical characteristics of granitoids in contrasting arcs and comments on magma sources. *J Geol Soc* 141:413–426
- Bucholz CE, Jagoutz O, Schmidt MW, Sambuu O (2014) Fractional crystallization of high-K arc magmas: biotite- versus amphibole-dominated fractionation series in the Dariv Igneous Complex, western Mongolia. *Contrib Miner Petrol* 168:1072–1100
- Campbell IH, Compston DM, Richards JP, Johnson JP, Kent AJR (1998) Review of the application of isotopic studies to the genesis of Cu–Au mineralization at Olympic Dam and Au mineralization at Porgera, the Tennant Creek district and Yilgarn Craton. *Aust J Earth Sci* 45:201–218
- Campbell IH, Stepanov AS, Liang HY, Allen CM, Norman MD, Zhang YQ, Xie YW (2014) The origin of shoshonites: new insights from the Tertiary high-potassium intrusions of eastern Tibet. *Contrib Miner Petrol* 167:983–1005
- Chen JL, Xu JF, Wang BD, Yang ZM, Ren JB, Yu HX, Liu H, Feng Y (2015) Geochemical differences between subduction- and collision-related copper-bearing porphyries and implications for metallogenesis. *Ore Geol Rev* 70:424–437
- Chevychev VY, Botcharnikov RE, Holtz F (2008) Partitioning of Cl and F between fluid and hydrous phonolitic melt of Mt. Vesuvius at 850–1000 °C and 200 MPa. *Chem Geol* 256:172–184
- Churikova T, Dorendorf F, Wörner G (2001) Sources and fluids in the mantle wedge below Kamchatka, evidence from across-arc geochemical variation. *J Petrol* 42:1567–1593
- Civetta L, Innocenti F, Manetti P, Peccerillo A, Poli G (1981) Geochemical characteristics of potassic volcanic from Mts. Ernici, southern Latium Italy. *Contrib Miner Petrol* 78:37–47
- Class C, Miller DM, Goldstein SL, Langmuir CH (2000) Distinguishing melt and fluid subduction components in Umnak volcanics, Aleutian Arc. *Geochem Geophys Geosyst* 1(6):Paper number 1999GC000010
- Colasanti CV, Johnson EA, Manning CE (2011) An experimental study of OH solubility in rutile at 500–900 °C, 0.5–2 GPa, and a range of oxygen fugacities. *Am Mineral* 96:1291–1299
- Costa FG, Oliveira EP, McNaughton NJ (2011) The Fazenda Gavião granodiorite and associated potassic plutons as evidence for Paleoproterozoic arc-continent collision in the Rio Itapicuru greenstone belt, Brazil. *J S Am Earth Sci* 32:127–141
- Coulon C, Megartsi M, Fourcade S, Maury RC, Bellon H, Louni-Hacini A, Cotton J, Coutelle A, Hermitte D (2002) Post-collisional transition from calc-alkaline to alkaline volcanism during the Neogene in Oranie (Algeria): magmatic expression of a slab breakoff. *Lithos* 62:87–110
- Cox KG, Hawkesworth CJ, O’Nions RK (1976) Isotopic evidence for the derivation of some Roman Region volcanics from anomalously enriched mantle. *Contrib Miner Petrol* 56:173–180
- Cundari A (1973) Petrology of the leucite-bearing lavas in New South Wales. *J Geol Soc Aust* 20:465–492
- Cundari A (1979) Petrogenesis of leucite-bearing lavas in the Roman volcanic region, Italy. The Sabatini lavas. *Contrib Miner Petrol* 70:9–21
- Cundari A, Matthias PP (1974) Evolution of the Vico lavas, Roman volcanic region, Italy. *Bull Volcanol* 38:98–114
- Curry JR, Shor GG, Raitt RW, Henry M (1977) Seismic refraction and reflection studies of crustal structure of the eastern Sunda and western Banda arcs. *J Geophys Res* 82:2479–2489
- Dal Piaz GV, Venturelli G, Scolari A (1979) Calc-alkaline to ultrapotassic postcollisional volcanic activity in the internal northwestern Alps. *Memorias del Instituto de Geologia et Mineralogia, University of Padova* 32:4–16

- Dalpè C, Baker DR (2000) Experimental investigation of large-ion-lithophile-element-, high-field-strength-element- and rare-earth-element-partitioning between calcic amphibole and basaltic melt: the effects of pressure and oxygen fugacity. *Contrib Miner Petrol* 140:233–250
- Dawod S, Al-Mishwat A, Bilal A (2010) Alkaline magmatic rocks from the Late Triassic to Early Cretaceous Qastal Almaaf Melange, northwest Syria. *Kuwait J Sci Eng* 37:135–157
- De Min A, Rosset A, Tunis G, Kocmann C, Tosone A, Lenaz D (2007) Igneous rock clasts from the Bovec Maastrichtian flysch (Slovenia): petrology and geodynamic aspects. *Geol Carpath* 58:1–11
- De Paolo DJ, Johnson RW (1979) Magma genesis in the New Britain island arc: constraints from Nd and Sr isotopes and trace element patterns. *Contrib Miner Petrol* 70:367–379
- Deruelle B (1982) Petrology of the Plio-Quaternary volcanism of the south-central and meridional Andes. *J Volcanol Geotherm Res* 14:77–124
- Deutsch A (1984) Young Alpine dykes south of the Tauern Window (Austria): a K–Ar and Sr isotope study. *Contrib Miner Petrol* 85:45–57
- Dixon TH, Batiza R (1979) Petrology and chemistry of Recent lavas in the N-Marianas: implications for the origin of island-arc basalts. *Contrib Miner Petrol* 70:167–181
- Dodge FCW, Moore JG (1981) Late Cenozoic volcanic rocks of the southern Sierra Nevada, California: II. Geochemistry. *Bull Geol Soc Am* 92:1670–1761
- Dostal J, Dupuy C, Lefevre C (1977a) Rare earth element distribution in Plio-Quaternary volcanic rocks from southern Peru. *Lithos* 10:173–183
- Dostal J, Zentilli M, Caelles JC, Clark AH (1977b) Geochemistry and origin of volcanic rocks of the Andes (26–28° S). *Contrib Miner Petrol* 63:113–128
- Duncker KE, Wolff JA, Harmon RS, Leat PT, Dockin AP, Thompson RN (1991) Diverse mantle and crustal components in lavas of the NW Cerros del Rio volcanic field, Rio Grande Rift, New Mexico. *Contrib Miner Petrol* 108:331–345
- Edgar AD (1987) The genesis of alkaline magmas with emphasis on their source regions: inferences from experimental studies. In: Fitton JG, Upton BGJ (eds) *Alkaline Igneous Rocks* (vol 30). Geological Society Special Publication, pp 29–52
- Edgar AD, Arima M (1985) Fluorine and chlorine contents of phlogopites crystallized from ultrapotassic rock compositions in high pressure experiments: implications for halogen reservoirs in source regions. *Am Mineral* 70:529–536
- Edwards CMH, Menzies MA, Thirlwall MF, Morrid JD, Leeman WP, Harmon RS (1994) The transition to potassic alkaline volcanism in island arcs: the Ringgit-Beser Complex, East Java, Indonesia. *J Petrol* 35:1557–1595
- Ellam RM, Hawkesworth CJ (1988) Elemental and isotopic variations in subduction-related basalts: evidence for a three component model. *Contrib Miner Petrol* 98:72–80
- Ellam RM, Hawkesworth CJ, Menzies MA, Rogers NW (1989) The volcanism of Southern Italy: role of subduction and the relationship between potassic and sodic alkaline magmatism. *J Geophys Res* 94:4589–4601
- Eyuboglu Y, Santosh M, Keewook Y, Tuysuz N, Korkmaz S, Akaryali E, Dudas FO, Bektas O (2014) The eastern Black Sea-type volcanogenic massive sulphide deposits: geochemistry, zircon U–Pb geochronology and an overview of the geodynamics of ore genesis. *Ore Geol Rev* 59:29–54
- Farahkhan N, Razavi MH, Masoudi F, Eskandary A (2010) Potassic nature of Karaj Dam Sill and its association with Cu, Au, Mo mineralization of Senj deposit, Iran. In: *The 1st International Applied Geological Congress*, Islamic Azad University, Iran 26–28 Apr 2010, pp 168–173
- Floyd PA, Winchester JA (1975) Magma type and tectonic setting discrimination using immobile elements. *Earth Planet Sci Lett* 27:211–218
- Foden JD (1979) The petrology of some young volcanic rocks from Lombok and Sumbawa, Lesser Sunda islands. Unpl. PhD Thesis, University of Tasmania, Hobart
- Foden JD, Varne R (1980) The petrology and tectonic setting of Quaternary-Recent volcanic centres of Lombok and Sumbawa, Sunda arc. *Chem Geol* 30:201–226
- Foley SF (1992) Petrological characterization of the source components of potassic magmas: geochemical and experimental constraints. *Lithos* 28:187–204
- Foley SF (1994) Geochemische und experimentelle Untersuchungen zur Genese der kalireichen Magmatite. *Neues Jahrbuch Mineralogie Abhandlungen* 167:1–55
- Foley SF, Peccerillo A (1992) Potassic and ultrapotassic magmas and their origin. *Lithos* 28:181–185
- Foley SF, Wheller GE (1990) Parallels in the origin of the geochemical signatures of island arc volcanics and continental potassic igneous rocks: the role of residual titanites. *Chem Geol* 85:1–18
- Foley SF, Venturelli G, Green DH, Toscani L (1987) The ultrapotassic rocks: characteristics, classification, and constraints for petrogenetic models. *Earth-Sci Rev* 24:81–134
- Foley SF, Jacob DE, O'Neill HSC (2011) Trace element variations in olivine phenocrysts from Ugandan potassic rocks as clues to the chemical characteristics of parental magmas. *Contrib Miner Petrol* 162:1–20
- Fornaseri M, Scherillo A, Ventriglia U (1963) *La regione vulcanica dei Colli Albani; vulcano Laziale*. Consiglio Nazionale Ricerche, Centro Mineralogia e Petrografia, Rome: 561
- Franz L, Romer RL (2010) Different styles of metasomatic veining in ultramafic xenoliths from the TUBAF seamount (Bismarck microplate, Papua New Guinea). *Lithos* 114:30–53

- Franz L, Becker KP, Kramer W, Herzig PM (2002) Metasomatic mantle xenoliths from the Bismarck Microplate (Papua New Guinea) – thermal evolution, geochemistry and extent of slab-induced metasomatism. *J Petrol* 43:315–343
- Fuge R, Andrews MJ, Johnson CC (1986) Chlorine and iodine, potential pathfinder elements in exploration geochemistry. *Appl Geochem* 1:111–116
- Gaffney AM, Blichert-Toft J, Nelson BK, Bizzarro M, Rosing M, Albarede F (2007) Constraints on source-forming processes of West Greenland kimberlites inferred from Hf–Nd isotope systematic. *Geochim Cosmochim Acta* 71:2820–2836
- Garcia MO, Liu NWK, Muenow DW (1979) Volatiles in submarine volcanic rocks from the Mariana island arc and trough. *Geochimica et Cosmochimica Acta* 43:305–312
- Gest DE, McBirney AR (1979) Genetic relationships of shoshonitic and absarokitic magmas, Absaroka Mountains, Wyoming. *J Volcanic Geoth Res* 6:85–104
- Ghasemi H, Rezaei-Kahkhaei M (2015) Petrochemistry and tectonic setting of the Davarzan-Abbasabad Eocene volcanic (DAEV) rocks, NE Iran. *Miner Petrol* 109:235–252
- Ghiara MR, Lirer L (1976) Mineralogy and geochemistry of the “low potassium” series of the Roccamonfina volcanic suite (Campania, S-Italy). *Bull Volcanol* 40:39–56
- Gibson SA, Thompson RN, Leat PT, Morrison MA, Hendry GL, Dickin AP, Mitchell JG (1993) Ultrapotassic magmas along the flanks of the Oligo-Miocene Rio Grande Rift, USA: monitors of the zone of lithospheric mantle extension and thinning beneath a continental rift. *J Petrol* 34:187–228
- Gill JB (1970) Geochemistry of Viti Levu, Fiji, and its evolution as an island arc. *Contrib Miner Petrol* 27:179–203
- Gill JB, Whelan P (1989) Early rifting of an oceanic island arc (Fiji) produced shoshonitic to tholeiitic basalts. *J Geophys Res* 94:4561–4578
- Gorton MP (1977) The geochemistry and origin of Quaternary volcanism in the New Hebrides. *Geochim Cosmochim Acta* 41:1257–1270
- Gregoire M, Moine BN, O’Reilly SY, Cottin JY, Giret A (2000) Trace element residence and partitioning in mantle xenoliths metasomatized by highly alkaline, silicate- and carbonate-rich melts (Kerguelen Islands, Indian Ocean). *J Petrol* 41:477–509
- Grove TL, Parman S, Bowring S (2002) The role of an H₂O-rich fluid component in the generation of primitive basaltic andesites and andesites from the Mt. Shasta region, N California. *Contrib Miner Petrol* 142:375–396
- Grove TL, Chatterjee N, Parman SW, Medard E (2006) The influence of H₂O on mantle wedge melting. *Earth Planet Sci Lett* 249:74–89
- Guo Z, Wilson M, Liu J, Mao Q (2006) Post-collisional, potassic and ultrapotassic magmatism of the northern Tibetan plateau: constraints on characteristics of the mantle source, geodynamic setting and uplift mechanisms. *J Petrol* 47:1177–1220
- Guo Z, Wilson M, Zhang M, Cheng Z, Zhang L (2013) Post-collisional, K-rich mafic magmatism in south Tibet: constraints on Indian slab-to-wedge transport processes and plateau uplift. *Contrib Miner Petrol* 165:1311–1340
- Halliday AN, Davidson JP, Holden P, DeWolf C, Lee DC, Fitton JG (1990) Trace element fractionation in plumes and the origin of HIMU mantle beneath the Cameroon Line. *Nature* 347:523–528
- Hellman PL, Smith RE, Henderson P (1979) The mobility of the rare earth elements: evidence and implications from selected terrains affected by burial metamorphism. *Contrib Miner Petrol* 71:23–44
- Holm PM, Lou S, Nielsen A (1982) The geochemistry and petrogenesis of the lavas of the Vulsinian district, Roman Province, Central Italy. *Contrib Miner Petrol* 80:367–378
- Hou Z, Yang Z, Qu X, Rui Z, Meng X, Gao Y (2009) The Miocene Gangdese porphyry copper belt generated during post-collisional extension in the Tibetan Orogen. *Ore Geol Rev* 36:25–51
- Hou Z, Zhang H, Pan X, Yang Z (2011) Porphyry Cu (–Mo–Au) deposits related to melting of thickened mafic lower crust: examples from the eastern Tethyan metallogenic domain. *Ore Geol Rev* 39:21–45
- Hudgins TR, Mukasa SB, Simon AC, Moore G, Barifajio E (2015) Melt inclusion evidence for CO₂-rich melts beneath the western branch of the East African rift: implications for long-term storage of volatiles in the deep lithospheric mantle. *Contrib Miner Petrol* 169 (in press)
- Hutchison CS, Jezek PA (1978) Banda Arc of eastern Indonesia: petrography, mineralogy and chemistry of the volcanic rocks. Proceedings of 3rd regional conference on the geology and mineral resources of Southeast Asia. Smithsonian Institution, Department of Mineral Science, Washington DC, pp 607–619
- Ionov DA, Hofmann AW (1995) Nb–Ta-rich mantle amphiboles and micas: implications for subduction-related metasomatic trace element fractionations. *Earth Planet Sci Lett* 131:341–356
- Ishimaru S, Arai S, Ishida Y, Shirasaka M, Okrugin VM (2007) Melting and multi-stage metasomatism in the mantle wedge beneath a frontal arc inferred from highly depleted peridotite xenoliths from the Avacha Volcano, southern Kamchatka. *J Petrol* 48:395–433
- Iwamori H (2007) Transportation of H₂O beneath the Japan arcs and its implications for global water circulation. *Chem Geol* 239:182–198
- Jakes P, Smith IE (1970) High-potassium calc-alkaline rocks from Cape Nelson, eastern Papua. *Contrib Miner Petrol* 28:259–271
- Jamali H, Mehrabi B (2015) Relationships between arc maturity and Cu–Mo–Au porphyry and related epithermal mineralization at the Cenozoic Arasbaran magmatic belt. *Ore Geol Rev* 65:487–501
- Jaques AL (1976) High-K₂O island-arc volcanic rocks from the Finisterre and Adelbert Ranges, northern Papua New Guinea. *Bulletin of the Geological Society of America* 87:861–867

- Jiang YH, Wang GC, Liu Z, Ni CY, Qing L, Zhang Q (2015) Repeated slab advance-retreat of the Paleo-Pacific plate underneath SE China. *International Geology Reviews* 57:472–491
- Joplin GA (1968) The shoshonite association—a review. *J Geol Soc Aust* 15:275–294
- Kalfoun F, Ionov D, Merlet C (2002) HFSE residence and Nb/Ta ratios in metasomatised, rutile-bearing mantle peridotites. *Earth Planet Sci Lett* 199:49–65
- Kay SM, Abbruzzi JM (1996) Magmatic evidence for Neogene lithospheric evolution of the central Andean “flat-slab” between 30°S and 32°S. *Tectonophysics* 259:15–28
- Kay SM, Mpodozis C (2001) Central Andean ore deposits linked to evolving shallow subduction systems and thickening crust. *GSA Today* 11:4–9
- Kay SM, MaksaeV V, Moscoso R, Mpodozis C, Nasi C (1987) Probing the evolving Andean lithosphere: mid-late Tertiary magmatism in Chile (29°–30°30'S) over the modern zone of subhorizontal subduction. *J Geophys Res* 92:6173–6189
- Kay SM, Godoy E, Kurtz A (2005) Episodic arc migration, crustal thickening, subduction erosion, and magmatism in the south-central Andes. *Geol Soc Am Bull* 117:67–88
- Kelemen PB, Johnson KTM, Kinzler RJ, Irving AJ (1990) High field strength element depletions in arc basalts due to mantle-magma interactions. *Nature* 345:521–524
- Keller J (1974) Petrology of some volcanic rock series of the Aeolian Arc, southern Tyrrhenian Sea: calc-alkaline and shoshonitic associations. *Contrib Miner Petrol* 46:29–47
- Kirchner JG (1979) Petrographic significance of a carbonate-rich lamprophyre from Squaw Creek, northern Black Hills, South Dakota. *Am Mineral* 64:986–992
- Kogiso T, Hirschmann MM, Reiners PW (2004) Length scales of mantle heterogeneities and their relationship to ocean island basalt geochemistry. *Geochim Cosmochim Acta* 68:345–360
- Kontak DJ, Clark AH, Farrar E, Pearce TH, Strong DF, Baadsgaard H (1986) Petrogenesis of a Neogene shoshonite suite, Cerro Moromoni, Puno, southeastern Peru. *Can Mineral* 24:117–135
- Kontinen A, Huhma H, Lahaye Y, O'Brien H, Torppa A (2013) Shoshonitic and alkaline 1.86–1.85 Ga magmatism at the contact of the Svecofennian and Karelian domains in the Pyhäntä area, Central Finland. *Geological Survey of Finland, Report of Investigation* 198:75–84
- Kuritani T, Kimura J, Ohtani E, Miyamoto H, Furuyama K (2013) Transition zone origin of potassic basalts from Wudalianchi Volcano, northeast China. *Lithos* 156:1–12
- Lange RA, Carmichael ISE, Renne PR (1993) Potassic volcanism near Mono basin, California: evidence for high water and oxygen fugacities inherited from subduction. *Geology* 21:949–952
- Le Maitre RW (1962) Petrology of volcanic rocks, Gough Island, South Atlantic. *Bulletin of the Geological Society of America* 73:1309–1340
- Le Maitre RW (1982) Numerical petrology: statistical interpretation of geochemical data. Elsevier Developments in Petrology 8: 291 pp
- Le Maitre RW (ed) (1989) A classification of igneous rocks and glossary of terms: recommendations of the International Union Of Geological Sciences Subcommittee on the systematics of igneous rocks. Blackwell Scientific Publications, Oxford, 193 pp
- Le Roex A (1985) Geochemistry, mineralogy and magmatic evolution of the basaltic and trachytic lavas from Gough Island, South Atlantic. *J Petrol* 26:149–186
- Leat PT, Thompson RN, Morrison MA, Hendry GL, Dickin AP (1988) Silicic magma derived by fractional-crystallization from Miocene minette, Elkhed Mountain, Colorado. *Mineral Mag* 52:577–586
- Leech ML (2001) Arrested orogenic development: eclogitization, delamination, and tectonic collapse. *Earth Planet Sci Lett* 185:149–159
- Lehmann St, Barcikowski J, von Quadt A, Gallhofer D, Peytcheva I, Heinrich CA, Serafimovski T (2013) Geochronology, geochemistry and isotope tracing of the Oligocene magmatism of the Buchim-Damjan-Borov Dol ore district: implications for timing, duration and source of the magmatism. *Lithos* 181:216–233
- Li XH, Li ZX, Li WX, Wang XC, Gao Y (2013) Revisiting the “C-type adakites” of the Lower Yangtze River Belt, central eastern China: in-situ zircon Hf–O isotope and geochemical constraints. *Chemical Geology* 345:1–15
- Lin PN, Stern RJ, Bloomer SH (1989) Shoshonitic volcanism in the northern Marianas arc: 2. LILE and REE abundances: evidence for the source of incompatible element enrichments in intra-oceanic arcs. *J Geophys Res* 94:4497–4514
- Liu D, Zhao Z, Zhu DC, Niu Y, DePaolo DJ, Harrison TM, Mo X, Dong G, Zhou S, Sun C, Zhang Z, Liu J (2014) Postcollisional potassic and ultrapotassic rocks in southern Tibet: mantle and crustal origins in response to India-Asia collision and convergence. *Geochim Cosmochim Acta* 143:207–231
- Liu Z, Jiang Y, Jia R, Zhao P, Zhou Q (2015) Origin of Late Triassic high-K calc-alkaline granitoids and their potassic microgranular enclaves from the western Tibet Plateau, northwest China: implications for Paleo-Tethys evolution. *Gondwana Res* 27:326–341
- Lu YJ, Kerrich R, McCuaig TC, Li ZX, Hart CJR, Cawood PA, Hou ZQ, Bagas L, Cliff J, Belousova EA, Tang S (2013a) Geochemical, Sr–Nd–Pb, and zircon Hf–O isotopic compositions of Eocene-Oligocene shoshonitic and potassic adakite-like felsic intrusions in western Yunnan, SW China: petrogenesis and tectonic implications. *J Petrol* 54:1309–1348
- Lu YJ, Kerrich R, Kemp AIS, McCuaig TC, Hou ZQ, Hart CJR, Li ZX, Cawood PA, Bagas L, Yang ZM, Cliff J, Belousova EA, Jourdan F, Evans NJ (2013b) Intracontinental Eocene-Oligocene porphyry Cu mineral systems of Yunnan, western Yangtze Craton, China: compositional characteristics, sources, and implications for continental collision metallogeny. *Econ Geol* 108:1541–1576

- Luhr JF, Kyser TK (1989) Primary igneous analcime: the Colima minettes. *American Mineralogist* 74:216–223
- Luhr JF, Allan JF, Carmichael ISE, Nelson SA, Hasegawa T (1989) Primitive calc-alkaline and alkaline rock types from the western Mexican volcanic belt. *Journal of Geophysical Research* 94:4515–4530
- Mallik A, Nelson J, Dasgupta R (2015) Partial melting of fertile peridotite fluxed by hydrous rhyolitic melt at 2–3 GPa: implications for mantle wedge hybridization by sediment melt and generation of ultrapotassic magmas in convergent margins. *Contrib Miner Petrol* 169:1–24
- Marcelot G, Dupuy C, Girod M, Maury RC (1983) Petrology of Futuna Island lavas (New Hebrides): an example of calc-alkaline magmatism associated with the initial stages of back-arc spreading. *Chemical Geology* 38:23–37
- Maughan DT, Keith JD, Christiansen EH, Pulsipher T, Hattori K, Evans NJ (2002) Contributions from mafic alkaline magmas to the Bingham porphyry Cu–Au–Mo deposit, Utah, USA. *Mineral Deposita* 37:14–37
- McDonald R, Upton BJ, Collerson KD, Hearn BC, James D (1992) Potassic mafic lavas of the Bearpaw Mountains, Montana: mineralogy, chemistry and origin. *J Petrol* 33:305–346
- McKenzie DE, Chappell BW (1972) Shoshonitic and calc-alkaline lavas from the highlands of Papua New Guinea. *Contrib Miner Petrol* 35:50–62
- McLennan SM, Taylor SR (1981) Role of subducted sediments in island arc magmatism: constraints from REE patterns. *Earth Planet Sci Lett* 54:423–430
- Meen JK (1987) Formation of shoshonites from calc-alkaline basalt magmas: geochemical and experimental constraints from the type locality. *Contrib Miner Petrol* 97:333–351
- Meijer A, Reagan M (1981) Petrology and geochemistry of the island of Sarigan in the Mariana arc; calc-alkaline volcanism in an oceanic setting. *Contrib Miner Petrol* 77:337–354
- Melluso L, de Gennaro R, Fedele L, Franciosi L, Morra V (2012) Evidence of crystallization in residual, Cl-F-rich, apatitic, trachyphonolitic magmas and primitive Mg-rich basalt-trachyphonolite interaction in the lava domes of the Phlegrean Fields (Italy). *Geol Mag* 149:532–550
- Menzies MA, Hawkesworth CJ (eds) (1987) *Mantle metasomatism*. Academic Press, London, pp 472
- Mikulski SZ (2007) The late Variscan gold mineralization in the Kaczawa Mountains, Western Sudetes. *Polish Geol Inst Spec Pap* 22:1–162
- Miller C, Schuster R, Klötzli U, Frank W, Purtscheller F (1999) Post-collisional potassic and ultrapotassic magmatism in SW Tibet: geochemical and Sr–Nd–Pb–O isotopic constraints for mantle source characteristics and petrogenesis. *J Petrol* 40:1399–1424
- Mitchell AHG, Garson MS (1981) *Mineral deposits and global tectonic setting*. Academic Press, London, p 421
- Montelli R, Nolet G, Dahlen FA, Masters G, Engdahl ER, Hung S-H (2004) Finite-frequency tomography reveals a variety of plumes in the mantle. *Science* 303:338–343
- Morrison MA (1978) The use of “immobile” trace elements to distinguish the paleotectonic affinities of metabasalts: applications to the Palaeocene basalts of Mull and Skye, Northwest Scotland. *Earth Planet Sci Lett* 39:407–416
- Morrison GW (1980) Characteristics and tectonic setting of the shoshonite rock association. *Lithos* 13:97–108
- Müller D (2002) Preface—Gold-copper mineralization in alkaline rocks. *Mineral Deposita* 37:1–3
- Müller D, Groves DI (1993) Direct and indirect associations between potassic igneous rocks, shoshonites and gold-copper deposits. *Ore Geol Rev* 8:383–406
- Müller D, Rock NMS, Groves DI (1992a) Geochemical discrimination between shoshonitic and potassic volcanic rocks from different tectonic settings: a pilot study. *Miner Petrol* 46:259–289
- Müller D, Stumpfl EF, Taylor WR (1992b) Shoshonitic and alkaline lamprophyres with elevated Au and PGE concentrations from the Kreuzeck Mountains, Eastern Alps, Austria. *Miner Petrol* 46:23–42
- Müller D, Franz L, Herzig PM, Hunt S (2001) Potassic igneous rocks from the vicinity of epithermal gold mineralization, Lihir Island, Papua New Guinea. *Lithos* 57:163–186
- Nelson DR, McCulloch MT, Sun SS (1986) The origins of ultrapotassic rocks as inferred from Sr, Nd and Pb isotopes. *Geochim Cosmochim Acta* 50:231–245
- Nicholls J (1969) *Studies of the volcanic petrology of the Navajo-Hopi area, Arizona*. Unpl. PhD Thesis, University of California, Berkeley
- Nicholls J, Carmichael ISE (1969) A commentary on the absarokite-shoshonite-banakite series of Wyoming, USA. *Schweizerische Mineralogische und Petrologische Mitteilungen* 49:47–64
- Nowell GM, Pearson DG, Bell DR, Carlson RW, Smith CB, Kempton PD, Noble SR (2004) Hafnium isotope systematic of kimberlites and their megacrysts: new constraints on their source regions. *J Petrol* 45:1583–1612
- Orozco-Garza A, Dostal J, Keppie JD, Paz-Moreno FA (2013) Mid-Tertiary (25–21 Ma) lamprophyres in NW Mexico derived from subduction-modified subcontinental lithospheric mantle in an extensional backarc environment following steepening of the Benioff zone. *Tectonophysics* 590:59–71
- Oyhantçabal P, Siegesmund S, Wemmer K, Frei R, Layer P (2007) Post-collisional transition from calc-alkaline to alkaline magmatism during transcurrent deformation in the southernmost Dom Feliciano Belt (Braziliano-Pan-African, Uruguay). *Lithos* 98:141–159
- Pan YM, Fleet ME (2002) Compositions of the apatite-group minerals: substitution mechanisms and controlling factors. *Rev Mineral Geochem* 48:13–49
- Pearce JA (1976) Statistical analysis of major element patterns in basalt. *J Petrol* 17:15–43
- Pearce JA (1982) Trace element characteristics of lavas from destructive plate boundaries. In: Thorpe RS (ed) *Andesites*. Wiley, New York, pp 525–548
- Pearce JA (1983) Role of sub-continental lithosphere in magma genesis at active continental margins. In:

- Hawkesworth CJ, Norry MJ (eds) Continental basalts and mantle xenoliths. Shiva, Nantwich, pp 230–249
- Pearce JA (1987) An expert system for the tectonic characterization of ancient volcanic rocks. *J Volcanol Geoth Res* 32:51–65
- Pearce JA, Cann JR (1973) Tectonic setting of basaltic volcanic rocks determined using trace element analysis. *Earth Planet Sci Lett* 19:290–300
- Pearce JA, Norry MJ (1979) Petrogenetic implications of Ti, Zr, Y, and Nb variations in volcanic rocks. *Contrib Miner Petrol* 69:33–47
- Pearce JA, Peate D (1995) Tectonic implications of the composition of volcanic arc magmas. *Annual Reviews of Earth and Planetary Sciences* 23:251–285
- Pearce JA, Harris NBW, Tindle AG (1984) Tectonic interpretation of granitic rocks. *J Petrol* 25:956–983
- Peccerillo A (1985) Roman comagmatic province (central Italy): evidence for subduction-related magma genesis. *Geology* 13:103–106
- Peccerillo A (1992) Potassic and ultrapotassic rocks: compositional characteristics, petrogenesis, and geologic significance. *IUGS Episodes* 15:243–251
- Peccerillo A, Taylor SR (1976a) Rare earth elements in east Carpathian volcanic rocks. *Earth Planet Sci Lett* 32:121–126
- Peccerillo A, Taylor SR (1976b) Geochemistry of Eocene calc-alkaline volcanic rocks from the Kastamonu area, northern Turkey. *Contrib Miner Petrol* 58:63–81
- Pe-Piper G (1980) Geochemistry of Miocene shoshonites, Lesbos, Greece. *Contrib Miner Petrol* 72:387–396
- Piercey SJ (2009) Litho-geochemistry of volcanic rocks associated with volcanogenic massive sulphide deposits and applications to exploration. In: Cousens B, Piercey SJ (eds) *Submarine volcanism and mineralization: modern through ancient*. Geological Association of Canada Short Course, Quebec, Canada, 29–30 May 2008, pp 15–40
- Pitcher WS (1983) Granite type and tectonic environment. In: Hsu K (ed) *Mountain building process*. Academic Press, London, pp 19–40
- Poli G, Frey FA, Ferrara G (1984) Geochemical characteristics of the South Tuscany (Italy) volcanic province: constraints on lava petrogenesis. *Chemical Geology* 43:203–221
- Pourtier E, Devidal JL, Gibert F (2010) Solubility measurements of synthetic neodymium monazite as a function of temperature at 2 kbars, and aqueous neodymium speciation in equilibrium with monazite. *Geochim Cosmochim Acta* 74:1872–1891
- Prelevic D, Foley SF, Romer RL, Cvetkovic V, Downes H (2005) Tertiary ultrapotassic volcanism in Serbia: constraints on petrogenesis and mantle source characteristics. *J Petrol* 46:1443–1487
- Prelevic D, Stracke A, Foley SF, Romer RL, Conticelli S (2010) Hafnium isotope compositions of Mediterranean lamproites: mixing of melts from asthenosphere and crustally contaminated mantle lithosphere. *Lithos* 119:297–312
- Rao NVC, Srivastava RK, Sinha AK, Ravikant V (2014) Petrogenesis of Kerguelen mantle plume-linked Early Cretaceous ultrapotassic intrusive rocks from the Gondwana sedimentary basins, Damodar Valley, Eastern India. *Earth Sci Rev* 136:96–120
- Reagan MK, Gill JB (1989) Coexisting calc-alkaline and high-Nb-basalts from Turrialba volcano, Costa Rica: implications for residual titanites in arc magma sources. *J Geophys Res* 94:4619–4633
- Righter K, Dyar MD, Delaney JS, Vennemann TW, Hervig RL, King PL (2002) Correlations of octahedral cations with OH⁻, O²⁻, Cl⁻, and F⁻ in biotite from volcanic rocks and xenoliths. *Am Mineral* 87:142–153
- Ringwood AE (1990) Slab-mantle interactions, 3: petrogenesis of intraplate magmas and structure of the upper mantle. *Chemical Geology* 82:187–207
- Rock NMS (1988) *Numerical Geology. Lecture notes in earth sciences*. Springer, Heidelberg, Berlin, vol 18, 427 p
- Rock NMS (1991) *Lamprophyres*. Blackie, Glasgow, p 285
- Rock NMS, Finlayson EJ (1990) Petrological affinities of intrusive rocks associated with the giant mesothermal gold deposit at Porgera, Papua New Guinea. *J SE Asian Earth Sci* 4:247–257
- Rock NMS, Syah HH, Davis AE, Hutchison D, Styles MT, Rahayu L (1982) Permian to Recent volcanism in northern Sumatra, Indonesia: a preliminary study of its distribution, chemistry and peculiarities. *Bull Volc* 45:127–152
- Roden MF (1981) Origin of coexisting minette and ultramafic breccias, Navajo volcanic field. *Contrib Miner Petrol* 77:195–206
- Roden MF, Smith D (1979) Field geology, chemistry and petrology of Buell Park diatreme, Apache County, Arizona. In: Boyd FR, Meyer HAO (eds) *Kimberlites, Diatremes and Diamonds*. In: *Proceedings of 2nd international kimberlite conference*. American Geophysical Union, Washington, vol 1, pp 364–381
- Rogers NW, Setterfield TN (1994) Potassium and incompatible-element enrichment in shoshonitic lavas from the Tavua volcano, Fiji. *Chem Geol* 118:43–62
- Rogers NW, Bachinsky SW, Henderson P, Parry SJ (1982) Origin of potash-rich basic lamprophyres: trace element data from Arizona minettes. *Earth Planet Sci Lett* 57:305–312
- Rogers NW, Hawkesworth CJ, Parker RJ, Marsh JS (1985) The geochemistry of potassic lavas from Vulsini, central Italy, and implications for mantle enrichment processes beneath the Roman Region. *Contrib Miner Petrol* 90:244–257
- Rudnick R, Fountain D (1995) Nature and composition of the continental crust: a lower crustal perspective. *Reviews in Geophysics* 33:267–309
- Sajona FG, Maury RC, Pubellier M, Leterrier J, Bellon H, Cotton J (2000) Magmatic source enrichment by slab-derived melts in a young post-collision setting, central Mindanao (Philippines). *Lithos* 54:173–206

- Saunders AD, Tarney J, Weaver SD (1980) Transverse geochemical variations across the Antarctic peninsula: implications for the genesis of calc-alkaline magmas. *Earth Planet Sci Lett* 46:344–360
- Saunders AD, Norry MJ, Tarney J (1991) Fluid influence on the trace element compositions of subduction zone magmas. *Transactions of the Royal Society of London* A335:377–392
- Savelli C (1967) The problem of rock assimilation by Somma-Vesuvius magma: I. composition of Somma and Vesuvius lavas. *Contrib Miner Petrol* 16:328–353
- Schiano P, Birck J-L, Allègre CJ (1997) Osmium-strontium-neodymium-lead isotopic covariations in mid-ocean ridge basalt glasses and the heterogeneity of the upper mantle. *Earth Planet Sci Lett* 150:363–379
- Shen P, Shen Y, Liu T, Li G, Zeng Q (2008) Geology and geochemistry of the Early Carboniferous Eastern Sawur caldera complex and associated gold epithermal mineralization, Sawur Mountains, Xinjiang, China. *J Asian Earth Sci* 32:259–279
- Smith IE (1972) High-potassium intrusions from south-eastern Papua. *Contrib Miner Petrol* 34:167–176
- Smith RE, Smith SE (1976) Comments on the use of Ti, Zr, Y, Sr, K, P, and Nb in classification of basaltic magmas. *Earth Planet Sci Lett* 32:114–120
- Soloviev SG (2014a) The Metallogeny of Shoshonitic Magmatism (Volume I). Scientific World Publications, Moscow: 1–528 pp (in Russian)
- Soloviev SG (2014b) The Metallogeny of Shoshonitic Magmatism (Volume II). Scientific World Publications, Moscow: 1–472 pp (in Russian)
- Soloviev SG (2015) Geology, mineralization, and fluid inclusion characteristics of the Kumbel oxidized W–Cu–Mo skarn and Au–W stockwork deposit in Kyrgyzstan, Tien Shan. *Mineral Deposita* 50:187–220
- Soloviev SG, Krivoschekov NN (2011) Petrochemistry of rocks in the Chorukh-Dairon monzonite-syenite-granite pluton, northern Tajikistan. *Geochem Int* 49:691–710
- Soloviev SG, Kryazhev SG, Dvurechenskaya SS (2013) Geology, mineralization, stable isotope geochemistry, and fluid inclusion characteristics of the Novogodnee-Monto oxidized Au-(Cu) skarn and porphyry deposit, Polar Ural, Russia. *Mineral Deposita* 48:603–627
- Sombroek H (1985) Igneous petrology of the Porgera intrusive “complex”. Unpl. BSc Honours Thesis, University of Sydney
- Spies O, Lensch G, Mihm A (1984) Petrology and geochemistry of the post-ophiolitic Tertiary volcanic between Sabzevar and Quchan, NE-Iran. *Neues Jahrbuch für Geologie und Paläontologie Abhandlungen* 16:389–408
- Srivastava RK, Rao NV, Sinha AK (2009) Cretaceous potassic intrusive with affinities to aillikites from Jharia area: magmatic expression of metasomatically veined and thinned lithospheric mantle beneath Singhbhum Craton, Eastern India. *Lithos* 112:407–418
- Stern RJ (1979) On the origin of andesite in the northern Mariana island arc: implications from Agrigan. *Contrib Miner Petrol* 68:207–219
- Stern RJ, Bloomer SH, Lin PG, Ito E, Morris J (1988) Shoshonitic magmas in nascent arcs: new evidence from submarine volcanoes in the northern Marianas. *Geology* 16:426–430
- Stern CR, Skewes MA, Arevalo A (2011) Magmatic evolution of the giant El Teniente Cu–Mo deposit, Central Chile. *J Petrol* 52:1591–1617
- Sun SS, McDonough WF (1989) Chemical and isotopic systematic of oceanic basalts: implications for mantle composition and processes. In: Saunders AD, Norry MJ (eds) *Magmatism in the ocean basins* (vol 42). Geological Society of London Special Publication, pp 313–345
- Tan J, Wei JH, Shi WJ, Wang MZ, Li YJ, Fu LB, Li H (2013a) Formation of Wulong mafic dykes via mixing of enriched lithospheric mantle-derived and crustal magmas, eastern North China Craton. *J Geol* 121:517–535
- Tan J, Wei JH, Shi WJ, Feng B, Li YJ, Fu LB (2013b) Origin of dyke swarms by mixing of metasomatized subcontinental lithospheric mantle-derived and lower crustal magmas in the Guocheng fault belt, Jiaodong Peninsula, North China Craton. *Geol J* 48:516–530
- Taylor SR, Capp AC, Graham AL, Blake DH (1969) Trace element abundances in andesites II: Saipan, Bougainville, and Fiji. *Contrib Miner Petrol* 23:1–26
- Taylor WR, Rock NMS, Groves DI, Perring CS, Golding SD (1994) Geochemistry of Archaean shoshonitic lamprophyres from the Yilgarn Block, Western Australia: Au abundance and association with gold mineralization. *Appl Geochem* 9:197–222
- Teiber H, Scharrer M, Marks MAW, Arzamastev AA, Wenzel T, Markl G (2015) Equilibrium partitioning and subsequent re-distribution of halogens among apatite-biotite-amphibole assemblages from mantle-derived plutonic rocks: complexities revealed. *Lithos* 223:221–237
- Thompson RN (1977) Primary basalts and magma genesis; III. Alban Hills, Roman comagmatic province, Central Italy. *Contrib Miner Petrol* 60:91–108
- Thompson RN (1982) Magmatism of the British Tertiary volcanic province. *Scott J Geol* 18:50–107
- Thompson RN, Morrison MA, Hendry GL, Parry SJ (1984) An assessment of the relative roles of crust and mantle in magma genesis: an elemental approach. *Philosophical Transactions of the Royal Society of London* A310:549–590
- Thorpe RS, Potts PJ, Francis PW (1976) Rare earth data and petrogenesis of andesite from the North Chilean Andes. *Contrib Miner Petrol* 54:65–78
- Tiepolo M, Vannucci R, Oberti R, Foley S, Bottazzi P, Zanetti A (2000) Nb and Ta incorporation and

- fractionation in titanian pargasite and kaersutite: crystal-chemical constraints and implications for natural systems. *Earth Planet Sci Lett* 176:185–201
- Till CB, Grove TL, Withers AC (2012) The beginnings of hydrous mantle wedge melting. *Contrib Miner Petrol* 163:669–688
- Tommasini S, Avanzinelli R, Conticelli S (2011) The Th/La and Sm/La conundrum of the Tethyan realm lamproites. *Earth Planet Sci Lett* 301:469–478
- Toplis MJ, Carroll MR (1995) An experimental study of the influence of oxygen fugacity on Fe–Ti oxide stability, phase relations, and mineral–melt equilibria in ferro-basaltic systems. *J Petrol* 36:1137–1170
- Torabi G (2011) Middle Eocene volcanic shoshonites from the western margin of the Central-East Iranian micro-continent (CEIM), a mark of previously subducted CEIM-confining oceanic crust. *Petrology* 19:675–689
- Torabi G, Arai S, Abbasi H (2014) Eocene continental dyke swarm from Central Iran (Khur area). *Petrology* 22:617–632
- Tropper P, Manning CE, Harlov DE (2011) Solubility of CePO_4 monazite and YPO_4 xenotime in H_2O and $\text{H}_2\text{O-NaCl}$ at 800°C and 1 GPa: implications for REE and Y transport during high-grade metamorphism. *Chem Geol* 282:58–66
- Van Bergen MJ, Ghezzo C, Ricci CA (1983) Minette inclusions in the rhyodacitic lavas of Mt. Amiata (central Italy): mineralogical and chemical evidence of mixing between Tuscan and Roman type magmas. *J Volcanol Geoth Res* 19:1–35
- Van Kooten G (1980) Mineralogy, petrology and geochemistry of an ultrapotassic basalt suite, Central Sierra Nevada, California, U.S.A. *J Petrol* 21:651–684
- Venturelli G, Fragipane M, Weibel M, Antiga D (1978) Trace element distribution in the Cainozoic lavas of Nevado Caropuna and Andagna Valley, Central Andes of Southern Peru. *Bull Volc* 41:213–228
- Venturelli G, Thorpe RS, Dal Piaz GV, Del Moro A, Potts PJ (1984) Petrogenesis of calc-alkaline, shoshonitic and associated ultrapotassic Oligocene volcanic rocks from the Northwestern Alps, Italy. *Contrib Miner Petrol* 86:209–220
- Vigouroux N, Wallace PJ, Kent AJR (2008) Volatiles in high-K magmas from the western Trans-Mexican volcanic belt: evidence for fluid fluxing and extreme enrichment of the mantle wedge by subduction processes. *J Petrol* 49:1589–1618
- Villemant B, Michaud V, Metrich N (1993) Wall rock-magma interactions in Etna, Italy, studied by U–Th disequilibrium and rare earth element systematic. *Geochim Cosmochim Acta* 57:1169–1180
- Wakabayashi J, Sawyer TL (2001) Stream incision, tectonics, uplift, and evolution of topography of the Sierra Nevada, California. *J Geol* 109:539–562
- Wallace DA, Johnson RW, Chappell BW, Arculus RJ, Perfit MR, Crick IH (1983) Cainozoic volcanism of the Tabar, Lihir, Tanga, and Feni islands, Papua New Guinea: geology, whole-rock analyses, and rock-forming mineral compositions. Bureau of Mineral Resources of Australia, BMR Report, vol 243, 138 pp
- Wang H, Wu YB, Li CR, Zhao TY, Qin ZW, Zhu LQ, Gao S, Zheng JP, Liu XM, Zhou L, Zhang Y, Yang SH (2014) Recycling of sediment into the mantle source of K-rich mafic rocks: Sr–Nd–Hf–O isotopic evidence from the Fushui complex in the Qinling orogen. *Contrib Miner Petrol* 168:1062–1081
- Weaver BL, Wood DA, Tarney J, Joron JL (1987) Geochemistry of ocean island basalts from the South Atlantic: Ascension, Bouvet, St.Helena, Gough and Tristan da Cunha. In: Fitton JG, Upton BGJ (eds) *Alkaline Igneous Rocks* (vol 30). Geological Society of London Special Publication, pp 253–267
- Wheller GE (1986) Petrogenetic studies of basalt-andesite-dacite volcanism at Batur volcano, Bali, and the causes of K-variation in Sunda-Banda-Arc basalts. Unpl. PhD Thesis, University of Tasmania, Hobart
- Wheller GE, Varne R, Foden JD, Abbott M (1986) Geochemistry of Quaternary volcanism in the Sunda-Banda arc, Indonesia, and three-component genesis of island arc basaltic magmas. *J Volcanol Geoth Res* 32:137–160
- Whitford DJ (1975) Geochemistry and petrology of volcanic rocks from the Sunda arc, Indonesia. Unpl. PhD Thesis, The Australian National University, Canberra
- Whitford DJ, Jezek PA (1979) Origin of Late-Cenozoic lavas from the Banda arc, Indonesia: trace element and Sr isotope evidence. *Contrib Miner Petrol* 68:141–150
- Whitford DJ, Nicholls IA, Taylor SR (1979) Spatial variations in the geochemistry of Quaternary lavas across the Sunda Arc in Java and Bali. *Contrib Miner Petrol* 70:341–356
- Wilson M (1989) *Igneous petrogenesis. A Global Tectonic Approach*. Unwin Hyman, London 466 pp
- Wood DA, Joron JL, Treuil M (1979) A re-appraisal of the use of trace elements to classify and discriminate between magma series erupted in different tectonic settings. *Earth Planet Sci Lett* 45:326–336
- Woodhead JD, Eggins S, Gamble JA (1993) High field strength and transition element systematic in island arc and back-arc basin basalts: evidence for multi-phase melt extraction and a depleted mantle wedge. *Earth Planet Sci Lett* 114:491–504
- Woodhead JD, Hergt JM, Davidson JP, Eggins SM (2001) Hafnium isotope evidence for ‘conservative’ element mobility during subduction zone processes. *Earth Planet Sci Lett* 192:331–346
- Yang XM, Lentz DR (2005) Chemical composition of rock-forming minerals in gold-related granitoid intrusions, southwestern New Brunswick, Canada: implications for crystallization conditions, volatile exsolution, and fluorine-chlorine activity. *Contrib Miner Petrol* 150:287–305
- Yang ZM, Lu YJ, Hou ZQ, Chang ZS (2015) High-Mg diorite from Qulong in Southern Tibet: implications for the genesis of adakite-like intrusions and

- associated porphyry Cu deposits in collisional orogens. *J Petrol* 56:227–254
- Zajacz Z, Seo JH, Candela PA, Piccoli PM, Heinrich CA, Guillong M (2010) Alkali metals control the release of gold from volatile-rich magmas. *Earth Planet Sci Lett* 297:50–56
- Zhang M, Suddaby P, Thompson RN, Thirlwall MF, Menzies MA (1995) Potassic volcanic rocks in NE China: geochemical constraints on mantle source and magma genesis. *J Petrol* 36:1275–1303

4.1 Roman Province (Italy): Example from a Continental Arc Setting

4.1.1 Introduction

The volcanic rocks of Central Italy (Fig. 4.1) are divided into three magmatic provinces (van Bergen et al. 1983; Peccerillo 2005):

- In the north, predominantly acid igneous rocks of Amiata, Roccastrada, San Vincenzo, and Elba represent the *Tuscan* Province.
- In central Italy, along the western side of the Apennine Fold Belt, the highly potassic volcanic centres of Vulsini, Vico, Sabatini, and Alban Hills form the *Roman* Province (see also Holm et al. 1982; Rogers et al. 1985; Boari et al. 2009).
- Potassic volcanoes such as Roccamonfina and Vesuvius, and the lavas of the Phlegrean Fields and Vulture form the *Campanian* Province in the south (van Bergen et al. 1983; D'Antonio and Di Girolamo 1994; Melluso et al. 2012).

The Pliocene-Quaternary volcanic rocks from the Roman Province, Italy, are considered to be

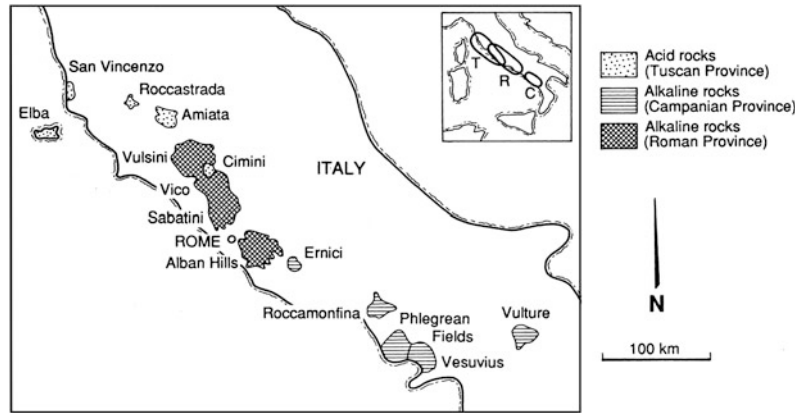
typical examples of orogenic ultrapotassic rocks as defined by Foley et al. (1987).

4.1.2 Regional Geology

Despite the potassic igneous rocks of the Roman Province having been studied by many petrologists (e.g. Appleton 1972; Cundari 1979; Civetta et al. 1981; Holm et al. 1982; van Bergen et al. 1983; Di Girolamo 1984; Poli et al. 1984), their petrogenesis has been the subject of controversy for many years (Rogers et al. 1985; Boari et al. 2009). There has also been considerable debate concerning the tectonic setting of these rocks. Most workers have interpreted the potassic igneous rocks to be related to subduction beneath the Calabrian Arc (Ninkovich and Hays 1972; Edgar 1980), but this has been contested by Cundari (1979). Modern studies based on stable isotopes (Rogers et al. 1985) seem to confirm the importance of subduction processes in the genesis of these rocks.

The Vulsinian District of the Roman Province is by far the largest in the region, covering 2280 km² (von Pichler 1970), and is the most intensively studied (Holm et al. 1982; Rogers et al. 1985; Peccerillo 2005). The volcanic activity is represented by lava flows and

Fig. 4.1 Geological overview of the Roman Province, Central Italy. Geological provinces: Tuscan; Roman; Campanian. Modified after Holm et al. (1982) and van Bergen et al. (1983)



pyroclastic rocks such as tuffs and ignimbrites (Holm et al. 1982; Boari et al. 2009).

4.1.3 Mineralogy and Petrography of the Potassic Igneous Rocks

The potassic igneous rocks from the Roman Province consist mainly of latites, tephrites, trachytes, phonolites and leucites (Holm et al. 1982; Boari et al. 2009).

Most of the lavas have porphyritic textures with phenocrysts of clinopyroxene, plagioclase, and leucite, with minor sanidine and olivine, in a fine-grained groundmass consisting of plagioclase, leucite, and clinopyroxene (Holm et al. 1982; Boari et al. 2009). The more silica-saturated latites and trachytes are characterized by similar assemblages, although leucite is absent and sanidine and quartz present; they also have biotite phenocrysts and apatite microphenocrysts (Holm et al. 1982; Rogers et al. 1985; Peccerillo 2005).

4.1.4 Geochemistry of the Potassic Igneous Rocks

Most of the lavas from the Roman Province are highly potassic (Conticelli and Peccerillo 1992; Peccerillo 2005), and some can be defined as ultrapotassic with K_2O and $MgO > 3$ wt%, and

K_2O/Na_2O ratios > 2 (Foley et al. 1987). The compositions (Table 4.1) normally vary from silica-undersaturated to silica-saturated with moderate SiO_2 contents (47.0–56.0 wt%); TiO_2 contents are low (< 0.8 wt%) and Al_2O_3 contents are variable (12.0–17.0 wt%), but can be as high as 19.9 wt% (e.g. Rogers et al. 1985), which is typical for subduction-related potassic igneous rocks (Morrison 1980; Campbell et al. 2014).

The rocks have high concentrations of LILE (e.g. up to 636 ppm Rb, up to 1812 ppm Sr), intermediate LREE (e.g. < 100 ppm La, < 200 ppm Ce), and low HFSE (< 0.8 wt% TiO_2 , < 26 ppm Y, < 14 ppm Nb, < 6 ppm Hf; see Table 4.1), when compared to those potassic igneous rocks derived from within-plate tectonic settings (Müller et al. 1992b). Based on their geochemistry, the rocks are interpreted to be subduction-related and they occur in a continental-arc setting, as previously suggested by most petrologists concerned with the area (e.g. Edgar 1980; Rogers et al. 1985; Boari et al. 2009). This interpretation is not consistent with studies by Cundari (1979), who proposes a within-plate tectonic setting for the igneous rocks from the Roman Province. Potassic igneous rocks from such within-plate settings are typically characterized by very high HFSE concentrations (cf. Müller et al. 1993), which is not the case in the rocks from the Roman Province (see Table 4.1).

Table 4.1 Representative whole-rock major- and trace-element geochemistry of potassic igneous rocks from the Roman Province, Central Italy

Province/deposit	Vulsini, Roman	Vulsini, Roman	Sabatini, Roman	Mount Ernici, Roman	Mount Ernici, Roman
Location	Italy	Italy	Italy	Italy	Italy
Rock type	Leucitite	Leucitite	Tephrite	Trachybasalt	Leucitite
Tectonic setting	Continental arc	Continental arc	Continental arc	Continental arc	Continental arc
Reference	Holm et al. (1982)	Rogers et al. (1985)	Coticelli and Peccerillo (1992)	Civetta et al. (1981)	Civetta et al. (1981)
SiO ₂	47.16	47.52	48.36	48.52	47.39
TiO ₂	0.74	0.87	0.70	0.77	0.72
Al ₂ O ₃	12.46	14.52	16.80	16.35	17.85
Fe ₂ O ₃ (tot)	7.49	8.44	6.95	6.87	6.03
MnO	0.11	0.14	0.13	0.15	0.13
MgO	9.22	7.38	6.57	9.03	6.36
CaO	15.41	13.15	9.85	12.03	10.53
Na ₂ O	0.68	0.96	1.30	2.79	2.51
K ₂ O	4.67	5.14	8.33	2.60	7.36
P ₂ O ₅	0.22	0.33	0.61	0.27	0.54
LOI	1.46	1.45	0.40	0.62	0.57
Total	99.62	99.90	100.00	100.00	99.99
V	225	243	n.a.	233	233
Cr	295	138	316	490	151
Ni	116	61	74	87	58
Rb	356	425	636	112	335
Sr	784	1122	1812	848	1412
Y	23	26	26	n.a.	n.a.
Zr	187	180	266	86	218
Nb	11	6	14	8	9
Ba	853	592	1202	500	892
La	62	56	88	n.a.	n.a.
Ce	112	127	202	n.a.	n.a.
Th	25	22	46	10	28
Ta	n.a.	0.6	0.6	n.a.	n.a.
Hf	n.a.	5	6	3	6

Major elements are in wt%, and trace elements are in ppm. Fe₂O₃ (tot) = total iron calculated as ferric oxide. Data from Civetta et al. (1981), Holm et al. (1982), Rogers et al. (1985), and Coticelli and Peccerillo (1992)

4.2 Kreuzeck Mountains, Eastern Alps (Austria): Example from a Postcollisional Arc Setting

4.2.1 Introduction

This region is described in more detail because data for the potassic igneous rocks were collected specifically for this study (cf. Müller 1993), the tectonic setting of the rocks is complex, and their precious-metal contents are discussed in Chap. 5.

The major components of the Eastern Alps in Austria, and adjoining areas of Switzerland, Italy, and Yugoslavia, are the Northern and Southern Calcareous Alps and the Central Alps (Fig. 4.2).

European-African plate collision and Alpine nappe emplacement in the late Cretaceous-Eocene were followed by a significant phase of mafic to felsic Oligocene dyke magmatism, mostly concentrated along a major (700 km), east-west-trending Tertiary suture, the Periadriatic Lineament (Exner 1976; Michálek et al. 2011; Konzett et al. 2012; Bartel et al. 2014). This lineament, also known as the Insubric Line, forms a dextrally transpressive intracontinental branch of the Europe-Africa plate boundary (Laubscher 1988). The Periadriatic fault separates the Austro-Alpine and South-Alpine units in the Eastern Alps, both of which belong to the

Adriatic microplate *sensu lato* (Bartel et al. 2014).

Dykes cut Austro-Alpine, South Alpine, and, rarely, Penninic units. They range in composition from basaltic to rhyolitic, but are mainly calc-alkaline andesitic and basaltic. Their compositions change across broad zones, from tholeiitic and calc-alkaline in the Southeastern Alps, to high-K calc-alkaline in the Central Alps, and shoshonitic and ultrapotassic in the northwestern and western sector (Beccaluva et al. 1983). The transition from calc-alkaline to high-K alkaline magmatism during transcurrent deformation is common in postcollisional arc-settings, probably suggesting the break-off of the subducting oceanic slab shortly after collision (cf. Oyhantçabal et al. 2007).

4.2.2 Regional Geology

The Kreuzeck Mountains, southern Austria, are composed of rocks of the middle Austro-Alpine unit of the Central Alps (Fig. 4.2). These consist of polymetamorphic crystalline basement rocks, which are partly overlain by a lower Palaeozoic volcanosedimentary sequence metamorphosed to greenschist facies (Reimann and Stumpfl 1981, 1985). The area studied covers more than 600 km² between the Möll Valley in the north and the Drau Valley in the south, and east-west from Iselsberg to Möllbrücke (Fig. 4.3).

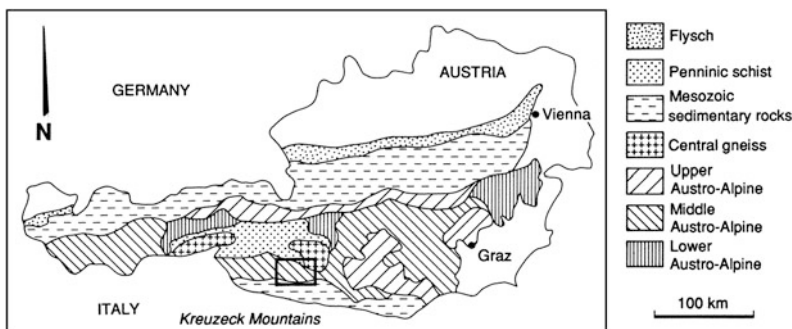


Fig. 4.2 Geological overview of the Eastern Alps, Austria, showing the location of the Kreuzeck Mountains. Modified after Reimann and Stumpfl (1985)

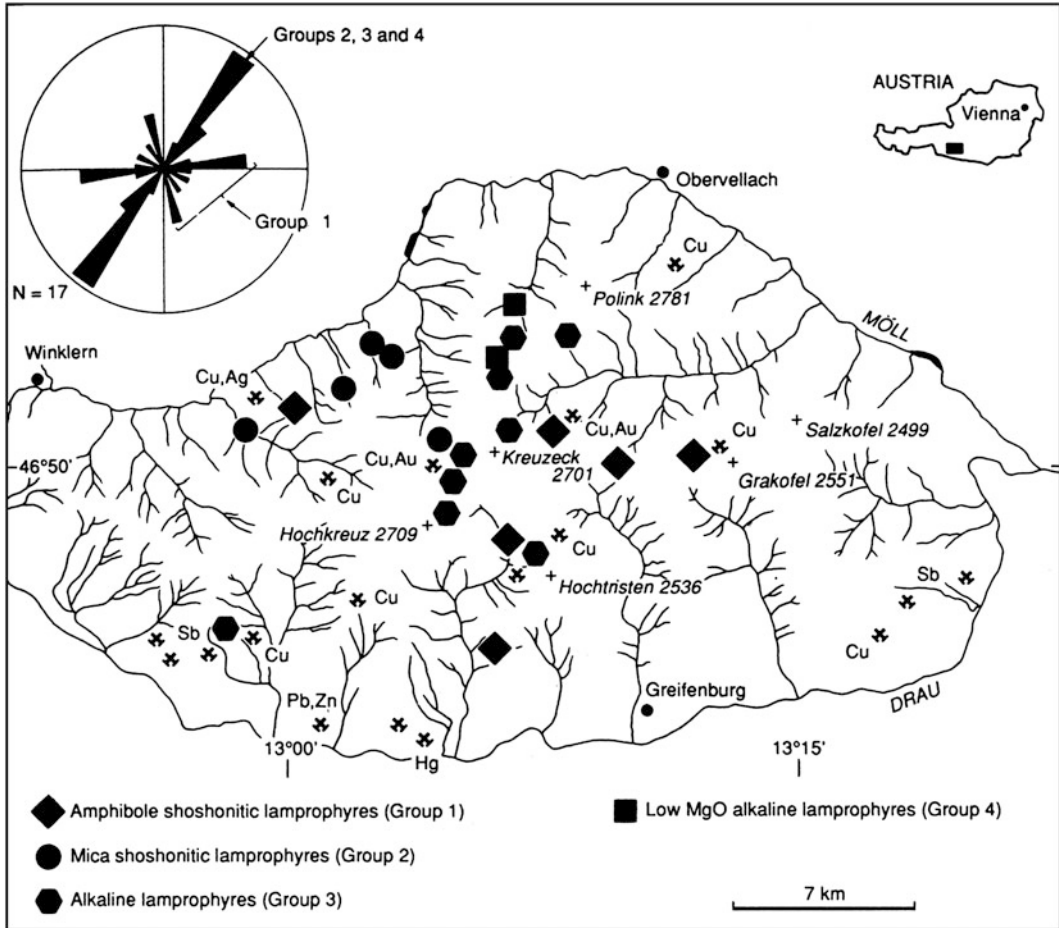


Fig. 4.3 Geographic map of the Kreuzeck Mountains, Austria, showing major mining areas and the location of shoshonitic and alkaline lamprophyres. Modified after Müller et al. (1992a)

The Kreuzeck Mountains are a wedge-shaped segment of the Austro-Alpine basement units of the Eastern Alps, south of the Penninic Tauern Window, and situated in the suture zone between the African and the European plates (Hoke 1990; Bartel et al. 2014). The Kreuzeck Mountains are subdivided into the Polinik Unit and the Strieden Unit, which make up the northern and southern parts, respectively (Hoke 1990; Konzett et al. 2012). These units are separated by a mylonitic fault zone, with K/Ar mica cooling ages indicating that tectonic transport along this fault zone commenced at about 90 Ma and continued until about 60 Ma (Hoke 1990). The Polinik Unit mainly consists of medium-grade quartzo-feldspathic

schists, gneisses and metapelites with lenses of amphibolites of up to several hundred metres in length (Konzett et al. 2012). The Strieden Unit in the south is composed of sillimanite-bearing metapelites, but without any evidence for eclogite-facies metamorphism (Konzett et al. 2012). Although no quantitative age data are available, the protoliths are estimated to be older than Permo-Carboniferous (Lahusen 1972; Michálek et al. 2011). In the prevailing plate tectonic models, the Kreuzeck Mountains form part of the Adriatic plate which overrode South Penninic units during the Eocene continent-continent collision. These Penninic units, with oceanic metasedimentary rocks, are exposed in the Tauern

Window to the north (Konzett et al. 2012). The Oligocene is characterized by several generations of dykes and local granodioritic plutons during a phase of extensional tectonics. This inhomogeneous extensional regime is followed by Miocene compression (Laubscher 1988).

The rocks of the Kreuzeck Mountains reveal a homogeneous pattern of deformation. Only in the northeastern area, which is nearest to the southern edge of the Tauern Window, are different phases of deformation detectable (Oxburgh 1966). Predominant tectonic features are faults and fractures, which show a dominant east-west trend. This correlates with the strike direction of most felsic dykes and some of the mafic dykes investigated here, which follow zones of weakness or fracture zones in the host rock, and implies a close connection with the east-west-striking Periadriatic Lineament.

The entire period of Oligocene orogenic magmatism is linked to continent-continent collision of the African and the European plates after the subduction of the Penninic oceans (Deutsch 1986). This includes the Western Alps (Venturelli et al. 1984), and dyke swarms along the southern margin of the European plate that are believed to be related to northwesterly dipping subduction of African oceanic lithosphere (Beccaluva et al. 1983). This event also produced back-arc spreading in the southwestern area (Provence, Balearic Basin, Sardinia).

More than 60 former prospects and mines are known from the Kreuzeck area (Friedrich 1963; Feitlinger et al. 1995). Mining activities date back to the Middle Ages and were mainly directed at stratabound ores of antimony-tungsten, mercury, and copper-silver-gold (Reimann and Stumpf 1981; Feitlinger et al. 1995). The precious metal mineralization occurs as sheeted quartz veins that were mined over a distance of 200 m along strike and dip. The quartz veins typically display colloform banding and/or cockade textures and contain abundant silver sulphosalts (Feitlinger et al. 1995). Most ore deposits are in the southern part of the Kreuzeck Mountains within a sequence of metavolcanic and metasedimentary rocks (Lahusen 1972) which extends, with tectonic

interruptions, for over 40 km along the Drau Valley (Fig. 4.3).

Early work by Friedrich (1963) suggested a relationship between ore deposits and Tertiary felsic porphyritic dykes in the Kreuzeck Mountains. He believed the mineralization to be of epigenetic hydrothermal origin, related to a hypothetical Tertiary pluton underlying the area. Friedrich (1963) interpreted numerous small granodioritic intrusions, as well as the lamprophyres and felsic dykes, as an indication of the presence of this postulated pluton. Later investigations by Höll and Maucher (1968) interpreted most of the antimony deposits to be submarine-exhalative, synsedimentary in origin (lower Palaeozoic age) and partly remobilized during Variscian and Alpine metamorphism, an opinion supported by Lahusen (1972). More recently, Feitlinger et al. (1995) suggested a metamorphic origin of the hydrothermal ore fluids, based on stable isotope data.

4.2.3 Mineralogy and Petrography of the Lamprophyres

Dyke rocks of the northern and central Kreuzeck Mountains are dominated by mafic types (lamprophyres, basaltic dykes), whereas in the southern part, most dykes are felsic (microdioritic). The lamprophyres of the Kreuzeck Mountains are unfoliated dykes that normally cut their host rocks discordantly. The dykes mainly strike northeast-southwest, although some strike east-west, parallel to the Periadriatic Line, which is about 15 km south of the Kreuzeck Mountains (Müller et al. 1992a). The thickness of the mafic dykes normally varies from 0.5 to 5.0 m, although dykes of intermediate composition can be up to 10 m thick.

Three petrographic types, based on phenocryst mineralogy, can be recognized (cf. Müller et al. 1992a):

- Type 1, amphibole-clinopyroxene \pm mica phyrlic.
- Type 2, mica-clinopyroxene \pm amphibole phyrlic.

- Type 3, mica-olivine \pm clinopyroxene \pm amphibole phyric.

Mica and amphibole phenocrysts are generally about 0.5–4 mm long, and commonly show compositional zonation (Fig. 4.4). The lamprophyres are characterized by a fine-grained microcrystalline groundmass comprising plagioclase, clinopyroxene, amphibole, and mica, with less common K-feldspar and apatite. Plagioclase is typically saussuritized and the mafic minerals are commonly altered to chlorite. Partially re-sorbed quartz xenocrysts, presumably derived from basement rocks, are present in some samples, particularly those of petrographic type 1.

According to the classification scheme of Mogessie et al. (1990), amphiboles from rocks of petrographic type 1 are tschermakitic hornblendes and tschermakites with 0.8–2.4 wt% TiO₂ (Table 4.2). According to Rock (1991), tschermakitic amphiboles are characteristic of calc-alkaline lamprophyres whereas Ti-rich amphiboles, especially kaersutite, are diagnostic of alkaline lamprophyres. Amphibole mineral chemistry thus indicates that dykes of both alkaline and calc-alkaline affinity are present in the Kreuzeck area.

Micas analyzed from rocks of petrographic types 2 and 3 are phlogopites with mg# > 75 (Table 4.2). They have high TiO₂ contents (~4.0–6.0 wt%), which are more typical of those for alkaline lamprophyres (see Rock 1991; Fig. 4.5).

4.2.4 Geochemistry of the Lamprophyres

Major- and trace-element chemistry is listed in Table 4.3. The dykes have a range of SiO₂ contents (42.6–57.0 wt%), and on a total alkalis versus silica plot (Fig. 4.5) they cluster into a mostly *nepheline*-normative alkaline group (<48.0 wt% silica, 4.0–7.0 wt% alkalis) and a *hypersthene*-normative calc-alkaline group (>48.0 wt% silica, 3.0–5.5 wt% alkalis). On the basis of their major- and trace-element chemistry

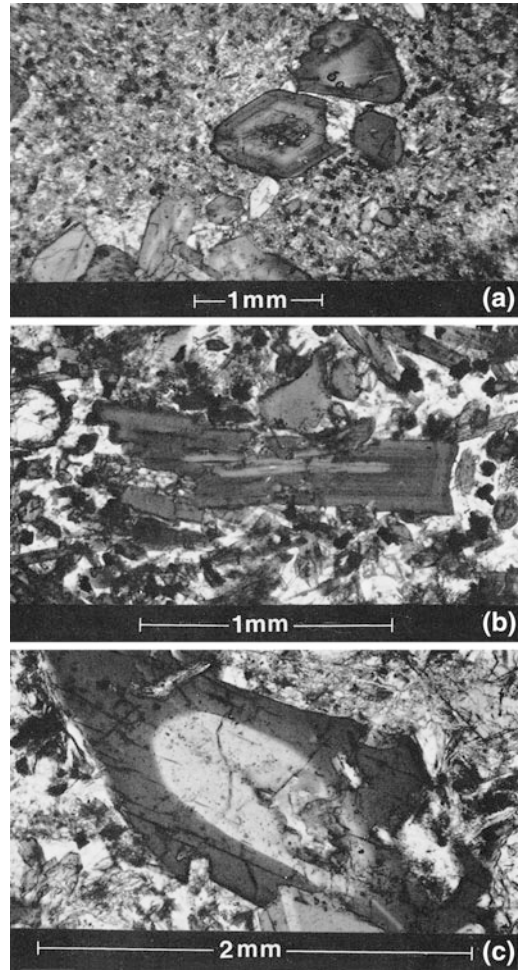


Fig. 4.4 Photomicrographs (crossed nicols) of typical lamprophyre samples from the Kreuzeck Mountains, Austria. The field of view (FOV) is given in square brackets. **a** Porphyritic texture of tschermakite-bearing shoshonitic lamprophyre (119050) [FOV 3.5 mm]; the tschermakite phenocrysts show multiple zoning with Fe-rich rims and Mg-rich cores. **b** Porphyritic texture of phlogopite-bearing alkaline lamprophyre (119040) [FOV 2.0 mm]; the phlogopite phenocryst is zoned with dark brown Fe-rich rim and pale Mg-rich core. **c** Zoned tschermakite with Fe-rich rim and Mg-rich core (119051) [FOV 2.0 mm]. Sample numbers refer to specimens held in the Museum of the Department of Geology and Geophysics, The University of Western Australia

and petrographic character, the rocks can be further subdivided into geochemical groups as described below (cf. Müller et al. 1992a).

Table 4.2 Microprobe (energy-dispersive spectra—EDS) analyses of selected phenocrysts from lamprophyres and basaltic dykes from the Kreuzeck Mountains, Eastern Alps, Austria

Sample no.	119036	119037	119049	119050	119051 ^a	119051 ^b	119055	119059	119061	119036	119042	119054	119056
Petrographic type	3	1	1	1	1	1	3	3	1	3	3	3	2
Geochemical group	3	1	1	1	1	1	3	2	1	3	3	3	4
SiO ₂	39.35	43.85	43.52	41.85	42.42	41.94	40.95	45.19	43.48	38.21	36.64	38.22	37.13
TiO ₂	4.63	2.47	0.79	1.81	1.77	2.20	2.80	2.21	1.78	4.05	6.18	5.24	6.11
Al ₂ O ₃	13.10	11.25	14.04	13.91	13.59	10.53	14.95	10.14	13.41	15.94	16.25	15.91	15.57
Cr ₂ O ₃	0.10	0.43	0.10	0.09	0.21	0.10	0.09	0.10	0.10	1.09	0.10	0.23	0.09
FeO (tot)	12.18	8.40	8.12	15.98	8.88	18.68	14.71	8.59	7.81	6.85	9.94	8.56	10.41
MnO	0.12	0.10	0.11	0.32	0.11	0.42	0.26	0.11	0.11	0.11	0.12	0.10	0.10
MgO	11.60	16.33	16.03	10.63	15.66	10.26	8.67	16.85	15.98	20.05	17.42	19.34	17.89
CaO	11.82	11.47	11.59	10.24	11.92	10.45	10.17	11.05	11.82	0.08	0.09	0.08	0.08
Na ₂ O	1.98	2.20	1.58	1.62	2.01	2.02	2.28	2.01	1.91	0.38	0.82	0.70	0.42
K ₂ O	1.55	0.36	0.49	0.70	0.89	0.68	2.26	1.04	1.25	9.52	8.79	8.78	9.25
Cl	0.05	0.04	0.05	0.05	0.04	0.04	0.04	0.05	0.05	0.05	0.05	0.04	0.04
Total	96.48	96.90	96.42	97.20	97.50	97.32	97.18	97.34	97.70	96.33	96.40	97.20	97.09
Name	Kaersutite	Tsch. Hbl	Tscherm.	Tscherm.	Tscherm.	Tscherm.	Pargasite	Tsch. Hbl	Tscherm.	Phlogopite	Phlogopite	Phlogopite	Phlogopite
mg#	62.9	77.5	77.9	54.2	75.8	50.5	51.2	77.7	78.5	83.4	75.7	80.1	75.4
Ox. form.	23	23	23	23	23	23	23	23	23	22	22	22	22
Atoms													
Si	5.949	6.276	6.335	6.272	6.061	6.397	6.173	6.562	6.289	5.457	5.304	5.426	5.351
Ti	0.527	0.267	0.087	0.204	0.189	0.253	0.317	0.241	0.194	0.434	0.673	0.559	0.662
Al	2.334	1.899	2.409	2.457	2.292	1.892	2.652	1.736	2.285	2.684	2.772	2.661	2.644

(continued)

Table 4.2 (continued)

Sample no.	119036	119037	119049	119050	119051 ^a	119051 ^b	119055	119059	119061	119036	119042	119054	119056
Petrographic type	3	1	1	1	1	1	3	3	1	3	3	3	2
Geochemical group	3	1	1	1	1	1	3	2	1	3	3	3	4
Cr	0.009	0.052	–	–	0.026	0.012	0.009	–	–	0.124	–	0.026	–
Fe	1.544	1.006	0.988	2.003	1.064	2.383	1.856	1.044	0.945	0.818	1.204	1.016	1.255
Mn	0.018	0.017	–	0.041	0.017	0.054	0.036	–	–	–	–	–	–
Mg	2.615	3.473	3.477	2.374	3.339	2.332	1.946	3.648	3.445	4.268	3.758	4.091	3.842
Ca	1.916	1.762	1.808	1.643	1.829	1.708	1.639	1.718	1.832	–	–	–	–
Na	0.581	0.611	0.444	0.472	0.558	0.596	0.669	0.565	0.535	0.107	0.231	0.192	0.118
K	0.301	0.069	0.091	0.131	0.163	0.132	0.435	0.193	0.231	1.735	1.623	1.591	1.699
Cl	–	–	–	–	–	–	–	–	–	–	–	–	–
Total	15.794	15.432	15.641	15.597	15.538	15.761	15.732	15.709	15.756	15.627	15.565	15.562	15.571

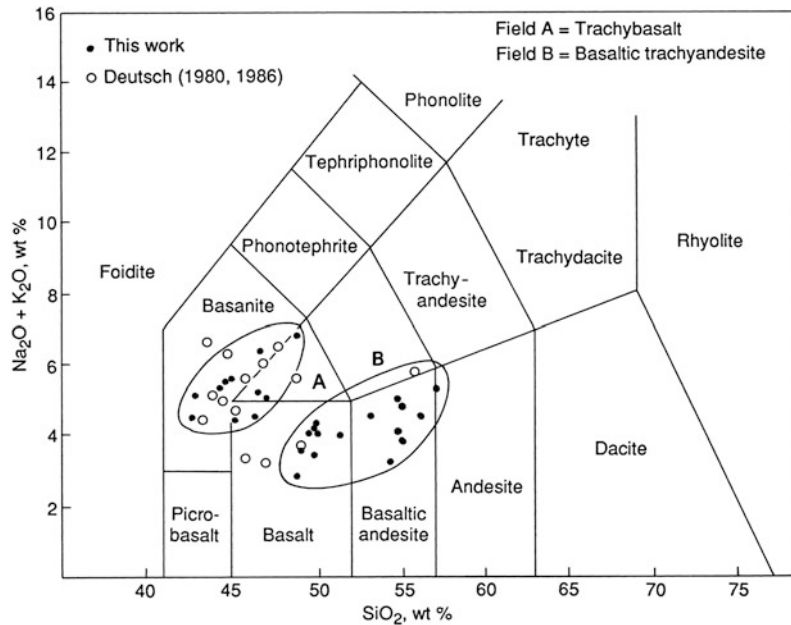
Oxides and Cl are in wt%. FeO (tot) = total iron calculated as ferrous oxide, Hbl. = Hornblende, Tsch. = tschermakitic, Tscherm. = tschermakitic, Ox. form. = oxygen formula.

Sample numbers refer to specimens held in the Museum of the Department of Geology and Geophysics, The University of Western Australia. From Müller et al. (1992a)

^aCore

^bRim

Fig. 4.5 ($\text{Na}_2\text{O} + \text{K}_2\text{O}$) versus SiO_2 (TAS) plot of dykes in the Kreuzeck Mountains, Austria, from this study and Deutsch (1980, 1986). The dykes are clearly divided into two groups: a SiO_2 -rich calc-alkaline to shoshonitic group and a less SiO_2 -rich alkaline group. Modified from Müller et al. (1992a)



Group 1, amphibole-bearing shoshonitic lamprophyres (petrographic type 1). These rocks have variable K_2O ($\sim 0.8\text{--}2.6$ wt%) and Rb (36–200 ppm) contents, suggesting some alkali loss. This is consistent with the generally altered nature of the groundmass in these dykes: that is, groundmass phlogopite is completely altered to chlorite in all samples except one, and feldspars are partially saussuritized in all samples. The low F content (<10 ppm) of one sample is also consistent with alteration of mica to chlorite. MgO contents range from 3.6 to 9.8 wt %, mg# is $\sim 50\text{--}70$, and Ni contents vary from <5 to 116 ppm, indicating that Group 1 dykes include both evolved and relatively primitive compositions. Group 1 dykes have 0.5–1.0 wt% TiO_2 and <13 ppm Nb. Barium contents are <400 ppm, resulting in the low Ba/Rb (<10) and Ba/Nb (<43) ratios characteristic of potassic magmas derived in postcollisional arc-settings.

Group 2, mica-bearing shoshonitic lamprophyres (petrographic types 2 and 3). As with Group 1, these rocks have somewhat variable K_2O contents ($\sim 0.8\text{--}2.2$ wt%) and $\text{K}_2\text{O}/\text{Na}_2\text{O}$ ratios ($\sim 0.2\text{--}1.2$) mainly reflecting alteration of groundmass mica and K-feldspar. Whole-rock F

contents (<500 ppm) are low for typical mica-phyric lamprophyres and suggest F loss. Olivine-phyric samples have high MgO contents (>10 wt%), mg# (>70), and Ni contents (>400 ppm), indicating that they represent primitive magma compositions. Other Group 2 rocks are more evolved: one sample has a mg# of ~ 65 and Ni contents of ~ 120 ppm. TiO_2 and Nb abundances are 1.0–1.5 wt% and <17 ppm, respectively. The high Ba contents result in high Ba/Rb (>20) and Ba/Nb (>100) ratios, which clearly distinguish them from Group 1 rocks. Such ratios are typical of mica-phyric shoshonitic magmas generated in subduction zone settings (e.g. Luhr et al. 1989; Bucholz et al. 2014).

Group 3, alkaline lamprophyres (petrographic type 3). The alkaline lamprophyres are mostly nepheline-normative in composition, and they have high alkali contents with $\text{K}_2\text{O}/\text{Na}_2\text{O} > 1$. Mg# is consistently $\sim 62\text{--}67$ and Ni content is ~ 150 ppm, suggesting that magma compositions are only slightly evolved. The HFSE contents are high (1.5–2.1 wt% TiO_2 , >200 ppm Zr, 30–55 ppm Nb), which clearly distinguishes these rocks from those of Groups 1 and 2. K/Nb ratios are ~ 500 and Ba/Nb ratios are ~ 35 , higher than

Table 4.3 Representative whole-rock major- and trace-element geochemistry of investigated lamprophyres from the Kreuzeck Mountains, Austria. Major elements are in wt%, trace elements are in ppm, and precious metals are in ppb

Province/deposit	Kreuzeck Mountains	Kreuzeck Mountains	Kreuzeck Mountains	Kreuzeck Mountains
Location	Austria	Austria	Austria	Austria
Rock type	Lamprophyre	Lamprophyre	Lamprophyre	Lamprophyre
Sample no.	119049	119045	119052	119053
Geochemical group	1	2	3	4
Tectonic setting	Postcollisional arc	Postcollisional arc	Postcollisional arc	Postcollisional arc
Reference	Müller et al. (1992a)			
SiO ₂	55.91	54.53	46.50	46.40
TiO ₂	0.45	1.38	2.01	2.41
Al ₂ O ₃	19.83	14.56	14.14	15.33
Fe ₂ O ₃ (tot)	6.17	7.21	9.54	11.73
MnO	0.13	0.08	0.15	0.20
MgO	3.94	5.67	8.20	5.69
CaO	6.04	4.43	8.32	8.06
Na ₂ O	1.97	4.30	2.33	2.55
K ₂ O	2.56	1.76	2.93	3.84
P ₂ O ₅	0.11	0.24	0.53	0.45
LOI	3.13	5.89	5.46	3.30
Total	100.18	99.98	100.10	99.91
ne%	0.00	0.00	0.00	3.40
mg#	59.8	64.7	66.7	53.1
F	n.a.	210	150	520
Sc	9	7	15	18
V	148	183	303	347
Cr	49	272	326	133
Ni	5	121	186	20
Cu	7	11	18	14
Zn	62	74	100	97
As	2	2	3	2
Rb	208	40	87	70
Sr	286	690	794	998
Y	17	19	37	29
Zr	92	183	259	215
Nb	8	16	33	17
Sb	0.4	11.0	0.7	0.3
Ba	284	2821	1212	1327
W	120	130	81	100

(continued)

Table 4.3 (continued)

Province/deposit	Kreuzeck Mountains	Kreuzeck Mountains	Kreuzeck Mountains	Kreuzeck Mountains
Location	Austria	Austria	Austria	Austria
Rock type	Lamprophyre	Lamprophyre	Lamprophyre	Lamprophyre
Sample no.	119049	119045	119052	119053
Geochemical group	1	2	3	4
Tectonic setting	Postcollisional arc	Postcollisional arc	Postcollisional arc	Postcollisional arc
Reference	Müller et al. (1992a)			
Pb	23	32	25	25
Th	29	11	25	16
Pd	<1	3	3	<1
Pt	<5	<5	<5	<5
Au	<3	26.8	15.5	<3

Fe₂O₃ (tot) = total iron calculated as ferric oxide, n.a. = not analyzed, ne% = nepheline-normative content in wt% (calculated by CIPW-Norm) based on whole-rock geochemistry. Sample numbers refer to specimens held in the Museum of the Department of Geology and Geophysics, The University of Western Australia. From Müller et al. (1992a)

those present in most non-Dupal-type oceanic island basalt (OIB) sources which have K/Nb ratios of ~180 and Ba/Nb ratios of ~6 (Weaver et al. 1987; Sun and McDonough 1989). The trace-element ratios of Group 3 alkaline lamprophyres are, however, similar to, or slightly more elevated than, potassic, Dupal-type (EM2-type) OIB sources; for example, Gough Island rocks which have K/Nb ratios of ~430 and Ba/Nb ratios of ~16. It is thought that Dupal-type OIB sources involve recycled sedimentary material, ancient continental lithosphere, or subduction-zone metasomatized lithosphere (Sun and McDonough 1989). An important difference between Dupal-type OIBs and the Group 3 lamprophyres is the much lower TiO₂ contents of the latter: <2.1 wt% compared with >2.5 wt% for Dupal-type OIB.

Group 4, low mg# alkaline lamprophyres (petrographic type 2). These lamprophyres are characterized by low mg# (53–56) and low Ni contents (~20 ppm), indicating that they represent evolved magmas. TiO₂ contents are ~2.5

wt% and Zr and Nb contents are ~200 and ~20 ppm, respectively. Because Zr and Nb contents are lower than in Group 3 lamprophyres, Group 4 rocks cannot be derived from Group 3 by fractional crystallization processes, and must have evolved from a separate primary magma. Group 3 dykes are clearly alkaline since they have >5 wt% total alkalis and >2 wt% normative-nepheline component, yet their low Nb contents are typical of magmas derived from subduction zones. K/Nb (>1300) and Ba/Nb (>55) ratios are extreme for basic alkaline magmas but similar to those of some highly potassic arc volcanoes such as Batu Tara in the Sunda Arc of Indonesia (Stolz et al. 1988; Foley and Wheller 1990; Soeria-Atmadja et al. 1998). The TiO₂ contents of Group 4 lamprophyres are, however, significantly higher than those of subduction-zone derived potassic magmas, which typically have <1.5 wt% TiO₂.

A plot of Ba/Rb versus TiO₂ (Fig. 4.6) is effective in separating the dyke rocks into Groups 1–4.

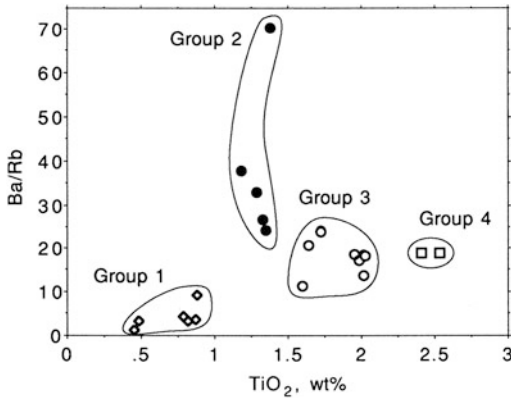


Fig. 4.6 Ba/Rb versus TiO_2 plot showing the four geochemical groups of investigated dykes. From Müller et al. (1992a)

K-Ar ages (Müller et al. 1992a) are between ca. 27 and 36 Ma (Table 4.4). The older shoshonitic lamprophyres (ca. 36 Ma) imply subduction-related features with low HFSE contents, whereas the younger alkaline lamprophyres (ca. 30 Ma) show transitional characteristics with higher HFSE contents (see Table 4.3). The older age for a Group 1 lamprophyre is also consistent with the greater degree of alteration and evidence for recrystallization in the Group 1 samples, suggesting emplacement during the latter stages of Alpine metamorphism. Their mainly east-west dyke orientations also distinguish them from the slightly younger Group 2–4 lamprophyres.

The largely Oligocene age of these lamprophyres is much younger than the supposed age of mineralization in the area (older than Permo-Carboniferous; Feitzinger et al. 1995).

4.3 Northern Mariana Arc (West Pacific): Example from an Initial Oceanic Arc Setting

4.3.1 Introduction

Intra-oceanic island arcs such as the Mariana Arc are restricted to the circum-Pacific region (Stern 1979). The Mariana Arc is located about 2000 km north of the mainland of Papua New Guinea in the West Pacific (Fig. 4.7) and consists of 21 major volcanoes and seamounts (Garcia et al. 1979; Meijer and Reagan 1981; Hole et al. 1984; Stern et al. 1988), from Nishino Shima in the north to Guam in the south. The subduction trench is situated in the west of the island arc.

Following the geographic distribution of volcanic islands and seamounts, the Mariana Arc is divided into three provinces: the Northern Seamount Province, the Central Island Province, and the Southern Seamount Province (Stern 1979; Lin et al. 1989).

4.3.2 Regional Geology

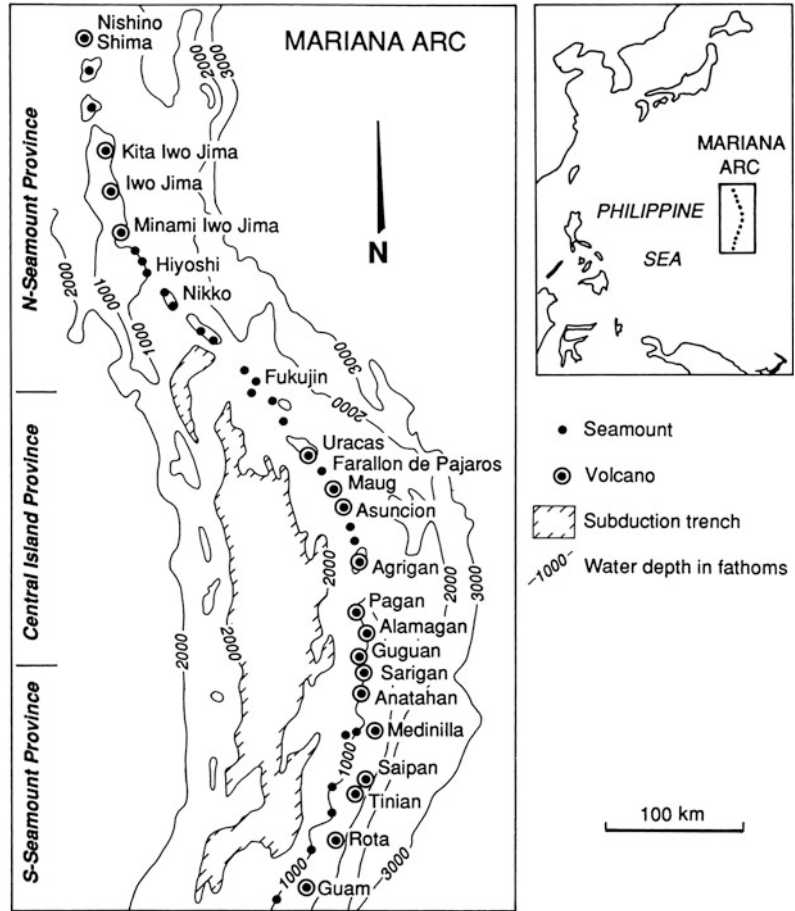
The magmatic system of the Mariana Arc formed by the subduction of the Pacific plate beneath the Philippine Sea plate (Lin et al. 1989). Volcanoes in the northern Mariana Arc between Uracas (latitude 20°N) and Minami Iwo Jima (24°N) are still active, yet entirely submarine (Stern et al. 1988). In contrast to the mainly low-K basalts and andesites of the subaerially exposed volcanoes in the Central Island Province (Meijer and Reagan 1981), the northern and southern parts

Table 4.4 Whole-rock K-Ar dating on lamprophyres and basaltic dykes from the Kreuzeck Mountains, Austria

Geochemical group	Sample no.	K-Ar age (Ma)	Rb-Sr age (Ma)	Initial $^{87}\text{Sr}/^{86}\text{Sr}$ (whole rock)	Orientation
1	119050	36 ± 1	–	–	E-W
2	119058	27 ± 0.5	31 ± 2	0.7079	NE-SW
3	119042	32 ± 0.7	29 ± 4	0.7055	NE-SW
4	119053	29 ± 0.7	–	–	NE-SW

The Rb-Sr data are from Deutsch (1984). The error on ages is quoted as $\pm 2\sigma$. From Müller et al. (1992a)

Fig. 4.7 Geographic overview of the Mariana Island Arc, West Pacific. Modified after Stern (1979) and Bloomer et al. (1989)



are dominated by high-K igneous rocks which have been classified as shoshonites by Stern et al. (1988) and Bloomer et al. (1989). The shoshonites apparently represent the youngest volcanic products of arc evolution, and were previously interpreted to be products of an episode of back-arc rifting (Stern et al. 1988; Bloomer et al. 1989; Lin et al. 1989). However, recent studies have demonstrated that the region now defined by the shoshonitic rocks occupies a “pre-rift” position (Baker et al. 1996; Gribble et al. 1998). The term *initial oceanic arc* reflects the unique tectonic setting of the shoshonites in the Mariana Arc. They were formed *early* during arc

evolution and they occur along the magmatic front, which is unusual for an oceanic island arc (De Long et al. 1975) because high-K calc-alkaline rocks and shoshonites normally occur farthest from the trench and above the highest parts of the Benioff Zone (Morrison 1980). More recent work (Till et al. 2012) interprets the unique compositions of the shoshonites in the northern Mariana Arc as the product of chlorite dehydration melting in a relatively cool subduction zone.

Andesites from Sarigan, an island in the Central Island Province, have been dated at 0.5 ± 0.2 Ma (Meijer and Reagan 1981).

4.3.3 Mineralogy and Petrography of the Potassic Igneous Rocks

The rocks are densely phyrlic and have highly porphyritic textures (Bloomer et al. 1989), and basalt and andesite dominate. The typical phenocryst assemblages are plagioclase, clinopyroxene, orthopyroxene, \pm olivine, \pm titanomagnetite, \pm apatite (Bloomer et al. 1989; Gribble et al. 1998) in a groundmass comprising mainly plagioclase and clinopyroxene, and minor K-feldspar and orthopyroxene (Meijer and Reagan 1981). Olivine is most common in the trachybasalts of the Southern Seamount Province. Hornblende phenocrysts are rare and mainly restricted to the andesitic rocks (Meijer and Reagan 1981).

The shoshonitic trachybasalts from the Northern and Southern Seamount Provinces contain phenocrysts of plagioclase, clinopyroxene, olivine, and biotite, which are set in a fine-grained groundmass of K-feldspar and plagioclase (Bloomer et al. 1989).

4.3.4 Geochemistry of the Potassic Igneous Rocks

The whole-rock geochemistry of the volcanic rocks from the Mariana Arc has been studied by Dixon and Batiza (1979), Stern et al. (1988), Bloomer et al. (1989), Lin et al. (1989), and Woodhead (1989).

The shoshonitic rocks, which are of interest here, are characterized by high K/Na ratios (>0.6), high K_2O (up to 2.54 wt%), and relatively high Al_2O_3 contents (up to 18 wt%); see Table 4.5. They are further characterized by very low concentrations of LILE (e.g. commonly <700 ppm Ba, <34 ppm Rb), and very low LREE (e.g. <40 ppm La, <50 ppm Ce) and HFSE (e.g. <90 ppm Zr, <5 ppm Nb, <2 ppm Hf) contents. These very low element abundances for the Mariana Arc shoshonites are distinct among the potassic igneous rock clan, and, in combination with their unusual generation during the initial stages of arc evolution (De Long et al. 1975;

Stern et al. 1988; Till et al. 2012), define those high-K rocks from initial oceanic arcs (Müller et al. 1992b).

4.4 Vanuatu (Southwest Pacific): Example from a Late Oceanic Arc Setting

4.4.1 Introduction

Vanuatu (formerly New Hebrides) is an isolated island arc about 2000 km east of Australia and forms part of the outer Melanesian Arc (Coleman 1970; Gorton 1977; Peate et al. 1997; Pelletier et al. 1998). The Vanuatu Arc marks the boundary between the Australian and the Pacific plates. The Vanuatu island arc consists of nine major islands and the subduction trench is situated to the west of the islands (Fig. 4.8). The islands are dominated by dome-shaped basaltic shield volcanoes (Coleman 1970).

4.4.2 Regional Geology

The oldest rocks on the islands of Vanuatu are Oligocene submarine lavas (Coleman 1970). Magmatism in the active volcanic arc (Central Chain) began in the late Miocene at about 6 Ma and was initially focused on Erromango, Tanna, and Anneityum in the south (Peate et al. 1997). Volcanism subsequently developed along the entire length of the arc and shifted closer to the trench due to a steepening of the subduction zone to its present inclination of about 70° (Peate et al. 1997). The arc was apparently rejuvenated in the Pliocene by a major period of submarine basaltic volcanism (Gorton 1977). In the Pleistocene and Recent, a third period of volcanism produced subaerial high-K olivine-trachybasalts on Gaua, Aoba, and Ambrym (Fig. 4.8; Mitchell and Warden 1971; Gorton 1977; Peate et al. 1997).

Modern studies suggest that the relative motion between the Fiji platform and the Australian plate is small and not yet quantified,

Table 4.5 Representative whole-rock major- and trace-element geochemistry of potassic igneous rocks from the Mariana Island arc, West Pacific

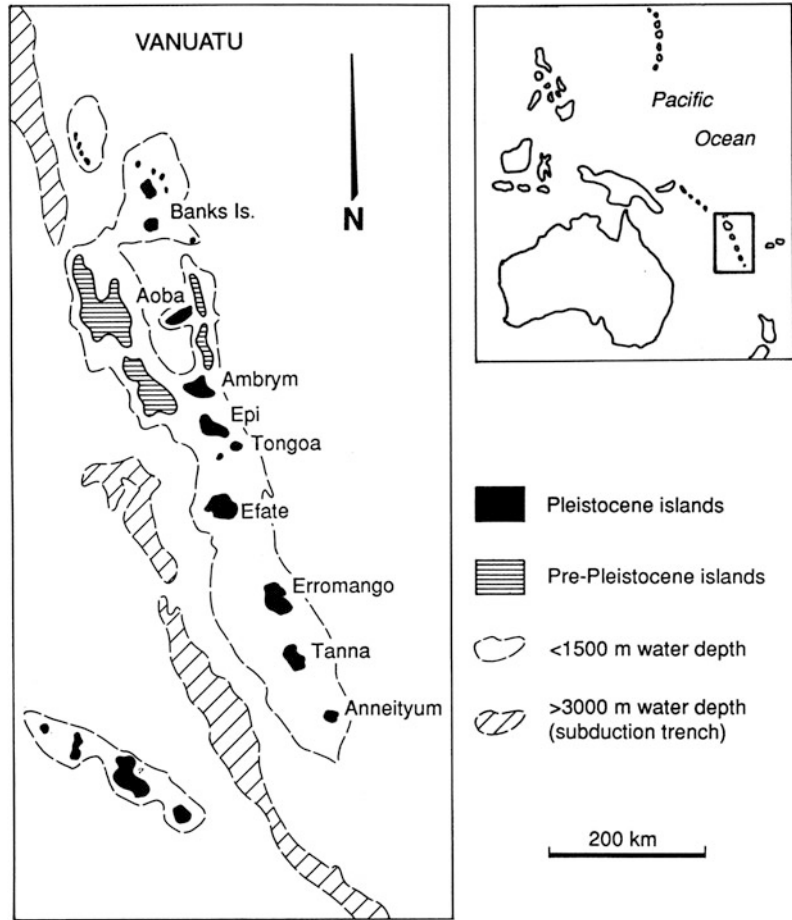
Province/deposit	Northern Seamount	Northern Seamount	Northern Seamount
Location	Mariana Islands	Mariana Islands	Mariana Islands
Rock type	Basalt	Basalt	Basalt
Tectonic setting	Initial oceanic arc	Initial oceanic arc	Initial oceanic arc
Reference	Batiza (1979)	Bloomer et al. (1989)	Woodhead (1989)
SiO ₂	53.37	50.25	54.60
TiO ₂	0.73	0.80	0.86
Al ₂ O ₃	16.01	18.54	16.78
Fe ₂ O ₃ (tot)	9.21	8.54	11.03
MnO	0.16	0.21	0.24
MgO	4.90	4.23	3.29
CaO	9.93	9.31	8.07
Na ₂ O	3.00	2.97	3.34
K ₂ O	1.05	2.54	1.43
P ₂ O ₅	0.19	0.34	0.27
LOI	0.35	1.80	0.10
Total	98.90	99.53	100.01
V	n.a.	398	213
Cr	38	49	4
Ni	n.a.	30	5
Rb	17	26	34
Sr	375	305	347
Y	n.a.	21	29
Zr	47	31	90
Nb	n.a.	n.a.	1
Ba	337	714	237
La	7	n.a.	42
Ce	16	n.a.	33
Th	1	n.a.	n.a.
Hf	2	n.a.	n.a.

Major elements are in wt%, and trace elements are in ppm. Fe₂O₃ (tot) = total iron calculated as ferric oxide. Data from Dixon and Batiza (1979), Bloomer et al. (1989), and Woodhead (1989)

and the Fiji platform can thus be considered as part of the Australian plate (Pelletier et al. 1998). Therefore, the convergence rate at the southern Vanuatu Arc is equal to the opening rate in the

southern North Fiji basin. Based on GPS data, Pelletier et al. (1998) estimate an average convergence rate of about 10 cm/year near 18° S in the southern part of the Vanuatu Arc.

Fig. 4.8 Geographic overview of Vanuatu, Southwest Pacific. Modified after Gorton (1977)



4.4.3 Mineralogy and Petrography of the Potassic Igneous Rocks

The submarine volcanic rocks consist entirely of pillow lavas. They are characterized by porphyritic textures with phenocrysts of hypersthene, augite, plagioclase, and rare olivine in a glassy groundmass. Phenocrysts of biotite and amphiboles are normally absent (Gorton 1977).

The subaerial potassic olivine-trachybasalts have porphyritic textures, with phenocrysts of olivine, augite, and plagioclase that are set in a groundmass dominated by K-feldspar and plagioclase with minor normative nepheline (Gorton 1977).

4.4.4 Geochemistry of the Potassic Igneous Rocks

The high-K olivine-trachybasalts from Vanuatu are characterized by high K_2O (up to 2.3 wt%), relatively high Al_2O_3 (up to 16.0 wt%), high CaO (up to 12.7 wt%), and high Na_2O (up to 3.5 wt%) contents (Gorton 1977; Peate et al. 1997): see Table 4.6. They have moderate mg# (<70) and moderate concentrations of mantle-compatible elements (e.g. <124 ppm Co, <260 ppm Cr, <250 ppm V) due to fractionation (Gorton 1977; Peate et al. 1997).

The very low concentrations of LILE (e.g. <80 ppm Rb, <540 ppm Sr), and low LREE (e.g. <30 ppm La, <70 ppm Ce) and HFSE (e.g. <0.8 wt%

Table 4.6 Representative whole-rock major- and trace-element geochemistry of potassic igneous rocks from Vanuatu, Southwest Pacific

Rock type	Basalt	Andesite
Tectonic setting	Late oceanic arc	Late oceanic arc
Reference	Gorton (1977)	Gorton (1977)
SiO ₂	49.42	60.74
TiO ₂	0.60	0.86
Al ₂ O ₃	13.14	15.24
Fe ₂ O ₃ (tot)	10.99	7.64
MnO	0.20	0.13
MgO	9.37	2.92
CaO	12.77	4.94
Na ₂ O	1.76	3.59
K ₂ O	1.45	3.48
P ₂ O ₅	0.30	0.46
LOI	0.64	1.28
Total	100.05	99.08
V	250	150
Cr	260	31
Ni	46	9
Rb	35	81
Sr	539	441
Y	17	34
Zr	57	176
Nb	1	4
Ba	160	1350
La	9	29
Ce	21	69
Th	2	5

Major elements are in wt%, and trace elements are in ppm. Fe₂O₃ (tot) = total iron calculated as ferric oxide. From Gorton (1977)

TiO₂, <176 ppm Zr, <4 ppm Nb) contents (Table 4.6) of the potassic rocks are typical for those derived in a late oceanic-arc setting (Müller et al. 1992b).

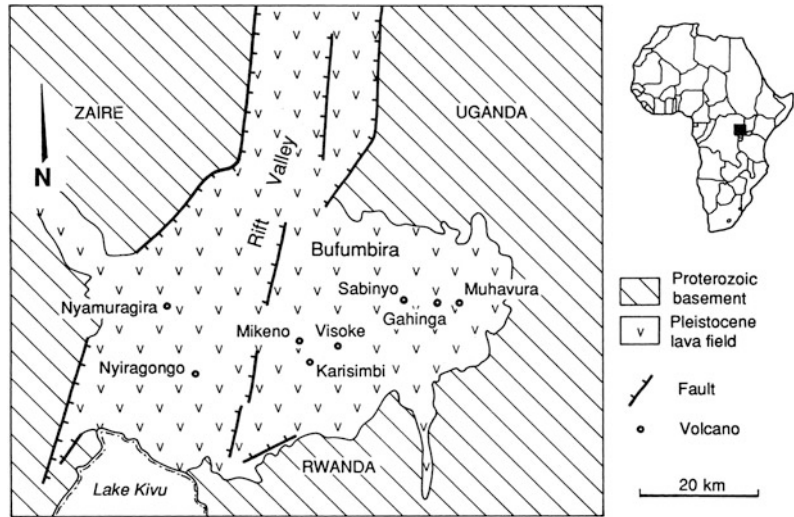
4.5 African Rift Valley (Rwanda, Uganda, Democratic Republic of Congo): Example from a Within-Plate Setting

4.5.1 Introduction

The Virunga volcanic province (Fig. 4.9) occupies an area of more than 3000 km² at the

junction of Rwanda, Uganda, and the Democratic Republic of the Congo (De Mulder et al. 1986; Rogers et al. 1992; Foley et al. 2011). The highly potassic lavas of the province, in the western branch of the East African rift system, have long attracted interest (Thompson 1985). The Virunga igneous complex is widely regarded as one of the classic within-plate potassic provinces (Rogers et al. 1992, 1998). However, the question remains as to whether the rocks were derived from lithospheric mantle sources (De Mulder et al. 1986), or by the input of a deep asthenospheric mantle plume (Thompson 1985). The extreme compositions of some melilite-bearing

Fig. 4.9 Geological overview of the Virunga Volcanic Province, African Rift Valley, Uganda. Modified after De Mulder et al. (1986)



lavas from Bufumbira seem to necessitate a high $\text{CO}_2/\text{H}_2\text{O}$ ratio in their mantle sources, if this was lherzolite (Thompson 1985). These high CO_2 contents are indicative of asthenospheric mantle plumes (Thompson 1985; Nelson et al. 1986; Wyllie 1988; Holm et al. 2006).

4.5.2 Regional Geology

Early Pliocene to late Pleistocene volcanic activity in the Virunga province produced eight major volcanoes (Fig. 4.9), two of which are still active (Rogers et al. 1992), and numerous minor vents (Cundari and Le Maitre 1970). The major volcanoes are situated in a large lava field. The volcanic activity is structurally related to graben-faulting during the development of a branch, known as the Bufumbira embayment, in the rift (De Mulder et al. 1986; Rogers et al. 1992). The Virunga volcanic rocks are underlain by metasedimentary rocks of the Karagwe-Ankolean System which was deposited about 2.1 Ga ago and deformed during the Kibaran Orogeny (1300–800 Ma; Vollmer and Norry 1983).

Karisimbi is the largest of the volcanoes and has been active during the last 0.1 Ma (Rogers et al. 1992). It was apparently formed during three phases, which are summarized by De Mulder et al. (1986) and Rogers et al. (1992). The initial phase formed a shield volcano comprising potassic basanites: this was followed by an eastward

migration of volcanic activity and the development of a caldera complex. The second phase was characterized by potassic mugearite lavas. The final volcanic activity is manifested by highly potassic latite and trachyte lava flows.

4.5.3 Mineralogy and Petrography of the Potassic Igneous Rocks

The majority of the Virunga volcanic rocks are silica-deficient, leucite-bearing potassic rocks (Vollmer and Norry 1983; Demant et al. 1994; Foley et al. 2011). However, the Nyriragongo volcano also consists of nephelinites and melilitites (Demant et al. 1994). The potassic basanites, which have the most primitive compositions, are characterized by pronounced porphyritic or glomeroporphyritic textures with abundant phenocrysts of olivine, diopside, and chromite in a fine-grained or glassy groundmass comprising plagioclase, K-feldspar or leucite, olivine, titaniferous salite, and titanomagnetite (Ferguson and Cundari 1975; Rogers et al. 1992). Despite the high modal content of olivine in the rocks with 16–22 wt% MgO, less than 10 volume percent of the olivines appear to be xenocrysts (Foley et al. 2011). Investigated olivine phenocrysts show common, but relatively subtle zonation, particularly decreasing Ni and Cr, and increasing Mn and Sc towards the rims (Foley et al. 2011).

The mugearites consist mainly of K-feldspar and diopside phenocrysts in a fine-grained groundmass of plagioclase, K-feldspar, olivine, and diopside (De Mulder et al. 1986). Grading into the late-stage latites and trachytes, K-feldspar joins plagioclase, biotite, and titanite as phenocrysts and commonly rims the plagioclase. Leucite cannot be optically identified in the groundmass (Ferguson and Cundari 1975).

4.5.4 Geochemistry of the Potassic Igneous Rocks

The whole-rock geochemistry of the Virunga potassic igneous rocks has been discussed by Mitchell and Bell (1976), De Mulder et al. (1986), and Rogers et al. (1992, 1998), and representative analyses are shown in Table 4.7.

Table 4.7 Representative whole-rock major- and trace-element geochemistry of potassic igneous rocks from the Virunga volcanic field, Uganda

Province/deposit	Karisimbi, Virunga	Karisimbi, Virunga	Karisimbi, Virunga
Location	Uganda	Uganda	Uganda
Rock type	Basanite	Mugearite	Trachyte
Tectonic setting	Within-plate	Within-plate	Within-plate
Reference	De Mulder et al. (1986)	De Mulder et al. (1986)	De Mulder et al. (1986)
SiO ₂	46.18	48.52	59.57
TiO ₂	2.98	2.70	1.08
Al ₂ O ₃	13.19	16.07	18.27
Fe ₂ O ₃ (tot)	11.13	11.08	5.15
MnO	0.19	0.21	0.12
MgO	7.05	4.23	0.97
CaO	10.83	6.76	2.30
Na ₂ O	2.91	3.63	4.39
K ₂ O	3.44	4.48	6.87
P ₂ O ₅	0.81	0.75	0.30
LOI	0.70	1.10	1.01
Total	99.41	99.53	100.03
V	n.a.	n.a.	n.a.
Cr	228	77	2
Ni	n.a.	n.a.	n.a.
Rb	115	151	242
Sr	1286	1280	698
Y	n.a.	n.a.	n.a.
Zr	311	341	414
Nb	60	n.a.	n.a.
Ba	1321	1445	1200
La	120	126	137
Ce	231	240	276
Th	20	26	42
Ta	9	10	10
Hf	8	8	10

Major elements are in wt%, and trace elements are in ppm. Fe₂O₃ (tot) = total iron calculated as ferric oxide. From De Mulder et al. (1986)

Rogers et al. (1992) divided the rocks into two groups mainly based on their MgO contents. The older basanites which formed the shield volcano have primitive compositions with high MgO contents (>6.3 wt%) and high mantle-compatible element concentrations (e.g. up to 1158 ppm Cr, up to 59 ppm Co; De Mulder et al. 1986). This can be compared to the mugearites with lower MgO contents (<4.2 wt%) and lower mantle-compatible element concentrations (e.g. <77 ppm Cr, <33 ppm Co; De Mulder et al. 1986). The late-stage trachytes are characterized by more evolved compositions with very low MgO (<1 wt%), Cr (<2 ppm) and Co (<5 ppm) contents. Crustal assimilation of the trachytes during uprise can be excluded based on the relatively high Ce/Pb ratios (>10) of the Virunga rocks which are similar to those of MORB and OIB (Hofmann et al. 1986; Rogers et al. 1992). Many MORBs and OIBs have low Pb contents and high Ce/Pb ratios (~20) when compared to those melts derived from the continental crust (Ce/Pb <6; Hofmann et al. 1986). The high HFSE concentrations (e.g. up to 4 wt% TiO₂, up to 91 ppm Nb, up to 18 ppm Hf; De Mulder et al. 1986; Rogers et al. 1992) of the Virunga rocks are typical for potassic igneous rocks derived in a within-plate setting (Müller et al. 1992b).

Stable-isotope studies by Rogers et al. (1992) indicate that the Virunga lavas were derived from the lithospheric mantle, and the evidence for a contribution from deep asthenospheric mantle sources, as proposed by Thompson (1985), is very limited.

References

- Appleton JD (1972) Petrogenesis of potassium-rich lavas from the Roccamonfina Volcano, Roman region, Italy. *J Petrol* 13:425–456
- Baker N, Fryer P, Martinez F, Yamazaki T (1996) Rifting history of the northern Mariana trough: SeaMARC II and seismic reflection surveys. *J Geophys Res* 101:11427–11455
- Bartel EM, Neubauer F, Genser J, Heberer B (2014) States of paleostress north and south of the Periadriatic fault: comparison of the Drau range and the Friuli Southalpine wedge. *Tectonophysics* 637:305–327
- Beccaluva L, Bigioggero LB, Chiesa S, Colombo A, Fanti G, Gatto GO, Gregnanin A, Montrasio A, Piccirillo EM, Tunesi A (1983) Postcollisional orogenic dyke magmatism in the Alps. *Memorias Soc Geol Italy* 26:341–359
- Bloomer SH, Stern RJ, Fisk E, Geschwind CH (1989) Shoshonitic volcanism in the northern Marianas Arc. 1. Mineralogic and major and trace element characteristics. *J Geophys Res* 94:4469–4496
- Boari E, Avanzinelli R, Melluso L, Giordano G, Mattei M, De Benedetti AA, Morra V, Conticelli S (2009) Isotope geochemistry (Sr-Nd-Pb) and petrogenesis of leucite-bearing volcanic rocks from “Colli Albani” volcano, Roman Magmatic Province, Central Italy: inferences on volcano evolution and magma genesis. *Bull Volc* 71:977–1005
- Bucholz CE, Jagoutz O, Schmidt MW, Sambuu O (2014) Fractional crystallization of high-K arc magmas: biotite- versus amphibole-dominated fractionation series in the Dariv Igneous Complex, western Mongolia. *Contrib Miner Petrol* 168:1072–1100
- Campbell IH, Stepanov AS, Liang HY, Allen CM, Norman MD, Zhang YQ, Xie YW (2014) The origin of shoshonites: new insights from the tertiary high-potassium intrusions of eastern Tibet. *Contrib Miner Petrol* 167:983–1005
- Civetta L, Innocenti F, Manetti P, Peccerillo A, Poli G (1981) Geochemical characteristics of potassic volcanic from Mts. Ernici, southern Latium, Italy. *Contrib Mineral Petrol* 78:37–47
- Coleman PJ (1970) Geology of the Solomon and New Hebrides islands as part of the Melanesian re-entrant, southwest Pacific. *Pac Sci* 24:289–314
- Conticelli S, Peccerillo A (1992) Petrology and geochemistry of potassic and ultrapotassic volcanism in Central Italy: petrogenesis and inferences on the evolution of the mantle sources. *Lithos* 28:221–240
- Cundari A (1979) Petrogenesis of leucite-bearing lavas in the Roman volcanic region, Italy. The Sabatini lavas. *Contrib Miner Petrol* 70:9–21
- Cundari A, Le Maitre RW (1970) On the petrogenesis of the leucite-bearing rocks of the Roman and Birunga volcanic regions. *J Petrol* 11:33–47
- D’Antonio M, Di Girolamo P (1994) Petrological and geochemical study of mafic shoshonitic volcanics from Procida-Vivara and Ventotene Islands (Campanian Region, South Italy). *Acta Vulcanologia* 5:69–80
- Demant A, Lestrade B, Lubala RT, Kampunzu AB, Durieux J (1994) Volcanological and petrological evolution of Nyiragongo volcano, Virunga volcanic field, Zaire. *Bull Volcanol* 56:47–61
- De Long SE, Hodges FN, Arculus RJ (1975) Ultramafic and mafic inclusions, Kanaga Island, Alaska, and the occurrence of alkaline rocks in island arcs. *J Geol* 83:721–736
- De Mulder M, Hertogen J, Deutsch S, Andre L (1986) The role of crustal contamination in the potassic suite of the Karisimbi Volcano (Virunga, African Rift Valley). *Chem Geol* 57:117–136

- Deutsch A (1980) Alkalibasaltische Ganggesteine aus der westlichen Goldeckgruppe (Kärnten/Österreich). *Tschermaks Mineralogische Petrographische Mitteilungen* 27:17–34
- Deutsch A (1984) Young Alpine dykes south of the Tauern window (Austria): a K-Ar and Sr isotope study. *Contrib Miner Petrol* 85:45–57
- Deutsch A (1986) Geochemie oligozäner shoshonitischer Ganggesteine aus der Kreuzeckgruppe (Kärnten/Osttirol). *Mitteilungen Gesellschaft der Geologie und Bergbaustudenten Österreich* 32:105–124
- Di Girolamo P (1984) Magmatic character and geotectonic setting of some tertiary-quaternary Italian volcanic rocks: orogenic, anorogenic and transitional association—a review. *Bull Volc* 47:421–432
- Dixon TH, Batiza R (1979) Petrology and chemistry of Recent lavas in the N-Marianas: implications for the origin of island-arc basalts. *Contrib Miner Petrol* 70:167–181
- Edgar AD (1980) Role of subduction in the genesis of leucite-bearing rocks: discussion. *Contrib Miner Petrol* 73:429–431
- Exner C (1976) Die geologische Position der Magmatite des Periadriatischen Lineamentes. *Verhandlungen der Geologischen Bundesanstalt Wien, Austria* 1976:3–64
- Feitzinger G, Paar WH, Tarkian M, Reche R, Weinzierl O, Prochaska W, Holzer H (1995) Vein type Ag-(Au)-Pb, Zn, Cu-(W, Sn) mineralization in the southern Kreuzeck Mountains, Carinthia Province, Austria. *Miner Petrol* 53:307–332
- Ferguson AK, Cundari A (1975) Petrological aspects and evolution of the leucite-bearing lavas from Bufumbira, SW Uganda. *Contrib Miner Petrol* 50:25–46
- Foley SF, Wheller GE (1990) Parallels in the origin of the geochemical signatures of island arc volcanics and continental potassic igneous rocks: the role of residual titanites. *Chem Geol* 85:1–18
- Foley SF, Venturelli G, Green DH, Toscani L (1987) The ultrapotassic rocks: characteristics, classification, and constraints for petrogenetic models. *Earth Sci Rev* 24:81–134
- Foley SF, Jacob DE, O'Neill HSC (2011) Trace element variations in olivine phenocrysts from Ugandan potassic rocks as clues to the chemical characteristics of parental magmas. *Contrib Miner Petrol* 162:1–20
- Friedrich OM (1963) Die Lagerstätten der Kreuzeck-Gruppe. *Monographien Kärntner Lagerstätten, 3. Teil. Archiv für Lagerstättenforschung in den Ostalpen, Band 1, Mining University Leoben*
- Garcia MO, Liu NWK, Muenow DW (1979) Volatiles in submarine volcanic rocks from the Mariana Island Arc and trough. *Geochim Cosmochim Acta* 43:305–312
- Gorton MP (1977) The geochemistry and origin of quaternary volcanism in the New Hebrides. *Geochim Cosmochim Acta* 41:1257–1270
- Gribble RF, Stern RJ, Newman S, Bloomer SH, O'Hearn T (1998) Chemical and isotopic composition of lavas from the northern Mariana trough: implications for magma genesis in back-arc basins. *J Petrol* 39:125–154
- Hofmann AW, Jochum KP, Seufert PM, White WM (1986) Nb and Pb in oceanic basalts: new constraints on mantle evolution. *Earth Planet Sci Lett* 79:33–45
- Hoke L (1990) The Altkristallin of the Kreuzeck Mountains, SE Tauern Window, Eastern Alps; basement crust in a convergent plate boundary zone. *Jahrbuch Geologische Bundesanstalt Wien* 133:5–87
- Hole MJ, Saunders AD, Marriner GF, Tarney J (1984) Subduction of pelagic sediments: implications for the origin of Ce-anomalous basalts from the Mariana Islands. *J Geol Soc* 141:453–472
- Höll R, Maucher A (1968) Genese und Alteration der Scheelit-Magnetit-Lagerstätte Tux. *Sitzber Bayerische Akademie der Wissenschaften, Mathematik und Naturwissenschaften, München Kl* 1967:1–11
- Holm PM, Lou S, Nielsen A (1982) The geochemistry and petrogenesis of the lavas of the Vulsinian district, Roman Province, Central Italy. *Contrib Miner Petrol* 80:367–378
- Holm PM, Wilson JR, Christensen BP, Hansen L, Hansen SL, Hein KM, Mortensen AK, Pedersen R, Plesner S, Runge MK (2006) Sampling the Cape Verde mantle plume: evolution of melt compositions on Santo Antão, Cape Verde Islands. *J Petrol* 47:145–189
- Konzett J, Krenn K, Hauzenberger C, Whitehouse M, Hoinkes G (2012) High-pressure tourmaline formation and fluid activity in Fe-Ti-rich eclogites from the Kreuzeck Mountains, Eastern Alps, Austria. *J Petrol* 53:99–125
- Lahusen L (1972) Schicht- und zeitgebundene Antimonit-Scheelit-Vorkommen und Zinnobervererzung in Kärnten Osttirol/Österreich. *Miner Deposita* 7:31–60
- Laubscher H (1988) Material balance in Alpine Orogeny. *Bull Geol Soc Am* 100:1313–1328
- Lin PN, Stern RJ, Bloomer SH (1989) Shoshonitic volcanism in the northern Marianas Arc: 2. LILE and REE abundances: evidence for the source of incompatible element enrichments in intra-oceanic arcs. *J Geophys Res* 94:4497–4514
- Luhr JF, Kyser TK (1989) Primary igneous analcime: the Colima minettes. *Am Min* 74:216–223
- Meijer A, Reagan M (1981) Petrology and geochemistry of the island of Sarigan in the Mariana Arc; calc-alkaline volcanism in an oceanic setting. *Contrib Miner Petrol* 77:337–354
- Melluso L, de Gennaro R, Fedele L, Franciosi L, Morra V (2012) Evidence of crystallization in residual, Cl-F-rich, aegaitic, trachyphonolitic magmas and primitive Mg-rich basalt-trachyphonolite interaction in the lava domes of the Phlegrean fields (Italy). *Geol Mag* 149:532–550
- Michàlek M, Putiš M, Hauzenberger CA (2011) P-T data of Ky-St-Grt gneisses hosting HP amphibolites and eclogites from the Austroalpine Polinik complex, Kreuzeck Mountains, Eastern Alps, Austria. *Central Eur J Geosci* 3:197–206
- Mitchell RH, Bell K (1976) Rare earth element geochemistry of potassic lavas from the Birunga and

- Toro-Ankole Regions of Uganda, Africa. *Contrib Miner Petrol* 58:293–303
- Mitchell AHG, Warden AJ (1971) Geological evolution of the New Hebrides Island Arc. *J Geol Soc* 127:501–529
- Mogessie A, Tessadri R, Veltman CB (1990) EMP-AMPH—a hypercard program to determine the name of an amphibole from electron microprobe analysis according to the international mineralogical association scheme. *Comput Geosci* 16:309–330
- Morrison GW (1980) Characteristics and tectonic setting of the shoshonite rock association. *Lithos* 13:97–108
- Müller D (1993) Shoshonites and potassic igneous rocks: indicators for tectonic setting and mineralization potential of modern and ancient terranes. Unpublished PhD Thesis, The University of Western Australia, Perth
- Müller D, Stumpfl EF, Taylor WR (1992a) Shoshonitic and alkaline lamprophyres with elevated Au and PGE concentrations from the Kreuzeck Mountains, Eastern Alps, Austria. *Mineral Petrol* 46:23–42
- Müller D, Rock NMS, Groves DI (1992b) Geochemical discrimination between shoshonitic and potassic volcanic rocks from different tectonic settings: a pilot study. *Mineral Petrol* 46:259–289
- Müller D, Morris BJ, Farrand MG (1993) Potassic alkaline lamprophyres with affinities to lamproites from the Karinya Syncline, South Australia. *Lithos* 30:123–137
- Nelson DR, McCulloch MT, Sun SS (1986) The origins of ultrapotassic rocks as inferred from Sr, Nd and Pb isotopes. *Geochim Cosmochim Acta* 50:231–245
- Ninkovich D, Hays JD (1972) Mediterranean Island Arcs and origin of high potash volcanoes. *Earth Planet Sci Lett* 16:331–345
- Oxburgh E (1966) Superimposed fold system in the Altkristallin rocks of the southeast margin of the Tauern window. *Verhandlungen der Geologischen Bundesanstalt Wien, Austria* 1966:33–46
- Oyhantgabal P, Siegesmund S, Wemmer K, Frei R, Layer P (2007) Post-collisional transition from calc-alkaline to alkaline magmatism during transcurrent deformation in the southernmost Dom Feliciano Belt (Braziliano-Pan-African, Uruguay). *Lithos* 98:141–159
- Peate DW, Pearce JA, Hawkesworth CJ, Colley H, Edwards CMH, Hirose K (1997) Geochemical variations in Vanuatu Arc lavas: the role of subducted material and a variable mantle wedge composition. *J Petrol* 38:1331–1358
- Peccerillo A (2005) Plio-quadernary volcanism in Italy: petrology, geochemistry, geodynamics. Springer, Berlin, p 365
- Pelletier B, Calmant S, Pillet R (1998) Current tectonics of the Tonga-New Hebrides Region. *Earth Planet Sci Lett* 164:263–276
- Poli G, Frey FA, Ferrara G (1984) Geochemical characteristics of the South Tuscany (Italy) volcanic province: constraints on lava petrogenesis. *Chem Geol* 43:203–221
- Reimann C, Stumpfl EF (1981) Geochemical setting of strata-bound stibnite mineralization in the Kreuzeck Mountains, Austria. *Trans Ins Mining Metallurgy* 90:126–132
- Reimann C, Stumpfl EF (1985) Paleozoic amphibolites, Kreuzeck Mountains, Austria: geochemical variations in the vicinity of mineralization. *Miner Deposita* 20:69–75
- Rock NMS (1991) *Lamprophyres*. Blackie, Glasgow, p 285
- Rogers NW, Hawkesworth CJ, Parker RJ, Marsh JS (1985) The geochemistry of potassic lavas from Vulcini, Central Italy, and implications for mantle enrichment processes beneath the Roman region. *Contrib Miner Petrol* 90:244–257
- Rogers NW, De Mulder M, Hawkesworth CJ (1992) An enriched mantle source for potassic basanites: evidence from Karisimbi Volcano, Virunga Volcanic Province, Rwanda. *Contrib Miner Petrol* 111:543–556
- Rogers NW, James D, Kelley SP, De Mulder M (1998) The generation of potassic lavas from the eastern Virunga Province, Rwanda. *J Petrol* 39:1223–1247
- Soeria-Atmadja R, Sunarya Y, Sutanto Hendaryono S (1998) Epithermal gold-copper mineralization associated with late Neogene-magmatism and crustal extension in the Sunda-Banda Arc. *Geol Soc Malays Bull* 42:257–268
- Stern RJ (1979) On the origin of andesite in the northern Mariana Island Arc: implications from Agrigan. *Contrib Miner Petrol* 68:207–219
- Stern RJ, Bloomer SH, Lin PG, Ito E, Morris J (1988) Shoshonitic magmas in nascent arcs: new evidence from submarine volcanoes in the northern Marianas. *Geology* 16:426–430
- Stolz AJ, Varne R, Wheller GE, Foden JD, Abbott MJ (1988) The geochemistry and petrogenesis of K-rich alkaline volcanic from the Batu Tara Volcano, eastern Sunda arc. *Contrib Miner Petrol* 98:374–389
- Sun SS, McDonough WF (1989) Chemical and isotopic systematic of oceanic basalts: implications for mantle composition and processes. In: Saunders AD, Norry MJ (eds), *Magmatism in the ocean basins*, vol 42. Geological Society of London Special Publication, pp 313–345
- Thompson RN (1985) Asthenospheric source of Ugandan ultrapotassic magma? *J Geol* 93:603–608
- Till CB, Grove TL, Withers AC (2012) The beginnings of hydrous mantle wedge melting. *Contrib Miner Petrol* 163:669–688
- Van Bergen MJ, Ghezzo C, Ricci CA (1983) Minette inclusions in the rhyodacitic lavas of Mt. Amiata (Central Italy): mineralogical and chemical evidence of mixing between Tuscan and Roman type magmas. *J Volcanol Geotherm Res* 19:1–35
- Venturelli G, Thorpe RS, Dal Piaz GV, Del Moro A, Potts PJ (1984) Petrogenesis of calc-alkaline, shoshonitic and associated ultrapotassic Oligocene volcanic rocks from the Northwestern Alps, Italy. *Contrib Miner Petrol* 86:209–220

- Vollmer R, Norry MJ (1983) Possible origin of K-rich volcanic rocks from Virunga, East Africa, by metasomatism of continental crustal material: Pb, Nd and Sr isotopic evidence. *Earth Planet Sci Lett* 64:374–385
- Von Pichler H (1970) *Italienische Vulkangebiete I. Somma-Vesuv, Latium, Toscana*. Gebrüder Bonträger, Berlin
- Weaver BL, Wood DA, Tarney J, Joron JL (1987) Geochemistry of ocean island basalts from the South Atlantic: Ascension, Bouvet, St.Helena, Gough and Tristan da Cunha. In: Fitton JG, Upton BGD (eds), *Alkaline igneous rocks*, vol 30. Geological Society of London Special Publication, pp 253–267
- Woodhead JD (1989) Geochemistry of the Mariana Arc (western Pacific): source composition and processes. *Chem Geol* 76:1–24
- Wyllie PJ (1988) Solidus curves, mantle plumes, and magma generation beneath Hawaii. *J Geophys Res* 93:4171–4181

5.1 Introduction

Controversy continues to surround the relative contributions of magmatic versus metamorphic, and crustal versus mantle, components to the fluids which are responsible for the origin of orogenic (Groves et al. 1998) gold deposits (e.g. Rock et al. 1989). The recognition that the products of deep-seated alkaline magmatism, such as lamprophyres, are spatially associated with many orogenic gold deposits (Rock et al. 1989; Rock 1991) has resulted in the detailed study of primary precious-metal contents in these rocks (e.g. Wyman and Kerrich 1989; Taylor et al. 1994). This chapter reviews some recent studies on primary precious-metal contents in shoshonitic and alkaline lamprophyres, and other potassic igneous rocks.

5.2 Theoretical Discussion

It has long been suspected that K-enriched melts are efficient carriers of Au (Mutschler et al. 1985; Rock and Groves 1988; Müller and Groves 1993; Müller 2002; Mavrogenes et al. 2006; Li and Audetat 2013). Recent experimental studies by Mavrogenes et al. (2006) reveal that the addition of K₂O to hydrous rhyolitic glasses at constant water content, temperature, pressure, and oxygen fugacity (fO₂) increases Au solubility by nearly an order of magnitude. In experimental runs with

FeS only, the Au content increased from 0.08 ppm Au (at 1.6 wt% K₂O) to 0.66 ppm Au (at 6.8 wt% K₂O; Mavrogenes et al. 2006). Ore deposits associated with potassic igneous rocks tend to be particularly Au-rich and various models have been proposed to explain this phenomenon (cf. Li and Audetat 2013), including: (1) partial melting of Au-enriched, metasomatized lithospheric mantle (McInnes et al. 1999); (2) partial re-melting of sulphide-bearing cumulates at the crust-mantle boundary (Richards 2009); (3) high Au solubility in S- and Cl-bearing magmas (Botcharnikov et al. 2011; Zajacz et al. 2010, 2012; Jago and Pichavant 2012); (4) high Au solubility in thiosulphate and alkali-chloride bearing fluids (Zajacz et al. 2010); and (5) lack of sulphides in the mantle source region due to the high oxygen fugacities of these magmas (Müller and Groves 1993; Sillitoe 1997; Mungall 2002).

The occurrence of all primary PGE deposits in mafic-ultramafic intrusions points to a congruent enrichment of precious metals in parts of the mantle (Rock et al. 1988a). Cabri (1981) and Maier et al. (2009) consider most of the terrestrial precious-metal budget to have been partitioned into the deep mantle and core during the early differentiation of the planet. The ideal magma-type to transport these elements into the crust is, therefore, one with an ultrabasic character and an exceptionally deep origin (i.e. alkaline rocks such as lamprophyres; cf. Rock et al. 1988a). Lamprophyres also have magmatic compositions (high CO₂ and halogen contents) potentially suitable for

transporting Au from the mantle into the crust (Rock et al. 1988a; Rock 1991).

Reviews have shown that mantle-derived lamprophyric melts have very high primary PGE contents (e.g. Crocket 1979). A compilation of precious-metal contents of potassic igneous rocks, such as lamprophyres and related rocks (Table 5.1), has been given by Rock et al. (1988a, 1989). For example, lamproites from the Ellendale Field, Western Australia, contain up to 56 ppb Pd (Lewis 1987). The Wessleton and Frank Smith kimberlites, South Africa, contain up to 19 ppb Pd (Paul et al. 1979), and discrete grains of platinum-group metals have been detected in these kimberlites (Mitchell 1986). The precious-metal concentrations in lamproites and kimberlites, which normally occur in within-plate settings and represent the deepest forms of magmatism, suggest the presence of precious-metal-enriched source regions within the upper mantle (Rock et al. 1988a). Their precious-metal enrichments are interpreted to be primary magmatic features (see below), since lamproites and kimberlites are rapidly erupted through the crust and commonly show little

evidence of significant fractionation during ascent, as reflected in their high mg# and the occurrence of mantle xenoliths (Rock et al. 1988a; Rock 1991).

The association in space and time between shoshonitic lamprophyres and orogenic (previously incorrectly termed mesothermal) gold deposits has been documented in many Archean greenstone-belt terrains (Hallberg 1985; Taylor et al. 1994). Platinum-group elements such as Ir, Os, and Ru are mantle compatible, and they remain as sulphide blebs in the olivine (forsterite)-bearing residue of the mantle during partial melting (Brügmann et al. 1987; Gueddari et al. 1996). Originally sulphur-rich magmas such as MORB are generally PGE-poor, because the sulphide-hosted PGE are removed during fractionation. By contrast, the elements Cu, Au, Pt, and Pd behave incompatibly during partial melting of a strongly depleted mantle source (Brügmann et al. 1987; Stanton 1994) forming sulphur-undersaturated melts (Hamlyn et al. 1985). Copper, Au, Pt, and Pd behave as mantle-incompatible elements (Gueddari et al. 1996) and are partitioned into the first

Table 5.1 Compilation of precious metal abundances in potassic igneous rocks

Individual intrusion	Reference	Method	Au (ppb)	Pt (ppb)	Pd (ppb)
<i>Kimberlites</i>					
South Africa					
Wessleton	Paul et al. (1979)	NAA	n.a.	n.a.	18
Frank Smith	Paul et al. (1979)	NAA	n.a.	n.a.	18
<i>Lamproites</i>					
Kimberley, Australia					
Ellendale 9	Lewis (1987)	ICP	n.a.	3	1
Ellendale 11	Lewis (1987)	ICP	n.a.	4	56
<i>Lamprophyres</i>					
Borneo					
Linhsaisai minette	Bergman et al. (1988)	NAA	15	n.a.	n.a.
Canada					
Malpeque	Greenough et al. (1988)	NAA	45	n.a.	n.a.
Papua New Guinea					
Fu lamprophyre	Finlayson et al. (1988)	NAA	29	n.a.	n.a.

NAA neutron activation analysis, ICP inductively coupled plasma mass spectrometry, n.a. not analyzed. After Rock et al. (1988a, 1989)

silicate-melt increments, rather than into a separate sulphide-liquid fraction (Taylor et al. 1994). Thus first-stage arc-magmas tend to generate Cu-rich melts (Richards 2009). Fractionation of these precious-metal enriched, but sulphur-undersaturated, parent magmas can lead to further Au and PGE enrichment provided the melt does not become sulphur saturated (Hamlyn et al. 1985; Brüggmann et al. 1987; Taylor et al. 1994). Gold probably behaves incompatibly during olivine fractionation, because the Au²⁺ oxidation state is not known from natural systems (Togashi and Terashima 1997). Native Au, Au⁺, or Au³⁺ are the most stable species, but their charges and their large ionic radii preclude their partitioning into olivine (Brüggmann et al. 1987).

Recent work suggests that small sulphide blebs can act as a reservoir of sulphur and ore metals such as Cu and Au (Keith et al. 1997; Halter et al. 2002; Nadeau et al. 2010). Based on melt inclusion studies on the Bajo de la Alumbrera porphyry Cu-Au deposit in Argentina, Halter et al. (2002) argue that the parental magma was probably sulphide-saturated, but that the early formed sulphide blebs were destabilized during volatile exsolution and that the Cu, Au, and S from the sulphide blebs then migrated into the ore-forming hydrothermal fluid. In accord with this interpretation, Nadeau et al. (2010) studied sulphide and melt inclusions in volcanic rocks from the Merapi Volcano, Indonesia, reporting numerous partially or almost completely dissolved sulphide inclusions associated with silicate melt inclusions and fluid inclusions. The authors interpret these textures as evidence for the interaction between sulphide blebs and a hydrothermal fluid (Nadeau et al. 2010). Park et al. (2015) suggest that the relative timing of sulphide saturation is a critical factor to form a magma enriched in chalcophile elements. Once a mantle-derived basaltic magma rises into the crust, its temperature, oxygen fugacity, and FeO content control sulphur solubility in the silicate melt (Park et al. 2015). Assimilation of reducing material from the wall-rocks and mixing with crust-derived silicic magmas are the most likely processes to result in sulphide saturation during open-system fractionation, whereas reduction

produced by magnetite crystallization is likely to be the dominant process in closed systems (Park et al. 2015). A magma that reaches sulphide saturation early and precipitates a significant amount of sulphides before it becomes volatile-saturated is unlikely to produce an economic porphyry copper-gold deposit, because ore metals, such as Cu and Au, will be held as cumulates at the base of the fractionating magma chamber, leading to a residual magma that is depleted in these elements (Richards 2011; Park et al. 2015).

Under conditions of relatively high fO_2 , sulphide species become unstable with respect to sulphates in the magma and the segregation of an immiscible sulphide-melt phase is impossible (Richards 1995, 2011). Under such conditions, the chalcophile elements behave as incompatible components in the melt, becoming steadily enriched during fractionation (Wyborn, pers. comm., 1995). Additionally, the high fO_2 may delay sulphur saturation until after the onset of volatile saturation, thus generating chalcophile-enriched hydrothermal fluids (Richards 1995, 2011; Park et al. 2015). Hence, the observed Au and PGE enrichments of many potassic lamprophyres (see Sect. 5.3) could be primary features. Trace element data for potassic igneous rocks such as shoshonites suggest that they are also enriched in Cu (Kesler 1997). The fact that not all potassic igneous rock suites are mineralized, and that not all shoshonitic lamprophyres are Au- or PGE-enriched (see Chap. 8), probably indicates the heterogeneity of mantle metasomatism processes (Taylor et al. 1994). It is not yet clear whether the oxidized nature of late oceanic-arc basalts is a source characteristic or whether it is caused by secondary processes such as degassing (Ballhaus 1993). For instance, the rapid loss of hydrogen by diffusion, with an attendant increase in the H_2O/H_2 ratio, increases fO_2 (Haggerty 1990), and has been modeled as the mechanism to account for oxidized crusts in ponded lava lakes (Sato and Wright 1966). Late oceanic-arc basalts, which are commonly more enriched in volatiles than other basalts (Muenow et al. 1990), are more susceptible to those degassing processes.

Generally, there are two mechanisms for the generation of sulphur-undersaturated precious-

metal-rich magmas (Sun et al. 1991): (1) high temperature (>1400 °C), large degree (>25 %) of mantle melting related to asthenospheric mantle plume activity; and (2) lower temperature, small degree of partial melting of mantle wedge material (<4 ppb Pt, Pd; <1 ppb Au; <250 ppm S) in subduction arcs.

The second process might produce potassic lamprophyres and shoshonites with primary precious-metal enrichments (S.S. Sun, pers. comm. 1996). However, too small a degree of partial melting (<10 %) will leave sulphides in the mantle residue, and hence retain the precious metals during such partial melting (Sun et al. 1991). As noted above, the conditions in subduction zones are considered to be too oxidizing for the generation of sulphur-saturated magmas (Taylor et al. 1994; Richards 2011).

Silicate minerals have low mineral/melt distribution coefficients for Pd, Pt, and Au (Keays 1982), when compared to the very high partition coefficients for PGE into sulphides (Campbell et al. 1983). Thus, the PGE tend to form sulphides if sufficient sulphur is present in the melt. These relatively dense sulphides are strongly affected by gravitational fractionation, which means that the resulting melt will be gradually depleted in precious metals *en route* to surface (cf. Richards 2011; Park et al. 2015). As a consequence, efficient precious-metal concentration in a magma chamber (Sun et al. 1991) requires fertile basic magmas with high PGE background levels (e.g. >15 ppb Pd), but low sulphur contents (<1000 ppm S).

Obvious exceptions to the rule regarding correlation between sulphur-undersaturation and precious-metal abundances in basic magmas are the sulphur-saturated lamproites and kimberlites which may contain significant precious-metal concentrations (Mitchell and Keays 1981). However, this can be explained by the volatile-driven rapid uprise of these potassic magmas, which might sample some precious-metal-enriched mantle sulphide droplets, in addition to mantle xenoliths, *en route* to surface (Sun et al. 1991).

Theoretically, on the basis of the discussion above, primary Au and PGE enrichment of

lamprophyric magmas should be characterized by elevated concentrations of all incompatible metals such as Cu, Au, Pt, and Pd. If Au peaks are decoupled from Cu, Pt, and Pd peaks in distribution plots of metal contents in the lamprophyres normalized to primitive mantle, it is likely that the anomalous Au contents are secondary features (Wyman and Kerrich 1989).

5.3 Case Study: Potassic Alkaline Lamprophyres with Elevated Gold Concentrations from the Karinya Syncline, South Australia

5.3.1 Introduction

During extensive base-metal exploration in the Karinya Syncline, which forms part of the Adelaide Geosyncline in South Australia, a lamprophyre province has been mapped in the area between Truro and Frankton about 80 km northeast of Adelaide (Fig. 5.1; Morris 1990; Müller et al. 1993). The investigated dykes from the Karinya Syncline have been classified as alkaline lamprophyres (Müller et al. 1993), but they also show transitional features to lamproites. Potassic lamprophyres with lamproitic affinity are known from several localities worldwide (e.g. Wagner and Velde 1986; Venturelli et al. 1991a; Sheppard and Taylor 1992; Semiz et al. 2012), but their petrogenesis is still poorly understood (Foley et al. 1987).

The potassic lamprophyres from the mineralized Karinya Syncline have high Au contents (Müller et al. 1993). As they have also been analyzed for other base- and precious-metals (Cu, Ni, Pt, Pd) and for elements commonly associated with hydrothermal gold deposits (As, Sb, W), it is informative to use them as a test of primary Au enrichment of these rocks as proposed, for example, by Rock and Groves (1988a, b). However, before doing this, the mineralogy, petrology and geochemistry of the suite must be documented to determine whether the rocks are hydrothermally altered or not. It is also informative to use the

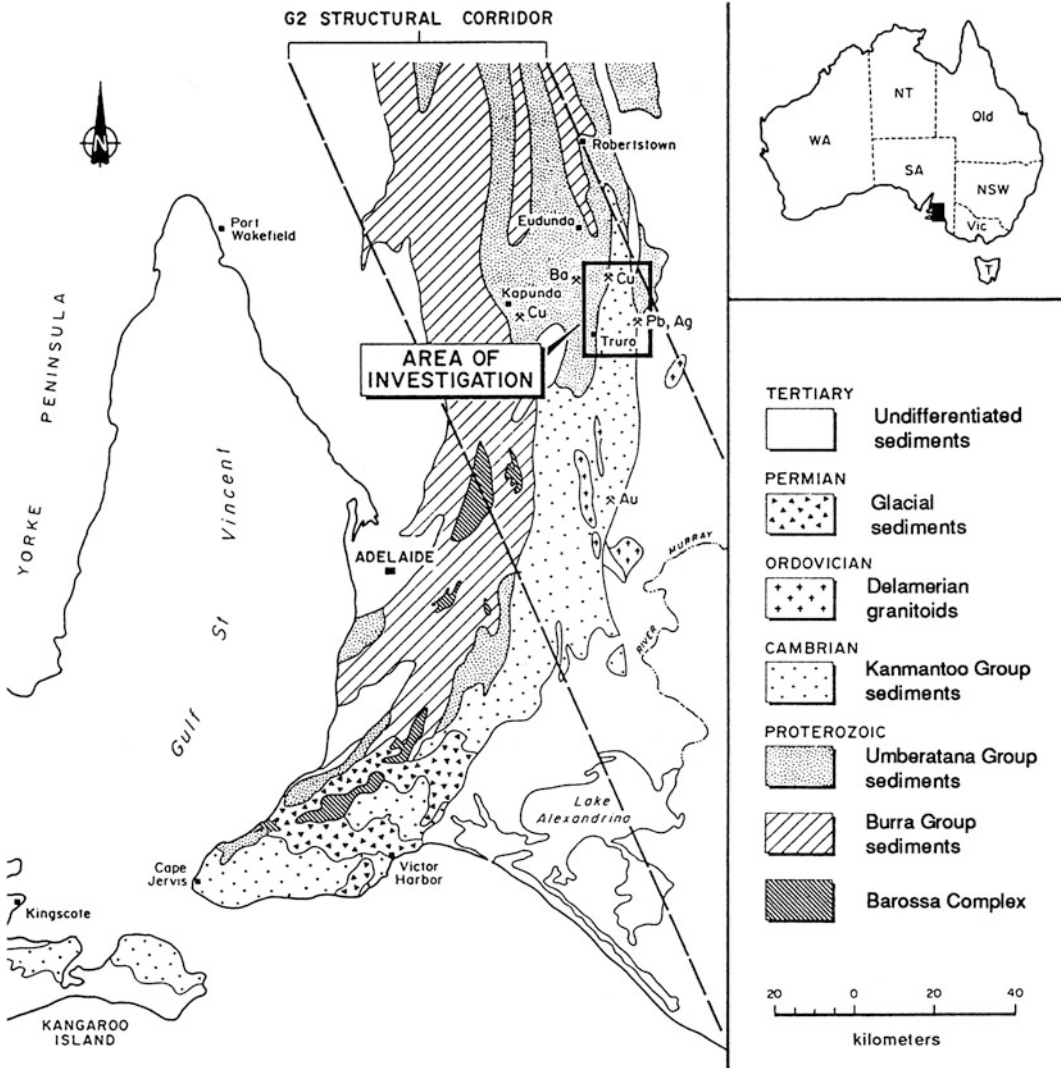


Fig. 5.1 Geological overview of the southern part of the Adelaide Geosyncline, South Australia, showing the study area, which includes the Karinya Syncline. Modified after Müller et al. (1993)

geochemical data as a test of the tectonic discrimination diagrams presented in Chap. 3. A more complete description is provided by Müller et al. (1993).

5.3.2 Regional Geology and Tectonic Setting

The Adelaide Geosyncline is a 700 km-long fold belt comprising late Proterozoic to middle Cambrian sedimentary rocks which were folded,

metamorphosed, and uplifted during the Delamerian Orogeny in the late Cambrian (Thomson 1969, 1970; Foden et al. 2002). No reliable indicators for an ancient subduction event (i.e. blueschists, ophiolites, mélanges) have been recorded in the Adelaide Geosyncline, and Preiss (1987) has suggested a within-plate origin for the igneous activity, perhaps related to deep-seated crustal fractures.

The Karinya Syncline, forming the northern part of the Kanmantoo Trough (southern part of

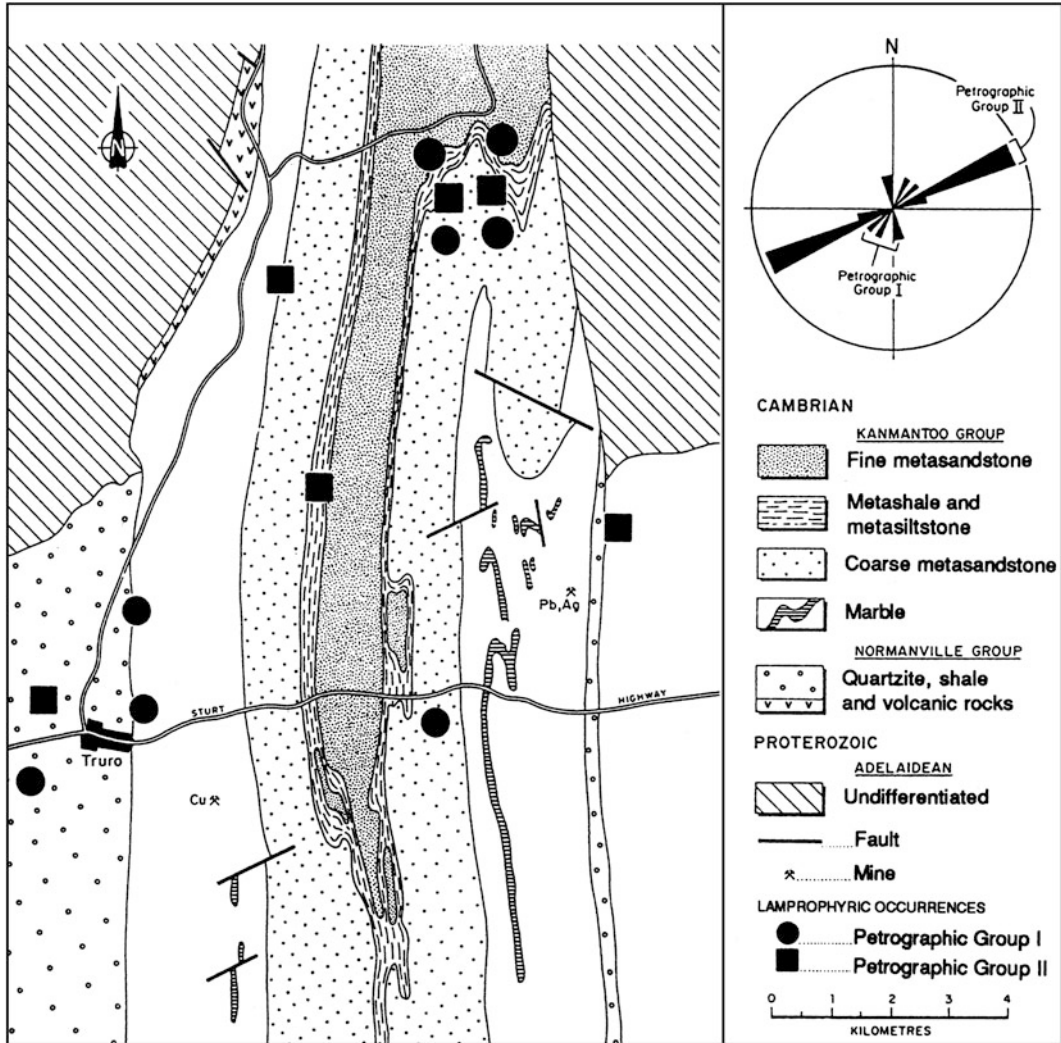


Fig. 5.2 Geological overview of the investigated area within the Karinya Syncline, South Australia. The map shows lamprophyre localities and two former base-metal mines in the area; circles represent samples from

petrographic group 1 and squares represent those from petrographic group 2. The rose diagram shows the different strike directions of the two distinctive petrographic groups. Modified after Müller et al. (1993)

the Adelaide Geosyncline), consists of Cambrian metasedimentary rocks which were intruded by the lamprophyre swarm during the Ordovician (Fig. 5.2).

5.3.3 Mineralization in the Vicinity of the Lamprophyres

In the Adelaide Geosyncline, mineral deposits of various kinds and different ages are situated

either in, or at the edges of, major north-northwest-trending lineaments or at their intersections (O'Driscoll 1983). O'Driscoll (1983) has shown that the largest lineaments coincide with small base-metal deposits at Kanmantoo and Kapunda, as well as with the giant iron-oxide copper-gold-uranium deposit at Olympic Dam (Creaser 1996). These deposits are, however, older than the lamprophyres discussed here (Müller et al. 1993). The area also

hosts several smaller gold mines, where shallow alluvial goldfields and some reefs were developed (e.g. Moppa and Hamilton areas south of Truro), as well as barite deposits (e.g. northwest of Dutton, west of Truro; Horn et al. 1989).

The occurrence of mineral deposits, in combination with the presence of crustal-scale lineaments which represent zones of deep-seated crustal weakness, reflects the potentially high prospectivity of the area for further gold and base-metal discoveries (cf. Rock et al. 1988a), although to date there are no clear indications of mineralization directly related to the lamprophyres.

5.3.4 Nature of the Lamprophyres

Most of the dykes strike northeasterly, as shown in Fig. 5.2. The thickness of the dykes varies from 0.1 to 1.5 m, and, in general, they have intruded joint planes of the country rock (Müller et al. 1993). The lamprophyre dykes show typical porphyritic textures, with phlogopite phenocrysts in a fine-grained groundmass. Most lamprophyre dykes show flow textures, with a parallel alignment of phlogopite phenocrysts, and several have chilled margins at lithological contacts with their host rocks. In the Truro area there is also a lamproitic diatreme (Müller et al. 1993). All samples are affected to varying extents by secondary alteration. The carbonate host rocks at Robertstown are strongly altered to talc, asbestos, and tourmaline.

The investigated lamprophyres were emplaced at a shallow depth during the Ordovician after the Delamerian Orogeny. Two different K-Ar ages of 458 ± 2 and 480 ± 3 Ma (Table 5.2) are consistent with two distinctive petrographic

groups of lamprophyres (see below) as discussed by Müller et al. (1993).

The large (1–6 mm), euhedral phlogopite phenocrysts are sited in a groundmass of mainly felsic components (e.g. orthoclase, leucite, plagioclase, quartz). The phlogopites commonly show battlement structures (Fig. 5.3c) and parallel orientations (i.e. flow textures; Fig. 5.3a, b). An older phenocryst generation is represented by large (up to 6 mm), zoned, Na-rich phlogopite crystals, and a younger generation by smaller (<1 mm) phlogopite crystals. Several rocks also have apatite and titanite microphenocrysts.

Based on phenocryst mineralogy, two petrographic types of lamprophyres can be distinguished, one is *phlogopite phyric* and the other is *apatite-phlogopite phyric* (Müller et al. 1993). Primary ferromagnesian phenocrysts other than phlogopite are generally absent. However, one sample also contains alkali-amphibole (i.e. riebeckite), and others show secondary amphibole (i.e. cummingtonite) resulting from intense alteration. Phenocryst mineralogy is dominated by large zoned phlogopites with very high mg# of 89–90, variable TiO₂ contents (1.71–4.06 wt%), and Al₂O₃ contents between 12.0 and 13.0 wt% (cf. Rock 1991). The phlogopite phenocrysts are characterized by relatively high F concentrations (up to 3.79 wt% F) compared to average values of typical lamproites (Table 5.3). For example, Miocene olivine-lamproites from the West Kimberley of Australia have F concentrations of only about 1.71 wt% (Jaques et al. 1986; Mitchell and Bergman 1991). Mica compositions, plotted on a Al-Mg-Fe triangular diagram (Mitchell and Bergman 1991; Sheppard and Taylor 1992), show some overlap between values typical for lamproites and lamprophyres (Fig. 5.4a).

Table 5.2 Whole-rock K-Ar dating on lamprophyres from the Karinya Syncline, South Australia

Sample no.	Petrographic group	K (wt%)	K-Ar age (Ma)
119068	I	7.33	458 ± 2
119072	II	7.84	478 ± 3
119078	II	8.29	481 ± 3

Analyses performed by Analabs Laboratories, Adelaide, South Australia. The error on ages is quoted as $\pm 2\sigma$. Sample numbers refer to specimens held in the Museum of the Department of Geology and Geophysics, The University of Western Australia. From Müller et al. (1993)

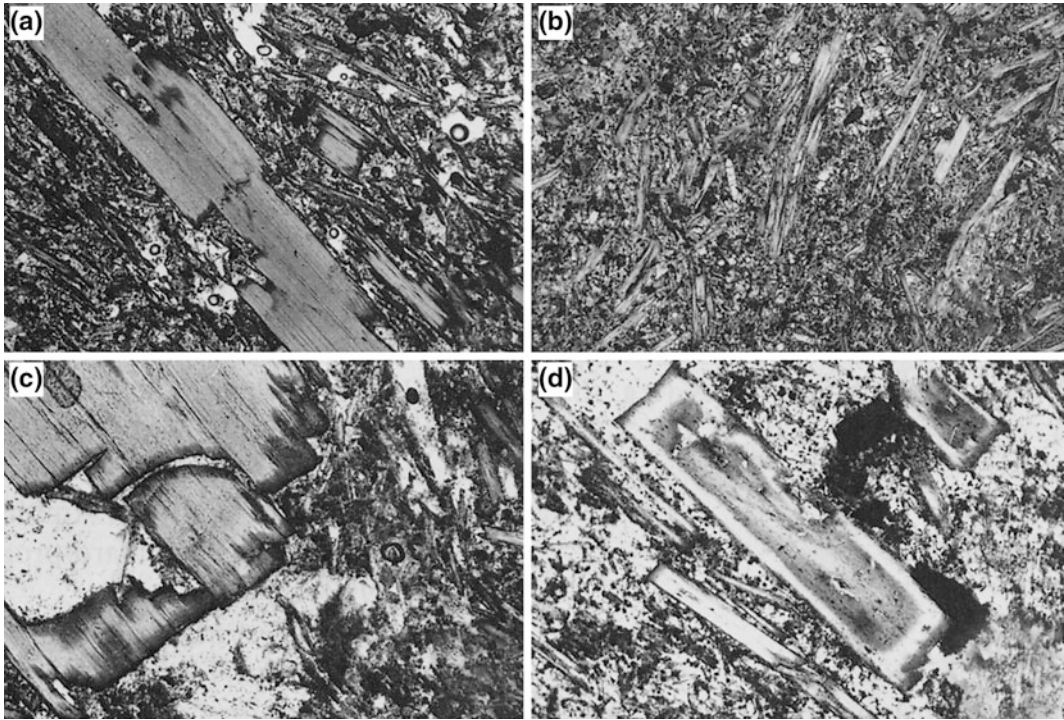


Fig. 5.3 Photomicrographs (crossed nicols) of typical lamprophyre samples from the Karinya Syncline, South Australia. **a** Two generations of mica phenocrysts with varying size (119068) [FOV 4.0 mm]. **b** Flow textures displayed by phlogopite phenocrysts (119072) [FOV 2.0 mm]. **c** Battlement structures in phlogopite phenocryst

(119068) [FOV 2.0 mm]. **d** Zoned phlogopite (119079) [FOV 3.0 mm]. Sample numbers refer to specimens held in the Museum of the Department of Geology and Geophysics, The University of Western Australia. From Müller et al. (1993)

Groundmass minerals are mainly orthoclase, leucite, plagioclase, and quartz. Potassic feldspars, plotted on a Fe_2O_3 versus orthoclase biaxial diagram (e.g. Sheppard and Taylor 1992), show transitional features between lamproites and alkaline lamprophyres (Fig. 5.4b). Lamproites *sensu stricto*, which commonly show leucite, do not contain plagioclase (Velde 1975; Bergman 1987). They are also characterized by the presence of Cr-spinels, which have not been detected in the described lamprophyres (Müller et al. 1993).

Several dykes have an extremely fine-grained, cryptocrystalline, and partly glassy groundmass. Two lamprophyres show syenitic ocelli, mainly consisting of orthoclase, which are irregular shaped globular structures and gradational with their host-rocks (cf. Rock et al. 1988b; Perring et al. 1989; Rock 1991; Taubald et al. 2004).

Importantly for the study of precious-metal concentrations, some samples are affected by secondary alteration. Alteration consists mainly of saussuritization of groundmass feldspars producing secondary epidote, or secondary carbonate replacement. Three samples are strongly altered, forming magnesio-cummingtonites with a fibrous character and anomalous birefringence; their felsic groundmass minerals are completely altered to secondary talc and epidote (Müller et al. 1993).

5.3.5 Petrology and Geochemistry of the Lamprophyres

The major- and trace-element chemistry of representative samples is given in Tables 5.4 and 5.5. The dykes show SiO_2 contents between 39.6 and 63.1 wt% (Fig. 5.5) and mg# varies from 35

Table 5.3 Microprobe (wavelength dispersive spectrum—WDS) analyses of mica phenocrysts from lamprophyres from the Karinya Syncline, South Australia

Sample no.	119068	119072	119073	119074	119076	119079	119080	119070	119081
Petrographic type	I	II	II	II	I	II	I	I	I
SiO ₂	39.58	40.24	37.51	40.07	39.86	39.54	40.36	40.04	52.90
TiO ₂	2.21	2.18	4.06	1.71	1.68	2.15	1.79	1.73	5.32
Al ₂ O ₃	13.35	12.46	12.94	11.89	11.41	12.14	12.30	14.25	0.42
Cr ₂ O ₃	0.10	0.13	0.02	0.42	0.17	0.33	0.18	0.26	0.02
FeO (tot)	5.87	6.15	12.42	6.35	6.01	6.22	6.02	11.20	17.16
MnO	0.06	0.05	0.10	0.05	0.05	0.06	0.05	0.27	0.05
MgO	22.79	22.83	17.34	22.28	23.33	22.23	22.52	28.42	12.77
CaO	0.03	0.03	0.04	0.03	0.02	0.03	0.03	0.56	0.80
Na ₂ O	0.32	0.12	0.21	0.08	0.29	0.15	0.26	0.59	6.71
K ₂ O	10.09	10.22	9.74	10.31	10.04	10.46	9.51	0.35	0.42
SrO	0.11	0.12	0.09	0.10	0.09	0.11	0.09	0.12	0.18
BaO	0.28	0.46	0.65	0.31	0.25	0.36	0.33	0.13	0.11
Cl	0.03	0.02	0.02	0.02	0.02	0.02	0.02	0.09	0.02
F	1.32	1.55	0.83	3.24	3.79	2.76	3.02	0.40	0.27
Total	95.56	95.89	95.60	95.48	95.40	95.38	95.19	98.15	97.02
Name	Phlogopite	Cummingtonite	Riebeckite						
mg#	90	89	76	89	90	89	90	85	63
Ox. form.	22	22	22	22	22	22	22	23	23
Atoms									
Si	5.728	5.823	5.612	5.895	5.943	5.817	5.900	5.720	7.811
Ti	0.241	0.237	0.456	0.189	0.184	0.237	0.197	0.186	0.591
Al	2.277	2.124	2.282	2.061	1.956	2.104	2.118	2.400	0.074

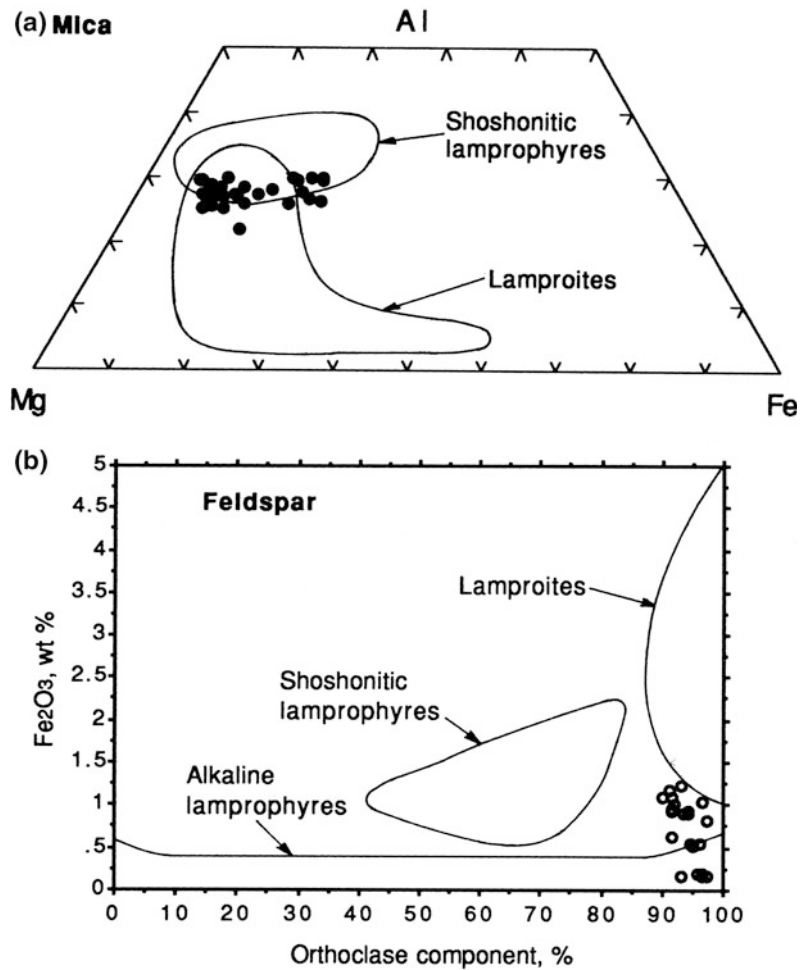
(continued)

Table 5.3 (continued)

Sample no.	119068	119072	119073	119074	119076	119079	119080	119070	119081
Cr	0.011	0.015	0.001	0.049	0.019	0.038	0.021	–	0.001
Fe	0.710	0.744	1.553	0.781	0.730	0.765	0.735	1.338	2.118
Mn	0.007	0.005	0.012	0.003	0.005	0.007	0.007	–	0.002
Mg	4.912	4.921	3.864	4.883	5.053	4.870	4.904	6.052	2.809
Ca	0.002	0.005	0.007	0.002	0.002	0.004	0.001	0.085	0.127
Na	0.090	0.034	0.059	0.023	0.081	0.042	0.072	0.163	1.919
K	1.863	1.885	1.858	1.934	1.862	1.962	1.772	0.063	0.079
Sr	0.007	0.010	0.005	0.008	0.008	0.009	0.007	0.011	–
Ba	0.016	0.026	0.038	0.018	0.014	0.021	0.019	–	0.006
Cl	–	–	–	–	–	–	–	–	–
F	–	–	–	–	–	–	–	–	–
Total	15.864	15.829	15.749	15.847	15.857	15.877	15.753	16.018	15.537

FeO (tot) = total iron calculated as ferrous oxide, *Cumm.* cummingtonite, *Ox. form* oxygen formula. Sample numbers refer to specimens held in the Museum of the Department of Geology and Geophysics, The University of Western Australia. From Müller et al. (1993)

Fig. 5.4 **a** Al-Mg-Fe triangular plot showing 47 representative mica analyses from the Karinya Syncline, South Australia. **b** Fe_2O_3 versus orthoclase biaxial plot showing 21 representative K-feldspar analyses for lamprophyres from the Karinya Syncline, South Australia. The orthoclase component of the investigated feldspar phases is given in %. Data from Müller et al. (1993). Modified from Sheppard and Taylor (1992)



to 73. Most samples have high K_2O (>3 wt%) and MgO (>3 wt%) contents, and $\text{K}_2\text{O}/\text{Na}_2\text{O}$ ratios >2, and can be classified as ultrapotassic (Foley et al. 1987). However, the most-altered samples have relatively low K_2O contents (<1.23 wt%) due to mobilization of K during alteration (Müller et al. 1993). The lamprophyres are characterized by very high F concentrations (1050–5800 ppm). Their high halogen contents (i.e. Cl and F) are consistent with the occurrence of phlogopite phenocrysts, probably indicating hydrous melting of the mantle source (Bizimis et al. 2000; Guo et al. 2013).

Dykes of petrographic type 2 show P_2O_5 values >1.4 wt%, whereas those of petrographic type 1 are characterized by P_2O_5 values <1.4 wt

% (Müller et al. 1993). Petrographic type 2 dykes show distinctive Nb concentrations between 20 and 30 ppm, whereas those of type 1 have very variable Nb concentrations, between 10 and 70 ppm. However, distinction between the two petrographic groups using spidergram patterns is equivocal.

The relatively low mg# of the rocks suggest that the lamprophyres are derived from primitive mantle melts via olivine ± clinopyroxene ± phlogopite ± apatite fractionation. This is consistent with their relatively low Ni concentrations. Spitz ratios, such as $(\text{Na} + \text{K})/\text{Al}$, show that the samples tend towards peralkaline character (Table 5.4). The relatively high TiO_2 contents of the investigated lamprophyres (up to 2.02 wt%;

Table 5.4 Selected major-element analyses (in wt%) of lamprophyres from the Karinya Syncline, South Australia

Sample no.	Fresh samples		Altered samples	
	119067	119072	119070	119078
Petrographic group	I	II	I	II
SiO ₂	56.30	56.00	40.01	48.00
TiO ₂	2.02	1.86	1.82	1.75
Al ₂ O ₃	12.29	12.10	12.84	9.50
Fe ₂ O ₃ (tot)	9.59	8.50	13.03	9.81
MnO	0.02	0.06	0.02	0.25
MgO	4.83	6.70	17.96	6.20
CaO	0.40	2.08	0.42	6.68
Na ₂ O	0.30	1.42	1.51	0.39
K ₂ O	9.10	7.55	1.08	7.69
P ₂ O ₅	0.48	1.60	0.31	1.80
LOI	3.98	2.13	10.71	6.57
Total	99.31	100.00	99.70	98.64
mg#	50	61	73	56
(Na+K)/Al	0.84	0.87	0.28	0.94

Sample numbers refer to specimens held in the Museum of the Department of Geology and Geophysics, The University of Western Australia. From Müller et al. (1993)

Müller et al. 1993) and their high Zr concentrations (up to 818 ppm) reflect their alkaline geochemistry (see Sect. 4.2; Müller et al. 1992a; Karsli et al. 2014). Two samples have very low SiO₂ contents (<41.0 wt%) and very high MgO contents (>17.0 wt%), suggesting an affinity to lamproites. However, despite their high MgO contents, they have only relatively low Ni (<345 ppm), Co (<55 ppm), and Cr (<145 ppm) contents. This clearly distinguishes them from typical olivine-lamproites (Müller et al. 1993), and suggests that the high MgO contents are not primary, but caused by secondary alteration processes.

The geochemistry of the investigated lamprophyres is atypical of lamproites (cf. Mitchell and Bergman 1991), because of their unusually low LREE abundances (e.g. <84 ppm La, <157 ppm Ce). The lamprophyres from the Karinya Syncline also have relatively high Al₂O₃ (~12.0 wt%) and low Ba contents (~2800 ppm in fresh samples) compared with average values

for lamproites of 4–10 wt% and 1–3 wt%, respectively (Bergman 1987).

In order to determine the tectonic setting of the investigated potassic lamprophyres, they were plotted on the TiO₂ versus Al₂O₃, Y versus Zr, and Zr/Al₂O₃ versus TiO₂/Al₂O₃ biaxial discrimination plots of Müller et al. (1992b). The fresh potassic lamprophyres from the Karinya Syncline are characterized by very high LILE, LREE, and HFSE concentrations, and plot in the fields of within-plate types in Fig. 5.6. This implies that the rocks were generated in a within-plate setting, consistent with previous tectonic interpretations of the area (Preiss 1987).

5.3.6 Precious Metal Abundance and Significance

Potassic igneous rocks are established as being closely related with certain types of gold and base-metal deposits (Mitchell and Garson 1981; Mutschler et al. 1985; Müller and Groves 1993;

Table 5.5 Selected trace-element analyses of lamprophyres from the Karinya Syncline, South Australia

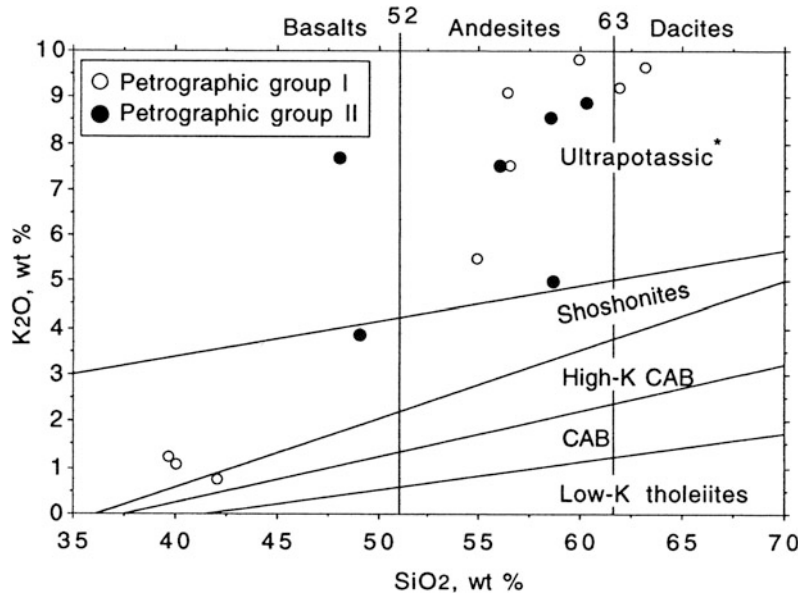
Sample no.	Fresh samples		Altered samples	
	119067	119072	119070	119078
Petrographic group	I	II	I	II
F	4300	5500	4500	n.a.
Li	62	123	62	43
Sc	20	17	33	16
V	587	544	327	502
Cr	70	105	145	100
Co	10	40	55	25
Ni	120	265	345	185
Cu	160	35	65	300
Zn	90	205	155	155
As	13	9	2	2
Rb	575	496	10	411
Sr	614	451	91	740
Y	89	64	36	27
Zr	777	810	165	818
Nb	26	28	11	20
Sb	1.4	2.0	0.2	3.2
Ba	2878	2494	165	2538
La	57.5	51.6	6.9	83.5
Ce	120	100	16	157
Nd	50	40	9	56
Sm	8.9	7.3	2.5	8.8
Yb	3.5	3.4	2.8	1.1
Hf	18	21	3.5	19
W	3.0	1.2	1.7	2.5
Pb	5	59	2	114
Pd	13	9	5	49
Pt	<5	<5	<5	19
Au	12	4	<3	23

Trace elements are in ppm, and precious metals are in ppb. *n.a.* not analyzed. Sample numbers refer to specimens held in the Museum of the Department of Geology and Geophysics, The University of Western Australia. From Müller et al. (1993)

Sillitoe 1997, 2002). Previous work shows that lamprophyres, too, can contain elevated concentrations of precious metals, as discussed above. As documented in Table 5.5, the lamprophyres from the Karinya Syncline contain up to 23 ppb Au, up to 19 ppb Pt, and up to 49 ppb Pd (Müller et al. 1993). These are well above the normal background levels of these elements for

basic igneous rocks, which are commonly less than 2 ppb (Taylor et al. 1994). Figure 5.7 shows that Au enrichment of the South Australian lamprophyres is not decoupled from Cu and Pd peaks in primitive mantle-normalized distribution plots (after Brüggmann et al. 1987), suggesting that the anomalous Au contents are primary features (Wyman and Kerrich 1989).

Fig. 5.5 K_2O versus SiO_2 plot (after Peccerillo and Taylor 1976) showing the potassic or ultrapotassic chemistry of the lamprophyres from the Karinya Syncline, South Australia. * = ultrapotassic, as defined by Foley et al. (1987); CAB = calc-alkaline basalts. From Müller et al. (1993)



The high correlation (>0.6 , <0.9) of the elements Cu, Au, Pd, and Pt is also shown in the correlation matrix for these elements, further supporting a primary precious-metal enrichment of the lamprophyres (Table 5.6). A precious-metal enrichment of the dykes by crustal assimilation during uprise (see Sect. 4.2) is improbable, and enrichment by hydrothermal fluids after their emplacement (see Sect. 8.2) seems unlikely because there is a poor correlation (<0.2) between Au and the pathfinder elements for hydrothermal mineralization (Table 5.6). Thus, the lamprophyres appear to be examples where there is a primary enrichment of precious metals (cf. Rock and Groves 1988a, b; Rock et al. 1988a; Wyman et al. 1995; Wang et al. 2001).

5.4 Comparison of Precious Metal Abundances for Lamprophyres from the Karinya Syncline and Kreuzeck Mountains

This section compares the precious-metal abundances of potassic lamprophyres from the Karinya Syncline, South Australia (Sect. 5.3) with

those from the Kreuzeck Mountains, Eastern Alps, Austria (Sect. 4.2). The Alpine lamprophyres are also characterized by elevated precious-metal concentrations (Table 4.3) but, importantly, these are not primary features, as discussed below.

All lamprophyre samples from the Kreuzeck Mountains, Eastern Alps, were analyzed for Au and PGE using Pb-fire-assay and graphite-furnace atomic-absorption spectroscopy (AAS) techniques at the Institute of Geology, Mining University Leoben, Austria. Samples were prepared for analysis according to the method of Sighinolfi et al. (1984). The detection limit was 3 ppb for Au, 5 ppb for Pt, and 1 ppb for Pd, and the results were checked against a SARM-7 standard.

The Kreuzeck lamprophyres contain up to 27 ppb Au and 19 ppb Pd (cf. Müller et al. 1992a), with one calc-alkaline basaltic dyke containing 34 ppb Au. This can be compared with the 0.5–2.5 ppb Au content that is the typical background level for basic igneous rocks (Taylor et al. 1994; Pitcairn 2011). The Au-bearing samples from the Kreuzeck Mountains are mainly exposed in the central part of the area, where massive sulphides with significant Au and Ag concentrations were mined. The lamprophyres enriched in

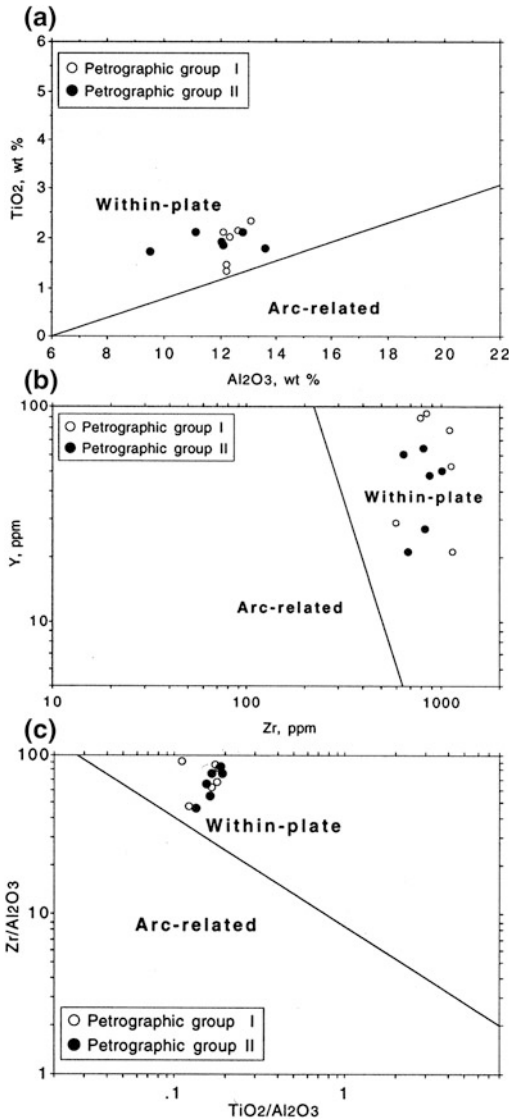


Fig. 5.6 Discrimination diagrams for potassic igneous rocks (see Chap. 3) indicating a within-plate tectonic setting for the investigated lamprophyres. **a** TiO_2 versus Al_2O_3 plot. **b** Y versus Zr plot. **c** Zr/Al_2O_3 versus TiO_2/Al_2O_3 plot. From Müller et al. (1993)

Au normally show Na_2O contents of more than 2.30 wt%, and commonly have high LOI.

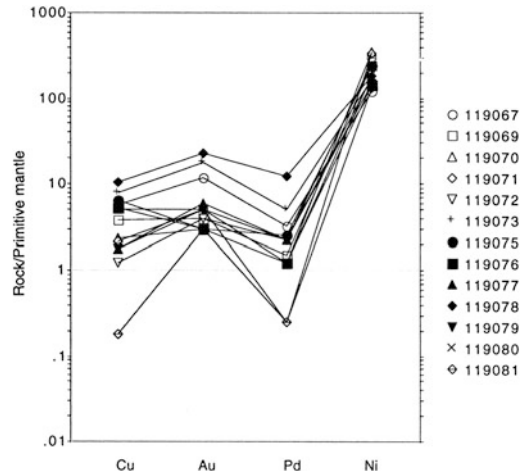


Fig. 5.7 Abundances of chalcophile elements in lamprophyres from the Karinya Syncline, South Australia, relative to primitive mantle. Normalizing factors after Brüggmann et al. (1987)

A Cu versus Au biaxial plot for these rocks (Fig. 5.8) shows no linear correlation between the two elements as would be expected if the magmas had a primary metal enrichment (Taylor et al. 1994). Figure 5.9a, b illustrate that elevated Au values of the dykes are decoupled from Cu, Pt, and Pd values in distribution plots of metal contents normalized to primitive mantle (after Brüggmann et al. 1987), contrasting with data for the lamprophyres from the Karinya Syncline (Fig. 5.7). Again, this suggests that the anomalous Au contents are secondary features (cf. Wyman and Kerrich 1989). Figure 5.9b indicates that the Au concentrations of dykes from the central parts of the Kreuzcek Mountains are slightly higher than those of dykes from the northern and southern parts of the area (Fig. 5.9a). Table 5.7 shows a correlation matrix for precious metals (Au, Pt, Pd), Cu, and pathfinder elements (As, Sb, W) for hydrothermal gold deposits, illustrating the weak correlation between these elements. If the

Table 5.6 Correlation matrix for precious metals (Au, Pd, Pt), Cu, and gold pathfinder elements (As, Sb, W) of lamprophyres from the Karinya Syncline, South Australia

	Cu	Au	Pt	Pd	As	Sb	W
Cu	1						
Au	0.772	1					
Pt	0.730	0.604	1				
Pd	0.786	0.900	0.849	1			
As	-0.140	-0.188	-0.363	-0.254	1		
Sb	0.410	0.136	0.050	0.115	0.316	1	
W	-0.234	-0.238	-0.088	-0.220	0.264	0.117	1

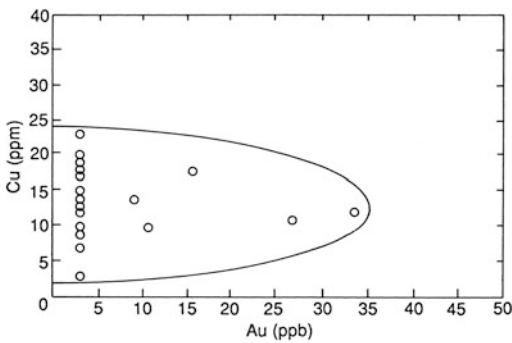


Fig. 5.8 Plot of Cu versus Au for lamprophyres from the Kreuzeck Mountains, Austria

elevated precious-metal contents in some of the lamprophyres were direct enrichments related to hydrothermal gold mineralization, a better correlation between gold and its normal pathfinder elements would be expected. Therefore, the available data support neither a primary magmatic enrichment model nor a hydrothermal enrichment model. Müller et al. (1992a) suggest that, in this case, the high Au and PGE contents are related to assimilation of the Au-enriched massive-sulphide deposits in the area during uprise and emplacement of the lamprophyric magmas.

The above interpretation is consistent with recent studies of shoshonitic lamprophyres from the Hillgrove gold-antimony mining district, New South Wales, Australia (Ashley et al. 1994; Ashley and Craw 2004), where the lamprophyres are enriched in the elements of the mineralization that they cut.

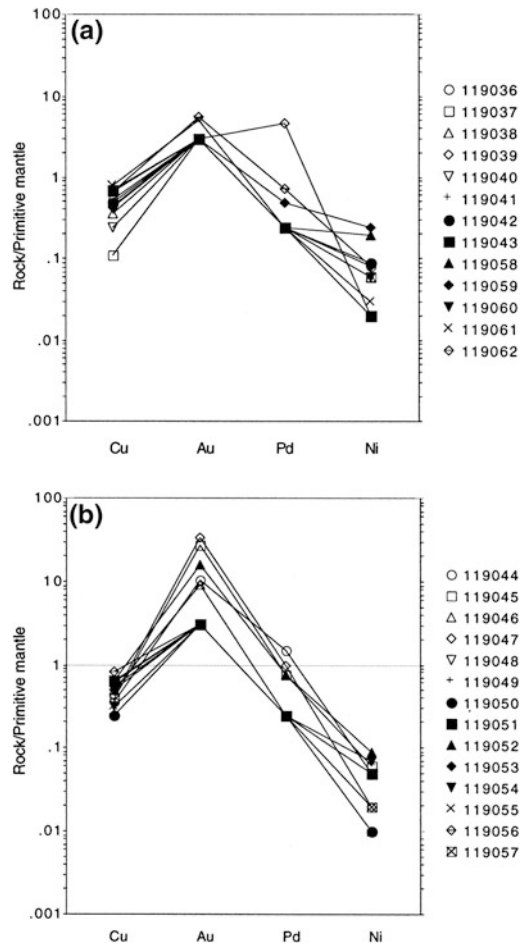


Fig. 5.9 Abundances of chalcophile elements in dykes from the Kreuzeck Mountains, Austria, relative to the primitive mantle. Normalizing values after Brüggmann et al. (1987). **a** Dykes from the northern and southern parts of the area. **b** Dykes from the central part of the area where most former gold mines are located

Table 5.7 Correlation matrix for precious metals (Au, Pd, Pt), Cu, and gold pathfinder elements (As, Sb, W) of dykes from the Kreuzeck Mountains, Austria

	Cu	Au	Pt	Pd	As	Sb	W
Cu	1						
Au	-0.043	1					
Pt	-	-	1				
Pd	0.229	0.142	-	1			
As	0.229	-0.170	-	-0.125	1		
Sb	-0.125	0.519	-	0.022	-0.035	1	
W	-0.028	0.473	-	-0.025	-0.289	-0.138	1

References

- Ashley PM, Craw D (2004) Structural controls on hydrothermal alteration and gold-antimony mineralization in the Hillgrove area, NSW, Australia. *Mineral Depos* 39:223–239
- Ashley PM, Cook NDJ, Hill RL, Kent AJR (1994) Shoshonitic lamprophyre dykes and their relation to mesothermal Au-Sb veins at Hillgrove, New South Wales, Australia. *Lithos* 32:249–272
- Ballhaus C (1993) Redox states of lithospheric and asthenospheric upper mantle. *Contrib Miner Petrol* 114:331–348
- Bergman SC (1987) Lamproites and other potassium-rich igneous rocks: a review of their occurrence, mineralogy and geochemistry. In: Fitton JG, Upton BGJ (eds) *Alkaline igneous rocks*. Geological society, vol 30. London, Geological Society Special Publication, pp 103–190
- Bergman SC, Dunn DP, Krol LG (1988) Rock and mineral chemistry of the Linhaisai minette and the origin of Borneo diamonds, Central Kalimantan, Indonesia. *Can Mineral* 26:23–44
- Bizimis M, Salters VJM, Bonatti E (2000) Trace and REE content of clinopyroxenes from supra-subduction zone peridotites. Implications for melting and enrichment processes in island arcs. *Chem Geol* 165:67–85
- Botcharnikov RE, Linnen RL, Wilke M, Holtz F, Jugo PJ, Berndt J (2011) High gold concentrations in sulphide-bearing magma under oxidizing conditions. *Nat Geosci* 4:112–115
- Brügmann GE, Arndt NT, Hofmann AW, Tobschall HJ (1987) Noble metal abundances in komatiite suites from Alexo, Ontario, and Gorgona Island, Colombia. *Geochim Cosmochim Acta* 51:2159–2169
- Cabri LJ (1981) Platinum-group elements: mineralogy, geology, recovery. *Can Inst Min Metall Spec*, vol 23, p 267
- Campbell IH, Naldrett AJ, Barnes SJ (1983) A model for the origin of the platinum-rich sulphide horizons in the Bushveld and Stillwater complexes. *J Petrol* 24:133–165
- Creaser RA (1996) Petrogenesis of a Mesoproterozoic quartz latite-granitoid suite from the Roxby Downs area, South Australia. *Precamb Res* 79:371–394
- Crocket JH (1979) Platinum-group elements in mafic and ultramafic rocks: a survey. *Can Mineral* 17:391–402
- Deino A, Keith JD (1997) Ages of volcanic and intrusive rocks in the Bingham mining district, Utah. *Econ Geol Guidebook* 29:91–100
- Finlayson EJ, Rock NMS, Golding SD (1988) Deformation and regional carbonate metasomatism of turbidite-hosted Cretaceous alkaline lamprophyres, northwestern Papua New Guinea. *Chem Geol* 69:215–233
- Foden J, Song SH, Turner S, Elburg M, Smith PB, van der Steldt B, van Penglis D (2002) Geochemical evolution of lithospheric mantle beneath S.E. South Australia. *Chem Geol* 182:663–695
- Foley SF, Venturelli G, Green DH, Toscani L (1987) The ultrapotassic rocks: characteristics, classification, and constraints for petrogenetic models. *Earth Sci Rev* 24:81–134
- Greenough JD, Hayatsu A, Papezik VS (1988) Mineralogy, petrology and geochemistry of the alkaline Malpeque sill, Prince Edward Island. *Can Mineral* 26:97–108
- Groves DI, Goldfarb RJ, Gebre-Mariam M, Hagemann SG, Robert F (1998) Orogenic gold deposits: a proposed classification in the context of their crustal distribution and relationship to other gold deposit types. *Ore Geol Rev* 13:7–27
- Gueddari K, Piboule M, Amosse J (1996) Differentiation of platinum-group elements (PGE) and of gold during partial melting of peridotites in the Iherzolitic massifs of the Bético-Rifean Range (Ronda and Beni Bousera). *Chem Geol* 134:181–197
- Guo Z, Wilson M, Zhang M, Cheng Z, Zhang L (2013) Post-collisional, K-rich mafic magmatism in south Tibet: constraints on Indian slab-to-wedge transport processes and plateau uplift. *Contrib Miner Petrol* 165:1311–1340
- Haggerty SE (1990) Redox state of the continental lithosphere. In: Menzies MA (ed) *Continental mantle*. Clarendon Press, Oxford, pp 87–109
- Hallberg JA (1985) *Geology and mineral deposits of the Leonora-Laverton area, northeastern Yilgarn Block, Western Australia*. Hesperian Press, Perth, p 89
- Halter WE, Pettke T, Heinrich CA (2002) The origin of Cu/Au ratios in porphyry-type ore deposits. *Science* 296:1844–1846

- Hamlyn PR, Keays RR, Cameron WE, Crawford AJ, Waldron HM (1985) Precious metals in magnesian low-Ti lavas: implications for metallogenesis and sulphur saturation in primary magmas. *Geochim Cosmochim Acta* 49:1797–1811
- Horn CM, Pain AM, Newton AW (1989) Mineral resources of the Kapunda district council area. South Australian Department of Mines and Energy Report 89/44
- Jaques AL, Lewis JD, Smith CB (1986) The kimberlites and lamproites of Western Australia. *Geol Surv W Austr Bull* 132:121
- Jego S, Pichavant M (2012) Gold solubility in arc magmas: experimental determination of the effect of sulphur at 1000 °C and 0.4 GPa. *Geochim Cosmochim Acta* 84:560–592
- Karsli O, Dokuz A, Kaliwoda M, Uysal I, Aydin F, Kandemir R, Fehr K-T (2014) Geochemical fingerprints of Late Triassic calc-alkaline lamprophyres from the Eastern Pontides, NE Turkey: a key to understanding lamprophyre formation in a subduction-related environment. *Lithos* 197:181–197
- Keays RR (1982) Palladium and iridium in komatiites and associated rocks: application to petrogenetic problems. In: Arndt NT, Nisbet EG (eds) *Komatiites*. Allen and Unwin, London, pp 435–457
- Kesler SE (1997) Metallogenic evolution of convergent margins: selected ore deposit models. *Ore Geol Rev* 12:153–171
- Lewis JD (1987) The geology and geochemistry of the lamproites of the Ellendale Field, West Kimberley Region, Western Australia. Unpl. MSc. thesis, The University of Western Australia, Perth
- Li Y, Audetat A (2013) Gold solubility and partitioning between sulfide liquid, monosulfide solid solution and hydrous mantle melts: implications for the formation of Au-rich magmas and crust-mantle differentiation. *Geochim Cosmochim Acta* 118:247–262
- Maier WD, Barnes SJ, Campbell IH, Fiorentini ML, Peltonen P, Barnes S-J, Smithies RH (2009) Progressive mixing of meteoritic veneer into the early Earth's deep mantle. *Nature* 460:620–623
- Mavrogenes JA, Scaillet B, Pichavant M, England RN (2006) The connection between high-K melts and Au deposits: evidence from natural and experimental systems. *Geochim Cosmochim Acta* 70:A404
- McInnes BIA, McBride JS, Evans NJ, Lambert DD, Andrew AS (1999) Osmium isotope constraints on ore metal recycling in subduction zones. *Science* 286:512–516
- Mitchell RH (1986) *Kimberlites: mineralogy, geochemistry, and petrology*. Plenum Press, New York, p 442
- Mitchell RH, Bergman SC (1991) *Petrology of lamproites*. Plenum Press, New York, p 447
- Mitchell AHG, Garson MS (1981) Mineral deposits and global tectonic setting. Academic Press, London, p 421
- Mitchell RH, Keays RR (1981) Abundance and distribution of gold, palladium and iridium in some spinel and garnet lherzolites: implications for the nature and origin of precious metal-rich intergranular components in the upper mantle. *Geochim Cosmochim Acta* 45:2425–2442
- Morris BJ (1990) Kanmantoo trough geological investigations, Karinya Syncline: Truro lamprophyres. South Australian Department of Mines and Energy Report 91/29
- Muenow DW, Garcia MO, Aggrey KE, Bednarz U, Schmincke HU (1990) Volatiles in submarine glasses as a discriminant of tectonic origin: application to the Troodos ophiolite. *Nature* 343:159–161
- Müller D (2002) Preface—Gold-copper mineralization in alkaline rocks. *Mineral Depos* 37:1–3
- Müller D, Groves DI (1993) Direct and indirect associations between potassic igneous rocks, shoshonites and gold-copper deposits. *Ore Geol Rev* 8:383–406
- Müller D, Stumpfl EF, Taylor WR (1992a) Shoshonitic and alkaline lamprophyres with elevated Au and PGE concentrations from the Kreuzeck Mountains, Eastern Alps, Austria. *Mineral Petrol* 46:23–42
- Müller D, Rock NMS, Groves DI (1992b) Geochemical discrimination between shoshonitic and potassic volcanic rocks from different tectonic settings: a pilot study. *Mineral Petrol* 46:259–289
- Müller D, Morris BJ, Farrand MG (1993) Potassic alkaline lamprophyres with affinities to lamproites from the Karinya Syncline, South Australia. *Lithos* 30:123–137
- Mungall JE (2002) Roasting the mantle: slab melting and the genesis of major Au and Au-rich Cu deposits. *Geology* 30:915–918
- Mutschler FE, Griffin ME, Scott-Stevens D, Shannon SS (1985) Precious-metal deposits related to alkaline rocks in the North American Cordillera—an interpretative view. *Trans Geol Soc S Afr* 88:355–377
- Nadeau O, Williams-Jones AE, Stix J (2010) Sulphide magma as a source of metals in arc-related magmatic hydrothermal ore fluids. *Nat Geosci* 3:501–505
- O'Driscoll EST (1983) Deep tectonic foundations of the Eromanga basin. *Aust Petrol Explor Assessments J* 23:5–17
- Park J-W, Campbell ICH, Kim J, Moon J-W (2015) The role of late sulfide saturation in the formation of a Cu- and Au-rich magma: insights from the platinum group element geochemistry of Niutahi-Motutahi lavas, Tonga rear arc. *J Petrol* 56:59–81
- Paul DK, Crocket JH, Nixon PH (1979) Abundance of palladium, iridium and gold in kimberlites and associated nodules. In: Boyd FR, Meyer HAO (eds) *Kimberlites, Diatremes and Diamonds*. Proceedings of 2nd International Kimberlite Conference, vol 1. American Geophysical Union, Washington, pp 272–279
- Peccerillo A, Taylor SR (1976) Geochemistry of Eocene calc-alkaline volcanic rocks from the Kastamonu area, northern Turkey. *Contrib Miner Petrol* 58:63–81
- Perring CS, Rock NMS, Golding SD, Roberts DE (1989) Criteria for the recognition of metamorphosed or altered lamprophyres: a case study from the Archaean of Kambalda, Western Australia. *Precamb Res* 43:215–237

- Pitcairn IK (2011) Background concentrations of gold in different rock types. *Appl Earth Sci* 120:31–38
- Preiss WV (1987) The Adelaide geosyncline—late proterozoic stratigraphy, sedimentation, palaeontology and tectonics. *Bull Geol Surv S Aust* 53:1–438
- Richards JP (1995) Alkalic-type epithermal gold deposits—a review. In: Thompson JFH (ed) *Magma, fluids, and ore deposits*, vol 23. Mineralogical association of Canada, Toronto, Short Course Handbook, pp 367–400
- Richards JP (2009) Postsubduction porphyry Cu-Au and epithermal Au deposits: products of remelting of subduction-modified lithosphere. *Geology* 37:247–250
- Richards JP (2011) High Sr/Y arc magmas and porphyry Cu±Mo±Au deposits: just add water. *Econ Geol* 106:1075–1081
- Rock NMS (1991) *Lamprophyres*. Blackie, Glasgow, p 285
- Rock NMS, Groves DI (1988a) Do lamprophyres carry gold as well as diamonds? *Nature* 332:253–255
- Rock NMS, Groves DI (1988b) Can lamprophyres resolve the genetic controversy over mesothermal gold deposits? *Geology* 16:538–541
- Rock NMS, Groves DI, Ramsay RR (1988a) Lamprophyres: a girl's best friend? In: Ho SE, Groves DI (eds) *Advances in understanding precambrian gold deposits volume II*, vol 12. Geology Department and University Extension, The University of Western Australia Publication, pp 295–308
- Rock NMS, Hallberg JA, Groves DI, Mather PJ (1988b) Archaean lamprophyres in the goldfields of the Yilgarn Block, Western Australia: new indications of their widespread distribution and significance. In: Ho SE, Groves DI (eds), *Advances in Understanding Precambrian Gold Deposits Volume II*. Geology Department & University Extension, The University of Western Australia Publication, pp 245–275
- Rock NMS, Groves DI, Perring CS, Golding SD (1989) Gold, lamprophyres, and porphyries: what does their association mean? In: Keays RR, Ramsay WRH, Groves DI (eds) *The Geology of gold deposits: the perspective in 1988*. *Econ Geol Monogr* 6:609–625
- Sato M, Wright TC (1966) Oxygen fugacity directly measured in magmatic gases. *Science* 153:1103–1105
- Semiz B, Coban H, Roden MF, Özpınar Y, Flower MFJ, McGregor H (2012) Mineral composition in cognate inclusions in late miocene-early pliocene potassic lamprophyres with affinities to lamproites from the Denizli region, western Anatolia, Turkey: implications for uppermost mantle processes in a back-arc setting. *Lithos* 135:253–272
- Sheppard S, Taylor WR (1992) Barium- and LREE-rich, olivine-mica lamprophyres with affinities to lamproites, Mt. Bunday, Northern Territory, Australia. *Lithos* 28:303–325
- Sighinolfi GP, Gorgoni C, Mohamed AH (1984) Comprehensive analysis of precious-metals in some geological standards by flameless atomic absorption spectroscopy. *Geostand Newsl* 8:25–29
- Sillitoe RH (1997) Characteristics and controls of the largest porphyry copper-gold and epithermal gold deposits in the circum-Pacific region. *Aust J Earth Sci* 44:373–388
- Sillitoe RH (2002) Some metallogenic features of gold and copper deposits related to alkaline rocks and consequences for exploration. *Mineral Depos* 37:4–13
- Stanton RL (1994) Ore elements in arc lavas, vol 29. Clarendon Press, New York, Oxford Monographs in Geology and Geophysics, 391 p
- Sun SS, Wallace DA, Hoatson DM, Glikson AY, Keays RR (1991) Use of geochemistry as a guide to platinum-group element potential of mafic-ultramafic rocks: examples from the western Pilbara and Halls Creek Mobile Zone, Western Australia. *Precamb Res* 50:1–35
- Taubald H, Morteani G, Satir M (2004) Geochemical and isotopic (Sr, C, O) data from the alkaline complex of Grønødal-Ika (South Greenland): evidence for unmixing and crustal contamination. *Int J Earth Sci* 93:348–360
- Taylor WR, Rock NMS, Groves DI, Perring CS, Golding SD (1994) Geochemistry of Archaean shoshonitic lamprophyres from the Yilgarn Block, Western Australia: Au abundance and association with gold mineralization. *Appl Geochem* 9:197–222
- Thomson BP (1969) Precambrian crystalline basement. In: Parkin LW (ed) *Handbook of South Australian geology*. Geological Survey of South Australia, Adelaide, pp 21–48
- Thomson BP (1970) A review of the Precambrian and lower Paleozoic tectonics of South Australia. *Trans Roy Soc S Aust* 94:193–221
- Togashi S, Terashima S (1997) The behavior of gold in unaltered island arc tholeiitic rocks from Izu-Oshima, Fuji, and Osoreyama volcanic areas, Japan. *Geochim Cosmochim Acta* 61:543–554
- Velde D (1975) Armalcolite-Ti phlogopite-diopside-analcite-bearing lamproites from Smoky Butte, Montana. *Am Mineral* 60:566–573
- Venturelli G, Capedri S, Barbieri M, Toscani L, Salvioli-Mariani E, Zerbi M (1991) The Jumilla lamproite revisited: a petrological oddity. *Eur J Mineral* 3:123–145
- Wagner C, Velde D (1986) Lamproites in North Vietnam? A re-examination of cocites. *J Geol* 94:770–776
- Wang J, Qi L, Yin A, Xie G (2001) Emplacement age and PGE geochemistry of lamprophyres in the Laowangzhai gold deposit, Yunnan, SW China. *Sci Chin Ser D* 44:146–154
- Wyman D, Kerrich R (1989) Archaean shoshonitic lamprophyres associated with Superior Province gold deposits: distribution, tectonic setting, noble metal abundances and significance for gold mineralization. In: Keays RR, Ramsay WRH, Groves DI (eds) *The geology of gold deposits: the perspective in 1988*. *Econ Geol Monogr* 6:651–667

- Wyman D, Kerrich R, Sun M (1995) Noble metal abundances of late Archaean (2.7 Ga) accretion-related shoshonitic lamprophyres, Superior Province, Canada. *Geochim Cosmochim Acta* 59:47–57
- Zajacz Z, Seo JH, Candela PA, Piccoli PM, Heinrich CA, Guillong M (2010) Alkali metals control the release of gold from volatile-rich magmas. *Earth Planet Sci Lett* 297:50–56
- Zajacz Z, Candela PA, Piccoli PM, Wälle M, Sanchez-Valle C (2012) Gold and copper in volatile saturated mafic to intermediate magmas: solubilities, partitioning, and implications for ore deposit formation. *Geochim Cosmochim Acta* 91:140–159

6.1 Direct Associations in Specific Tectonic Settings: Introduction

An overview of spatial associations between potassic igneous rocks and gold-copper deposits in the Southwest Pacific area is shown in Fig. 6.1. Examples of direct associations between potassic igneous rocks and copper-gold deposits investigated in this study are, in order of increasing age:

- The Quaternary Ladolam gold deposit, Lihir Island, Papua New Guinea (Wallace et al. 1983; Plimer et al. 1988; Moyle et al. 1990; Dimock 1993; Hoogvliet 1993; Carman 1994, 2003; Müller et al. 2001, 2002a, b; Müller 2003; Simmons and Brown 2006; Blackwell et al. 2014).
- The Tertiary Emperor gold deposit, Viti Levu, Fiji (Gill 1970; Colley and Greenbaum 1980; Anderson and Eaton 1990; Setterfield 1991; Setterfield et al. 1992; Pals et al. 2003; Scherbarth and Spry 2006).
- The Pliocene Grasberg copper-gold deposit, Irian Jaya, Indonesia (Van Nort et al. 1991; McMahon 1994; MacDonald and Arnold 1994; Pollard and Taylor 2002; Pollard et al. 2005).
- The Pliocene Misima gold deposit, Misima Island, Papua New Guinea (Lewis and Wilson 1980; Appleby et al. 1995).
- The Miocene Porgera gold deposit, Papua New Guinea (Handley and Henry 1990; Richards 1990a, b, 1992; Richards et al. 1990, 1991; Ronacher et al. 2002, 2004; Peterson and Mavrogenes 2014).
- The Miocene Bajo de la Alumbrera copper-gold deposit, Catamarca Province, Argentina (Müller and Forrestal 1998; Ulrich et al. 2001; Ulrich and Heinrich 2002; Proffett 2003; Harris et al. 2004a, b, 2006).
- The Miocene Dinkidi copper-gold deposit, Didipio district, Philippines (Haggman 1997a, b; Garrett 1996; Wolfe et al. 1998; Wolfe 2001; Wolfe and Cooke 2011).
- The Miocene El Indio gold deposit, El Indio-Pascua belt, Chile (Siddeley and Arandeda 1986; Jannas et al. 1990; Bissig et al. 2001, 2002, 2003; Deyell et al. 2005).
- The Miocene Skouries copper-gold deposit, Chalkidiki Peninsula, Greece (Magri et al. 1998; Tobey et al. 1998; Kroll 2001; Kroll et al. 2002).
- The Oligocene Cripple Creek gold deposit, Colorado, USA (Lindgren and Ransome 1906; Thompson et al. 1985; Kelley et al. 1998; Kelley and Ludington 2002; Jensen 2003).
- The Eocene Bingham copper-gold deposit, Utah, USA (Lanier et al. 1978a, b; Warnaars et al. 1978; Bowman et al. 1987; Deino and Keith 1997; Waite et al. 1997; Maughan et al. 2002; Redmond et al. 2004; Gruen et al. 2010; Landtwing et al. 2010; Redmond and Einaudi 2010).
- The Cretaceous Peschanka copper-gold deposit, Siberia, Russia (Volkov et al. 2006;

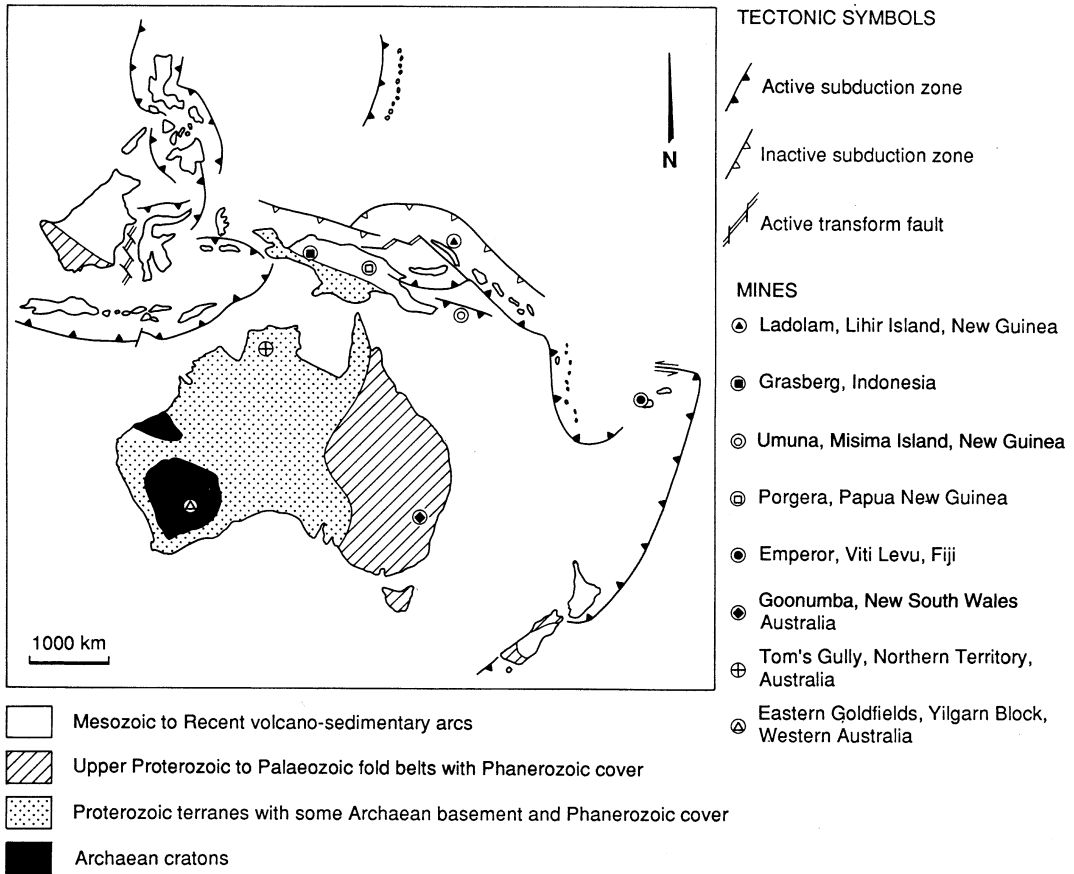


Fig. 6.1 Overview in terms of gross tectonic setting of some major gold and base-metal deposits hosted by potassic igneous rocks in the Southwest Pacific area.

Modified after Müller and Groves (1993). See Fig. 1.1 for a more complete overview of the entire Pacific Rim

- Nagornaya 2010; Chitalin et al. 2012; Bakshev et al. 2013; Marushchenko 2013; Nikolaev et al. 2013, 2014; Soloviev 2014).
- The Devonian Hugo Dummett (Oyu Tolgoi) porphyry copper-gold deposit, Mongolia (Perello et al. 2001; Kavalieris and Wainwright 2005; Kashgerel et al. 2006, 2009; Wainwright et al. 2011; Crane and Kavalieris 2012).
- The Ordovician Ridgeway (Cadia) copper-gold deposit, New South Wales, Australia (Harper 2000; Blevin 2002; Holliday et al. 2002; Wilson et al. 2003, 2007).

- The Ordovician Northparkes (Goonumbla) copper-gold deposit, New South Wales, Australia (Jones 1985; Heithersay 1986; Heithersay et al. 1990; Perkins et al. 1990a, b, 1992; Müller et al. 1994; Heithersay and Walshe 1995; Blevin 2002; Lickfold et al. 2003; Harris and Holcombe 2014).

A database comprising representative petrological and geochemical data from the high-K calc-alkaline and shoshonitic intrusive rocks from these mineralized localities was compiled (GOLD1), and the sources are listed in Tables 6.1 and 6.2. Available samples were

Table 6.1 Some representative major and base-metal deposits associated with potassic igneous rocks through time

Age	Deposit/mineral field	Location	Mineralization	Host rocks	Geochemistry	Alteration	Tectonic setting	References
Pleistocene	Ladolam	Lihir Island, New Ireland Province, Papua New Guinea	Epithermal gold	Monzodiorites, trachybasalts	High LILE	Potassic, argillic, propylitic	Late oceanic arc	Moyle et al. (1990) Carman (1994, 2003) Müller et al. (2001, 2002a, b) Simmons and Brown (2006)
					Low LREE			
					Low HFSE			
Pliocene	Emperor	Viti Levu, Fiji	Epithermal gold	Monzonites, trachybasalts	High LILE	Potassic, propylitic, sericite ± carbonate	Late oceanic arc	Ahmad and Walshe (1990) Setterfield et al. (1991, 1992) Pals et al. (2003) Scherbarth and Spry (2006)
					Low LREE			
					Low HFSE			
Pliocene	Grasberg	Irian Jaya, Indonesia	Porphyry copper-gold	Monzodiorites, monzonites	High LILE	Potassic, propylitic	Postcollisional arc	Van Nort et al. (1991) McMahon (1994) MacDonald and Arnold (1994) Pollard and Taylor (2002), Pollard et al. (2005)
					Low LREE			
					Low HFSE			
Pliocene	Misima	Lousiade Archipelago, Papua New Guinea	Epithermal gold	Lamprophyres	High LILE	Potassic, sericite, propylitic	Postcollisional arc	Appleby et al. (1995)
					Mod. LREE			
					High Nb			

(continued)

Table 6.1 (continued)

Age	Deposit/mineral field	Location	Mineralization	Host rocks	Geochemistry	Alteration	Tectonic setting	References	
Miocene	Porgera	Enga Province, Papua New Guinea	Epithermal gold	Trachybasalts	High LILE	Carbonate, roscoelite	Postcollisional arc	Handley and Henry (1990)	
					Low LREE				Richards (1990a, b, 1992)
					High Nb				
Miocene	Bajo de la Alumbra	Catamarca Province, Argentina	Porphyry copper-gold	Dacites	High LILE	Potassic, sericite, propylitic	Continental arc	Müller and Forrestal (1998)	
					Mod. LREE				Ulrich et al. (2001)
					Low HFSE				
Miocene	Dinkidi	Didipio District, Philippines	Epithermal gold	Monzonites, syenites	High LILE	Potassic, silica-carbonate	Late oceanic arc	Haggman (1997a, b)	
					Low LREE				Wolfe et al. (1998)
					Low HFSE				
Miocene	Skouries	Chalkidiki Province, Greece	Porphyry copper-gold	Monzonites	High LILE	Potassic, sericite, propylitic	Continental arc	Tobey et al. (1998)	
					Low LREE				Kroll (2001)
					Low HFSE				

(continued)

Table 6.1 (continued)

Age	Deposit/mineral field	Location	Mineralization	Host rocks	Geochemistry	Alteration	Tectonic setting	References	
Eocene	Bingham	Utah, USA	Porphyry copper-gold	Monzonites, latites	High LILE	Potassic, sericite, weak propylitic	Continental arc	Lanier et al. (1978a, b)	
					Low LREE				Wamaars et al. (1978)
					Low HFSE				Waite et al. (1997)
Cretaceous	Peschanka	Siberia, Russia	Porphyry copper-gold	Monzonites	High LILE	Potassic, sericite, propylitic	Late oceanic arc	Chitalin et al. (2012)	
					Low LREE			Bakshiev et al. (2013)	
					Low HFSE			Nikolaev et al. (2013, 2014)	
								Soloviev (2014)	
Devonian	Oyu Tolgoi	Mongolia	Porphyry copper-gold	Monzodiorites, monzonites, augite-basalt	High LILE	Potassic, sericite, propylitic	Late oceanic arc	Perello et al. (2001)	
					Low LREE			Kashgerel et al. (2006, 2009)	
					Low HFSE			Wainwright et al. (2011)	
								Crane and Kavalieris (2012)	

(continued)

Table 6.1 (continued)

Age	Deposit/mineral field	Location	Mineralization	Host rocks	Geochemistry	Alteration	Tectonic setting	References
Ordovician	Cadia	New South Wales, Australia	Porphyry copper-gold	Monzonites, latites	High LILE	Potassic, sericite, propylitic	Late oceanic arc	Harper (2000)
					Low LREE			Blevin (2002)
					Low HFSE			Holliday et al. (2002)
								Wilson et al. (2003, 2007)
Ordovician	Northparkes	New South Wales, Australia	Porphyry copper-gold	Monzonites, latites	High LILE	Potassic, sericite, propylitic	Late oceanic arc	Heithersay et al. (1990)
					Low LREE			Müller et al. (1994)
					Low HFSE			Heithersay and Walshe (1995)
								Lickfold et al. (2003)
								Harris and Holcombe (2014)

Table 6.2 Whole-rock data sources for samples in database GOLD1

1. Continental arcs	2. Postcollisional arcs	3. Late oceanic arcs	4. Within-plate settings
<i>El Indio, Chile</i>	<i>Misima, Papua New Guinea</i>	<i>Viti Levu, Fiji</i>	<i>Mount Bunday, Northern Territory, Australia</i>
Bissig et al. (2003) [5]	Appleby (pers. comm., 1996) [5]	Gill (1970) [10] Setterfield (1991) [27]	Sheppard and Taylor (1992) [6]
<i>Bajo de la Alumbraera, Argentina</i>	<i>Porgera, Papua New Guinea</i>		
Müller and Forrester (1998) [4]	Richards (1990a) [6]	<i>Northparkes, NSW, Australia</i>	
	Richards (1990b) [13]	Müller et al. (1994) [3]	
<i>Bingham, Utah, USA</i>	Richards et al. (1990) [4]		
Waite et al. (1997) [3]		<i>Ladolam, Lihir Island, Papua New Guinea</i>	
	<i>Superior Province, Canada</i>	Wallace et al. (1983) [16]	
	Wyman (1990) [20]	Kennecott Exploration (pers. comm., 1992) [2]	
	Wyman and Kerrich (1989) [31]		
		<i>Dinkidi, Didipio, Philippines</i>	
	<i>Yilgarn Block, Western Australia</i>	Wolfe (pers. comm., 1999) [3]	
	Taylor et al. (1994) [18]		
	Univ. of Western Australia (unpubl. data) [15]		

The number in square brackets refers to the number of analyses from that reference in the database. From Müller and Groves (1993)

filtered and geochemical discrimination diagrams developed. The data were plotted on the K_2O versus SiO_2 biaxial diagram of Peccerillo and Taylor (1976a) to illustrate the potassic affinities of the igneous rocks (Fig. 6.2). Rocks from the gold deposits at Emperor, Tom's Gully (Mount Bunday), Ladolam, and Porgera generally show the highest K_2O contents (Fig. 6.2). Mount Bunday is a potassic pluton close to the Tom's Gully gold deposit and both are associated with potassic lamprophyres.

Nearly all of the potassic igneous rocks and shoshonites from mineralized environments investigated in this study are arc-related (cf. Müller and Groves 1993), as illustrated by their geological setting and confirmed by their position

on the TiO_2 versus Al_2O_3 and Y versus Zr biaxial plots (Figs. 6.3 and 6.4). However, spatial associations between some potassic lamprophyres and orogenic gold mineralization, for example at the Tom's Gully deposit in the Proterozoic Pine Creek Geosyncline, Northern Territory, Australia (see Sect. 7.3), are recorded from within-plate tectonic settings as illustrated in Figs. 6.3 and 6.4.

6.2 Erection of Database GOLD1

A new database (GOLD1) has been constructed so that geochemical discrimination diagrams—based on the filtered database SHOSH2—can be applied

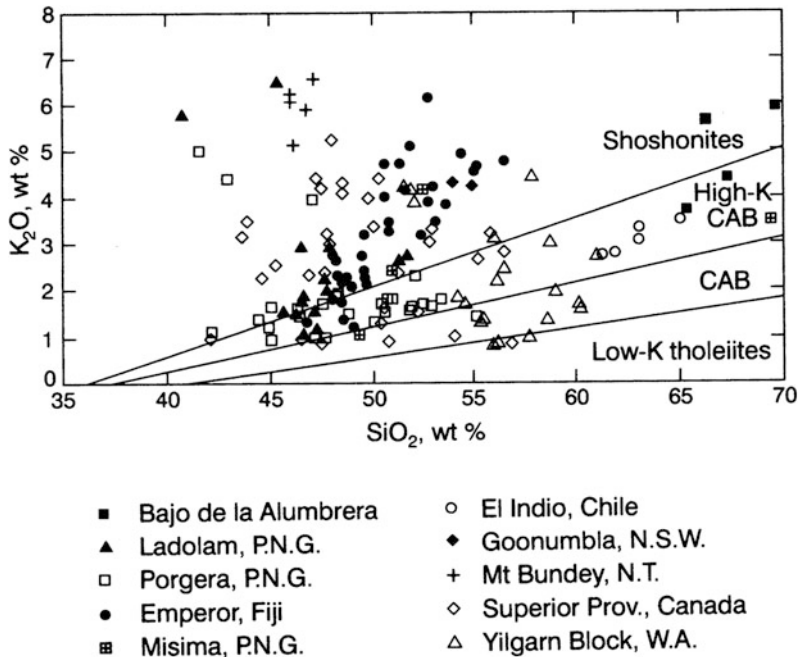


Fig. 6.2 K_2O versus SiO_2 plot (after Peccerillo and Taylor 1976a) showing data from database GOLD1. CAB = calc-alkaline basalts. Adapted from Müller and Groves (1993)

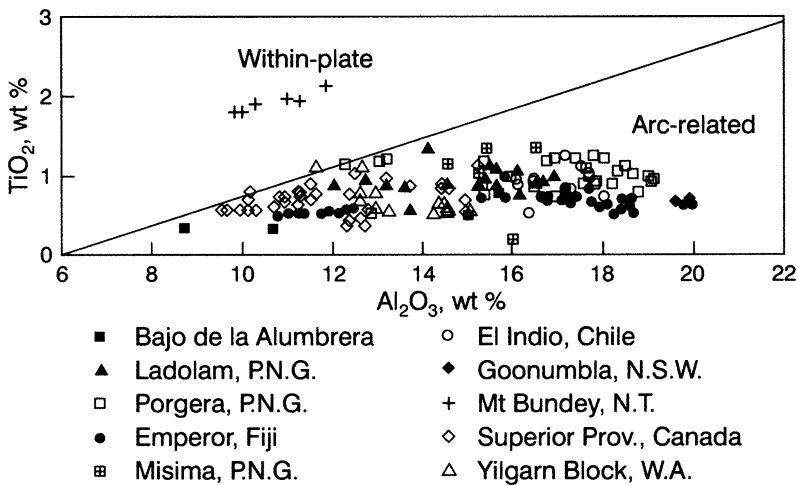


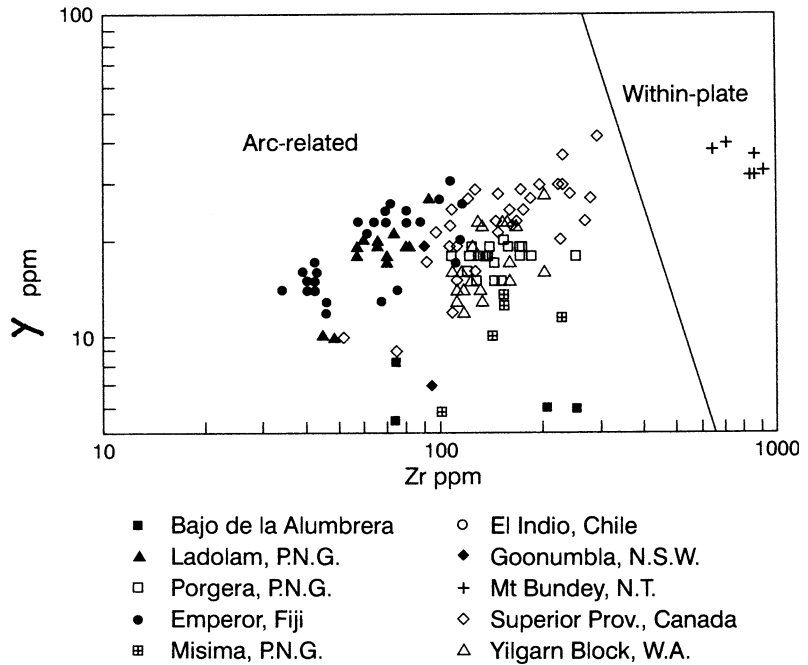
Fig. 6.3 TiO_2 versus Al_2O_3 diagram (see Chap. 3) showing discriminant fields and the position of shoshonitic and potassic igneous rocks associated with gold-copper mineralization. Mount Bunday is the

intrusion adjacent to the Tom's Gully gold deposit, Northern Territory, Australia. Adapted from Müller and Groves (1993)

to mineralized tectonic settings. The database comprises only geochemical data for potassic igneous rocks from mineralized localities such as the Emperor, Ladolam, and Porgera gold deposits,

and major porphyry-copper districts such as the Chilean Andes and the Goonumbla and Cadia areas, Lachlan Fold Belt, as listed in Table 6.2. The data were taken from the literature or derived from

Fig. 6.4 Y versus Zr diagram (see Chap. 3) showing discriminant fields and the position of shoshonitic and potassic igneous rocks associated with gold-copper mineralization. Adapted from Müller and Groves (1993)



analyses undertaken for this study. Using the procedure given in Chap. 3, samples were filtered and discrimination diagrams developed. Although several samples from highly mineralized settings (e.g. Porgera) have high LOI values (i.e. >5 wt%), and slightly higher CaO (up to 2.4 wt%) and Na₂O (up to 5.3 wt%) contents than recommended for the use of the discrimination diagrams, they were left in the database GOLD1.

6.3 Late Oceanic Arc Associations

Generally, the samples from those mineralized arcs described below are characterized by the lowest Zr and Nb concentrations (<110 and <8 ppm, respectively, see Fig. 6.4) and hence are typical of potassic igneous rocks from oceanic arc settings (Chap. 3). Figure 6.5 clearly discriminates them from high-K rocks typical of continental and postcollisional arc settings, which are also characterized by higher Zr and Nb contents (up to 300 ppm and >10 ppm, respectively; see Fig. 6.4). As demonstrated in Fig. 6.6—the

(TiO₂/10)–(10 × La)–(P₂O₅/10) triangular plot of Chap. 3—all mineralized potassic island-arc rocks discussed here are from late oceanic arcs, with the implication that initial oceanic arcs may be barren of gold or base-metal mineralization in association with high-K igneous rocks.

6.3.1 Ladolam Gold Deposit, Lihir Island, Papua New Guinea

Introduction The Southwest Pacific hosts some of the world's premier gold and gold-copper deposits (Andrews 1995). One example is Ladolam, on Lihir Island, which is hosted by Quaternary high-K calc-alkaline rocks (Wallace et al. 1983; Moyle et al. 1990; Carman 1994; Müller et al. 2001). Lihir Island is in the New Ireland Province of Papua New Guinea, and has an area of about 192 km². The island has a rugged and deeply incised topography rising to about 700 m above sea level (Moyle et al. 1990). Lihir Island is one of four volcanic island groups which form an island chain extending for more than 260 km, located to the northeast and subparallel to the

Fig. 6.5 ($\text{TiO}_2/100$)-La-($\text{Hf} \times 10$) triangular diagram (see Chap. 3) discriminating between samples from oceanic arcs (*black symbols*) and those from continental or postcollisional arc settings (*white symbols*). The symbols are the same as in Figs. 6.2, 6.3 and 6.4. Adapted from Müller and Groves (1993)

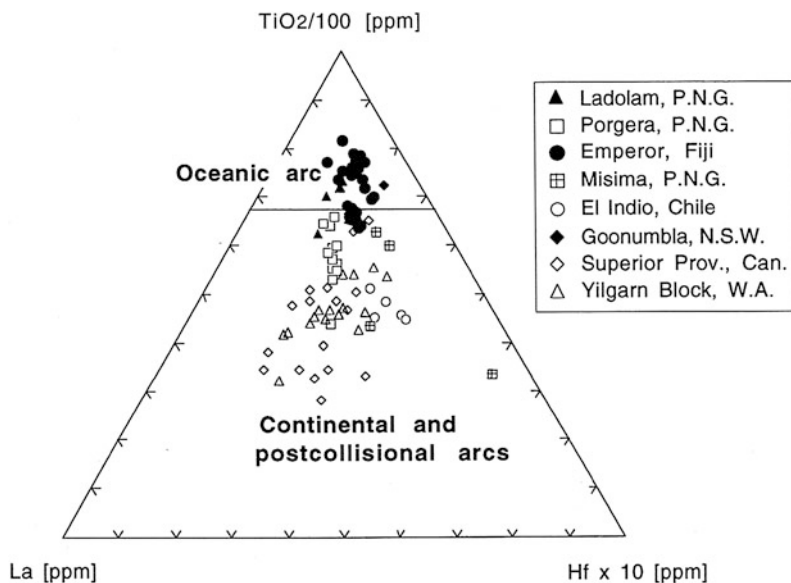
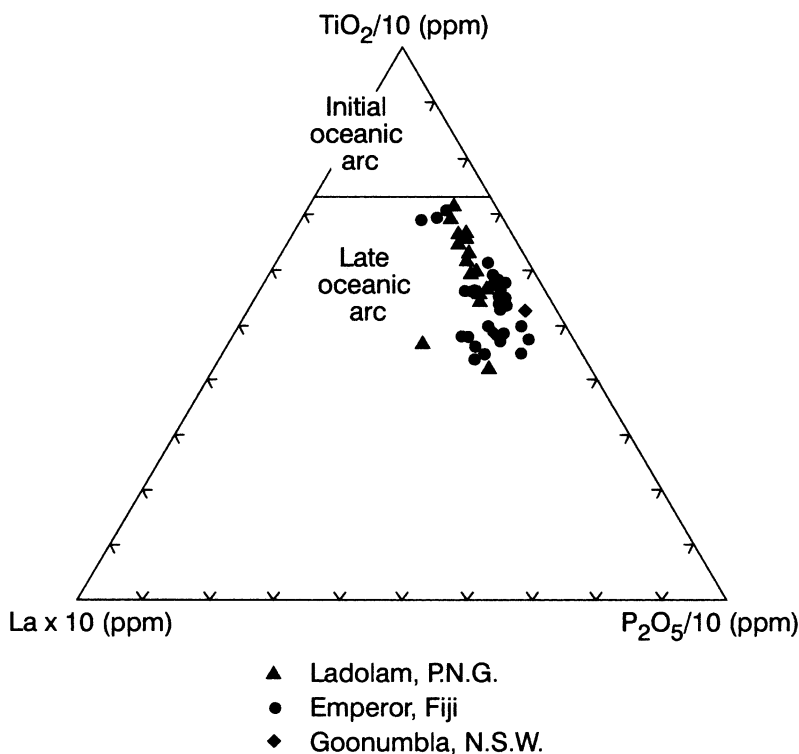


Fig. 6.6 Samples from oceanic arcs (Lihir Island, Viti Levu, Goonumbla) plotted on the ($\text{TiO}_2/10$)-($\text{La} \times 10$)-($\text{P}_2\text{O}_5/10$) triangular diagram (see Chap. 3) suggesting their genesis in a late oceanic arc. From Müller and Groves (1993)



New Ireland coast line (Fig. 6.7). The other islands are Tabar to the northwest and Tanga and Feni to the southeast (Wallace et al. 1983). Volcanic activity started at about 3.6 Ma on Tabar

(Rytuba et al. 1993) and the most recent on-land eruption was recorded on Feni Island about 2300 year ago (Licence et al. 1987). There are a number of small volcanic edifices on the seafloor

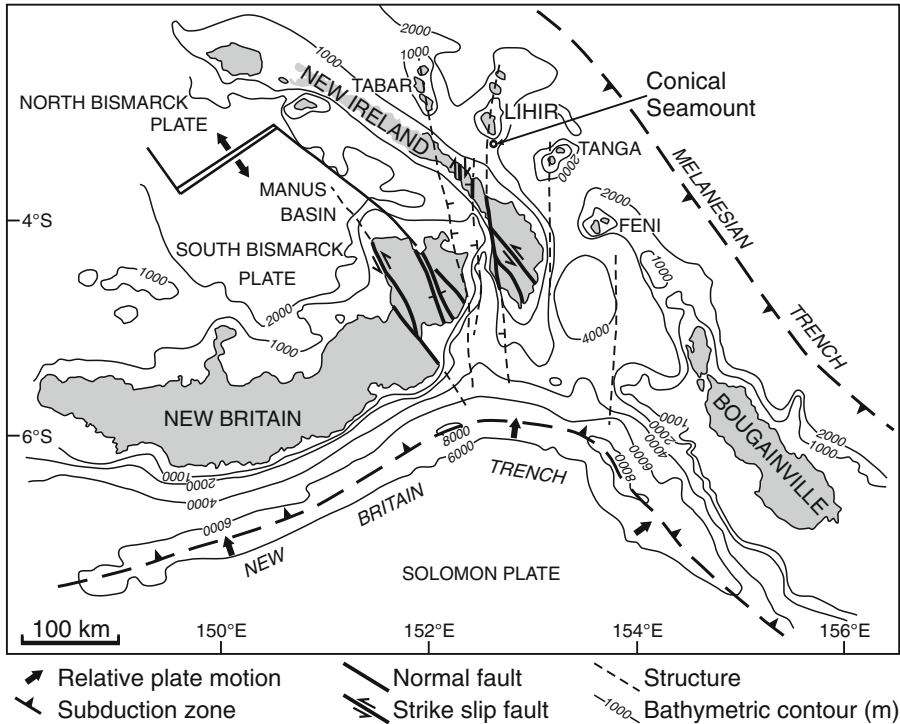


Fig. 6.7 Structural map of the New Britain arc-trench complex, showing major structures and the locations of Lihir Island and Conical Seamount, respectively. Edison

and TUBAF seamounts, which are close together, are located about 20 km southwest of Lihir Island (not shown). Modified after Lindley (1988)

to the south of Lihir Island (Franz et al. 2002; Franz and Romer 2010), the largest of which is called Conical Seamount (Petersen et al. 2002). Conical Seamount (Fig. 6.7) is located about 10 km to the south of Lihir Island (Müller et al. 2003; Gemell et al. 2004). Submarine grab samples from this seamount contain the highest gold concentrations yet reported from the modern seafloor (max. 230 ppm Au, avg. 26 ppm, $n = 40$). The exceptionally large Ladolam gold deposit contains >46 Moz of gold and is located on the east coast of Lihir Island (Fig. 6.8). The deposit was discovered in 1982 by the Kennecott Explorations and Niugini Mining Joint Venture (Hoogvliet 1993).

Regional Geology Lihir Island is composed of Pliocene-Pleistocene alkaline lavas, volcanic breccias, and pyroclastic and epiclastic rocks derived from five volcanoes that dominate the

island (Müller et al. 2001). These are, in chronological order, the Huniho, Wurtol, Luise, Londolovit, and Kinami volcanoes. Whereas the Londolovit and Huniho volcanoes form the northern part of the island, the central part is dominated by the Wurtol and Luise volcanoes and the southern part by Kinami, which represents the youngest volcano on Lihir Island. The volcanic rocks include porphyritic trachybasalts, trachyandesites, latites, and pyroclastic rocks with high K_2O contents (Wallace et al. 1983; Müller et al. 2001). In places, the lavas are intruded by small monzodiorite and monzonite plugs (Müller et al. 2002a).

The Pleistocene Luise stratovolcano consists of an elongate elliptical crater, about 5.5 by 3.5 km, where the northeastern margin has collapsed into the sea. Based on the presence of two overlapping circular demagnetized zones, the

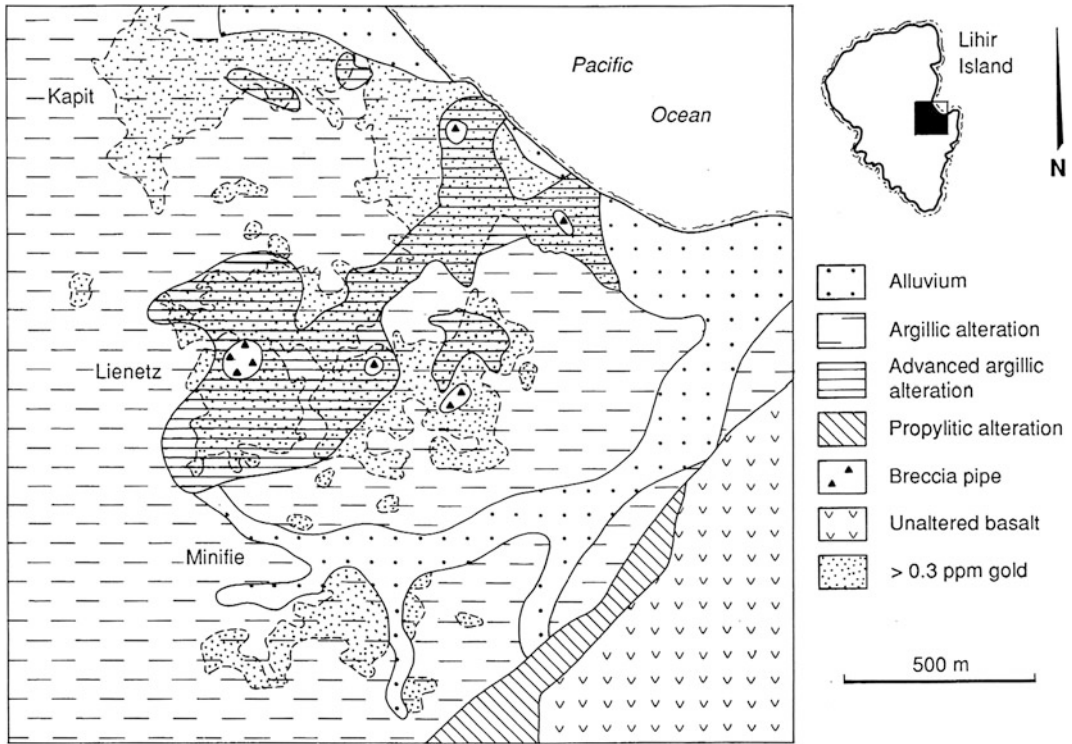


Fig. 6.8 Alteration map of the Ladolam gold deposit, Lihir Island, Papua New Guinea. Modified after Dimock et al. (1993)

volcano probably consisted of two active centers (Komyshan 1999). Extensive diamond drilling indicates that the Luise collapse amphitheatre does not represent a caldera as was suggested by previous workers (e.g. Wallace et al. 1983; Davies and Ballantyne 1987; Moyle et al. 1990). Instead, the feature is interpreted as a partial volcanic slope failure (cf. Lopez and Williams 1993; Voight and Elsworth 1997) of the original stratovolcano. Failure of the northeastern slope of the Luise volcano may have been triggered by an earthquake or by phreatic explosions. The resulting agglomeratic debris avalanche slipped seaward along east-west striking, spoon-shaped, listric faults (Müller et al. 2000b). Lithostatic unloading during this process (cf. Carman 1994) would have led to widespread hydraulic brecciation of the host rocks that were saturated with hydrothermal fluid. These breccias were healed by anhydrite and calcite precipitation at depth (Müller et al. 2002a), a common characteristic of

gold deposits in the Southwest Pacific (R. Sillitoe pers. comm., 2012).

Conical Seamount consists of massive trachybasaltic lava flows, pillows, and talus breccias comprising moderately vesicular fragments and scoria (Müller et al. 2003). The volcano has a basal diameter of about 2.8 km and rises about 600 m above the seafloor to a water depth of 1050 m (Petersen et al. 2002). The seamount is characterized by a small summit plateau extending over 100×200 m and hosting an elongate, 100 m-long and east-west oriented eruptive fissure.

The plate tectonic setting in this area was characterized by the southwestward subduction of the Pacific plate beneath the Melanesian trench and contemporaneous calc-alkaline volcanism on New Ireland (Müller et al. 2001; Franz et al. 2002). About 15 m.y. ago, the southwestward subduction ceased due to the collision of the Ontong-Java plateau with the Kilinailau trench

(Coleman and Kroenke 1981). This resulted in plate rotation and stress relocation. As a consequence, the northward movement of both the Solomon and the Australian plates generated the presently active north-dipping New Britain trench (Fig. 6.7). Back-arc spreading then developed in the Manus basin and separated the Bismarck microplate into northern and southern segments. Partial melting of subduction-modified upper mantle sources beneath Lihir Island was probably triggered by adiabatic decompression melting along deep-seated extensional structures either related to the back-arc rifting of the Manus basin (Taylor 1979) or, more likely, to a north-trending flexure and a resulting slab tear in the subducting Solomon plate (Müller et al. 2002b). Slab tears may play a dominant role in the formation of porphyry copper-gold deposits globally (Logan and Mihalynuk 2014). Abundant north-trending structures have been mapped in the open pit of the Ladolam gold mine and they are referred to as Letomazien structures by Corbett (1999). Several high gold-grade late-stage chalcidony-illite-adularia veins also follow this trend (Corbett et al. 2001). Additionally, Lihir Island lies along a northerly trend of shallow seismicity, which may be related to a fault of similar orientation on New Ireland (Shatwell 1987). The Londolovit, Luise, and Kinami volcanoes as well as Conical Seamount are aligned along a north-south-trending structure (Müller et al. 2002b). Kinks or flexures in the subducting oceanic slab are also interpreted to control the location of other major deposits such as the porphyry copper-gold deposits at Bajo de la Alumbrera, Argentina (Müller and Forrester 1998), Batu Hijau, Sumbawa Island, Indonesia (Kerrick et al. 2000), and the porphyry gold systems of the Maricunga belt, Chile (Vila and Sillitoe 1991).

Nature of Epithermal Gold Mineralization

The Ladolam gold deposit (Fig. 6.8) consists of four orebodies, all of which occupy the center of the extinct Luise volcano: Minifie, Lienetz, Kapit, and Coastal (Moyle et al. 1990; Diemock et al. 1993; Carman 1994). Minifie and Lienetz represent the largest orebodies being separated

by a major fault with a vertical offset in excess of 100 m (Müller et al. 2002b). Mining commenced in late-1997 with two individual open pits exploiting the Minifie and Lienetz orebodies. However, both pits were eventually combined into the large open pit that is currently in operation. Minifie and Lienetz form tabular ore zones covering about 2 km² and extending from the surface to 400 m below sea level (Simmons and Brown 2006). They lie in the middle of a breached crater that formed in response to sector collapse and unroofing of the volcanic edifice about 400,000 years ago (Moyle et al. 1990). The resulting explosive depressurization of the magmatic-hydrothermal system produced a large breccia complex and highly permeable rocks, which now host the ore (Müller et al. 2002a; Simmons and Brown 2006; Blackwell et al. 2014). The Ladolam gold deposit represents a transition from porphyry-style to epithermal mineralization (Carman 1994, 2003; Müller et al. 2002a, b; Blackwell et al. 2014). Three stages of gold mineralization and hydrothermal alteration have been documented at Ladolam (Carman 1994; Müller et al. 2002a, b): (1) an early-stage porphyry gold ± copper system (Fig. 6.9a), (2) a transitional stage between porphyry and epithermal styles (Fig. 6.9b), and (3) an epithermal gold mineralization event (Fig. 6.9c). An early-stage porphyry gold ± copper system is indicated by clasts of strongly potassic-altered monzodiorite and propylitic-altered trachyandesite that are preserved in the abundant breccias (Müller et al. 2002a). These breccias also contain clasts of silicified and potassic-altered monzodiorite with disseminated pyrite ± chalcopyrite and poorly developed pyrite ± quartz stockwork veins (Fig. 6.9a). Additionally, deep exploration drilling under the open pit area intersected monzodiorite intrusions with strong potassic alteration and trachyandesite lavas with strong propylitic alteration. The transitional stage is indicated by poorly sorted, clast-supported heterolithic breccias containing angular to subangular fragments of monzodiorite, trachyandesite, tuffs, minor laminated mudstones, as well as juvenile clasts. The matrix of these breccias (Fig. 6.9b) is normally strongly mineralized with fine-grained

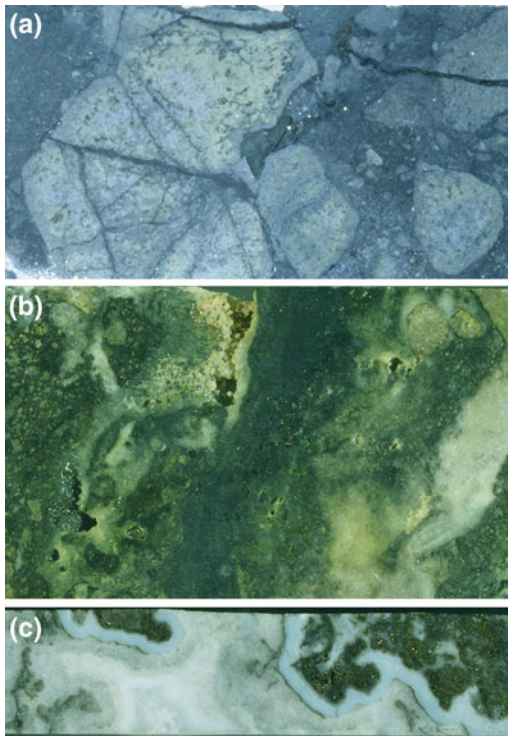


Fig. 6.9 Representative ore samples from the Ladolam gold deposit, Lihir Island, Papua New Guinea (photos taken by D. Müller): **a** hydrothermal breccia containing large clast of silicified and potassic altered monzodiorite with disseminated pyrite \pm chalcopyrite and cut by pyrite \pm quartz stockwork veining (early-stage porphyry-style mineralization) [FOV 4×8 cm]; **b** bulk ore of strongly mineralized and poorly sorted heterolithic hydrothermal breccia containing approximately 20 vol.% of fine-grained auriferous pyrite in the matrix (transitional style) [FOV 4×8 cm]; **c** hydrothermal breccia cut by blue quartz-chalcedony-illite-adularia-pyrite vein (late-stage low-sulphidation epithermal style) [FOV 3×12 cm]

auriferous pyrite (Müller et al. 2002b). The mineralization consists mainly of pyrite with minor marcasite and rare chalcopyrite \pm galena \pm tetrahedrite. The hydrothermal breccias contain uniform gold grades of about 5 g/t and represent the bulk of the ore at Ladolam. Argillic alteration is poorly developed at the Minifie orebody but is well developed in the top parts of the Lienetz, Coastal, and Kapit orebodies (Moyle et al. 1990). The hydrothermal breccias of the transitional stage are cut by late-stage gray to blue quartz-chalcedony-illite-adularia-arsenian pyrite veins (Fig. 6.9c) that may contain isolated

bonanza gold grades of up to 120 g/t (Müller et al. 2002a). Blue and chalcedonic quartz in the late-stage veins is normally fine-grained and has collomorph textures, whereas coarse euhedral dog-tooth quartz is commonly white.

At the deeper levels of the Minifie orebody, the monzodiorites and trachyandesite lavas are brecciated and healed with anhydrite-calcite veins, locally referred to as the “anhydrite seal” (Corbett et al. 2001). The anhydrite-calcite healed breccias are monolithic in composition and, thus, different from the heterolithic breccias which host the bulk mineralization at Ladolam (Müller et al. 2002b).

Ladolam represents a gold resource of about 46 Moz with an average grade of 2.52 g/t (Blackwell et al. 2014) and the hydrothermal system is still geothermally active (Moyle et al. 1990). A number of deep geothermal wells were drilled under the open pit in order to explore the hydrology of the system and to remove hot water from the mine site. The deep well cuttings, containing orthoclase, phlogopite, quartz, magnetite, pyrite, calcite, and anhydrite, indicate a near-neutral pH of 6–7 at hydrothermal conditions (Simmons and Brown 2006). The deep geothermal sulfate-chloride brine thus resembles the ore-forming fluid. It contains high gold concentrations of 13–16 ppb, and except for Sb and Pb, the proportions of Au, Ag, Cu, Mo, Zn, and As match those in the ore (Müller et al. 2002a; Simmons and Brown 2006). Simmons and Brown (2006) estimate an overall gold flux of 24 kg/year, and only about 55,000 years would be required to account for all the known gold in the Ladolam ores assuming a constant aqueous gold concentration and fluid flow (50 kg/s), and 100 % deposition.

Submarine gold mineralization at Conical Seamount is confined to the summit and along its eruptive fissure (Petersen et al. 2002; Müller et al. 2003). Grab samples from the area reveal three mineralization styles: (1) a pyrite stockwork with locally intense clay-silica alteration overprinting trachybasalt, (2) auriferous pyrite-bearing silica veins and disseminated polymetallic sulphides, and (3) a late-stage fracture-filling As-Sb mineralization.

Although Sr isotopic data indicate some involvement of seawater, high-precision lead isotopic measurements conducted with a plasma multi-collector ICP-MS on ores, lavas, and sediments from Lihir Island and Conical Seamount suggest that neither seawater nor the sediments in the area have significantly contributed to the metal budget of the ore at Ladolam and Conical Seamount (Kamenov et al. 2005). The data imply that the ores and lavas from both locations share similar Pb isotopic compositions suggesting that the Pb in both hydrothermal systems was ultimately derived from the alkaline magmas (Kamenov et al. 2005, 2008).

Petrology and Geochemistry of the Potassic Host Rocks The five volcanoes that form Lihir Island consist of a suite of high-K calc-alkaline rocks, mainly trachybasalts, trachyandesites, and latites, which are locally intruded by monzodiorite stocks (Wallace et al. 1983). Several late-stage trachyandesitic and latitic porphyry stocks and dykes have been intersected in drill holes (Moyle et al. 1990). More rarely, phonolites and olivine-clinopyroxene cumulates are recognized (Müller et al. 2002b).

The upper parts of the Luise volcano consist of trachyandesite and latite lavas and related tuffs. The central part of the volcano is dominated by breccias and trachyandesite lavas that are locally cut by hypabyssal monzodiorite stocks. The volcanic rocks have porphyritic textures with phenocrysts of plagioclase, augite, and minor phlogopite and hornblende in a fine-grained feldspathic groundmass (Moyle et al. 1990). A few samples have a very fine-grained or glassy groundmass as in a trachybasalt sample which also contains abundant vesicles (Müller et al. 2001). Hypabyssal monzodiorite intrusions are porphyritic with phenocrysts of plagioclase, brown and/or green hornblende and phlogopite that are set in a medium-grained, quartz-poor, groundmass. Igneous phlogopite contains very high F contents of up to 5.60 wt%. In contrast, hydrothermal biotite is restricted to zones with potassic

alteration and it is characterized by very low F contents (<0.08 wt%), but high Cl concentrations of up to 0.15 wt% (Müller et al. 2001).

The alkaline rocks from Lihir Island (Table 6.3; cf. Müller et al. 2001) range in geochemical composition from primitive to relatively evolved compositions, as reflected by SiO₂ (45.77–54.97 wt%), MgO (1.40–15.30 wt%) contents, and variable concentrations of the mantle-compatible elements (130–328 ppm V, 1–186 ppm Ni). These data are consistent with the wide range of mg# (31–79) that are calculated using an Fe²/(Fe² + Fe³) ratio set at 0.15, common in potassic igneous rocks (cf. Müller et al. 1992b). Most samples are hypersthene-normative, but those samples with the highest total alkali contents (>5.64 wt%) are nepheline-normative (Müller et al. 2001). Previous studies by Kennedy et al. (1990), which suggest that the Luise lavas may be separated into primitive and relatively evolved groups, with two distinct fractionation trends, were not confirmed. For comparison, compositions of samples from the Luise, Huniho, Wurtol, and Londolovit volcanoes as well as Conical Seamount are plotted as MgO versus Al₂O₃ (Fig. 6.10); all samples, including the cumulates, plot along the fractionation trend outlined by the arrow in Fig. 6.10, suggesting that the melts from all volcanoes are related to a single common parental magma, probably derived from an underlying magma chamber (Müller et al. 2003). Note that the three samples with the highest MgO contents are augite-olivine cumulates. They also fall on the fractionation trend.

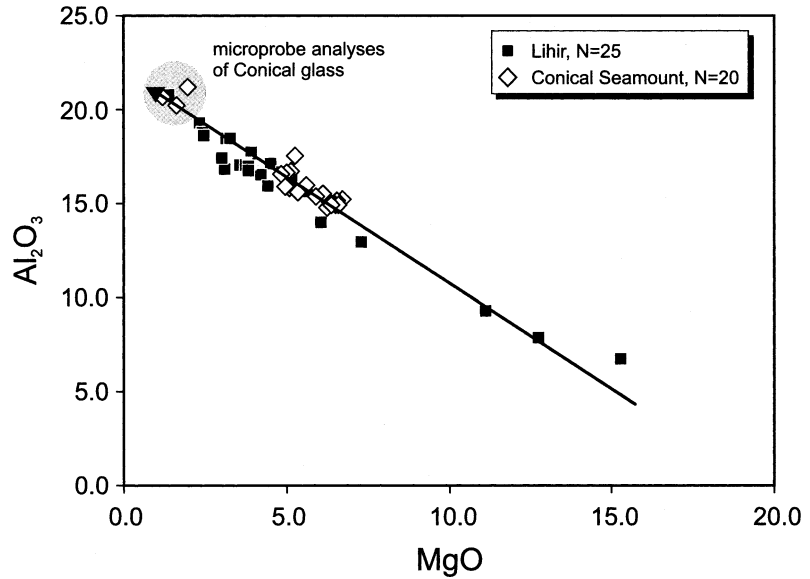
The rocks from Lihir Island are characterized by high K₂O contents (up to 4.68 wt%), high average K₂O/Na₂O ratios (0.8), and high average Ce/Yb ratios (14.1), which are typical of high-K calc-alkaline rocks transitional to shoshonites (Pearce 1982). However, the rocks are not comparable to shoshonites *sensu stricto* (Morrison 1980), as suggested by previous workers (e.g. Moyle et al. 1990). The high LILE (e.g. Rb 186 ppm, Sr 1461 ppm, Ba 760 ppm), low LREE (e.g. La < 20.3 ppm and Ce < 38.4 ppm), and very low HFSE concentrations (e.g.

Table 6.3 Major- and trace-element analyses of potassic igneous rocks from Lihir Island and Conical Seamount, New Ireland Province, Papua New Guinea

Province/deposit	Lihir Island	Lihir Island	Lihir Island	Conical Seamount	Conical Seamount
Location	Papua New Guinea				
Rock type	Monzodiorite	Monzodiorite	Monzodiorite	Trachybasalt	Trachybasalt
Tectonic setting	Late oceanic arc				
Reference	Müller et al. (2001)	Müller et al. (2001)	Müller et al. (2001)	Müller et al. (2003)	Müller et al. (2003)
SiO ₂	51.12	49.08	49.57	47.32	47.75
TiO ₂	1.01	1.10	1.07	0.74	0.73
Al ₂ O ₃	17.08	17.67	16.48	15.58	15.07
Fe ₂ O ₃	10.51	10.32	9.90	5.00	4.24
FeO	n.a.	n.a.	n.a.	4.54	5.57
MnO	0.20	0.21	0.18	0.17	0.18
MgO	4.55	3.94	4.23	5.35	6.34
CaO	8.93	9.05	9.73	11.08	11.63
Na ₂ O	3.02	3.37	3.76	2.24	2.82
K ₂ O	2.75	1.47	1.88	3.31	3.03
P ₂ O ₅	0.36	0.43	0.35	0.42	0.38
LOI	1.00	3.40	3.10	2.98	1.05
Total	100.70	100.23	100.42	98.73	98.79
mg#	46	43	46	51	55
K ₂ O/Na ₂ O	0.91	0.44	0.5	1.5	1.1
Sc	n.a.	n.a.	n.a.	n.a.	n.a.
V	224	296	222	n.a.	n.a.
Co	29	26	27	40	37
Ni	10	4	8	29	33
Rb	48	19	40	51	60
Sr	969	1107	1116	1050	940
Y	27	25	26	19	19
Zr	76	87	87	56	57
Nb	2	3.3	3.3	1.4	1.3
Ba	291	278	270	220	210
La	14.9	15.0	14.2	9.7	9.6
Ce	28.9	29.7	30.0	20	20
Sm	4.6	5.0	4.9	3.8	3.9
Yb	2.30	2.25	2.42	1.6	1.6
Hf	2.0	2.3	2.5	1.5	1.4
Ta	0.1	0.1	0.2	0.09	0.09
Th	1.4	1.3	1.7	0.89	0.85
U	0.6	1.0	1.1	0.69	0.61

The samples from Conical Seamount were dredged during *Sonne* cruise SO133 in 1998. Major elements are in wt%, and trace elements are in ppm. Fe₂O₃ (tot) = total iron for samples from Lihir Island are calculated as ferric oxide. Ferric iron for samples from Conical Seamount is determined using the Wilson method. From Müller et al. (2001) and Müller et al. (2003)

Fig. 6.10 MgO versus Al_2O_3 biaxial diagram showing one single fractionation trend for the potassic igneous rocks from Lihir Island and Conical Seamount. Adapted from Müller et al. (2003)



Zr < 132 ppm, Nb < 4.2 ppm, and Hf < 3.7 ppm) are typical for potassic igneous rocks from oceanic (island)-arc settings (Müller et al. 1992b). The late oceanic (island)-arc affiliation is confirmed by plotting the data on Zr versus Y and La-TiO₂/100-Hfx10 discrimination diagrams (Figs. 6.5 and 6.6).

The lavas from Conical Seamount are defined by geochemically similar, but more primitive compositions (Müller et al. 2003). The rocks have high K₂O contents (up to 3.31 wt%), high average K₂O/Na₂O ratios (1.19), and high average Ce/Yb ratios (13.0), which are characteristic features of potassic igneous rocks transitional to shoshonites (Morrison 1980; Pearce 1982). The elevated LILE (e.g. Rb, Sr, Ba up to 65, 1540, and 320 ppm, respectively), low LREE (e.g. La < 15.0 ppm, Ce < 33.0 ppm), and very low HFSE concentrations (e.g. TiO₂ < 0.83 wt%, Zr < 75 ppm, Nb < 1.7 ppm, and Hf < 2.1 ppm) are typical for potassic igneous rocks from late oceanic (island)-arc settings (Müller et al. 1992b).

Magmatic phlogopites from Conical Seamount have low concentrations of F and Cl (<0.3 wt% and <0.05 wt%) pointing to high H₂O contents of up to 4.1 wt% (Müller et al. 2003).

Elevated oxygen fugacities (Müller et al. 2001, 2003) of 0.7–2.5 log units above the FMQ buffer are recorded for lavas from Conical Seamount, which is quite similar to samples from Lihir Island ($\Delta \log (f_{\text{O}_2})^{\text{FMQ}} = 1.4\text{--}4.8$). This high magma f_{O_2} , as also indicated by abundant igneous magnetite in the rocks from Lihir Island (>5 vol.% magnetite), is a prerequisite for the enrichment of large quantities of gold in arc magmas (Sillitoe 1979; Mungall 2002; Müller 2002b).

6.3.2 Emperor Gold Deposit, Viti Levu, Fiji

Introduction Epithermal gold mineralization in a late oceanic arc setting occurs at the Emperor mine, Viti Levu, Fiji (Fig. 6.11). The mine is located at the northern tip of the main island of Viti Levu, in the Nakaudavadra Mountains about 100 km northwest of Suva and 8 km inland from the coast (Smith et al. 2008). Mineralization is hosted by Pliocene shoshonitic volcanic rocks (Ahmad 1979; Anderson and Eaton 1990; Setterfield 1991; Setterfield et al. 1991, 1992; Pals and Spry 2003; Pals et al. 2003; Scherbarth and Spry 2006; Smith et al. 2008).

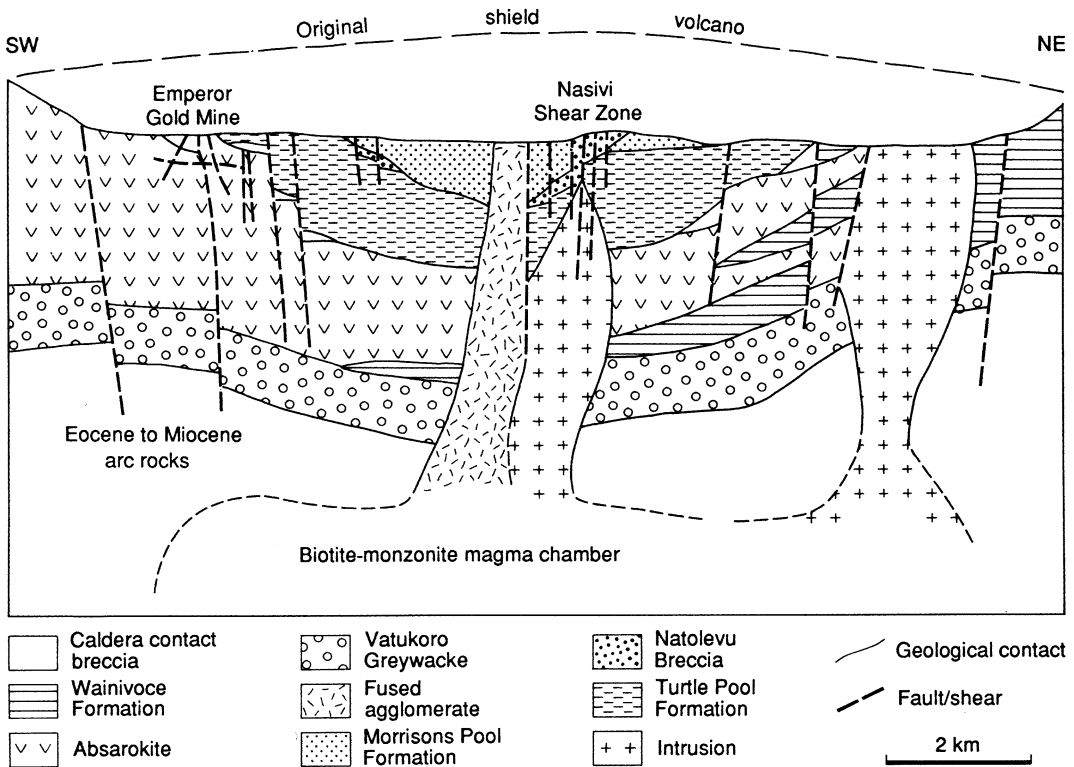


Fig. 6.11 Geological overview of the Emperor gold deposit, Fiji. Modified after Setterfield et al. (1991)

Emperor was 100 % owned and operated as an open pit and underground operation by Emperor Mines Limited until 2006 when the mine was shut down due to low gold prices and the high level of capital required to sustain the mining operation. The mine was later sold to River Diamonds Plc (now re-named to Vatukoula Gold Mines Plc) and re-opened in April 2008. Operating for over 80 years since 1933, the Emperor mine has produced >7 Moz of Au (Smith et al. 2008).

Regional Geology Fiji is situated at the boundary between the Indo-Australian and Pacific plates, midway between the west-dipping Tonga-Kermadec Trench and the east-dipping Vanuatu Trench (Gill and Whelan 1989). Magmatism in Fiji is largely derived from subduction along the now-inactive Vitiaz Trench (Setterfield et al. 1992).

Viti Levu was formed during three periods of volcanism, with the igneous rock series erupted, in order, from tholeiites, to calc-alkaline, and finally shoshonitic rocks (Gill 1970; Setterfield 1991; Pals et al. 2003; Scherbarth and Spry 2006).

The Emperor deposit supports the country's largest operating gold mine and is located in northern Viti Levu at the caldera margin of a Tertiary shoshonitic shield volcano (Anderson and Eaton 1990). The second gold mine in Fiji is the Tuvatu gold-silver telluride deposit with reserves of about 13 t Au (Scherbarth and Spry 2006). The Emperor gold deposit is situated at the intersection of a northwest-trending shear zone with a major, 250 km long, northeast-trending lineament (Setterfield et al. 1991) that also controls the Tuvatu gold deposit, located about 50 km to the southwest (Scherbarth and Spry 2006). Both gold deposits are

genetically related to monzonite intrusions with almost identical ages (5.4–4.6 Ma) and shoshonitic affinities (Scherbarth and Spry 2006). The Emperor deposit occurs along the margins of the shoshonitic Tavua shield volcano, whereas the Tuvatu deposit occurs adjacent to an eroded shoshonitic volcano.

Nature of Epithermal Gold Mineralization

Gold mineralization in Fiji includes various types of volcanogenic massive-sulphide (VMS) deposits, disseminated porphyry copper-gold deposits and epithermal gold-tellurium-silver deposits, most of which are associated with high-K calc-alkaline and shoshonitic rocks (Colley and Greenbaum 1980). Low-sulphidation epithermal gold telluride and auriferous pyrite mineralization occurs in flat-lying quartz-sericite \pm carbonate veins, steep faults, shatter zones, stockworks, and hydrothermal breccias at the western flank of the Tavua Caldera (Setterfield et al. 1992; Pals and Spry 2003), a similar mineralization style as documented at the Tuvatu gold deposit (Scherbarth and Spry 2006). The unusually high Au content of Te-bearing arsenian pyrite at Emperor is probably due to the presence of lamellae of Au-bearing marcasite and arsenopyrite (Pals et al. 2003). Epithermal gold mineralization is accompanied by propylitic alteration (Setterfield et al. 1992) and, in places, potassic alteration of the host rocks (Ahmad and Walshe 1990; Anderson and Eaton 1990; Pals et al. 2003). Mineralization in both deposits formed in multiple stages and is characterized by the presence of quartz-roscoelite telluride veins in which gold-rich tellurides were deposited prior to silver-rich tellurides (Scherbarth and Spry 2006). Gold tellurides and vanadium micas were deposited at approximately 250 °C from moderately saline fluids. ^{40}Ar - ^{39}Ar dating indicates that epithermal gold mineralization at Emperor was formed at 3.71 ± 0.13 Ma, whereas shoshonite emplacement and the less important porphyry-style mineralization were earlier at ca. 4.3 Ma (Setterfield 1991). Oxygen and hydrogen isotope compositions of ore fluids at Emperor and Tuvatu are similar to the

composition of waters exsolved from arc magmas (Scherbarth and Spry 2006). The isotopic $\delta^{34}\text{S}$ values of sulphides from Emperor (-20.3 to $+3.9$ ‰) are similar to those obtained from the Tuvatu deposit (-15.3 to -3.2 ‰) and indicate, along with mineral assemblages, that the hydrothermal fluids were oxidizing (Pals et al. 2003; Scherbarth and Spry 2006). Both stable isotope and fluid inclusion studies suggest that the gold mineralization and potassic alteration were produced by ascending magmatic fluids mixed with heated meteoric waters (Ahmad and Walshe 1990; Anderson and Eaton 1990; Kwak 1990), with the magmatic source being a high-K monzonite stock at depth (Ahmad 1979; Pals and Spry 2003).

Petrology and Geochemistry of the Shoshonitic Host Rocks The trachybasaltic host rocks at Emperor have a shoshonitic geochemistry and consist of plagioclase, augite, and olivine phenocrysts, with minor biotite and hornblende, in a fine-grained feldspathic groundmass (Gill 1970; Ahmad and Walshe 1990; Setterfield et al. 1991; Scherbarth and Spry 2006). Magma evolution was controlled solely by fractional crystallization of titanomagnetite, olivine, clinopyroxene, and plagioclase (Setterfield 1991). All volcanic rocks plot in the late oceanic-arc magma series on Figs. 6.5 and 6.6.

Fractional crystallization resulted in low concentrations of mantle-compatible trace-elements (e.g. <198 ppm V, <11 ppm Cr, <6 ppm Ni). The rocks (Setterfield 1991) which are highly potassic (up to 6.13 wt% K_2O , and high $\text{K}_2\text{O}/\text{Na}_2\text{O}$ ratios of up to 2.04), also contain high concentrations of Al_2O_3 (up to 19.71 wt%) and Na_2O (up to 3.69 wt%). Their trace-element composition (Table 6.4), is characterized by very high LILE (e.g. up to 142 ppm Rb, up to 1812 ppm Sr, up to 1209 ppm Ba), moderate LREE (e.g. ~ 20 ppm La, ~ 40 ppm Ce), and very low HFSE (e.g. <0.60 wt% TiO_2 , <23 ppm Y, <87 ppm Zr, <4 ppm Nb, ~ 2 ppm Hf) contents, which are typical for shoshonitic rocks derived in a late oceanic-arc setting (Müller et al. 1992b).

Table 6.4 Major- and trace-element analyses of shoshonitic rocks from the Emperor gold deposit, Fiji

Province/deposit	Emperor	Emperor
Location	Fiji	Fiji
Rock type	Trachybasalt	Trachybasalt
Tectonic setting	Late oceanic arc	Late oceanic arc
Reference	Setterfield (1991)	Setterfield (1991)
SiO ₂	51.29	52.73
TiO ₂	0.60	0.54
Al ₂ O ₃	17.87	19.71
Fe ₂ O ₃	7.92	6.29
FeO	n.a.	n.a.
MnO	0.17	0.15
MgO	3.15	1.98
CaO	6.51	5.84
Na ₂ O	3.69	3.00
K ₂ O	4.70	6.13
P ₂ O ₅	0.53	0.48
LOI	3.18	2.73
Total	99.61	99.58
mg#	48	42
K ₂ O/Na ₂ O	1.27	2.04
Sc	n.a.	n.a.
V	198	146
Cr	11	3
Ni	6	2
Rb	142	105
Sr	1571	1812
Y	21	23
Zr	85	87
Nb	2	4
Ba	1209	1145
Hf	2	2.1
La	23	18
Ce	39	34

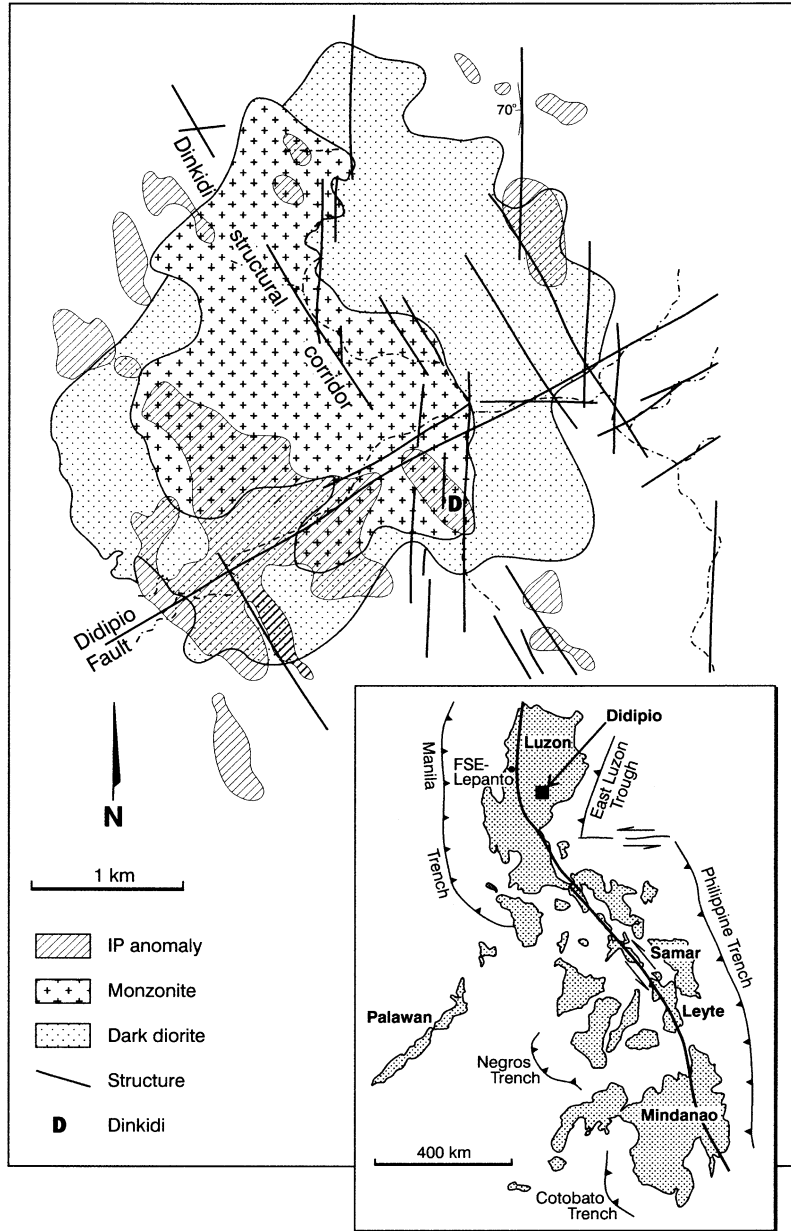
Major elements are in wt%, and trace elements are in ppm. Fe₂O₃ (tot) = total iron calculated as ferric oxide. From Setterfield (1991)

6.3.3 Dinkidi Copper-Gold Deposit, Didipio, Philippines

Introduction The Philippines are well endowed with porphyry copper-gold deposits (Sillitoe and Gappe 1984). The Philippines are a collage of tectonic elements, and porphyry-style deposits

have formed in discrete provinces within this collage at various times since the Cretaceous (Sillitoe and Gappe 1984). The Dinkidi porphyry copper-gold deposit is located in the Didipio area (Fig. 6.12) about 270 km north of Manila, at an elevation of 700 m above sea level, in the remote Sierra Madre Mountains of the Nueva Vizcaya

Fig. 6.12 Geological overview of the Dinkidi copper-gold deposit, Didipio, Philippines. Modified after Haggman (1997b) and Wolfe et al. (1998)



Province of northern Luzon, Philippines (Haggman 1997a; Wolfe et al. 1998). Access to the site is via logging roads from Cabarroguis (Garrett 1996). The region was mined for alluvial gold for many years, as Dinkidi forms a razorback ridge protruding from an alluvial valley floor (Haggman 1997a). On the ridge there are narrow quartz-stockwork veins and zones with argillic

alteration, which overprints monzodioritic to monzonitic intrusions (Haggman 1997a; Wolfe 2001). Systematic exploration of the ridge surface revealed abundant copper-oxide minerals. A 300 m by 500 m-wide anomaly was identified by a subsequent IP survey, and diamond drilling intersected porphyry copper-gold mineralization (Haggman 1997a). Detailed geological mapping

of the area suggests that Dinkidi forms part of a monzonitic caldera complex measuring about 8 km in diameter (Haggman 1997b).

Dinkidi was discovered in 1988 during a systematic soil sampling program by Climax Arimco Corporation when following up on an aeromagnetic anomaly. In 2006, Climax Mining merged with the much larger New Zealand-based OceanaGold Corporation which brought the mine into production in April 2013 and is the current operator. Dinkidi is a combined open pit and underground operation and, over its projected 16-year mine life, will produce about 100,000 oz of Au and 14,000 t of Cu annually. The Dinkidi deposit consists of a measured and indicated resource of about 2.06 Moz of Au and 272.4 Kt of Cu (McIntyre et al. 2010), including a high-grade zone of 7.9 million tonnes at 6 ppm Au equivalent (Haggman 1997b). Oxidized ore represents only three percent of the total resource.

Regional Geology The Didipio area consists of late-Cretaceous to mid-Miocene volcanosedimentary and volcanoclastic rocks that were derived in an oceanic (island) arc setting (Haggman 1997a; Wolfe 2001).

Dinkidi is thought to be related to the change from Miocene westward subduction along the northern Luzon Trench to eastward subduction along the Manila Trench (Corbett and Leach 1998). Dinkidi occurs in a back arc basin that trends north-south along the Cagayan Valley (Haggman 1997b). The Didipio Igneous Complex represents several potassic igneous intrusions that are localized by the intersection of east-northeast-trending transfer structures with north-northwest fractures parallel to the Philippine Fault (Haggman 1997b).

Stratigraphically, the Didipio area is formed by a pre-Tertiary basement complex of tonalites and schists, which are covered by Eocene andesitic lavas and basaltic tuffs interlayered with sedimentary rocks (Haggman 1997b). This Eocene Caraballo Group is unconformably overlain by the Late Oligocene Mamparang Formation, which comprises high-K calc-alkaline

to shoshonitic lavas and related volcanoclastic rocks that have been intruded by the early-Miocene Didipio Igneous Complex (Wolfe et al. 1998; Wolfe and Cooke 2011).

The Didipio Igneous Complex consists of a series of early clinopyroxene cumulates, diorites, and monzodiorites that were intruded by a large, composite monzonite pluton (Wolfe et al. 1998; Wolfe 2001). The Dinkidi deposit is hosted by a large, 800 m by 200 m wide, elongate biotite- and amphibole-phyric monzonite stock and a thin diopside-phyric syenitic pegmatite dyke at the southern margin of this composite monzonite pluton (Wolfe 2001). The syenite pegmatite is interpreted to represent a volatile-rich late-stage felsic differentiate from the monzonitic magma (Wolfe et al. 1998). Recent studies suggest that these intrusions are broadly co-magmatic and both the monzonite porphyry stock and the syenite pegmatite host the bulk of the quartz stockwork mineralization at Dinkidi (Wolfe 2001; Wolfe and Cooke 2011).

Nature of Porphyry Copper-Gold Mineralization Emplacement of the monzonite porphyry was temporally and spatially associated with pervasive biotite-magnetite-orthoclase alteration, while the pegmatite emplacement was accompanied by a diopside-actinolite-orthoclase alteration assemblage (Wolfe and Cooke 2011). Both intrusions host an intense quartz-chalcopyrite-bornite vein stockwork, including A-type and B-type veins.

The alteration intensity varies broadly throughout the deposit (Garrett 1996). The deep core of the porphyry system is characterized by an intense whitish clay-carbonate-muscovite-silica-sericite alteration, which overprinted the monzonite porphyry. The alteration is accompanied by weak disseminations of magnetite-pyrite-chalcopyrite and, more rarely, fine veinlets of quartz-pyrite-chalcopyrite (Garrett 1996). This alteration type grades vertically upward into a potassic alteration assemblage (Garrett 1996; Wolfe 2001). Within the potassic alteration zone, the plagioclase phenocrysts are typically altered to white sericite-clay-carbonate assemblages,

whereas the groundmass fraction is flooded by pinkish-grey orthoclase (Garrett 1996). The potassic alteration at Dinkidi is dominated by secondary orthoclase (Corbett and Leach 1998). The less abundant clinopyroxene, biotite, and amphibole phenocrysts of the monzonite porphyry are weakly altered to chlorite-magnetite assemblages (Garrett 1996; Wolfe 2001).

The principal copper-sulphides are chalcopyrite and, to a lesser extent, bornite, and they commonly occur as fine disseminations and within quartz stockwork veins (Haggman 1997b; Wolfe 2001; Wolfe and Cooke 2011). Bornite occurs as alteration rims around and within chalcopyrite grains (Haggman 1997b). Native gold occurs as inclusions within chalcopyrite and, less commonly, within bornite. Native gold and electrum are rare inclusions in silicates (Garrett 1996; Wolfe 2001).

High-grade porphyry copper-gold mineralization (>1 wt% Cu, >3 ppm Au) is either associated with potassic alteration (Wolfe and Cooke 2011) or occurs within the silica-carbonate-epidote-chalcopyrite zone surrounding the core of the deposit (Haggman 1997b). Outside the potassic alteration zone, the grades are commonly lower (Garrett 1996).

In places, hydrothermal brecciation overprints the potassic alteration zone. These small hydrothermal breccias generally contain the highest copper-gold grades due to remobilization of these metals and their concentration within the breccia matrix (Garrett 1996; Wolfe 2001). The hydrothermal brecciation is consistent with the high volatile contents of the parental melts (cf. Kamenetsky et al. 1999).

The porphyry copper-gold mineralization is interpreted to be genetically related to the late-stage release of volatiles and monzonitic melt from the fractionating magma chamber beneath the caldera. The fractal nature of the biotite- and hornblende-phyric monzonite porphyry and the syenite pegmatite is consistent with the release of increasingly more-evolved melt fractions from a larger magma chamber at depth (Wolfe 2001).

Dinkidi has several similarities with the Cadia and Northparkes porphyry copper-gold deposits

in New South Wales, Australia (Sects. 6.3.4 and 6.3.5). All three deposits are hosted by porphyritic monzonite intrusions that represent the late-stage melts derived from an underlying crustal magma chamber. At all three deposits, the monzonites have high-K calc-alkaline to shoshonitic compositions and are interpreted to have formed in late oceanic arcs.

Petrography and Geochemistry of the Potassic Host Rocks

The mineralized monzonite porphyry is a pinkish-grey, medium-grained, intrusive rock consisting of phenocrysts of plagioclase, clinopyroxene, biotite, and hornblende, which are set in a holocrystalline granular feldspathic groundmass (Garrett 1996; Wolfe 2001). The monzonite also contains apatite microphenocrysts. The rock has a vughy texture, but is intensely and pervasively biotite-magnetite altered. In places, its groundmass is flooded by hydrothermal orthoclase (Garrett 1996). The vughy relic texture is interpreted to reflect the volatile-rich nature of the parental melt (Wolfe 2001), a common feature of most porphyry copper-gold deposits hosted by potassic igneous rocks. The syenite pegmatite forms a thin, 2–30 m-wide, intrusion composed mainly of K-feldspar, plagioclase, and clinopyroxene, with accessory apatite, magnetite, and titanite (Kamenetsky et al. 1999; Wolfe 2001). The pegmatite dyke displays remarkable textural variation, from equigranular intergrowths of clinopyroxene and perthite to coarsely (2–5 cm) clinopyroxene-phyric porphyries with a mosaic-textured perthitic groundmass (Kamenetsky et al. 1999; Wolfe 2001). Detailed studies on fluid and melt inclusions derived from the syenitic pegmatite confirm the high volatile contents of the parental melt (Kamenetsky et al. 1999; Wolfe 2001).

Table 6.5 shows representative whole-rock analyses of the potassic igneous rocks from the Didipio Igneous Complex (Wolfe 2001). The rocks are characterized by enriched LILE concentrations (e.g. up to 4.38 wt% K₂O; up to 79 ppm Rb, 1005 ppm Sr, 1100 ppm Ba), low LREE contents (e.g. <15 ppm La, <29 ppm Ce),

Table 6.5 Major- and trace-element analyses of potassic igneous rocks from the Dinkidi copper-gold deposit, Didipio, Philippines

Province/deposit	Dinkidi	Dinkidi	Dinkidi
Location	Philippines	Philippines	Philippines
Rock type	Monzodiorite	Monzonite	Qtz-monzonite
Tectonic setting	Late oceanic arc	Late oceanic arc	Late oceanic arc
Reference	Wolfe (2001)	Wolfe (2001)	Wolfe (2001)
SiO ₂	51.81	57.55	61.40
TiO ₂	0.65	0.45	0.37
Al ₂ O ₃	18.66	18.29	19.19
Fe ₂ O ₃	8.28	5.44	4.11
MnO	0.19	0.13	0.07
MgO	3.86	2.09	1.40
CaO	9.54	5.65	2.97
Na ₂ O	3.75	4.87	5.58
K ₂ O	2.57	4.13	4.38
P ₂ O ₅	0.46	0.37	0.23
LOI	0.23	0.76	0.99
Total	100.01	99.73	100.69
mg#	52	47	44
K ₂ O/Na ₂ O	0.68	0.85	0.78
Cr	6	3	2
Ni	7	3	1
Rb	49	70	79
Sr	1005	872	864
Y	20	18	13
Zr	66	100	72
Nb	1.5	1.9	1.7
Ba	502	484	1100
La	11	15	9
Ce	24	29	20
Yb	2.0	1.8	1.3

Major elements are in wt%, and trace elements are in ppm. Fe₂O₃ (tot) = total iron calculated as ferric oxide. Data from Wolfe (2001)

and very low HFSE abundances (e.g. TiO₂ < 0.65 wt%, <100 ppm Zr, <20 ppm Y, <2 ppm Nb). Fractional crystallization resulted in low mg# (<52), and very low concentrations of mantle-incompatible trace-elements (e.g. <6 ppm Cr, <7 ppm Ni). The rocks have elevated P₂O₅

concentrations (up to 0.46 wt%), consistent with the presence of apatite microphenocrysts (Kamenetsky et al. 1999; Wolfe 2001).

The samples have not been plotted on geochemical discriminant diagrams due to a lack of Hf analyses. However, based on their

geochemical compositions, the rocks are interpreted to be derived in a late oceanic-arc setting (Müller et al. 1992b).

6.3.4 Northparkes (Goonumbla) Copper-Gold Deposit, New South Wales, Australia

Introduction In the Lachlan Fold Belt of southeastern Australia, porphyry copper-gold deposits are associated with a compositional variety of Ordovician igneous rock suites, in contrast to voluminous later Silurian-Devonian and Carboniferous magmatism, which as a group is dominantly associated with W, Sn and Mo mineralization (Blevin and Chappell 1992, 1995; Blevin 2002). An example of ancient mineralization hosted by shoshonitic rocks in a late oceanic-arc setting is the Ordovician Goonumbla porphyry copper-gold deposit in New South Wales, Australia (Heithersay et al. 1990; Müller et al. 1994; Heithersay and Walshe 1995; Hooper et al. 1996; Blevin 2002; Lickfold et al. 2003). It is described in some detail here because many of the primary data were collected specifically for this study (cf. Müller 1993). The Goonumbla igneous complex is situated within a collapsed caldera and hosts the world-class Northparkes copper-gold mine. This igneous suite forms one of several mineralized Ordovician shoshonitic centres in the Lachlan Fold Belt (Thompson et al. 1986; Perkins et al. 1992; Wyborn 1992; Blevin 2002). Eleven centres of volcanic-hosted mineralization can be distinguished at Goonumbla (Hooper et al. 1996). The four largest deposits are Endeavour 22, E27, E26 North, and E48 (Fig. 6.13). They were discovered by Geopeko geologists in the late-eighties and early-nineties. The Northparkes project was developed by North Limited after the takeover of Geopeko and production commenced with two open pits at the E22 and E27 orebodies in 1993. Both pits have been exploited and the larger E26 North and E48 deposits are currently mined as underground block-caving operations by a joint venture between the Rio Tinto and Sumitomo Groups, respectively. Northparkes, including the four

orebodies E22, E27, E26N, and E48, has an estimated resource base of 287.8 Mt at 0.57 wt% Cu and 0.26 g/t Au, as well as significant Ag credits (Butcher et al. 2011).

Regional Geology Many igneous provinces of Ordovician age are known from southeastern Australia (Horton 1978; Powell 1984; Thompson et al. 1986; Perkins et al. 1992; Wyborn 1992; Müller et al. 1993; Blevin 2002). The Lachlan Fold Belt in New South Wales is divided into several north-south trending synclinal and anticlinal tectonic zones composed of Paleozoic igneous and sedimentary rocks (Scheibner 1972). The Goonumbla district is situated in the northeastern part of the Bogan Gate synclinal zone (Scheibner 1974). This north-trending trough forms a broad tectonic boundary within the Lachlan Fold Belt, separating two Proterozoic terranes to the west and east of the Parkes area—the Wagga Metamorphic Belt and the Kosciusko Terrane, respectively—and comprises a zone of Paleozoic sedimentary rocks with associated late Ordovician to early Silurian igneous rocks (Jones 1985; Perkins et al. 1992; Blevin 2002). In the Parkes area, a sequence of latitic lavas, interlayered flows and pyroclastic units with minor volcanoclastic rocks and limestones comprises the Goonumbla igneous complex (Jones 1985). The rocks are generally unmetamorphosed, but are commonly gently folded with relatively gentle dips (Heithersay 1986; Heithersay et al. 1990). Compositions of the igneous rocks, which are locally intruded by monzodiorite, monzonite and quartz-monzonite stocks, range from trachyandesitic to latitic, and they exhibit typical shoshonitic geochemistry (Joplin et al. 1972; Morrison 1980). As discussed by previous workers, the Goonumbla igneous rocks are probably related to a former subduction event (Müller et al. 1994; Blevin 2002). Porphyry copper-gold mineralization is typically hosted by quartz-monzonite intrusions (Müller et al. 1994; Heithersay and Walshe 1995). Uranium-Pb zircon dating of the intrusions has established that they do not represent a single magmatic episode, but three distinct episodes at about 482, 450 and 440 Ma, respectively (Butera

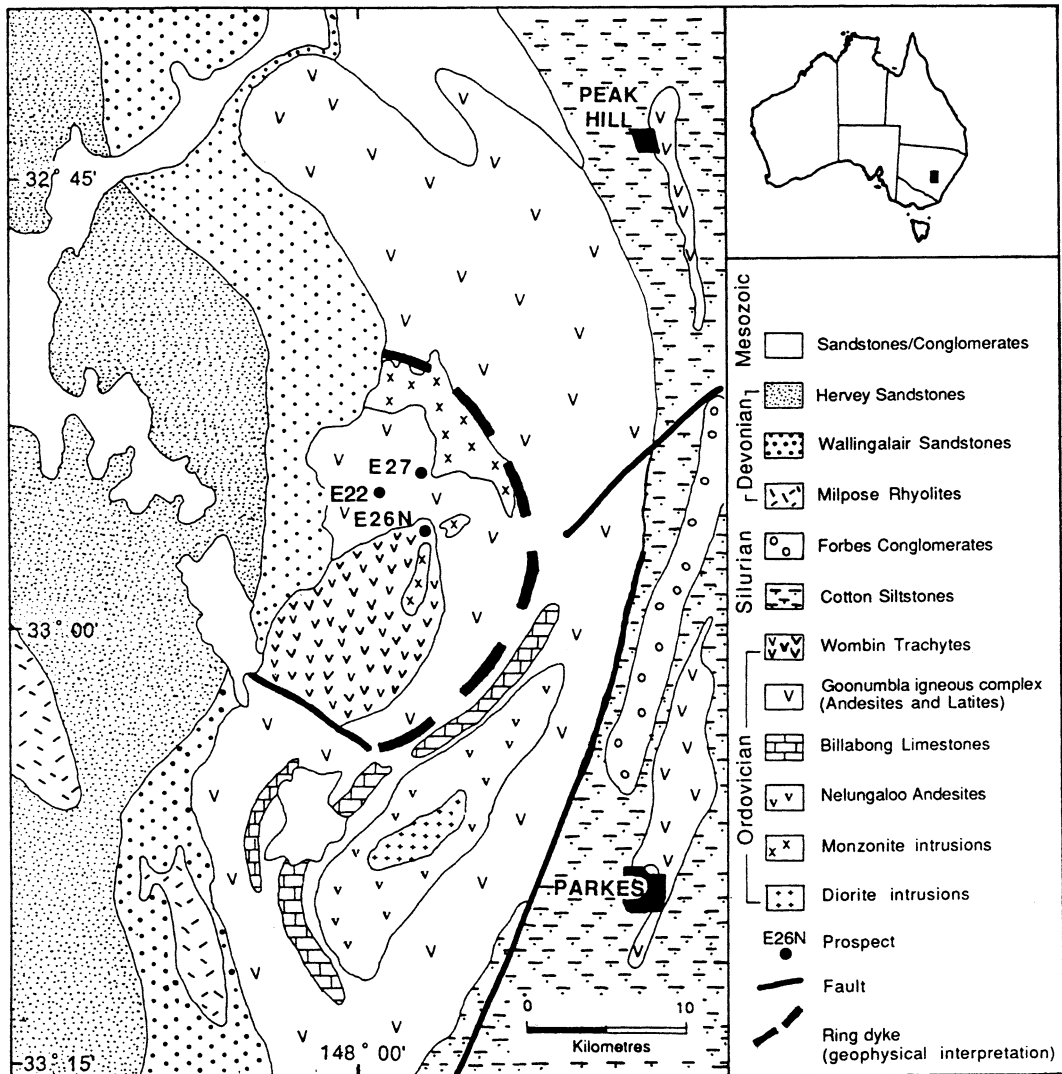


Fig. 6.13 Geological overview of the Northparkes copper-gold deposits, Goonumbla igneous complex, New South Wales, Australia. Modified after Heithersay et al. (1990)

et al. 2001; Blevin 2002). Empirical studies suggest a direct relationship between increasing mineral deposit size and the degree of K-enrichment in the related igneous progenitor in the Lachlan Fold Belt (Blevin 2002; Holliday et al. 2002). More specifically, the Ordovician igneous suites that host the world-class Cadia and Northparkes porphyry copper-gold deposits in the Lachlan Fold Belt contrast markedly from those of the Silurian, Devonian and Carboniferous in that the former are typically more

oxidized, and are significantly less compositionally evolved (Blevin 2002).

Nature of Porphyry Copper-Gold Mineralization Within the Goonumbla district, eleven centres of mineralization are located within a circular feature which is some 22 km in diameter (Fig. 6.13). It is partly bounded by a monzonitic ring dyke, and is interpreted to be a collapsed caldera formed as a result of regional extension (Jones 1985). The Goonumbla igneous rocks

consist mainly of andesites, latites, and the slightly younger Wombin trachytes locally intruded by monzonite stocks and minor basaltic dykes. The igneous rocks represent a cogenetic suite with shoshonitic geochemistry as defined by Morrison (1980).

The mineralized igneous host rocks comprise a repetitive sequence of andesitic lavas, latites and trachytes, with associated epiclastic rocks. Porphyry copper-gold mineralization in the Goonumbla district is generally associated with relatively small pipe-like intrusive bodies of quartz-rich monzonite. These monzonite stocks can have diameters up to 100 m and vertical extensions up to 900 m (Perkins et al. 1992), and were probably formed as late-stage differentiates of trachyandesitic parental melts. These late-stage quartz-monzonites form fractal, finger-like intrusions which commonly have crowded porphyritic centres that grade outward, through zones with mosaic textures, into sparsely porphyritic margins (G. Morrison pers. comm., 1996). The highest volatile concentrations appear to be in the mosaic-textured zones. Internal zoning is present in some intrusions, and is pronounced in the small, strongly porphyritic, mineralized bodies that are intruded off larger, and more mafic, plutonic bodies with monzodioritic and/or mafic monzonitic composition at depth (Heithersay and Walshe 1995). Diamond drilling suggests that the deep plutonic batholiths have biotite-poor and hornblende-phyric, mafic monzonitic compositions, while younger intrusions tend to be more felsic, in accord with the progressively more felsic nature of the younger volcanic units (Müller et al. 1994; Blevin 2002).

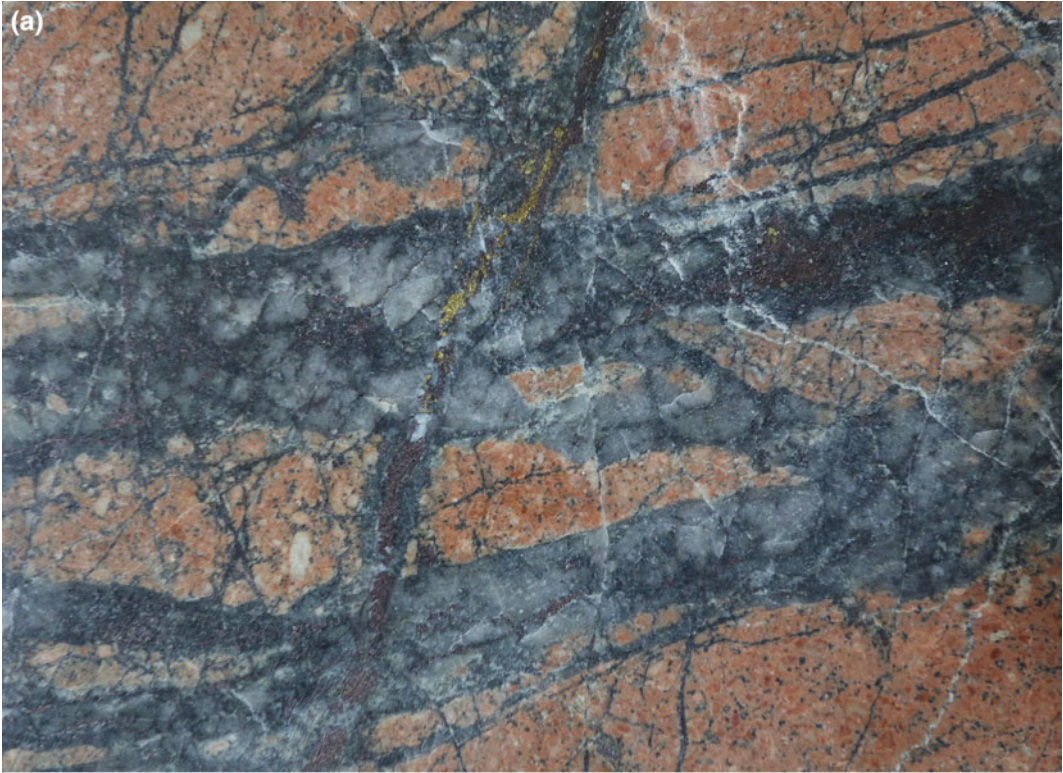
Primary copper and zinc mineralization consists of disseminated and vein sulphides, notably chalcopyrite, bornite, chalcocite, sphalerite and minor pyrite, and is generally associated with quartz vein stockworks which occur both within the intrusive bodies and the surrounding volcanic host rocks (Heithersay and Walshe 1995; Lickfold et al. 2003; Harris and Holcombe 2014). Sulphide mineralization is commonly accompanied by disseminated grains of hematite and magnetite. Pervasive hematite-sericite alteration

is peripheral to the mineralization (Müller et al. 1994).

Native gold occurs mainly as minute grains within silicates of the host rock, and more rarely as fine inclusions in the sulphides (Jones 1985). The highest gold values are present in the potassic alteration zone (see below), and are closely associated with chalcopyrite and bornite mineralization.

No large pervasive alteration zones that typify many other porphyry copper deposits (e.g. Bajo de la Alumbrera, Argentina; see Gonzales 1975) are present in the Goonumbla igneous complex (Heithersay et al. 1990). However, mineralization is generally associated with potassic alteration zones, characterized by either pervasive secondary biotite flakes and magnetite grains, or hydrothermal sericite or orthoclase veins. Pink hydrothermal orthoclase also forms dense granular replacements, or occurs as alteration selvages around quartz veins, comparable to the Skouries porphyry copper-gold deposit in Greece (Kroll et al. 2002). Secondary biotite is most commonly developed as dark pervasive zones within the more mafic trachyandesites. The stockwork at the Goonumbla deposits includes A-type and B-type veins (Fig. 6.14). Detailed studies on the quartz-vein emplacement mechanisms at the E26 North deposit reveal a broad range of vein orientations that define a conical distribution around a vertical axis (Harris and Holcombe 2014). Hydraulically driven deformation was locally important, contributing to the formation of the irregular fracture stockwork immediately adjacent to the small intrusive bodies (Harris and Holcombe 2014).

Regional zones of propylitic alteration in the Goonumbla district are mainly characterized by irregular secondary grains of epidote, chlorite, and carbonate in igneous rocks. Epidote also forms fine-grained aggregates which have replaced primary mica and plagioclase phenocrysts. This pervasive alteration style, which commonly obliterates primary volcanic textures, is developed only on a local scale, and is apparently related to major structures and/or contact zones of the intrusive monzonites. Oxide mineralization blankets comprising malachite,



◀ **Fig. 6.14** Representative ore samples from the Northparkes copper-gold deposits, E48 orebody, Goonumbla igneous complex, New South Wales, Australia (photos taken by C. Stegman): **a** potassic altered quartz-monzonite porphyry cut by intense quartz-bornite (A-type) stockwork veining; note the cross-cutting

late-stage S-type vein [FOV 5×12 cm]. **b** Quartz-monzonite porphyry cut by intense quartz-bornite-chalcocopyrite (A-type) stockwork veining, locally with hydrothermal orthoclase flooding; note that the original potassic alteration is overprinted by a late-stage pervasive sericite alteration [FOV 5×12 cm]

azurite, and libethenite, were well developed over the E22 and E27 deposits.

Hydrothermal sericite associated with mineralization yields an $^{40}\text{Ar}/^{39}\text{Ar}$ step-heating age of 439.2 ± 1.2 Ma (Perkins et al. 1990a). Uranium-Pb dating by ion microprobe on magmatic zircons from diorites near the Goonumbla deposits yields an age of 438 ± 3.5 Ma (Perkins et al. 1990b). These ages indicate that mineralization at Northparkes was synchronous with magmatism and broadly contemporaneous with the formation of other gold deposits in the Lachlan Fold Belt (e.g. Glendale and Sheahan-Grants) as dated by Perkins et al. (1992).

Petrography and Geochemistry of the Shoshonitic Host Rocks The Goonumbla igneous complex comprises mainly volcanic rocks with porphyritic textures which are intruded by monzonite stocks with equigranular textures. The grey trachyandesitic host rocks consist mainly of labradorite as euhedral crystals up to 5 mm long and commonly intensely affected by saussuritization or dusting by sericite, with minor olivine and apatite microphenocrysts. The groundmass consists of plagioclase and K-feldspar (Müller et al. 1994). The latites consist of phenocrysts of labradorite, K-feldspar, augite, and apatite microphenocrysts which are set in a fine-grained groundmass of quartz, K-feldspar, and plagioclase. The trachytes consist mainly of K-feldspar, labradorite, augite, and biotite phenocrysts set in an orange-red groundmass of K-feldspar, plagioclase, and quartz. The trachytes commonly contain apatite microphenocrysts (Müller et al. 1994). The intrusive, medium-grained, pink, quartz-rich monzonite

bodies are holocrystalline rocks, comprising principally K-feldspar, plagioclase, quartz, and biotite. Monzodioritic intrusive bodies are composed of plagioclase and clinopyroxene with minor late K-feldspar (Blevin 2002). Apatite microphenocrysts and magnetite are also present, suggestive of high volatile contents and high oxygen fugacities of the parental melts (cf. Kroll et al. 2002). Amphibole is present in places as a late-stage minor phase with rare quartz. The mafic monzonites from the underlying batholiths comprise plagioclase and more rarely K-feldspar phenocrysts with clinopyroxene phenocrysts set in a groundmass of K-feldspar (Blevin 2002). Biotite phenocrysts are restricted to, and occur in place of clinopyroxene in, the more evolved quartz-monzonites (Müller et al. 1994). Quartz intergrown with K-feldspar may be locally abundant in the groundmass in these rocks.

Whole-rock analyses cover the petrographic spectrum from basaltic to dacitic rocks (i.e. SiO_2 contents between 46.8 and 64.9 wt%), as shown in Table 6.6. The samples are characterized by high, but variable, Al_2O_3 contents (13.4–19.9 wt %), very high K_2O contents (up to 6.8 wt%) and high $\text{K}_2\text{O}/\text{Na}_2\text{O}$ ratios (0.58–1.48) which are typical for the shoshonite association (Joplin et al. 1972; Morrison 1980; Lu et al. 2013). The rocks also have enriched LILE concentrations (e.g. up to 1200 ppm Ba, 1350 ppm Sr), low HFSE contents (<0.67 wt% TiO_2 , <20 ppm Y, <125 ppm Zr, <10 ppm Nb, <3.4 ppm Hf) and very low LREE abundances (<22.4 ppm La, <31 ppm Ce). Low mg# (<63) suggest that the rocks were generated from evolved magmas, probably affected by clinopyroxene-biotite \pm apatite fractionation. All volcanic and intrusive

Table 6.6 Major- and trace-element analyses of shoshonitic rocks from the Northparkes copper-gold deposits, Goonumbla igneous complex, New South Wales, Australia

Province/deposit	Northparkes (Goonumbla)				
Location	E27 (NSW, Australia)	E27 (NSW, Australia)	E26N (NSW, Australia)	E26N (NSW, Australia)	E27 (NSW, Australia)
Rock type	Trachyandesite	Trachyandesite	Monzonite	Monzonite	Latite
Tectonic setting	Late oceanic arc				
Reference	Müller et al. (1994)				
SiO ₂	54.90	54.00	64.60	64.90	60.10
TiO ₂	0.67	0.67	0.36	0.36	0.48
Al ₂ O ₃	19.60	19.90	17.50	17.10	18.40
Fe ₂ O ₃	5.69	5.51	1.89	2.13	4.60
FeO	n.a.	n.a.	n.a.	n.a.	n.a.
MnO	0.10	0.12	0.03	0.03	0.18
MgO	2.65	2.92	1.38	1.04	1.45
CaO	3.93	3.76	0.87	1.15	2.16
Na ₂ O	4.99	4.92	5.76	6.39	5.93
K ₂ O	4.21	4.29	4.68	3.99	5.31
P ₂ O ₅	0.54	0.56	0.18	0.15	0.28
LOI	2.91	3.07	2.80	3.12	1.50
Total	100.13	99.69	100.12	100.35	100.35
mg#	52	55	63	53	42
K ₂ O/Na ₂ O	0.84	0.87	0.81	0.62	0.89
Sc	n.a.	n.a.	n.a.	n.a.	n.a.
V	170	170	120	110	80
Cr	n.a.	n.a.	n.a.	n.a.	n.a.
Ni	4	4	5	4	4
Rb	75	75	90	70	85
Sr	1250	1350	680	650	450
Y	19	19	16	12	20
Zr	90	90	100	95	125
Nb	3	2	5	2	7
Ba	1050	1200	810	850	800
Hf	1.8	1.8	1.9	1.8	3.1
La	16.4	16.3	14.3	13	22.4
Ce	31	29	22	20	31
Sm	n.a.	n.a.	n.a.	n.a.	n.a.
Yb	1.8	1.6	1.3	1.3	2.1
Th	n.a.	n.a.	n.a.	n.a.	n.a.
U	n.a.	n.a.	n.a.	n.a.	n.a.

Major elements are in wt%, and trace elements are in ppm. Fe₂O₃ (tot) = total iron calculated as ferric oxide. Samples were derived from diamond drill cores of the E26N or E27 orebodies. Sample numbers refer to specimens held in the Museum of the Department of Geology and Geophysics, The University of Western Australia. Data from Müller et al. (1994)

rocks plot in the field of late oceanic-arc magmas in Figs. 6.5 and 6.6.

6.3.5 Cadia Ridgeway Copper-Gold Deposit, New South Wales, Australia

Introduction Another example of ancient mineralization hosted by shoshonitic rocks in a late oceanic-arc setting is the group of Ordovician Cadia porphyry gold-copper deposits in New South Wales, Australia (Holliday et al. 2002; Wilson et al. 2003). The mineralized intrusive complexes of the Late Ordovician in the Lachlan Fold Belt can be viewed as a continuum of progressive K and other incompatible element enrichment, with the Cadia porphyry gold-copper deposits representing the youngest, most enriched and the most strongly mineralized example (Blevin 2002; Holliday et al. 2002). The Cadia system represents a cluster of porphyry gold-copper deposits, including Cadia Hill, Cadia Quarry, Cadia East, Cadia Ridgeway, and Cadia Far East. The deposits are situated about 20 km south of Orange in the central tablelands of the Lachlan Fold Belt in New South Wales, Australia, about 200 km to the west of Sydney. The existence of economic mineralization at Cadia was demonstrated in the early-1990s, when Newcrest geologists recognized the large-tonnage, low-grade openpit potential of sheeted-vein mineralization at Cadia Hill (Wood and Holliday 1995). Additional gold-copper mineralization at Cadia Quarry was discovered at the same time, followed by Cadia East in 1994, and Cadia Ridgeway (Holliday et al. 1999) and Cadia Far East in 1996 (Tedder et al. 2001). Pre-mine resources at Cadia were >19.5 Moz of contained gold and 2.3 Mt of contained copper, making the Cadia district, as a whole, the largest gold deposit in eastern Australia (Holliday et al. 2002). In 2002, the underground resource at the Ridgeway porphyry gold-copper deposit was 54 Mt at 2.5 g/t Au and 0.77 wt% Cu.

Regional Geology The Cadia gold-copper deposits are hosted by a late Ordovician to early Silurian shoshonitic volcano-intrusive

complex, which forms part of a larger zone of oceanic island arc-related volcanic and associated intrusive rocks in the eastern Lachlan Fold Belt (Fig. 6.15). The Ordovician volcano-intrusive complexes are one of four main components of the Lachlan Fold Belt in New South Wales, the others being Cambrian greenstones, Ordovician to early Silurian quartz turbidites, and Silurian to early Devonian volcanic and sedimentary rocks (Suppel et al. 1998). The Lachlan Fold Belt is interpreted to have formed by complex accretionary processes from mid Cambrian to Carboniferous times, related to the closure of a back-arc basin (Scheibner and Basden 1998) and associated collision of an oceanic-arc along the Pacific margin of Gondwana (Foster et al. 1999). The Ordovician arc-related igneous rocks were accreted during the early Silurian, and the current geometry of the volcanic rocks as four separate belts is attributed to splitting of a single arc (Glen et al. 1998). Despite multiple tectonic events, the Ordovician volcanic belts that host the Cadia and Northparkes porphyry copper-gold deposits are largely undeformed and probably acted as buttresses during deformation (Holliday et al. 2002).

Mineralization at Cadia is hosted by mid to late Ordovician Forest Reefs Volcanics and underlying Weemalla Formation, and by the late Ordovician-early Silurian Cadia Intrusive Complex (Holliday et al. 2002). The Forest Reefs Volcanics in the Cadia area are dominated by trachyandesites and latitic volcanoclastic units. All Ordovician volcanics are cut by feldspar porphyry and pyroxene porphyry dykes. Post-mineralization cover comprises Silurian shales, at least 200 m thick in the Cadia area and becoming thicker further to the east, and a thin layer of Tertiary basalts and gravel (Holliday et al. 2002). Both the Forest Reefs Volcanics and the Weemalla Formation are intruded by the Cadia Intrusive Complex, a 3 × 1.5 km wide, composite stock. Strong compositional zonation is present in this Complex, grading from monzoniorite, diorite and minor gabbro in the west to coarse-grained K-feldspar and plagioclase-phyric quartz-monzonite porphyry in the east (Holliday

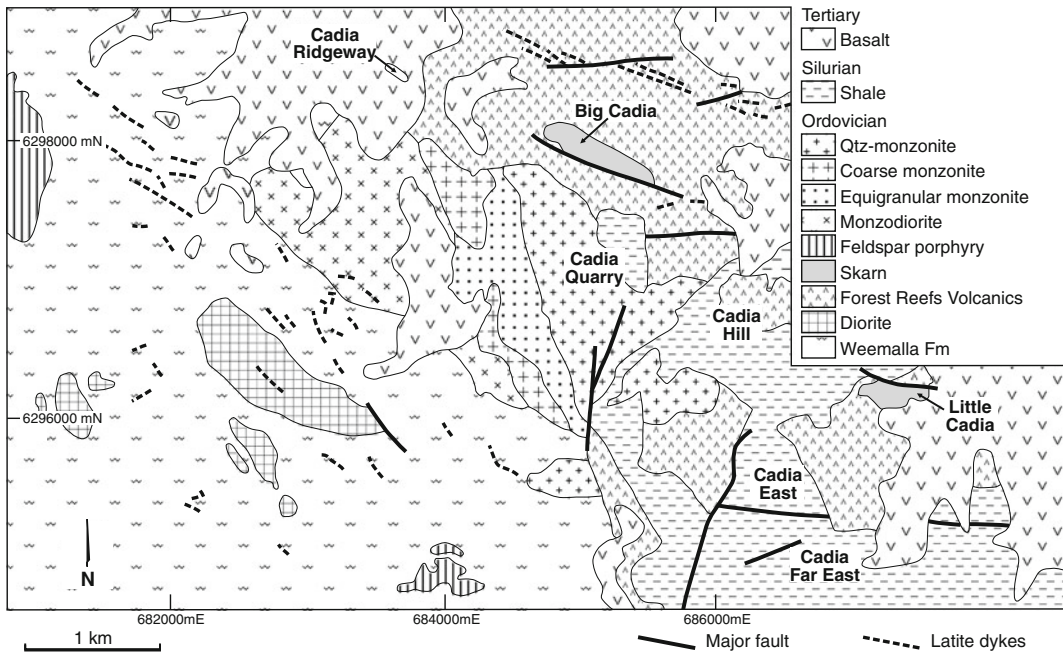


Fig. 6.15 Geological overview of the Cadia copper-gold deposits, Cadia igneous complex, New South Wales, Australia. Modified after Holliday et al. (2002)

et al. 2002). A plug of quartz-monzonite at Cadia Hill, and unexposed monzodioritic to monzonitic intrusions at Cadia Far East and Cadia Ridgeway, are compositionally identical with the exposed section of the Cadia Intrusive Complex. A swarm of trachyte dykes to the north of the Cadia Intrusive Complex are interpreted to be more evolved, late-stage, differentiates of the underlying magma chamber. The Cadia monzonites and quartz-monzonites also cut the above-mentioned feldspar porphyry and pyroxene porphyry dykes that have intruded the Forrest Reefs Volcanics (Holliday et al. 2002).

Emplacement of the Cadia Intrusive Complex was probably facilitated by a major northwest-trending dilational structure which is apparent in regional magnetic data (Holliday et al. 2002). Its northwestern trend is also reflected in the orientation of mineralized sheeted quartz veins at Cadia Hill, Cadia Quarry, Cadia East, and Cadia Far East.

Nature of Porphyry Gold-Copper Mineralization

There are six components to the Cadia porphyry cluster: (1) intrusion- and volcanic-hosted, mainly sheeted quartz-vein mineralization at Cadia Hill; (2) volcanic-hosted disseminated and sheeted quartz-vein mineralization at Cadia East; (3) volcanic- and intrusion-hosted mainly sheeted quartz-vein mineralization at Cadia Far East; (4) intrusion-hosted mainly sheeted quartz-vein mineralization at Cadia Quarry; (5) intrusion- and volcanic-hosted quartz-stockwork vein mineralization at Cadia Ridgeway; and (6) Fe-rich skarns at Big and Little Cadia (Holliday et al. 2002). The Cadia Ridgeway deposit is an upright, bulbous body of quartz vein stockworks (250–300 m across and 600 m vertical extent) that is centered on a small (50–100 m diameter) composite plug of quartz-monzonite porphyry. The top of the composite plug occurs at 450 m depth below the present-day surface and the

compositional and textural characteristics of the individual intrusive phases are documented by Wilson et al. (2003). The plug has intruded relatively flat-lying, volcanoclastic breccia of the Forest Reefs Volcanics and the conformably underlying Weemalla Formation, to the west of the main Cadia Intrusive Complex (Holliday et al. 2002). Intense silicification and local garnet-epidote alteration related to the Ridgeway deposit have rendered the original composition of the Weemalla siltstones unrecognizable at Ridgeway, although outcrops of the units to the south of the deposit are relatively fresh and only weakly carbonaceous (Wilson et al. 2003). The most strongly developed quartz vein stockworks and potassic alteration, as well as the highest gold and copper grades, occur immediately adjacent to the quartz-monzonite. The highest-grade portion of the orebody occurs above the quartz-monzonite. The intensity of veins and potassic alteration decreases both outwards and inwards from the monzonite porphyry margin (Holliday et al. 2002). Ore minerals are native gold, bornite, chalcopyrite and covellite, typically occurring within A-type and B-type quartz veins, but also as disseminations throughout the rock (Fig. 6.16). Potassic alteration assemblages consist of hydrothermal biotite and magnetite, as well as local orthoclase flooding and selvages around B-type veins.

Hydrothermal magnetite also occurs within quartz veins, particularly in the massive, laminated quartz veins that occur immediately outside the lithological contact between the quartz-monzonite porphyry and its volcanic wall rocks (Holliday et al. 2002). Propylitic alteration includes secondary epidote, chlorite, calcite, and hematite dusting (Harper 2000).

Intrusions hosting the Ridgeway deposit were emplaced at 456 ± 6 Ma, as were weakly mineralized intrusions at Cadia Quarry and Cadia East (Wilson et al. 2007). A second episode of intrusive activity occurred at 437 ± 4 Ma, based on a $^{206}\text{Pb}/^{238}\text{U}$ weighted average age for quartz-monzonite stocks and dykes that host mineralization at Cadia Quarry, Cadia Hill, and Cadia East (Wilson et al. 2007). Hence, the porphyry gold-copper deposits of the Cadia district formed in two mineralizing episodes separated by 18 m.y., from the Late Ordovician to Early Silurian. This represents one of the longest recognized time spans for porphyry copper deposits within a single district (Wilson et al. 2007) and might suggest multiple replenishment of the fractionating magma chamber at depth. The intrusions at Cadia Ridgeway were emplaced within a northwest-oriented pre-existing structural corridor. Although the system is cut by northwest-striking fractures, there has been little

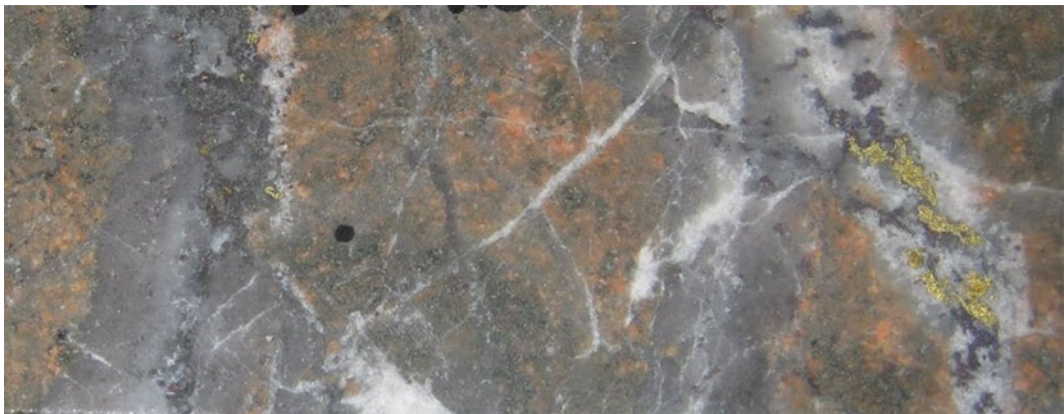


Fig. 6.16 Representative ore from the Cadia Ridgeway copper-gold deposit, Cadia igneous complex, New South Wales, Australia (photo taken by M. Foster). Potassic

altered quartz-monzonite porphyry cut by quartz-bornite-chalcopyrite (A-type) stockwork veining [FOV 8×15 cm]

syn- or post-mineral movement on any of these structures and the orebody has no major offsets (Holliday et al. 2002). Cadia Ridgeway is a small, but high-grade, porphyry gold-copper system and is comparable in this sense to the Goonumbla porphyries (cf. Heithersay et al. 1990; Heithersay and Walshe 1995). It represents the highest-grade porphyry gold-copper deposit discovered to date in the Lachlan Fold Belt.

Petrography and Geochemistry of the Shoshonitic Host Rocks With increasing fractionation of the magma, pyroxene decreases in abundance in company with the appearance of amphibole. The grain size of the rocks decreases from equigranular coarse in the mafic portions to medium-grained in the felsic portions, coupled with the appearance of K-feldspar, and more rarely, plagioclase phenocrysts in the monzonites and quartz-monzonites (Holliday et al. 2002). Where fresh, the monzonites are salmon pink, but they range in colour to green, dependant on alteration, with large (up to 2 cm) pink K-feldspar phenocrysts within a seriate textured groundmass of plagioclase, biotite and amphibole. With the exception of thin, <20 cm wide, syenogranite aplitic dykes, no cross-cutting intrusions are documented in the Cadia Intrusive Complex (Holliday et al. 2002). The presence of magmatic biotite, the replacement of pyroxene by amphibole, the presence of aplites, and vapour cavities infilled by interstitial melt, indicate a rapid build-up of volatiles within the melt during fractionation (cf. Burnham 1979). Petrographic and textural evidence suggest high oxygen fugacities during magma crystallization (Holliday et al. 2002). The more mafic units of the Cadia Intrusive Complex contain 1–2 vol.% primary magmatic magnetite, and magmatic biotite phenocrysts have high Mg/(Mg + Fe) ratios of >0.59. Whole-rock Fe₂O₃/FeO ratios are also elevated, generally in the range of 1.0–1.5 (Holliday et al. 2002).

Representative whole-rock analyses of the Cadia Intrusive Complex are provided in Table 6.7. The rocks range in composition from 48.0 to 65.0 wt% SiO₂ and exhibit a well-defined

fractionation trend ranging from trachybasalts through latites to trachytes (cf. Holliday et al. 2002). Compositionally, the Cadia Intrusive Complex conforms to the definition of shoshonite in terms of its modal mineralogy and textures, as well as its geochemical composition (Holliday et al. 2002). The igneous rocks have high K₂O contents (4.00–5.84 wt%), and high K₂O/Na₂O ratios (0.92–1.54) which are typical for the shoshonite association (cf. Joplin et al. 1972; Morrison 1980; Lu et al. 2013). Molecular K/Na ratios for all unaltered samples are consistently >1 (i.e. potassic; Müller et al. 1992b). Additionally, all samples fall within the shoshonite field on Ce/Yb versus Ta/Yb and Th/Yb versus Ta/Yb biaxial plots (Pearce 1982; Holliday et al. 2002). The samples also have enriched LILE concentrations (e.g. up to 1040 ppm Ba, 101 ppm Rb, 843 ppm Sr), low HFSE contents (<0.60 wt% TiO₂, <19 ppm Y, <126 ppm Zr, <7 ppm Nb, <8 ppm Hf) and very low LREE abundances (<27 ppm La, <35 ppm Ce) which are typical for potassic igneous rocks derived in late oceanic arc settings (Müller et al. 1992b). Carr et al. (1995) demonstrated that Pb isotope data from the mineralized Ordovician intrusions in the Lachlan Fold Belt fall into the field of modern mantle reservoirs typified by oceanic island basalts, with little to no evidence of crustal input. The elevated P₂O₅ contents of the Cadia rocks of up to 0.43 wt% are consistent with the presence of abundant apatite microphenocrysts (Wilson et al. 2003).

6.3.6 Hugo Dummett (Oyu Tolgoi) Copper-Gold Deposit, Mongolia

Introduction The Hugo Dummett porphyry copper-gold deposit is the highest grade part of the Oyu Tolgoi porphyry district in the southern Gobi desert of Mongolia (Crane and Kavalieris 2012; Dolgopolova et al. 2013). The Oyu Tolgoi porphyry district is located about 650 km south of the Mongolian capital Ulaanbaatar and about 80 km from the Chinese border (Perello et al. 2001). It comprises six copper-gold deposits including Hugo Dummett, Central Oyu, South

Table 6.7 Major- and trace-element analyses of shoshonitic rocks from the Cadia copper-gold deposits, New South Wales, Australia

Province/deposit	Cadia Ridgeway	Cadia Ridgeway	Cadia Hill	Cadia East	Cadia Far East
Location	NSW, Australia				
Rock type	Monzonite	Monzodiorite	Monzonite	Monzonite	Trachyte dyke
Tectonic setting	Late oceanic arc				
Reference	Holliday et al. (2002)				
SiO ₂	61.59	52.84	60.05	60.32	53.15
TiO ₂	0.44	0.60	0.46	0.46	0.53
Al ₂ O ₃	16.05	14.94	16.55	16.60	13.88
Fe ₂ O ₃	2.91	5.98	3.10	3.07	3.34
FeO	2.79	4.21	2.81	2.73	5.35
MnO	0.03	0.10	0.03	0.04	0.14
MgO	2.22	3.96	1.99	1.88	7.06
CaO	1.74	5.65	1.80	3.69	6.03
Na ₂ O	4.46	4.32	4.01	3.94	2.77
K ₂ O	4.89	4.00	5.84	4.33	4.27
P ₂ O ₅	0.21	0.43	0.23	0.21	0.38
LOI	2.67	2.97	3.13	2.73	3.10
Total	100.00	100.00	100.00	100.00	100.00
mg#	42	44	39	38	60
K ₂ O/Na ₂ O	1.09	0.92	1.45	1.09	1.54
Sc	14	26	14	14	30
V	87	206	113	103	192
Cr	9	17	9	10	348
Ni	6	12	5	6	94
Rb	65	56	101	64	59
Sr	455	843	565	785	785
Y	14	19	14	19	14
Zr	117	63	126	115	58
Nb	7	4	7	7	5
Ba	669	818	1040	1036	874
Hf	6	8	n.a.	8	2
La	10	16	27	16	16
Ce	20	35	25	35	30
Sm	n.a.	n.a.	n.a.	n.a.	n.a.
Yb	n.a.	n.a.	n.a.	n.a.	n.a.
Th	6	3	7.5	5	4
U	1	1	3	1	1

Major elements are in wt%, and trace elements are in ppm. Fe₂O₃ (tot) = total iron calculated as ferric oxide. Data from Holliday et al. (2002)

and Southwest Oyu, Heruga North and Heruga (Kavalieris et al. 2011) containing a total metal content exceeding 41.7 million metric tons of copper and 49.8 million oz of gold (Crane and Kavalieris 2012). The Oyu Tolgoi porphyry district forms part of the mid- to late Paleozoic Gurvansayhan island-arc terrane (Lamb and Badarch 1997), which represents an east-west trending belt through southern Mongolia, about 200 km wide and about 750 km long (Kashgerel et al. 2008). The morphology of the area is flat and widely covered by sand and gravel, with rare undulating hills. Oyu Tolgoi is the Mongolian name for Turquoise Hill, an area with old workings targeting outcropping copper oxides. Identification of porphyry copper mineralization in the area is accredited to Magma Copper geologists who visited the area in September 1996. After the take-over of Magma Copper by BHP, the latter company completed the geochemical and geophysical surveys and conducted 23 diamond drill holes, culminating in the identification of the Oyu Tolgoi North, Central, and South mineralized zones (cf. Crane and Kavalieris 2012). However, BHP's exploration strategy was focused on the discovery of large chalcocite blankets and their drill holes were limited to a depth of 350 m (D. Kirwin, pers. comm., 2004). Hence, they did not discover the largest deposit, Hugo Dummett, which is concealed beneath >800 m of unmineralized rock (Crane and Kavalieris 2012). In 1999, BHP offered the tenements for joint venture and a resulting agreement with Ivanhoe Mines allowed acquisition of up to 100 % of the properties. Exploration by Ivanhoe Mines began in May 2000, and exploration is still ongoing. More than 2400 drill holes totaling over 1000 km have been drilled at Oyu Tolgoi and the exploration history is documented in detail by Kirwin et al. (2005) and Crane and Kavalieris (2012). In January 2012, Rio Tinto took a majority stake in Ivanhoe Mines and the project is currently operated by Turquoise Hill Resources, a majority-owned subsidiary of Rio Tinto with 66 % ownership and the Government of Mongolia holding 34 %. The mine is a combined underground and open pit operation which shipped its first batch of

copper in July 2013. Copper production is scheduled to reach about 450,000 tonnes (500,000 short tons) annually.

Regional Geology The Oyu Tolgoi district is situated within the Altaid Tectonic Belt (Khain et al. 2003). The Altaid Tectonic Belt represents a complex pattern of accreted microcontinental blocks and mobile belts and it stretches for almost 5000 km across Asia from the Siberian Craton and the Tarim to the North China Craton (Kröner et al. 2007). During the Paleozoic, southern Mongolia grew through accretion of subduction-related oceanic island-arcs and continental blocks (Dolgoplova et al. 2013). The Oyu Tolgoi area consists of Silurian to Carboniferous polydeformed arcs that are intruded by Devonian to Permian granitoids (Wainwright et al. 2011). The region represents an ancient analogue to active ore-forming environments associated with arc magmatism, not unlike the modern situation in the southwest Pacific (Blight et al. 2010).

The Late-Devonian porphyry copper-gold deposits of the Oyu Tolgoi district occur in a 22 km-long north-northeast trending zone (Fig. 6.17) and are hosted by high-K calc-alkaline quartz-monzodiorite and quartz-monzonite intrusions emplaced in porphyritic augite-basalt lavas (Kashgerel et al. 2008). The local geology comprises Late-Devonian basaltic to dacitic volcanosedimentary units of the Alagbayan Group which are unconformably overlain by Early-Carboniferous basalts and minor sedimentary rocks of the Sainshandhudag Formation (Kashgerel et al. 2006). The Devonian-Carboniferous units record the existence of an oceanic island arc (Perello et al. 2001). Arc construction commenced in the Late-Silurian with subduction of oceanic crust beneath the Tuva Mongol arc (Sengör and Natalin 1996). The large Tuva Mongol arc was active for much of the Paleozoic. By the Permian, a very complicated collage of tectonic units had formed throughout Central Asia by collision, shortening, and strike-slip displacement (Sengör and Natalin 1996; Perello et al. 2001).

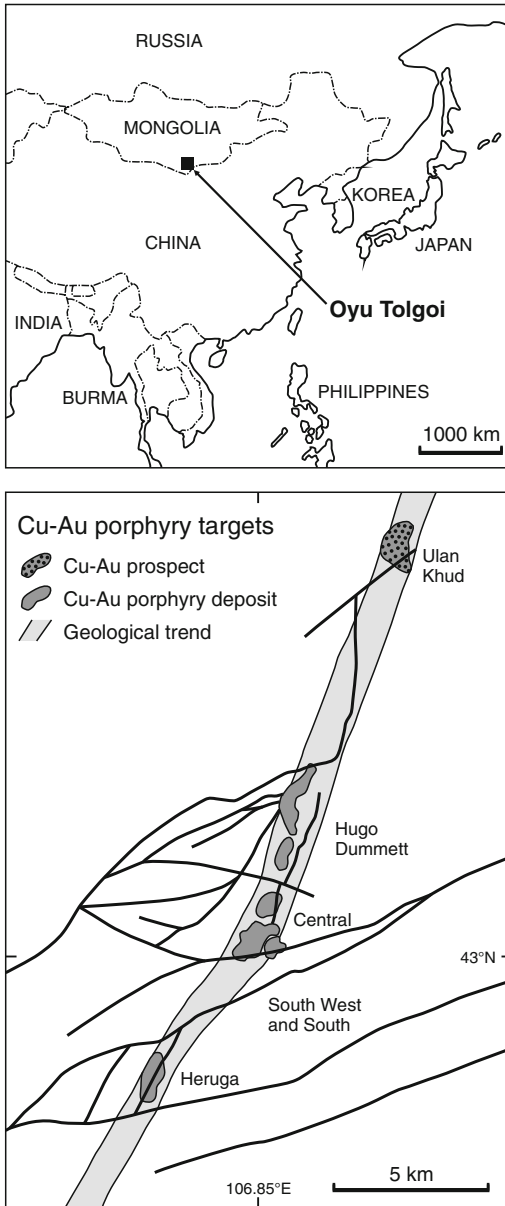


Fig. 6.17 Location of the Oyu Tolgoi porphyry copper-gold district including the Hugo Dummett, Central, South West, South, and Heruga copper-gold deposits and the Ulan Khud prospect, Mongolia. Adapted from Kashgerel et al. (2008)

The Oyu Tolgoi area is intersected by several major northwest- and northeast-striking lineaments. A large northeast-striking lineament can

be traced for several kilometers across the border and into the Inner Mongolia Province of North China where it controls the Oblaga copper-gold skarn deposit (Sen et al. 2005). Oblaga is genetically associated with sheeted quartz-monzonite dykes of high-K calc-alkaline composition (Sen et al. 2005). The most distinctive structural feature at Oyu Tolgoi is the sheeted nature of some of the northwest-trending quartz-magnetite veinlet exposures, aligned with old workings at South Oyu that exploited high-grade copper mineralization, and a series of pebble dykes in Central Oyu (Perello et al. 2001).

The high-K calc-alkaline quartz-monzodiorite and quartz-monzonite intrusions which host the Hugo Dummett porphyry copper-gold deposit occur as dykes and stocks, a few tens of meters wide, and formed in a mid-Paleozoic oceanic island-arc setting (Kashgerel et al. 2006; Wainwright et al. 2011). The quartz-monzodiorites are dated at 369 ± 2 Ma (Kashgerel et al. 2009). Southwest of the Hugo Dummett deposit, there is a large barren quartz-monzodiorite pluton that is considered to be related to the small mineralized porphyry intrusions, although a definitive link cannot be established due to the lack of outcrop (Wainwright et al. 2011). However, airborne geophysics and limited drilling suggest that the large intrusion has an elliptical shape with the long axis oriented north-northeast over a 5×8 km area (Kashgerel et al. 2006), dimensions that approach those of batholiths known to underlie world-class porphyry copper districts (Dilles et al. 2000).

Nature of Porphyry Copper-Gold Mineralization

Porphyry copper-gold mineralization is genetically related to a series of small polyphase quartz-monzodiorite and quartz-monzonite intrusions which are similar at all deposits at Oyu Tolgoi (Kashgerel et al. 2006). In places, granodiorite phases truncate strongly mineralized quartz-monzodiorites forming chilled margins adjacent to quartz- and sulphide-rich zones. The granodiorite intrusions postdate the main porphyry copper-gold system, but are locally

accompanied by pervasive hydrothermal alteration and weak copper mineralization (Wainwright et al. 2011). Barren post-mineral intrusions in the Oyu Tolgoi area are dominated by multiple-phase rhyolite and syenite dykes and small plugs that are locally exposed at the surface and intersected by drill holes (Perello et al. 2001). In places, the dykes have chilled margins along their lithological contacts with the country rocks and they contain xenoliths and large blocks of mineralized quartz-monzodiorites (Perello et al. 2001). Hydrothermal breccias are not common and volumetrically insignificant at Oyu Tolgoi (Crane and Kavalieris 2012). They typically contain about 25 vol.% of strongly altered, subrounded lithic fragments of undefined composition plus subangular quartz veinlet clasts in a fine-grained, flow-banded and laminated, sand-sized clastic matrix of rock flour and disseminated clastic pyrite (Perello et al. 2001).

Hugo Dummett is divided into two deposits, Hugo Dummett North and Hugo Dummett South that are composed of multiple intrusions and may be broadly separated into two intrusive centers. Each of the centers has a similar structure, with small intensely quartz-veined dykes (high-grade ore: >2.5 wt% Cu) on the eastern margin, flanking larger quartz-monzodiorite intrusions presumed to form the center of the intrusive complex (Kashgerel et al. 2009). The complex tectonic history, as well as extensive cover rocks, obscures fundamental characteristics of the early island arc terrane that hosts the Oyu Tolgoi deposits (Crane and Kavalieris 2012). Post-mineral deformation has modified the original intrusive structure and ductile deformation of sulphides is common in the Hugo Dummett deposits. A schematic reconstruction of Hugo Dummett shows that the core of the system is made up of a dome-shaped intrusion overprinted by concentric zones of alteration and mineralization (Kashgerel et al. 2009). The Hugo Dummett deposits are the richest and deepest porphyry system at Oyu Tolgoi, locally characterized by high-grade copper (>2.5 wt% Cu) and gold (0.5–2.0 g/t) mineralization associated with intense A-type quartz

veins and multiple phases of quartz-monzodiorite and quartz-monzonite stocks and dykes (Crane and Kavalieris 2012). The intrusions are emplaced into a coarse-grained porphyritic augite-basalt (Kashgerel et al. 2006). The high iron content of this basalt had a reducing effect on the hydrothermal fluids, thus precipitating the ores with very high copper-gold grades that define the Hugo Dummett deposits, but are highly unusual for typical porphyry Cu-Au deposits. The high-grade zone along the lithological contact of the augite-basalt is best developed at Hugo Dummett North, where it forms a lens up to 90 m wide and about 600 m in vertical extent, and with a strike length of >1.5 km (Crane, pers. comm., 2011). The high-grade zone is defined by intense A-type quartz-bornite veins (in places up to 5 wt % Cu), locally termed the Qv90 zone for >90 vol. % quartz veins (Fig. 6.18). This zone is closely enveloped by advanced argillic alteration and deeply overprinted by a quartz-sericite assemblage. Hypogene bornite typically impregnates quartz, filling spaces and fractures within the Qv90 zone (Fig. 6.18). Enargite-pyrite occurs as veins in the outer parts of the Hugo Dummett deposits and associated with advanced argillic alteration. Parts of the Hugo Dummett North deposit have unusually high Au (g/t)/Cu(%) ratios >1, corresponding to areas with native gold recorded in polished section (Crane and Kavalieris 2012).

An early and regional sodic-calcic alteration is overprinted by younger wall-rock biotite-magnetite alteration along with orthoclase alteration, the latter two largely restricted to the host quartz-monzodiorite intrusions (Crane and Kavalieris 2012). High-grade bornite mineralization is commonly associated with intense sericite alteration, which overprints earlier potassic alteration assemblages (Kashgerel et al. 2009). Sulphide minerals are zoned outward from a bornite-dominated core to chalcopyrite, upward to pyrite ± enargite and covellite at shallower depth. The latter high-sulphidation state sulphides are hosted by advanced argillic alteration that overprints the sericite alteration (Kashgerel et al. 2009).

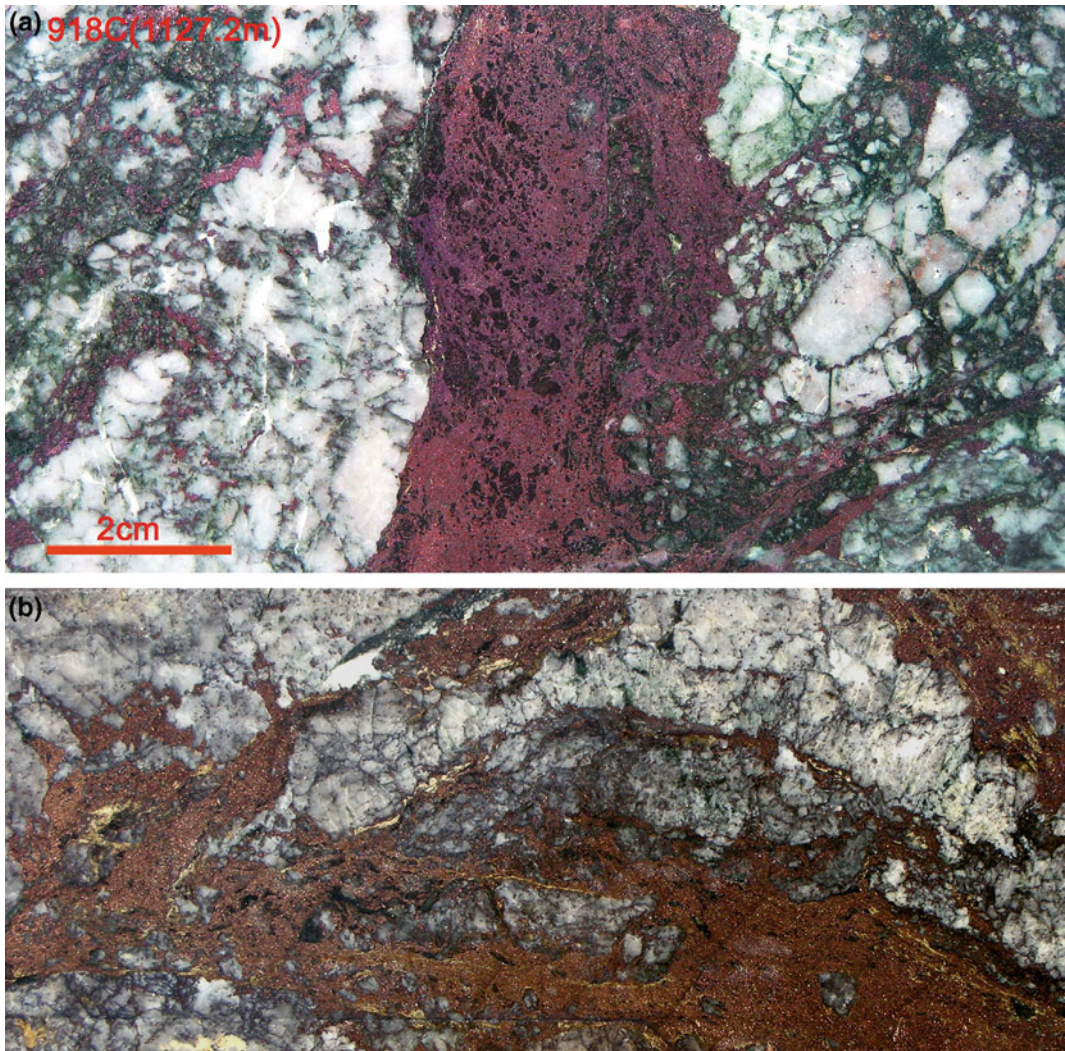


Fig. 6.18 High-grade ore samples from the Qv90 zone, Hugo Dummett copper-gold deposit, Mongolia (photos taken by B.E. Khashgerel): **a** intense quartz-bornite mineralization from the Qv90 high-grade zone [FOV

6×10 cm]. **b** Intense quartz-bornite \pm chalcopyrite mineralization from the Qv90 zone; note that bornite impregnates quartz, filling spaces and fractures within the Qv90 zone [FOV 6×12 cm]

Petrology and Geochemistry of the Potassic

Host Rocks Quartz-monzodiorites and quartz-monzonites are medium-grained and consist of subhedral hornblende and biotite ferromagnesian phenocrysts, plagioclase phenocryst-crowded textures, and with potassic feldspar exclusively in the matrix (Kavalieris and Wainwright 2005). The rocks also contain accessory magnetite, zircon and apatite (Dolgo-polova et al. 2013; Wainwright et al. 2011). Where unaltered, these rocks are characterized by

a distinct brick-red tint, comparable to the Goonumbla intrusions in New South Wales (Müller et al. 1994). The granodiorite suite is subdivided into a coarse-grained and sparsely porphyritic phase with plagioclase and biotite phenocrysts as well as apatite microphenocrysts which are set in a distinctive brown aphanitic groundmass, and, more rarely, a crowded porphyritic phase dominated by plagioclase and minor quartz phenocrysts set in a grey-brown to beige-yellow feldspathic groundmass (Wainwright et al. 2011).

The abundance of hydrous minerals, such as biotite and hornblende phenocrysts, as well as apatite microphenocrysts suggests volatile-rich magmas (Wainwright et al. 2011).

Table 6.8 shows representative whole-rock analyses for the potassic igneous rocks from Oyu Tolgoi (Kavalieris and Wainwright 2005). Geochemically, the rocks belong to the high-K calc-alkaline suite with high, but variable Al_2O_3 contents (16.64–19.19 wt%), high K_2O contents (up to 3.88 wt%), and high $\text{K}_2\text{O}/\text{Na}_2\text{O}$ ratios (0.55–1.05). The rocks have enriched LILE (up to 495 ppm Ba, up to 96 ppm Rb, up to 208 ppm Sr), low HFSE (<0.79 wt% TiO_2 , <136 ppm Zr, <8.9 ppm Nb, <21 ppm Y), very low LREE abundances (<18.1 ppm La, <34.1 ppm Ce), and high Ba/La ratios that exceed 25, which are typical for potassic igneous rocks derived from oceanic island arc settings (Müller et al. 1992; Kavalieris and Wainwright 2005). The Ce/Yb (10.5–17.2) and Th/Yb ratios (1.26–1.63) of the quartz-monzodiorites from Oyu Tolgoi confirm their high-K calc-alkaline affinities (cf. Pearce 1982). Mineralized quartz-monzodiorites are characterized by relatively flat, spoon-shaped, patterns in mantle-normalized REE spidergram diagrams (Kavalieris and Wainwright 2005), generally considered to indicate metasomatic hydrous alteration of the peridotitic mantle sources (Navon and Stolper 1987; Takazawa et al. 1992). The lack of negative Eu anomalies indicates high oxygen fugacities of the magmas, and is conducive for gold-rich porphyry systems (Kavalieris and Wainwright 2005).

The augite-basalt hosting the Hugo Dummett porphyry copper-gold deposit is very coarse-grained and porphyritic containing large augite phenocrysts (35 vol.%, 5–8 mm) that are set in a dark-gray to black fine-grained groundmass consisting of plagioclase, augite and magnetite (Kashgerel et al. 2009). Geochemically, the augite-basalt has primitive tholeiitic compositions with about 1.37 wt% TiO_2 , 12.46 wt% Al_2O_3 , 10.77 wt% MgO, and 0.6 wt% K_2O , and it is defined by relatively flat REE patterns on

mantle-normalized spidergram diagrams (Kavalieris and Wainwright 2005; Wainwright et al. 2011).

6.3.7 Peschanka Copper-Gold Deposit, Siberia, Russia

Introduction The Peschanka deposit is another example of copper-gold mineralization hosted by potassic igneous rocks that were derived in a late oceanic arc setting. It probably represents the most isolated copper-gold deposit of significant grade and tonnage (Chitalin et al. 2012). Peschanka is situated in the Chukotka Autonomous Region near the Arctic circle, about 250 km southwest of the small town of Bilibino and 425 km from the small seasonal port of Pevek in the far north of eastern Siberia (Marushchenko 2013). The area comprises undulating hills that are largely covered by vast pine forests. Annual average temperatures are well below 0 °C.

The Peschanka deposit forms part of the Baimka ore district that is confined to the eastern margin of the large Egdygkych pluton, a composite mafic intrusion of early Cretaceous age (Baksheev et al. 2013; Nikolaev et al. 2014; Soloviev 2014). The mineral potential of the Baimka district was discovered during large regional stream sediment and soil sampling surveys in the nineteen seventies and early-eighties (Nokleberg et al. 2005; Chitalin et al. 2012). Contour maps plotting the elements Cu, Mo, Pb, and Zn revealed subtle, but perfectly zoned anomalies in the permafrost soils (Nokleberg et al. 2005). The Baimka district represents a cluster of porphyry copper-gold systems, probably related to a fractionating magma chamber at depth. The best explored deposit is Peschanka which crops out at surface and it is well defined by deep diamond drilling. Peschanka represents the largest porphyry copper-gold deposit in Russia, comprising a resource of >1350 Mt at 0.61 wt% Cu, 0.015 wt% Mo, 0.32 g/t Au, and 3.7 g/t Ag accounting for a total metal content of

Table 6.8 Major- and trace-element analyses of potassic igneous rocks from the Oyu Tolgoi copper-gold deposits, Mongolia

Province/deposit	Oyu Tolgoi	Oyu Tolgoi	Oyu Tolgoi	Oyu Tolgoi
Location	Mongolia	Mongolia	Mongolia	Mongolia
Rock type	Quartz-Monzodiorite	Quartz-Monzonite	Quartz-Monzonite	Granodiorite
Tectonic setting	Late oceanic arc	Late oceanic arc	Late oceanic arc	Late oceanic arc
Reference	Kavalieris and Wainwright (2005)			
SiO ₂	56.73	66.31	65.78	63.54
TiO ₂	0.79	0.32	0.49	0.45
Al ₂ O ₃	19.19	16.64	17.01	17.79
Fe ₂ O ₃	4.69	3.77	4.53	3.83
FeO	n.a.	n.a.	n.a.	n.a.
MnO	0.06	0.02	0.01	0.05
MgO	3.28	1.27	0.84	0.62
CaO	0.92	0.41	0.32	1.91
Na ₂ O	5.24	5.15	3.27	4.03
K ₂ O	3.88	2.84	3.43	3.12
P ₂ O ₅	0.42	0.12	0.19	0.23
LOI	4.59	3.96	4.49	4.23
Total	99.79	100.81	100.36	99.8
mg#	58	40	38	26
K ₂ O/Na ₂ O	0.74	0.55	1.05	0.77
Sc	14	3	4	5
V	74	240	99	89
Cr	n.a.	n.a.	<20	<20
Ni	6	1	<20	<20
Rb	62	96	94	77
Sr	208	176	81	262
Y	9.6	17.8	21	15
Zr	102	115	136	94
Nb	5.2	4.8	8.9	6.8
Ba	237	300	495	231
La	7.5	11	18.1	16
Ce	14.5	21.9	34.1	31
Sm	1.67	3.51	3.87	2.9
Yb	1.19	2.09	2.4	1.8
Th	1.61	2.71	3.93	2.28
U	0.63	0.64	2.03	0.87

Major elements are in wt%, and trace elements are in ppm. Fe₂O₃ (tot) = total iron calculated as ferric oxide. Data from Kavalieris and Wainwright (2005)

8.3 Mt Cu, 200 kt Mo, >14 Moz of Au, and >116 Moz of Ag (Seltmann et al. 2010). The exploration potential of the area is high and regional exploration is ongoing. There is also potential for the discovery of additional, but concealed, high-grade zones as one of the drill holes in the Nakhodka area has intersected an interval averaging 1.5 wt% Cu and 2.1 g/t Au over 147 m (cf. Soloviev 2014, and references therein). The Peschanka property is 100 % owned by Millhouse Capital Ltd., the British investment arm of Roman Abramovich Holdings in London.

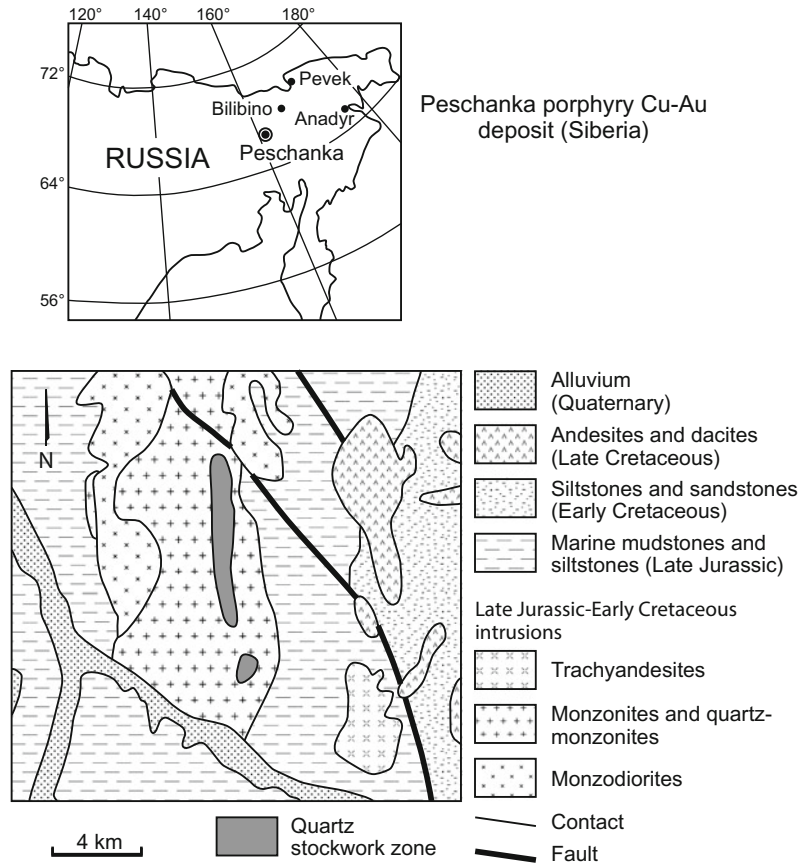
Regional Geology The geology of eastern Siberia is complex and it incorporates several large tectonic terranes: (1) the Siberian Craton; (2) the Western Siberian Lowland; (3) the Proterozoic-Paleozoic orogenic belts; (4) the Late Paleozoic-Mesozoic orogenic belts; and (5) the Cretaceous-Tertiary Okhotsk-Chukotka volcanic belt overprinting easterly orogenic belts (Parfenov et al. 2003; Seltmann et al. 2010). The Baimka ore district is hosted by Paleozoic-Mesozoic orogenic belts adjoining the Siberian Craton to the east, which are interpreted as an amalgamation of late Paleozoic to early Cretaceous island arcs (Sidorov and Eremin 1994; Volkov et al. 2006). Its geological and metallogenic evolution is comparable to the Lachlan Fold Belt in New South Wales, Australia. The Chukotka Autonomous Region does not only host significant low-sulphidation epithermal Au-Te deposits such as the alkaline rock-hosted Dvoynoi (1.1 Moz of Au) and Kupol (2.5 Moz) mines (Nikolaev et al. 2013), but also world-class porphyry copper-gold deposits such as Peschanka and Vetka that are hosted by high-K intrusions (Baksheev et al. 2010).

The polyphase Early Cretaceous Egdygkych pluton has been dated at 138–141 Ma based on U/Pb zircon ages (Baksheev et al. 2013). It represents a composite intrusion that was formed during at least three phases, ranging from (1) a mafic early-stage monzogabbro and monzodiorite phase, through a (2) monzodiorite and monzonite phase, to a (3) late-stage, and more evolved, quartz-monzonite porphyry phase

(Marushchenko 2013; Soloviev 2014). The last is associated with porphyry copper-gold mineralization (Soloviev 2014). The Egdygkych pluton is emplaced within Upper Jurassic marine sedimentary rocks, including mudstones, siltstones, sandstones and conglomerates (Migachev et al. 1995; Soloviev 2014). The pluton has an elongated shape, extending over >25 km with a north-south orientation (Fig. 6.19), and it is structurally controlled by a deep extensional fault zone of similar orientation and with a dextral displacement, locally known as the Baimka Fault (Chitalin et al. 2012). The Egdygkych pluton was formed by progressively more evolved pulses of high-K calc-alkaline melt derived from the cupola of a fractionating magma chamber in the lower crust, comparable to the geological setting of the Goonumbla and Cadia districts in eastern Australia (cf. Heithersay and Walshe 1995; Holliday et al. 2002). The Peschanka deposit is intersected by a series of dykes, including pre- and post-mineral lamprophyres (Volchkov et al. 1982; Maraeva et al. 1988), and post-mineral andesite porphyries (Nikolaev et al. 2014).

Nature of Porphyry Copper-Gold Mineralization Stockwork mineralization is confined to a north-south trending, eastward dipping, sheet-like quartz-monzonite porphyry stock of late Jurassic age that cuts the polyphase Egdygkych pluton and splits into a series of dyke-like apophyses at surface (Seltmann et al. 2010; Soloviev 2014). Mineralization comprises disseminated sulphides and quartz-sulphide stockwork veining including A-type and B-type veins (Fig. 6.20). Typical ore minerals are bornite, chalcopyrite, pyrite, magnetite, molybdenite, and rare native gold (Nagornaya 2010). The stockwork veins are conformal to the quartz-monzonite porphyry phases that merge together at depth, but also extends for tens to, locally, several hundred meters into the surrounding country rocks of the Egdygkych pluton (Baksheev et al. 2012; Soloviev 2014). Deep exploration drilling defines a north-south oriented, elongated stockwork zone of about 7000 m by 1500 m in size and economic mineralization extends to a vertical depth of >700 m (Chitalin et al. 2012; Nikolaev et al. 2014). The quartz

Fig. 6.19 Geological overview of the Peschanka copper-gold deposit, Siberia, Russia. Adapted from Nokleberg et al. (2005) and Chitalin et al. (2012)



stockwork zone extends almost continuously from the south to the north, and the deposit was formed by hydraulic fracturing in the stress field of near-horizontal latitudinal extension (Chitalin et al. 2012). The following vein types can be distinguished: (1) quartz-magnetite-pyrite; (2) quartz-molybdenite; (3) quartz-pyrite-chalcopyrite; (4) high-grade quartz-chalcopyrite-bornite-tennantite; (5) late-stage polymetallic quartz-carbonate-sphalerite-galena-chalcopyrite; and (6) post-mineral carbonate-anhydrite veins, the latter suggesting high oxygen fugacities of the system (cf. Chap. 10). The quartz-molybdenite veins are restricted to the core of the system and its vein density increases with depth. Molybdenite phases are dated at about 140 Ma using Re–Os methods (Baksheev et al. 2013). Sulphide veinlets and stringer veins are

commonly lenticular, *en echelon*-shaped, and clearly controlled by extensional, northeast-striking, strike-slip faults that are related to the regional north-south trending Baimka structure (Chitalin et al. 2012). Late-stage hydrothermal breccias are common in the high-grade core of the system and consist of angular to subangular clasts of quartz-monzonite porphyry cemented by barren quartz. The breccias are typically associated with, but post-date, early hydrothermal biotite-magnetite alteration. Hydrothermal orthoclase alteration rarely occurs as flooding, and more commonly as alteration selvages around quartz veins. The potassic alteration assemblages are overprinted by a late-stage and pervasive sericite alteration, particularly along the lithological contacts between the mineralized quartz-monzonite stock and its

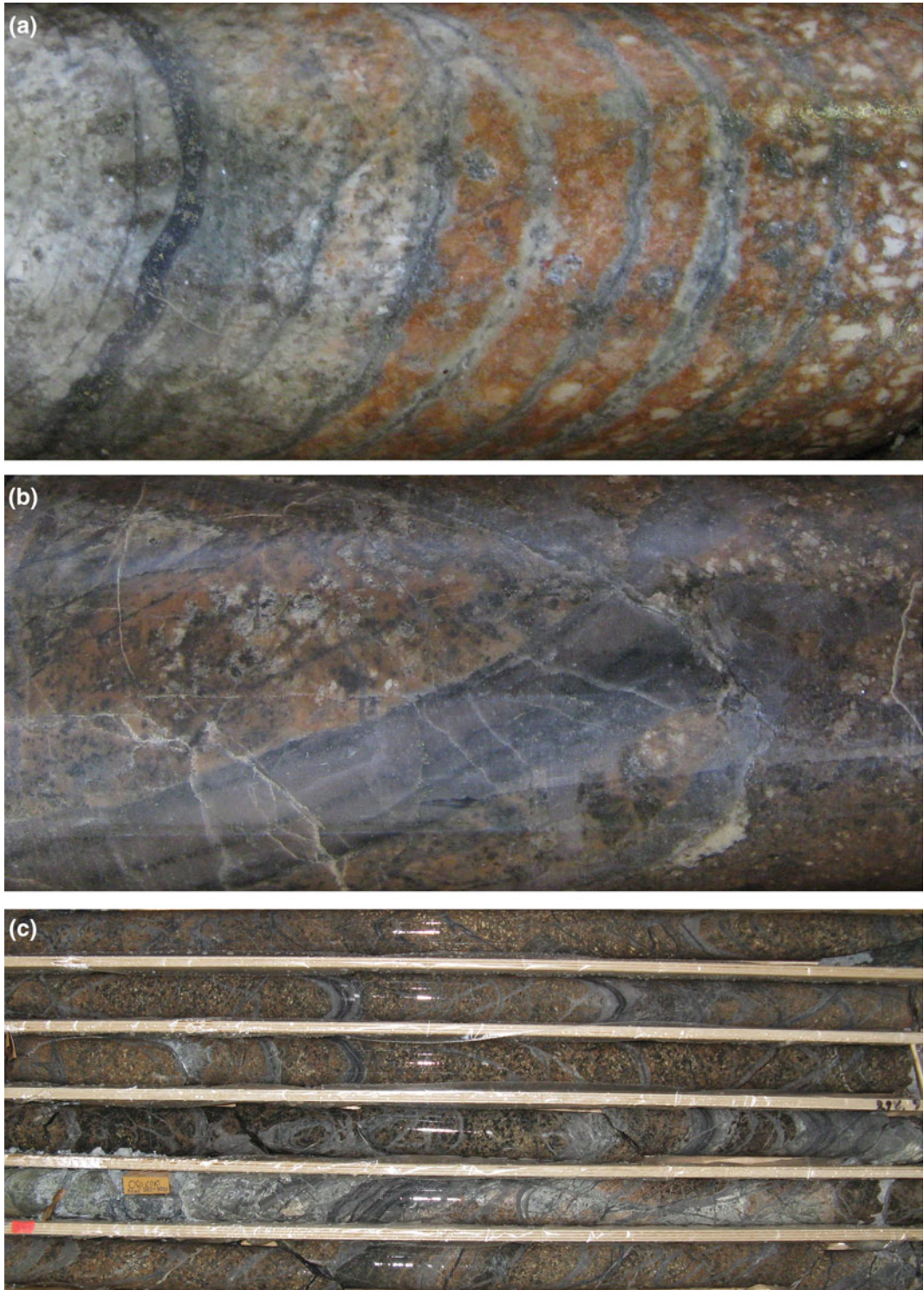


Fig. 6.20 Representative ore samples from the Peschanka copper-gold deposit, Siberia, Russia (photos taken by A. Chitalin): **a** potassic altered quartz-monzonite porphyry cut by sheeted quartz-bornite-chalcopyrite veining [FOV 4×10 cm]. **b** Potassic altered quartz-monzonite

porphyry cut by quartz-molybdenite veins [FOV 4×8 cm]. **c** Drill core box (HQ size) with potassic altered quartz-monzonite porphyry cut by intense quartz-bornite (A- and B-type) stockwork veining from Peschanka

Table 6.9 Major-element analyses (in wt%) of potassic igneous rocks from the Peschanka copper-gold deposit, Siberia, Russia

Province/deposit	Peschanka	Peschanka	Peschanka	Peschanka
Location	Siberia	Siberia	Siberia	Siberia
Rock type	Monzonite	Monzonite	Monzonite	Monzonite
Tectonic setting	Late oceanic arc	Late oceanic arc	Late oceanic arc	Late oceanic arc
Reference	Volchkov et al. (1982)			
SiO ₂	58.23	59.12	58.73	60.02
TiO ₂	0.69	0.69	0.67	0.64
Al ₂ O ₃	18.31	18.12	18.66	18.19
Fe ₂ O ₃	3.24	2.88	2.69	2.17
FeO	2.56	2.26	2.63	2.68
MnO	0.14	0.10	0.14	0.12
MgO	2.60	2.50	1.99	2.09
CaO	4.88	4.37	4.12	4.41
Na ₂ O	4.50	4.68	4.72	5.00
K ₂ O	3.48	3.68	4.57	3.98
P ₂ O ₅	0.27	0.24	0.22	0.22
LOI	0.74	0.83	0.70	0.58
Total	99.64	99.47	99.84	100.10
mg#	46	48	42	45
K ₂ O/Na ₂ O	0.77	0.78	0.97	0.8

Ferric iron is determined using the Wilson method. Data from Volchkov et al. (1982)

wall rocks. However, sericite alteration and abundant D-type veins are also controlled by fractures and faults (Chitalin et al. 2012). The highest Cu and Au grades of the orebody are related to north- and northeast-trending zones where original potassic alteration is overprinted by sericite alteration, suggesting that the extensional strike-slip setting provided by the regional Baimka Fault did not only control the intrusion emplacement, but it remained active during stockwork development and hydrothermal alteration (Chitalin et al. 2012). The extensional northeast-trending strike-slip faults, that also host a series of post-mineral andesite porphyry dykes, are interpreted as Riedel structures related to the Baimka Fault (Chitalin et al. 2012). Propylitic alteration is well developed within the mafic intrusive wall rocks of the Egdygkych pluton, represented by epidote-actinolite-chlorite-albite-tourmaline assemblages (Marushchenko

2013). A thin supergene cap is present on top of the orebody, but largely eroded and <30 m thick. Sulphur isotopic compositions of sulphide phases derived from quartz veins range from -6.4 to +4.8‰, indicating a magmatic sulphur source (Baksheev et al. 2013).

Petrography and Geochemistry of the Potassic Host Rocks The quartz-monzonite porphyry is medium-grained and comprises phenocrysts of K-feldspar, plagioclase, quartz, biotite, clinopyroxene, and amphibole that are set in a feldspathic groundmass with interstitial quartz (Nagornaya 2010). Accessory minerals are rutile, titanite, calcite, and prehnite (Marushchenko 2013).

Whole-rock analyses of monzodiorites and monzonites from the Egdygkych pluton are presented in Table 6.9 (cf. Volchkov et al. 1982;

Soloviev 2014). The samples are characterized by high K₂O contents (up to 4.57 wt%), high K₂O/Na₂O ratios (0.7–0.9), high Al₂O₃ (>18.1 wt%), and low TiO₂ contents (<0.7 wt%) which are typical for high-K calc-alkaline intrusions (Peccerillo and Taylor 1976a, b; Müller et al. 1992b). Distinctly low HFSE, such as TiO₂ (<0.7 wt%), suggest a late oceanic island arc setting, as proposed by Sidorov and Eremin (1994) and Volkov et al. (2006). Unfortunately, no trace element compositions of the rocks have been published to date.

However, high volatile contents of the intrusions are indicated by the presence of high-salinity fluid inclusions in quartz veins and fluorite veins in different parts of the deposit (Chitalin et al. 2012; Nikolaev et al. 2014). Abundant primary magnetite contents of the monzonites and quartz-monzonites, as well as numerous gypsum and anhydrite veins, are suggestive of high oxygen fugacities of the melts (Volkov et al. 2006; Chitalin et al. 2012). This is consistent with high whole-rock Fe₂O₃/FeO ratios of the rocks (0.8–1.27).

6.4 Continental Arc Associations

Porphyry copper-gold and epithermal gold deposits hosted by high-K igneous rocks are known from both the North American Cordillera and the South American Andes (Clark 1993; Kelley and Ludington 2002; Maughan et al. 2002; Sillitoe 2002). The Andes are considered in more detail here because the geochemistry of the host rocks is better documented in the literature. Generally, the host rocks of porphyry copper deposits in continental arcs of the western hemisphere are more felsic than those in late oceanic arcs of the Southwest Pacific (Titley 1975; Sillitoe 1997, 2002). This might be explained by a greater role of crustal assimilation during magma uprise and emplacement in continental arcs (Müller and Groves 1993).

Although there are exceptions, porphyry copper deposits in continental arcs commonly are more Mo-rich, but Au-poor, than those in late oceanic arcs (Sillitoe 1997, 2002).

6.4.1 Bajo de La Alumbraera Copper-Gold Deposit, Catamarca Province, Argentina

Introduction The Bajo de la Alumbraera porphyry copper-gold deposit is located in the Catamarca Province in northwest Argentina (Figs. 6.21 and 6.22). The closest towns are Belen, about 100 km to the southwest, and Tucuman, about 300 km to the northeast. The area belongs to the eastern Cordillera, situated at an altitude of about 2500 m above sea level near the border to Chile, with an arid climate and highly variable temperatures ranging between 0 and 35 °C during the year.

The deposit forms an oval-shaped topographic low below the edges of the unaltered, and thus more resistant, units of the surrounding Farallon Negro Formation. Outcrops of potassic and phyllic alteration in the center of the deposit form a distinct colour anomaly on satellite images. Small copper occurrences in the Farallon Negro area were known since the nineteen seventies, but no systematic exploration was undertaken. Significant porphyry copper-gold mineralization was discovered and subsequently developed by MIM Holdings Ltd in the early-nineties. Commercial production commenced as an open pit operation in February 1998 and the project's current ownership structure is 50 % Glencore (the operator), 37.5 % Goldcorp, and 12.5 % Yamana Gold Inc.

Bajo de la Alumbraera ranks among the ten largest porphyry copper-gold deposits in the world, and it is one of the biggest gold producers in South America. The total resource, before mining, was 806 Mt at 0.53 wt% Cu and 0.64 g/t Au (D. Keough, pers. comm., 1998). In

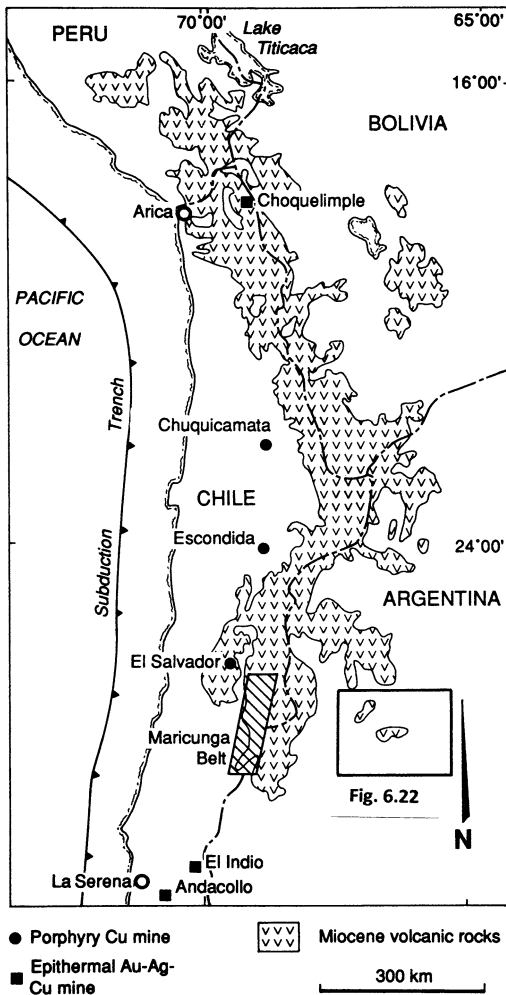


Fig. 6.21 Geographic overview of the major copper-gold deposits of the Chilean and Argentinian Andes that are hosted by high-K calc-alkaline rocks. Modified after Vila and Sillitoe (1991)

December 2013, proven ore reserves were 178 Mt at 0.35 wt% Cu and 0.35 g/t Au (cf. GlencoreX-strata—Resources & Reserves Report 2013).

Regional Geology Northwest Argentina consists of three geological provinces: (1) the Puna, (2) the Cordillera Oriental, and (3) the Sierras Pampeanas. The high-K calc-alkaline rocks that host the Bajo de la Alumbrera deposit belong to the Farallon Negro Formation and are situated in the northernmost Sierras Pampeanas (Figs. 6.21 and 6.22).

The Sierras Pampeanas comprise a series of subparallel, north-trending, reverse fault-bounded, mountain ranges of Upper Proterozoic to Lower Paleozoic basement rocks which are separated by wide flat valleys in the foreland of the Central Andes (Caelles 1979). The thrusts and reverse faults commonly dip at about 60° to the east and have throws in excess of 7000 m (Strecker et al. 1989). The basement rocks are predominantly amphibolites-facies mica schists and paragneisses which, in places, have been intruded by Upper Ordovician to Silurian granitoids (Caelles 1979). The Upper Ordovician to Silurian period in the Sierras Pampeanas was characterized by widespread plutonic activity and compressional deformation. This is consistent with modern plate-tectonic reconstructions of that time, implying collision between the eastern part of the North American continent and the western part of the South American continent during the Ordovician (Dalziel 1995).

The basement blocks have been uplifted along reverse faults during the Pliocene and early Pleistocene (Strecker et al. 1989), thus forming the intramontane basins of both the Puna and Sierras Pampeanas of northwest Argentina (Schwab and Lippolt 1974). The Pampean structural style is similar to that of the Laramide Ranges in western North America (Kay and Gordillo 1994), and has been suggested to be characteristic of foreland deformation over shallow subduction zones (Jordan and Allmendinger 1986; Introcaso et al. 1987).

In the Andes, the subduction angle varies along strike, and Recent volcanism is restricted to zones where the dip is about 30° (Kay et al. 1987, 1988, 2005). Miocene to Pliocene magmatism in the Sierras Pampeanas has been derived from the so-called “flat-slab zone”, which represents the segment of the subducting oceanic Nazca Plate between 28° and 33°S (Kay et al. 1987, 2005; Kay and Abbruzzi 1996). In this zone, the subduction angle increasingly shallowed during the Miocene and Pliocene, beginning at ca. 18 Ma (Caelles 1979), probably caused by the subduction of a bend in the Juan-Fernandez Ridge (Pilger 1984). The shallowing subduction angle was accompanied by a

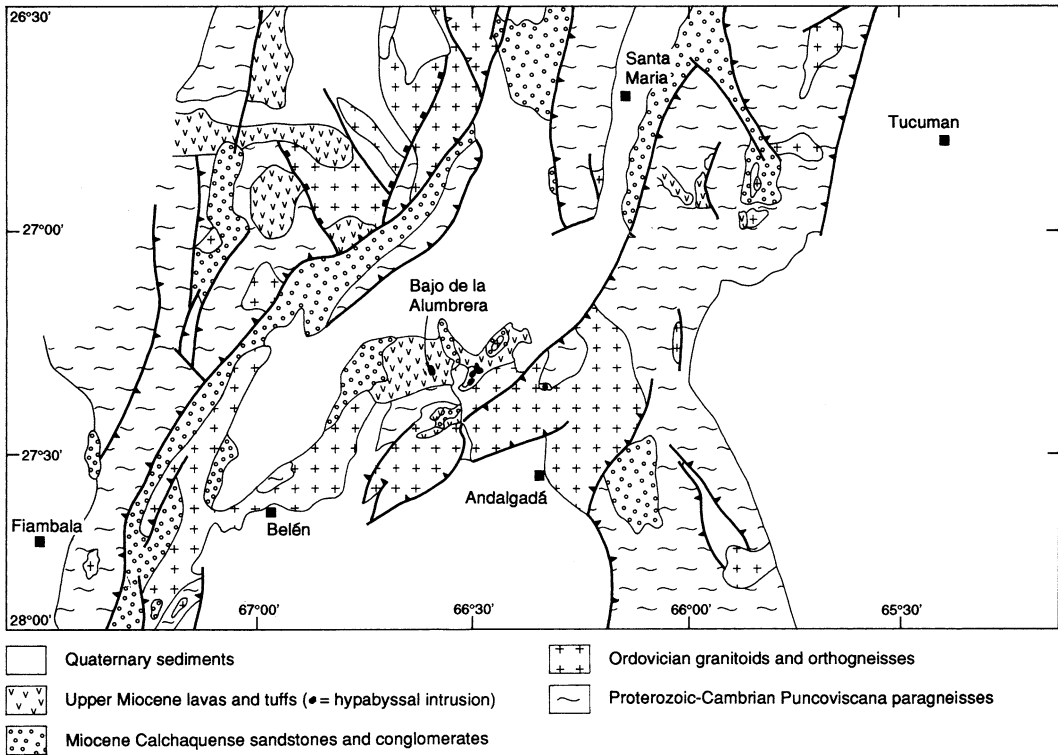


Fig. 6.22 Geological overview of the Catamarca Province, northwest Argentina, showing the location of the Bajo de la Alumbra copper-gold deposit. Modified after

Allmendinger et al. (1983), Allmendinger (1986), and Strecker et al. (1989)

progressive enrichment of the mantle wedge in LILE, and an increase in Pb and Σ Nd values, resulting in enrichment of melts from the Upper Miocene relative to those from the Lower Miocene (Kay and Abbruzzi 1996). Quaternary and present-day volcanism is lacking in the flat-slab zone (Kay and Gordillo 1994; Kay et al. 2005; Stern et al. 2011).

The present subduction angle in this zone has been estimated to be about 10° , in contrast to the normal angle of about 30° to the north and south of the flat-slab zone (Caelles 1979) where Quaternary volcanism has been recorded (e.g. Strecker et al. 1989). The seismic transition between the flat-slab zone and the more steeply dipping subduction zone further to the north occurs between 25° and 28° S, and is characterized by a flexure below the 100-km depth contour for the Benioff Zone (Strecker et al. 1989). Progressive subduction of kinks or flexures in the

downgoing oceanic slab might eventually lead to tears, thus promoting the uprise of deep asthenospheric mantle melts that are normally blocked off by the subducting slab (cf. M ller et al. 2002b; Logan and Mihalynuk 2014). The K-rich calc-alkaline Farallon Negro Formation, which hosts Bajo de la Alumbra (Ulrich and Heinrich 2002), is situated within this “transitional zone”, immediately to the north of the gently dipping segment where the shallow subduction angle gradually increases again to 30° (Caelles 1979). The brief history of the Farallon Negro volcanic complex hosting the Bajo de la Alumbra deposit differs from that of other Andean provinces hosting porphyry copper deposits (Harris et al. 2004a). For example, at the El Salvador porphyry copper district in Chile, magmatism related to copper mineralization was episodic in regional igneous activity that occurred over tens of millions of years. By contrast,

Bajo de la Alumbraera resulted from the superposition of multiple porphyry-related hydrothermal systems, temporally separated by only a million years (Harris et al. 2004a).

The emplacement of the Cenozoic potassic igneous complexes of northwest Argentina, such as the Farallon Negro Formation, was controlled by major northwest-striking lineaments (Allmendinger et al. 1983; Salfity 1985). Allmendinger et al. (1983) postulated a sinistral strike-slip movement of up to 20 km along the lineaments, which are characterized by small negative gravity anomalies (Götze et al. 1987), probably related to young volcanic activity which extends along these structures far to the east of the main volcanic chain (Schreiber and Schwab 1991).

Nature of Porphyry Copper-Gold Mineralization Reconstruction of the volcanic structure suggests that the top of the exposed orebody was originally emplaced beneath about 2500 m of andesite, but not directly beneath the vent of a stratovolcano (Proffett 2003; Harris et al. 2006). Detailed mapping suggests that porphyry copper-gold mineralization is centered on a closely spaced cluster of small dacite porphyry stocks and dykes, emplaced into andesites during seven phases of intrusion (Proffett 2003). Geochronological work has divided the porphyry intrusions into two temporally distinct events: (1) one group emplaced at ca. 8.0 Ma (early porphyries), and another intruded about a million years later (late porphyries; Harris et al. 2004b). Both groups of intrusions are associated with varying degrees of hydrothermal alteration (Proffett 2003; Harris et al. 2004b).

Bajo de la Alumbraera is characterized by a classical alteration zonation, ranging from a potassic core which typically contains the most intense quartz-vein stockworks and the highest gold grades (~ 2 g/t Au), surrounded by propylitization and an annular phyllic overprint (Müller and Forrestal 1998; Ulrich et al. 2001; Proffett 2003; Ford et al. 2015). High-grade stockwork mineralization includes A-type and B-type quartz-sulphide veins, hosted by the earlier dacite

porphyries and associated with abundant hydrothermal orthoclase, both occurring as flooding and alteration selvages around quartz veins (Ulrich et al. 2001; Ulrich and Heinrich 2002; Proffett 2003). These zones are typically overprinted by a later phase of stockwork veins introduced by subsequent porphyry intrusions and accompanied by hydrothermal biotite-magnetite-anhydrite assemblages (Proffett 2003). Chalcopyrite and auriferous pyrite represent the most dominant ore minerals, with rare bornite and enargite, occurring both in the quartz veins and as disseminations (Ulrich and Heinrich 2002). Originally, the central zone with potassic alteration and stockwork mineralization cropped out at surface due to a high erosion level, and was the focal point when open pit mining commenced in 1998. The argillic cap of the system has been removed by erosion. Potassic alteration is focused on the dacite porphyries, but biotite-magnetite assemblages locally extend into the andesitic wall rocks within up to 100 m of the intrusions (Ulrich and Heinrich 2002). Abundant hydrothermal magnetite (up to 10 vol.%), that is both disseminated and in small veins, as well as abundant anhydrite and gypsum veins (cf. Proffett 2003), imply high oxygen fugacities of the hydrothermal fluids.

Metallurgical studies have shown that native gold occurs mainly as inclusions within pyrite and chalcopyrite. Interestingly, no gold occurs within the structure of the magnetite (S. Brown, pers. comm., 1994), which is a known host mineral of gold in many porphyry copper-gold deposits in the Philippines (I. Kavalieris, pers. comm., 1996).

Petrography and Geochemistry of the Potassic Host Rocks The Upper Miocene (i.e. 6–10 Ma) Farallon Negro Formation forms an igneous complex of lava flows, tuff breccias, and agglomerates, which, in places, are intruded by comagmatic hypabyssal stocks and domes (Müller and Forrestal 1998). Petrographically, both lava flows and tuffs vary from basaltic through latitic to rhyolitic in composition. The comagmatic intrusions (ca. 7.9 Ma) consist of monzonite stocks and dykes and hypabyssal trachyandesites and dacites (Stults 1985). The entire volcanic succession represents the basal

remnants of a large, formerly up to 6 km high, stratovolcano some 16 km in diameter (Llambias 1972), and covers about 700 km² (Caelles 1979). The complex is situated within a tectonic depression bounded by uplifted Lower Paleozoic basement rocks of the Sierra de Quilmes to the north and the Sierra de Aconquija to the east. The igneous rocks were erupted through a crystalline basement comprising amphibolites-facies metasedimentary rocks and granitoid batholiths (Müller and Forrestal 1998).

Porphyry copper-gold mineralization at Bajo de la Alumbrera was coeval with the emplacement of a hypabyssal dacite dome (H. Salgado, pers. comm., 1994), and several other prospects for porphyry copper-gold (e.g. Cerro Durazno, Agua Rica) and epithermal gold (e.g. Cerro Atajo) are known within the Farallon Negro Formation (Müller and Forrestal 1998; Landtwing et al. 2002). The hypabyssal dacite has a porphyritic texture consisting of phenocrysts of plagioclase, quartz, and biotite, with minor amphiboles and accessory apatite and magnetite, within a fine-grained groundmass mainly comprising feldspar and quartz (Müller and Forrestal 1998; Harris et al. 2004b). There are two petrographically distinct types of quartz eyes in the mineralized dacite porphyries (Harris et al. 2004b). Type 1 consists of typical quartz phenocrysts that are large, up to 8 mm in diameter, rounded and irregular anhedral crystals. Type 2 quartz eyes are elliptical, small (<2 mm), and consist of saccharoidal aggregates of anhedral quartz crystals (Harris et al. 2004b). They are distinctly different from the quartz phenocrysts in that they are intergrown with crystals of feldspar and magnetite. In places, narrow, anastomosing zones of graphic quartz-K-feldspar intergrowths and ragged biotite connect type-2 quartz eyes (Harris et al. 2004b). This connectivity can be over as much as 10 cm, but more commonly, these interconnected miarolitic cavities are approximately 1–2 mm across and 5 cm or less in length (Harris et al. 2004b). The presence of hydrous phenocrysts such as biotite and hornblende, as well as miarolitic cavities, suggests high volatile contents (H₂O, Cl, SO₂,

SO₃) of the parental melts. Accessory magmatic magnetite in the samples is indicative of high oxygen fugacities of the high-K calc-alkaline magmas (Sillitoe 1979; Müller et al. 2001). Proximal to the orebody, the rocks are overprinted by intense secondary biotite-magnetite alteration, in which the magnetite content of the dacites may be as high as 10 vol.% (Brown, pers. comm., 1994).

The lava flows and pyroclastic deposits of the Farallon Negro Formation have typical high-K calc-alkaline compositions, whereas the shallow comagmatic dacite porphyry intrusions, that are genetically associated with the mineralization at Bajo de la Alumbrera, are derived from fractionated high-K calc-alkaline magmas, transitional to shoshonites (Müller and Forrestal 1998; Harris et al. 2004b). The samples are characterized geochemically (Table 6.10) by very high Ce/Yb ratios (22–54) that are typical for shoshonitic rocks (Pearce 1982; Müller et al. 1992b) and rather low, but variable, Al₂O₃ contents (8.82–15.90 wt%). Fractional crystallization resulted in low mg# (<27) and low concentrations of mantle-compatible trace-elements (e.g. <142 ppm Cr, <7 ppm Ni). The rocks are characterized by high concentrations of LILE (e.g. up to 5.81 wt% K₂O; up to 113 ppm Rb, 181 ppm Sr, 504 ppm Ba), moderate LREE (e.g. up to 32 ppm La, 65 ppm Ce), and low HFSE (e.g. <0.60 wt% TiO₂, <115 ppm Zr, <9 ppm Y, <11 ppm Nb, <4 ppm Hf). Their geochemical fingerprints are typical for potassic igneous rocks derived in a mature continental arc setting (Figs. 6.2, 6.3, 6.4, 6.5 and 6.23).

6.4.2 Bingham Copper-Molybdenum Deposit, Utah, USA

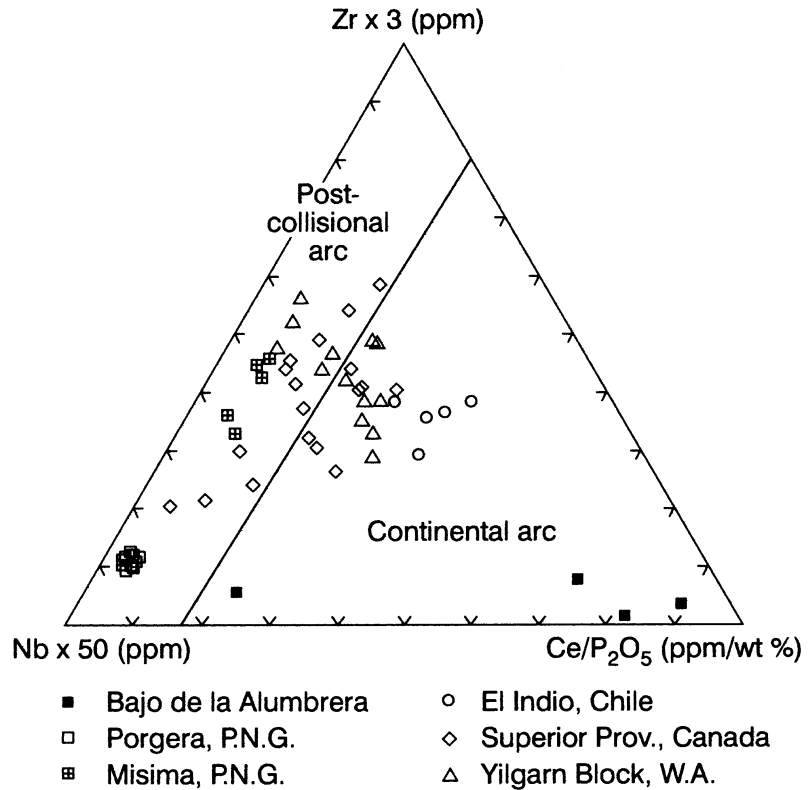
Introduction The Bingham porphyry copper ± gold deposit (Fig. 6.24) is located about 32 km southwest of Salt Lake City, in the central Oquirrh Mountains, Utah (Bowman et al. 1987; Waite et al. 1997). With a production of 1300 million tonnes of 0.85 wt% copper ore from 1904 to 1976, the Bingham mining district represents the largest porphyry copper deposit of North

Table 6.10 Major- and trace-element analyses of dacitic rocks from the Bajo de la Alumbraera copper-gold deposit, Catamarca Province, Argentina

Province/deposit	Bajo de la Alumbraera			
Location	Argentina	Argentina	Argentina	Argentina
Rock type	Dacite porphyry	Dacite porphyry	Dacite porphyry	Dacite porphyry
Tectonic setting	Continental arc	Continental arc	Continental arc	Continental arc
Reference	Müller and Forrestal (1998)			
SiO ₂	69.90	67.30	65.10	66.80
TiO ₂	0.35	0.60	0.51	0.30
Al ₂ O ₃	10.30	15.90	15.00	8.82
Fe ₂ O ₃	2.45	4.40	5.81	4.49
FeO	3.36	0.69	1.19	7.12
MnO	0.15	0.01	0.01	0.07
MgO	0.99	0.77	0.83	0.92
CaO	1.56	0.09	0.30	0.91
Na ₂ O	0.80	0.20	0.20	0.45
K ₂ O	5.81	4.32	3.85	5.67
P ₂ O ₅	0.10	0.11	0.04	0.01
LOI	3.98	5.49	6.88	4.29
Total	99.75	99.88	99.72	99.85
mg#	27	26	21	15
Ce/Yb	22.5	29	54.1	25.7
Sc	n.a.	n.a.	n.a.	n.a.
V	79	93	81	195
Cr	124	69	62	142
Ni	7	6	4	6
Rb	113	87	75	74
Sr	181	30	24	158
Y	8.6	6	6	5.6
Zr	78	111	115	72
Nb	11	3	3	7
Ba	504	243	134	487
Hf	2.9	3.9	4	2.4
La	9	32	31	10
Ce	18	61	65	18
Sm	n.a.	n.a.	n.a.	n.a.
Yb	0.8	2.1	1.2	0.7

Major elements are in wt%, and trace elements are in ppm. Data from Müller and Forrestal (1998)

Fig. 6.23 $(Zr \times 3)$ - $(Nb \times 50)$ - (Ce/P_2O_5) triangular diagram (see Chap. 3) showing only samples from continental and postcollisional arcs. Samples from the latter tectonic setting show some overlap due to P mobilization in altered Archean shoshonitic lamprophyres. Adapted from Müller and Groves (1993)



America and the world's largest skarn copper deposit with significant by-products of molybdenum, gold, and silver (Einaudi 1982). As of 2004, Bingham yielded more than 17 million tons of copper, 23 million oz of gold, 190 million oz of silver, and 850 million pounds of molybdenum (M. Landtwing, pers. comm., 2004). Copper oxide mineralization in the area was first discovered in 1848 by two Mormon settlers, sons of Erastus Bingham, who lend their name to the deposit. However, it was not until 1863 that extraction of the first ore began and the mineral potential of Bingham Canyon began to be widely recognized. Industrial mining commenced in 1906 by the Utah Copper Corporation which was taken over by Kennecott Copper Corporation in 1936. The mine is now 100 % owned and operated by the Rio Tinto Group.

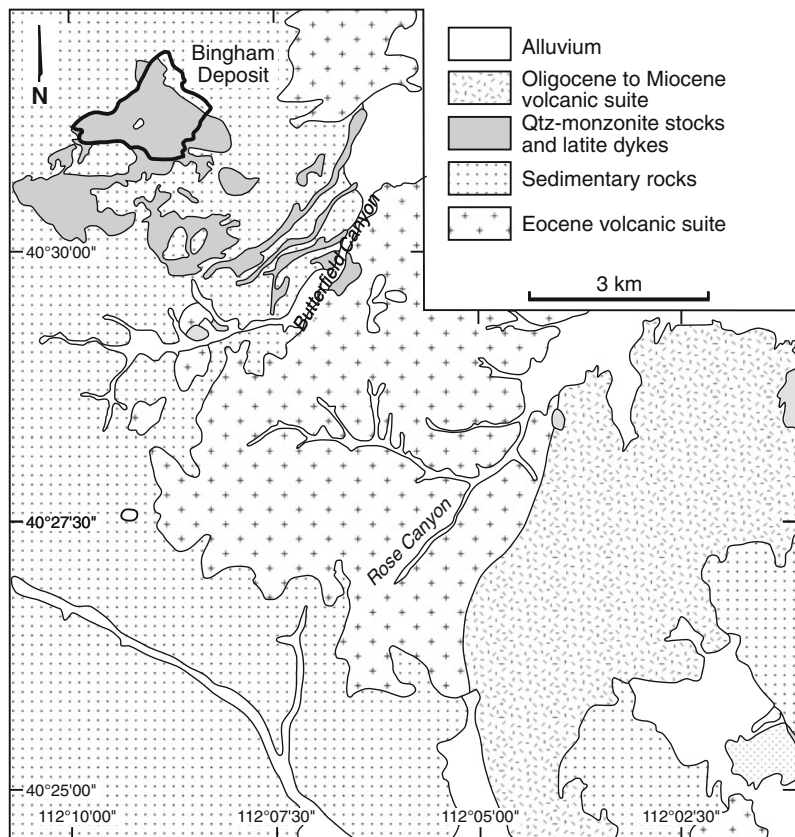
Regional Geology A series of Eocene mineralized intrusions in northern Utah, including the

polyphase quartz-monzonites from Bingham, occur along an east-west lineament, locally known as the Uinta-Cortez Axis (Roberts et al. 1965). This lineament is considered to represent an Archean-Proterozoic plate suture (Presnell 1997). After suturing of the Archean-Proterozoic plates, a rifted continental margin formed, and Proterozoic and Paleozoic sediments were deposited (Hintze 1988). The sedimentary basin in which the rocks accumulated is known as the Oquirrh Basin and contains up to 7.5 km of Late Pennsylvanian to Early Permian quartzites, shales and limestones (Jordan and Douglas 1980). Folding and thrusting of the sedimentary units occurred during the Jurassic and Cretaceous, respectively (Constenius 1996) and is characterized by large, open, northwest-striking anticlines and synclines (Lanier et al. 1978a). The dominant fold within the mining area strikes northwest and plunges 45° northwest, with the igneous intrusions and porphyry copper

mineralization localized along the southwestern limb (Bowman et al. 1987). Presnell (1997) suggests that two extensional episodes occurred during the Tertiary. Northeast-striking faults that formed during the extensional tectonics host a significant portion of the vein-related late-Eocene mineralization, implying that these faults were open at least during the Bingham mineralization, dated at 39.8–37.5 Ma (Warnaars et al. 1978). The Bingham system is comprised of several small, polyphase and mineralized late-Eocene quartz-monzonite and latite porphyry stocks (Fig. 6.24) and dykes emplaced in older equigranular monzonite as well as Paleozoic quartzites and limestones (Maughan et al. 2002; Landtwing et al. 2010). The Bingham stock has a surface extent of about 3 km. Most of the Bingham quartz-monzonites are steep-walled intrusions that may have vented just as readily

as the coeval latite dykes (Moore 1973). Maughan et al. (2002) document that rare mineralized minette dykes within the ore body (37.74 ± 0.11 Ma) have the same age as the youngest ore-related intrusion, the quartz-latite porphyry (37.72 ± 0.09 Ma). Trace elements of sapphire crystals (<1 mm in diameter) are present in the Bingham quartz-monzonite porphyry, nearby latite porphyry dykes, latitic minette clasts from block and ash flow deposits, and the ash and pumice portion of the block and ash flows (Maughan et al. 2002). These unusual characteristics strongly argue for a co-magmatic origin for the volcanic and intrusive rocks at Bingham. The quartz-monzonites show ample evidence of prior magma mixing and recent studies suggest that Bingham may be only world-class because of substantial contributions of sulphur and metals from a basic alkaline

Fig. 6.24 Simplified geologic map of the eastern Oquirrh Mountains in relation to Bingham intrusive units, Utah, USA. The location of the Bingham copper-gold deposit is outlined in *black*. Modified after Maughan et al. (2002)



magma injected into an otherwise unremarkable calc-alkaline magma chamber (Maughan et al. 2002).

Nature of Porphyry Copper Mineralization

Porphyry copper \pm gold mineralization probably took place during several pulses of hydrothermal activity which started at 39.8 Ma and continued until the emplacement of minette and latite dykes at about 37.7 Ma (Warnaars et al. 1978; Maughan et al. 2002). Mineralization is focused on a hydrothermally altered composite stock of quartz-monzonite intrusions, first referred to as the Bingham stock by Butler (1920). Three alteration zones can be distinguished: (1) a central potassic alteration zone, (2) a surrounding propylitic alteration zone, and (3) a late-stage and mainly fault-controlled sericitic alteration zone (Lanier et al. 1978a).

Porphyry-type mineralization occurs mainly within the potassic alteration zone which overprints the quartz-monzonite stocks and latite porphyry dykes. Potassic alteration typically consists of hydrothermal biotite-magnetite assemblages, partially replacing the groundmass of the porphyries, and less common orthoclase selvages around quartz veins (Bowman et al. 1987; Landtwing et al. 2005, 2010). Mineralization consists of a high-grade core with pyrite and chalcopyrite, a molybdenite stockwork zone, and an outermost pyrite zone (Bowman et al. 1987). The surrounding propylitic alteration zone partially overlaps potassic alteration and its typical minerals include actinolite, chlorite, and epidote (Keith et al. 1997). The late-stage sericitic alteration comprises sericite that has replaced plagioclase and mafic minerals, and is developed most prominently in the southwestern part of the Bingham deposit, overprinting all dyke types as well as sedimentary rocks (Gruen et al. 2010; Landtwing et al. 2010). Quartz stockworks include A-type and B-type veins and within an area of about 1×2 km² centered in the quartz-monzonite stock, total vein density exceeds 4 vol.%, locally rising to >10 vol.% in the center (Gruen et al. 2010). The central

high-grade orebody contains an average of 0.8 wt % Cu and 0.6 g/t Au. The highest Au concentrations correlate systematically with the presence of bornite and digenite as the dominant Cu minerals (Gruen et al. 2010). Many veins show multiple generations of successively opened and quartz-filled fractures of changing and random orientation. Quartz-chalcopyrite \pm bornite veins are typically 2–10 mm wide and can be followed for tens of centimeters, but wider and more extensive veins occur sporadically (Gruen et al. 2010). Quartz-molybdenite veins form a distinct later vein generation that consistently crosscuts all quartz stockwork veins and even the latest porphyry dykes (Redmond and Einaudi 2010). They commonly occur as single, laterally extensive veins with straight walls that are at least 1 cm wide. In contrast to the quartz stockwork veins, the quartz-molybdenite veins are commonly symmetrical with free-standing euhedral quartz crystals in the center (Gruen et al. 2010). Molybdenite occurs as a selvage that predates most quartz, as bands within the quartz, or as euhedral platelets overgrowing the quartz. Minor chalcopyrite in these veins predominantly occurs as late vug-filling crystals; bornite is absent. The quartz-molybdenite veins are typically associated with biotite-stable alteration extending at least tens of centimeters away but they lack hydrothermal orthoclase selvages (Gruen et al. 2010). The molybdenum ore shell broadly overlaps with the copper ore shell at its inner and lower rim, but it extends to greater depths. Although quartz-vein stockworks are most intensely developed in the quartz-monzonite porphyry, vein truncations at the intrusive contacts of later porphyries indicate that a similar sequence of vein formation was repeated with decreasing intensity after the emplacement of each porphyry intrusion (Redmond et al. 2004; Redmond and Einaudi 2010).

Structural observations on the evolving dyke and vein geometry of the Bingham porphyry copper system indicate that the concentrically zoned ore shell is a result of rock extension ahead of a broad fluid pressure front driven by a deep hydrous and volatile-rich magma chamber (Gruen et al. 2010).

Petrography and Geochemistry of the Potassic Host Rocks

The Bingham intrusive system consists of five separate mineralizing intrusions (Redmond and Einaudi 2010). From oldest to youngest they are quartz-monzonite porphyry (80 vol.%), latite porphyry (12 vol.%), biotite porphyry (1 vol.%), quartz-latite porphyry breccia (2 vol.%), and quartz-latite porphyry (5 vol.% of ore-forming intrusions). Additionally, two thin mineralized minette dykes are documented at the Bingham deposit. One of the minette dykes was dated at 37.74 ± 0.11 Ma (Deino and Keith 1997). Initial mapping of the Bingham stock revealed that the outer portions of the quartz-monzonite porphyry are more mafic, and darker grey, than the interior mass of the intrusion (Maughan et al. 2002). The internal part is locally known as “hybrid quartz-monzonite porphyry”, because it contains mafic xenoliths and early workers inferred that it had formed by assimilation of the more mafic, early-stage, monzonite (Lanier 1978a). Locally, these xenoliths contain up to 20 vol.% biotite phenocrysts indicating that the parental melt of the hybrid quartz-monzonite porphyry may have mixed with a more basic and volatile-rich component prior to its emplacement rather than assimilating large volumes of adjacent wall rock at epizonal levels (Maughan et al. 2002). Studies by Keith et al. (1995, 1997) suggest that the latites and quartz-monzonites at Bingham are the products of mixing of shoshonites and minettes with intermediate calc-alkaline melts. However, petrographic evidence of mixing was obscured by mineralization (Maughan et al. 2002). Prior to mining, the hybrid quartz-monzonite porphyry formed two large light grey rootless intrusions with abundant quartz phenocrysts (>20 vol.%), up to 250 m wide (Lanier et al. 1978a). Most of it has now been excavated and only a small portion remains. Both quartz-monzonite phases have more crowded phenocrysts at higher elevations and are more equigranular at deeper levels (Maughan et al. 2002). The Bingham quartz-monzonites are commonly grey. Phenocryst abundance is variable with about 20 vol.% K-feldspar (up to 8 mm), 10 vol.% quartz (1–2 mm), 5–10 vol.% plagioclase, and 5–8 vol.%

biotite (up to 5 mm). In places, the stocks are intersected by hypabyssal andesite porphyry dykes, which belong to a swarm of northeast-trending plagioclase-phyric dykes and sills cutting the northwest margin of the Bingham stock (Lanier et al. 1978a; Warnaars et al. 1978). High halogen (i.e. Cl and F) contents of the parental melts that formed the Bingham intrusive system are suggested by the presence of fluorapatite in the groundmass (Wilson 1978).

Table 6.11 shows representative whole-rock analyses for the potassic igneous rocks from Bingham (Waite et al. 1997; Maughan et al. 2002). The samples are defined by very high LILE concentrations (e.g. up to 6.63 wt% K₂O, up to 301 ppm Rb, 708 ppm Sr, 2100 ppm Ba), moderate LREE concentrations (e.g. <99 ppm La, <152 ppm Ce), and low HFSE abundances (e.g. <0.93 wt% TiO₂, <20 ppm Y, <229 ppm Zr, <16 ppm Nb). Fractional crystallization resulted in relatively low mg# (<63), and elevated concentrations of mantle-incompatible trace-elements (e.g. up to 49 ppm Th, up to 10 ppm U). The rocks have elevated P₂O₅ concentrations (up to 0.32 wt%), which is consistent with the presence of fluorapatite microphenocrysts (Wilson 1978). Plotting the samples on discrimination diagrams indicates that they were formed in a mature continental arc-setting (cf. Maughan et al. 2002). Note that several samples from the Nb-rich minette dykes show within-plate affinities, suggesting the input of a basic alkaline melt, probably derived from the deep asthenospheric mantle, into the fractionating magma chamber beneath Bingham (Maughan et al. 2002).

6.4.3 El Indio Gold Deposit, Chile

Introduction The Chilean Andes represent the largest copper province in the world (Sillitoe and Camus 1991). Since the discovery of the epithermal gold deposits El Indio, Tambo, Pascua-Llama, Choquelimpie, El Hueso, La Copia, Puren, and Veladero, Chile has also earned the status of a major gold province (Sillitoe 1991,

Table 6.11 Major- and trace-element analyses of potassic igneous rocks from the Bingham copper-gold deposit, Utah, USA

<i>Province/deposit</i>	Bingham	Bingham	Bingham	Bingham
<i>Location</i>	Utah, USA	Utah, USA	Utah, USA	Utah, USA
<i>Rock type</i>	Latite	Dacite	Quartz-Monzonite	Mafic xenolith within qtz-monzonite
<i>Tectonic setting</i>	Continental arc	Continental arc	Continental arc	Continental arc
<i>Reference</i>	Waite et al. (1997)	Waite et al. (1997)	Maughan et al. (2002)	Maughan et al. (2002)
SiO ₂	61.54	62.89	67.25	59.64
TiO ₂	0.69	0.69	0.62	0.93
Al ₂ O ₃	14.81	14.50	15.82	13.50
Fe ₂ O ₃	6.19	6.10	3.30	7.66
FeO	n.a.	n.a.	n.a.	n.a.
MnO	0.09	0.09	0.01	0.02
MgO	4.23	4.21	3.32	9.03
CaO	5.31	4.49	1.59	1.72
Na ₂ O	3.14	2.98	2.45	0.46
K ₂ O	3.67	3.76	5.28	6.63
P ₂ O ₅	0.34	0.32	0.25	0.32
LOI	1.30	2.37	0.54	0.69
Total	100.01	100.02	100.43	100.60
mg#	57	58	67	70
K ₂ O/Na ₂ O	1.17	1.26	2.15	14.41
Sc	n.a.	n.a.	7	24
V	142	130	82	163
Cr	166	853	66	473
Ni	52	45	59	157
Rb	105	216	170	301
Sr	708	203	529	202
Y	20	15	16	9
Zr	229	228	204	164
Nb	13	16	10	10
Ba	2074	2100	1601	767
La	76	99	66	57
Ce	117	152	132	135
Sm	n.a.	n.a.	9	9
Yb	n.a.	n.a.	1.6	n.a.
Th	n.a.	n.a.	49	11
U	n.a.	n.a.	9	10

Major elements are in wt%, and trace elements are in ppm. Fe₂O₃ (tot) = total iron calculated as ferric oxide. Data from Waite et al. (1997) and Maughan et al. (2002)

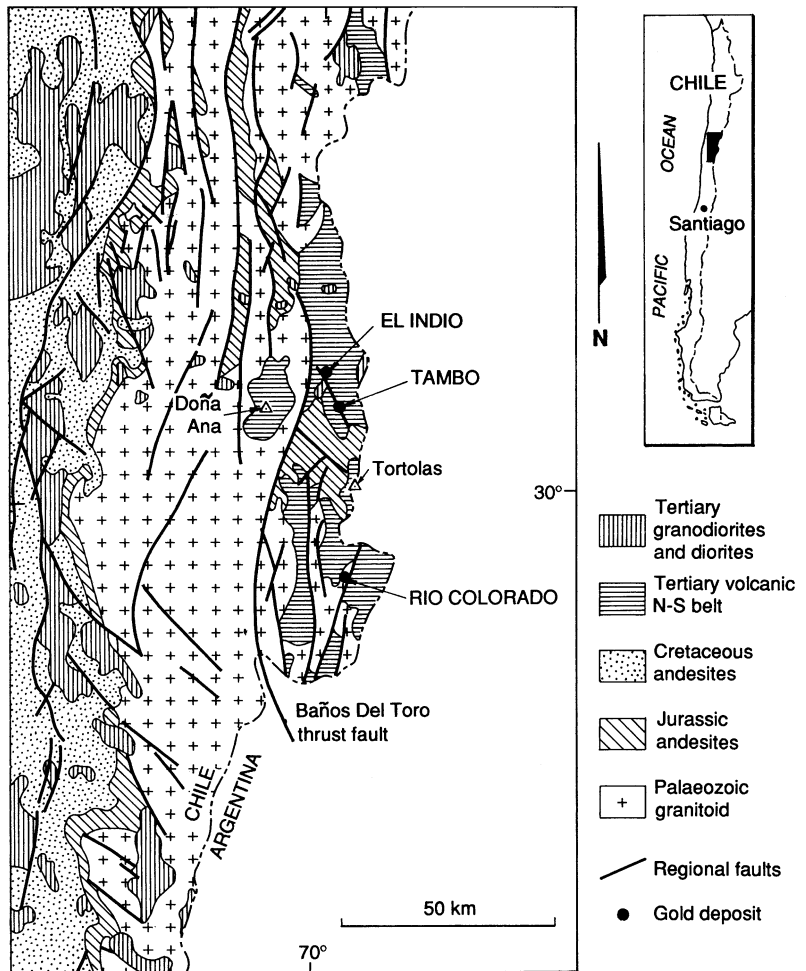
2008; Clark 1993). Most of the principal epithermal- or porphyry-type gold deposits with more than 10 tonnes of contained gold are associated with Miocene stratovolcanoes and/or dome complexes (Arribas pers. comm., 2013). These gold deposits are concentrated in northern and central Chile, commonly at altitudes in excess of 4000 m above mean sea level (Sillitoe 1991, 2008).

El Indio (Fig. 6.25) is located about 500 km north of Santiago and 180 km east of La Serena in a rugged mountainous terrain close to the Argentinian border. The mine workings reach 4150 m above sea level (Siddeley and Araneda 1986; Jannas et al. 1990). In 1994, the El Indio

gold-silver mine was acquired by Barrick Gold, which operated the mine until its closure in 2002 as a combined open pit and underground operation. Regional exploration in the vicinity of El Indio by Barrick Gold geologists led to the discovery of the additional gold deposits Pascua-Llama, Tambo, and Veladero, and the district became locally known as the El Indio-Pascua Au-Ag belt (Bissig et al. 2001, 2002; Deyell et al. 2005).

El Indio is one of a number of epithermal gold deposits related to high-K calc-alkaline rocks within the Main Cordillera of the Chilean Andes (Kay et al. 1987; Kay and Mpodozis 2001). The mine produced about 5.5 Moz of gold, 24 Moz of silver, and 500,000 tonnes of copper (Robert,

Fig. 6.25 Geological overview of the high Andes of north-central Chile showing the locations of the El Indio and Tambo gold deposits. Modified after Siddeley and Araneda (1986)



pers. comm., 2014) and, together with its neighboring deposits, Pascua-Llama (17 Moz of Au), Tambo (1 Moz Au), and Veladero (11 Moz Au), El Indio was one of the most important gold-silver producers in Chile (Bissig et al. 2003; Deyell et al. 2005).

Regional Geology The Chilean copper-gold deposits are part of a series of linear volcano-plutonic arcs that were generated progressively farther eastward during subduction of the oceanic Nazca plate beneath the continental South American plate from Mesozoic to Recent (Sillitoe 1991, 2008). Most of the copper-gold deposits hosted by high-K calc-alkaline rocks are Upper Cretaceous to Miocene in age (Davidson and Mpodozis 1991; Gröpper et al. 1991; Reyes 1991; Clark 1993; Sillitoe 2008). The Cretaceous-Upper Tertiary volcanic and pyroclastic rocks in the high Andes of north-central Chile form a regional north-south-trending belt over 150 km long, which is underlain by Carboniferous to Lower Triassic medium-K calc-alkaline granodioritic batholiths (Fig. 6.25; Jannas et al. 1990). These basement rocks have been thrust over the Cretaceous-Tertiary volcanic rocks by the steeply west-dipping Baños del Toro Fault, which defines the western boundary of the volcanic belt (Jannas et al. 1990).

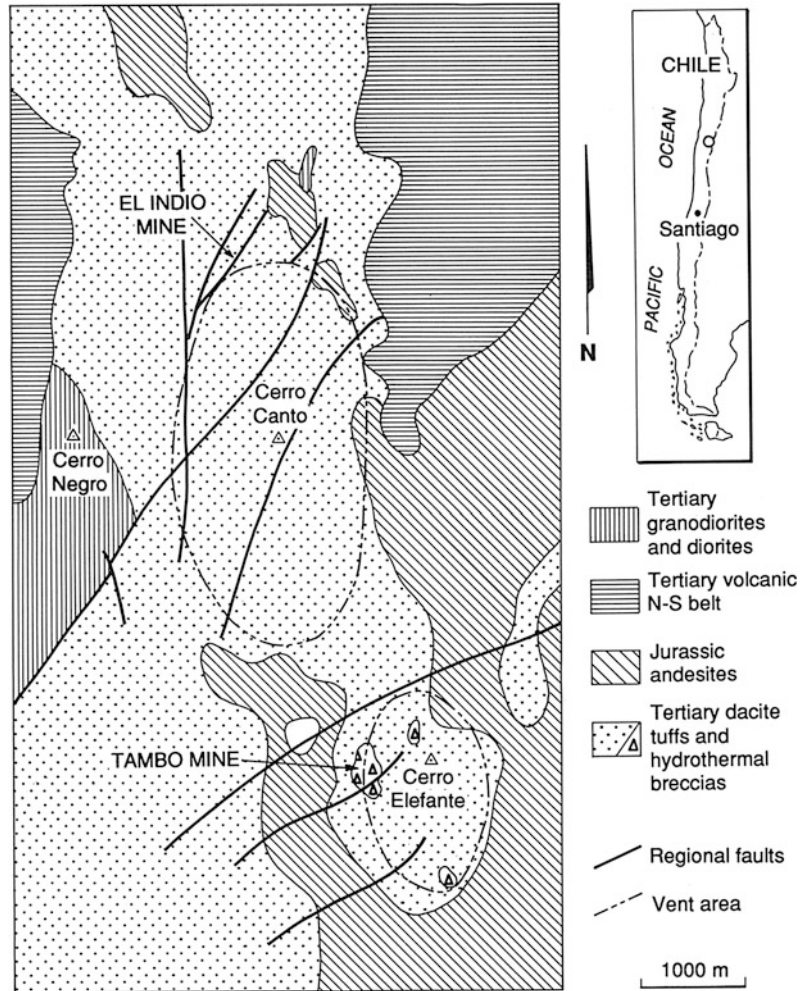
As recognized by Barazangi and Isacks (1976) and confirmed by Cahill and Isacks (1992), the subducting Nazca plate includes nearly flat segments with a shallow subduction angle of about 10°, above which there is no volcanism (Kay and Gordillo 1994), that are flanked by relatively steeper segments associated with active volcanism (Kay et al. 1987; Kay and Mpodozis 2001). The El Indio-Pascua Au-Ag belt is located above the center of the Chilean flat slab zone between 28° and 33°S, with the Maricunga-Farallon Negro district above the northern transition to a zone with steep subduction angle (i.e. ~30°), and the El Teniente district situated above the southern transition to a steep subduction angle further south (Kay and Mpodozis 2001; Stern et al. 2011). Epithermal gold-silver mineralization in the El Indio-Pascua

belt took place above the flat-slab zone while the subduction angle was shallowing and probably enhancing mantle hydration above the subducting slab (James and Sacks 1999; Kay and Mpodozis 2001).

The Eocene to Miocene volcanic and hypabyssal rocks of the El Indio-Pascua Au-Ag-Cu belt are high-K calc-alkaline arc suites, ranging in composition from andesite to rhyolite (Bissig et al. 2003). El Indio is located within the Upper Oligocene to Lower Miocene Doña Ana Formation (Fig. 6.25), a sequence of intensely fractured volcanic and volcanoclastic rocks which belong to the volcanic belt of the High Cordillera (Deyell et al. 2005). Epithermal gold mineralization at El Indio is mainly hosted by lavas and intercalated pyroclastic units with dacitic compositions (Jannas et al. 1990). Mineralization is spatially related to hypabyssal dioritic and monzodioritic stocks and dykes of the Infiernillo Unit (ca. 16.7 Ma), which intruded the bimodal andesite-rhyolite sequence (ca. 18–27 Ma) of the Doña Ana Formation (Kay et al. 1987, 1988; Jannas et al. 1990). However, new $^{40}\text{Ar}/^{39}\text{Ar}$ laser step-heating plateau ages suggest that epithermal gold mineralization both at El Indio and Tambo is younger than these intrusions (Bissig et al. 2001; Deyell et al. 2005). Hydrothermal activity occurred at least from the late Eocene to the late Miocene, but economic gold-silver mineralization was confined to the 6.0–9.5 Ma interval, the only recorded contemporaneous igneous unit being the hypabyssal Pascua Formation (Bissig et al. 2001). The Pascua Formation comprises small hypabyssal bodies of dacite porphyry, dated at 5.0–9.5 Ma (Bissig et al. 2002, 2003). The widespread argillic alteration in the district indicates that the availability of hydrothermal fluid was not the controlling factor for ore formation, emphasizing instead the role of the metal content of the magmas associated with epithermal gold mineralization and/or the requirement for favorable physiographic conditions at the site of ore deposition (Bissig et al. 2001).

The regional structural setting of El Indio is dominated by north-south-trending faults sub-parallel to the main Andean trend (Walthier et al. 1985). The major portion of the exploited

Fig. 6.26 Simplified geologic map of the El Indio-Pascua belt showing the locations of the El Indio and Tambo gold deposits, Chile. Modified after Siddeley and Araneda (1986)



gold-silver \pm copper mineralization occurred within a structural block only 150 m wide by 500 m long. This block contained more than 40 mineralized veins and was bounded by two northeast-striking principal faults, which dip steeply to the northwest (Jannas et al. 1990). Individual veins extended more than 400 m and their thickness varied between a few centimeters and 20 meters (Jannas et al. 1990). The veins had commonly lenticular shapes (Siddeley and Araneda 1986).

Nature of Epithermal Gold Mineralization

The epithermal gold deposits in Chile (Sillitoe 1991, 2008) include both high- and low-sulphidation types, and range from vein-

dominated systems at El Indio through hydrothermal breccia-dominated systems at Choquelimpie, to complex systems combining vein stockworks, disseminated zones, hydrothermal breccias, and veins. The epithermal gold-silver deposits of the El Indio-Pascua belt (Fig. 6.26) range from high-sulphidation (Tambo, Pascua-Llama) to complex associations of high-, intermediate- and, even, low-sulphidation (El Indio) systems (Bissig et al. 2003).

El Indio is characterized by argillic alteration and silicification (Jannas et al. 1990), both of which are typical features for many high-sulphidation epithermal gold deposits worldwide (White et al. 1995; Arribas et al. 1995).

The argillic alteration affects mainly the dacitic pyroclastic units, converting feldspars to kaolinite, sericite and dickite, with minor pyrophyllite and montmorillonite (Siddeley and Araneda 1986). Regional silicification occurs in patchy, pervasive zones, locally obliterating wallrock textures, and it predominated in the vicinity of high-grade ores (Jannas et al. 1990), now mined out. The local replacement of feldspars by alunite and jarosite is a minor, late-stage feature (Siddeley and Araneda 1986). Propylitic alteration is virtually absent at El Indio, although it is dominant outside the two major, northeast-striking, faults that bound the deposit (Walthier et al. 1985).

All mineralization at El Indio was structurally controlled (Fig. 6.26), along extensive tensional features, and two major ore types could be distinguished (Siddeley and Araneda 1986): (1) massive sulphide veins; and (2) quartz-gold veins. The bulk ore at El Indio was derived from the massive sulphide veins, which consisted mainly of enargite and pyrite, together forming about 90 vol.% of the vein material (Siddeley and Araneda 1986). The remaining 10 vol.% of the massive sulphide veins consisted of argillic altered wallrock fragments. The richer gold ores consisted of younger quartz veins which, in places, intersected the massive sulphide veins (Siddeley and Araneda 1986). Gold in these veins occurred predominantly in the native state, as thin trails or disseminated within the quartz, and could be accompanied by minor pyrite, enargite, and tennantite (Siddeley and Araneda 1986). The average gold content of these quartz veins ranged between 18 and 25 ppm, but locally exceeded 200 ppm (Jannas et al. 1990). The quartz gangue material was typically grey, cryptocrystalline, banded, colloform, cherty or drusy (Siddeley and Araneda 1986).

Bissig et al. (2002) propose that changes of the surficial hydrodynamic environment in the El Indio-Pascua district, including a rapid lowering of the water table, increased the lateral

ground-water flow, and fluid boiling and mixing, all favoring ore deposition.

Petrography and Geochemistry of the Potassic Host Rocks

The hypabyssal porphyritic dacite stocks of the Pascua Formation are medium-grained and contain phenocrysts of quartz, plagioclase, clinopyroxene, biotite, and hornblende, which are set in a grey fine-grained feldspathic groundmass. Geochemically (Table 6.12; Bissig et al. 2003), the dacites are characterized by high whole-rock K_2O/Na_2O ratios (0.62–0.84), high LILE concentrations (e.g. up to 3.60 wt% K_2O ; up to 834 ppm Ba, 153 ppm Rb, 508 ppm Sr, respectively) and relatively low LREE contents (e.g. <25 ppm La, <51 ppm Ce). The investigated samples (Bissig et al. 2003) also have low HFSE contents (e.g. <0.67 wt% TiO_2 , <131 ppm Zr, <10 ppm Y, <4 ppm Hf, <3.2 ppm Ta) that are typical for high-K calc-alkaline rocks derived in continental arc settings (Müller et al. 1992b). Low mantle-compatible element abundances (<103 ppm V and <2 ppm Cr) are consistent with high degrees of fractionation of the rocks, probably associated with crustal assimilation during their emplacement, as suggested by elevated Th (up to 11.7 ppm) and U (up to 5.2 ppm) concentrations (Bissig et al. 2003).

El Indio is only one example of Chilean gold deposits associated with high-K calc-alkaline rocks. In fact, many of the Chilean gold deposits, such as Andacollo (Reyes 1991), Choquelimpie (Gröpper et al. 1991), and those of the Maricunga Belt (Dostal et al. 1977; Vila and Sillitoe 1991), are hosted by high-K calc-alkaline rocks interpreted to have formed during subduction in a continental arc setting (Kay et al. 1987, 1988; Levi et al. 1988; Clark 1993). In places, copper-gold mineralization is associated with widespread potassic alteration. However, whole-rock geochemical analyses from unaltered volcanic host rocks (e.g. Gröpper et al. 1991) suggest that the original intrusions were

Table 6.12 Major- and trace-element analyses of potassic igneous rocks from the El Indio gold deposit, Chile

Province/deposit	El Indio	El Indio
Location	Chile	Chile
Rock type	Dacite	Dacite
Tectonic setting	Continental arc	Continental arc
Reference	Bissig et al. (2003)	Bissig et al. (2003)
SiO ₂	63.94	70.66
TiO ₂	0.67	0.36
Al ₂ O ₃	17.23	15.94
Fe ₂ O ₃	4.51	1.83
FeO	n.a.	n.a.
MnO	0.27	0.07
MgO	2.10	0.59
CaO	5.76	2.18
Na ₂ O	2.98	4.26
K ₂ O	1.86	3.60
P ₂ O ₅	0.19	0.10
LOI	0.49	1.11
Total	100.00	100.70
mg#	48	39
K ₂ O/Na ₂ O	0.62	0.84
Sc	7.3	3.3
V	103	42
Cr	1.4	1.2
Ni	n.a.	n.a.
Rb	78.2	153
Sr	336	508
Y	9.4	9.2
Zr	123	131
Nb	n.a.	n.a.
Ba	387	834
Hf	2.7	3.9
Ta	3.2	1.2
La	24.7	24.2
Ce	51.2	42.8
Sm	4.1	2.9
Yb	0.96	0.76
Th	8	11.7
U	2.4	5.2

Major elements are in wt%, and trace elements are in ppm. Fe₂O₃ (tot) = total iron calculated as ferric oxide. Data from Bissig et al. (2003)

characterized by high-K calc-alkaline affinities *before* potassic alteration took place.

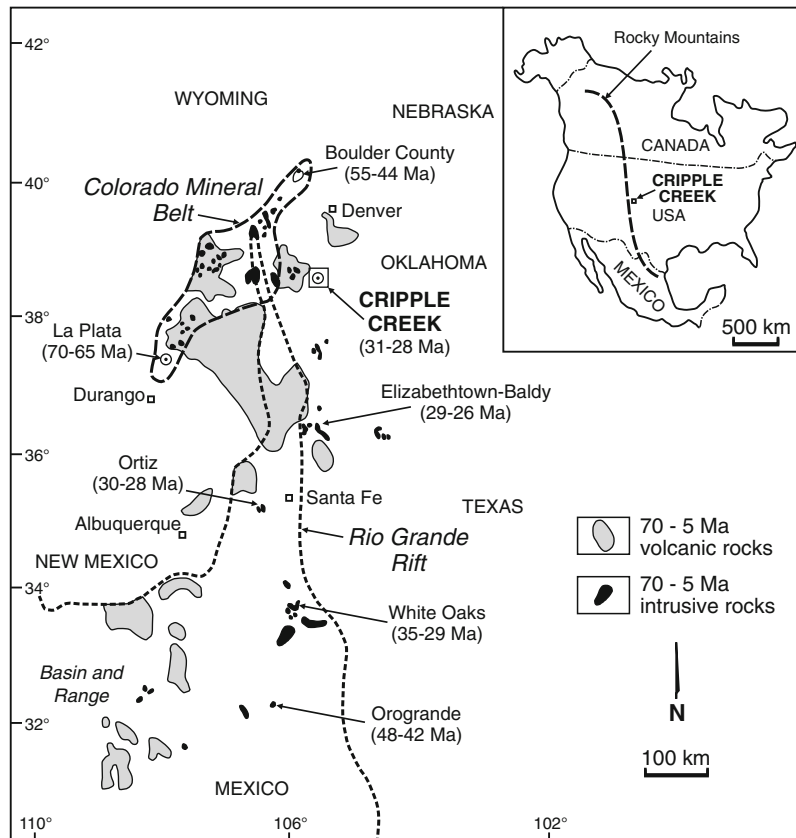
6.4.4 Cripple Creek Gold Deposit, Colorado, USA

Introduction The Cripple Creek district is located in the Rocky Mountains, about 30 km southwest of Colorado Springs, at an elevation of about 2890 m above sea level (Fig. 6.27). In October 1890, a local prospector discovered a high-grade gold vein in the area and triggered the great Colorado gold rush. By 1900, Cripple Creek had grown into a substantial mining community. High-grade gold veins were originally targeted by small shafts and workings, and later by underground mines that reached depths of 1150 m below the surface (e.g. Portland shafts). In 1994, large-scale open pit mining began in the district, along with an aggressive

exploration drilling program (Jensen 2003). Current mining is conducted by CC&V Gold Mining Company who exploit low-grade disseminated gold ores from large-scale openpits (e.g. Cresson pits). Since its discovery in 1890, the Cripple Creek district has produced about 23.5 Moz of gold (Kelley and Ludington 2002).

Regional Geology. The Cripple Creek district is situated in the Rocky Mountains that form part of the Laramides in western North America (Fig. 6.27). The Laramide orogeny began during the Late Cretaceous at about 70 Ma (Kelley and Ludington 2002) and ended about 35 Ma ago. Laramide subduction was characterized by northeast-directed regional compression, shortening, and uplift, and by emplacement of a varied suite of plutonic and volcanic rocks that were largely restricted to the Colorado Mineral Belt (Mutschler et al. 1988). Magmatism was active

Fig. 6.27 Simplified map illustrating locations of major gold deposits hosted by high-K alkaline rocks in Colorado and New Mexico, their relative ages and their distribution to Laramide or Tertiary igneous rocks; the locations of the Colorado Mineral belt and the Rio Grande rift are also shown. Modified after Kelley and Ludington (2002)



from 70 to about 55 Ma. Most of these igneous rocks are calc-alkaline, but high-K alkaline rocks were emplaced in the northeastern and southwestern ends of the Colorado Mineral Belt (Kelley and Ludington 2002). From about 55 to 40 Ma, magmatic activity waned, although it did not cease. This has been attributed to an increasing subduction rate and temporary flattening of the subducting slab to a low angle (Dickinson and Snyder 1978; Lipman 1981), comparable to the “flat-slab zone” of central Chile (cf. Kay et al. 1987; see Sects. 6.4.1 and 6.4.3). The alkaline magmatism at Cripple Creek took place in a continental arc setting at a time when the region was experiencing a transition between a period of compressional tectonics (i.e. Laramide orogeny), and an extensional phase during the Oligocene, probably related to the Rio Grande rift (Kelley and Ludington 2002; Jensen 2003). Cripple Creek is located in the center of an eroded alkaline diatreme complex, dated at ca. 30 Ma, and emplaced into Precambrian and Proterozoic wall rocks (Thompson et al. 1985; Fears et al. 1986). The Cripple Creek diatreme complex is located on a north-trending regional structure formed during the Proterozoic, but subsequently reactivated in late Paleozoic and Tertiary time (Kelley and Ludington 2002).

Geological mapping of the area shows evidence for multiple stages of igneous and hydrothermal activity (Jensen 2003). The volcanic complex contains a series of intrusions and volcanic vents filled with volcanic breccias, the largest of which is an elliptical-shaped feature about 5 km in diameter, interpreted as a diatreme complex (Thompson et al. 1985). The diatreme contact with the surrounding Precambrian wall rocks is erosive and irregular (Jensen 2003). In addition to the volcanic breccias, coherent bodies of high-K alkaline volcanic rocks are present throughout the area, including dykes, sills, laccoliths, and composite flows (Jensen 2003). Multiple phases of small-volume alkaline intrusions are recorded within the main diatreme complex. These are phonolites, tephrites, hypabyssal trachybasalts, syenites, and ultramafic lamprophyres (Jensen 2003). Phonolite stocks

and sills are dated at 32.5–31.5 Ma and form the oldest intrusive rocks at Cripple Creek (Kelley et al. 1998), locally intersecting the volcanic breccias in the diatreme. They were closely followed by more mafic intrusions including tephrite and trachyandesite porphyries. The porphyritic intrusions are locally intersected by nepheline-bearing syenite dykes that, in turn, are cut by trachybasaltic dykes. These events were followed by a widespread phonolitic magmatism that represents the largest volume of Tertiary rocks outside the diatreme (Jensen 2003). In contrast with many other igneous complexes, the intrusions at Cripple Creek show a trend towards more mafic compositions with time, as well as successively smaller volumes of intrusions (Jensen 2003). Hence, the youngest intrusions are a series of narrow ultramafic lamprophyres dykes and related small breccia pipes. The lamprophyre dykes commonly have north-northwesterly orientations, and they bifurcate, anastomose, and pinch and swell along strike. Locally, they form sets of *en echelon* dykes, trending subparallel and adjacent to structures. No igneous rocks have been recorded to cut lamprophyres (Jensen 2003).

Nature of Epithermal Gold Mineralization

The Cripple Creek district exhibits a complex history of magmatic and hydrothermal activity. Two different styles of gold mineralization may be distinguished (Kelley et al. 1998; Jensen 2003): (1) high-grade Au-Te veins that were the source of most of the historic gold production, and (2) low-grade, disseminated gold deposits that are currently being mined. The high-grade low-sulphidation epithermal Au-Te veins consist of early-stage quartz-K-feldspar-fluorite-pyrite assemblages followed by base-metal sulphides, and late-stage telluride mineralization, locally with roscelite (Lindgren and Ransome 1906; Loughlin and Koschmann 1935; Thompson et al. 1985). Low-grade deposits comprise disseminated pyrite with microcrystalline native gold and pervasive adularia alteration (Jensen and Barton 1997; Jensen 2003). Both mineralization styles are spatially associated with alkaline intrusions (Lindgren and Ransome 1906; Kelley

and Ludington 2002), and $^{206}\text{Pb}/^{204}\text{Pb}$ compositions of vein galena almost entirely overlap those of phonolites suggesting a direct genetic relationship between alkaline magmatism and gold mineralization (Kelley et al. 1998).

Hydrothermal alteration began with the emplacement of the earliest phonolite intrusions and continued past the last, lamprophyre-dominated intrusive events along with the introduction of gold (Jensen 2003). Alteration types range from minor early pyroxene-stable varieties through biotite-bearing assemblages into voluminous K-feldspar-stable types. Economic gold mineralization is intimately associated with the late-stage voluminous K-feldspar-pyrite alteration (Jensen 2003). Deep exploration drilling reveals that hydrothermal alteration emanates as splays or spurs off lithological contacts at depth (Jensen 2003), suggesting that these lithological contacts acted as conduits for hydrothermal fluids. This is consistent with the development of high-grade veins along the margins of early lamprophyre dykes (e.g. at Conundrum mine; cf. Loughlin and Koschmann 1935).

Geological mapping reveals that the most productive Au-Te veins show a preference for the southern half of the volcanic complex (Jensen 2003). These veins typically have subvertical orientations and upward flaring morphologies. Locally, they consist of networks of veins and veinlets occupying sheeted fracture zones that link together to form coherent structural trends. However, a smaller portion of the veins is hosted by lower-angle structures and they are locally referred to as “flats” even though they dip as much as 60° (Jensen 2003). They are commonly developed in the near-surface environment, and become less abundant at depth. The most productive mines comprise intrusive phases from all major igneous events, indicating that structural conduits were continuously reopened during the evolution of the igneous complex (Jensen 2003). As recognized by Lindgren and Ransome (1906), the presence of late-stage lamprophyre dykes is particularly favorable, suggesting that structural conduits were dilated during the waning stages of igneous activity. In places, north-northwest

striking phonolite dykes and lamprophyres appear to have formed impermeable barriers for hydrothermal fluids, or served as conduits for migrating fluids (Jensen 2003). Outside of the main diatreme complex, satellite phonolite dykes serve as the main controls for mineralization and alteration.

Petrography and Geochemistry of the

Potassic Host Rocks The ultramafic lamprophyres at Cripple Creek are melanocratic rocks, typically with coarsely porphyritic textures (Jensen 2003). Phenocrysts include olivine, clinopyroxene, and phlogopite, the latter locally up to 3 cm in diameter. Feldspar phenocrysts are not recorded and amphibole phenocrysts are very rare. The fine-grained, dark green groundmass consists mainly of clinopyroxene with minor K-feldspar, plagioclase, biotite and magnetite (Jensen 2003). The lamprophyres exhibit textures suggestive of exsolution of a low-density, carbonate-rich phase (Thompson et al. 1985). Their high volatile contents (e.g. CO_2 , H_2O , Cl, F) are reflected both in their mineralogy (i.e. abundant phlogopite; fluorite veinlets) and their whole-rock geochemistry (e.g. CaO contents of up to 14.49 wt%, see below). Recent studies on melt inclusions hosted by phonolites from Cripple Creek reveal significant halogen contents of 0.35 wt% Cl and 0.52 wt% F, respectively (Webster et al. 2014). Oval-shaped ocelli are common in the less coarse-grained lamprophyres and are filled by carbonate, K-feldspar, analcime, quartz, clinopyroxene, fluorite, and phlogopite assemblages. Ocelli are common in lamprophyres (cf. Rock 1991). Lamprophyre breccia pipes form dark green masses comprising subangular clasts of lamprophyres that are set in a matrix of reworked rock flour, carbonate, analcime and K-feldspar (Jensen 2003).

Geochemically, the alkaline rocks (Table 6.13) are characterized by high K_2O contents (up to 3.22 wt%) and very high Ce/Yb ratios (37–168), reflecting their high-K alkaline compositions (Pearce 1982; Müller et al. 1992b). The igneous rocks from Cripple Creek (Jensen 2003) are nepheline-normative, contain high LILE (e.g. up

Table 6.13 Major- and trace-element analyses of potassic igneous rocks from the Cripple Creek gold deposit, Colorado, USA

Province/deposit	Cripple Creek	Cripple Creek	Cripple Creek	Cripple Creek
Location	Colorado, USA	Colorado, USA	Colorado, USA	Colorado, USA
Site	Portland Mine	Dolly Varden	Gold King Mine	Gold King Mine
Rock type	Tephritic breccia	Trachybasalt	Ultramafic lamprophyre	Ultramafic lamprophyre
Tectonic setting	Continental arc	Continental arc	Continental arc	Continental arc
Reference	Jensen (2003)	Jensen (2003)	Jensen (2003)	Jensen (2003)
SiO ₂	47.41	50.54	34.24	34.89
TiO ₂	1.09	1.62	2.02	1.99
Al ₂ O ₃	13.89	16.54	9.84	9.84
Fe ₂ O ₃	10.19	9.92	11.05	10.78
FeO	n.a.	n.a.	n.a.	n.a.
MnO	0.15	0.16	0.18	0.19
MgO	4.68	4.36	9.20	9.02
CaO	4.90	9.47	14.38	14.49
Na ₂ O	5.19	3.70	2.12	2.34
K ₂ O	3.22	2.48	3.13	2.93
P ₂ O ₅	0.40	0.82	1.94	1.80
LOI	8.29	0.68	11.09	9.88
Total	99.41	100.29	99.19	98.15
Ce/Yb	37	62	152	168
Sc	24	27	22	21
V	182	219	241	238
Cr	151	15	294	276
Ni	31	21	104	93
Rb	131	75.4	191	253
Sr	1089	1730	1820	2052
Y	21	24	26	25
Zr	175	184	218	137
Nb	31	46	65	67
Ba	819	1250	1223	1272
Hf	4.9	5	5	5.3
Ta	2	3	3	4
La	41.2	68.5	125	132
Ce	74	142	213	219
Sm	5.5	11.1	16.1	17
Yb	2	2.3	1.4	1.3
Th	12.2	23.6	19.3	21.1
U	2.4	5	4.1	3.9

Major elements are in wt%, and trace elements are in ppm. Fe₂O₃ (tot) = total iron calculated as ferric oxide. Data from Jensen (2003)

to 1250 ppm Ba, up to 131 ppm Rb, up to 1730 ppm Sr), high LREE (e.g. up to 68.5 ppm La, up to 142 ppm Ce), and variable HFSE contents. While some HFSE, such as Y (<24 ppm), Hf (<5 ppm), and Ta (<3 ppm) have low concentrations, the other HFSE, such as TiO₂ (up to 1.62 wt%), Zr (up to 184 ppm), and Nb (up to 46 ppm) have high concentrations. By contrast, late-stage, ultramafic lamprophyres from Cripple Creek, also nepheline-normative, are defined by very high LILE (e.g. up to 1272 ppm Ba, up to 253 ppm Rb, up to 2052 ppm Sr), very high LREE (e.g. up to 132 ppm La, up to 219 ppm Ce), and very high HFSE (e.g. up to 2.02 wt% TiO₂; up to 218 ppm Zr, up to 67 ppm Nb).

The lithospheric mantle source above the subducted slab in the Rocky Mountains region during the Laramide orogeny was probably oxidized and volatile-enriched (Kelley and Ludington 2002), when adiabatic decompression melting produced small increments of fertile alkaline melts during the onset of the Rio Grande Rift (Jensen 2003). This would explain the unique geochemical fingerprints of the alkaline rocks from Cripple Creek, reflecting their derivation in a mature continental arc setting, but with distinctly elevated HFSE contents such as TiO₂ (up to 2.02 wt%) and Nb (up to 67 ppm) inherited from the rifting processes during their evolution. Initial ⁸⁷Sr/⁸⁶Sr ratios of the alkaline rocks from Cripple Creek average about 0.7055 (Kelley and Ludington 2002; Jensen 2003), suggesting an upper mantle source of the melts and very minor crustal contamination during emplacement (Kelley et al. 1998; McLemore 1996).

6.4.5 Skouries Copper-Gold Deposit, Chalkidiki, Greece

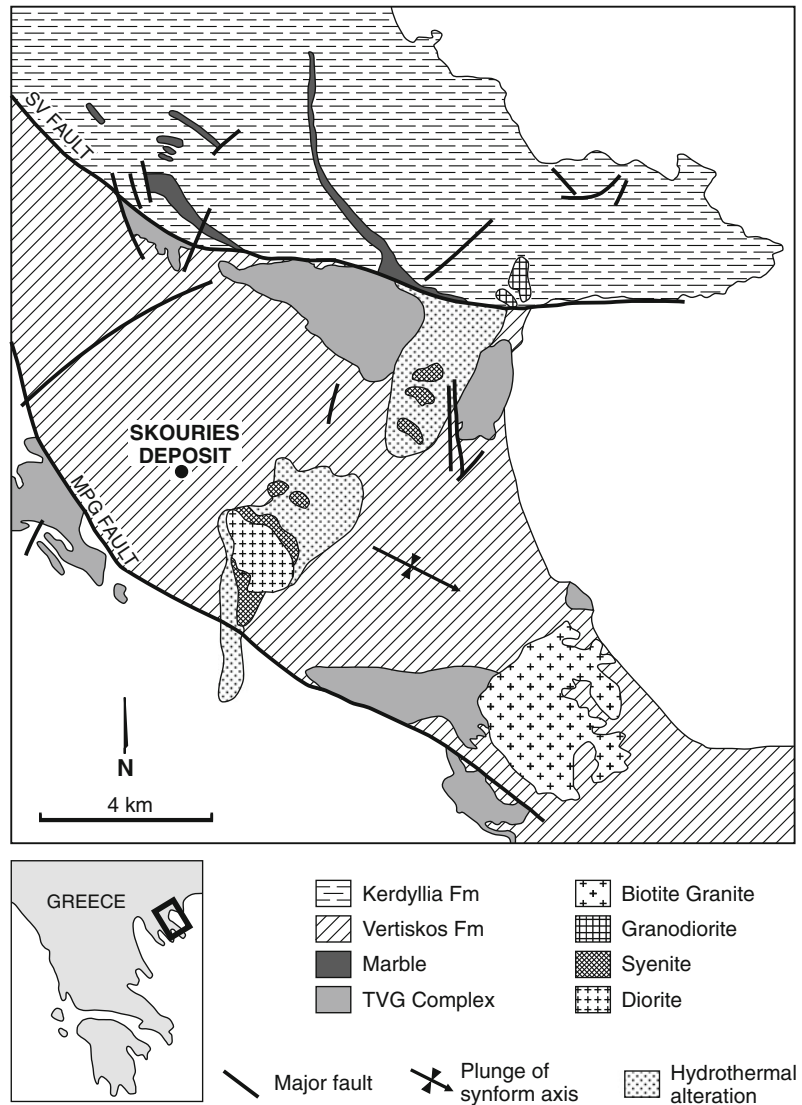
Introduction Mining has a long history in Greece and has contributed significantly to its economic power during ancient times. Lead-silver ore from the famous polymetallic Lavrion mining district, located about 50 km southeast of Athens, has been exploited since prehistoric times (Voudouris et al. 2008). By

contrast, the northeastern part of Greece has long been known for copper occurrences hosted by high-K igneous rocks such as the Kassandra mining district that includes Limnos and Lesbos islands as well as the Chalkidiki peninsula (Kroll et al. 2002; Fornadel et al. 2012; Bristol et al. 2015). This district lies within the Serbomacedonian metallogenic province, which, in turn, is part of the Serbomacedonian Massif (Economou-Eliopoulos 2005). The topography is dominated by undulating hills, the higher parts of which are about 600 m above sea level and largely covered by forests.

The Skouries porphyry copper-gold deposit is situated on the Chalkidiki Peninsula of north-eastern Greece (Fig. 6.28), approximately 90 km southeast of Thessaloniki, and forms part of the Kassandra mining district (Kroll et al. 2002). Systematic exploration and resource drilling at Skouries was originally conducted by TVX Gold Inc. during 1996–1998, defining an indicated reserve of 206 Mt grading at 0.54 % Cu and 0.8 g/t Au (Magri et al. 1998; Tobey et al. 1998). In 2012, Eldorado Gold acquired the property and further developed the project. As of 2015, Eldorado Gold defined a proven reserve of 3.7 Moz at 0.76 g/t Au and 767 Kt at 0.51 % Cu with measured and indicated resources of 5.4 Moz at 0.6 g/t Au and 1.2 Mt at 0.43 % Cu. Skouries also has important Pd credits of up to 480 ppb that are interpreted to be intrinsic to the system (Tarkian and Stribny 1999). Mine construction has commenced in 2013 and the first production is planned for 2016.

Regional Geology The Serbomacedonian Massif forms a northwest-oriented tectono-magmatic belt perpendicular to the closure of the western Tethys; that is, the northeast-trending collision zone between Africa and Europe (Kockel et al. 1975; Frei 1995). The massif consists of a crystalline series which has undergone almandine-amphibolite facies metamorphism during Paleozoic and Pre-Paleozoic times. The crystalline basement consists of gneisses and amphibolites which are unconformably overlain by late Paleozoic sedimentary

Fig. 6.28 Simplified geologic map of northeast Chalkidiki Peninsula, Greece, showing the location of the Skouries copper-gold deposit. Modified after Frei (1995) and Kroll et al. (2002)



rocks. During Mesozoic orogeny, these sedimentary rocks were interfolded with the basement rocks and metamorphosed to the greenschist facies (Kockel et al. 1975). The crystalline basement includes two stratigraphic units, the lower Kerdyllia Formation and the upper Vertiskos Formation, separated by the northwest-striking Stratoni-Varvara fault (Fig. 6.28). The upper Vertiskos Formation consists of muscovite-garnet-biotite-staurolite-tourmaline schists, amphibolites lenses and two-mica schists. It has suffered retrograde

metamorphism to the greenschist facies. The lower Kerdyllia Formation is at higher metamorphic grade and comprises biotite, biotite-plagioclase and hornblende-biotite gneisses, amphibolites and marble lenses (cf. Frei 1992).

The Serbomacedonian massif represents an important metallogenic province within the eastern Alpine belt and hosts numerous Pb-Zn-(Cu-Mo-Sb) deposits, mainly comprising Pb-Zn replacement, fracture-controlled Sb-vein-,

Cu-Mo porphyry, and stratiform volcano-sedimentary deposits which are interpreted to be genetically related to Tertiary magmatism (Frei 1992). During the Early Oligocene, the schists and gneisses of the northeastern Chalkidiki Peninsula were intruded by a series of dioritic to andesitic porphyry stocks (Frei 1995). Some of these stocks are accompanied by characteristic sericitic alteration halos. The Skouries porphyry intrusions (Fig. 6.29) consist of monzonites and quartz-monzonites with shoshonitic compositions (Kroll et al. 2002), dated at about 19 Ma (Frei 1995). The multiple intrusions have pipe-like shapes and were emplaced into lower amphibolite facies mica schists and gneisses of the Vertiskos Formation (Kockel et al. 1975; Kalogeropoulos 1986; Tobey et al. 1998). The composite intrusions were emplaced along a deep-seated northwest-striking fault system (Veranis 1994), extend at surface over an area of about 200 × 200 m, and have a vertical extent of 700 m (Tobey et al. 1998; Kroll et al. 2002).

Nature of Porphyry Copper-Gold Mineralization Porphyry copper-gold mineralization at Skouries consists of quartz-vein stockworks, comprising pyrite, chalcopyrite, and bornite, that are centered on multiple phase monzonite intrusions (Kroll et al. 2002). The orebody measures about 300 m across with a vertical extent of approximately 750 m (Tobey, pers. comm., 2001). Typically, the veins contain 2–3 vol.% sulphides (Perantonis 1982). However, chalcopyrite can also occur as fine-grained disseminations in the host rocks and, locally, has replaced mafic phenocrysts. Early-stage A-type quartz veinlets, about 1–2 mm in thickness, can be distinguished from B-type veins. The A-type veinlets have discontinuous and curvilinear shapes and contain disseminated chalcopyrite-bornite assemblages (Fig. 6.29e). By contrast, B-type veins are characteristically regular and continuous with variable thicknesses, from 0.5 to 8.0 mm. They are defined by internal banding consisting of quartz with fine trails of chalcopyrite (Fig. 6.29f). The B-type veins

commonly have orthoclase selvages. Both vein types are intersected by late-stage pyrite veins, <2 mm in thickness, with sericitic halos. These D-type veins normally occupy continuous, though locally irregular, systematically oriented fractures (Kroll 2001; Kroll et al. 2002).

High-grade ore is characterized by intense potassic alteration, including secondary orthoclase and biotite-magnetite assemblages. In places, hydrothermal biotite crystals, up to 1 cm in length, occur along small veins associated with hydrothermal magnetite. Large hydrothermal biotite crystals of up to 1.2 cm length are also recorded at the Grasberg porphyry copper-gold deposit in Indonesia, where they are locally known as “pseudo-pegmatites” (Kavalieris, pers. comm., 1997). However, typically the hydrothermal biotite-magnetite assemblage occurs as fine-grained pervasive disseminated grains. Hydrothermal orthoclase ranges from patchy replacements of plagioclase phenocrysts, through cross-cutting veinlets, to zones with pervasive flooding (Kroll et al. 2002). The large propylitic and phyllic alteration zones, that are common in many porphyry copper deposits, are not present at Skouries (Tobey et al. 1998). Propylitic alteration at Skouries consists of a narrow, <50 m wide, halo around the host intrusions, comprising mainly chlorite and albite with rare epidote (Kroll 2001). Phyllic alteration is mainly developed along structures and late-stage barren dykes, and post-dates both the potassic and propylitic alteration assemblages (Kroll et al. 2002).

Petrology and Geochemistry of the Shoshonitic Host Rocks Porphyry copper-gold mineralization is hosted by at least four hypabyssal monzonite-porphyry phases. In decreasing age, they are: (1) pink monzonite, (2) main monzonite, (3) intra-mineral monzonite, and (4) late-stage porphyry. The monzonites have porphyritic textures with phenocrysts of plagioclase, K-feldspar, biotite and amphibole, as well as apatite and titanite microphenocrysts, that are set in a fine-grained and feldspar-dominated groundmass (Kroll 2001). The Skouries

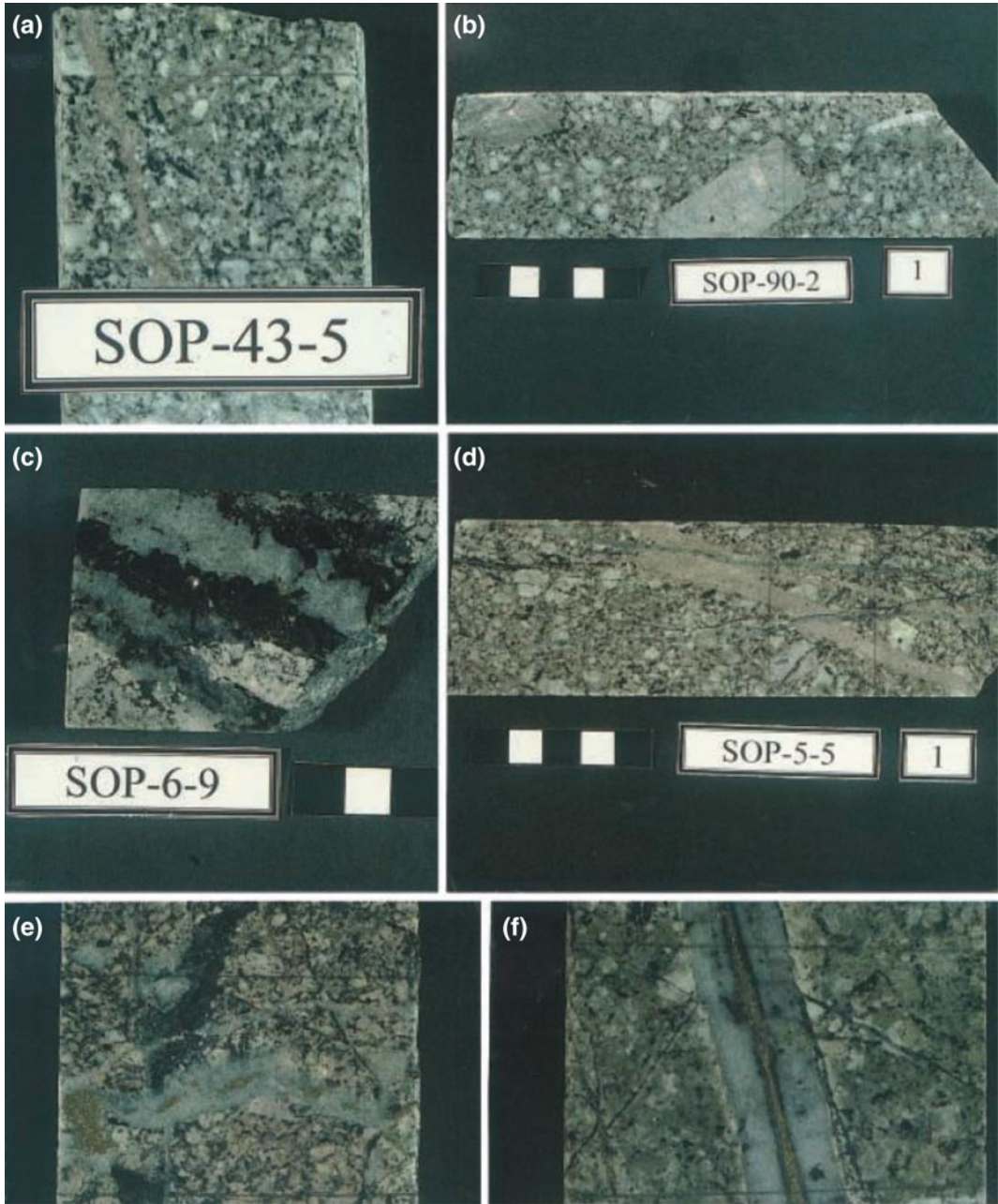


Fig. 6.29 Representative ore samples from the Skouries copper-gold deposit, Chalkidiki, Greece (photos taken by T. Kroll): **a** late-stage monzonite porphyry cut by hydrothermal orthoclase veinlet [FOV 4×6 cm]. **b** Pink monzonite porphyry with large, up to 4 cm, K-feldspar phenocrysts [FOV 4×16 cm]. **c** Main monzonite porphyry with quartz-chalcopyrite vein containing large, up to 1 cm, crystals of hydrothermal biotite [FOV 4×6 cm]. **d** Main monzonite porphyry intersected by

hydrothermal orthoclase veinlet and cross-cutting quartz veinlets [FOV 4×17 cm]. **e** Main monzonite porphyry cut by A-type quartz-chalcopyrite-bornite veins which intersect an earlier black biotite-magnetite veinlet [FOV 4×6 cm]. **f** Main mineral porphyry cut by B-type quartz-chalcopyrite-biotite vein; note that the original potassic alteration assemblage is overprinted by a late-stage pervasive sericite alteration [FOV 4×6 cm]

monzonites are characterized by a pink colour, probably due to the presence of Fe in the K-feldspar structure as also documented at the Cadia (Holliday et al. 2002) and Northparkes porphyry copper-gold deposits in New South Wales, Australia (Müller et al. 1994; Heithersay and Walshe 1995).

All four monzonite phases have relatively evolved compositions (Table 6.14), as reflected by their high SiO₂ (62.0–68.0 wt%) and low MgO (1.1–2.2 wt%) contents, and by variable, but low concentrations of mantle-compatible elements (<92 ppm V, <103 ppm Ni, <18 ppm Co). The relatively high degrees of fractionation are consistent with the relatively low mg# of the rocks (36–52), calculated using a molecular Fe²⁺ (Fe²⁺ + Fe³⁺) set at 0.15, a common ratio in potassic igneous rocks (Müller et al. 1992b). The pink monzonite porphyry, which represents the oldest phase of the Skouries intrusions, has the highest mg# (52), whereas the mineralized main quartz-monzonite porphyry has relatively low mg# (36–39) implying higher degrees of fractionation (Kroll et al. 2002). This is consistent with other alkaline rock-hosted porphyry copper-gold systems, such as Grasberg, Indonesia (Pollard and Taylor 2002), and Northparkes, Australia (Müller et al. 1994), that each consist of a series of interconnected intrusions ranging from mafic to increasingly more fractionated compositions. Typically, the stockwork mineralization is directly associated with the relatively evolved quartz-monzonite phase. The high K₂O contents (4.4–5.8 wt%) and high K₂O/Na₂O ratios (>1) of the least altered samples are typical of alkaline rocks of the shoshonite association (cf. Joplin 1968; Morrison 1980; Müller et al. 1992b; Lu et al. 2013). This relationship is confirmed by the high Ce/Yb (>34) and Th/Yb (>21) ratios of the Skouries intrusions (Pearce 1982; Kroll et al. 2002). All investigated samples also plot on the “shoshonite” field on the K₂O versus SiO₂ diagram of Peccerillo and Taylor (1976a, b). The Skouries intrusions have very high U and Th concentrations (up to 18.9 and 62 ppm, respectively), consistent with accessory allanite and

thorite in several samples (Tobey et al. 1998). Gill and Williams (1990) suggest that the mantle-incompatible elements U and Th are metasomatically added to the mantle wedge above subduction zones by fluids derived from dehydration of the subducted slab.

Relatively high initial ⁸⁷Sr/⁸⁶Sr ratios of the rocks average at about 0.7082 suggesting crustal contamination of their parental melts during emplacement (Kroll et al. 2002). Plotting the analyzed samples on the geochemical discrimination diagrams of Müller et al. (1992b) unequivocally assigns them to a continental arc-setting (Kroll et al. 2002), an interpretation that agrees with studies by Veranis (1994).

The high halogen contents of the Skouries intrusions are reflected in the high Cl and F concentrations of biotite phenocrysts (up to 0.19 and 2.48 wt%, cf. Kroll et al. 2002). The presence of magmatic magnetite in all intrusive phases implies high oxygen fugacities of the parental melts (see Sect. 10.3.2).

6.5 Postcollisional Arc Associations

6.5.1 Grasberg Copper-Gold Deposit, Irian Jaya, Indonesia

Introduction The Pliocene Grasberg porphyry copper-gold deposit (Fig. 6.30) is situated in the Ertsberg Mineral District of Irian Jaya, at 4°S latitude in the western (Indonesian) part of the New Guinea mainland. The rugged Ertsberg district is about 70 km inland from the Arafura Sea at an altitude of 3500–4500 m above sea level (Van Nort et al. 1991). The area is one of only three in the world having permanent mountain glaciers at equatorial latitudes (MacDonald and Arnold 1994). The mineral potential of the area has been first recognized in 1936 with the discovery of the small, but very high-grade, Ertsberg bornite-skarn deposit, but both the remote location and the outbreak of the Second World War delayed its development. Hence,

Table 6.14 Major- and trace-element analyses of shoshonitic rocks from the Skouries copper-gold deposit, Chalkidiki, Greece

Province/deposit	Skouries	Skouries	Skouries
Location	Greece	Greece	Greece
Rock type	Monzonite	Monzonite	Monzonite
Tectonic setting	Continental arc	Continental arc	Continental arc
Reference	Kroll et al. (2002)	Kroll et al. (2002)	Kroll et al. (2002)
SiO ₂	64.80	64.79	63.60
TiO ₂	0.35	0.34	0.43
Al ₂ O ₃	16.90	17.20	17.60
Fe ₂ O ₃	4.90	4.89	4.91
FeO	n.a.	n.a.	n.a.
MnO	0.16	0.05	0.05
MgO	1.28	1.37	1.80
CaO	1.60	1.69	2.08
Na ₂ O	3.62	3.88	3.74
K ₂ O	5.20	4.80	4.50
P ₂ O ₅	0.24	0.28	0.26
LOI	0.13	0.04	0.21
Total	99.18	99.35	99.18
mg#	38	39	46
Ce/Yb	53	62	55
V	71	75	86
Co	7	7	10
Ni	19	18	13
Rb	155	94	106
Sr	1173	1155	1440
Zr	320	322	310
Nb	n.a.	n.a.	n.a.
Ba	2300	2100	2000
Hf	8	9	8
Ta	1.2	0.5	0.5
La	38	56.1	39.8
Ce	69	106	83
Yb	1.3	1.7	1.5
Th	61.7	62.0	55.3
U	18.9	16.1	11.8

Major elements are in wt%, and trace elements are in ppm. Fe₂O₃ (tot) = total iron calculated as ferric oxide. Data from Kroll et al. (2002)

systematic and helicopter-supported, regional exploration in the area by Freeport Mining Corporation only commenced in 1967. The Grasberg porphyry copper-gold deposit was discovered less than 3 km from the Ertsberg mine in 1988 at

an elevation of 4270 m above sea level. The history of early exploration at Grasberg has been described in detail by Wilson (1981).

Mining operations at Grasberg commenced as an open pit in 1990 and the mine is now a combined

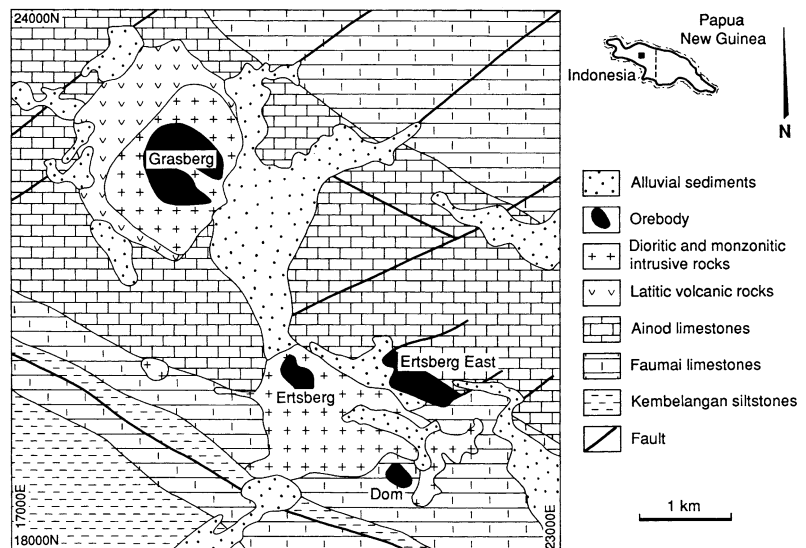
open pit and underground block-caving operation managed by Freeport McMoRan Inc. In 2002, total recoverable reserves were estimated as 51 billion pounds of copper, 62.4 Moz of gold, and 135.5 Moz of silver (Pollard and Taylor 2002).

Regional Geology The island of New Guinea has long been recognized as the product of Miocene collision between the north-moving Australian plate and the southwest-migrating Pacific plate (e.g. Puntodewo et al. 1994). Undeformed continental crust (Van Nort et al. 1991) of the Australian plate extends northward from beneath the Arafura Sea along the southern coastal plain to the southern edge of the Papuan Fold Belt, commonly referred to as the “highland mountainbelt” in the literature (e.g. Richards et al. 1991).

Both the Ertsberg copper skarn and Grasberg copper-gold porphyry mineralization are hosted by igneous intrusive rocks of intermediate composition (Fig. 6.30), ranging from diorite to quartz-monzonite with high-K calc-alkaline to shoshonitic compositions (Van Nort et al. 1991; McMahon 1994; Pollard and Taylor 2002). The intrusions cut Tertiary limestones of the New Guinea Group (MacDonald and Arnold 1994) and several large copper-gold skarns are recorded

along their lithological contacts, the largest of which being the discovery outcrop of the entire district, the Ertsberg (Jowitt et al. 2013). The limestones have been compressed into a series of tight isoclinal folds with nearly vertical axial planes. Pluton emplacement, as well as subsequent copper-gold mineralization, may have been controlled by the intersections of steep, northwest-trending reverse faults and northeast-trending sinistral strike-slip faults (MacDonald and Arnold 1994). The Grasberg Intrusive Complex is dated at ca. 3 ± 0.5 Ma using conventional K-Ar methods (MacDonald and Arnold 1994). More accurate $^{40}\text{Ar}/^{39}\text{Ar}$ ages of magmatic and hydrothermal micas from the Grasberg Igneous Complex range from 3.33 ± 0.12 to 3.01 ± 0.06 Ma (Pollard et al. 2005). Both the ages of intrusive rocks and paragenetic relationships between intrusions and hydrothermal alteration indicate that the Grasberg Igneous Complex formed during several cycles (Pollard and Taylor 2002). Each cycle of intrusion and alteration appears to have lasted around 0.1 m.y. or less and indicates that the huge size and high grade of Grasberg did not result from an unusually prolonged period of hydrothermal activity (Pollard et al. 2005). The $^{40}\text{Ar}/^{39}\text{Ar}$ ages of equigranular diorite from the Ertsberg intrusion (2.67 ± 0.03 Ma) and

Fig. 6.30 Geological overview of the Grasberg copper-gold deposit, Irian Jaya, Indonesia. Modified after MacDonald and Arnold (1994)



phlogopite from the Ertsberg copper skarn deposit (2.59 ± 0.15 Ma) suggest that intrusion and mineralization at Ertsberg are slightly younger than in the Grasberg Igneous Complex (Pollard et al. 2005).

Nature of Porphyry Copper-Gold Mineralization

The bulk of the high-grade copper-gold mineralization is hosted by intense, and multi-phase, quartz-vein stockworks associated with potassic alteration (Fig. 6.31). Stockwork mineralization has been delineated from the original surface at 4200 m and is still open below 2500 m (Pollard and Taylor 2002). The primary hypogene sulphide mineralogy consists mainly of chalcopyrite, bornite, and minor pyrite (Van Nort et al. 1991) which occur in A-type and B-type quartz veins, S-type veins, or as disseminations in the intrusions (Fig. 6.31). Chalcopyrite also occurs as late-stage fracture fillings and as sulphide veinlets (“S-type veins”) throughout the porphyry. Vein quartz from the Grasberg deposit displays a wide range of features in scanned cathodoluminescence images, including concentric growth zoning, quartz-filled microfractures, dark luminescence near sulphides, turbid growth zoning, and the truncation of concentric growth zoning (Penniston-Dorland 2001). MacDonald and Arnold (1994) recognized three major episodes of hydrothermal alteration and mineralization that are genetically linked to successive Dalam Diatreme, Main Grasberg Stock and South Kali Dyke phases of intrusion. However, more recent studies (Pollard and Taylor 2002) reveal numerous overprinting stages of alteration and infill with two main episodes of copper-gold deposition, both of which post-date intrusive rocks within the Grasberg Igneous Complex. The major quartz-chalcopyrite-bornite vein system is developed towards the center of the intrusive complex, while the later disseminated chalcopyrite-bornite-pyrite \pm covellite \pm enargite system is best developed towards the periphery of the Grasberg Igneous Complex (Pollard and Taylor 2002). Molybdenite is rare and either occurs as thin stringer veins (~ 1 mm) or along the margins of anhydrite-quartz veins in the

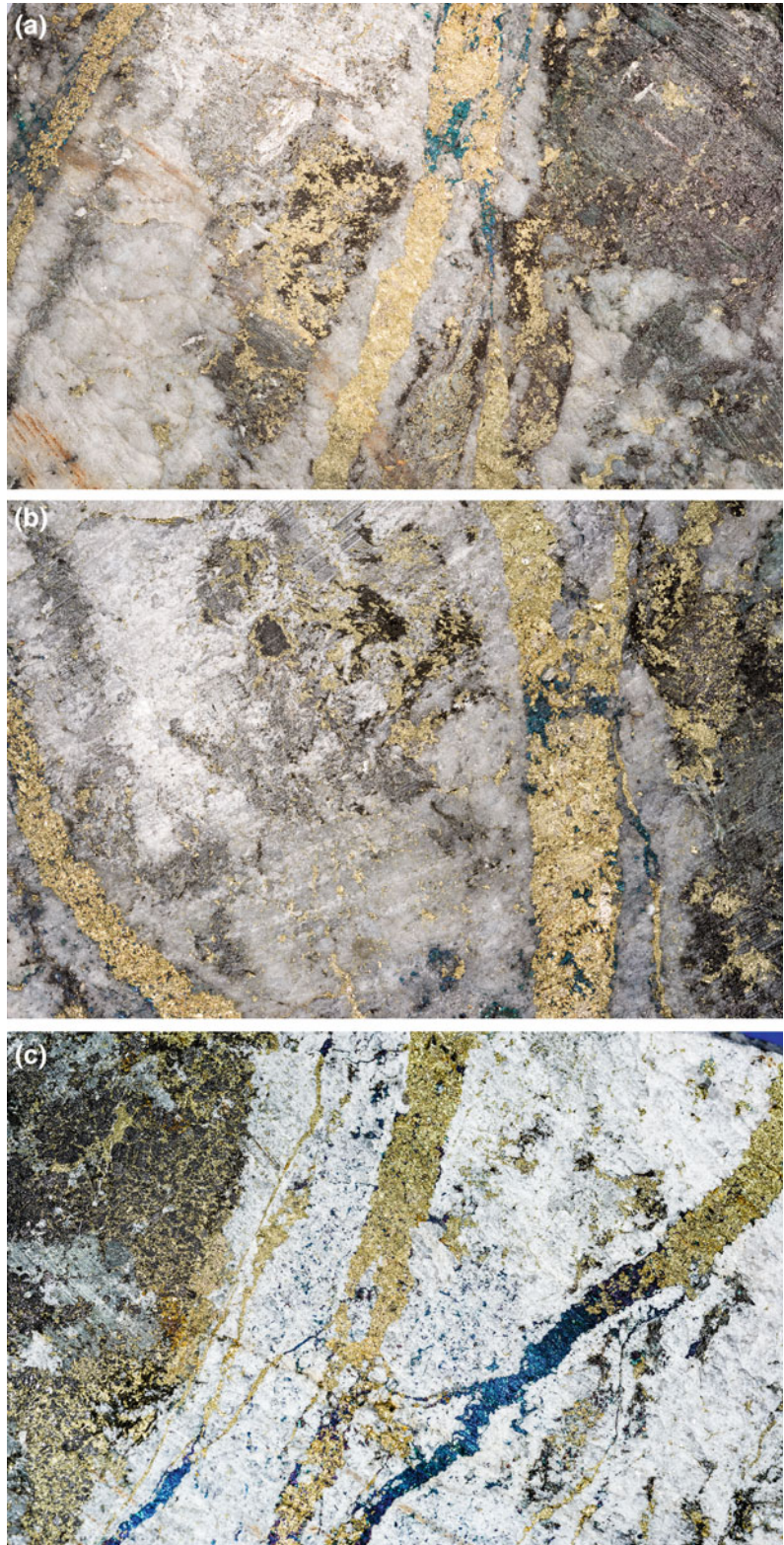
deeper parts of the orebody (Pollard and Taylor 2002). Gold is closely associated with chalcopyrite and bornite, and gold values appear to increase with depth (Van Nort et al. 1991). The native gold is characterized by high Pd contents of up to 3500 ppm (I. Kavalieris, pers. comm., 1996). Major ore reserves are also hosted by skarn-type mineralization formed at contact zones between igneous intrusions and the dolomitic country rocks (Hickson 1991; Jowitt et al. 2013). Typical skarn ore bodies at Grasberg are chalcopyrite-bornite-magnetite-silicate-rich replacements of dolomite (Hickson 1991).

The central potassic alteration zone, with associated quartz-vein stockworks, grades outward into phyllic alteration and then into a thin propylitic zone near the intrusive contact with the limestone country rocks (Hickson 1991). The potassic alteration zone is characterized by hydrothermal, very fine-grained biotite and orthoclase (Van Nort et al. 1991). Anhydrite development is also characteristic as small patches and veins and typically accompanies potassic alteration (MacDonald and Arnold 1994). Phyllic alteration surrounds the potassic zone, and consists mainly of sericite, kaolinite, and pyrite. Primary (magmatic) disseminated magnetite survives potassic alteration, but is absent in the phyllic alteration zone (MacDonald and Arnold 1994). Propylitic alteration is not well developed at Grasberg and, where recorded, rock textures are preserved but feldspar and mafic phenocrysts are altered to either clay or chlorite, with minor epidote (Van Nort et al. 1991). Supergene effects are minimal, with the development of only a weak, thin (about 5 m), leached cap characterized by secondary chalcocite, digenite, and covellite. However, the area has gone through several glacial ice advances over the past one million years, and most of the leached cap was probably scoured off (Van Nort et al. 1991).

Petrology and Geochemistry of the Potassic Host Rocks

The porphyry copper-gold mineralization in the Grasberg-Ertsberg Mineral District is hosted by two major and several minor

Fig. 6.31 Representative high-grade ore samples from the Grasberg copper-gold deposit, Irian Jaya, Indonesia (photos taken by F. Sumarwan and P. Warren): **a** potassic altered monzodiorite porphyry with intense disseminated chalcopyrite mineralization and cut by (S-type) chalcopyrite-bornite veinlets [FOV 5×12 cm]. **b** Potassic altered monzodiorite porphyry with intense disseminated chalcopyrite \pm bornite mineralization and cut by (S-type) chalcopyrite-bornite veinlets [FOV 4×8 cm]. **c** Potassic altered monzodiorite porphyry with intense disseminated chalcopyrite-bornite mineralization and cut by (S-type) bornite-chalcopyrite veinlets; note the *brown patches* of hydrothermal biotite alteration intergrown with fine-grained chalcopyrite [FOV 5×11 cm]



intrusions ranging in composition from monzodiorite to quartz-monzodiorite (Hickson 1991; MacDonald and Arnold 1994). The economically most important intrusions are the Grasberg Igneous Complex, and the Ertzberg and Dom stocks (Fig. 6.30). The intrusions that make up the Grasberg Igneous Complex and the hydrothermal fluids responsible for the porphyry copper-gold mineralization appear to have been derived from a deep crustal magma chamber (Pollard et al. 2005). The Grasberg Igneous Complex (3.33–3.01 Ma) was formed during at least three major intrusive episodes, which are, in successive order: (1) the Dalam Diatreme, (2) the Main Grasberg Stock, consisting of monzodiorite porphyry, and (3) the South Kali quartz-monzodiorite dykes (MacDonald and Arnold 1994; Pollard and Taylor 2002). The youngest intrusive phase is a cross-cutting post-mineral diorite dyke, more mafic than the preceding Kali quartz-monzodiorite intrusions, and suggesting that the magma chamber was periodically replenished by basic magma (Pollard et al. 2005).

The Grasberg Stock, which hosts the porphyry copper-gold deposit, is a medium- to coarse-grained monzodiorite porphyry containing 35–55 vol.% plagioclase, 3–5 vol.% biotite, 2–4 vol.% hornblende phenocrysts, with local quartz eyes that are set in an equigranular groundmass of quartz, biotite and feldspar (Hickson 1991; Van Nort et al. 1991). The rock also contains abundant disseminated magmatic magnetite (up to 5 vol.%; MacDonald and Arnold 1994), suggesting high oxygen fugacities of the parental melts.

Geochemically, the igneous host rocks at Grasberg are strongly evolved (Table 6.15), as reflected by high SiO₂ (>59.5 wt%) and low MgO (<3.4 wt%) contents, low mg# (<60), and low concentrations of the mantle-compatible trace elements (e.g. <100 ppm V, <60 ppm Cr, <35 ppm Ni). The rocks are generally characterized by very high K₂O contents (up to 8.23 wt%), high K₂O/Na₂O ratios (up to 6.8), and high LILE (up to 170 ppm Rb, up to 303 ppm Sr, up to 1554 ppm Ba), intermediate LREE (<49 ppm La, <79 ppm Ce), and low HFSE

(<0.50 wt% TiO₂; <13 ppm Y, <168 ppm Zr) contents. The rocks contain elevated Nb concentrations (up to 15 ppm), which are consistent with those of potassic igneous rocks from many other postcollisional arc settings (Müller et al. 1992b).

Due to the limited data set (e.g. no Hf data) available to the authors, the rocks could not be plotted on the discrimination diagrams of Chap. 3. However, based on the geological setting and the whole-rock geochemistry of the Grasberg igneous suite, it is interpreted to be the product of a postcollisional arc setting.

6.5.2 Misima Gold Deposit, Misima Island, Papua New Guinea

Introduction The Misima gold deposit is located on Misima Island in the Louisiade Archipelago, some 670 km east-southeast of Port Moresby and about 240 km east-southeast of the Papua New Guinea mainland (Lewis and Wilson 1990; Fallon et al. 2002). Misima Island is about 40 km long and up to 9 km wide, comprising an area of 202 km². The topography of the island ranges from coral reefs along the coast (Fallon et al. 2002) to a rugged mountainous topography covered by dense tropical vegetation, rising to 1050 m above sea level in the central part (Lewis and Wilson 1990).

The Misima gold mine is located in the eastern part of the island (Fig. 6.32). Mine construction commenced in 1988, with total mineable reserves of 55.9 million tonnes at 1.38 g/t Au and 21.0 g/t Ag at a cutoff grade of 0.7 g/t Au equivalent (Lewis and Wilson 1990). The mine was an open pit operation, managed by a joint venture between Placer Dome (80 %) and state-owned Orogen Minerals (20 %), that produced about 3.7 Moz of Au and 20 Moz of Ag until its closure in 2004. Regional exploration for epithermal gold and porphyry copper-gold targets at Misima Island is currently undertaken by WCB Resources Ltd.

Regional Geology The geology of Misima Island (Fig. 6.32) is dominated by Eocene or older metamorphic rocks (Appleby et al. 1995),

Table 6.15 Major- and trace-element analyses of potassic igneous rocks from the Grasberg copper-gold deposit, Irian Jaya, Indonesia

Province/deposit	Grasberg	Grasberg
Location	Indonesia	Indonesia
Rock type	Monzodiorite	Monzodiorite
Tectonic setting	Postcollisional arc	Postcollisional arc
Reference	Freeport Mining Co. (unpubl. Data, 1993)	Freeport Mining Co. (unpubl. Data, 1993)
SiO ₂	59.45	66.75
TiO ₂	0.38	0.50
Al ₂ O ₃	10.79	13.74
Fe ₂ O ₃	15.57	3.22
FeO	n.a.	n.a.
MnO	0.05	0.01
MgO	3.35	2.09
CaO	0.42	0.62
Na ₂ O	1.16	1.20
K ₂ O	6.31	8.23
P ₂ O ₅	0.27	0.23
LOI	1.32	2.57
Total	99.07	99.16
mg#	33	60
K ₂ O/Na ₂ O	5.4	6.8
Sc	n.a.	n.a.
V	97	87
Cr	13	56
Ni	11	35
Rb	150	170
Sr	179	303
Y	13	11
Zr	86	168
Nb	10	15
Ba	277	1554
Hf	n.a.	n.a.
La	9	49
Ce	15	79

Major elements are in wt%, and trace elements are in ppm. Fe₂O₃ (tot) = total iron calculated as ferric oxide. Data from Freeport Mining Co. (unpl. data, 1993)

which have been subdivided into the higher-grade Awaibi Association and the lower-grade Sisa Association (Lewis and Wilson 1990). These two

metamorphic units are separated by an extensional, low-angle detachment fault with a mylonitic fabric (Fig. 6.22; Appleby et al. 1995). The Awaibi Association amphibolite-facies metamorphic rocks structurally underlie the less-metamorphosed Sisa Association rocks of upper greenschist facies, which occur on the eastern part of the island and contain the gold mineralization (Lewis and Wilson 1990). The Sisa Association is a conformable sequence of dominantly psammopelitic schists enclosing fine-grained, massive to foliated greenstones (de Keyser 1961; Clark et al. 1990).

The Sisa Association units are gently dipping and are folded into an east-trending, east-plunging antiform (Appleby et al. 1995). The rocks are overprinted by a penetrative deformation which resulted in foliation, crenulation fabrics, and isoclinal to chevron folding (Clark 1988). The schists and greenstones of the Sisa Association have been intruded by hypabyssal andesitic to dacitic stocks, sills, and dykes known as the Boiou microgranodiorite (Fig. 6.22; Clark et al. 1990), which postdates the deformation (Clark 1988). SHRIMP II U-Pb dating of magmatic zircons from this granodiorite yields a crystallization age of 8.1 ± 0.4 Ma (Appleby et al. 1995).

At least three phases of faulting can be identified, the best-known relationships being in the Umuna Fault Zone, a 50–200 m-wide zone of subparallel and anastomosing fractures (Lewis and Wilson 1990) in which the Misima gold deposit is situated (A.K. Appleby written comm., 1996). The epithermal gold mineralization at Misima is spatially associated with contemporaneous shoshonitic lamprophyres, and both the mineralization and lamprophyre dykes have been K-Ar dated at 3.5 Ma (A.K. Appleby, written comm., 1996).

Nature of Epithermal Gold Mineralization

Two mineralization events can be distinguished at Misima (Appleby et al. 1995): (1) early-stage uneconomic *porphyry-style* pyrite-chalcopyrite-bornite-molybdenite mineralization with both weak (potassic) biotite-magnetite and (propylitic) chlorite-albite-epidote alteration assemblages

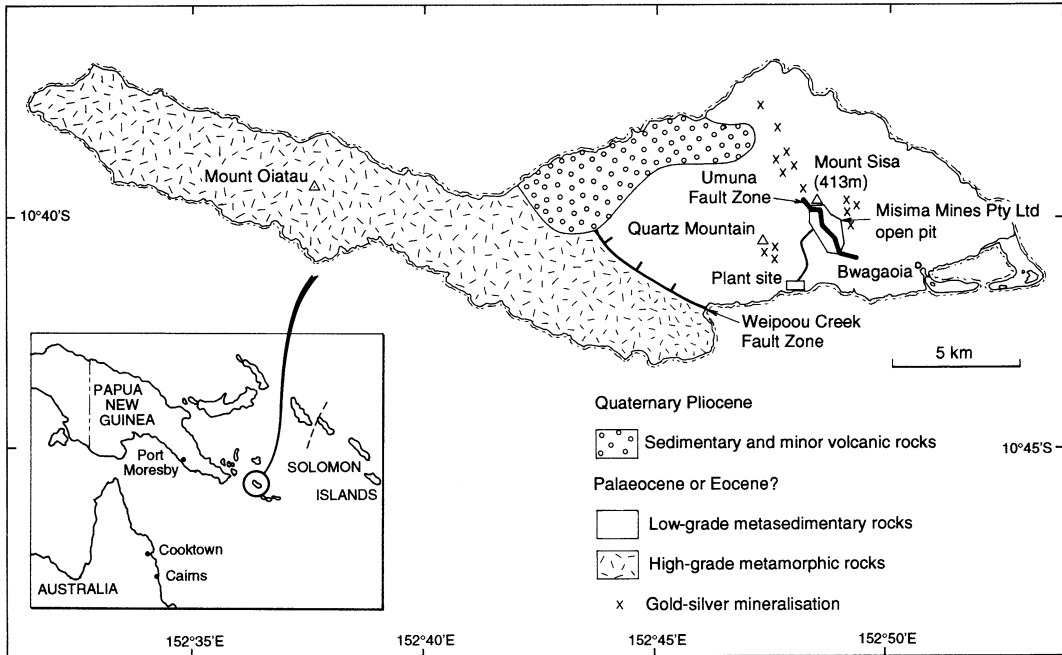


Fig. 6.32 Geological overview of Misima Island, Louisiade Archipelago, Papua New Guinea, showing gold-silver mineralization. Modified after Appleby et al. (1995)

associated with the Boiou microgranodiorite; and (2) late economic *epithermal* precious-metal mineralization with auriferous pyrite-sphalerite-galena-chalcopyrite \pm gold \pm silver associated with quartz and quartz-carbonate gangue as fracture fill. The epithermal gold-silver mineralization is focused in high- and low-angle structures in the upper plate of the detachment fault (Appleby et al. 1995).

The north-northwest-striking Umuna Fault Zone is the most significant known locus of mineralization on Misima Island (Fig. 6.33). The orebody is about 100–200 m wide, 500 m deep, and has a 3 km strike length (Appleby et al. 1995). The high-grade gold mineralization is sited in *en echelon* dilational sites, indicating normal movement with dextral slip along the Umuna Fault Zone at the time of mineralization (Appleby et al. 1995).

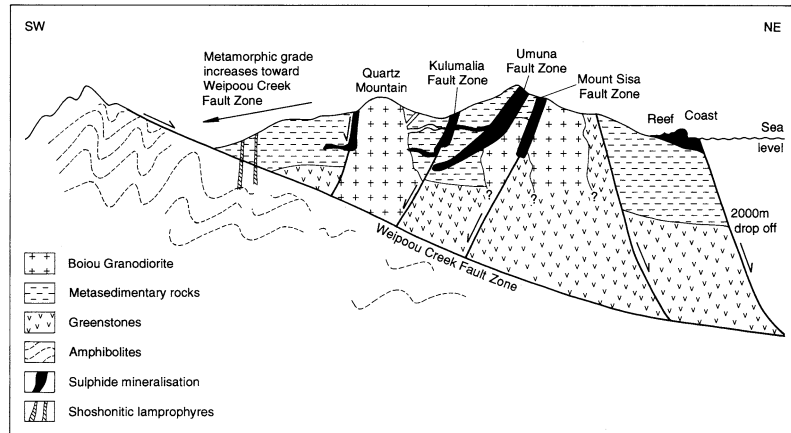
The vein mineralogy is dominated by quartz or carbonate gangue with galena, sphalerite, pyrite, and chalcopyrite. Gold shows a distinctive correlation with galena (Appleby et al. 1995).

The upper levels of the deposit are dominated by <20 m-wide silica veins with minor barite, whereas carbonate veins and breccia infill are more common at depth (Lewis and Wilson 1990). The alteration associated with mineralization is confined to narrow vein selvages of sericite-chlorite-pyrite \pm epidote. Sericitic alteration is dominant (Appleby written comm., 1996). The vein mineralogy, texture, and associated alteration are characteristic of epithermal gold mineralization in a low-sulphidation hydrothermal system (Appleby et al. 1995; White et al. 1995).

In summary, the epithermal gold-silver mineralization at Misima is attributed to coeval Pliocene extensional and transpressional tectonics, the unroofing of a metamorphic core complex, and mantle-derived potassic magmatism (A.K. Appleby written comm., 1996).

Petrography and Geochemistry of the Associated Potassic Rocks The Miocene (8 Ma) Boiou microgranodiorite stocks and dykes vary texturally from porphyritic to even

Fig. 6.33 Geological cross-section (SW-NE) of Misima Island, Louisiade Archipelago, Papua New Guinea. Modified after Appleby et al. (1995)



grained, with phenocrysts of plagioclase (<5 mm long), quartz (~1 mm long), biotite (<2 mm long), and amphibole (<2 mm long) within a fine-grained groundmass consisting of quartz and feldspar (Lewis and Wilson 1990).

The Pliocene (3.5 Ma) lamprophyre dykes at Misima consist of up to 40 vol.% amphibole phenocrysts (~1 mm long) within a very fine-grained groundmass dominated by plagioclase and secondary chlorite (A.K. Appleby, written comm., 1996), and thus can be classified as spessartites as defined by Rock (1991). The spessartites near the Umuna Fault Zone are strongly carbonate altered (Appleby et al. 1995).

Geochemically, the microgranodiorites (Table 6.16) are characterized by evolved compositions with high SiO₂ (up to 69.5 wt%) contents, and very low TiO₂ (~0.25 wt%), Fe₂O₃ (i.e. ~1.98 wt%), and MgO (~0.99 wt%) concentrations (A.K. Appleby written comm., 1996). On a total alkalis versus silica plot (Le Maitre 1989), the samples plot on the boundary between trachytes and dacites due to their high alkali contents (i.e. ~4.64 wt% Na₂O, ~3.06 wt% K₂O).

The spessartites (Table 6.16) have typical shoshonitic compositions (A.K. Appleby written comm., 1996), with relatively low SiO₂ (<52.20 wt%) abundances, low but variable Al₂O₃ (14.50–16.60 wt%), high LILE (up to 4.20 wt% K₂O; up to 1540 ppm Ba, up to 65 ppm Rb, up to 1600 ppm Sr), relatively low LREE (<50 ppm

La, <95 ppm Ce), and, except for TiO₂ and Nb, low HFSE (<220 ppm Zr, <15 ppm Y, ~6 ppm Hf) contents. The TiO₂ and Nb concentrations are slightly elevated (up to 1.47 wt% TiO₂, up to 15 ppm Nb). Their compositions are consistent with those of potassic igneous rocks from other postcollisional arc settings (see Sects. 4.2, 6.5.1 and 6.5.3).

Based on both structural considerations (A.K. Appleby written comm., 1996) and their geochemical fingerprints, the lamprophyres are interpreted to have been intruded into a postcollisional arc (Fig. 6.23).

6.5.3 Porgera Gold Deposit, Papua New Guinea

Introduction The Miocene Porgera gold deposit is situated about 600 km to the northwest of Port Moresby and about 130 km to the west of Mount Hagen, the capital of the Enga Province, in the rugged highlands of Papua New Guinea (Fig. 6.34). Porgera is an example of modern gold mineralization hosted by volatile-rich potassic igneous rocks in a postcollisional arc setting. The Porgera mine is host to exceptionally high-grade low-sulphidation epithermal gold mineralization, locally containing abundant visible gold and exceeding 1000 g/t (MacMahon, pers. comm., 1997; Ronacher et al. 2002). Porgera was discovered by Placer Dome geologists

Table 6.16 Major- and trace-element analyses of potassic igneous rocks from the Misima gold deposit, Louisiade Archipelago, Papua New Guinea

Province/deposit	Misima	Misima	Misima	Misima
Location	Papua New Guinea	Papua New Guinea	Papua New Guinea	Papua New Guinea
Rock type	Microgranodiorite	Spessartite	Spessartite	Spessartite
Tectonic setting	Postcollisional arc	Postcollisional arc	Postcollisional arc	Postcollisional arc
Reference	Appleby (written comm., 1996)			
SiO ₂	69.50	52.20	50.90	50.70
TiO ₂	0.25	1.20	1.27	1.47
Al ₂ O ₃	16.00	14.50	15.10	16.60
Fe ₂ O ₃	1.98	6.60	6.40	6.60
FeO	n.a.	n.a.	n.a.	n.a.
MnO	0.15	0.19	0.15	0.15
MgO	0.99	5.25	5.80	5.65
CaO	2.26	8.15	6.10	4.58
Na ₂ O	4.64	2.50	3.94	4.68
K ₂ O	3.06	4.20	2.38	2.34
P ₂ O ₅	0.20	1.32	0.66	0.73
LOI	1.58	4.06	7.95	7.00
Total	100.61	100.17	100.65	100.50
mg#	54	65	68	66
K ₂ O/Na ₂ O	0.66	1.7	0.6	0.5
Sc	n.a.	n.a.	n.a.	n.a.
V	40	160	170	170
Cr	130	150	180	60
Ni	<50	100	100	<50
Rb	70	65	45	45
Sr	1040	1600	320	260
Y	6	13	11	15
Zr	100	220	150	160
Nb	10	15	10	15
Ba	930	1540	760	940
Hf	5	8	6	6
La	6	50	20	25
Ce	11	95	40	45

Major elements are in wt%, and trace elements are in ppm. Fe₂O₃ (tot) = total iron calculated as ferric oxide. Data from A.K. Appleby (written comm., 1996)

in the late-eighties and its exploration history is well documented by Handley and Henry (1990). Since the take-over of Placer Dome Inc. in 2006, the Porgera gold mine has been operated by

Barrick Gold Ltd. With 10.3 Moz of Au recovered between the start of production in 1990 and June 2001, Porgera is one of the largest gold producers in the Southwest Pacific region

(Ronacher et al. 2004). Reserves and resources in June 2001 amount to 113 Mt of ore at a grade of 3.5 g/t. The total contained gold at Porgera is about 22.9 Moz (Ronacher et al. 2004).

Regional Geology Porgera is located in a highland mountainbelt (Fig. 6.34) which was formed by Late Miocene continent-island arc collision (Richards et al. 1991). The region is cut by the Lagaip Fault Zone, which trends west-northwest, and separates deformed and metamorphosed volcanosedimentary rocks to the northeast from unmetamorphosed Jurassic and Cretaceous sedimentary rocks to the southwest (Richards et al. 1991). These supracrustal rocks were affected by rapid uplift during the Early Pliocene following the Late Miocene collision event (Hill and Gleadow 1989). The intrusion of the Porgera Igneous Complex immediately predates the main stage of tectonism in the highlands (Richards et al. 1991). The Porgera Igneous Complex is of middle to late Miocene age (Fleming et al. 1986; Handley and Henry 1990), comprising a series of small volatile-rich plugs,

stocks, and dykes of potassic alkaline composition and relatively high oxygen fugacities (Richards et al. 1991; Peterson and Mavrogenes 2014). The intrusions were emplaced at ca. 6 Ma at a paleo-depth of about 2.5 km (Richards and McDougall 1990) and are coeval, within error, with mineralization (Ronacher et al. 2002). The intrusions form small balloon-shaped stocks with narrow contact halos, ranging from a few meters to a few tens of meters, in the sedimentary wall rocks. They are interpreted to be apophyses derived from a much larger pluton at depth, as indicated by a circular aeromagnetic anomaly, about 5 km in diameter (Ronacher et al. 2002). Intrusions and gold-quartz veins are hosted in a thick, regionally extensive sequence of Cretaceous black carbonaceous shales (Ronacher et al. 2004; Peterson and Mavrogenes 2014). The deposit is intersected by the north-northeast striking Roamane fault zone, a late and dominantly extensional, normal fault that post-dates all intrusions and controls the late-stage high-grade gold-quartz veins (Ronacher et al. 2002; Peterson and Mavrogenes 2014).

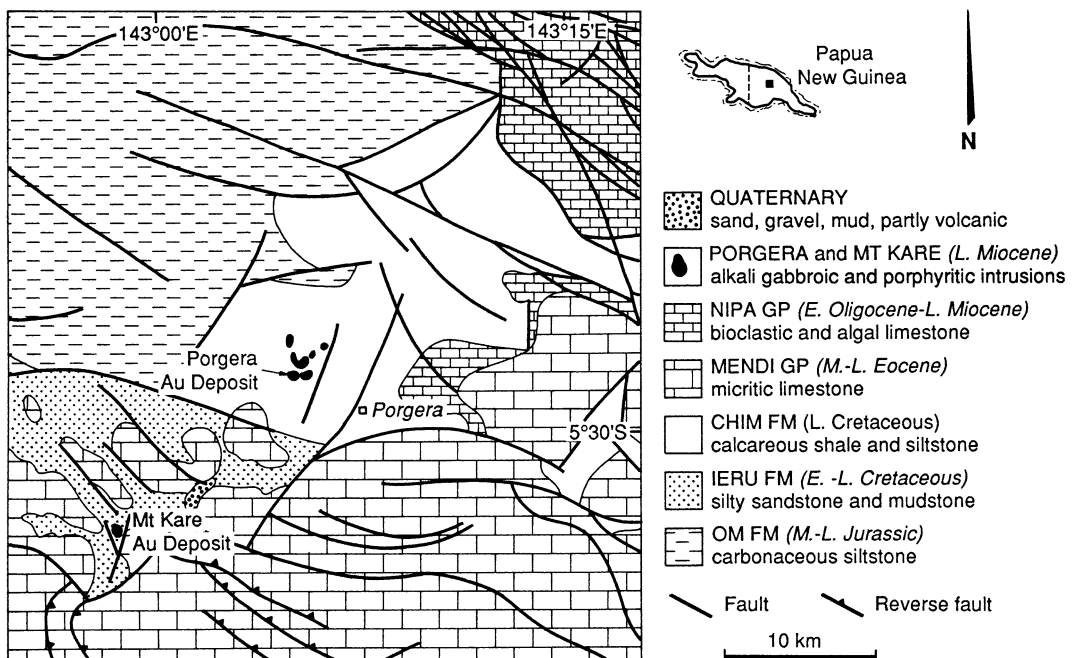


Fig. 6.34 Geological overview of the Porgera and Mount Kare (see Sect. 11.2.19) gold deposits, Enga Province, Papua New Guinea. Modified after Richards and Kerrich (1993)

Nature of Epithermal Gold Mineralization

The Porgera deposit combines characteristics of porphyry, epithermal, and structurally controlled lode-gold deposits (Peterson and Mavrogenes 2014). However, although the richest gold contents in porphyry-type deposits are normally in the potassic alteration zone (Hollister 1975), no such alteration zone has been recorded at Porgera (Richards 1992). Gold mineralization was episodic (Handley and Henry 1990), with several overlapping stages of mineralization from early, low-grade gold disseminations to late, high-grade epithermal gold veins (Richards 1990a, b). A magmatic association between gold mineralization and the high-K Porgera Intrusive Complex is evident (Richards et al. 1991; Ronacher et al. 2004; Peterson and Mavrogenes 2014). Richards (1990a) provides evidence for the evolution of a volatile phase during magma crystallization, suggesting that gold and other elements were partitioned into a magmatic fluid. These magmatic-hydrothermal fluids probably caused the initial stage of gold enrichment (Richards 1990b). A late influx of fresh magma into the underlying magma chamber might have resulted in the emplacement of a late suite of feldspar porphyry dykes and the release of a final pulse of hydrothermal fluid (Richards 1990a). Gold at the Porgera complex is predominantly in structurally controlled veins and faults with lesser, low-grade arsenian pyrite disseminated in altered wall rocks (Peterson and Mavrogenes 2014). Three types of gold-bearing vein assemblages occur at Porgera (Ronacher et al. 2004): (1) magnetite-sulphide-carbonate veins with minor gold, (2) base metal-sulfide \pm gold-carbonate veins, and (3) late-stage quartz-roscoelite-pyrite-gold veins. In places, the latter phase hosts bonanza gold grades and is economically the most significant. The quartz-roscoelite-pyrite-gold veins mainly occur within or in the splays of the Roamane fault zone, the high-grade domain of which is locally referred to as “Zone VII”, where abundant visible gold and up to 1000 g/t Au occurred in quartz-roscoelite breccias (MacMahon pers. comm., 1997; Ronacher et al. 2002). Disruption of the Roamane fault zone significantly altered hydrothermal fluid pressure and

flow regimes, initiating the high-grade quartz-roscoelite-pyrite-gold mineralization (Peterson and Mavrogenes 2014). Studies on the V-rich roscoelite micas by Wall et al. (1995) and Cameron (1998) suggested that mixing of an oxidized magmatic fluid and a reduced fluid expelled from carbonaceous sedimentary rocks was responsible for the formation of high-grade zones. The interpretation that gold may have been concentrated in an oxidized magmatic fluid phase is supported by the presence of hypersaline fluid inclusions and stable isotope compositions of mineralization-related minerals consistent with the involvement of magmatic volatiles (Richards 1992), and evidence for high halogen concentrations in biotite phenocrysts of the magmatic host rocks (Müller and Groves, 1993; see Chap. 9). Detailed studies on fluid inclusions from Porgera imply that boiling was, at least locally, responsible for gold deposition (Ronacher et al. 2004). More recent studies reveal an intricate zonation within pyrite crystals derived from the high-grade zone at Porgera, documenting a rapid and complete switching of alternating bands of two distinct pyrite types within a single vein system (Peterson and Mavrogenes 2014). This cyclicity of the hydrothermal fluids and the resulting sequential evolution of the mineralization is interpreted as the manifestation of a fault-valve system providing rapid pressure drops during rupture that either caused flash boiling or allowed separate fluids to be focused through faults during earthquake aftershocks (Peterson and Mavrogenes 2014). Laser $^{40}\text{Ar}/^{39}\text{Ar}$ age dating of magmatic biotite and hornblende (5.99 ± 0.08 Ma), representing the intrusive event, and of hydrothermal biotite (5.98 ± 0.13 Ma) and roscoelite (5.92 ± 0.08 Ma), representing the mineralizing event, show that the life-span of the magmatic and mineralizing system at Porgera was less than 0.1 million years (Ronacher et al. 2002).

Petrology and Geochemistry of the Potassic Host Rocks

The intrusions of the Porgera Intrusive Complex range from fine- to medium-grained, porphyritic through euhedral granular to ophitic textures, due to different rates

of crystallization, in smaller and larger intrusive bodies, respectively. The rocks consist of olivine, diopside, feldspar, hornblende, biotite, phlogopite, fluorapatite, chromite and magnetite (Richards 1990a; Richards and Ledlie 1993). The presence of miarolitic cavities and vesicles in fine-grained mafic dykes and chilled margins, as well as magmatic biotite, phlogopite and fluorapatite, reflect the high volatile contents of the melts (Richards 1990a). Fluorapatite microphenocrysts are locally up to 2 mm wide (Richards pers. comm., 2003). Fresh olivine has not been recorded at Porgera, but its original presence in mafic rocks is inferred from the occurrence of characteristically shaped pseudomorphs (Richards 1990a). Plagioclase crystallization was delayed until shortly after hornblende crystallization (Richards and Kerrich 1993), with the result that a small window of compositions exists within rocks which texturally resemble lamprophyres (i.e. non-plagioclase phyric, clinopyroxene-hornblende porphyries). However, the rare lamprophyre-textured samples within a much larger continuum of non-lamprophyric rocks indicates that the entire Porgera suite cannot be classified as lamprophyric as originally proposed by Rock and Finlayson (1990).

The potassic host rocks at Porgera are characterized by a primitive geochemistry (Table 6.17) with low SiO₂ (<48.3 wt%), high Na₂O (up to 3.2 wt%) and high MgO (up to 12.2 wt%) contents, high mg# (up to 75), and high concentrations of mantle-compatible trace elements (e.g. >200 ppm V, up to 780 ppm Cr, up to 380 ppm Ni). The rocks have high LILE (e.g. ~650 ppm Sr, ~400 ppm Ba), moderate LREE (e.g. ~30 ppm La, ~60 ppm Ce), and, with the exception of Nb, low HFSE (<1.20 wt% TiO₂, ~125 ppm Zr, ~3 ppm Hf) contents. Richards (1990b) interpreted the geochemistry of the Porgera intrusive suite in terms of within-plate magmatism resulting from localized melting in the subcontinental mantle. In terms of the available database, potassic igneous rocks from such within-plate settings have very high HFSE concentrations (Chap. 3). The Porgera volcanic rocks

(Fig. 6.23), indeed, have very high Nb concentrations (~50 ppm), but the remaining HFSE have abundances which are far too low to be considered as reliable geochemical fingerprints of within-plate potassic volcanism (<170 ppm Zr, <19 ppm Y, <3.6 ppm Hf). Potassic igneous rocks from many mature postcollisional arc settings do tend to show a transition from a calc-alkaline or shoshonitic geochemistry to a more alkaline geochemistry during the later stages of magmatism (e.g. Sect. 4.2; Müller et al. 1992a, b), which might apply at Porgera.

On balance, the relatively low HFSE (with the exception of Nb) contents of the Porgera intrusive suite implicate a subduction-related postcollisional arc setting rather than a within-plate tectonic setting. Moreover, a genetic model proposing that within-plate magmatism was responsible for the intrusion of the Porgera Intrusive Complex at 6 Ma would require the uprise of a deep asthenospheric mantle plume with OIB-type geochemistry. Tectonic reconstructions of the area imply the presence of an oceanic slab subducting southwestward beneath the continental crust of the Papua New Guinea main island at this time (Cooper and Taylor 1987), which would have blocked the ascent of rising mantle plumes. Therefore, a postcollisional arc setting is suggested on the basis of both geological and geochemical data.

6.6 Synthesis of Direct Genetic Associations

As discussed above, there are spatial and probably genetic associations between copper-gold mineralization and high-K igneous suites in late oceanic (island) arc, continental arc and postcollisional arc settings (cf. Müller and Groves 1993). It is apparent that Tertiary epithermal gold deposits (e.g. Ladolam, Emperor, Porgera; see Fig. 6.1) can be hosted by potassic igneous rocks in *late oceanic arcs*, in places within, or at the margin of, a collapsed caldera structure (Anderson and Eaton 1990; Haggman 1997b). The

Table 6.17 Major- and trace-element analyses of potassic igneous rocks from the Porgera gold deposit, Enga Province, Papua New Guinea

Province/deposit	Porgera	Porgera
Location	Papua New Guinea	Papua New Guinea
Rock type	Trachybasalt	Trachybasalt
Tectonic setting	Postcollisional arc	Postcollisional arc
Reference	Richards (1990a)	Richards (1990a)
SiO ₂	48.25	45.08
TiO ₂	0.88	1.19
Al ₂ O ₃	15.50	13.03
Fe ₂ O ₃	7.07	9.47
FeO	n.a.	n.a.
MnO	0.16	0.17
MgO	5.73	12.23
CaO	9.61	11.41
Na ₂ O	3.27	2.14
K ₂ O	1.90	1.63
P ₂ O ₅	0.34	0.64
LOI	7.29	3.01
Total	100.00	100.00
mg#	64	85
K ₂ O/Na ₂ O	0.58	0.76
Sc	n.a.	n.a.
V	230	240
Cr	170	785
Ni	59	388
Rb	44	45
Sr	665	630
Y	15	16
Zr	127	120
Nb	59	49
Ba	415	330
Hf	2.8	2.9
La	31	32
Ce	59	65
Sm	n.a.	n.a.
Yb	n.a.	n.a.

Major elements are in wt%, and trace elements are in ppm. Fe₂O₃ (tot) = total iron calculated as ferric oxide. Data from Richards (1990a)

Au-bearing sulphide mineralization in these settings is generally disseminated or occurs as quartz-vein stockworks within the K-rich host rocks. The high-salinity fluid inclusions in these deposits suggest that the ore fluids were of

magmatic origin (Kwak 1990; Moyle et al. 1990; Richards 1995), and the mineralization and potassic magmatism are coeval. Older porphyry-style deposits at Northparkes (Goonumbla) and Ridgeway (Cadia) are from a similar tectonic

setting, formed from high salinity fluids (Heithersay et al. 1990; Heithersay and Walshe 1995; Wilson et al. 2003), and were coeval with high-K igneous rocks (e.g. Perkins et al. 1990a).

Many Cretaceous to Cenozoic epithermal (e.g. El Indio) and porphyry-type (e.g. Bajo de la Alumbrera; El Teniente) copper-gold deposits in the Chilean and Argentinian Andes are hosted by high-K calc-alkaline igneous rocks (e.g. Stults 1985; Tschischow 1989; Gröpper et al. 1991; Reyes 1991; Kay et al. 2005; Stern et al. 2011), and a direct genetic link between potassic magmatism and mineralization in this *continental arc* has been proposed.

A similar genetic association between epithermal gold and porphyry copper-gold mineralization and potassic igneous host rocks is also assumed at the Miocene Porgera and Pliocene Misima gold deposits, and the Pliocene Grasberg copper-gold deposit, which occur in a *postcollisional arc*. Both hypersaline fluid inclusions and stable isotope data provide evidence for the involvement of magmatic volatiles in ore formation (Richards 1992), and gold mineralization occurred within 1 million years of magmatism (Richards et al. 1991; Ronacher et al. 2002; Pollard and Taylor 2002; A.K. Appleby written comm., 1996).

There is growing evidence that high-K igneous rocks also may be an important component of the setting of VMS deposits in late oceanic arcs (e.g. Fiji: Colley and Greenbaum 1980; Flin Flon, Manitoba, Canada: Syme and Bailes 1993; Stern et al. 1995) and postcollisional arc (e.g. western Tasmania: Crawford et al. 1992) settings. The role of the high-K rocks is not defined, and hence these associations are not discussed in detail in this book. One possibility is that the high-K igneous rocks mark tectonic settings significantly inboard of subduction where there is a greater chance of preservation of the deposits.

There is also evidence for an association between molybdenum mineralization and high-K igneous rocks in island arc settings (e.g. Polillo Island, Philippines: Knittel and Burton 1985) and between iron-oxide-Cu-Au (IOCG) mineralization and volatile-rich potassic igneous rocks in

within-plate settings (e.g. Olympic Dam, South Australia: Skirrow et al. 2007; Pirajno 2008; Groves et al. 2010). This is discussed in more detail in Chap. 7.

References

- Ahmad M (1979) Fluid inclusion and geochemical studies at the Emperor gold mine, Fiji. Unpublished Ph.D., thesis, University of Tasmania, Hobart
- Ahmad M, Walshe JL (1990) Wall-rock alteration at the Emperor gold-silver telluride deposit, Fiji. *Aust J Earth Sci* 37:189–199
- Allmendinger RW (1986) Tectonic development, south-eastern border of the Puna Plateau, northwestern Argentine Andes. *Bull Am Geol Soc* 97:1070–1082
- Allmendinger RW, Ramos VA, Jordan TE, Palma M, Isacks BL (1983) Paleogeography and Andean structural geometry, Northwestern Argentina. *Tectonics* 2:1–16
- Anderson WB, Eaton PC (1990) Gold mineralization at the Emperor mine, Vatukoula, Fiji. *J Geochem Expl* 36:267–296
- Andrew RL (1995) Porphyry copper-gold deposits of the Southwest Pacific. *Min Eng* 47:33–38
- Appleby AK, Circosta G, Fanning M, Logan K (1995) A new model for controls on Au-Ag mineralization on Misima Island, Papua New Guinea. *Proceedings of 101st Annual Northwest Mining Association Convention*. Northwest Mining Association, Spokane, pp 122–127
- Arribas A (1995) Characteristics of high-sulphidation epithermal deposits, and their relation to magmatic fluid. In: Thompson JFH (ed) *Magmas, fluids, and ore deposits*. Mineralogical Association of Canada Short Course, vol 23, pp 419–454
- Baksheev IA, Chitalin AF, Yapaskurt VO, Vigasina MF, Bryzgalov IA, Ustinov VI (2010) Tourmaline in the Vetka porphyry copper-molybdenum deposit of the Chukchi Peninsula of Russia. *Mosc Univ Geol Bull* 65:27–38
- Baksheev IA, Prokof'ev VY, Zaraisky GP, Chitalin AF, Yapaskurt VO, Nikolaev YN, Tikhomirov PL, Nagornaya EV, Rogacheva LI, Gorelikova NV, Kononov OV (2012) Tourmaline as a prospecting guide for porphyry-style deposits. *Eur J Mineral* 24:957–979
- Baksheev IA, Nikolaev YN, Prokof'ev VY, Nagornaya EV, Sidorina YN, Maruschenko LI, Kal'ko IA, Chitalin AF (2013) Porphyry-epithermal system of the Baimka Cu-Au trend, western Chukchi Peninsula, Russia. *SGA Newsletter* 2013:A193
- Barazangi M, Isacks BL (1976) Spatial distribution of earthquakes and subduction of the Nazca plate beneath South America. *Geology* 4:686–692

- Bissig T, Lee JKW, Clark AH, Heather KB (2001) The Cenozoic history of volcanism and hydrothermal alteration in the Central Andean flat-slab region: new ^{40}Ar - ^{39}Ar constraints from the El Indio-Pascua Au (-Ag, Cu) Belt, 29°20'-30°30' S. *Int Geol Rev* 43: 312-340
- Bissig T, Clark AH, Lee JKW, Hodgson CJ (2002) Miocene landscape evolution and geomorphologic controls on epithermal processes in the El Indio-Pascua Au-Ag-Cu belt, Chile and Argentina. *Econ Geol* 97:971-996
- Bissig T, Clark AH, Lee JKW, von Quadt A (2003) Petrogenetic and metallogenetic responses to Miocene slab flattening: new constraints from the El Indio-Pascua Au-Ag-Cu belt, Chile/Argentina. *Mineral Deposita* 38:844-862
- Blackwell JL, Cooke DR, McPhie J, Simpson KA (2014) Lithofacies associations and evolution of the volcanic host succession to the Minifie ore zone: Ladolam gold deposit, Lihir Island, Papua New Guinea. *Econ Geol* 109:1137-1160
- Blevin PL (2002) The petrographic and compositional character of variably K-enriched magmatic suites associated with Ordovician porphyry Cu-Au mineralization in the Lachlan Fold Belt, Australia. *Mineral Deposita* 37:87-99
- Blevin PL, Chappell BW (1992) The role of magma sources, oxidation states and fractionation in determining the granite metallogeny of eastern Australia. *Trans Roy Soc Edinb Earth Sci* 83:205-316
- Blevin PL, Chappell BW (1995) Chemistry, origin, and evolution of mineralized granites in the Lachlan Fold Belt, Australia: the metallogeny of I- and S-type granites. *Econ Geol* 90:1604-1619
- Blight JHS, Crowley QG, Petterson MG, Cunningham D (2010) Granites of the Southern Mongolia Carboniferous arc: new geochronological and geochemical constraints. *Lithos* 116:35-52
- Bowman JR, Parry WT, Kropp WP, Krueger SA (1987) Chemical and isotopic evolution of hydrothermal solutions at Bingham, Utah. *Econ Geol* 82:395-428
- Bristol SK, Spry PG, Voudouris PC, Melfos V, Mathur RD, Fornadel AP, Sakellaris GA (2015) Geochemical and geochronological constraints on the formation of shear-zone hosted Cu-Au-Bi-Te mineralization in the Stanos area, Chalkidiki, northern Greece. *Ore Geol Rev* 66:266-282
- Burnham CW (1979) Magmas and hydrothermal fluids. In: Barnes HL (ed) *Geochemistry of hydrothermal ore deposits*, 2nd edn. Wiley Interscience, New York, pp 71-136
- Butcher A, Cunningham R, Edwards K, Lye A, Simmons J, Stegman C, Wyllie A (2011) Northparkes mines. In: *Australasian Mining and Metallurgical Operating Practices*. AusIMM Monograph, vol 28, pp 861-878
- Butera KM, Williams IS, Blevin PL, Simpson CJ (2001) Zircon U-Pb dating of early Paleozoic monzonitic intrusives from the Goonumbla area, NSW. *Aust J Earth Sci* 48:457-464
- Butler BS (1920) Oquirrh range. In: *The ore deposits of Utah*. US Geol Surv Prof Paper 111:335-362
- Caelles JC (1979) The geological evolution of the Sierras Pampeanas Massif, La Rioja and Catamarca Provinces, Argentina. Unpublished Ph.D., thesis, Queen's University, Kingston
- Cahill TA, Isacks BL (1992) Seismicity and shape of the subducted Nazca plate. *J Geophys Res* 97:503-529
- Cameron GH (1998) The hydrothermal evolution and genesis of the Porgera gold deposit, Papua New Guinea. Unpublished Ph.D., thesis, Australian National University, Canberra
- Carman GD (1994) Genesis of the Ladolam gold deposit, Lihir Island, Papua New Guinea. Unpublished Ph.D., thesis, Monash University, Melbourne
- Carman GD (2003) Geology, mineralization and hydrothermal evolution of the Ladolam gold deposit, Lihir Island, Papua New Guinea. *Econ Geol Spec Publ* 10:247-284
- Carr GR, Dean JA, Suppel DW, Heithersay PS (1995) Precise lead isotope fingerprinting of hydrothermal activity associated with Ordovician to Carboniferous metallogenetic events in the Lachlan Fold Belt of New South Wales. *Econ Geol* 90:1467-1505
- Chitalin AF, Fomichev E, Usenko V, Agapitov D, Shtengelov A (2012) Structural model of the Peschanka porphyry Cu-Au-Mo deposit, western Chukotka, Russia. In: Vearncombe J (ed) *Structural geology and resources—2012*. Australian Institute of Geosciences Symposium, Kalgoorlie, 26-28 Sept 2012, pp 21-27
- Clark AH (1993) Are outsize porphyry copper deposits either anatomically or environmentally distinctive? In: Whiting BH, Hodgson CJ, Mason R (eds) *Giant ore deposits*. *Econ Geol Spec Publ* 2:213-283
- Clark DS (1988) Lateral zonation within epithermal gold mineralization, Misima Island, Papua New Guinea. *Australas Inst Min Metall Bull Proc* 293:63-66
- Clark DS, Lewis RW, Waldron HM (1990) Geology and trace-element geochemistry of the Umuna gold-silver deposit, Misima Island, Papua New Guinea. *J Geochem Explor* 36:201-223
- Coleman PJ, Kroenke LW (1981) Subduction without volcanism in the Solomon island arc. *Geo-Mar Lett* 1:129-134
- Colley H, Greenbaum D (1980) The mineral deposits and metallogenesis of the Fiji platform. *Econ Geol* 75:807-829
- Constenius KW (1996) Late Paleogene extensional collapse of the Cordilleran Foreland fold and thrust belt. *Geol Soc Am Bull* 108:20-39
- Cooper P, Taylor B (1987) Seismotectonics of New Guinea: a model for arc reversal following arc-continent collision. *Tectonics* 6:53-67
- Corbett GJ (1999) Comments on the structural controls and styles of gold mineralization in the Minifie pit, Lihir Island. Unpl report to Lihir Management Company, Port Moresby
- Corbett GJ, Leach TM (1998) Southwest Pacific Rim and Gold-Copper Systems: structure, alteration, and mineralization. *Econ Geol Spec Publ* 6:1-236

- Corbett GJ, Hunt S, Cook A, Tamaduk P, Leach T (2001) Geology of the Ladolam gold deposit, Lihir Island, from exposures in the Minifie open pit. PNG Geology, Exploration and Mining Conference June 2001, Port Moresby, pp 69–77
- Crane D, Kavalieris I (2012) Geologic overview of the Oyu Tolgoi porphyry Cu-Au-Mo deposits, Mongolia. *Econ Geol Spec Publ* 16:187–213
- Crawford AJ, Corbett KD, Everard JL (1992) Geochemistry of the Cambrian volcanic-hosted massive sulphide-rich Mount Read Volcanics, Tasmania, and some tectonic implications. *Econ Geol* 87:597–619
- Dalziel IWD (1995) Earth before Pangea. *Sci Am* 272:58–63
- Davidson JP, Mpodozis C (1991) Regional geologic setting of epithermal gold deposits, Chile. *Econ Geol* 86:1174–1186
- Davies RM, Ballantyne GH (1987) Geology of the Ladolam gold deposit, Lihir Island, Papua New Guinea. *Pacific Rim Congr* 87:943–949
- Deino A, Keith JD (1997) Ages of volcanic and intrusive rocks in the Bingham mining district, Utah. *Econ Geol Guidebook* 29:91–100
- Deyell CL, Rye RO, Landis GP, Bissig T (2005) Alunite and the role of magmatic fluids in the Tambo high-sulphidation deposit, El Indio-Pascua belt, Chile. *Chem Geol* 215:185–218
- Dickinson WR, Snyder WS (1978) Plate tectonics of the Laramide orogeny. *Geol Soc Am Mem* 151:355–366
- Dilles JH, Einaudi MT, Profett JM, Barton MD (2000) Overview of the Yerrington porphyry copper district: magmatic to non-magmatic sources of hydrothermal fluids: their flow paths and alteration effects on rocks and Cu-Mo-Fe-Au ores. In: Thompson TB (ed) *Econ Geol Guidebook* 32:55–66
- Dimock RR, Carter CJ, Forth JR, Hoogvliet H, Jacobsen WL, Ketcham VJ, Probert TI, Thiel KF, Watson DL, Zavodni ZM (1993) Proposed gold ore mining and treatment operations at the Lihir Island Project, New Ireland Province, Papua New Guinea. *Australas Inst Min Metall Monogr* 19:913–922
- Dolgoplova A, Seltmann R, Armstrong R, Belousova E, Pankhurst RJ, Kavalieris I (2013) Sr-Nd-Pb-Hf isotope systematic of the Hugo Dummett Cu-Au porphyry deposit (Oyu Tolgoi, Mongolia). *Lithos* 167:47–64
- Dostal J, Zentilli M, Caelles JC, Clark AH (1977) Geochemistry and origin of volcanic rocks of the Andes (26–28°S). *Contrib Miner Petrol* 63:113–128
- Economou-Eliopoulos M (2005) Mineralogical and geochemical characteristics of the Skouries porphyry-Cu-Au-Pd-Pt deposit (Greece): evidence for the precious metal. In: Economou-Eliopoulos M, Eliopoulos DG (eds) *Mineral deposit research: meeting the global challenge*, vol 935–938
- Einaudi MT (1982) Description of skarns associated with porphyry copper plutons. In: Titley SR (ed) *Advances in Geology of the Porphyry Copper Deposits, Southwestern North America*. University of Arizona Press, Tucson, pp 139–183
- Fallon SJ, White JC, McCulloch MT (2002) Porite corals as recorders of mining and environmental impacts: Misima Island, Papua New Guinea. *Geochim Cosmochim Acta* 66:45–62
- Fears DW, Mutschler FE, Larson EE (1986) Cripple Creek, Colorado - a petrogenetic model. *Geological Society of America 99th Annual Meeting Abstracts, San Antonio*, vol 18, p 599
- Fleming AW, Handley GA, Williams KL, Hills AL, Corbett GJ (1986) The Porgera gold deposit, Papua New Guinea. *Econ Geol* 81:660–680
- Ford A, Hagemann SG, Fogliata AS, Miller JM, Mol A, Doyle PJ (2015) Porphyry, epithermal, and orogenic gold prospectivity of Argentina. *Ore Geol Rev* (in press)
- Fornadel AP, Voudouris PC, Spry PG, Melfos V (2012) Mineralogical, stable isotope, and fluid inclusion studies of spatially related porphyry Cu and epithermal Au-Te mineralization, Fakos Peninsula, Limnos Island, Greece. *Mineral Petrol* 105:85–111
- Franz L, Romer RL (2010) Different styles of metasomatic veining in ultramafic xenoliths from the TUBAF seamount (Bismarck microplate, Papua New Guinea). *Lithos* 114:30–53
- Franz L, Becker KP, Kramer W, Herzig PM (2002) Metasomatic mantle xenoliths from the Bismarck Microplate (Papua New Guinea)—thermal evolution, geochemistry and extent of slab-induced metasomatism. *J Petrol* 43:315–343
- Frei R (1992) Isotope (Pb-Rb-Sr-S-O-C-U-Pb) geochemical investigations on Tertiary intrusions and related mineralizations in the Serbo-Macedonian (Pb-Zn, Sb +Cu-Mo metallogenic) Province in northern Greece. Unpubl Ph.D. Thesis, ETH Zürich, Switzerland
- Frei R (1995) Evolution of mineralizing fluid in the porphyry copper system of the Skouries deposit, northeast Chalkidiki (Greece): evidence from combined Pb-Sr and stable isotope data. *Econ Geol* 90:746–762
- Garrett S (1996) The geology and mineralization of the Dinkidi porphyry-related Au-Cu deposit. In: *Porphyry-related copper and gold deposits of the Asia Pacific Region*. Australian Mineral Foundation, Cairns, pp 6.0–6.15
- Gemmell JB, Sharpe R, Jonasson IR, Herzig PM (2004) Sulfur isotope evidence for magmatic contributions to submarine and subaerial gold mineralization: conical seamount and the Ladolam gold deposit, Papua New Guinea. *Econ Geol* 99:1711–1725
- Gill JB (1970) Geochemistry of Viti Levu, Fiji, and its evolution as an island arc. *Contrib Miner Petrol* 27:179–203
- Gill JB, Whelan P (1989) Early rifting of an oceanic island arc (Fiji) produced shoshonitic to tholeiitic basalts. *J Geophys Res* 94:4561–4578
- Gill JB, Williams RW (1990) The isotope and U-series studies of subduction-related volcanic rocks. *Geochim Cosmochim Acta* 54:1427–1442
- Glen RA, Walshe JL, Barron LM, Watkins JJ (1998) Ordovician convergent-margin volcanism and tectonism in the Lachlan sector of East Gondwana. *Geology* 26:751–754

- Gonzalez OE (1975) Geología y alteración en el cobre porfídico “Bajo de la Alumbreira”, República Argentina. II Congreso Ibero-Americano de Geología Económica 2:247–270
- Götze HJ, Lahmeier B, Schmidt S, Strunk S (1987) Gravity field and megafault-system of the Central Andes (20°–26°S). *Terra Cognita* 7:57
- Gröpper H, Calvo M, Crespo H, Bisso CR, Cuadra WA, Dunkerley PM, Aguirre E (1991) The epithermal gold-silver deposit of Choquelimpie, Northern Chile. *Econ Geol* 86:1206–1221
- Groves DI, Bierlein FP, Meinert LD, Hitzman MW (2010) Iron oxide copper-gold (IOCG) deposits through earth history: implications for origin, lithospheric setting, and distinction from other epigenetic iron oxide deposits. *Econ Geol* 105:641–654
- Gruen G, Heinrich CA, Schroeder K (2010) The Bingham Canyon porphyry Cu-Mo-Au deposit. II. Vein geometry and ore shell formation by pressure-driven rock extension. *Econ Geol* 105:69–90
- Haggman JA (1997a) Philippines exploration: discovery of the Dinkidi gold-copper porphyry. *Min Eng* 49:34–39
- Haggman (1997b) The discovery, exploration and future development of the Didipio Project. In: World Gold '97 Conference. Australasian Institute of Mining and Metallurgy Publication Series, vol 2/97, pp 183–188
- Handley GA, Henry DD (1990) Porgera gold deposit. In: Hughes FE (ed) *Geology of the mineral deposits of Australia and Papua New Guinea*. Australasian Institute of Mining and Metallurgy, Parkville, Monograph, vol 14, pp 1717–1724
- Harper BL (2000) Hydrothermal alteration at the Ridge-way porphyry gold-copper deposit, NSW Unpublished Honours Thesis, University of Tasmania, Hobart
- Harris AC, Holcombe RJ (2014) Quartz vein emplacement at the E26 porphyry Cu-Au deposit, New South Wales. *Econ Geol* 109:1035–1050
- Harris AC, Allen CM, Bryan SE, Campbell IH, Holcombe RJ, Palin JM (2004a) ELA-ICP-MS U-Pb zircon geochronology of regional volcanism hosting the Bajo de la Alumbreira Cu-Au deposit: implications for porphyry-related mineralization. *Mineral Deposita* 39:46–67
- Harris AC, Kamenetsky VS, White NC, Steele DA (2004b) Volatile phase separation in silicic magmas at Bajo de la Alumbreira porphyry Cu-Au deposit, NW Argentina. *Resour Geol* 54:341–356
- Harris AC, Bryan SE, Holcombe RJ (2006) Volcanic setting of the Bajo de la Alumbreira porphyry Cu-Au deposit, Farallon Negro Volcanics, Northwest Argentina. *Econ Geol* 101:71–94
- Heithersay PS (1986) Endeavour 26 North copper-gold deposit, Goonumbla, NSW—paragenesis and alteration zonation. In: Berkman DA (ed) 13th CMMI congress, geology and exploration. Australasian Institute of Mining and Metallurgy, Parkville, vol 2, pp 181–189
- Heithersay PS, Walshe JL (1995) Endeavour 26 North: a porphyry copper-gold deposit in the Late Ordovician shoshonitic Goonumbla volcanic complex, New South Wales, Australia. *Econ Geol* 90:1506–1532
- Heithersay PS, O'Neill WJ, van der Helder P, Moore CR, Harbon PG (1990) Goonumbla porphyry copper district—Endeavour 26 North, Endeavour 22 and Endeavour 27 copper-gold deposits. In: Hughes FE (ed) *Geology of the mineral resources of Australia and Papua New Guinea*. Australasian Institute of Mining and Metallurgy, Parkville, Monograph, vol 14, pp 1385–1398
- Hickson RJ (1991) Grasberg open-pit: Ertzberg's big brother comes onstream in Indonesia. *Min Eng* 43:385–391
- Hill KC, Gleadow AJW (1989) Uplift and thermal history of the Papuan Fold Belt, Papua New Guinea: apatite fission track analysis. *Aust J Earth Sci* 36:515–539
- Hintze LF (1988) *Geologic History of Utah*. Brigham Young University, Provo, Geological Studies Special Publication, vol 7, 134 p
- Holliday JR, McMillan C, Tedder I (1999) Discovery of the Cadia Ridgeway gold-copper deposit. New generation gold mines—case histories of discovery. Australian Mineral Foundation, Perth, pp 101–107
- Holliday JR, Wilson AJ, Blevin PL, Tedder IJ, Dunham PD, Pfitzner M (2002) Porphyry gold-copper mineralization in the Cadia district, eastern Lachlan Fold Belt, New South Wales, and its relationship to shoshonitic magmatism. *Mineral Deposita* 37:100–116
- Hollister VF (1975) An appraisal of the nature and source of porphyry copper deposits. *Miner Sci Eng* 7:225–233
- Hoogvliet H (1993) The Ladolam gold deposit—at least two major events. *Aust J Min*, p 20 (Sept 1993)
- Hooper B, Heithersay PS, Mills MB, Lindhorst JW, Freyberg J (1996) Shoshonite-hosted Endeavour 48 porphyry copper-gold deposit, Northparkes, central New South Wales. *Aust J Earth Sci* 43:279–288
- Horton DJ (1978) Porphyry-type copper-molybdenum mineralization belts in Eastern Queensland, Australia. *Econ Geol* 73:904–921
- Introcaso A, Liou A, Ramos VA (1987) La estructura profunda de las Sierras de Cordoba. *Rev Asoc Geol Argent* 42:177–187
- James DE, Sacks JW (1999) Cenozoic formation of the central Andes: a geophysical perspective. *Econ Geol Spec Publ* 7:1–25
- Jannas RR, Beane RE, Ahler BA, Brosnahan DR (1990) Gold and copper mineralization at the El Indio deposit, Chile. *J Geochem Explor* 36:233–266
- Jensen EP (2003) Magmatic and hydrothermal evolution of the Cripple Creek gold deposit, Colorado, and comparisons with regional and global magmatic-hydrothermal systems associated with alkaline magmatism. Unpublished Ph.D., thesis, The University of Arizona, Tucson
- Jensen EP, Barton MD (1997) Types of potassium silicate alteration and related base metal mineralization in the Cripple Creek district, Colorado. *Geol Soc Am Abstr Programs* 29:207
- Jones GJ (1985) The Goonumbla porphyry copper deposits, NSW. *Econ Geol* 80:591–613

- Joplin GA (1968) The shoshonite association—a review. *J Geol Soc Aust* 15:275–294
- Joplin GA, Kiss E, Ware NG, Widdowson JR (1972) Some chemical data on members of the shoshonite association. *Mineral Mag* 38:936–945
- Jordan TE, Allmendinger RW (1986) The Sierras Pampeanas of Argentina: a modern analogue of rocky mountain foreland deformation. *Am J Sci* 286:737–764
- Jordan TE, Douglas RC (1980) Paleogeography and structural development of the Late Pennsylvanian to Early Permian Oquirrh Basin, northwestern Utah. In: Fouch TD, Mahathan ER (eds) *Paleozoic Paleogeography of the west-central United States; Rocky Mountain Paleogeography Symposium 1*. Society of Economic Paleontologists and Mineralogists, Rocky Mountain Section, Denver, pp 217–230
- Jowitz SM, Mudd GM, Weng Z (2013) Hidden mineral deposits in Cu-dominated porphyry-skarn systems: how resource reporting can occlude important mineralization types within mining camps. *Econ Geol* 108:1185–1193
- Kalogeropoulos SI (1986) The Skouries porphyry copper deposit, Chalkidiki Peninsula, northern Greece. In: *International South European symposium on exploration geochemistry*. Association of Exploration Geochemists, Field Trips Guide Book, Athens, pp 33–42
- Kamenetsky VS, Wolfe RC, Eggins SM, Mernagh TP, Bastrakov E (1999) Volatile exsolution at the Dinkidi Cu-Au porphyry deposit, Philippines: a melt-inclusion record of the initial ore-forming process. *Geology* 27:691–694
- Kamenov GD, Perfit MR, Jonasson IR, Mueller PA (2005) High-precision Pb isotope measurements reveal magma recharge as a mechanism for ore deposit formation: examples from Lihir Island and Conical Seamount, Papua New Guinea. *Chem Geol* 219:131–148
- Kamenov GD, Perfit MR, Mueller PA, Jonasson IR (2008) Controls on magmatism in an island arc environment: study of lavas and sub-arc xenoliths from the Tabar-Lihir-Tanga-Feni island chain, Papua New Guinea. *Contrib Miner Petrol* 155:635–656
- Kashgerel BE, Rye RO, Hedenquist JW, Kavalieris I (2006) Geology and reconnaissance stable isotope study of the Oyu Tolgoi porphyry Cu-Au system, South Gobi, Mongolia. *Econ Geol* 101:503–522
- Kashgerel BE, Kavalieris I, Hayashi KI (2008) Mineralogy, textures, and whole-rock geochemistry of advanced argillic alteration: Hugo Dummett porphyry Cu-Au deposit, Oyu Tolgoi mineral district, Mongolia. *Mineral Deposita* 43:913–932
- Kashgerel BE, Rye RO, Kavalieris I, Hayashi KI (2009) The sericitic to advanced argillic transition: stable isotope and mineralogical characteristics from the Hugo Dummett porphyry Cu-Au deposit, Oyu Tolgoi District, Mongolia. *Econ Geol* 104:1087–1110
- Kavalieris I, Wainwright A (2005) Whole-rock geochemistry of Late-Devonian island arc and intrusive suites from Oyu Tolgoi, South Gobi, Mongolia. In: Seltmann R, Gerel O, Kirwin D (eds) *Geodynamics and metallogeny of Mongolia with a special emphasis on copper and gold deposits*. IAGOD Guidebook Series, vol 11, pp 169–174
- Kavalieris I, Rinchin O, Gombojav J, Gombosuren N, Crane D, Orssich C, Khashgerel BE (2011) Characteristics of the Oyu Tolgoi porphyry deposits, South Gobi, Mongolia. In: *Abstract volume, 11th SGA Biennial Meeting, Antofagasta, Chile, 26–29 Sept 2011*, p A111
- Kay SM, Abbruzzo JM (1996) Magmatic evidence for Neogene lithospheric evolution of the central Andean “flat-slab” between 30°S and 32°S. *Tectonophysics* 259:15–28
- Kay SM, Gordillo CE (1994) Pocho volcanic rocks and the melting of depleted continental lithosphere above a shallowly dipping, subduction zone in the Andes. *Contrib Miner Petrol* 117:25–44
- Kay SM, Mpodozis C (2001) Central Andean ore deposits linked to evolving shallow subduction systems and thickening crust. *GSA Today* 11:4–9
- Kay SM, Maksiyev V, Moscoso R, Mpodozis C, Nasi C (1987) Probing the evolving Andean lithosphere: mid-late Tertiary magmatism in Chile (29°–30°30'S) over the modern zone of subhorizontal subduction. *J Geophys Res* 92:6173–6189
- Kay SM, Maksiyev V, Moscoso R, Mpodozis C, Nasi C, Gordillo CE (1988) Tertiary Andean magmatism in Chile and Argentina between 28°S and 33°S: correlation of magmatic chemistry with a changing Benioff Zone. *J S Am Earth Sci* 1:21–38
- Kay SM, Godoy E, Kurtz A (2005) Episodic arc migration, crustal thickening, subduction erosion, and magmatism in the south-central Andes. *Geol Soc Am Bull* 117:67–88
- Keith JD, Whitney JA, Cannan TM, Hook C, Hattori K (1995) The role of magmatic sulphides and mafic alkaline magmatism in the formation of giant porphyry and vein systems: examples from the Bingham and Tintic mining districts, Utah. In: Clark AH (ed) *Giant Ore Deposits - II*. QMinEx Department of Geological Sciences, Queens University, Kingston, pp 316–339
- Keith JD, Whitney JA, Hattori K, Ballantyne GH, Christiansen EH, Barr DL, Cannan TM, Hook CJ (1997) The role of magmatic sulphides and mafic alkaline magmas in the Bingham and Tintic mining districts, Utah. *J Petrol* 38:1679–1690
- Kelley KD, Ludington S (2002) Cripple Creek and other alkaline-related gold deposits in the Southern Rocky Mountains, USA: influence of regional tectonics. *Mineral Deposita* 37:38–60
- Kelley KD, Romberger SB, Beaty DW, Pontius JA, Snee LW, Stein HJ, Thompson TB (1998) Geochemical and geochronological constraints on the genesis of Au-Te deposits at Cripple Creek, Colorado. *Econ Geol* 93:981–1012
- Kennedy AK, Grove TL, Johnson RW (1990) Experimental and major element constraints on the evolution of lavas from Lihir Island, Papua New Guinea. *Contrib Mineral Petrol* 104:722–734

- Kerrich R, Goldfarb R, Groves DI, Garwin S (2000) The geodynamics of world-class gold deposits: characteristics, space-time distribution, and origins. *Economic Geology Reviews* 13:501–551
- Keyser F (1961) Misima Island—geology and gold mineralization. Bureau of Mineral Resources, Australia, BMR report, vol 57, pp 1–36
- Khain EV, Bibikova EV, Salnikova EB, Kröner A, Gibsher AS, Didenko AN, Degtyarev KE, Fedotova AA (2003) The Paleo-Asian ocean in the Neoproterozoic and early Paleozoic: new geochronological data and paleotectonic reconstructions. *Precambrian Res* 122:329–358
- Kirwin D, Forster CN, Kavalieris I, Crane D, Orsich C, Panther C, Garamjav D, Minkhbat TO, Niislekhuu G (2005) The Oyu Tolgoi copper-gold porphyry deposits, South Gobi, Mongolia. In: Seltmann R, Gerel O, Kirwin D (eds) *Geodynamics and metallogeny of Mongolia with a special emphasis on copper and gold deposits*, SEG-IAGOD Field Trip, 14–16 August 2005. 8th Biennial SGA Meeting; CERCAMS/NHM, London, IAGOD Guidebook Series, vol 11, pp 155–168
- Knittel U, Burton CK (1985) Polillo Island (Philippines): molybdenum mineralization in an island arc. *Econ Geol* 80:2013–2018
- Kockel F, Mollat H, Gundlach H (1975) Hydrothermally altered and (copper) mineralized porphyritic intrusions in the Serbomacedonian Massif (Greece). *Mineral Deposita* 10:195–204
- Komyshan P (1999) Geological interpretations of Lihir Island. Consulting Scientists of Australia (CSA Australia Pty Ltd), Unpl report R8.99
- Kroll T (2001) Petrographic-geochemical studies on monzonite intrusions hosting the Skouries porphyry Cu-Au deposit: barren versus mineralized. Unpubl M.Sc. Thesis, TU Bergakademie Freiberg, Freiberg
- Kroll T, Müller R, Seifert T, Herzog PM, Schneider A (2002) Petrology and geochemistry of the shoshonite-hosted Skouries porphyry Cu-Au deposit, Chalkidiki, Greece. *Mineral Deposita* 37:137–144
- Kröner A, Windley BF, Badarch G, Tomurtogoo O, Hegner E, Jahn BB, Grushka S, Khain EV, Demoux A, Wingate MTD (2007) Accretionary growth and crust-formation in the Central Asian Orogenic Belt and comparison with the Arabian-Nubian shield. *Geol Soc Am Mem* 200:181–209
- Kwak TAP (1990) Geochemical and temperature controls on ore mineralization at the Emperor gold mine, Vatukoula, Fiji. *J Geochem Explor* 36:297–337
- Lamb MA, Badarch G (1997) Paleozoic sedimentary basins and volcanic arc systems of Southern Mongolia: new stratigraphic and sedimentologic constraints. *Int Geol Rev* 39:342–576
- Landtwing MR, Dillenbeck ED, Leake MH, Heinrich CA (2002) Evolution of the breccias-hosted porphyry Cu-Mo-Au deposit at Agua Rica, Argentina: progressive unroofing of a magmatic hydrothermal system. *Econ Geol* 97:1273–1292
- Landtwing MR, Pettke T, Halter WE, Heinrich CA, Redmond PB, Einaudi MT, Kunze K (2005) Copper distribution during quartz dissolution by cooling magmatic-hydrothermal fluids: the Bingham porphyry. *Earth Planet Sci Lett* 235:229–243
- Landtwing MR, Furrer C, Pettke T, Guillong M, Heinrich CA (2010) The Bingham Canyon porphyry Cu-Mo-Au deposit: III. Zoned copper-gold ore deposition by magmatic vapor expansion. *Econ Geol* 105:91–118
- Lanier G, John EC, Swensen AJ, Reid J, Bard CE, Cadday SW, Wilson JC (1978a) General geology of the Bingham mine, Bingham Canyon, Utah. *Econ Geol* 73:1228–1241
- Lanier G, Raab WJ, Folsom RB, Cone S (1978b) Alteration of equigranular monzonite, Bingham mining district, Utah. *Econ Geol* 73:1270–1286
- Le Maitre RW (ed) (1989) *A classification of igneous rocks and glossary of terms: recommendations of the international union of geological sciences subcommission on the systematics of igneous rocks*. Blackwell Scientific Publications, Oxford, 193 p
- Levi B, Nyström JO, Thiele R, Aberg G (1988) Geochemical trends in mesozoic-tertiary volcanic rocks from the Andes in central Chile and its tectonic implications. *J SE Asian Earth Sci* 1:63–74
- Lewis RW, Wilson GI (1990) Misima gold deposit. In: Hughes FE (ed) *Geology of the mineral resources of Australia and Papua New Guinea*. Australasian Institute of Mining and Metallurgy, Parkville, Monograph, vol 14, pp 1741–1745
- Licence PS, Terril JE, Fergusson LJ (1987) Epithermal gold mineralization, Ambittle Island, Papua New Guinea. *Pacific Rim Congr* 87:273–278
- Lickfold V, Cooke DR, Smith SG, Ullrich TD (2003) Endeavour Cu-Au porphyry deposits, Northparkes, NSW: intrusive history and fluid evolution. *Econ Geol* 98:1607–1636
- Lindgren W, Ransome FL (1906) Geology and gold deposits of the Cripple Creek district, Colorado. *US Geol Surv Prof Pap* 541–516
- Lindley D (1988) Early Cainozoic stratigraphy and structure of the Gazelle peninsula, east New Britain: an example of extensional tectonics in the New Britain arc-trench complex. *Aust J Earth Sci* 35:231–244
- Lipman PW (1981) Volcano-tectonic setting of Tertiary ore deposits, southern rocky mountains. In: Dickinson WR, Payne WD (eds) *Relations of tectonics to ore deposits in the Southern Cordillera*. *Ariz Geol Soc Digest* 14:199–213
- Llambias EG (1972) Estructura del grupo volcánico Farallon Negro, Catamarca, República Argentina. *Rev Asoc Geol Argent* 27:161–169
- Logan JM, Mihalyuk MG (2014) Tectonic controls on early Mesozoic paired alkaline porphyry deposit belts (Cu-Au±Ag-Pt-Pd-Mo) within the Canadian Cordillera. *Econ Geol* 109:827–858
- Lopez DL, Williams SN (1993) Catastrophic volcanic collapse: relation to hydrothermal processes. *Science* 260:1794–1796

- Loughlin GF, Koschmann AH (1935) Geology and ore of the Cripple Creek District, Colorado. *Proc Colorado Sci Soc* 13:217–435
- Lu YJ, Kerrich R, McCuaig TC, Li ZX, Hart CJR, Cawood PA, Hou ZQ, Bagas L, Cliff J, Belousova EA, Tang S (2013) Geochemical, Sr-Nd-Pb, and zircon Hf-O isotopic compositions of Eocene-Oligocene shoshonitic and potassic adakite-like felsic intrusions in Western Yunnan, SW China: petrogenesis and tectonic implications. *J Petrol* 54:1309–1348
- MacDonald GD, Arnold LC (1994) Geological and geochemical zoning of the Grasberg igneous complex, Irian Jaya, Indonesia. *J Geochem Explor* 50:143–178
- Magri E, Tschischow N, Quiroga J, Lorca G, Couble A, Berenguela A (1998) Skouries Project—geological resource estimation—feasibility study. Unpubl TVX company report
- Maraeva RN, Migachev IF, Sapozhnikov VG, Shishakov VB (1988) Geological settings of copper-porphyry mineralization in the western Chukotka. In: Migachev IF (ed) *Mineralization of porphyry type in the far East of Russia*. Far East Branch of the USSR Academy of Science Publishing 1988, pp 94–105
- Marushchenko LI (2013) The mineralogy of propylites of the large Peschanka porphyry copper deposit (West Chukotka). *Moscow Univ Geol Bull* 68:79–88
- Maughan DT, Keith JD, Christiansen EH, Pulsipher T, Hattori K, Evans NJ (2002) Contributions from mafic alkaline magmas to the Bingham porphyry Cu-Au-Mo deposit, Utah, USA. *Mineral Deposita* 37:14–37
- McIntyre J, Moore J, Wyche J (2010) Technical report for the Didipio gold-copper project, Luzon, Philippines. Unpubl OceanaGold company report, pp 171
- McLemore VT (1996) Great Plains Margin (alkaline-related) gold deposits in New Mexico. In: Coyner AR, Fahey PL (eds) *Geology and ore deposits of the American Cordillera*. *Geol Soc Nevada Symp Proceed* 2:935–950
- McMahon T (1994) Pliocene intrusions in the Gunung Bijih (Ertsberg) Mining District, Irian Jaya, Indonesia: major and trace element chemistry. *Int Geol Rev* 36:925–946
- Migachev IF, Girfanov MM, Shishakov VB (1995) The Peschanka copper porphyry deposit. *Ore and Metals* 3:48–58 (in Russian)
- Moore WJ (1973) Igneous rocks in the Bingham mining district, Utah. *US Geol Soc Prof Paper* 629-B
- Morrison GW (1980) Characteristics and tectonic setting of the shoshonite rock association. *Lithos* 13:97–108
- Moyle AJ, Doyle BJ, Hoogvliet H, Ware AR (1990) Ladolam gold deposit, Lihir Island. In: Hughes FE (ed) *Geology of the mineral resources of Australia and Papua New Guinea*. Australasian Institute of Mining and Metallurgy, Parkville, Monograph, vol 14, pp 1793–1805
- Müller D (1993) Shoshonites and potassic igneous rocks: indicators for tectonic setting and mineralization potential of modern and ancient terranes. Unpubl Ph.D. Thesis, The University of Western Australia, Perth
- Müller D (2003) Geochemical variations of alkaline rocks as vector to epithermal gold mineralization at the giant Ladolam gold deposit, Lihir Island, Papua New Guinea. Unpubl. Habilitation Thesis, TU Bergakademie Freiberg, Freiberg
- Müller D, Forrester P (1998) The shoshonite porphyry Cu-Au association at Bajo de la Alumbrera, Catamarca Province, Argentina. *Mineral Petrol* 64:47–64
- Müller D, Groves DI (1993) Direct and indirect associations between potassic igneous rocks, shoshonites and gold-copper deposits. *Ore Geol Rev* 8:383–406
- Müller D, Rock NMS, Groves DI (1992a) Geochemical discrimination between shoshonitic and potassic volcanic rocks from different tectonic settings: a pilot study. *Mineral Petrol* 46:259–289
- Müller D, Stumpff EF, Taylor WR (1992b) Shoshonitic and alkaline lamprophyres with elevated Au and PGE concentrations from the Kreuzeck Mountains, Eastern Alps, Austria. *Mineral Petrol* 46:23–42
- Müller D, Morris BJ, Farrand MG (1993) Potassic alkaline lamprophyres with affinities to lamproites from the Karinya Syncline, South Australia. *Lithos* 30:123–137
- Müller D, Heithersay PS, Groves DI (1994) The shoshonite porphyry Cu-Au association in the Goonumbula district, NSW, Australia. *Miner Petrol* 51:299–321
- Müller D, Franz L, Herzig PM, Hunt S (2001) Potassic igneous rocks from the vicinity of epithermal gold mineralization, Lihir Island, Papua New Guinea. *Lithos* 57:163–186
- Müller D, Kaminski K, Uhlig S, Graupner T, Herzig PM, Hunt S (2002a) The transition from porphyry- to epithermal-style gold mineralization at Ladolam, Lihir Island, Papua New Guinea: a reconnaissance study. *Mineral Deposita* 37:61–74
- Müller D, Herzig PM, Scholten JC, Hunt S (2002b) Ladolam gold deposit, Lihir Island, Papua New Guinea: gold mineralization hosted by alkaline rocks. *Econ Geol Spec Publ* 9:367–382
- Müller D, Franz L, Petersen S, Herzig PM, Hannington MD (2003) Comparison between magmatic activity and gold mineralization at Conical Seamount and Lihir Island, Papua New Guinea. *Mineral Petrol* 79:259–283
- Mungall JE (2002) Roasting the mantle: slab melting and the genesis of major Au and Au-rich Cu deposits. *Geology* 30:915–918
- Mutschler FE, Larson EE, Bruce RM (1988) Laramide and younger magmatism in Colorado—new petrologic and tectonic variations on old themes. *Col School Min* 82:1–47
- Nagornaya EV (2010) Wall-rock alteration at the porphyry copper-molybdenum deposits of the Baimka ore cluster, Chukchi Peninsula. In: *International Conference on Geochemistry of Alkaline Rocks, Moscow, 12–16 Sept 2010*
- Navon O, Stolper E (1987) Geochemical consequences of melt percolation: the upper mantle as a chromatographic column. *J Petrol* 95:285–307

- Nikolaev YN, Prokof'ev VY, Apletalin AV, Vlasov EA, Baksheev IA, Kal'ko IA, Komarova YS (2013) Gold-telluride mineralization of the western Chukchi Peninsula, Russia: mineralogy, geochemistry, and formation conditions. *Geol Ore Dep* 55:96–124
- Nikolaev YN, Prokof'ev VY, Baksheev IA, Chitalin AF, Marushchenko LI, Kal'ko IA (2014) The first data on the zoned distribution of fluid inclusions in the ore-forming system of the Peschanka gold-copper porphyry deposit (Northeast Russia). *Dokl Earth Sci* 459:1615–1618
- Nokleberg WJ, Bundtzen TK, Eremin RA, Ratkin VV, Dawson KM, Shpikerman VI, Goryachev NA, Byalobzhesky SG, Frolov YF, Khanchuk AI, Koch RD, Monger JWH, Pozdeev AI, Rozenblum IS, Rodionov SM, Parfenov LM, Scotese CR, Sidorov AA (2005) Metallogeny and tectonics of the Russian Far East, Alaska, and the Canadian Cordillera. USGS Professional Paper, Denver, vol 1697, 380 p
- Pals DW, Spry PG (2003) Telluride mineralogy of the low-sulfidation epithermal Emperor gold deposit, Vatukoula, Fiji. *Mineral Petrol* 79:285–307
- Pals DW, Spry PG, Chryssoulis S (2003) Invisible gold and tellurium in arsenic-rich pyrite from the Emperor gold deposit, Fiji: implications for gold distribution and deposition. *Econ Geol* 98:479–493
- Parfenov LM, Berzin NA, Khanchuk AI (2003) Model for formation of orogenic belts in Central and Northeastern Asia. *Pac Geol* 6:7–41 (in Russian)
- Pearce JA (1982) Trace element characteristics of lavas from destructive plate boundaries. In: Thorpe RS (ed) *Andesites*. Wiley, New York, pp 525–548
- Peccerillo A, Taylor SR (1976a) Geochemistry of Eocene calc-alkaline volcanic rocks from the Kastamonu area, Northern Turkey. *Contrib Miner Petrol* 58:63–81
- Peccerillo A, Taylor SR (1976b) Rare earth elements in east Carpathian volcanic rocks. *Earth and Planetary Science Letters* 32:121–126
- Penniston-Dorland SC (2001) Illumination of quartz vein textures in a porphyry copper ore deposit using scanned cathodoluminescence: Grasberg igneous complex, Irian Jaya, Indonesia. *Am Mineral* 86:652–666
- Perantonis GI (1982) Genesis of porphyry copper deposits in the Chalkidiki Peninsula and Western Thrace, Greece. Unpubl Ph.D. Thesis, University of Athens, Athens
- Perello J, Cox D, Garamjav D, Sanjdorj S, Diakov S, Schissel D, Munkhbat TO, Oyun G (2001) Oyu Tolgoi, Mongolia: Siluro-Devonian porphyry Cu-Au-(Mo) and high-sulfidation Cu mineralization with a Cretaceous chalcocite blanket. *Econ Geol* 96:1407–1428
- Perkins C, McDougall I, Clauouè-Long J, Heithersay PS (1990a) $^{40}\text{Ar}/^{39}\text{Ar}$ and U-Pb geochronology of the Goonumbla porphyry Cu-Au deposits, NSW Australia. *Econ Geol* 85:1808–1824
- Perkins C, McDougall I, Clauouè-Long J (1990b) Dating of ore deposits with high precision: examples from the Lachlan Fold Belt, NSW, Australia. Pacific Rim Congress 90. Australasian Institute of Mining and Metallurgy, Parkville, pp 105–112
- Perkins C, McDougall I, Walshe JL (1992) Timing of shoshonitic magmatism and gold mineralization, Sheahan-Grants and Glendale, New South Wales. *Aust J Earth Sci* 39:99–110
- Petersen S, Herzig PM, Hannington MD, Jonasson IR, Arribas A (2002) Submarine vein-type gold mineralization near Lihir Island, New Ireland fore-arc, Papua New Guinea. *Econ Geol* 97:1795–1813
- Peterson EC, Mavrogenes JA (2014) Linking high-grade gold mineralization to earthquake-induced fault-valve processes in the Porgera gold deposit, Papua New Guinea. *Geology* 42:383–386
- Pilger RH (1984) Cenozoic plate kinematics, subduction and magmatism: South American Andes. *J Geol Soc Lond* 141:793–802
- Pirajno F (2008) Hydrothermal processes and mineral systems. Springer, Berlin, 1250 p
- Plimer IR, Andrew AS, Jenkins R, Lottermoser BG (1988) The geology and geochemistry of the Lihir gold deposit, Papua New Guinea. *Geol Soc Aust Abstr* 22:139–143
- Pollard PJ, Taylor RG (2002) Paragenesis of the Grasberg Cu-Au deposit, Irian Jaya, Indonesia: results from logging section 13. *Mineral Deposita* 37:117–136
- Pollard PJ, Taylor RG, Peters L (2005) Ages of intrusion, alteration, and mineralization at the Grasberg Cu-Au deposit, Papua, Indonesia. *Econ Geol* 100:1005–1020
- Powell CMcA (1984) Ordovician to earliest Silurian: marginal sea and island arc. In: Veevers JJ (ed) *Phanerozoic earth history of Australia*. Clarendon Press, Oxford, pp 290–312
- Presnell RD (1997) Structural controls on the plutonism and metallogeny in the Wasatch and Oquirrh Mountains, Utah. *Econ Geol Guidebook* 29:1–14
- Proffett JM (2003) Geology of the Bajo de la Alumbrera porphyry copper-gold deposit, Argentina. *Econ Geol* 98:1535–1574
- Puntodewo SSO, McCaffrey R, Calais E, Bock Y, Rais J, Subarya C, Poewariardi R, Stevens C, Genrich J, Fauzi Zwick P, Wdowinski S (1994) GPS measurements of crustal deformation within the Pacific-Australia plate boundary zone in Irian Jaya, Indonesia. *Tectonophysics* 237:141–153
- Redmond PB, Einaudi MT (2010) The Bingham Canyon porphyry Cu-Mo-Au deposit: I. Sequence of intrusion, vein formation, and sulfide deposition. *Econ Geol* 105:43–68
- Redmond PB, Einaudi MT, Inan EE, Landtwing MR, Heinrich CA (2004) Copper deposition by fluid cooling in intrusion-centered systems: new insights from the Bingham porphyry ore deposit, Utah. *Geology* 32:217–220
- Reyes M (1991) The Andacollo strata-bound gold deposit, Chile, and its position in a porphyry copper-gold system. *Econ Geol* 86:1301–1316
- Richards JP (1990a) The Porgera gold deposit, Papua New Guinea: geology, geochemistry and geochronology. Unpubl Ph.D. Thesis, The Australian National University, Canberra

- Richards JP (1990b) Petrology and geochemistry of alkaline intrusive at the Porgera gold deposit, Papua New Guinea. *J Geochem Explor* 35:141–199
- Richards JP (1992) Magmatic-epithermal transitions in alkali systems: Porgera gold deposit, Papua New Guinea. *Geology* 20:547–550
- Richards JP (1995) Alkalic-type epithermal gold deposits—a review. In: Thompson JFH (ed) *Magmas, fluids, and ore deposits*. Mineralogical Association of Canada, Toronto, Short Course Handbook, vol 23, pp 367–400
- Richards JP, Kerrich R (1993) The Porgera gold mine, Papua New Guinea: magmatic hydrothermal to epithermal evolution of an alkali-type precious-metal deposit. *Econ Geol* 88:1017–1052
- Richards JP, Ledlie I (1993) Alkalic intrusive rocks associated with the Mount Kare gold deposit, Papua New Guinea: comparison with the Porgera intrusive complex. *Econ Geol* 88:755–781
- Richards JP, McDougall I (1990) Geochronology of the Porgera gold deposit, Papua New Guinea: resolving the effects of excess argon on K-Ar and $^{40}\text{Ar}/^{39}\text{Ar}$ age estimates for magnetism and mineralization. *Geochim Cosmochim Acta* 54:1397–1415
- Richards JP, Chappell BW, McCulloch MT (1990) Intraplate-type magmatism in a continent-island-arc collision zone: Porgera intrusive complex, Papua New Guinea. *Geology* 18:958–961
- Richards JP, McCulloch MT, Chappell BW, Kerrich R (1991) Sources of metals in the Porgera gold deposit, Papua New Guinea: evidence from alteration, isotope, and noble metal geochemistry. *Geochim Cosmochim Acta* 55:565–580
- Roberts RJ, Crittenden MD, Tooker EW, Morris HT, Hose RK, Cheney TM (1965) Pennsylvanian and Permian basins in northwestern Utah, northwestern Nevada, and south-central Idaho. *Am Assoc Petrol Geol Bull* 49:1926–1956
- Rock NMS (1991) *Lamprophyres*. Blackie, Glasgow, p 285
- Rock NMS, Finlayson EJ (1990) Petrological affinities of intrusive rocks associated with the giant mesothermal gold deposit at Porgera, Papua New Guinea. *J SE Asian Earth Sci* 4:247–257
- Ronacher E, Richards JP, Villeneuve ME, Johnston MD (2002) Short life-span of the ore-forming system at the Porgera gold deposit, Papua New Guinea: laser $^{40}\text{Ar}/^{39}\text{Ar}$ dates for roscoelite, biotite, and hornblende. *Mineral Deposita* 37:75–86
- Ronacher E, Richards JP, Reed MH, Bray CJ, Spooner ETC, Adams PD (2004) Characteristics and evolution of the hydrothermal fluid in the North Zone high-grade area, Porgera gold deposit, Papua New Guinea. *Econ Geol* 99:843–867
- Rytuba JJ, McKee EH, Cox D (1993) Geochronology and geochemistry of the Ladolam gold deposit, Lihir Island, and gold deposits and volcanoes of Tabar and Tatau, Papua New Guinea. *US Geol Surv Bull* 2039:119–126
- Salfity JA (1985) Lineamentos transversales al rumbo Andino en el noroeste Argentino. In: Arias FJ, Camano BP, Espinoza RS (eds) *Proceedings IV Congreso Geologica Chileno*, 19–24 Aug 1985, Antofagasta, Chile. Universidad del Norte Chile, Departamento de Geociencias, Antofagasta, pp 119–137
- Scheibner E (1972) Tectonic concepts and tectonic mapping. *NSW Geol Surv Rec* 14, pp 37–83
- Scheibner E (1974) Lachlan fold belt. Definition and review of structural elements. In: Markham NL, Basden H (eds) *The mineral deposits of New South Wales*. *NSW Geol Surv Rec* 16, pp 109–113
- Scheibner E, Basden H (1998) *Geology of New South Wales—synthesis*. *Geol Surv New South Wales*, Sydney
- Scherbarth NL, Spry PG (2006) Mineralogical, petrological, stable isotope, and fluid inclusion characteristics of the Tuvatu gold-silver telluride deposit, Fiji: comparisons with the Emperor deposit. *Econ Geol* 101:135–158
- Schreiber U, Schwab K (1991) Geochemistry of Quaternary shoshonitic lavas related to the Calama-Olacapato-El Toro lineament, NW-Argentina. *J S Am Earth Sci* 4:73–85
- Schwab K, Lippolt H (1974) K-Ar mineral ages and late Cenozoic history of the Salar de Canchari area (Argentine Puna). In: Gonzalez FO (ed) *Proceedings of the IAVCEI symposium on andean and antarctic volcanology problems*, September 1974, Santiago, Chile. International Association of Volcanology and Chemistry of the Earth's Interior, Rome, pp 698–714
- Seltmann R, Solovieva R, Shatov V, Pirajnoa F, Naumov E, Cherkasov S (2010) Metallogeny of Siberia: tectonic, geologic and metallogenic settings of selected significant deposits. *Aust J Earth Sci* 57:655–706
- Sen SNC, Mauk JL, Müller D (2005) Hydrothermal alteration of the Oblaga Cu-Au skarn deposit and the Oblaga porphyry Cu-Au prospect, Inner Mongolia, China. In: *Proceedings of the 2005 New Zealand Minerals Conference*, pp 398–406
- Sengör AMC, Natalin BA (1996) Paleotectonics of Asia: fragment of a synthesis. In: An, Yin, Harrison TM (eds) *The Tectonic Evolution of Asia*. Cambridge University Press, Cambridge, pp 486–640
- Setterfield TN (1991) Evolution of the Tavua caldera and associated hydrothermal systems. Fiji. Unpubl Ph.D. Thesis, University of Cambridge, Cambridge
- Setterfield TN, Eaton PC, Rose WJ, Sparks RSJ (1991) The Tavua caldera, Fiji: a complex shoshonitic caldera formed by concurrent faulting and downsagging. *J Geol Soc* 148:115–127
- Setterfield TN, Mussett AE, Oglethorpe RDJ (1992) Magmatism and associated hydrothermal activity during the evolution of the Tavua caldera: $^{40}\text{Ar}/^{39}\text{Ar}$ dating on the volcanic, intrusive and hydrothermal events. *Econ Geol* 87:1130–1140

- Shatwell D (1987) Epithermal gold mineralization and Late Cenozoic magmatism in the Melanesian outer arc. *Pacific Rim Congr* 87:393–398
- Sheppard S, Taylor WR (1992) Barium- and LREE-rich, olivine-mica lamprophyres with affinities to lamprophytes, Mt. Bunday, Northern Territory, Australia. *Lithos* 28:303–325
- Siddeley G, Araneda R (1986) The El Indio—Tambo gold deposits, Chile. In: Macdonald AJ (ed) *Proceedings of Gold '86 international symposium on the geology of gold deposits*, Toronto, pp 445–456
- Sidorov AA, Eremin RA (1994) Metallogeny and gold lode deposits of northeastern Russia. In: ICAM-94 *Proceedings*, pp 247–256
- Sillitoe RH (1979) Some thoughts on gold-rich porphyry copper deposits. *Mineral Deposita* 14:161–174
- Sillitoe RH (1991) Gold metallogeny of Chile—an introduction. *Econ Geol* 86:1187–1205
- Sillitoe RH (1997) Characteristics and controls of the largest porphyry copper-gold and epithermal gold deposits in the circum-Pacific region. *Aust J Earth Sci* 44:373–388
- Sillitoe RH (2002) Some metallogenic features of gold and copper deposits related to alkaline rocks and consequences for exploration. *Mineral Deposita* 37:4–13
- Sillitoe RH (2008) Special paper: major gold deposits and belts of the North and South American Cordillera: distribution, tectonomagmatic settings, and metallogenic considerations. *Econ Geol* 103:663–687
- Sillitoe RH, Camus F (1991) A special issue devoted to the gold deposits in the Chilean Andes—preface. *Econ Geol* 86:1153–1154
- Sillitoe RH, Gappe IM (1984) Philippine porphyry copper deposits: geologic setting and characteristics. U.N.-ESCAP, CCOP Tech Publ, vol 14, 89 pp
- Simmons SF, Brown KL (2006) Gold in magmatic hydrothermal solutions and rapid formation of a giant ore deposit. *Science* 314:288–291
- Skirrow RG, Bastrakov EN, Barovich K, Fraser GL, Creaser RA, Fanning CM, Raymond OL, Davidson GJ (2007) Timing of iron oxide Cu-Au-U hydrothermal activity and Nd isotopic constraints on metal sources in the Gawler Craton, South Australia. *Econ Geol* 102:1441–1470
- Smith B, Smith C, Wilson EW (2008) The Emperor mine, Vatukoula, Viti Levu, Fiji. *Mineral Rec* 39:397–301
- Soloviev SG (2014) *The Metallogeny of Shoshonitic Magmatism*, vol I. Scientific World Publications, Moscow, pp 1–528 (in Russian)
- Stern RA, Syme EC, Bailes AH, Lucas SB (1995) Paleoproterozoic (1.90–1.86 Ga) arc volcanism in the Flin Flon belt, Trans-Hudson Orogen, Canada. *Contrib Miner Petrol* 119:117–141
- Stern CR, Skewes MA, Arevalo A (2011) Magmatic evolution of the giant El Teniente Cu-Mo deposit, Central Chile. *J Petrol* 52:1591–1617
- Strecker MR, Cervený P, Bloom AL, Malizia D (1989) Late Cenozoic tectonism and landscape development in the foreland of the Andes: Northern Sierras Pampeanas (26°–28°S), Argentina. *Tectonics* 8:517–534
- Stults A (1985) Geology of the Bajo de la Alumbraera porphyry copper-gold prospect, Catamarca Province, Argentina. Unpubl M.Sc. Thesis, The University of Arizona, Tucson
- Suppel DW, Barnes RG, Scheibner E (1998) The Paleozoic in New South Wales: geology and mineral resources. *J Aust Geol Geophys* 17(3):87–105
- Syme EC, Bailes AH (1993) Stratigraphic and tectonic setting of early proterozoic volcanogenic massive sulphide deposits, Flin Flon, Manitoba. *Econ Geol* 88:566–589
- Takazawa E, Frey FA, Shimizu N, Obata M, Bodinier JL (1992) Geochemical evidence for melt migration and reaction in the upper mantle. *Nature* 359:55–58
- Tarkian M, Stribny B (1999) Platinum-group elements in porphyry copper deposits: a reconnaissance study. *Mineral Petrol* 65:161–183
- Taylor B (1979) Bismarck Sea: evolution of a back arc basin. *Geology* 7:171–174
- Taylor WR, Rock NMS, Groves DI, Perring CS, Golding SD (1994) Geochemistry of Archaean shoshonitic lamprophyres from the Yilgam Block, Western Australia: Au abundance and association with gold mineralization. *Appl Geochem* 9:197–222
- Tedder IJ, Holliday JR, Hayward S (2001) Discovery and evaluation drilling of the Cadia Far East gold-copper deposit. In: *NewGen Gold 2001*. Australian Mineral Foundation, Perth, pp 212–216
- Thompson TB, Trippel AD, Dwelley PC (1985) Mineralized veins and breccias of the Cripple Creek District, Colorado. *Econ Geol* 80:1669–1688
- Thompson JFH, Lessman J, Thompson AJB (1986) The Temora gold-silver deposit: a newly recognized style of high sulphur mineralization in the lower Paleozoic of Australia. *Econ Geol* 81:732–738
- Titley SR (1975) Geological characteristics and environment of some porphyry copper occurrences in the Southwestern Pacific. *Econ Geol* 70:499–514
- Tobey E, Schneider A, Alegria A, Olcay L, Perantonis G, Quiroga J (1998) Skouries porphyry copper-gold deposit, Chalkidiki, Greece. In: Porter TM (ed) *Porphyry and hydrothermal Cu-Au deposits. A global perspective*. Australian Mineral Foundation Conference Proceedings, Glenside, South Australia, pp 159–168
- Tschischow N (1989) *Geología y geoquímica de El Indio, IV Region, Coquimbo, Chile: implicancias genéticas*. Unpubl B.Sc. Thesis, Universidad de Chile, Santiago
- Ulrich T, Heinrich CA (2002) Geology and alteration geochemistry of the porphyry Cu-Au deposit at Bajo de la Alumbraera, Argentina. *Econ Geol* 97:1865–1888
- Ulrich T, Günther D, Heinrich CA (2001) The evolution of a porphyry Cu-Au deposit, based on LA-ICP-MS analysis of fluid inclusions: Bajo de la Alumbraera, Argentina. *Econ Geol* 96:1743–1774
- Van Nort SD, Atwood GW, Collinson TB, Potter DR (1991) The geology and mineralization of the

- Grasberg porphyry copper-gold deposit, Irian Jaya, Indonesia. *Min Eng* 43:300–303
- Veranis N (1994) Geological structure and primary raw materials in the Chalkidiki Peninsula. IGME Report, Athens (in Greek)
- Vila T, Sillitoe RH (1991) Gold-rich porphyry systems in the Maricunga Belt, Northern Chile. *Econ Geol* 86:1238–1260
- Voight B, Elsworth D (1997) Failure of volcano slopes. *Geotechnique* 47:1–31
- Volchkov AG, Sokirkin GI, Shishakov VB (1982) Geological setting and ore composition of the Anyiskoe copper-porphyry deposit. *Geol Ore Deposits* 4:89–94
- Volkov AV, Savva NE, Sidorov AA, Egorov VN, Shapovalov VS, Prokof'ev VY, Kolova EE (2006) Spatial distribution and formation conditions of Au-bearing porphyry Cu-Mo deposits in the Northeast of Russia. *Geol Ore Deposits* 48:448–472
- Voudouris P, Melfos V, Spry PG, Bonsall T, Tarkian M, Solomon C (2008) Carbonate-replacement Pb-Zn-Ag-Au mineralization in the Kamariza area, Lavrion, Greece: mineralogy and thermochemical conditions of formation. *Mineral Petrol* 94:85–106
- Wainwright AJ, Tosdal RM, Wooden JL, Mazdab FK, Friedman RM (2011) U-Pb (zircon) and geochemical constraints on the age, origin, and evolution of Paleozoic arc magmas in the Oyu Tolgoi porphyry Cu-Au district, Southern Mongolia. *Gondwana Res* 19:764–787
- Waite KA, Keith JD, Christiansen EH, Whitney JA, Hattori K, Tingey DG, Hook CJ (1997) Petrogenesis of the volcanic and intrusive rocks associated with the Bingham Canyon porphyry Cu-Au-Mo deposit, Utah. In: John DA, Ballantyne GH (eds) *Geology and ore deposits of the Oquirrh and Wasatch Mountains, Utah*. *Econ Geol Guidebook* 29:69–90
- Wall VJ, Munroe SM, Cameron GH, Heinrich CA, Cox SF, Walshe JL (1995) Porgera: plumbing and processes of gold mineralization. In: Clark AH (ed) *Giant ore deposits—II. Proceedings of the second giant ore deposits workshop*, Queen's University, Kingston, Ontario, pp 649–667
- Wallace DA, Johnson RW, Chappell BW, Arculus RJ, Perfit MR, Crick IH (1983) Cainozoic volcanism of the Tabar, Lihir, Tanga, and Feni Islands, Papua New Guinea: geology, whole-rock analyses, and rock-forming mineral compositions. Bureau of Mineral Resources of Australia. BMR report, vol 243, p 138
- Walthier TN, Sirvas E, Araneda R (1985) The El Indio gold, silver, copper deposit. *Eng Min J* 186:38–42
- Warnaars FW, Smith WH, Bray RE, Lanier G, Shafiqullah M (1978) Geochronology of igneous intrusions and porphyry copper mineralization at Bingham, Utah. *Econ Geol* 73:1242–1249
- Webster JD, Goldoff B, Sintoni MF, Shimizu N, Vivo BD (2014) C-O-H-Cl-S-F volatile solubilities, partitioning, and mixing in phonolithic-trachytic melts and aqueous-carbonic vapor±saline liquid at 200 MPa. *J Petrol* 55:2217–2248
- White NC, Leake MJ, McCaughey SN, Parris BW (1995) Epithermal gold deposits of the Southwest Pacific. *J Geochem Explor* 54:87–136
- Wilson JC (1978) Ore fluid-magma relationships in a vesicular quartz-late porphyry dyke at Bingham, Utah. *Econ Geol* 73:1287–1307
- Wilson F (1981) *The conquest of copper mountain*. Atheneum, New York, p 244
- Wilson AJ, Cooke DR, Harper BL (2003) The Ridgeway gold-copper deposit: a high-grade alkali porphyry deposit in the Lachlan Fold Belt, New South Wales, Australia. *Econ Geol* 98:1637–1666
- Wilson AJ, Cooke DR, Harper BJ, Deyell CL (2007) Sulfur isotopic zonation in the Cadia district, southeastern Australia: exploration significance and implications for the genesis of alkali porphyry gold-copper deposits. *Mineral Deposita* 42:465–487
- Wolfe RC (2001) *Geology of the Didipio region and paragenesis of the Dinkidi Cu-Au porphyry deposit*. Unpubl Ph.D. Thesis, University of Tasmania, Hobart
- Wolfe RC, Cooke DR (2011) *Geology of the Didipio region and genesis of the Dinkidi alkali porphyry Cu-Au deposit and related pegmatites, Northern Luzon, Philippines*. *Econ Geol* 106:1279–1315
- Wolfe RC, Cooke DR, Joyce P (1998) The Dinkidi Au-Cu porphyry—an alkaline porphyry deposit from North Luzon, Philippines. *Geol Soc Aust Abstr* 49:131
- Wood D, Holliday JR (1995) Discovery of the Cadia gold/copper deposit. In: *New South Wales: new generation gold mines—case histories of discovery*. Australian Mineral Foundation, Perth, pp 11.1–11.10
- Wyborn D (1992) The tectonic significance of Ordovician magmatism in the Eastern Lachlan Fold Belt. *Tectonophysics* 214:177–192
- Wyman D (1990) *Archaean shoshonitic lamprophyres of the Superior Province, Canada: petrogenesis, geodynamic setting, and implications for lode gold deposits*. Unpubl Ph.D. Thesis, University of Saskatchewan, Saskatoon
- Wyman D, Kerrich R (1989) Archaean shoshonitic lamprophyres associated with Superior Province gold deposits: distribution, tectonic setting, noble metal abundances and significance for gold mineralization. In: Keays RR, Ramsay WRH, Groves DI (eds) *The geology of gold deposits: the perspective in 1988*. *Econ Geol Monogr* 6:651–667

Direct Associations Between Potassic Igneous Rocks and Copper-Gold Deposits on Craton Margins

7

7.1 Introduction

Although this book is mainly about potassic igneous rocks and hydrothermal gold and gold-copper mineralization in volcanic arc environments, there is increasing evidence for the genetic association between volatile-rich potassic igneous rocks and iron-oxide-Cu-Au (IOCG) deposits (e.g. Campbell et al. 1998; Groves et al. 2010; Haywood 2013; Fazel et al. 2015; Sarjoughian et al. 2015) and intrusion-related gold deposits (IRGD) in plume-related within-plate settings (e.g. Goldfarb et al. 2005; Mair et al. 2011). Recent studies suggest that both IOCG and IRGD systems form above metasomatized lithosphere from hydrothermal fluids connected to mixed basic to felsic alkaline to sub-alkaline intrusions that generated in sub-MOHO magma chambers (see summary by Groves and Santosh 2015). Such systems provide strong chemical potential gradients between greatly contrasting magma geochemistry (Fig. 7.1), allowing both metal and fluid migration from the hotter basic-ultrabasic melts to the less-dense overlying felsic melts, which then provide the source of ore fluid and metals to form the IOCG and IRGD systems (Groves and Santosh 2015). Additionally, both deposit types are interpreted to share a common within-plate tectonic setting, probably related to mantle plumes along near-vertical, partly fault-disrupted craton margins (Fig. 7.2). These long-lived sutures, where previous paleo-

subduction events have enriched the lithosphere with mantle-incompatible elements and metals during metasomatism, provided preferred pathways for uprising asthenospheric mantle plumes (Groves and Santosh 2015). Partial assimilation of the LILE- and volatile-enriched upper mantle sources by the basic and CO₂-rich asthenospheric plumes would provide the fertile melts capable of forming the complex geochemical fingerprints (i.e. high Cl, F, Co, Ni, Ba, LREE, HREE, U, elements related to high fO₂) of IOCG deposits. This process would also explain the unusually deep root zones of many IOCG deposits such as Olympic Dam and Fe-P deposits such as Kiruna (J. Bryant, pers. comm., 2011). Consequently, the giant IOCG deposits of Olympic Dam, Australia, and Salobo, Brazil, together with other world-class to giant deposits, are located on craton margins (Grainger et al. 2008; Groves et al. 2010; Haywood 2013). Additionally, the world-class to giant IRGD system at Fort Knox, Alaska, is related to hybrid monzogranite intrusions into shelf sedimentary sequences, situated adjacent to, and overlying, the western margin of the North American Craton (Groves and Santosh 2015). The giant Telfer gold deposit, between the Pilbara and Kimberley cratons in Western Australia, is another deposit that is probably an IRGD. The importance of cratonic margins, and other deep-seated discontinuities, as plumbing systems for major copper and gold deposits is also indicated by the detailed analysis of combined geological,

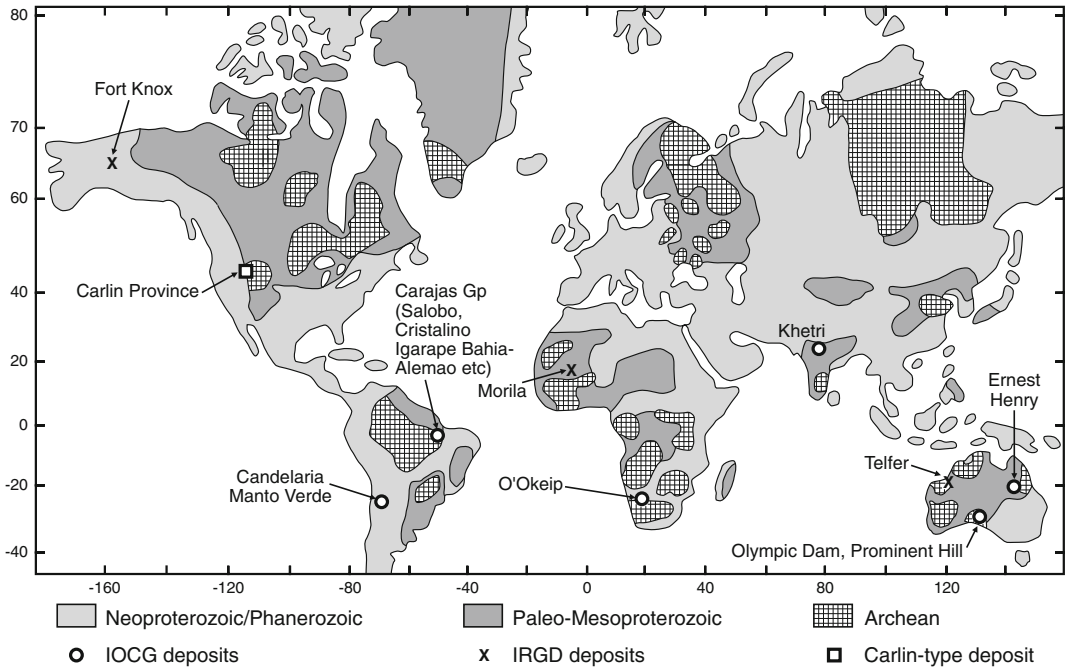


Fig. 7.1 Geographical distribution of IOCG and IRGD shown relative to the position of Archaean and Proterozoic cratons. Modified after Groves et al. (2010)

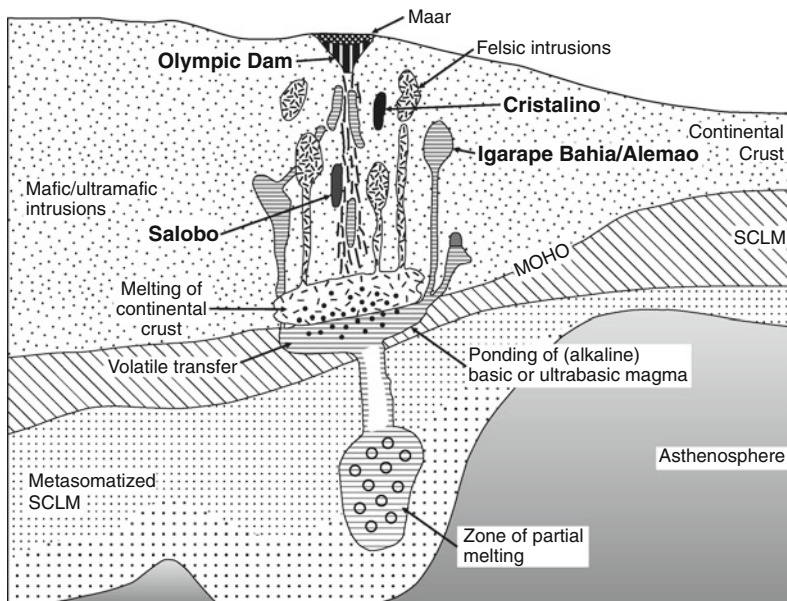


Fig. 7.2 Magmatic-hydrothermal model for IOCG deposits associated with high-K alkaline magmatism derived from metasomatized lithosphere on craton margins. SCLM = Subcontinental lithospheric mantle. Modified after Groves and Santosh (2015)

geophysical and isotopic data at the lithospheric scale (cf. Begg et al. 2010; Hronsky et al. 2012).

Interestingly, there have been recent suggestions (e.g. Cline et al. 2005; Muntean et al. 2011; Johnson et al. 2015) that the gold deposits of the giant Carlin province of Nevada, USA, on the same western margin of the North American Craton as Fort Knox, have at least an indirect association to high potassic magmatism. The Carlin deposits have an almost identical Eocene age to the giant Bingham porphyry copper deposit (see Sect. 6.4.2) to the east. However, they were deposited from low-temperature non-magmatic ore fluids, so the hot and high-potassic magmas can only have acted as a heat source driving the Carlin hydrothermal system, not as the primary fluid source as for Bingham (e.g. Cunningham et al. 2004).

The economically most significant examples of IOCG deposits (Olympic Dam, Australia) and IRGD associated with potassic igneous rocks (Fort Knox, Alaska, USA) are discussed in more detail below.

7.2 Iron-Oxide Copper-Gold (IOCG) Deposits and Potassic Igneous Rocks

7.2.1 Introduction

The iron-oxide copper-gold (IOCG) *sensu stricto* deposits are magmatic-hydrothermal deposits that contain economic copper and gold grades and are typically controlled by deep-seated structures or their intersections (e.g. Hitzman 2000; Williams et al. 2005; Groves et al. 2010). Most IOCG systems contain significant volumes of breccias, they may be accompanied by pre-sulphide alkali (K-feldspar-biotite) and/or sodic-calcic (albite-actinolite) alteration, but lack widespread quartz veins or silicification (Williams et al. 2005; Groves et al. 2010). Typically, the deposits show a temporal, but not close spatial, relationship to major alkaline to subalkaline intrusions that are derived from the mantle (Groves et al. 2010). The IOCG deposits

are defined by abundant low-Ti iron oxides (hematite and/or magnetite) and iron silicates that are intimately associated with, but may be paragenetically older than, Fe-Cu sulphides (Campbell et al. 1998; Williams et al. 2005; Groves et al. 2010). Copper-bearing sulphides tend to be paragenetically late and postdate the albite-actinolite alteration in the deeper seated deposits (Williams et al. 2005). Independent variation in fO_2 conditions during mineralization produced IOCG deposits ranging from pyrite-poor examples with abundant chalcopyrite, bornite, and chalcocite (e.g. Salobo, Brazil, and Olympic Dam, Australia), to others in which pyrite and chalcopyrite are the main sulphides (e.g. Candelaria, Chile). Fluid inclusion and stable isotope studies indicate that highly saline brines, probably directly sourced from mantle-derived volatile-rich basic magmas, were involved in the genesis of these deposits (Campbell et al. 1998; Williams et al. 2005; Groves et al. 2010). The exceptionally high REE contents of IOCG deposits of typically 10^4 times the chondritic value (Campbell et al. 1998) suggest high halogen (Cl and F) contents of the precipitating hydrothermal fluids as the REE are known to have higher solubilities in Cl- and F-rich solutions (Hellman et al. 1979; Oreskes and Einaudi 1990; Allen and Seyfried 2005; Tropper et al. 2011).

A likely source of the high Cu, Au, REE, and volatile contents of IOCG deposits are portions of the upper mantle that had been metasomatically enriched during previous paleo-subduction events (Groves et al. 2005; Haywood 2008). Haywood (2008) further suggest that mixing of these volatile- and metal-rich, alkaline, basic melts with oxidized silicic crustal melts produced sulphide-oxide immiscibility and volatile exsolution responsible for the formation of IOCG deposits. The complexity of associated magmatism, with mafic to felsic plutons, can be explained by mixing of alkaline parent mantle-derived magmas with felsic magmas derived from underplating of the parent magmas below continental crust (cf. Hart et al. 2004). A schematic model for the generation of IOCG deposits is presented in Fig. 7.2. The alkalic

dykes documented in numerous IOCG deposits are interpreted as apophyses from large hydrous alkaline magma chambers that underlay the respective orebodies at the time of their formation (Campbell et al. 1998). The existence of a large magma chamber would also explain the coincident magnetic and gravity anomalies associated with the Olympic Dam deposit (Roberts and Hudson 1983).

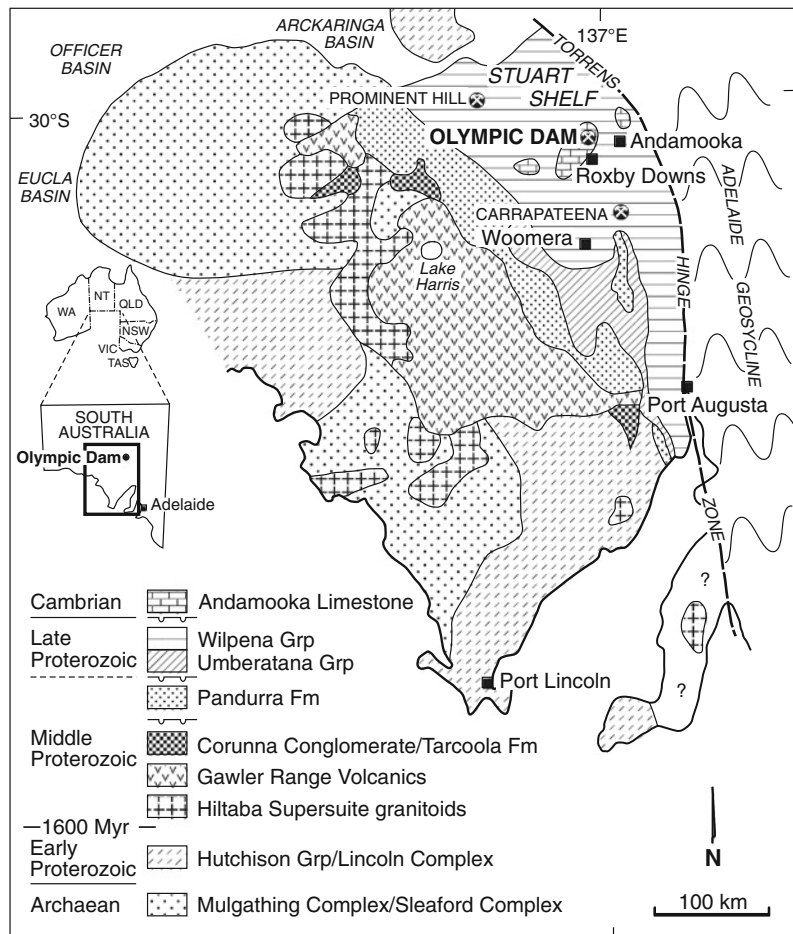
7.2.2 Olympic Dam Cu-Au-U-REE Deposit, South Australia

Introduction The Olympic Dam copper-uranium-gold-silver deposit (Fig. 7.3) is located about 520 km north-northwest of Adelaide in South Australia (Wang et al. 1999). The deposit was discovered by Western Mining Corporation

(WMC) in 1975 during an extensive multi-disciplinary exploration program. The discovery drill hole RD-1 was collared near the Olympic Dam stock watering hole on Roxby Downs station and intersected sub-economic copper minerals at depths of more than 300 m (J. Bryant, pers. comm., 2011). The follow-up drill holes were disappointing, but the persistence of WMC’s exploration team was rewarded with hole RD-10 intersecting >170 m at >2 wt% copper.

Olympic Dam has total indicated resources of 4571 Mt at 0.88 wt% copper, 0.34 g/t gold, 1.56 g/t Ag and 280 g/t U₃O₈ (mining-technology.com). The mine is currently operated as an underground operation by BHP Billiton. Olympic Dam does not only represent one of the largest copper deposits in the world, but it also contains economic by-products of silver and

Fig. 7.3 Regional geologic map of the Gawler Craton, South Australia. The Olympic Dam copper-gold-uranium-REE deposit lies in the northeast of the craton beneath the sedimentary units of the Stuart Shelf. Modified after Johnson and McCulloch (1995)



LREE (Oreskes and Einaudi 1990; Campbell et al. 1998; Williams et al. 2005). No other deposit is known to have the same metal association and similar grades (Johnson and McCulloch 1995). Consequently there has been much curiosity and speculation regarding possible genetic models for its origin and potential exploration strategies for further discoveries (Johnson and McCulloch 1995).

Regional Geology The Archaean Gawler craton, which underlies a large area of southern Australia, is separated from another cratonic block to the east, the Curnamona province, by Proterozoic continental supracrustal rocks preserved in the early Paleozoic Adelaide Fold Belt (Fig. 7.3). Olympic Dam is concealed beneath >300 m of Proterozoic and Cambrian sedimentary cover near the northeastern margin of the Gawler craton (Reeve et al. 1990; Williams et al. 2005). The deposit is hosted by Middle Proterozoic monzogranites and related breccias (Fig. 7.4). Several smaller IOCG systems occur in the vicinity of Olympic Dam (Skirrow et al. 2002) and other large deposits have been discovered at Prominent Hill to the north and Carrapateena to the south of Olympic Dam on the same craton margin. The mineralization at Olympic Dam (Fig. 7.4) occurs in a 7 by 5 km zone of brecciated and altered rock developed within the Hiltaba-Suite Roxby Downs granite that has been dated at 1588 ± 4 Ma (Oreskes and Einaudi 1990; Johnson and Cross 1995). The hematite-rich breccias contain large blocks of sedimentary rocks and have been interpreted to represent a diatreme-maar volcanic setting (e.g. Haynes et al. 1995).

Nature of Copper-Uranium-Gold-Silver Mineralization Hematite-rich breccias that host the bulk of the ore are generally matrix-supported with clast sizes mostly <20 cm, but ranging up to tens of meters (Reeve et al. 1990). The breccias typically form steeply dipping, northwest-striking, dyke-like bodies within fractured granite (Oreskes and Einaudi 1990). The vertical extent of these breccias extends to depths much greater than 1 km (Oreskes and Einaudi 1990). The dominant alteration

assemblage at Olympic Dam is sericite-hematite \pm chlorite \pm quartz \pm siderite (Williams et al. 2005). Hematite occurs as euhedral laths and fine-grained aggregates in the matrices of all breccias types (Oreskes and Einaudi 1990). By contrast, magnetite is subordinate, paragenetically earlier than the hematite-phyllsilicate alteration, and concentrated in the deeper parts of the system as suggested by deep exploration drilling (J. Bryant, pers. comm., 2011), suggesting that the widespread hematite alteration could represent a surficial oxidation product (i.e. martitization) overprinting an originally magnetite-dominated orebody.

Economic mineralization consists of breccia-hosted chalcopyrite-bornite-chalcocite \pm pyrite assemblages (Johnson and McCulloch 1995). The Cu-Fe sulphides commonly are intergrown with fluorite and locally rim corroded quartz grains (Oreskes and Einaudi 1990). Locally, the sulphides also occur as disseminated grains interstitial to hematite grains in breccia matrices (Campbell et al. 1998). Radiogenic isotope studies reveal that the sulphide-rich hematitic breccias share an initial Σ_{Nd} signature of about -2.5 , suggesting that these ore types are cogenetic (Johnson and McCulloch 1995). The host Roxby Downs granite has an initial Σ_{Nd} value of about -5.0 , and therefore cannot alone have been the source of the mineralizing fluids (Johnson and McCulloch 1995). The isotope data clearly suggest a contribution from a mantle-derived basic magma (Johnson and McCulloch 1995; Campbell et al. 1998). The hematite breccias also have high LREE and HREE contents, averaging about 5000 ppm and about 10^4 times the chondritic value, and the total LREE content and La/Lu ratios are positively correlated with hematite abundance (Oreskes and Einaudi 1990). Five hydrothermal REE-bearing mineral phases have been identified: bastnaesite, florencite, monazite, xenotime, and britholite (Oreskes and Einaudi 1990).

The orebody is intruded by numerous ultramafic, mafic, and felsic dykes which are temporally related to the hydrothermal activity (Williams et al. 2005). A post-mineral dyke has

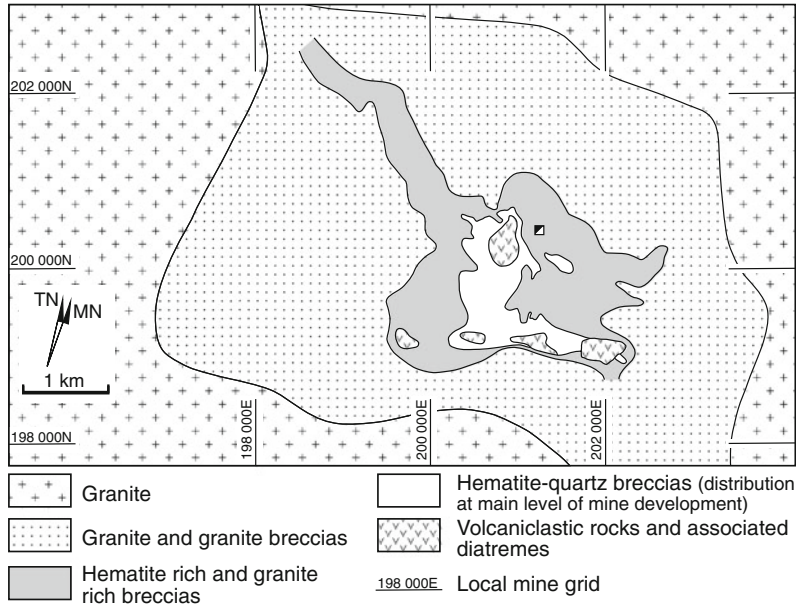


Fig. 7.4 Simplified geologic map of the Olympic Dam copper-gold-uranium-REE deposit, South Australia, at the main development level of the mine. The position of the Whenan Shaft is shown. Note the lithological zonation

from the host monzogranite at the margins to progressively more hematite-rich lithologies in the centre of the breccia complex. Modified after Johnson and McCulloch (1995)

been dated at 1592 ± 8 Ma (Johnson and Cross 1995), implying that the deposit formed soon after emplacement of the Roxby Downs granite (i.e. 1588 ± 4 Ma; Oreskes and Einaudi 1990). A pipe-like body of barren hematite-quartz breccias forms the centre of the orebody (Fig. 7.4), that is progressively surrounded by a complex zone of granite-rich breccias and hematite-altered granite (Reeve et al. 1990).

Petrography and Geochemistry of the Potassic Host Rocks The Olympic Dam IOCG mineralization is restricted to a hematitic breccia complex (Reeve et al. 1990), which occurs wholly within the Roxby Downs monzogranite (Fig. 7.4). Where unaltered, the monzogranite is a pink-red, medium- to coarse-grained rock with massive textures (Reeve et al. 1990; Johnson and McCulloch 1995). The K-feldspar commonly displays rapakivi textures, where K-feldspars are rimmed by albite. Geochemically, the rock is

characterized by high K_2O , LILE, LREE, HREE, HFSE, U, and F (Collins et al. 1982; Creaser 1989; Johnson and McCulloch 1995), reflecting a within-plate tectonic setting (cf. Müller et al. 1992). The hematitic breccias which host the bulk of mineralization vary from matrix-poor types showing crackle or jigsaw textures, to matrix-supported types with rotated clasts (Johnson and McCulloch 1995). Their compositional variability encompasses: (1) heterolithic breccias with abundant hematite and monzogranite clasts; (2) hematite breccias with dominantly hematite clasts; and (3) hematite-quartz breccias with clasts of hematite and granite-derived quartz. The matrix typically consists of reworked granite fragments and fine-grained hematite aggregates (Oreskes and Einaudi 1990). Minor components occurring as discrete clasts include sulphides \pm pitchblende, fluorite, barite and siderite (Johnson and McCulloch 1995).

7.3 Intrusion-Related Gold Deposits (IRGD) and Potassic Igneous Rocks

7.3.1 Introduction

Although many orogenic gold deposits have spatial, and more rarely temporal, associations, but no genetic link, with felsic plutons, intrusion-related gold deposits (IRGD) have a clear genetic relationship with host or adjacent plutons (Goldfarb et al. 2005) that are hybrid mantle-crustal high-K magmas (Mair et al. 2011). The IRGD systems differ from porphyry and skarn copper-gold and epithermal gold deposits in terms of the relatively low fO_2 of their associated intrusions when compared to arc magmas (see Sect. 10.3.2). Intrusion-related gold deposits represent a relatively new group of gold deposits that are hosted primarily within, or in the immediate wall rocks to, intrusions (Lang and Baker 2001). Exploration interest has been attracted to this group of deposits in the last decade due to their attributed global distribution (Fig. 7.2), although only a small number of undoubted IRGDs contain a significant gold resource of >3 Moz (Goldfarb et al. 2005). World-class to giant examples include Fort Knox (Bakke et al. 2000), and probably Telfer (Rowins et al. 1997) and Morila (McFarlane et al. 2011). Other world-class deposits such as Donlin Creek and Pogo in Alaska, as well as Kidston in Australia, Kori Kollo in Bolivia, and Vasilkovsky in Kazakhstan, described by Lang and Baker (2001), among others, as IRGDs are now considered unlikely to belong to this group (Goldfarb et al. 2005).

Intrusion-related gold deposits have several distinct characteristics including their associations with: (1) intermediate to felsic intrusions with relatively low fO_2 that were derived from potassic basic parent magmas sourced from the lithospheric mantle (2) carbonic, CO_2 -rich, hydrothermal fluids; (3) Bi-W-As-Te-Sb-Sn ore assemblages; (4) relatively low sulphide contents (<5 vol.%); (5) weak hydrothermal alteration zones; and (6) continental within-plate tectonic

settings (Thompson et al. 1999; Lang and Baker 2001; Goldfarb et al. 2005); on (7) craton margins (Mair et al. 2011; Groves and Santosh 2015).

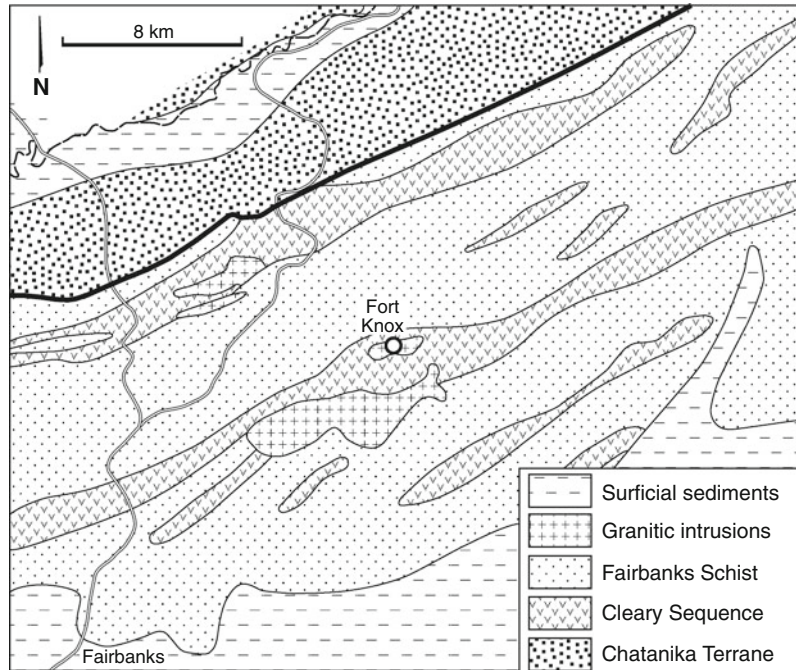
7.3.2 Fort Knox Gold Deposit, Alaska, USA

Introduction The Fort Knox gold deposit is situated about 40 km northeast of Fairbanks in eastern Alaska. Fort Knox represents the largest tonnage IRGD in the world (Bakke et al. 2000) and total resources now total about 7 Moz gold.

The Fort Knox area was actively explored for gold placer deposits from 1902 when a prospector discovered gold nuggets in the Fish Creek located downstream of the Fort Knox deposit (Quandt et al. 2008). Since that initial discovery, small placer deposits in the Fairbanks mining district have produced >8 Moz of gold. In 1980, two local prospectors recovered bismuthinite nuggets containing abundant gold. The demonstrated correlation between the gold and bismuth resulted in a systematic exploration program involving panning and trenching in the area (Quandt et al. 2008). In 1984, a consulting geologist noted the presence of native gold in quartz veins hosted by monzogranite in the Fort Knox area. Subsequently, the claims were leased to an exploration joint venture between Nye Minerals and Electrum Resources in 1987 which commenced a large exploration program. In 1992, Amax Gold purchased the Fort Knox project and established Fairbanks Gold Mining, a wholly-owned subsidiary, to operate the project (Quandt et al. 2008). The orebody was delineated by soil sampling and exploration drilling in late 1992. In 1998, Kinross Gold Corporation acquired the Fort Knox property as part of its merger with Amax Gold Inc. (Quandt et al., 2008). The deposit has been mined as an open-pit operation by Kinross Gold Corporation since 1998.

Regional Geology The Fairbanks district is situated on the western margin of the North American Craton in the northwestern part of the

Fig. 7.5 Simplified geologic map of the Fort Knox gold deposit, Alaska, USA, showing the dominant northeast-oriented regional structural trend. Modified after Quandt et al. (2008)



Yukon-Tanana Terrane, which consists of poly-metamorphic rocks of Precambrian to upper Paleozoic ages (Quandt et al. 2008). The dominant rock types are grey to brown, fine-grained mica schists and micaceous quartzites, locally known as the Fairbanks Schist, that is locally intruded by Cretaceous granodiorite and granite stocks (Fig. 7.5; Quandt et al. 2008). The Cleary Sequence, comprising bimodal meta-rhyolite and meta-basalt with actinolite schist, graphite schist, and marbles, is intercalated with the Fairbanks Schist. The northern part of the district contains outcrops of amphibolite-facies metamorphosed rocks of the Paleozoic Chatanika Terrane (Quandt et al. 2008).

Fort Knox belongs to the Tintina gold province which forms a broad Cretaceous (110–65 Ma) magmatic belt that continues for >1500 km, from southwestern Alaska, across central Alaska and Yukon, to the westernmost Northwest Territories (Hart et al. 2002; Goldfarb et al. 2005). The province contains both intrusion-related gold deposits including Fort Knox, Dublin Gulch, Brewery Creek and possibly Shotgun, and orogenic gold deposits such as Pogo and Donlin Creek (Goldfarb et al. 2005).

The gold deposits are generally situated in a northeast trending, structurally complex zone characterized by a series of folds, shear zones, high-angle faults, and rare low-angle faults (Quandt et al. 2008). Northeast-striking high-angle faults (Fig. 7.5), which display strike-slip displacements, influence the location of gold deposits that are related to movement along the regional north-bounding Tintina Fault system and the south-bounding Denali Fault system, respectively (Quandt et al. 2008). The Fairbanks Schist is intersected by several late Cretaceous to early Tertiary intrusions ranging from ultramafic to felsic compositions (Quandt et al. 2008), including lamprophyre dykes (Hart et al. 2004; Mair et al. 2011).

Nature of Gold Mineralization The Fort Knox gold deposit (Hart et al. 2004; Goldfarb et al. 2005) is hosted by a small elongate (1 km²), biotite- and hornblende-bearing composite granite stock (Fig. 7.5). Magmatic biotites from this intrusion are dated at about 88–86 Ma using ⁴⁰Ar/³⁹Ar methods (Selby et al. 2002). Radiogenic isotope data indicate a significant crustal component to the magmas (Lang et al. 2000), but

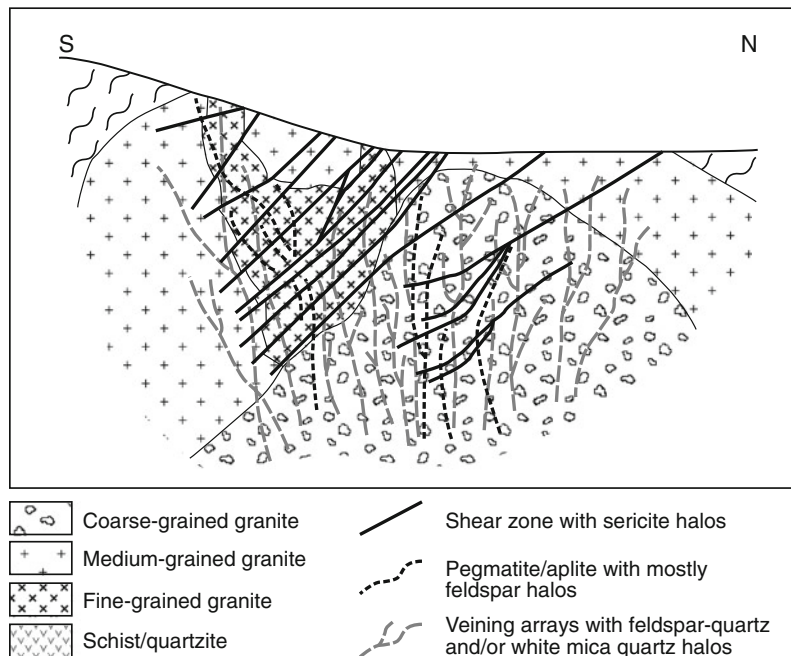
locally, there are also important contributions from ancient metasomatized mantle (Hart et al. 2004; Goldfarb et al. 2005). The surface exposure of the elongate composite intrusion measures approximately 1100 by 600 m across (Quandt et al. 2008). The intrusion is offset by two northeast-trending structures which display left-lateral strike slip movement. These structures, the Monte-Cristo Fault and Melba Fault, are regional in extent and also offset the Gilmore Dome pluton south of Fort Knox (Quandt et al. 2008). The gold mineralization mainly consists of fine-grained native gold and it has a distinctly low (<0.10 vol.%) sulphide content (Quandt et al. 2008). Typical sulphide phases documented at Fort Knox are rare maldonite, bismuthinite, bismite, tetradymite, and native bismuth (Quandt et al. 2008). Native gold grains measure <100 microns in diameter and typically occur in and along the margins of pegmatite veins, quartz stockwork veins and veinlets, quartz-veined shear zones, and fractures within the granite (Fig. 7.6). Pervasive hydrothermal alteration zones are lacking at Fort Knox (Goldfarb et al. 2005), but locally, quartz veins and veinlets can have thin albite and/or phyllic alteration selvages that range in thickness from 0.5 to 3.0 cm

(Quandt et al. 2008). The stockwork veins strike predominantly east and have steep dips (Quandt et al. 2008). The stockwork vein density generally increases with depth. Shear zones typically strike northwest and dip moderately to the southwest. Gold mineralization in the quartz-filled shears is distributed relatively evenly (Quandt et al. 2008).

Petrography and Geochemistry of the Potassic Host Rocks

The granite stock hosting the Fort Knox deposit has very variable textures and compositions, ranging from fine-grained granodiorite, through medium-grained biotite-granite, to coarse-grained biotite-monzogranite porphyry with phenocrysts of quartz, K-feldspar, biotite and hornblende (Quandt et al. 2008). The diverse textural and geochemical varieties as well as sharp to gradational intrusive contacts suggest that the Fort Knox pluton represents a composite, multi-phase intrusion (Quandt et al. 2008). The local occurrences of orthoclase megacrysts, resorbed quartz phenocrysts, and quartz glomero-phenocrysts support that interpretation (Quandt et al. 2008). Crenulated quartz layers (i.e. brain rock) and dendritic growths of quartz and K-feldspar documented in the Fort Knox

Fig. 7.6 Geological cross-section (N-S) of the Fort Knox gold deposit, Alaska, USA, showing the composite monzogranite stock that hosts the mineralization. At least three intrusive phases ranging from coarse- to fine-grained may be distinguished. The late-stage shear zones containing high-grade gold mineralization (up to 1.0 oz/t) are also shown. Adapted from Bakke et al. (2000)



intrusion assist to evaluate intrusive contacts and paragenesis (Bakke et al. 2000; Quandt et al. 2008). High whole-rock K_2O contents (>4.3 wt %), low Fe_2O_3/FeO ratios (0.15–0.3), and low magnetic susceptibilities, suggest a reduced oxidation state of the high-K parent magma (Hart et al. 2004), consistent with more detailed geochemical studies at the smaller IRGD-associated Scheelite Dome complex to the east (Mair et al. 2011).

References

- Allen DE, Seyfried WE (2005) REE controls in ultramafic hosted MOR hydrothermal systems: an experimental study at elevated temperature and pressure. *Geochim Cosmochim Acta* 69:675–683
- Bakke A, Morrell B, Odden J, Bergstrom T, Woodman J (2000) Kinross Gold USA's activities in the Fairbanks mining district. *British Columbia Yukon Chamber Mines Spec*, vol 2:89–98
- Begg GC, Hronsky JMA, Arndt NT, Griffin WL, O'Reilly SY, Haywood N (2010) Lithospheric, cratonic and geodynamic setting of Ni-Cu-PGE deposits. *Econ Geol* 105:1057–1070
- Campbell IH, Compston DM, Richards JP, Johnson JP, Kent AJR (1998) Review of the application of isotopic studies to the genesis of Cu-Au mineralization at Olympic Dam and Au mineralization at Porgera, the Tennant Creek district and Yilgarn Craton. *Aust J Earth Sci* 45:201–218
- Cline JS, Hofstra AH, Muntean JL, Tosdal RM, Hickey K (2005) Carlin-type deposits in Nevada: critical geological characteristics and viable models. *Econ Geol* 100:371–405
- Collins WJ, Beams SD, White AJR, Chappell BW (1982) Nature and origin of A-type granites with particular reference to southeastern Australia. *Contrib Miner Petrol* 80:189–200
- Creaser RA (1989) The geology and petrology of Middle Proterozoic felsic magmatism of the Stuart Shelf. South Australia. Unpublished PhD Thesis, La Trobe University, Melbourne
- Cunningham CG, Austin GW, Naeser CW, Rye RO, Ballantyne GH, Stamm RG, Barker CE (2004) Formation of a Paleothermal anomaly and disseminated gold deposits associated with the Bingham Canyon porphyry Cu-Au-Mo system, Utah *Econ Geol* 99:789–806
- Fazel ET, Mehrabi B, Shabani AAT (2015) Kuh-e Dom Fe-Cu-Au prospect, Anarak metallogenic complex, Central Iran: a geological, mineralogical and fluid inclusion study. *Miner Petrol* 109:115–141
- Goldfarb RJ, Baker T, Dubè B, Groves DI, Hart CJR, Gosselin P (2005) Distribution, character, and genesis of gold deposits in metamorphic terranes. *Econ Geol* 100:407–450
- Grainger CJ, Groves DI, Fletcher IR, Tallarico FMB (2008) Metallogenesis of the Carajas Mineral Province, southern Amazon Craton, Brazil: varying styles of Archaean through Neoproterozoic base- and precious-metal mineralization. *Ore Geol Rev* 33:451–489
- Groves DI, Condie KC, Goldfarb RJ, Hronsky JMA, Vielreicher RM (2005) Secular changes in global tectonic processes and their influence on the temporal distribution of gold-bearing mineral deposits. *Econ Geol* 100:203–224
- Groves DI, Bierlein FP, Meinert LD, Hitzman MW (2010) Iron oxide copper-gold (IOCG) deposits through earth history: implications for origin, lithospheric setting, and distinction from other epigenetic iron oxide deposits. *Econ Geol* 105:641–654
- Groves DI, Santosh M (2015) Province-scale commonalities of some world-class gold deposits: implications for mineral exploration. *Geosci Front* 6:389–399
- Hart CJR, McCoy D, Goldfarb RJ, Smith M, Roberts P, Hulstein R, Bakke AA, Bundtzen TK (2002) Geology, exploration and discovery in the Tintina gold province, Alaska and Yukon. *Econ Geol Spec Publ* 9:241–274
- Hart CJR, Mair JL, Goldfarb RJ, Groves DI (2004) Source and redox controls on metallogenic variations in ore systems, Tombstone-Tungsten Belt, Yukon, Canada. *Trans Royal Soc Edinburgh Earth Sci* 95:339–356
- Haynes DW, Cross KC, Bills RT, Reed MH (1995) Olympic Dam ore genesis: a fluid mixing model. *Econ Geol* 90:281–307
- Haywood N (2008) The geodynamic setting and magmatic controls on genesis of world-class IOCG ore deposits. *Geol Soc Aust Abstr* 89:130
- Haywood N (2013) Genesis and location of world-class iron oxide copper-gold deposits. In: Chang Z, Goldfarb RJ, Blenkinsop T, Placzek C, Cooke D, Carranza J (eds) *FUTORES Conference Abstracts*, vol 68. EGRU Contribution, p 20
- Hellman PL, Smith RE, Henderson P (1979) The mobility of the rare earth elements: evidence and implications from selected terrains affected by burial metamorphism. *Contrib Miner Petrol* 71:23–44
- Hitzman MW (2000) Iron oxide-Cu-Au deposits: what, where, when, and why? In: Porter TM (ed) *Hydrothermal iron oxide copper-gold and related deposits. A global perspective*, vol 2. Australian Mineral Foundation, Adelaide, pp 9–26
- Hronsky JMA, Groves DI, Loucks RR, Begg GC (2012) A unified model for gold mineralization in accretionary orogens and implications for regional-scale exploration targeting methods. *Mineral Deposita* 47:339–358

- Johnson JP, Cross KC (1995) U-Pb geochronological constraints on the genesis of the Olympic Dam Cu-U-Au-Ag deposit, South Australia. *Econ Geol* 90:1046–1063
- Johnson JP, McCulloch MT (1995) Sources of mineralizing fluids for the Olympic Dam deposit (South Australia): Sm-Nd isotopic constraints. *Chem Geol* 121:177–199
- Johnson CL, Dilles JH, Kent AJR, Farmer LP (2015) Petrology and geochemistry of the Emigrant Pass volcanics, Nevada: implications for a magmatic-hydrothermal origin of the Carlin gold deposits. In: Pennell WM, Garside LJ (eds) *New Concepts and Discoveries*, vol 1. Geol Soc Nevada 2015 Symposium, DEStech Publications Inc., Lancaster: 391–408
- Lang JR, Baker T, Hart CJR, Mortensen JK (2000) An exploration model for intrusion-related gold systems. *Econ Geol Newslett* 40:1, 6–15
- Lang JR, Baker T (2001) Intrusion-related gold systems: the present level of understanding. *Mineral Deposita* 36:477–489
- Mair JL, Farmer GL, Groves DI, Hart CJR, Goldfarb RJ (2011) Petrogenesis of postcollisional magmatism at Scheelite Dome, Yukon, Canada: evidence for a lithospheric mantle source for magmas associated with intrusion-related gold systems. *Econ Geol* 106:451–480
- McFarlane CRM, Mavrogenes J, Lentz D, King Ken, Allibone A, Holcombe R (2011) Geology and intrusion-related affinity of the Morila gold mine, southeast Mali. *Econ Geol* 106:727–750
- Müller D, Rock NMS, Groves DI (1992) Geochemical discrimination between shoshonitic and potassic volcanic rocks from different tectonic settings: a pilot study. *Miner Petrol* 46:259–289
- Muntean JL, Cline JS, Simon AC, Longo AA (2011) Magmatic-hydrothermal origin of Nevada's Carlin-type gold deposits. *Nat Geosci* 4:122–127
- Oreskes N, Einaudi MT (1990) Origin of rare earth element-enriched hematite breccias at the Olympic Dam Cu-U-Au-Ag deposit, Roxby Downs, South Australia. *Econ Geol* 85:1–28
- Quandt D, Ekstrom C, Triebel K, Henderson RD (2008) Technical report for the Fort Knox mine prepared for Kinross Gold Corporation and Fairbanks Gold Mining Incorporated, Fairbanks North Star Borough, Alaska, USA. Unpublished Report, March 2008, 79 p
- Reeve JS, Cross KC, Smith RN, Oreskes N (1990) Olympic Dam copper-uranium-gold-silver deposit. In: Hughes FE (ed) *Geology of the mineral deposits of Australia and Papua New Guinea*. Australasian Institute of Mining and Metallurgy, Melbourne, pp 1009–1035
- Roberts DE, Hudson GRT (1983) The Olympic Dam copper-uranium gold-silver deposit, Roxby Downs, South Australia. *Econ Geol* 78:799–822
- Rowins SM, Groves DI, McNaughton NJ, Palmer MR, Eldridge CS (1997) A reinterpretation of the role of granitoids in the genesis of Neoproterozoic gold mineralization in the Telfer Dome, Western Australia. *Econ Geol* 92:133–160
- Sarjoughian F, Kananian A, Ahmadian J, Murata M (2015) Chemical composition of biotite from the Kuh-e Dom pluton, Central Iran: implications for granitoid magmatism and related Cu-Au mineralization. *Arab J Geosci* 8:1521–1533
- Selby D, Creaser RA, Hart CJR, Rombach CS, Thompson JFH, Smith MT, Bakke AA, Goldfarb RJ (2002) Absolute timing of sulphide and gold mineralization: a comparison of Re-Os molybdenite and Ar-Ar mica methods from the Tintina gold belt, Alaska. *Geology* 30:791–794
- Skirrow RG, Raymond OL, Bastrakov E, Davidson G, Heathersay P (2002) The geological framework, distribution, and controls of Fe oxide Cu-Au mineralization in the Gawler Craton, South Australia. Part II: alteration and mineralization. In: Porter TM (ed) *Hydrothermal iron oxide copper-gold and related deposits: a global perspective*, vol 2. Australian Mineral Foundation, Adelaide, pp 33–47
- Thompson JFH, Sillitoe RH, Baker T, Lang JR, Mortensen JK (1999) Intrusion-related gold deposits associated with tungsten-tin provinces. *Mineral Deposita* 34:323–334
- Tropper P, Manning CE, Harlov DE (2011) Solubility of CePO_4 monazite and YPO_4 xenotime in H_2O and $\text{H}_2\text{O-NaCl}$ at 800 °C and 1 GPa: implications for REE and Y transport during high-grade metamorphism. *Chem Geol* 282:58–66
- Wang X, Xie X, Cheng Z, Liu D (1999) Delineation of regional geochemical anomalies penetrating through thick cover in concealed terrains—a case history from the Olympic Dam deposit, Australia. *J Geochem Explor* 66:85–97
- Williams PJ, Barton MD, Johnson DA, Fontbote L, de Haller A, Mark G, Oliver NHS, Marschik R (2005) Iron oxide copper-gold deposits: geology, space-time distribution, and possible modes of origin. *Econ Geol* 100:371–405

Indirect Associations Between Lamprophyres and Gold-Copper Deposits

8

8.1 Introduction

Lamprophyres (cf. Rock 1991) are recorded from many different tectonic settings worldwide, including the Eastern Alps, Austria (e.g. Müller et al. 1992a), Yilgarn Craton, Western Australia (e.g. Taylor et al. 1994), Karinya Syncline, South Australia (Müller et al. 1993), Bahia province (Rios et al. 2007) and São Francisco Craton, Brazil (Plà Cid et al. 2012), Superior Province, Canada (e.g. Wyman 1990), Sulu Orogen, E China (Guo et al. 2004), Yunnan Province, SW China (e.g. Lu et al. 2015b), NW Iran (Aghazadeh et al. 2015), NW Mexico (Orozco-Garza et al. 2013), Central Oman (Worthing and Nasir 2008), and Turkey (Asan and Ertürk 2013; Karsli et al. 2014).

Examples of associations between gold mineralization and high-K rocks in postcollisional arc settings include the spatial and temporal associations between Archaean shoshonitic lamprophyres and orogenic lode-gold deposits in the Superior Province, Canada (Wyman and Kerrich 1989a), including associations with very large gold deposits at Hollinger-McIntyre and Kerr Addison-Chesterville (Burrows and Spooner 1989; Spooner 1993), and in the Leonora-

Laverton and New Celebration-Kambalda regions of the eastern Yilgarn Block, Western Australia (Perring et al. 1989; Rock et al. 1989; Barley and Groves 1990; Taylor et al. 1994). These associations are discussed in Sects. 8.4 and 8.5, respectively. More recently, the association between lamprophyres and orogenic gold deposits has also been documented in the Yunnan Province, China (e.g. Wang et al. 2001; Chen et al. 2014; Lu et al. 2013b, 2015). Additionally, Štemprok et al. (2014) note their association with hydrothermal Sn–W mineralization in the Erzgebirge, East Germany. Lamprophyre dykes are also recorded at the giant Bingham, USA (Maughan et al. 2002), El Teniente, Chile (Stern et al. 2011), porphyry copper-gold, and the Yao'an, China (Lu et al. 2013a, b), porphyry gold deposits, respectively.

There are also spatial associations between lamprophyres and gold deposits in Proterozoic terrains, including those in the vicinity of the Goodall and Tom's Gully mines in the Pine Creek Geosyncline of the Northern Territory, Australia, as described in Sects. 8.2 and 8.3, respectively. In this chapter, it is shown that although there is a strong spatial correlation between lamprophyres and gold deposits, this is an indirect rather than a genetic relationship.

8.2 Shoshonitic Lamprophyres with Elevated Gold Concentrations from the Goodall Gold Deposit, Northern Territory, Australia (Proterozoic)

8.2.1 Introduction

This section describes and discusses lamprophyre dykes from the Goodall gold deposit in the Pine Creek Inlier, Northern Territory, Australia, because of their spatial association with gold mineralization. The Goodall deposit is described in some detail here because much of the data was collected specifically for this study (cf. Müller 1993), but have not been published elsewhere. Goodall mine has been operated by Western Mining Corporation since 1988. Bulk reserves were about 1 Mio oz of gold (D. Quick, pers. comm. 1992).

8.2.2 Regional Geology

The Pine Creek Geosyncline, which forms the major mineral province of the Northern Territory, consists of an Early Proterozoic (ca. 1900 Ma) metavolcanosedimentary sequence covering about 66,000 km² between Darwin and Katherine (Needham et al. 1988; Needham and De Ross 1990). Three main geological units of the Pine Creek Geosyncline can be distinguished (Needham and De Ross 1990):

- Early Proterozoic sedimentary rocks deposited in a shallow intra-cratonic geosyncline.
- Late Early Proterozoic rift-related felsic volcanic rocks.
- Subhorizontal platform sandstones of Middle Proterozoic age.

The Early Proterozoic sedimentary rocks consist of shales, siltstones, sandstones, conglomerates, and carbonates which were metamorphosed during the Top End Orogeny (ca. 1870–1690 Ma; Stuart-Smith et al. 1986; page 1988). Geophysical modeling by Tucker et al.

(1980) suggests that the basement is granitic throughout the whole region.

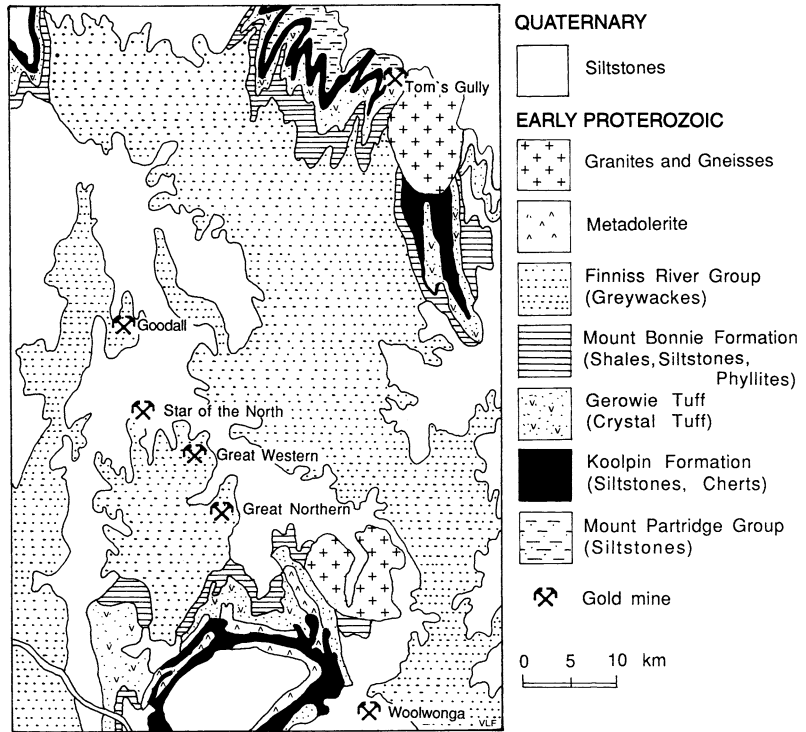
Regional metamorphism in the area decreases from upper amphibolites and granulite facies in the northeast, to lower greenschist facies in the centre, and increases to upper greenschist facies in the Rum Jungle area (Sheppard 1992). Most felsic and mafic intrusions in the area were emplaced during the Top End Orogeny (Needham et al. 1988). The earliest known granitoid intrusions are in the Nimbuwah domain to the east (ca. 1870 Ma) and in the Litchfield domain to the west (1850–1840 Ma; Needham et al. 1988). Lamprophyre intrusions are common in the central part of the Pine Creek Geosyncline (Stuart-Smith et al. 1986; Nicholson and Eupene 1990), and representative samples from the Mount Bundey area near Tom's Gully (Fig. 8.1) were dated via a Pb–Pb isochron at ca. 1831 ± 6 Ma (Sheppard and Taylor 1992).

Most economic deposits are restricted to the central part of the Pine Creek Geosyncline (Sheppard 1992). The area is notable as one of the world's largest and richest uranium provinces, as well as being a significant gold province within Australia (Needham and De Ross 1990). Despite the episodic nature of gold mineralization through Earth history, with production largely dominated by late Archean and Mesozoic to Recent deposits, and only few discovered Proterozoic deposits (Barley and Groves 1992), there are several large gold producers in the Pine Creek Geosyncline (Sheppard 1992). Three styles of gold mineralization can be distinguished:

- Gold associated with uranium ores.
- Stratiform gold ores.
- Epithermal quartz-vein stockwork gold mineralization which is commonly accompanied by lamprophyre dykes.

The last-mentioned forms the most economically important style (e.g. Goodall and Woolwonga mines; Nicholson and Eupene 1990; Smolonogov and Marshall 1993). The heat source, and possibly the fluid and metal source,

Fig. 8.1 Geological overview of the Pine Creek Geosyncline, Northern Territory, Australia, showing the Goodall and Tom's Gully gold deposits. The Mount Bonnie Formation, Gerowie Tuff, and Koolpin Formation comprise the South Alligator Group. Modified after Stuart-Smith et al. (1986)



for much of the vein-type deposits were probably the Middle Proterozoic granites, spanning the period 1870–1765 Ma (Needham and Roarty 1980; Wall 1990; Sheppard 1992).

8.2.3 Nature of Orogenic Gold Mineralization

The Goodall gold deposit is hosted by folded Early Proterozoic greywackes, siltstones, and shales of the Finnis River Group (Fig. 8.1) in the central part of the Pine Creek Geosyncline. Low-grade metamorphosed and folded sedimentary rocks are discordantly cut by lamprophyre dykes striking north-northwest. The sediment-hosted ore shoots also strike north-northwest. The thickness of dykes varies from 10 to 50 cm, and they are exposed in both the open pit and several diamond-drill holes. The lamprophyres appear to be broadly parallel to fold axial planes, and they either predate gold mineralization or have been intruded synchronously with it. All dykes are affected by hydrothermal alteration, which has produced secondary sericitization, and several

dykes in the open pit are mineralized. Most dyke rocks analyzed in this study were sampled from exploration drill holes, with one sample collected in the open pit.

Sulphide mineralization at Goodall occurs mainly as epigenetic quartz stockwork veining in bleached sericitized siltstones, and rarely as disseminated assemblages, and it consists mainly of arsenopyrite, pyrite, and chalcopyrite. Native gold appears to be entirely vein-related, occurring as visible gold accompanied by arsenopyrite.

8.2.4 Mineralogy of the Lamprophyres

Most Goodall lamprophyres are characterized by cognate mica phenocrysts in a groundmass of feldspar and quartz. One sample contains amphibole phenocrysts which are completely altered to chlorite. Only their typical shapes allow them to be classified as former amphiboles. Two generations of mica phenocrysts with different sizes can be distinguished: a phenocryst phase with large phenocrysts (up to 4 mm) and a

Table 8.1 Microprobe (WDS) analyses of mica phenocrysts from lamprophyres at Goodall gold deposit, Northern Territory, Australia

Province/deposit	Goodall	Goodall
Location	Northern Territory, Australia	Northern Territory, Australia
Sample no.	119115	119115
Reference	Müller (1993)	Müller (1993)
SiO ₂	40.91	44.63
TiO ₂	3.12	4.44
Al ₂ O ₃	27.68	29.74
FeO (tot)	9.93	3.82
Cr ₂ O ₃	0.02	0.02
MnO	0.04	0.04
MgO	6.55	3.33
NiO	0.06	0.05
BaO	0.29	0.31
CaO	0.03	0.03
SrO	0.12	0.10
K ₂ O	6.78	8.82
Na ₂ O	0.10	0.11
Cl	0.02	0.02
F	0.35	0.47
Total	96.00	96.24
mg#	60	67
Ox. form.	22	22
<i>Atoms</i>		
Si	5.861	6.037
Ti	0.323	0.451
Al	4.673	4.739
Fe	1.189	0.431
Cr	0.002	–
Mn	0.001	0.003
Mg	1.398	0.671
Ni	0.001	0.005
Ba	0.016	0.016
Ca	–	0.005
Sr	–	0.006
K	1.239	1.521
Na	0.028	0.030
Cl	–	–
F	–	–
Total	14.731	13.915

Ox. form. = oxygen formula. Sample numbers refer to specimens held in the Museum of the Department of Geology and Geophysics, The University of Western Australia. Data from Müller (1993)

groundmass phase with small, elongated mica flakes (~1 mm). The rocks have been hydrothermally altered after or during dyke emplacement, with chloritization of the mica and amphibole phenocrysts (Table 8.1), and sericitization of groundmass feldspars.

8.2.5 Geochemistry of the Lamprophyres

The whole-rock major- and trace-element geochemistry of the lamprophyres from Goodall gold mine is shown in Table 8.2. The investigated lamprophyres have andesitic compositions (51.4–63.1 wt% SiO₂) with low TiO₂ (<0.87 wt%), high but variable Al₂O₃ (14.13–18.46 wt%), and high K₂O (>2.3 wt%) contents. The K enrichment is probably due to secondary sericitization. The lamprophyres are characterized by extremely low Na₂O (<0.25 wt%) and very low CaO (<0.89 wt%) contents, which were probably caused by secondary alteration processes. The use of the K₂O versus SiO₂ biaxial plot of Pecerillo and Taylor (1976), in order to determine the shoshonitic geochemistry of the samples, is flawed due to the mobilization of alkali elements during hydrothermal alteration. However, all samples plot in the shoshonite fields of the Ce/Yb versus Ta/Yb and the Th/Yb versus Ta/Yb biaxial plots (Fig. 8.2). Since these elements are considered to be essentially immobile during secondary alteration processes (Pearce and Cann 1973; Pearce 1982), the plots allow the classification of the dykes as shoshonitic lamprophyres. For comparison, the lamprophyres from the Mount Bunday area, located about 40 km northeast of Goodall gold mine (Sheppard and Taylor 1992), have also been plotted on Fig. 8.2. They form a different dyke swarm with a distinctive geochemistry (see Sect. 8.3).

The lamprophyres range from fractionated to relatively primitive (mg# of 42–67), with high V (~160 ppm) and moderate Ni (~40 ppm) concentrations. The low Ba and Sr concentrations and the Ba/Nb ratios of <71, which are relatively low in comparison with mica-phyric shoshonitic magmas from other localities (e.g. Chap. 3), are

not primary features and are likely to have been caused by mobilization of these elements during secondary alteration processes. The original rocks were probably characterized by very high enrichments of LILE, a common feature of unaltered shoshonitic rocks (Morrison 1980; Müller et al. 1992b; Campbell et al. 2014).

The investigated lamprophyre dykes have a different geochemistry from those of the Mount Bunday area (Sheppard and Taylor 1992). In comparison, the Goodall lamprophyres are characterized by higher SiO₂ (>51 wt%) and Al₂O₃ (>14 wt%), and much lower P₂O₅ contents (<0.6 wt%) than those from the Mount Bunday suite (generally <50 wt%, <13 wt%, >0.7 wt%, respectively). The Goodall lamprophyres are also strongly affected by secondary alteration, as reflected in their extremely low Na₂O and CaO contents mentioned above. The suites differ in their trace-element geochemistry, with much lower LILE (<302 ppm Rb, <71 ppm Sr), lower LREE (<49 ppm La, <86 ppm Ce), and lower HFSE (<0.87 wt% TiO₂, <258 ppm Zr, <14 ppm Nb, <5.5 ppm Hf) concentrations for the Goodall lamprophyres. The Mount Bunday dykes, as described by Sheppard and Taylor (1992), contain very high LILE (up to 355 ppm Rb, up to 3635 ppm Sr), very high LREE (up to 340 ppm La, up to 750 ppm Ce), and higher HFSE (up to 2.1 wt% TiO₂, up to 932 ppm Zr, up to 75 ppm Nb, up to 21 ppm Hf) contents which are typical for potassic igneous rocks, such as lamprophyres, generated in a within-plate tectonic setting (Müller et al. 1993; Worthing and Nasir 2008). However, the use of the geochemical discrimination diagrams (see Chap. 3) in order to determine the tectonic setting of the Goodall lamprophyres is not appropriate because of the strong hydrothermal alteration.

8.2.6 Direct or Indirect Link Between Potassic Lamprophyres and Mineralization

A possible genetic link between shoshonitic lamprophyres and orogenic gold mineralization, as discussed above, has been proposed by Rock

Table 8.2 Major- and trace-element analyses of lamprophyres from Goodall gold deposit, Northern Territory, Australia

Province/deposit	Goodall						
Location	Northern Territory, Australia						
Sample no.	119111	119112	119113	119114	119115	119116	119117
Reference	Müller (1993)						
SiO ₂	51.40	54.80	63.10	54.10	56.00	60.10	54.80
TiO ₂	0.80	0.85	0.63	0.85	0.87	0.74	0.81
Al ₂ O ₃	15.60	14.13	18.46	16.66	17.06	16.25	16.02
Fe ₂ O ₃	16.07	10.47	5.18	13.93	9.58	9.20	14.28
FeO	n.a.						
MnO	0.31	0.06	0.02	0.04	0.05	0.02	0.04
MgO	5.01	9.29	2.95	5.72	7.18	4.96	5.72
CaO	0.37	0.89	0.17	0.26	0.24	0.03	0.27
Na ₂ O	0.16	0.25	0.15	0.12	0.16	0.16	0.13
K ₂ O	3.57	2.31	5.27	3.68	3.10	3.80	3.13
P ₂ O ₅	0.21	0.67	0.23	0.22	0.15	0.22	0.20
LOI	6.45	6.39	4.02	4.46	5.72	4.62	4.70
Total	99.96	100.14	100.13	100.02	100.11	100.10	100.07
mg#	42	67	57	49	63	55	48
V	164	227	107	185	166	206	167
Ni	38	68	28	12	59	81	42
Cu	171	67	20	265	20	20	20
Zn	109	92	60	62	105	78	48
As	n.a.	n.a.	32	250	34	75	61
Rb	164	89	302	139	140	209	147
Sr	16	71	39	9	11	11	11
Y	18	26	30	22	20	20	24
Zr	148	258	206	154	166	139	149
Nb	12	10	14	9	5	6	6
Sb	n.a.	n.a.	2.4	4.4	3.9	11	2.1
Ba	860	514	616	274	142	353	249
La	32.9	43.6	49.8	37	34.3	27.9	35
Ce	63	80	86	69	64	49	66
Yb	1.6	1.6	2.8	1.8	1.9	1.5	1.9
Hf	3.2	5.5	5.2	3.4	3.6	3	3.5
Ta	0.7	0.6	0.8	0.5	0.4	0.4	0.4
W	n.a.	n.a.	4.5	14	2	3	4.5
Th	15	17	18	14	13	8	14

(continued)

Table 8.2 (continued)

Province/deposit	Goodall						
Location	Northern Territory, Australia						
Sample no.	119111	119112	119113	119114	119115	119116	119117
Reference	Müller (1993)						
Pd	n.a.	n.a.	<1	<1	<1	<1	<1
Pt	n.a.	n.a.	<5	<5	<5	<5	<5
Au	59	5	28	54	5	5	5

Major elements are in wt%, trace elements are in ppm, and precious metals are in ppb. Fe₂O₃ (tot) = total iron calculated as ferric oxide. Precious-metal detection limits are: Au, Pt = 5 ppb, Pd = 1 ppb. Sample numbers refer to specimens held in the Museum of the Department of Geology and Geophysics, The University of Western Australia. Data from Müller (1993)

and Groves (1988a, b). The intrusion of lamprophyric magmas into the crust is capable of promoting hydrothermal circulation and initiating partial melting, thereby generating felsic high-K igneous rocks which are commonly associated with gold deposits (Sheppard 1992; Betsi and Lentz 2011; Lu et al. 2013b; Heidari et al. 2015). During crystallization, lamprophyres can generate S- and CO₂-rich fluids, analogous to those thought responsible for the genesis of orogenic gold deposits (e.g. Rock 1991).

Some lamprophyres from the Goodall deposit indeed show enrichments in Au of up to 59 ppb (Table 8.2). The elevated Au values are, however, unlike those of the potassic rocks from the Kariya Syncline (Chap. 5) in that they are *decoupled* from Cu and Pd peaks in primitive mantle-normalized distribution plots (Fig. 8.3; after Brüggemann et al. 1987), suggesting that the anomalous Au contents are secondary features (Wyman and Kerrich 1989a). The high Au enrichment compared to other chalcophile elements such as Cu and Pd is reflected in the high Au/Pd (up to 54) and Au/Cu ratios (up to 1.4), compared to primitive mantle ratios of 0.25 and 0.036, respectively (Brüggemann et al. 1987). Hydrothermal mineralizing fluids which overprinted the dykes *after* emplacement are thought to be responsible for the elevated gold concentrations in the dykes. This interpretation is consistent with the high

correlation between Au and its pathfinder elements (e.g. As, W), as shown in Table 8.3. In comparison to the Truro lamprophyres from South Australia (see Sect. 5.3), the lamprophyres at Goodall are situated in a major gold-mining area and were intensively altered (sericitization) by hydrothermal fluids after emplacement.

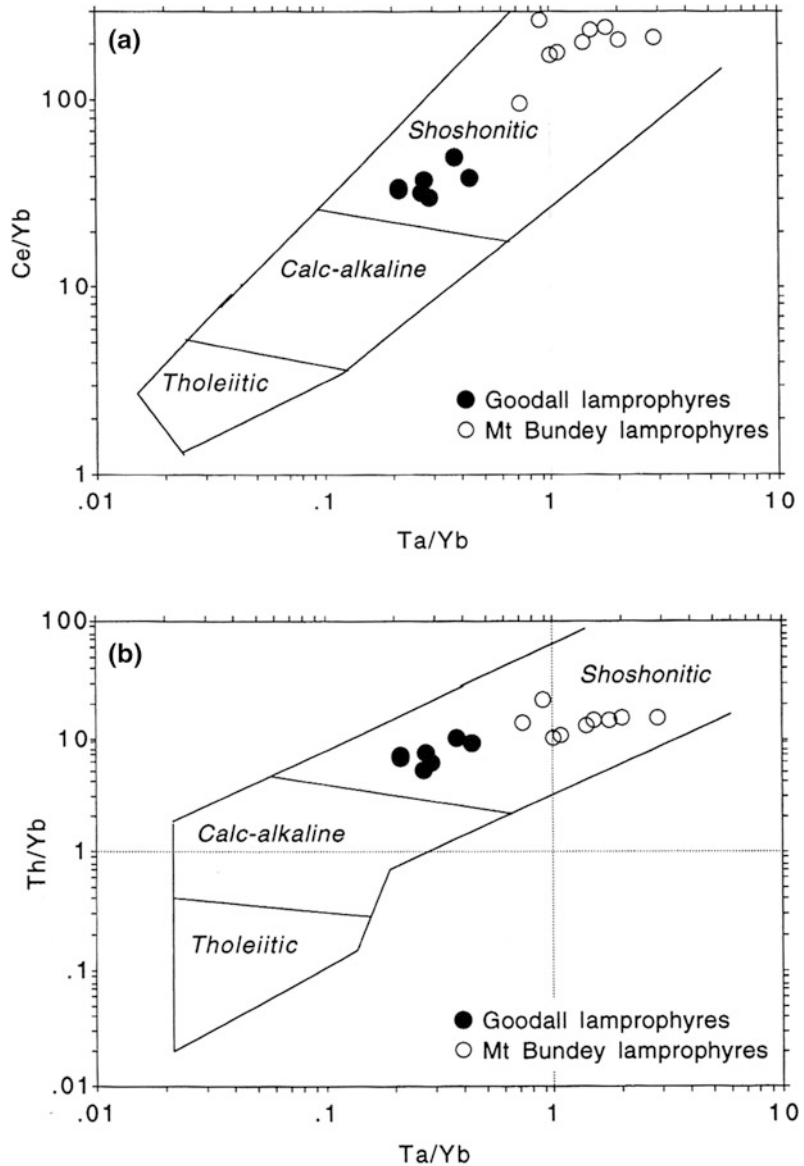
8.3 Shoshonitic Lamprophyres from the Tom's Gully Gold Deposit, Northern Territory, Australia (Proterozoic)

8.3.1 Introduction

No direct genetic associations between potassic igneous rocks from within-plate tectonic settings and economic epithermal gold or porphyry copper-gold mineralization have been reported to date. However, indirect associations, where both gold mineralization and potassic lamprophyre dykes were emplaced along major fault zones, are apparent in some areas, as discussed in Sect. 8.2 for the Goodall district.

A further example of a probable within-plate association is the Tom's Gully gold deposit in the Mount Bunday area, Northern Territory, Australia.

Fig. 8.2 Application of geochemical discrimination diagrams based on immobile trace elements (after Pearce 1982) in order to illustrate the shoshonitic character of the highly altered lamprophyres from Goodall, Northern Territory. **a** (Ce/Yb) versus (Ta/Yb) plot. **b** (Th/Yb) versus (Ta/Yb) plot. Data for the Goodall lamprophyres are from Müller (1993) and those for lamprophyres from the Mount Bunday area, about 40 km northeast, are from Sheppard and Taylor (1992)



8.3.2 Regional Geology

The Mount Bunday area is located in the northern part of the Pine Creek Geosyncline (Fig. 8.1). As described in Sect. 8.2, the Pine Creek Geosyncline consists of Early Proterozoic metasedimentary and minor metavolcanic rocks. Rocks of the Pine Creek Geosyncline unconformably overlie several Archaean granitic and gneissic complexes thought to form a continuous basement (Needham et al. 1988). The main period of

deformation and metamorphism is dated at 1885–1860 Ma (Page 1988).

The Mount Bunday pluton, covering about 80 km², consists of post-tectonic syenitic and granitic rocks which intrude shales and siltstones of the Early Proterozoic South Alligator Group (Fig. 8.1). The lamprophyre dykes are restricted to within 10 km of the Mount Bunday pluton, which is probably coeval with mineralization (Sheppard 1992). The dykes intrude the syenites

Fig. 8.3 Abundances of chalcophile elements in lamprophyres from the Goodall gold deposit, Northern Territory, relative to the primitive mantle. Normalizing factors after Brüggemann et al. (1987). Data from Müller (1993)

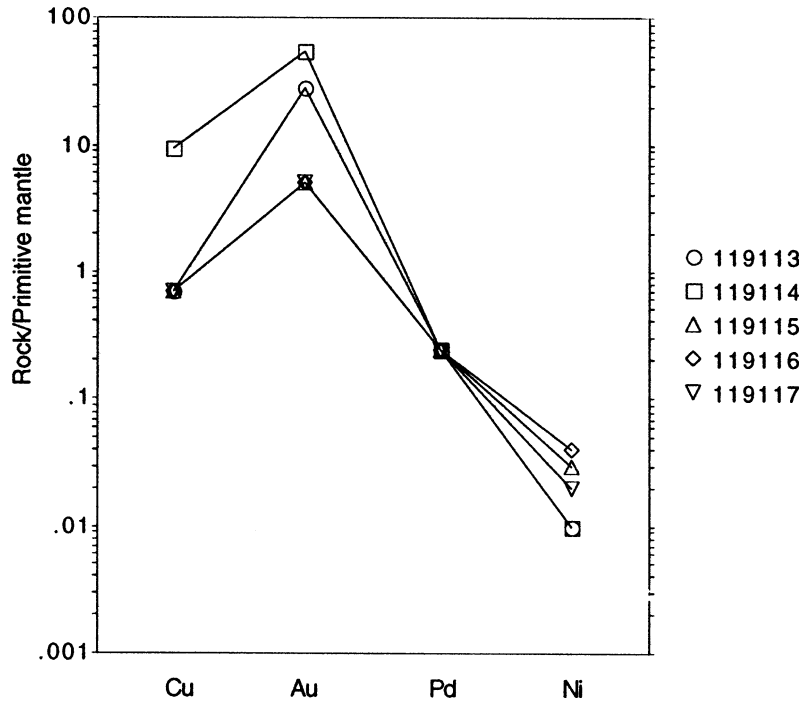


Table 8.3 Correlation matrix for precious metals (Au, Pd, Pt), Cu, and gold pathfinder elements (As, Sb, W) of lamprophyres from the Goodall gold deposit, Australia

	Cu	Au	Pt	Pd	As	Sb	W
Cu	1						
Au	0.889	1					
Pt	–	–	1				
Pd	–	–	–	1			
As	0.980	0.817	–	–	1		
Sb	–0.056	–0.228	–	–	0.084	1	
W	0.973	0.927	–	–	0.956	–0.151	1

Data from Müller (1993)

and I-type granites of the pluton, and postdate regional deformation and metamorphism (Sheppard 1992, 1995). The lamprophyres are dated via conventional U-Pb in zircon methods at 1831 ± 6 Ma (Sheppard 1992, 1995). The Mount Bunday pluton is dated at 1825 Ma (Rasmussen et al. 2006).

8.3.3 Nature of Orogenic Gold Mineralization

The Tom's Gully gold deposit is situated in the thermal aureole of the Mount Bunday pluton.

There are two sulphidic ore-shoots in a single, fault-controlled, shallowly-dipping quartz reef (Sheppard 1992). On average, the reef is 1.0–1.5 m thick, but it pinches and swells between 0 and 2.4 m. Ore was probably deposited at Tom's Gully during wrench shearing associated with emplacement of the granitic rocks (Sheppard 1992). The sulphidic ore-shoots consist mainly of pyrite-arsenopyrite \pm loellingite \pm gold (Sheppard 1992), which are hosted by graphitic siltstones and shales of the Wildman Siltstone Unit (Sheppard 1992). Loellingite is commonly replaced by arsenopyrite. Visible gold commonly

occurs as blebs of electrum within arsenopyrite. Minor wallrock alteration of the metasedimentary host rocks is expressed by the oxidation of graphitic pelites and formation of secondary sericite and potassic feldspar (Sheppard 1992).

8.3.4 Petrology and Geochemistry of the Lamprophyres

The lamprophyre dykes are 0.5–3.0 m thick and have chilled margins. Two petrographic types can be distinguished (Sheppard and Taylor 1992): one olivine-phlogopite-diopside-phyric and the other olivine-amphibole-diopside-phyric. Recent studies by Bucholz et al. (2014) indicate that phlogopite crystallization strongly depends on the degree of K enrichment in a melt, while amphibole crystallization requires a high H₂O content. However, both phases can coexist as they are not in direct “competition” as crystallizing phases (Bucholz et al. 2014). Both petrographic types contain apatite microphenocrysts and their groundmass is dominated by orthoclase.

Geochemically, the lamprophyres are characterized by very high F (up to 4900 ppm), very high P₂O₅ (~2.0 wt%), and K₂O (up to 7.4 wt%) contents (Table 8.4), and resulting high K₂O/Na₂O ratios (>2; Sheppard and Taylor 1992). The Mount Bunday lamprophyres have a primitive geochemistry (Sheppard and Taylor 1992) with relatively high mg# (63–66) and high mantle-compatible element concentrations (e.g. >107 ppm V, >205 ppm Cr, >157 ppm Ni). Their high LILE (e.g. up to 3635 ppm Sr, up to 5101 ppm Ba), high LREE (e.g. ~220 ppm La, ~500 ppm Ce) and very high HFSE (~2.0 wt% TiO₂, ~750 ppm Zr, ~60 ppm Nb, ~17 ppm Hf) contents are consistent with potassic igneous rocks emplaced in a within-plate tectonic setting (cf. Figs. 6.3 and 6.4).

The coincidence of lamprophyres, syenites, and granites is common in many localities worldwide (Rock 1991; Worthing and Nasir 2008; Karsli et al. 2014; Aghazadeh et al. 2015). Fractional crystallization of lamprophyric melts has been demonstrated to produce syenitic

magmas (McDonald et al. 1986; Leat et al. 1988), and granitic rocks associated with lamprophyres are interpreted to be generated by crustal assimilation triggered by the interaction of mantle-derived hot and volatile-rich lamprophyric melts with the lower crust (McDonald et al. 1986; Lu et al. 2013a). It is possible that the conduits for these magmas coincide with those for deeply sourced auriferous fluids.

8.3.5 Indirect Link Between Lamprophyres and Gold Mineralization

The lamprophyres, syenite and granite at Mount Bunday define a Pb-Pb isochron age of 1831 ± 6 Ma, suggesting that the three rock types form a co-magmatic suite (Sheppard and Taylor 1992) in which the syenite represents the fractionated product of lamprophyric magmatism. Although the gold mineralization at Tom’s Gully is bracketed in time by the lamprophyre dykes, the lamprophyres do not have intrinsically high Au contents and no direct genetic association is evident (Sheppard 1992). More recent work (Rasmussen et al. 2006) dates the gold mineralization at Tom’s Gully at 1780 ± 10 Ma and thus postdating the Mount Bunday pluton by about 45 m.y. Hence, the shoshonite-gold association at Tom’s Gully is interpreted to be indirect, representing only similar structural controls on both dyke intrusion and mineralization, as at Goodall in the same terrane.

8.4 Shoshonitic Lamprophyres from the Eastern Goldfields, Yilgarn Block, Western Australia (Archaean)

8.4.1 Introduction

In Australia, the ca. 2700 Ma granitoid-greenstone terrains of the Yilgarn Block are the most intensely mineralized with world-class gold deposits

Table 8.4 Major- and trace-element analyses of lamprophyres from the Mount Bunday district, Northern Territory, Australia

Province/deposit	Mount Bunday	Mount Bunday
Location	Northern Territory, Australia	Northern Territory, Australia
Rock type	Lamprophyre	Lamprophyre
Tectonic setting	Within-plate	Within-plate
Reference	Sheppard and Taylor (1992)	Sheppard and Taylor (1992)
SiO ₂	46.73	47.22
TiO ₂	2.13	1.92
Al ₂ O ₃	11.88	11.30
Fe ₂ O ₃	11.02	10.30
FeO	n.a.	n.a.
MnO	0.14	0.13
MgO	8.12	8.65
CaO	7.78	7.35
Na ₂ O	2.34	2.18
K ₂ O	5.82	6.49
P ₂ O ₅	2.08	2.18
LOI	2.07	2.01
Total	100.11	99.73
mg#	63	66
V	154	144
Cr	205	262
Ni	200	237
Rb	162	181
Sr	3136	3635
Y	40	37
Zr	722	866
Nb	59	70
Ba	5023	5101
La	220	228
Ce	483	514
Hf	16	19

Major elements are in wt%, and trace elements are in ppm. Fe₂O₃ (tot) = total iron calculated as ferric oxide. Data from Sheppard and Taylor (1992)

(Groves et al. 1994). Widespread shoshonitic lamprophyre dyke-swarms also represent a significant contribution to magmatism in the Yilgarn Block at ca. 2680–2660 Ma (Rock et al. 1988b; Vielreicher et al. 2015). Along with contemporaneous swarms from the Superior Province, Canada, and the Limpopo Belt, Zimbabwe, they may represent a global Archaean mantle event (Rock et al. 1988b). Many of these lamprophyre dykes

have been misclassified as “diorites”, “diabases” and “trachyandesites” in the past (Rock 1991).

8.4.2 Regional Geology

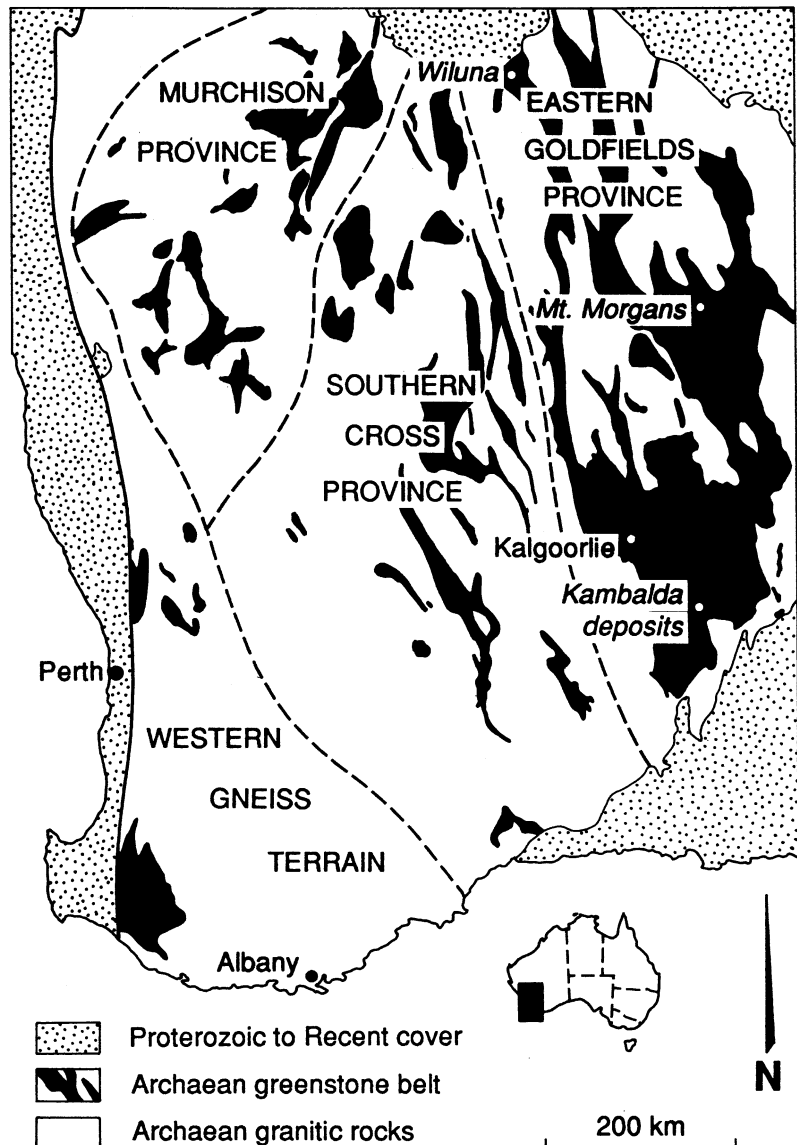
The Yilgarn Block comprises high-grade gneiss and supracrustal rocks in the west and granitoid-greenstone terrains in its central and eastern segments (Groves et al. 1994). The craton has

traditionally been subdivided into four main subprovinces: the Western Gneiss Terrain, and the Murchison, Southern Cross, and Eastern Goldfields Provinces (Gee et al. 1981; Fig. 8.4). Myers (1993) redefines the craton as a number of geologically distinct superterranes. However, the province terminology is well recognized in the literature so it is used here.

The Western Gneiss Terrain contains the oldest Archaean crust recognized to date in Australia (Groves et al. 1994). The granitoid-greenstone

terrains of the Murchison, Southern Cross, and Eastern Goldfields Provinces have a common history of granitoid intrusion, deformation, and metamorphism from ca. 2680–2630 Ma, although the trend of major fault and shear zones varies from one province to another (Groves et al. 1994). The Murchison Province, for example, is dominated by northeast-trending shear zones and greenstone belts, whereas most shear zones and greenstone belts trend north-northwest to northwest in the Eastern Goldfields Province.

Fig. 8.4 Geological overview of the Yilgarn Craton, Western Australia, showing the Eastern Goldfields Province and the Kambalda, Mount Morgans and Wiluna gold deposits, which are spatially associated with shoshonitic lamprophyres. After Gee et al. (1981)



Although there are only preliminary data, there appear to be two major supracrustal sequences in the greenstone belts. Older sequences, which are dominated by tholeiitic to high-magnesium basalts, contain abundant banded iron-formations (BIF). These sequences are dominant in the Murchison and Southern Cross Provinces, with only local occurrences in the Eastern Goldfields Province. By contrast, younger supracrustal sequences, dated at ca. 2700 Ma, dominate the Norseman-Wiluna Belt in the Eastern Goldfields Province, but are more restricted in the Murchison and Southern Cross Provinces (Groves et al. 1994). These sequences contain virtually no BIF, but there are thick sequences of komatiites and discrete felsic volcanic centres (e.g. Hallberg 1985). The volcanic rocks are commonly overlain by clastic sedimentary rocks in restricted structural basins. The ca. 2700 Ma volcanic sequences resemble those in modern subduction arcs (e.g. Barley et al. 1989). However, the volcanic rocks were apparently erupted through older continental crust because they commonly contain xenocrystic zircons older than 3000 Ma (Groves et al. 1994).

8.4.3 Nature of Orogenic Gold Mineralization

The Western Gneiss Terrain, like most high-grade gneiss terrains worldwide, contains only minor mineralization. By contrast, the granitoid-greenstone terrains are exceptionally well mineralized with widespread lode-gold and komatiite-hosted nickel-copper, and more restricted copper-zinc VMS deposits (Groves 1982; Groves et al. 1994).

With an output of about 68 Mio oz of gold to 1987, the Yilgarn Block has produced almost half of Australia's gold production from lode deposits of about 146 Mio oz to 1987 (Groves et al. 1994, 1998). The Norseman-Wiluna Belt is the most highly mineralized, followed by the Murchison Province, the Southern Cross Province, and the remainder of the Eastern Goldfields Province. About half of the total gold production has come from the Golden Mile at Kalgoorlie.

Although the physical appearance of the lode-gold deposits varies greatly, due to differences in structural style, host rock, and mineralogy of alteration assemblages, the deposits appear to represent a coherent genetic group (Groves 1993). Basically, they comprise structurally controlled gold \pm silver \pm arsenic \pm tellurium \pm antimony \pm tungsten deposits, associated with metasomatic zones representing K \pm CO₂ \pm Na \pm Ca addition, in a variety of ultramafics, mafic and felsic igneous rocks, and Fe-rich sedimentary rocks in greenstone belts of sub-greenschist to lower granulite-facies grade (normally greenschist-amphibolite; Groves 1993; Solomon and Groves 1994).

8.4.4 Lamprophyres and Their Association with Mineralization

Shoshonitic lamprophyres have been reported from the Eastern Goldfields (e.g. Kambalda and Leonora-Laverton areas) and Murchison Provinces (Rock et al. 1988b). Most of these lamprophyres (see Fig. 8.4) occur in the highly mineralized greenstone belts of the Eastern Goldfields Province (Hallberg 1985), in particular in association with the orogenic lode gold deposits at Wiluna (Hagemann et al. 1992; Kent and Hagemann 1996), Mount Morgan (Vielreicher et al. 1994) and Kambalda (Perring 1988). Mutually cross-cutting relationships between these dykes and mineralized quartz veins at several mines suggest that shoshonitic magmatism overlapped with, although it was commonly earlier than, the period of gold mineralization (Hallberg 1985; Barley and Groves 1990; Taylor et al. 1994). Both lamprophyres and gold mineralization appear to be spatially and genetically linked to subhorizontal oblique compression, and occur along major shear zones which are interpreted to have extended to the upper mantle (Perring et al. 1989; Wyman and Kerrich 1988, 1989a), thus providing favourable conduits for both lamprophyric magmas and deeply sourced mineralizing fluids.

8.4.5 Petrology and Geochemistry of the Lamprophyres

The shoshonitic lamprophyres comprise amphibole-phyric spessartites and mica-phyric kersantites (Perring 1988; Rock et al. 1988b). Generally, in lamprophyres the feldspars are restricted to the groundmass (Rock 1991). Spessartites normally consist of euhedral, zoned hornblende phenocrysts set in a groundmass of plagioclase with accessory apatite and titanite. Kersantites are characterized by battlemented phlogopite phenocrysts in a groundmass containing plagioclase and carbonate with accessory pyrite, apatite, and zircon. Felsic ocelli are common in the dykes and are composed of arborescent plagioclase (larger crystals show chessboard albite twinning) with minor carbonate (Perring 1988). Some kersantites also contain quartz xenocrysts (Perring 1988), which is indicative of volatile-driven rapid uprising of the lamprophyric magma (cf. Rock 1991).

The shoshonitic lamprophyres of the Eastern Goldfields Province are altered to various degrees. Fresh samples are characterized geochemically by relatively primitive compositions with relatively high, but variable, mg# (up to 67) and high concentrations of mantle-compatible elements (e.g. >100 ppm V, >300 ppm Cr, >100 ppm Ni; Taylor et al. 1994). They normally have high LILE (e.g. up to 740 ppm Sr, up to 1300 ppm Ba), low LREE (e.g. ~40 ppm La, ~75 ppm Ce), and very low HFSE (e.g. <0.7 wt % TiO₂, <160 ppm Zr, <8 ppm Nb, <5 ppm Hf) contents. Representative data of mineralogically fresh samples are presented in Table 8.5. It should be noted that the Au content of most Yilgarn lamprophyres is only elevated in those samples which were collected from the vicinity of orogenic gold deposits (Fig. 8.5). The gold values are decoupled from those of other chalcophile elements in primitive mantle-normalized distribution plots (Fig. 8.5b), suggesting that they are secondary features. This is consistent with the poor correlation between Au and the magmatic elements Cu, Pt, and Pd (Table 8.6). The significance of the gold contents of the rocks in

terms of an indirect or genetic association between lamprophyres and gold mineralization is discussed in Sect. 8.6.

8.5 Shoshonitic Lamprophyres from the Superior Province, Canada (Archean)

8.5.1 Introduction

The Superior Province, exposed over an area of >2 million km², represents the world's largest relatively undisturbed Archean craton (Card and Ciesielski 1986). Parts of it are buried beneath Phanerozoic strata of the Interior Plains and the Michigan, Hudson, and Moose River Basins, and beneath little-deformed Proterozoic cover sequences. The Superior Province is surrounded by Proterozoic orogenic belts: the Grenville Province on the southeast, the Churchill Province on the east, north and west, and the Southern Province on the south. The Superior Province is subdivided into several subprovinces, based on absolute and relative ages of rock units, major fault zones, as well as structural trends and styles (cf. Card and Ciesielski 1986).

8.5.2 Regional Geology

The Superior Province comprises a collage of granitoid-greenstone belts with intervening belts of metasedimentary rocks and tonalitic gneisses which are separated by major structural discontinuities such as shear zones and transcurrent fault systems (Wyman 1990). The greenstone belts show a similar age range to those of the Yilgarn Block described in Sect. 8.4, but there is much less evidence for eruption through continental crust (e.g. Wyman 1990). Alkaline igneous rocks are only a volumetrically minor component of the Archean Superior Province of Canada but, as in Western Australia, share important spatial and temporal distributions with orogenic lode-gold deposits (Wyman and Kerrich 1988). The alkalic magmatism comprises

Table 8.5 Major- and trace-element analyses of lamprophyres from the Eastern Goldfields Province, Yilgarn Craton, Western Australia

Province/deposit	Eastern Goldfields, Yilgarn Craton	Eastern Goldfields, Yilgarn Craton
Location	Western Australia	Western Australia
Rock type	Lamprophyre	Lamprophyre
Tectonic setting	Postcollisional arc	Postcollisional arc
Reference	Taylor et al. (1994)	Taylor et al. (1994)
SiO ₂	60.39	55.99
TiO ₂	0.55	0.69
Al ₂ O ₃	14.56	12.61
Fe ₂ O ₃	5.96	7.52
FeO	n.a.	n.a.
MnO	0.09	0.12
MgO	5.17	8.46
CaO	6.24	5.74
Na ₂ O	3.73	3.82
K ₂ O	1.84	3.10
P ₂ O ₅	0.22	0.36
LOI	1.37	2.47
Total	100.12	100.88
mg#	67	52
V	116	135
Cr	323	684
Ni	101	217
Rb	29	75
Sr	589	738
Y	14	23
Zr	131	154
Nb	5	8
Ba	359	1278
La	38	35
Ce	72	77
Hf	3.1	4.4

Major elements are in wt%, and trace elements are in ppm. Fe₂O₃ (tot) = total iron calculated as ferric oxide. Data from Taylor et al. (1994)

both shoshonitic lamprophyres and K-rich plutonic rocks which are sited along major structures and are late in the greenstone belt development (Wyman and Kerrich 1988; Blichert-Toft et al. 1996).

8.5.3 Nature of Orogenic Gold Mineralization

Superior Province lode-gold deposits systematically occur as late kinematic features, generally

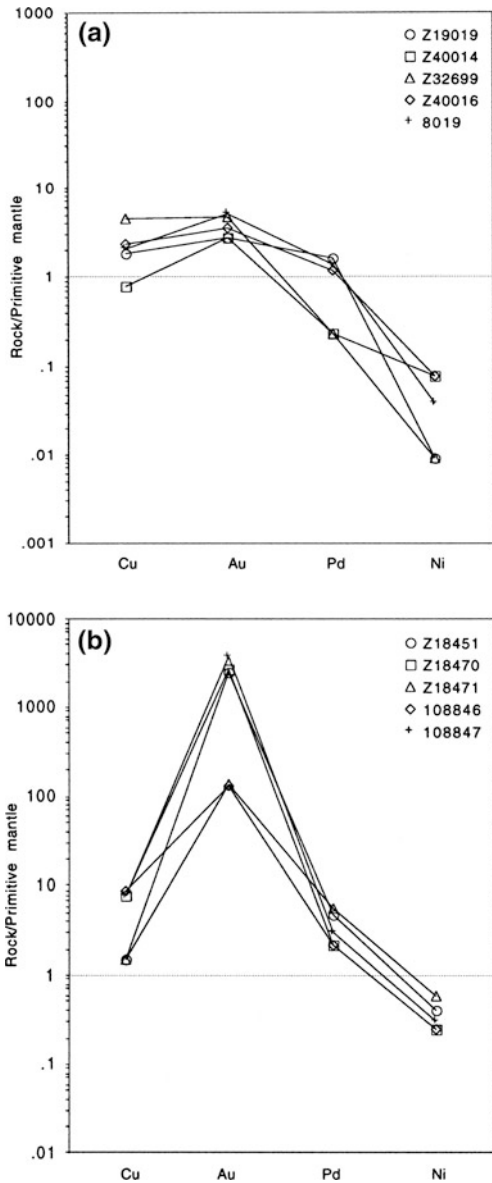


Fig. 8.5 Abundances of chalcophile elements in lamprophyres from the Yilgarn Craton relative to the primitive mantle. **a** Data for lamprophyres distal to gold deposits. **b** Data for lamprophyres from the vicinity of gold deposits. Normalizing factors after Brüggmann et al. (1987). Data from Taylor et al. (1994)

in proximity to crustal-scale structures called “breaks” (Wyman and Kerrich 1988). Similar to the lode-gold deposits in the Yilgarn Block, those in the Superior Province, also comprise mainly structurally controlled gold \pm silver \pm

arsenic \pm tellurium \pm antimony \pm tungsten deposits, which are associated with metasomatic zones representing K \pm CO₂ \pm Na \pm Ca addition. The orogenic lode-gold deposits are associated with a variety of ultramafic, mafic, and felsic igneous rocks and Fe-rich sedimentary rocks in greenstone belts of greenschist- to amphibolites-facies grade. An excellent summary is given by Colvine (1989).

8.5.4 Lamprophyres and Their Association with Mineralization

Shoshonitic lamprophyre dykes are abundant in areas such as Kirkland Lake, where several small syenite plutons are also prominent (Rowins et al. 1993), and in the Hemlo region, which is transected by regional-scale shear zones (Wyman and Kerrich 1988). Both orogenic gold mineralization and lamprophyre emplacement young to the south from Red Lake (ca. 2700 Ma) to the southern Abitibi Belt (ca. 2673 Ma; Wyman and Kerrich 1989a). The transgressive nature of these events is compatible with a series of accretionary events which resulted in generation of the greenstone belts in the Late Archaean (Wyman and Kerrich 1989a), implying that these processes were linked to a postcollisional arc setting.

The shoshonitic lamprophyres are typically restricted to granitoid-greenstone subprovinces and their tectonic boundaries with metasedimentary terranes (Wyman 1990; Blichert-Toft et al. 1996), a geological setting which they share with their Western Australian counterparts (Groves et al. 1994). The Superior Province lamprophyres are dated at ca. 2690–2675 Ma, and include minette, kersantite, and vogesite dykes (Wyman and Kerrich 1989a). The steeply dipping dykes contain phenocrysts of augite, phlogopite and/or hornblende in a primary carbonate-bearing, feldspathic groundmass (Wyman 1990), and their emplacement is interpreted to be spatially and genetically linked to subduction-like underthrusting within a largely transpressive tectonic regime (e.g. Wyman and Kerrich 1989a). The lamprophyre-gold spatial association is restricted to the final period of

Table 8.6 Correlation matrix for precious metals (Au, Pd, Pt), Cu, and gold pathfinder elements (As, Sb, W) of lamprophyres from the Yilgarn Craton, Western Australia

<i>(a) Data for samples distal to gold deposits</i>							
	Cu	Au	Pt	Pd	As	Sb	W
Cu	1						
Au	0.713	1					
Pt	0.312	0.409	1				
Pd	0.258	0.512	-0.091	1			
As	-0.399	0.023	-0.202	-0.434	1		
Sb	0.102	-0.123	-0.674	0.634	-0.525	1	
W	-0.304	-0.245	-0.627	0.682	-0.365	0.877	1
<i>(b) Data for samples proximal to gold deposits</i>							
	Cu	Au	Pt	Pd	As	Sb	W
Cu	1						
Au	0.228	1					
Pt	-0.563	0.082	1				
Pd	-0.342	-0.420	0.631	1			
As	-0.040	-0.067	0.154	-0.424	1		
Sb	0.286	0.631	0.012	0.182	-0.780	1	
W	0.092	0.791	-0.102	-0.173	-0.628	0.878	1

Data from Taylor et al. (1994)

stabilization of the Superior Province (Wyman 1990), being particularly well developed near major fault systems, as exemplified by the Kirkland Lake area (Fig. 8.6) and Abitibi Belt (Jensen 1978; Toogood and Hodgson 1985; Wyman 1990; Rowins et al. 1993). In the Kirkland Lake area, both lamprophyres and orogenic gold mineralization are also spatially associated with high-K syenitic plutons (Fig. 8.6; Mortensen 1993) which are dated at 2680 ± 1 Ma using conventional U-Pb in zircon techniques (Rowins et al. 1993). The syenitic plutons are believed to have been generated by fractional crystallization of a mantle-derived lamprophyric magma (Rowins et al. 1993).

8.5.5 Petrology and Geochemistry of the Lamprophyres

The dykes are all shoshonitic types, including minettes, kersantites, and vogesites. In contrast to the lamprophyres of the Yilgarn Block, spessartites have not been recorded to date in the Superior Province.

Geochemically, the lamprophyres are characterized by primitive compositions, which are comparable to their Western Australian counterparts (see Sect. 8.4.5), with high mg# (>70) and high concentrations of mantle-compatible elements (e.g. >110 ppm V, ~550 ppm Cr, ~150 ppm Ni; Table 8.7). They are highly potassic (up to 5.6 wt% K₂O), and they are characterized by high concentrations of LILE (e.g. up to 200 ppm Rb, up to 750 ppm Sr, up to 1600 ppm Ba), and intermediate LREE (e.g. ~80 ppm La, ~140 ppm Ce), and low HFSE (e.g. ~0.8 wt% TiO₂, ~250 ppm Zr, ~10 ppm Nb, ~5 ppm Hf) concentrations (Table 8.7). Only a few published precious-metal contents of lamprophyres from the Superior Province are available (Wyman and Kerrich 1989a). They were derived from fresh, unaltered samples distal from orogenic gold mineralization (Wyman and Kerrich 1989a) and no significant Au abundances were detected (Fig. 8.7). Table 8.8 shows the very low correlation between Au and the magmatic elements Cu, Pt, and Pd, and the normal pathfinder elements Sb and W although the

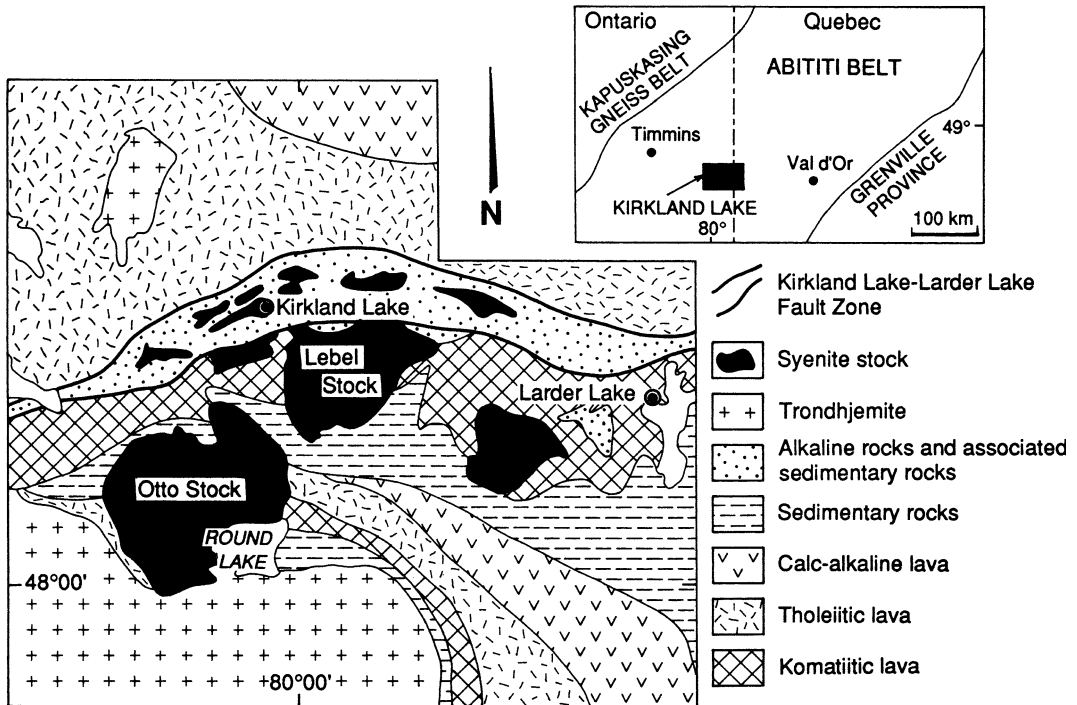


Fig. 8.6 Geological overview of the Kirkland Lake area, Superior Province, Canada. Modified after Rowins et al. (1993)

database is limited. The significance of the Au contents of the rocks is discussed in Sect. 8.6, together with those of counterparts in the Yilgarn Block.

8.6 Indirect Link Between Lamprophyres and Archaean Gold Mineralization

Many of the shoshonitic lamprophyres from the Superior Province, Canada, and the Yilgarn Block, Western Australia, plot in the postcollisional arc field (Fig. 6.15), consistent with their late-tectonic timing with respect to initial volcanism. However, discrimination is equivocal for several samples which plot in the continental arc field on the diagram. This could be explained by the high degree of alteration and extensive metamorphic recrystallization of most of the Archaean lamprophyres, which have been

affected by a complex history of metamorphism, deformation, and hydrothermal alteration (e.g. Taylor et al. 1994), resulting in the mobilization of P and an increase in the Ce/P₂O₅ ratios. The P depletion is also displayed by pronounced negative anomalies in their spidergram patterns (Taylor et al. 1994).

The lamprophyric magmas were probably mantle-derived from between 50 and 120 km depth beneath the continental crust, whereas the gold mineralizing systems were probably confined to the continental crust (Wyman and Kerrich 1989a). Data from Wyman and Kerrich (1989a) and Taylor et al. (1994) indicate that the Archaean shoshonitic lamprophyres do not have intrinsically high Au concentrations. Sporadically anomalous Au abundances are restricted to samples from the vicinity of orogenic gold deposits (Fig. 8.5b), and the Au values are decoupled from Cu and Pd peaks in primitive mantle-normalized distribution plots in the shoshonitic lamprophyres (Figs. 8.5 and 8.6),

Table 8.7 Major- and trace-element analyses of lamprophyres from the Superior Province, Canada

Province/deposit	Superior province	Superior province
Location	Canada	Canada
Rock type	Lamprophyre	Lamprophyre
Tectonic setting	Postcollisional arc	Postcollisional arc
Reference	Wyman (1990)	Wyman (1990)
SiO ₂	48.60	47.70
TiO ₂	0.79	0.75
Al ₂ O ₃	12.20	11.60
Fe ₂ O ₃	9.28	8.99
FeO	n.a.	n.a.
MnO	0.17	0.16
MgO	9.86	9.93
CaO	7.40	9.49
Na ₂ O	2.92	2.43
K ₂ O	4.03	2.37
P ₂ O ₅	0.65	0.68
LOI	4.08	4.54
Total	99.98	98.64
mg#	71	72
V	118	213
Cr	557	590
Ni	144	159
Rb	198	123
Sr	749	676
Y	23	28
Zr	275	244
Nb	10	12
Ba	765	1542
La	83	65
Ce	144	114
Hf	6.8	4.8

Major elements are in wt%, and trace elements are in ppm. Fe₂O₃ (tot) = total iron calculated as ferric oxide. Data from Wyman (1990)

suggesting that anomalous Au contents are secondary, not primary, features. This is consistent with the poor correlation between Au and the magmatic elements Cu, Pt, and Pd (Tables 8.6 and 8.8), although it is not supported by a good correlation between Au and the gold pathfinder elements As, Sb, and W.

Overall, the spatial but not genetic association of orogenic gold deposits and shoshonitic magmatism since the late Archaean appears to be related to their common requirement of Phanerozoic-style subduction followed by oblique collision (e.g. Barley et al. 1989; Wyman 1990).

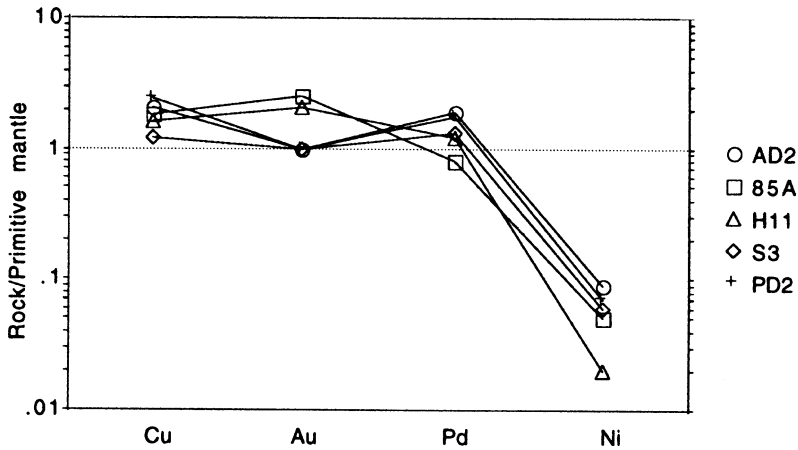


Fig. 8.7 Abundances of chalcophile elements in lamprophyres from the Superior Province relative to the primitive mantle. All data are from lamprophyres distal to gold deposits. Normalizing factors after Brüggmann et al. (1987). Data from Wyman and Kerrich (1989a)

Table 8.8 Correlation matrix for precious metals (Au, Pd, Pt), Cu, and gold pathfinder elements (As, Sb, W) of lamprophyres from the Superior Province, Canada

	Cu	Au	Pt	Pd	Sb	W
Cu	1					
Au	0.025	1				
Pt	0.878	-0.457	1			
Pd	0.819	-0.553	0.994	1		
Sb	-1.000	-0.052	-0.865	-0.803	1	
W	0.853	-0.500	0.999	0.998	-0.839	1

All samples are derived from localities distal to gold deposits. Data from Wyman and Kerrich (1989b)

8.7 Synthesis of Indirect Associations

Although lamprophyres are spatially and temporally related to gold mineralization in several ancient terranes, the association is interpreted to be an indirect one.

Proterozoic orogenic lode-gold mineralization and lamprophyre emplacement may be contemporaneous in several places, although no direct genetic relationships have been established yet. Both lamprophyres and mineralization commonly occur along major faults and shear zones which controlled their emplacement. The elevated Au contents in some Proterozoic lamprophyres from the vicinity of lode-gold deposits are decoupled from Cu and Pd peaks in primitive

mantle-normalized distribution plots suggesting that the anomalous Au contents are secondary features. The contamination *en route* to surface or caused by hydrothermal fluids overprinting the dykes after their emplacement.

Spatial associations also exist between Archaean orogenic gold deposits and potassic lamprophyre dykes in both postcollisional arc and within-plate settings. Rock and Groves (1988a, b) suggest that the volatile- and LILE-enriched fluids necessary to form a metasomatically enriched mantle capable of yielding potassic magmas would also be capable of transporting Au because they mimic hydrothermal fluids known to form gold deposits in the crust. However, recent studies argue against a direct genetic association, although lamprophyre intrusions may bracket the gold mineralization in time (Taylor et al. 1994;

Yeats et al. 1999). The orogenic gold deposits in these settings are not hosted by potassic igneous complexes, but they do occur along major faults and shear zones, which also represent the deep conduits for emplacement of lamprophyre intrusions (Wyman and Kerrich 1989a, b). As for the Proterozoic lamprophyres, the elevated Au contents of some Archaean lamprophyres are decoupled from Cu and Pd peaks in primitive mantle-normalized distribution plots, suggesting that the anomalous Au contents are secondary features, caused by either crustal contamination by mineralized wallrocks or overprinting by later hydrothermal fluids.

Indirect associations between shoshonitic lamprophyres and orogenic gold-antimony deposits have also been documented from the Permian Hillgrove district, New South Wales, Australia (Ashley et al. 1994; Ashley and Craw 2004). A similar direct relationship between shoshonitic lamprophyres and orogenic copper-gold-bismuth mineralization has been recorded for the Tennant Creek area, although recent $^{40}\text{Ar}/^{39}\text{Ar}$ age dating indicates that the lamprophyres significantly postdate the mineralization (Duggan and Jaques 1996). Based on available geochemical and geochronological data, the widespread spatial association of gold deposits and lamprophyres, worldwide (e.g. Rock et al. 1988a, 1989), is probably an indirect, rather than genetic, association, related to the siting of both adjacent to crustal-scale deformation zones.

References

- Aghazadeh M, Prelevic D, Badrzadeh Z, Braschi E, van den Bogaard P, Conticelli S (2015) Geochemistry Sr-Nd-Pb isotopes and geochronology of amphibole- and mica-bearing lamprophyres in northwestern Iran: implications for mantle wedge heterogeneity in a paleo-subduction zone. *Lithos* 217:352–369
- Asan K, Ertürk MA (2013) First evidence of lamprophyric magmatism from the Konya region, Turkey: a genetic link to high-K volcanism. *Acta Geol Sinica* 87:1617–1629
- Ashley PM, Craw D (2004) Structural controls on hydrothermal alteration and gold-antimony mineralization in the Hillgrove area, NSW, Australia. *Mineral Deposita* 39:223–239
- Ashley PM, Cook NDJ, Hill RL, Kent AJR (1994) Shoshonitic lamprophyre dykes and their relation to mesothermal Au-Sb veins at Hillgrove, New South Wales, Australia. *Lithos* 32:249–272
- Barley ME, Groves DI (1990) Deciphering the tectonic evolution of Archaean greenstone belts: the importance of contrasting histories to the distribution of mineralization in the Yilgarn Craton, Western Australia. *Precamb Res* 46:3–20
- Barley ME, Groves DI (1992) Supercontinent cycles and the distribution of metal deposits through time. *Geology* 20:291–294
- Barley ME, Eisenlohr BN, Groves DI, Perring CS, Vearncombe JR (1989) Late Archaean convergent margin tectonics and gold mineralization: a new look at the Norseman-Wiluna Belt, Western Australia. *Geology* 17:826–829
- Betsi TB, Lentz D (2011) Petrochemistry of subvolcanic dyke swarms associated with the Golden Revenue Au-Cu and the Stoddart Mo-Cu ± W mineralizations (Dawson Range, Yukon Territory, Canada) and implications for ore genesis. *Ore Geol Rev* 39:134–163
- Blichert-Toft J, Arndt NT, Ludden JN (1996) Precambrian alkaline magmatism. *Lithos* 37:97–111
- Brüggemann GE, Arndt NT, Hofmann AW, Tobschall HJ (1987) Noble metal abundances in komatiite suites from Alexo, Ontario, and Gorgona Island, Colombia. *Geochim Cosmochim Acta* 51:2159–2169
- Bucholz CE, Jagoutz O, Schmidt MW, Sambuu O (2014) Fractional crystallization of high-K arc magmas: biotite-versus amphibole-dominated fractionation series in the Dariv Igneous Complex, western Mongolia. *Contrib Miner Petrol* 168:1072–1100
- Burrows DR, Spooner ETC (1989) Relationships between Archaean gold quartz vein-shear zone mineralization and igneous intrusions in the Val d'Or and Timmins areas, Abitibi Subprovince, Canada. In: Keays RR, Ramsay WRH, Groves DI (eds) *The geology of gold deposits: the perspective in 1988*. *Econ Geol Monogr* 6:424–444
- Campbell IH, Stepanov AS, Liang HY, Allen CM, Norman MD, Zhang YQ, Xie YW (2014) The origin of shoshonites: new insights from the Tertiary high-potassium intrusions of eastern Tibet. *Contrib Miner Petrol* 167:983–1005
- Card KD, Ciesielski A (1986) Subdivisions of the Superior Province of the Canadian Shield. *J Geol Assoc Canada* 13:5–13
- Chen Y, Yao S, Pan Y (2014) Geochemistry of lamprophyres at the Daping gold deposit, Yunnan Province, China: constraints on the timing of gold mineralization and evidence for mantle convection in the eastern Tibetan Plateau. *J Asian Earth Sci* 93:129–145
- Colvine AC (1989) An empirical model for the formation of Archaean gold deposits: products of final cratonization of the Superior Province, Canada. In: Keays RR, Ramsay WRH, Groves DI (eds) *The geology of gold deposits: the perspective in 1988*. *Econ Geol Monogr* 6:37–53

- Duggan MB, Jaques AL (1996) Mineralogy and geochemistry of Proterozoic shoshonitic lamprophyres from the Tennant Creek Inlier, Northern Territory. *Aust J Earth Sci* 43:269–278
- Gee RD, Baxter JL, Wilde SA, Williams IR (1981) Crustal development in the Archaean Yilgarn Block, Western Australia. In: Glover JE, Groves DI (eds) *Archaean geology: Second International Symposium*, Perth, 1980. *Geol Soc Austr Spec Publ* 7:43–56
- Groves DI (1982) The Archaean and earliest Proterozoic evolution and metallogeny of Australia. *Rev Brasil Geosci* 12:135–148
- Groves DI (1993) The crustal continuum model for late-Archaean lode-gold deposits of the Yilgarn Block, Western Australia. *Miner Deposita* 28:366–374
- Groves DI, Barley ME, Shepherd JM (1994) Geology and mineralization of Western Australia. In: Dentith MC, Frankcombe KF, Ho SE, Shepherd JM, Groves DI, Trench A (eds) *Geophysical signatures of Western Australian mineral deposits. Geology and Geophysics Department & UWA Extension, University of Western Australia, Publication, vol 26, pp 3–28*
- Groves DI, Goldfarb RJ, Gebre-Mariam M, Hagemann SG, Robert F (1998) Orogenic gold deposits: a proposed classification in the context of their crustal distribution and relationship to other gold deposit types. *Ore Geol Rev* 13:7–27
- Guo F, Fan W, Wang Y, Zhang M (2004) Origin of early Cretaceous calc-alkaline lamprophyres from the Sulu orogen in eastern China: implications for enrichment processes beneath continental collisional belt. *Lithos* 78:291–305
- Hagemann SG, Groves DI, Ridley JR, Vearncombe JR (1992) The Archaean lode gold deposits at Wiluna, Western Australia: high-level brittle-style mineralization in a strike-slip regime. *Econ Geol* 87:1022–1053
- Hallberg JA (1985) Geology and mineral deposits of the Leonora-Laverton area, northeastern Yilgarn Block, Western Australia. Hesperian Press, Perth, p 89
- Heidari SM, Daliran F, Paquette J-L, Gasquet D (2015) Geology, timing, and genesis of the high sulphidation Au (-Cu) deposit of Touzlar, NW Iran. *Ore Geol Rev* 65:460–486
- Jensen LS (1978) Larder Lake synoptic mapping project, districts of Cochrane and Timiskaming. *Ontario Geol Surv Miscellaneous Pap* 94:64–69
- Karsli O, Dokuz A, Kaliwoda M, Uysal I, Aydin F, Kandemir R, Fehr K-T (2014) Geochemical fingerprints of Late Triassic calc-alkaline lamprophyres from the Eastern Pontides, NE Turkey: a key to understanding lamprophyre formation in a subduction-related environment. *Lithos* 197:181–197
- Kent AJR, Hagemann SG (1996) Constraints on the timing of lode-gold mineralization in the Wiluna greenstone belt, Yilgarn Craton, Western Australia. *Aust J Earth Sci* 43:573–588
- Leat PT, Thompson RN, Morrison MA, Hendry GL, Dickin AP (1988) Silicic magma derived by fractional-crystallization from Miocene minette, Elkhead Mountain, Colorado. *Mineral Mag* 52:577–586
- Lu YJ, Kerrich R, McCuaig TC, Li ZX, Hart CJR, Cawood PA, Hou ZQ, Bagas L, Cliff J, Belousova EA, Tang S (2013a) Geochemical, Sr-Nd-Pb, and zircon Hf-O isotopic compositions of Eocene-Oligocene shoshonitic and potassic adakite-like felsic intrusions in western Yunnan, SW China: petrogenesis and tectonic implications. *J Petrol* 54:1309–1348
- Lu YJ, Kerrich R, Kemp AIS, McCuaig TC, Hou ZQ, Hart CJR, Li ZX, Cawood PA, Bagas L, Yang ZM, Cliff J, Belousova EA, Jourdan F, Evans NJ (2013b) Intracontinental Eocene-Oligocene porphyry Cu mineral systems of Yunnan, western Yangtze Craton, China: compositional characteristics, sources, and implications for continental collision metallogeny. *Econ Geol* 108:1541–1576
- Lu YJ, McCuaig TC, Li ZX, Jourdan F, Hart CJR, Hou ZQ, Tang S (2015) Paleogene post-collisional lamprophyres in western Yunnan, western Yangtze Craton: mantle source and tectonic implications. *Lithos* (in press)
- Maughan DT, Keith JD, Christiansen EH, Pulsipher T, Hattori K, Evans NJ (2002) Contributions from mafic alkaline magmas to the Bingham porphyry Cu-Au-Mo deposit, Utah, USA. *Mineral Deposita* 37:14–37
- McDonald R, Rock NMS, Rundle CC, Russell OJ (1986) Relationships between late Caledonian lamprophyric and acidic magmas in a differentiated dyke, SW Scotland. *Mineral Mag* 50:547–557
- Morrison GW (1980) Characteristics and tectonic setting of the shoshonite rock association. *Lithos* 13: 97–108
- Mortensen JK (1993) U-Pb geochronology of the eastern Abitibi Subprovince, part 2: Noranda—Kirkland Lake area. *Can J Earth Sci* 30:29–41
- Müller D (1993) Shoshonites and potassic igneous rocks: indicators for tectonic setting and mineralization potential of modern and ancient terranes. Unpublished PhD Thesis, The University of Western Australia, Perth
- Müller D, Stumpfl EF, Taylor WR (1992a) Shoshonitic and alkaline lamprophyres with elevated Au and PGE concentrations from the Kreuzeck Mountains, Eastern Alps, Austria. *Mineral Petrol* 46:23–42
- Müller D, Rock NMS, Groves DI (1992b) Geochemical discrimination between shoshonitic and potassic volcanic rocks from different tectonic settings: a pilot study. *Mineral Petrol* 46:259–289
- Müller D, Morris BJ, Farrand MG (1993) Potassic alkaline lamprophyres with affinities to lamproites from the Karinya Syncline, South Australia. *Lithos* 30:123–137
- Myers JS (1993) Precambrian history of the Western Australian Craton and adjacent orogens. *Ann Rev Earth Planet Sci* 21:453–485
- Needham RS, De Ross GJ (1990) Pine Creek Inlier—regional geology and mineralization. In: Hughes FE (ed) *Geology of the mineral deposits of Australia and Papua New Guinea*. Australasian Institute of Mining and Metallurgy, Parville, Monograph, vol 14, pp 727–737

- Needham RS, Roarty MJ (1980) An overview of metallic mineralization in the Pine Creek Geosyncline. In: Ferguson J, Goleby AB (eds) Proceedings of international uranium symposium on the Pine Creek Geosyncline, Sydney, 1979. International Atomic Energy Agency, Vienna, pp 157–174
- Needham RS, Stuart-Smith PG, Page RW (1988) Tectonic evolution of the Pine Creek Inlier, Northern Territory. *Precambr Res* 41:543–564
- Nicholson PM, Eupene GS (1990) Gold deposits of the Pine Creek Inlier. In: Hughes FE (ed) *Geology of the mineral resources of Australia and Papua New Guinea*. Australasian Institute of Mining and Metallurgy, Parkville, Monograph, vol 14, pp 739–742
- Orozco-Garza A, Dostal J, Keppie JD, Paz-Moreno FA (2013) Mid-tertiary (25–21 Ma) lamprophyres in NW Mexico derived from subduction-modified subcontinental lithospheric mantle in an extensional backarc environment following steepening of the Benioff zone. *Tectonophysics* 590:59–71
- Pearce JA (1982) Trace element characteristics of lavas from destructive plate boundaries. In: Thorpe RS (ed) *Andesites*. Wiley, New York, pp 525–548
- Pearce JA, Cann JR (1973) Tectonic setting of basaltic volcanic rocks determined using trace element analysis. *Earth Planet Sci Lett* 19:290–300
- Peccerillo A, Taylor SR (1976) Geochemistry of Eocene calc-alkaline volcanic rocks from the Kastamonu area, northern Turkey. *Contrib Miner Petrol* 58:63–81
- Perring CS (1988) Petrogenesis of the lamprophyre-“porphyry” suite from Kambalda, Western Australia. In: Ho SE, Groves DI (eds) *Advances in understanding Precambrian gold deposits*, vol II. Geology Department & University Extension, The University of Western Australia, Perth, Publication, vol 12, pp 277–294
- Perring CS, Barley ME, Cassidy KF, Groves DI, McNaughton NJ, Rock NMS, Bettenay LF, Golding SD, Hallberg JA (1989) The association of linear orogenic belts, mantle-crustal magmatism and Archaean gold mineralization in the Eastern Yilgarn Block of Western Australia. In: Keays RR, Ramsay WRH, Groves DI (eds) *The geology of gold deposits: the perspective in 1988*. *Econ Geol Monogr* 6:571–584
- Plá Cid J, Campos CS, Nardi LVS, Florisbal L (2012) Petrology of Gameleira potassic lamprophyres, São Francisco Craton. *Anais de Academia Brasileira de Ciências* 84:377–398
- Rasmussen B, Sheppard S, Fletcher I (2006) Testing ore deposit models using in situ U-Pb geochronology of hydrothermal monazite: Paleoproterozoic gold mineralization in Northern Territory. *Geology* 34:77–80
- Rios DC, Conceição H, Davis DW, Plá Cid J, Rosa MLS, Macambira MJB, McReath I, Marinho MM, Davis WJ (2007) *Precambr Res* 154:1–30
- Rock NMS (1991) *Lamprophyres*. Blackie, Glasgow, p 285
- Rock NMS, Groves DI (1988a) Do lamprophyres carry gold as well as diamonds? *Nature* 332:253–255
- Rock NMS, Groves DI (1988b) Can lamprophyres resolve the genetic controversy over mesothermal gold deposits? *Geology* 16:538–541
- Rock NMS, Groves DI, Ramsay RR (1988a) Lamprophyres: a girl’s best friend? In: Ho SE, Groves DI (eds) *Advances in understanding Precambrian gold deposits*, vol II. Geology Department & University Extension, The University of Western Australia Publication, vol 12, pp 295–308
- Rock NMS, Hallberg JA, Groves DI, Mather PJ (1988b) Archaean lamprophyres in the goldfields of the Yilgarn Block, Western Australia: new indications of their widespread distribution and significance. In: Ho SE, Groves DI (eds) *Advances in understanding Precambrian gold deposits*, vol II. Geology Department & University Extension, The University of Western Australia Publication, vol 12, pp 245–275
- Rock NMS, Groves DI, Perring CS, Golding SD (1989) Gold, lamprophyres, and porphyries: what does their association mean? In: Keays RR, Ramsay WRH, Groves DI (eds) *The geology of gold deposits: the perspective in 1988*. *Econ Geol Monogr* 6:609–625
- Rowins SM, Cameron EM, Lalonde AE, Ernst RE (1993) Petrogenesis of the late Archaean syenitic Murdoch Creek pluton, Kirkland Lake, Ontario: evidence for an extensional tectonic setting. *Can Mineral* 31:219–244
- Sheppard S (1992) An early Proterozoic shoshonitic lamprophyre-granite association and its relationship to the Tom’s Gully gold deposit, Mt. Bundeley, Northern Territory, Australia. Unpublished PhD Thesis, The University of Western Australia, Perth
- Sheppard S (1995) Hybridization of shoshonitic lamprophyre and calc-alkaline granite magma in the Early Proterozoic Mt. Bundeley igneous suite, Northern Territory. *Aust J Earth Sci* 42:173–185
- Sheppard S, Taylor WR (1992) Barium- and LREE-rich, olivine-mica lamprophyres with affinities to lamprophyres, Mt. Bundeley, Northern Territory. *Australia. Lithos* 28:303–325
- Smolonoogov S, Marshall B (1993) A genetic model for the Woodcutters Pb-Zn-Ag orebodies, Northern Territory, Australia. *Ore Geol Rev* 8:65–88
- Solomon M, Groves DI (1994) *The geology and origin of Australia’s mineral deposits*. Oxford monographs in geology and geophysics, Clarendon Press, New York, vol 24, 951 pp
- Spooner ETC (1993) Magmatic sulphide/volatile interaction as a mechanism for producing chalcophile element-enriched, Archaean Au-quartz hydrothermal ore fluids. *Ore Geol Rev* 7:359–379
- Štemprok M, Dolejš D, Holub F (2014) Late Variscan calc-alkaline lamprophyres in the Krupka ore district, Eastern Krušné hory/Erzgebirge: their relationship to Sn-W mineralization. *J Geosci* 59:41–68

- Stern CR, Skewes MA, Arevalo A (2011) Magmatic evolution of the giant El Teniente Cu-Mo deposit, Central Chile. *J Petrol* 52:1591–1617
- Stuart-Smith PG, Needham RS, Wallace DA, Roarty MJ (1986) McKinley River, Northern Territory: 1:100,000 geological map commentary. Department of Mines and Energy Northern Territory, Darwin
- Taylor WR, Rock NMS, Groves DI, Perring CS, Golding SD (1994) Geochemistry of Archaean shoshonitic lamprophyres from the Yilgarn Block, Western Australia: Au abundance and association with gold mineralization. *Appl Geochem* 9:197–222
- Toogood DJ, Hodgson CJ (1985) A structural investigation between Kirkland Lake and Larder Lake gold camps. Ontario Geol Surv Miscellaneous Pap 127:200–205
- Tucker DH, Stuart DC, Hone IG, Sampath N (1980) The characteristics and interpretation of regional gravity, magnetic and radiometric surveys in the Pine Creek Geosyncline. In: Ferguson J, Goleby AB (eds) Proceedings of International Uranium Symposium on the Pine Creek Geosyncline, Sydney, 1979. International Atomic Energy Agency, Vienna, pp 101–140
- Vielreicher RW, Groves DI, Ridley JR, McNaughton NJ (1994) A replacement origin for the BIF-hosted gold deposit at Mt. Morgans, Yilgarn Block, Western Australia. *Ore Geol Rev* 9:325–347
- Vielreicher N, Groves DI, McNaughton N, Fletcher I (2015) The timing of gold mineralization across the eastern Yilgarn craton using U-Pb geochronology of hydrothermal phosphate minerals. *Mineral Deposita* 50:391–428
- Wall VJ (1990) Fluids and metamorphism. Unpublished PhD thesis, Monash University, Melbourne
- Wang J, Qi L, Yin A, Xie G (2001) Emplacement age and PGE geochemistry of lamprophyres in the Laowangzhai gold deposit, Yunnan, SW China. *Sci China (Ser D)* 44:146–154
- Worthing MA, Nasir S (2008) Cambro-Ordovician potassic (alkaline) magmatism in Central Oman: petrological and geochemical constraints on petrogenesis. *Lithos* 106:25–38
- Wyman D (1990) Archaean shoshonitic lamprophyres of the Superior Province, Canada: petrogenesis, geodynamic setting, and implications for lode gold deposits. Unpublished PhD thesis, University of Saskatchewan, Saskatoon
- Wyman D, Kerrich R (1988) Alkaline magmatism, major structures and gold deposits: implications for greenstone belt gold metallogeny. *Econ Geol* 83:454–461
- Wyman D, Kerrich R (1989a) Archaean shoshonitic lamprophyres associated with Superior Province gold deposits: distribution, tectonic setting, noble metal abundances and significance for gold mineralization. In: Keays RR, Ramsay WRH, Groves DI (eds) The geology of gold deposits: the perspective in 1988. *Econ Geol Monogr* 6:651–667
- Wyman D, Kerrich R (1989b) Archaean lamprophyre dykes of the Superior Province, Canada: distribution, petrology and geochemical characteristics. *J Geophys Res* 94:4667–4696
- Yeats CJ, McNaughton NJ, Ruettger D, Bateman R, Groves DI, Harris JL (1999) Evidence for diachronous Archaean lode-gold mineralization events in the Yilgarn Craton, Western Australia; a SHRIMP U-Pb study of intrusive rocks. *Econ Geol* 94:1259–1276

9.1 Introduction

Numerous studies have established the important role of halogens (Cl, F) for the transport of metals in ore deposits related to igneous rocks (Holland 1972; Kilinc and Burnham 1972; Gunow et al. 1980; Boudreau et al. 1986; Carten 1987; Webster and Holloway 1988, 1990; Richards 1990a; Richards et al. 1991; Webster 1992; Stanton 1994; Candela 1997; Heinrich 2005; Yang and Lentz 2005; Ulrich and Mavrogenes 2008; Richards 2009; Zajacz et al. 2010; Lesne et al. 2011; Vignerresse et al. 2014; Webster et al. 2014; Liang and Hoshino 2015; Zellmer et al. 2015). A recent review of fluid saturation and volatile partitioning between melts and hydrous fluids in crustal magmatic systems (Baker and Alletti 2012) indicates that, whenever a fluid phase first forms, it will strip not only Cl and S from the melt, but also metals associated with chlorine (e.g. Cu and Au) as previously discussed by Williams-Jones and Heinrich (2005). It seems likely that the development of hydrothermal ore deposits depends less on the relative abundance of the ore metals such as Au, Cu and Mo in the fluids than on the availability of appropriate mechanisms to concentrate, transport, and deposit the metals, as suggested by Roegge et al. (1974). Modern experimental studies on the solubility of Mo in KCl–H₂O solutions imply that base-metal concentration in aqueous fluids was not the controlling factor for ore formation.

The Mo solubility is temperature dependent and correlates positively with the KCl concentration of the hydrothermal fluid (Ulrich and Mavrogenes 2008). More recent work suggests that the availability and oxidation state of sulphur and the presence of sufficient halogens such as Cl and F in the magmas are important chemical parameters (Zajacz et al. 2010, 2012). Chlorine largely controls the abundances of chlorophile ore and associated elements (e.g. Fe, Mn, Na, K, Cu, Mo) in saline aqueous fluids that exsolve from a magma (Webster 1992), and it also increases PGE solubilities in both sulphide and silicate melts (Peach et al. 1994). In the rock-forming minerals, Cl generally occupies the hydroxyl sites of micas, amphiboles, and apatites (Fuge et al. 1986). The strong affinity of the halogens for potassium, particularly in micas, can be explained in terms of their electronic configurations (Cocco et al. 1972). The Cl–OH and F–OH exchange in the hydroxyl site of micas is susceptible to interaction with hydrothermal fluids, which may impact cations in the octahedral sites given the presence of correlation between (F–Cl–OH) and (Al + Ti + Fe³ + Cr) (see Righter et al. 2002; Yang and Lentz 2005; Teiber et al. 2015). Due to the similar ionic *radii* of F[–] (1.33 Å; Shannon 1976) and OH[–] (1.32–1.37 Å), F[–] is much easily incorporated into OH-bearing minerals than the larger Cl[–] (1.81 Å). Hence, at the magmatic-hydrothermal transition, F is largely retained in the melt whereas Cl preferentially partitions into the fluid

phase (Webster et al. 2009; Wang et al. 2014; Teiber et al. 2015).

The potential use of high Cl concentrations in mica phenocrysts as a prospecting tool to define mineralized volcanic and subvolcanic rocks was first suggested by Stollery et al. (1971). Comparisons between the halogen contents of micas from mineralized and barren intrusions showed that micas from the former are generally characterized by higher Cl and F concentrations than those from the latter (Stollery et al. 1971; Kesler et al. 1975; Jiang et al. 1994; Loferski and Ayuso 1995; Coulson et al. 2001; Müller et al. 2001; Kroll et al. 2002; Shabani et al. 2003; Yang and Lentz 2005; Sarjoughian et al. 2015). Although most of the preliminary studies did not focus on mica compositions of potassic igneous rocks, mica phenocrysts of unmineralized suites of these rocks are known to have intrinsically higher halogen contents than those of K-poor intrusions (Kesler et al. 1975), in agreement with studies showing that the Cl solubility in volatile-rich melts increases with the alkalinity of the melt (Metrich and Rutherford 1992; Dixon et al. 1997; Zajacz et al. 2012). Numerous studies have shown that alkaline magmas such as potassic melts are characteristically enriched in halogens (Bailey and Hampton 1990; Yang and Bodnar 1994; Foley 1994; Zhang et al. 1995; Müller et al. 2001; Kroll et al. 2002; Chevychelov et al. 2008; Melluso et al. 2012), suggesting that the strongest Cl enrichments of magmatic-hydrothermal fluids, and ore metals complexed with Cl, occur in fluids exsolved from magmas that are relatively enriched in K_2O (Webster 1992; Webster et al. 2014; Chen et al. 2015). This is consistent with experiments by Gammons and Williams-Jones (1997), which indicate that, at 500 °C, gold solubility as $AuCl_2^-$ is highest for fluids that are oxidized ($SO_2/H_2S > 1$), highly saline, and potassium-rich. Generally, the measured gold concentrations increase with increasing amounts of Cl and S dissolved in the silicate melt (Botcharnikov et al. 2010). The dependence of gold solubility on the concentrations of Cl and S at fixed redox conditions indicates that gold may not only form oxide- but also Cl- and S-bearing complexes in

silicate melts. Furthermore, it indicates that exsolution of S and Cl from the melt by degassing and crystallization processes may lead to the precipitation of gold into the sulphide phases (Botcharnikov et al. 2010). At low pressures, S is preferentially released over Cl, leading to a distinct increase in vapour S/Cl ratios (Lesne et al. 2011). Experimental work by Zajacz et al. (2010, 2012) implies that the stability of gold hydro-sulphide complexes is greatly increased by the presence of minute concentrations of KCl or NaCl (0.1–0.5 mol/kg H_2O). The amplifying effect of alkali chlorides on the solubility of gold in H_2S -bearing volatiles may explain the preferential association of many giant hydrothermal gold deposits with high-K igneous rocks, which exsolve volatiles that simultaneously contain both H_2S and alkali chlorides in significant concentrations (Zajacz et al. 2010). However, in the range of Cl and S concentrations realistic for natural systems, the role of Cl in gold solubility is far subordinate to that of reduced S (Zajacz et al. 2012).

Gold and Cu are both highly chalcophile elements whose behavior is controlled by the abundance and oxidation state of S, for example as a HS-bearing complex in fluids (Gibert et al. 1998; Sun et al. 2004, 2013). They can also partition into Cl-rich aqueous fluids, as a Cl-bearing complex (Gammons and Williams-Jones 1997). Given the high abundance of Cl in arc magmas, a Cl complex might be important in scavenging Au and Cu out of the magmas, but there are no experiments so far to demonstrate which complex is more important at magmatic temperature and pressures (Sun et al. 2004).

9.2 Erection of Database MICA1

The fact that most potassic igneous rocks contain mica phenocrysts, and that considerable mineral chemistry data have been published, led to compilation of a database of mica analyses—MICA1—from mineralized and barren potassic igneous rocks to test their potential as exploration guides. The halogen contents of

Table 9.1 Data sources of mica compositions from database MICA1

1. Continental arcs	2. Postcollisional arcs	3a. Late oceanic arcs	4. Within-plate settings
<i>American Cordillera</i>	<i>Eastern Alps</i>	<i>Northparkes, NSW, Australia</i>	<i>Karinya Syncline, South Australia</i>
(barren)	Müller (1993) [6]	Müller et al. (1994) [5]	Müller et al. (1993) [7]
Allan and Carmichael (1984) [12]			
	<i>Grasberg, Indonesia</i>	<i>Ladomal, Lihir Island, Papua New Guinea</i>	<i>Mount Bundey, Northern Territory, Australia</i>
<i>American Cordillera</i>	Müller (1993) [4]	Müller (1993) [9]	Müller (1993) [7]
(mineralized)			
Kesler et al. (1975) [28]	<i>Porgera, Papua New Guinea</i>		
	Müller (1993) [3]		
<i>Bingham, USA</i>	Richards (1990b) [2]		
Parry et al. (1978) [7]			
	<i>Superior Province, Canada</i>		
	Müller (1993) [6]		
	<i>Yilgarn Craton, Western Australia</i>		
	Müller (1993) [19]		

The number in square brackets refers to the number of analyses from that reference in the database. From Müller (1993) and Müller and Groves (1993)

representative fresh mica phenocrysts from the investigated localities were both collated from the literature and directly analyzed using a ARL-SEM-Q microprobe with attached WDS system at the Centre for Microscopy and Microanalysis, The University of Western Australia, Perth. All analyzed micas are homogeneous and unzoned. The available data are not filtered, and their sources are listed in Table 9.1. The significance of the data is discussed below.

9.3 Discussion

9.3.1 Behaviour of Halogens in Magmatic Hydrothermal Systems

During magma crystallization, trace elements and halogens partition between the melt and the crystallizing solids (Candela 1989; Cline and Bodnar

1991; Vigneresse 2009). At some stage during crystallization, bubbles of a magmatic aqueous phase nucleate and grow because the water concentration increases in the bulk melt as quartz and feldspar crystallize (Candela 1989; Lowenstern 1994). The exsolution of this aqueous fluid during the final stages of crystallization leads to vein stockworks due to hydraulic fracturing caused by expansion of the igneous pluton (Solomon and Groves 1994). This magmatic-hydrothermal transition occurs in response to decreasing pressure (first boiling) and crystallization (second boiling) as the melt approaches the surface (Cline and Bodnar 1991; Candela 1997). Studies by Webster (2004) suggest that chlorine solubility is a strong function of melt composition and varies with melt fractionation. More specifically, the chemical evolution of dioritic magmas to more-evolved quartz-monzonite compositions involves a dramatic reduction in Cl solubility that increases the probability of hydrosaline liquid exsolution (Webster 2004). Fractional

crystallization increases volatile abundances in the residual melt and increases silica and decreases CaO and MgO concentrations of the residual melt which reduces Cl solubility without influencing H₂O solubility appreciably (Webster 2004). Chlorine has a pronounced preference for the aqueous fluid relative to the silicate melt and silicate minerals, implying that a Cl-bearing fluid would form during the crystallization of a H₂O-saturated, Cl-bearing magma (Kullerud 1995; Shinohara 2009). Extreme enrichments in Cl and F may occur in these magmatic hydrothermal fluids during the end stages of crystallization (Webster and Holloway 1990), especially in potassic alkaline melts (Webster 2004). Experimental studies on volatile-rich high-K alkaline rocks hosting the epithermal gold mineralization at Cripple Creek, Colorado (Kelley and Ludington 2002; Jensen 2003), allow the estimation of the primary volatile (H₂O, CO₂, S, Cl, and F) compositions of the exsolved magmatic fluids (Webster et al. 2014). The bulk integrated magmatic fluid in equilibrium with Cripple Creek phonolitic melt contains high volatile contents of up to 3 wt% Cl (3 mol%), and 0.2 wt% F (0.2 mol%) at 200 MPa, the common pressure at which magmas pond, fractionate, and exsolve fluids (Webster et al. 2014). By contrast, the average concentrations of halogens and sulphur in the primitive, undepleted mantle are estimated to be only 1.4 ppm of Cl, 18 ppm of F, and 230 ppm of S, respectively (Lyubetskaya and Korenaga 2007; Baker and Alletti 2012). Significant quantities of ore elements such as Cu, Au, and Mo may be partitioned into these volatile-rich hydrothermal fluid phases and be removed from the pluton (Candela 1989; Vigneresse 2009).

It is likely, therefore, that such Cl-rich hydrothermal fluids, which exsolve during magma crystallization, also transport gold and/or base metals (Kilinc and Burnham 1972), particularly since ore-metal solubility as chloride complexes in aqueous fluids is a strong function of their Cl content (Webster 1997; Ulrich and Mavrogenes 2008; Zajacz et al. 2010, 2012). For example, the textures and geochemistry of plutons associated with Climax-type porphyry-molybdenum deposits indicate that Cl- and F-enriched magmatic

hydrothermal fluids were primarily responsible for the transport of ore constituents (White et al. 1981; Webster and Holloway 1990). The very high salinities of the ore fluids in most porphyry copper-gold systems, as indicated by fluid inclusion studies (e.g. Roedder 1984), suggest that base-metals were carried as chloride complexes, as was Au, at least at high temperatures (Hayba et al. 1985; Heald et al. 1987; Large et al. 1989).

More recent studies suggest that both Cu and Au preferentially partition into the volatile phase during magmatic devolatilization, being dissolved in that phase as chloride complexes (Hayashi and Ohmoto 1991; Heinrich 2005). Cooling will eventually result in the disproportionation of the SO₂ to sulphate and sulphide species, thus leading to the precipitation of Cu-bearing sulphide minerals (Richards 1995). Although some Au may also be deposited with these sulphides, much of it will remain in solution by conversion from chloride to bisulphide complexes at lower temperatures (Hayashi and Ohmoto 1991; Heinrich 2005). Most of the Au may be precipitated at shallower levels in the epithermal environment (Richards 1995, 2011), consistent with the decrease of Au grade downwards into increasingly Cu-rich mineralization, as was originally proposed by Bonham and Giles (1983).

An important prerequisite for the hydrothermal extraction of Au from the magma is that removal of chalcophile elements from the melt by sulphide-liquid segregation should not occur before volatile saturation (Richards 1995, 2011). This condition may be achieved by the suppression of sulphur saturation through a high oxidation state of the magma (see Sect. 10.3.2), thus promoting the presence of sulphur as sulphate, not sulphide, within the melt (Carmichael and Ghiorso 1986; Campbell et al. 1998; Müller et al. 2002). Recent work has shown that several barren granites of northern Mexico represent magmas that exsolved a fluid relatively early in their crystallization history (i.e. before 30% crystallization), but this study also concluded that these magmas did not generate mineralization primarily because of the low salinity of their exsolving fluids (Audetat and Pettke 2003).

Thus, Cl and F are important components of the hydrothermal system in that they represent an effective metal-transporting medium (Spear 1984; Loferski and Ayuso 1995; Richards 2011). Hence, it may be no coincidence that many gold deposits tend to be associated with the more volatile-rich potassic and calc-alkaline magmas (Spooner 1993), where a magmatic connection is indicated (Richards 1995; Sillitoe 2002; Mavrogenes et al. 2006; Li and Audetat 2013).

Chlorine is enriched, together with K_2O , in residual melts as a result of crystal-liquid differentiation of vapour-poor magmas, and a moderate correlation between these elements has been recorded for lavas from several localities (Anderson 1974). However, in vapour-rich lavas, Cl tends to partition into the vapour phase and hence is likely lost during degassing on magma ascent (Edgar, written comm. 1994). Fluorine contents increase regularly from tholeiites to potassic basalts (Aoki et al. 1981), and F is a significant element in potassic and ultrapotassic magmas (Edgar and Charbonneau 1991; Foley 1994; Kelley and Ludington 2002; Chevychelov et al. 2008). Experimental studies by Vukadinovic and Edgar (1993) suggest that F, in contrast to Cl (see Magenheim et al. 1995), behaves as a mantle-compatible element. This can be explained by the relatively small ionic *radius* of the F cation when compared to the larger and probably more incompatible Cl anion (Teiber et al. 2015). Although, under mantle conditions, F tends to remain in the solid phases rather than partitioning into the first melt increments during partial melting (Vukadinovic and Edgar 1993), alkaline rocks derived in within-plate settings such as OIB are defined by relatively high F concentrations of 900–1100 ppm (cf. Wang et al. 2014). During crystallization, F is partitioned into the hydrous phenocrysts rather than remaining in the melt (Edgar et al. 1994). In accord with this, Kesler et al. (1975) and Naumov et al. (1998) have shown that the average whole-rock halogen contents of potassic intrusions (>2 wt% K_2O) are higher (240 ppm Cl, 620 ppm F) than those for non-potassic (<2 wt% K_2O) intrusions (160 ppm Cl, 380 ppm F). High primary Cl and F contents

of potassic igneous rocks from Cripple Creek, Colorado, are also well documented in fluid (Thompson et al. 1985) and melt inclusions (Webster et al. 2014), respectively. In addition, micas from mineralized intrusions tend to be more Cl-enriched than those from barren igneous rocks (Munoz 1984; Coulson et al. 2001; Yang and Lentz 2005; Sarjoughian et al. 2015). The ions OH^- , Cl^- , F^- , and K^+ are fixed preferentially in hydrous minerals, in particular phlogopites, under subsolidus conditions (Aoki et al. 1981; Spear 1984; Foley 1992). Phlogopite-bearing metasomatized mantle peridotites are considered to be source materials for primitive potassic magmas (Tatsumi and Koyaguchi 1989; Foley 1992; Franz et al. 2002, 2010), and phlogopites provide the major sites of Cl and F in potassic igneous rocks (Aoki et al. 1981; Edgar and Arima 1985; Edgar et al. 1994). Mineralogical studies by Jiang et al. (1994) suggest that F is preferentially incorporated into micas with high Mg/Fe ratios, whereas Cl tends to be enriched in those with lower Mg/Fe ratios.

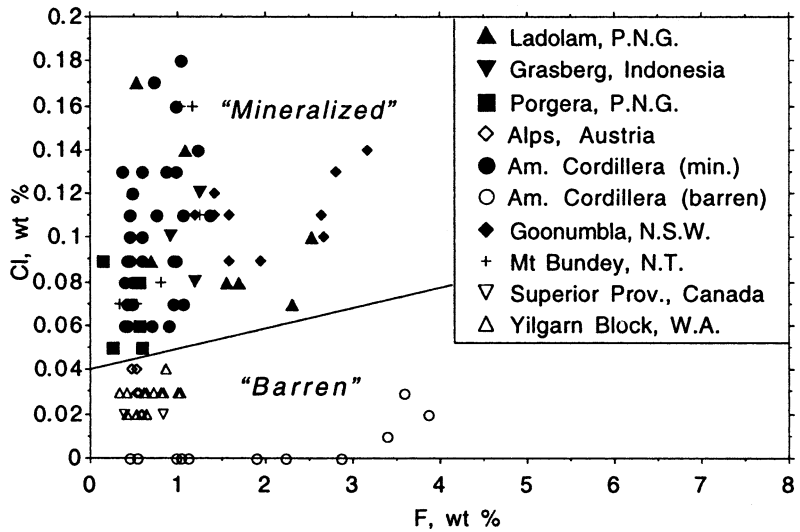
The common presence of primary biotite in most porphyries which host hydrothermal Cu–Au mineralization indicates that water loss to hydrous phases and enhancement of the Cl/ H_2O ratio occurs in all productive systems (e.g. Cline and Bodnar 1991). However, in more rare examples, such as the Ladolam gold deposit on Lihir Island, Papua New Guinea (see Sect. 6.3.1), biotite is restricted to secondary (hydrothermal) phases associated with potassic alteration, while phlogopite represents the primary magmatic phases (Müller et al. 2001).

Water-leach analyses of biotites and phlogopites suggest that less than 10 wt% of Cl and 1 wt% of F are present in fluid inclusions. The remainder is apparently present in the mica structure (Kesler et al. 1975).

9.3.2 Halogen Contents of Mica in Potassic Igneous Rocks

The halogen contents of representative, fresh mica phenocrysts from potassic igneous rocks associated with mineralization from the

Fig. 9.1 Chlorine and F compositions of mica phenocrysts from potassic igneous rocks from barren and mineralized environments (data sources are listed in Table 9.1). Adapted from Müller and Groves (1993)



investigated localities are plotted on a Cl versus F biaxial diagram in Fig. 9.1. Representative data for micas from potassic igneous rocks interpreted to be genetically associated with epithermal gold mineralization are listed in Tables 9.2 (Ladolam, Papua New Guinea) and 9.3 (Porgera, Papua New Guinea), and with porphyry copper-gold mineralization are listed in Tables 9.4 (Grasberg, Indonesia), and 9.5 (Northparkes, Australia). Data from such rocks only spatially related to mineralization are listed in Tables 9.6 (Eastern Goldfields Province, Yilgarn Block, Australia) and 9.7 (Kirkland Lake gold district, Superior Province, Canada).

Mica phenocrysts from shoshonitic lamprophyres from the Eastern Goldfields Province (Kambalda area, Mount Morgans gold mine) and Kirkland Lake gold district are generally characterized by very low halogen (<0.04 wt% Cl) concentrations (Fig. 9.1). This is consistent with the extremely low Cl concentrations (about 0.02 wt%) of apatite microphenocrysts in Superior Province lamprophyres (Kerrich, written comm. 1992). The low halogen contents of Yilgarn Block and Superior Province shoshonitic lamprophyres, when compared to those from mineralized high-K igneous rocks from equivalent postcollisional arc-settings (Fig. 9.1), lend

further credence to the arguments that the lamprophyres are not genetically related to the orogenic gold mineralization, as originally suggested by Rock et al. (1987) and Rock and Groves (1988), but have an indirect association (Wyman and Kerrich 1989; Taylor et al. 1994; see Sect. 8.6).

By contrast, mica phenocrysts from potassic igneous rocks which host epithermal gold or porphyry copper-gold mineralization are characterized by elevated halogen abundances (>0.04 wt% Cl). Examples are micas from the high-K igneous rocks associated with the epithermal gold deposits at Ladolam (up to 0.29 wt% Cl) and Porgera (up to 0.09 wt% Cl), and from the Grasberg (up to 0.24 wt% Cl) and Northparkes (up to 0.14 wt% Cl) porphyry copper-gold deposits.

Where mineralization is interpreted to be genetically associated with potassic igneous rocks, the host rocks were generated in continental, postcollisional or late oceanic island arcs (cf. Müller and Groves 1993). These three settings are the only tectonic settings in which mineralization genetically related to potassic igneous rocks is currently recognized. The high Cl concentrations (>0.04 wt% Cl) in mica phenocrysts from all mineralized potassic igneous

Table 9.2 (continued)

Province/deposit	Ladolam	Conical										
<i>Atoms</i>												
Si	5.770	5.805	5.653	5.580	5.744	5.659	2.769	2.709				
Ti	0.327	0.135	0.479	0.494	0.483	0.489	0.248	0.109				
Al	2.284	2.747	2.502	2.484	2.405	2.489	1.268	1.468				
Fe	1.593	1.420	1.384	1.437	1.659	1.647	1.132	0.637				
Cr	–	–	–	–	–	–	–	0.004				
Mn	–	–	–	–	–	–	0.025	0.004				
Mg	3.767	3.845	3.628	3.741	3.602	3.636	1.399	2.012				
Ni	–	–	–	–	–	–	–	–				
Ba	0.008	0.003	0.009	0.011	0.004	0.018	–	0.002				
Ca	0.007	0.005	0.013	0.013	0.005	0.001	0.002	0.001				
Sr	0.042	0.006	0.003	0.010	0.008	0.004	–	–				
K	1.814	1.932	1.744	1.734	1.854	1.860	0.962	0.909				
Na	0.113	0.123	0.144	0.100	0.081	0.078	0.049	0.092				
Cl	–	–	–	–	–	–	–	–				
F	–	–	–	–	–	–	–	–				
Total	15.725	16.021	15.559	15.604	15.845	15.881	7.854	7.946				

Ox. form. oxygen formula. Six-digit sample numbers refer to specimens held in the Museum of the Department of Geology and Geophysics, The University of Western Australia. Data from Müller (1993) and Müller et al. (2001, 2003)

Table 9.3 Microprobe (WDS) analyses of mica phenocrysts from potassic igneous rocks from the Porgera gold deposit, Papua New Guinea

Province/deposit	Porgera	Porgera	Porgera	Porgera	Porgera
Location	Papua New Guinea	Papua New Guinea	Papua New Guinea	Papua New Guinea	Papua New Guinea
Rock type	Trachybasalt	Trachybasalt	Trachybasalt	Trachybasalt	Trachybasalt
Sample no.	PO13	PO14	PO14	RJR-46-A	RJR-21-A
Reference	N.M.S. Rock (unpl. data)	N.M.S. Rock (unpl. data)	N.M.S. Rock (unpl. data)	Richards (1990b)	Richards (1990b)
<i>wt%</i>					
SiO ₂	35.62	36.07	37.25	36.13	36.63
TiO ₂	3.78	3.97	3.56	3.77	2.70
Al ₂ O ₃	14.58	14.94	14.94	14.31	15.23
FeO (tot)	15.70	14.64	13.19	14.41	11.50
Cr ₂ O ₃	0.03	0.03	0.03	0.03	0.09
MnO	0.39	0.27	0.24	0.27	0.13
MgO	14.84	15.86	17.07	16.93	18.64
NiO	0.09	0.10	0.09	–	–
BaO	0.18	0.18	0.18	0.20	0.80
CaO	0.03	0.04	0.03	0.02	0.01
SrO	0.16	0.16	0.15	–	–
K ₂ O	8.80	9.12	8.64	8.76	8.89
Na ₂ O	0.89	0.91	1.12	1.08	0.76
Cl	0.06	0.06	0.08	0.05	0.09
F	0.59	0.55	0.55	0.26	0.14
Total	95.48	96.66	96.89	96.21	95.63
mg#	68	71	75	73	79
Ox. form.	22	22	22	22	22
<i>Atoms</i>					
Si	5.410	5.380	5.475	5.389	5.423
Ti	0.432	0.445	0.393	0.423	0.300
Al	2.609	2.626	2.587	2.515	2.658
Fe	1.994	1.826	1.620	1.797	1.424
Cr	–	0.002	0.003	0.004	0.010
Mn	0.050	0.033	0.029	0.034	0.017
Mg	3.359	3.524	3.737	3.763	4.114
Ni	0.008	0.011	0.011	–	–
Ba	0.005	0.006	0.006	0.012	0.046
Ca	0.002	0.007	0.004	0.003	–
Sr	–	–	–	–	–
K	1.704	1.734	1.619	1.667	1.678
Na	0.261	0.262	0.319	0.313	0.217

(continued)

Table 9.3 (continued)

Province/deposit	Porgera	Porgera	Porgera	Porgera	Porgera
Cl	–	–	–	–	–
F	–	–	–	–	–
Total	15.834	15.856	15.803	16.052	15.979

Ox. form. oxygen formula. Samples are from the private collection of N.M.S. Rock, and other data are from Richards (1990b)

rocks further support a direct genetic relationship between magmatism and mineralizing fluids in these three specific tectonic settings.

Micas from the high-K calc-alkaline host rocks of the Ladolam epithermal gold (Table 9.2; see also Müller et al. 2001), and from shoshonites hosting the Northparkes porphyry copper-gold deposit (Table 9.5), both interpreted to have been generated in a late oceanic island-arc setting (Müller et al. 1994), are enriched in Cl and F (Fig. 9.1). This might be a specific feature of mineralized potassic igneous rocks from this setting, but it awaits confirmation from data on deposits such as the Emperor epithermal gold deposit, Fiji, which is in a similar tectonic setting.

Importantly, analyzed unmineralized potassic igneous suites from continental, postcollisional, and late oceanic island arcs contain low-Cl (\pm F) mica phenocrysts, and hence contrast with those from mineralized settings (Fig. 9.1). It should be noted, however, that analyzed phenocrysts from potassic igneous rocks from within-plate settings (e.g. Mount Bundey suite, Fig. 9.1) have high Cl contents equivalent to those of mineralized high-K rocks from continental, postcollisional, and late oceanic arc settings, although the rocks are interpreted to have no genetic relationship to gold mineralization in the area. It may also be significant that some potassic igneous rocks from within-plate settings (e.g. Karinya Syncline, Sect. 5.3) have intrinsically high Au contents although no direct relationships to mineralization have yet been established.

Potassic igneous rocks from the Mariana Arc (Sect. 4.3), an initial oceanic island arc, do not contain mica phenocrysts (Dixon and Batiza 1979) and cannot, therefore, be assessed in terms of halogen contents.

Mica phenocrysts from potassic igneous rocks generated in within-plate tectonic settings can contain elevated halogen concentrations. Studies by Naumov et al. (1998) suggest also that potassic rocks with high TiO₂ contents (\sim 3.23 wt%), which are typical for those from within-plate tectonic settings, have primary enrichments in F compared to the average F concentrations of basic melts. However, within-plate tectonic settings may have no known mineralization or there may be only an indirect association with known mineralization (e.g. Mount Bundey igneous suite and Tom's Gully gold deposit).

9.3.3 Significance of Halogen Data

From the above discussion, it appears that the halogen contents of mica phenocrysts from high-K igneous suites can be used, with due caution, as a measure of gold-copper mineralization potential in continental, postcollisional, and late oceanic island arcs (Müller and Groves 1993; Müller et al. 2001; Kroll et al. 2002; Yang and Lentz 2005). The threshold value for Cl concentration for such micas is about 0.04 wt% or 400 ppm, but F is a poor discriminant, being enriched up to about 4.0 wt% in potassic rocks

Table 9.4 Microprobe (WDS) analyses of mica phenocrysts from potassic igneous rocks from the Grasberg copper-gold deposit, Irian Jaya, Indonesia

Province/deposit	Grasberg	Grasberg	Grasberg	Grasberg
Location	Indonesia	Indonesia	Indonesia	Indonesia
Rock type	Monzodiorite	Monzodiorite	Monzodiorite	Monzodiorite
Sample no.	DM1	DM1	DM1	DM1
Reference	Müller (1993)	Müller (1993)	Müller (1993)	Müller (1993)
<i>wt%</i>				
SiO ₂	35.56	35.24	35.37	35.44
TiO ₂	5.01	5.02	5.27	4.61
Al ₂ O ₃	13.59	13.08	13.58	14.07
FeO (tot)	16.96	17.32	17.13	16.97
Cr ₂ O ₃	–	–	–	–
MnO	–	–	–	–
MgO	12.65	12.95	13.56	13.67
NiO	–	–	–	–
BaO	0.21	0.32	0.23	0.20
CaO	0.08	0.03	0.03	0.03
SrO	0.09	0.11	0.11	0.09
K ₂ O	9.43	9.46	9.67	9.79
Na ₂ O	0.40	0.33	0.26	0.28
Cl	0.12	0.26	0.08	0.10
F	1.30	1.42	1.23	1.31
Total	95.40	95.54	96.52	96.56
mg#	63	63	65	65
Ox. form.	22	22	22	22
<i>Atoms</i>				
Si	5.498	5.483	5.416	5.418
Ti	0.582	0.587	0.606	0.529
Al	2.475	2.397	2.449	2.535
Fe	2.192	2.253	2.192	2.168
Cr	–	–	–	–
Mn	–	–	–	–
Mg	2.913	3.001	3.093	3.114
Ni	–	–	–	–
Ba	0.013	0.019	0.014	0.012
Ca	0.013	0.001	0.001	0.005
Sr	0.006	–	–	0.005
K	1.859	1.877	1.888	1.909
Na	0.120	0.099	0.076	0.083
Cl	–	–	–	–
F	–	–	–	–
Total	15.671	15.717	15.735	15.778

Ox. form. oxygen formula. Sample numbers refer to specimens held in the Museum of the Department of Geology and Geophysics, The University of Western Australia. Data from Müller (1993)

Table 9.5 Microprobe (WDS) analyses of mica phenocrysts from shoshonitic rocks from the Northparkes copper-gold deposit E26 N, Goonumbla igneous complex, New South Wales, Australia

Province/deposit	Northparkes	Northparkes	Northparkes	Northparkes
Location	NSW, Australia	NSW, Australia	NSW, Australia	NSW, Australia
Rock type	Monzonite	Monzonite	Trachyte	Trachyte
Sample no.	119086	119086	119100	119102
Reference	Müller et al. (1994)			
<i>wt%</i>				
SiO ₂	36.10	37.12	36.53	35.46
TiO ₂	4.22	4.00	2.83	3.45
Al ₂ O ₃	14.35	14.17	16.42	16.59
FeO (tot)	11.65	11.50	13.03	13.33
Cr ₂ O ₃	0.02	0.02	0.02	0.02
MnO	0.10	0.16	0.16	0.22
MgO	16.57	16.35	15.65	15.32
BaO	0.28	0.19	0.14	0.14
CaO	0.03	0.03	0.03	0.03
SrO	0.15	0.16	0.15	0.16
K ₂ O	9.20	9.10	8.85	9.47
Na ₂ O	0.42	0.44	0.29	0.29
Cl	0.10	0.14	0.11	0.12
F	3.90	3.18	1.58	1.42
Total	95.88	95.83	95.85	95.53
mg#	77	77	74	73
Ox. form.	22	22	22	22
<i>Atoms</i>				
Si	5.136	5.290	5.242	5.120
Ti	0.452	0.428	0.306	0.374
Al	2.406	2.380	2.778	2.824
Fe	1.248	1.234	1.406	1.448
Cr	0.002	0.002	0.002	0.002
Mn	0.012	0.020	0.020	0.026
Mg	3.514	3.472	3.346	3.296
Ba	0.016	0.010	0.008	0.008
Ca	0.004	0.004	0.004	0.004
Sr	0.012	0.014	0.012	0.014
K	1.670	1.654	1.648	1.744
Na	0.116	0.122	0.080	0.082
Cl	–	–	–	–
F	–	–	–	–
Total	14.604	14.646	14.868	14.958

Ox. form. oxygen formula. Sample numbers refer to specimens held in the Museum of the Department of Geology and Geophysics, The University of Western Australia. Data from Müller et al. (1994)

Table 9.6 Microprobe (WDS) analyses of mica phenocrysts from shoshonitic lamprophyres from the Kambalda gold province and from Mount Morgans gold deposit, Yilgarn Craton, Western Australia

Province/deposit	Kambalda	Kambalda	Mount Morgans	Mount Morgans	Mount Morgans
Location	Western Australia				
Rock type	Lamprophyre	Lamprophyre	Lamprophyre	Lamprophyre	Lamprophyre
Sample no.	108370	108512	RV5	RV5	B64
Zonation	No	No	Core	Rim	No
Reference	Müller (1993)				
<i>wt%</i>					
SiO ₂	37.07	37.93	40.66	40.09	36.54
TiO ₂	2.27	2.31	1.37	1.84	2.28
Al ₂ O ₃	17.98	14.29	12.77	12.96	15.27
FeO (tot)	11.08	15.79	2.88	10.18	16.76
Cr ₂ O ₃	0.03	0.10	0.47	0.45	0.13
MnO	0.16	0.08	0.05	0.09	0.17
MgO	14.94	14.84	24.54	18.96	13.19
NiO	0.10	0.06	0.70	0.55	0.10
BaO	0.22	0.37	0.17	0.19	0.19
CaO	0.03	0.03	0.03	0.03	0.07
SrO	0.13	0.13	0.14	0.14	0.15
K ₂ O	10.14	9.35	10.68	10.27	9.06
Na ₂ O	0.10	0.21	0.03	0.03	0.09
Cl	0.03	0.03	0.03	0.03	0.02
F	1.02	0.41	0.81	0.64	0.58
Total	94.87	95.76	94.99	96.18	94.36
mg#	75	68	95	81	64
Ox. form.	22	22	22	22	22
<i>Atoms</i>					
Si	5.518	5.695	5.847	5.868	5.601
Ti	0.254	0.260	0.147	0.203	0.262
Al	3.153	2.528	2.163	2.235	2.758
Fe	1.378	1.981	0.347	1.246	2.148
Cr	0.001	0.012	0.053	0.052	0.016
Mn	0.019	0.010	0.006	0.011	0.022
Mg	3.313	3.319	5.256	4.134	3.012
Ni	0.012	0.007	0.081	0.065	0.012
Ba	0.011	0.022	0.006	0.004	0.007
Ca	0.002	0.030	–	0.001	0.012
Sr	0.011	0.011	0.007	0.007	0.002
K	1.924	1.790	1.958	1.916	1.772

(continued)

Table 9.6 (continued)

Province/deposit	Kambalda	Kambalda	Mount Morgans	Mount Morgans	Mount Morgans
Na	0.028	0.060	0.004	–	0.027
Cl	–	–	–	–	–
F	–	–	–	–	–
Total	15.624	15.725	15.875	15.742	15.651

Ox. form. oxygen formula. Sample numbers refer to specimens held in the Museum of the Department of Geology and Geophysics, The University of Western Australia. Data from Müller (1993)

Table 9.7 Microprobe (WDS) analyses of mica phenocrysts from shoshonitic lamprophyres from the Kirkland Lake gold district, Superior Province, Canada

Province/deposit	Kirkland Lake				
Location	Canada	Canada	Canada	Canada	Canada
Rock type	Lamprophyre	Lamprophyre	Lamprophyre	Lamprophyre	Lamprophyre
Sample no.	NMSR1	NMSR2	NMSR3	NMSR4	NMSR5
Zonation	No	No	No	No	No
Reference	Müller (1993)				
<i>wt%</i>					
SiO ₂	38.89	38.35	37.47	36.46	35.99
TiO ₂	1.76	2.01	1.73	3.39	3.16
Al ₂ O ₃	15.05	15.05	15.33	13.92	14.14
FeO (tot)	12.78	13.04	12.99	16.68	16.70
Cr ₂ O ₃	0.09	0.17	0.13	0.02	0.04
MnO	0.18	0.11	0.16	0.18	0.24
MgO	16.49	15.89	15.76	14.24	14.24
NiO	0.10	0.09	0.07	0.06	0.06
BaO	0.35	0.27	0.35	0.52	0.53
CaO	0.04	0.12	0.03	0.03	0.03
SrO	0.16	0.10	0.13	0.11	0.10
K ₂ O	10.03	9.52	10.01	9.27	9.44
Na ₂ O	0.04	0.09	0.09	0.22	0.17
Cl	0.02	0.04	0.04	0.04	0.05
F	0.38	0.36	0.33	0.37	0.44
Total	96.31	95.10	94.24	94.91	95.14
mg#	72	71	71	63	63
Ox. form.	22	22	22	22	22
<i>Atoms</i>					
Si	5.731	5.712	5.646	5.557	5.514
Ti	0.195	0.225	0.195	0.388	0.363
Al	2.612	2.641	2.722	2.499	2.553
Fe	1.574	1.623	1.637	2.125	2.138

(continued)

Table 9.7 (continued)

Province/deposit	Kirkland Lake				
Cr	0.010	0.019	0.015	0.002	0.004
Mn	0.022	0.014	0.020	0.023	0.031
Mg	3.618	3.526	3.537	3.232	3.249
Ni	0.011	0.010	0.008	0.004	0.004
Ba	0.020	0.016	0.021	0.031	0.031
Ca	0.006	0.019	0.002	0.004	0.003
Sr	0.013	0.008	0.011	0.003	0.004
K	1.884	1.808	1.923	1.802	1.845
Na	0.010	0.025	0.026	0.064	0.050
Cl	–	–	–	–	–
F	–	–	–	–	–
Total	15.710	15.649	15.764	15.738	15.792

Ox. form. oxygen formula. Samples are from the private collection of N.M.S. Rock

from both mineralized and unmineralized environments (Fig. 9.1).

References

- Allan JF, Carmichael ISE (1984) Lamprophyric lavas in the Colima graben, SW Mexico. *Contrib Miner Petrol* 88:203–216
- Anderson AT (1974) Chlorine, sulfur and water in magmas and oceans. *Bull Am Geol Society* 85:1485–1492
- Aoki K, Ishiwaka K, Kanisawa S (1981) Fluorine geochemistry of basaltic rocks from continental and oceanic regions and petrogenetic application. *Contrib Miner Petrol* 76:53–59
- Audetat A, Pettko T (2003) The magmatic-hydrothermal evolution of two barren granites: a melt and fluid inclusion study of the Rito del Medio and Canada Pinabete plutons in southern New Mexico (USA). *Geochim Cosmochim Acta* 67:97–122
- Bailey DK, Hampton CM (1990) Volatiles in alkaline magmatism. *Lithos* 26:157–165
- Baker DR, Alletti M (2012) Fluid saturation and volatile partitioning between melts and hydrous fluids in crustal magmatic systems: the contribution of experimental measurements and solubility models. *Earth Sci Rev* 114:298–324
- Bonham HF, Giles DL (1983) Epithermal gold/silver deposits: the geothermal connection. *Geotherm Resour Counc Spec Rep* 13:257–262
- Botcharnikov RE, Linnen RL, Holtz F (2010) Solubility of Au in Cl- and S-bearing hydrous silicate melts. *Geochimica Cosmochimica Acta* 74:2396–2411
- Boudreau AE, Mathez EA, McCallum IS (1986) Halogen geochemistry of the Stillwater and Bushveld complexes: evidence for transport of the platinum-group elements by Cl-rich fluids. *J Petrol* 27:967–986
- Campbell IH, Compston DM, Richards JP, Johnson JP, Kent AJR (1998) Review of the application of isotopic studies to the genesis of Cu–Au mineralization at Olympic Dam and Au mineralization at Porgera, the Tennant Creek district and Yilgarn Craton. *Aust J Earth Sci* 45:201–218
- Candela PA (1989) Felsic magmas, volatiles, and metallogenesis. In: Whitney JA, Naldrett AJ (eds) *Ore Deposition associated with Magmas*. *Rev in Econ Geol* 4:223–233
- Candela PA (1997) A review of shallow, ore-related granites: textures, volatiles, and ore metals. *J Petrol* 38:1619–1633
- Carmichael ISE, Ghiorso MS (1986) Oxidation-reduction relations in basic magma: a case for homogeneous equilibria. *Earth Planet Sci Lett* 78:200–210
- Carten RB (1987) Evolution of immiscible Cl- and F-rich liquids from ore magmas, Henderson porphyry molybdenum deposit Colorado. *Geol Soc Am Abstracts* 19:613
- Chen JL, Xu JF, Wang BD, Yang ZM, Ren JB, Yu HX, Liu H, Feng Y (2015) Geochemical differences between subduction- and collision-related copper-bearing porphyries and implications for metallogenesis. *Ore Geology Reviews* 70:424–437

- Chevychelov VY, Botcharnikov RE, Holtz F (2008) Partitioning of Cl and F between fluid and hydrous phonolitic melt of Mt. Vesuvius at 850–1000 °C and 200 MPa. *Chem Geol* 256:172–184
- Cline JS, Bodnar RJ (1991) Can economic porphyry copper mineralization be generated by a typical calc-alkaline melt? *J Geophys Res* 96:8113–8126
- Cocco G, Fanfani L, Zanazzi PF (1972) Potassium. In: Wedepohl KH (ed) *Handbook of Geochemistry Volume II-2*. Springer, Berlin
- Coulson IM, Dipple GM, Raudsepp M (2001) Evolution of HF and HCl activity in magmatic volatiles of the gold-mineralized Emerald Lake pluton, Yukon Territory, Canada. *Mineral Depos* 36:594–606
- Dixon TH, Batiza R (1979) Petrology and chemistry of Recent lavas in the N-Marianas: implications for the origin of island-arc basalts. *Contrib Miner Petrol* 70:167–181
- Dixon JE, Clague DA, Wallace P, Poreda R (1997) Volatiles in alkali basalts from the North Arch volcanic field, Hawaii: extensive degassing of deep submarine-erupted alkali series lavas. *J Petrol* 38:911–939
- Edgar AD, Arima M (1985) Fluorine and chlorine contents of phlogopites crystallized from ultrapotassic rock compositions in high pressure experiments: implications for halogen reservoirs in source regions. *Am Mineral* 70:529–536
- Edgar AD, Charbonneau HE (1991) Fluorine-bearing phases in lamproites. *Miner Petrol* 44:125–149
- Edgar AD, Lloyd FE, Vukadinovic D (1994) The role of fluorine in the evolution of ultrapotassic magmas. *Miner Petrol* 51:173–193
- Foley SF (1992) Petrological characterization of the source components of potassic magmas: geochemical and experimental constraints. *Lithos* 28:187–204
- Foley SF (1994) Geochemische und experimentelle Untersuchungen zur Genese der kalireichen Magmatite. *Neues Jahrbuch Mineralogie Abhandlungen* 167:1–55
- Franz L, Becker KP, Kramer W, Herzig PM (2002) Metasomatic mantle xenoliths from the Bismarck Microplate (Papua New Guinea)—Thermal evolution, geochemistry and extent of slab-induced metasomatism. *J Petrol* 43:315–343
- Fuge R, Andrews MJ, Johnson CC (1986) Chlorine and iodine, potential pathfinder elements in exploration geochemistry. *Appl Geochem* 1:111–116
- Gammons CH, Williams-Jones AE (1997) Chemical mobility of gold in the porphyry-epithermal environment. *Econ Geol* 92:45–59
- Gibert F, Pascal ML, Pichavant M (1998) Gold solubility and speciation in hydrothermal solutions: experimental study of the stability of hydrosulphide complex of gold (AuHS⁰) at 350 to 450 °C and 500 bars. *Geochimica Cosmochimica Acta* 62:2931–2947
- Gunow AJ, Ludington S, Munoz JL (1980) Fluorine in micas from the Henderson molybdenite deposit, Colorado. *Econ Geol* 75:1127–1136
- Hayashi KI, Ohmoto H (1991) Solubility of gold in NaCl- and H₂S-bearing aqueous solutions at 250–350 °C. *Geochim Cosmochim Acta* 55:2111–2126
- Hayba DO, Bethke PM, Heald P, Foley NK (1985) Geologic, mineralogic and geochemical characteristics of volcanic-hosted precious-metal deposits. In: Berger BR, Bethke PM (eds) *Geology and Geochemistry of Epithermal Systems*. *Rev in Econ Geol* 2:129–167
- Heald P, Foley NK, Hayba DO (1987) Comparative anatomy of volcanic-hosted epithermal deposits: acid-sulphate and adularia-sericite types. *Econ Geol* 82:1–24
- Heinrich CA (2005) The physical and chemical evolution of low-salinity magmatic fluids at the porphyry to epithermal transition: a thermodynamic study. *Mineral Deposita* 39:864–889
- Holland HD (1972) Granites, solutions, and base-metals. *Econ Geol* 67:281–301
- Jensen EP (2003) Magmatic and hydrothermal evolution of the Cripple Creek gold deposit, Colorado, and comparisons with regional and global magmatic-hydrothermal systems associated with alkaline magmatism. Unpl. PhD Thesis, The University of Arizona, Tucson
- Jiang SY, Palmer MR, Xue CJ, Li YH (1994) Halogen-rich scapolite-biotite rocks from the Tongmugou Pb–Zn deposit, Qinling, northwestern China: implications for the ore-forming processes. *Miner Mag* 58:543–552
- Kelley KD, Ludington S (2002) Cripple Creek and other alkaline-related gold deposits in the southern Rocky Mountains, USA: influence of regional tectonics. *Mineral Depos* 37:38–60
- Kesler SE, Issigonis MJ, Brownlow AH, Damon PE, Moore WJ, Northcote KE, Preto VA (1975) Geochemistry of biotites from mineralized and barren intrusive systems. *Econ Geol* 70:559–567
- Kilinc IA, Burnham CW (1972) Partitioning of chloride between a silicate melt and coexisting aqueous phase from 2 to 8 kilobars. *Econ Geol* 67:231–235
- Kroll T, Müller D, Seifert T, Herzig PM, Schneider A (2002) Petrology and geochemistry of the shoshonite-hosted Skouries porphyry Cu–Au deposit, Chalkidiki, Greece. *Mineral Depos* 37:137–144
- Kullerud K (1995) Chlorine, titanium and barium-rich biotites: factors controlling biotite composition and the implications for garnet-biotite geothermometry. *Contrib Miner Petrol* 120:42–59
- Large RR, Huston DL, McGoldrick PJ, Ruxton PA (1989) Gold distribution and genesis in Australian volcanogenic massive sulphide deposits and their significance for gold transport models. In: Keays RR, Ramsay WRH, Groves DI (eds) *The Geology of Gold Deposits: The Perspective in 1988*. *Econ Geol Monogr* 6:520–536
- Lesne P, Kohn SC, Blundy J, Witham F, Botcharnikov RE, Behrens H (2011) Experimental simulation of closed-system degassing in the system basalt–H₂O–CO₂–S–Cl. *J Petrol* 52:1737–1762

- Li Y, Audetat A (2013) Gold solubility and partitioning between sulfide liquid, monosulfide solid solution and hydrous mantle melts: implications for the formation of Au-rich magmas and crust-mantle differentiation. *Geochimica Cosmochimica Acta* 118:247–262
- Liang Y, Hoshino K (2015) Thermodynamic calculations of $\text{Au}_x\text{Ag}_{1-x}$ —fluid equilibria and their applications for ore-forming conditions. *Appl Geochem* 52:109–117
- Lofersky PJ, Ayuso RA (1995) Petrography and mineral chemistry of the composite Deboullie pluton, northern Maine, USA: implications for the genesis of Cu–Mo mineralization. *Chem Geol* 123:89–105
- Lowenstern JB (1994) Dissolved volatile concentrations in an ore-forming magma. *Geology* 22:893–896
- Lyubetskaya T, Korenaga J (2007) Chemical composition of Earth's primitive mantle and its variance: 1. Methods and results. *J Geophys Res* 112. <http://dx.doi.org/10.1029/2005JB004223>
- Magenheim AJ, Spivack AJ, Michael PJ, Gieskes JM (1995) Chlorine stable isotope composition of the oceanic crust: implications for Earth's distribution of chlorine. *Earth Planet Sci Lett* 131:427–432
- Mavrogenes JA, Scaillet B, Pichavant M, England RN (2006) The connection between high-K melts and Au deposits: evidence from natural and experimental systems. *Geochim Cosmochim Acta* 70:A404
- Melluso L, de Gennaro R, Fedele L, Franciosi L, Morra V (2012) Evidence of crystallization in residual, Cl–F-rich, apatitic, trachyphonolitic magmas and primitive Mg-rich basalt-trachyphonolite interaction in the lava domes of the Phlegrean Fields (Italy). *Geol Mag* 149:532–550
- Metrich N, Rutherford MJ (1992) Experimental study of chlorine behavior in hydrous silicic melts. *Geochim Cosmochim Acta* 56:607–616
- Müller D (1993) Shoshonites and potassic igneous rocks: indicators for tectonic setting and mineralization potential of modern and ancient terranes. Unpl. PhD Thesis, The University of Western Australia, Perth
- Müller D, Groves DI (1993) Direct and indirect associations between potassic igneous rocks, shoshonites and gold-copper deposits. *Ore Geol Rev* 8:383–406
- Müller D, Morris BJ, Farrand MG (1993) Potassic alkaline lamprophyres with affinities to lamproites from the Karinya Syncline, South Australia. *Lithos* 30:123–137
- Müller D, Heathersay PS, Groves DI (1994) The shoshonite porphyry Cu–Au association in the Goonumbra district, N.S.W., Australia. *Miner Petrol* 51:299–321
- Müller D, Franz L, Herzig PM, Hunt S (2001) Potassic igneous rocks from the vicinity of epithermal gold mineralization, Lihir Island, Papua New Guinea. *Lithos* 57:163–186
- Müller D, Herzig PM, Scholten JC, Hunt S (2002) Ladolam gold deposit, Lihir Island, Papua New Guinea: gold mineralization hosted by alkaline rocks. *Econ Geol Spec Publ* 9:367–382
- Müller D, Franz L, Petersen S, Herzig PM, Hannington MD (2003) Comparison between magmatic activity and gold mineralization at Conical Seamount and Lihir Island, Papua New Guinea. *Miner Petrol* 79:259–283
- Munoz JL (1984) F–OH and Cl–OH exchange in micas with applications to hydrothermal ore deposits. In: Bailey SW (ed) *Micas*. American Mineralogical Society, Michigan, *Reviews in Mineralogy* vol 13, pp 469–493
- Naumov VB, Kovalenko VI, Dorofeeva VA (1998) Fluorine concentration in magmatic melts: evidence from inclusions in minerals. *Geochem Int* 36:117–127
- Parry WT, Ballantyne GH, Wilson JC (1978) Chemistry of biotites and apatites from a vesicular quartz-lattice porphyry plug at Bingham, Utah. *Econ Geol* 73:1308–1314
- Peach CL, Mathez EA, Keays RR, Reeves SJ (1994) Experimentally determined sulphide melt-silicate melt partition coefficients for iridium and palladium. *Chem Geol* 117:361–377
- Richards JP (1990a) Petrology and geochemistry of alkaline intrusive at the Porgera gold deposit, Papua New Guinea. *J Geochem Explor* 35:141–199
- Richards JP (1990b) The Porgera gold deposit, Papua New Guinea: geology, geochemistry and geochronology. Unpl. Ph.D. thesis, The Australian National University, Canberra
- Richards JP (1995) Alkalic-type epithermal gold deposits—A review. In: Thompson JFH (ed) *Magmas, Fluids, and Ore Deposits*. Mineralogical Association of Canada, Toronto, *Short Course Handbook* vol 23, pp 367–400
- Richards JP (2009) Postsubduction porphyry Cu–Au and epithermal Au deposits: products of remelting of subduction-modified lithosphere. *Geology* 37:247–250
- Richards JP (2011) High Sr/Y arc magmas and porphyry Cu \pm Mo \pm Au deposits: just add water. *Econ Geol* 106:1075–1081
- Richards JP, McCulloch MT, Chappell BW, Kerrich R (1991) Sources of metals in the Porgera gold deposit, Papua New Guinea: evidence from alteration, isotope, and noble metal geochemistry. *Geochim Cosmochim Acta* 55:565–580
- Righter K, Dyar MD, Delaney JS, Vennemann TW, Hervig RL, King PL (2002) Correlations of octahedral cations with OH^- , O^{2-} , Cl^- , and F^- in biotite from volcanic rocks and xenoliths. *Am Miner* 87:142–153
- Rock NMS, Groves DI (1988) Do lamprophyres carry gold as well as diamonds? *Nature* 332:253–255
- Rock NMS, Duller P, Haszeldine S, Groves DI (1987) Lamprophyres as potential gold exploration targets: some preliminary observations and speculations. In: Ho SE, Groves DI (eds) *Recent Advances in Understanding Precambrian Gold Deposits*. Geology Department and University Extension, The University of Western Australia Publication vol 11, pp 271–286
- Roedder E (1984) Fluid Inclusions. *Mineralogical Society of America, Reviews in Mineralogy* 12:1–644
- Roegge JS, Logsdon MJ, Young HS, Barr HB, Borcsik M, Holland HD (1974) Halogens in apatites from the Providencia area, Mexico. *Econ Geol* 69:229–240

- Sarjoughian F, Kananian A, Ahmadian J, Murata M (2015) Chemical composition of biotite from the Kuh-e Dom pluton, Central Iran: implications for granitoid magmatism and related Cu–Au mineralization. *Arab J Geosci* 8:1521–1533
- Shabani AAT, Lalonde A, Whalen JB (2003) Composition of biotite from granitic rocks of the Canadian Appalachian orogen: a potential tectonomagmatic indicator? *Can Mineral* 41:1381–1396
- Shannon RD (1976) Revised effective ionic radii and systematic studies of interatomic distances in halides and chalcogenides. *Acta Crystallographica* 32:751–767
- Shinohara H (2009) A missing link between volcanic degassing and experimental studies on chloride partitioning. *Chem Geol* 263:51–59
- Sillitoe RH (2002) Some metallogenic features of gold and copper deposits related to alkaline rocks and consequences for exploration. *Mineral Depos* 37:4–13
- Solomon M, Groves DI (1994) *The Geology and Origin of Australia's Mineral Deposits* (vol 24). Clarendon Press, New York, Oxford Monographs in Geology and Geophysics, pp 951
- Spear JA (1984) Micas in igneous rocks. In: Bailey SW (ed) *Micas*. American Mineralogical Society, Michigan, *Reviews in Mineralogy* vol 13, pp 299–349
- Spooner ETC (1993) Magmatic sulphide/volatile interaction as a mechanism for producing chalcophile element-enriched, Archaean Au-quartz hydrothermal ore fluids. *Ore Geol Rev* 7:359–379
- Stanton RL (1994) Ore elements in arc lavas. Oxford Monographs in Geology and Geophysics, vol 29. Clarendon Press, New York, pp 391
- Stollery G, Borcsik M, Holland HD (1971) Chlorine in intrusions: a possible prospecting tool. *Econ Geol* 66:361–367
- Sun W, Arculus RJ, Kamenetsky VS, Binns RA (2004) Release of gold-bearing fluids in convergent margin magmas prompted by magnetite crystallization. *Nature* 431:975–978
- Sun WD, Liang HY, Ling MX, Zhan MZ, Ding X, Zhang H, Yang XY, Li YL, Ireland TR, Wei QR, Fan WM (2013) The link between reduced porphyry copper deposits and oxidized magmas. *Geochim Cosmochim Acta* 103:263–275
- Tatsumi Y, Koyaguchi T (1989) An absarokite from a phlogopite lherzolite source. *Contrib Miner Petrol* 102:34–40
- Taylor WR, Rock NMS, Groves DI, Perring CS, Golding SD (1994) Geochemistry of Archaean shoshonitic lamprophyres from the Yilgarn Block, Western Australia: Au abundance and association with gold mineralization. *Appl Geochem* 9:197–222
- Teiber H, Scharer M, Marks MAW, Arzamastev AA, Wenzel T, Markl G (2015) Equilibrium partitioning and subsequent re-distribution of halogens among apatite-biotite-amphibole assemblages from mantle-derived plutonic rocks: complexities revealed. *Lithos* 223:221–237
- Thompson TB, Trippel AD, Dwelley PC (1985) Mineralized veins and breccias of the Cripple Creek District, Colorado. *Econ Geol* 80:1669–1688
- Ulrich T, Mavrogenes J (2008) An experimental study of the solubility of molybdenum in H₂O and KCl–H₂O solutions from 500 °C to 800 °C, and 150 to 300 MPa. *Geochim Cosmochim Acta* 72:2316–2330
- Vigneresse JL (2009) Evaluation of the chemical reactivity of the fluid phase through hard-soft acid-base concepts in magmatic intrusions with applications to ore generation. *Chem Geol* 263:69–81
- Vigneresse JL, Truche L, Chattaraj PK (2014) Metal (copper) segregation in magmas. *Lithos* 209:462–470
- Vukadinovic D, Edgar AD (1993) Phase relations in the phlogopite-apatite system at 20 kbar—Implications for the role of fluorine in mantle melting. *Contrib Miner Petrol* 114:247–254
- Wang L, Marks MAW, Keller J, Markl G (2014) Halogen variations in alkaline rocks from the Upper Rhine Graben (SW Germany): insights into F, Cl and Br behavior during magmatic processes. *Chem Geol* 380:133–144
- Webster JD (1992) Water solubility and chlorine partitioning in Cl-rich granitic systems: effects of melt composition at 2 kbar and 800 °C. *Geochim Cosmochim Acta* 56:679–687
- Webster JD (1997) Chloride solubility in felsic melts and the role of chloride in magmatic degassing. *J Petrol* 38:1793–1807
- Webster JD (2004) The exsolution of magmatic hydroalaline chloride liquids. *Chem Geol* 210:33–48
- Webster JD, Holloway JR (1988) Experimental constraints on the partitioning of Cl between topaz rhyolite melt and H₂O and H₂O+CO₂ fluids: implications for granitic differentiation and ore deposition. *Geochim Cosmochim Acta* 52:2091–2105
- Webster JD, Holloway JR (1990) Partitioning of F and Cl between magmatic hydrothermal fluids and highly evolved granitic magmas. In: Stein HJ, Hannah JL (eds) *Ore-bearing granite systems; petrogenesis and mineralizing processes*. Geological Society of America Special Paper vol 246, pp 21–33
- Webster JD, Tappen CM, Mandeville CW (2009) Partitioning behavior of chlorine and fluorine in the system apatite-melt-fluid. II: felsic silicate systems at 200 MPa. *Geochim Cosmochim Acta* 73:559–581
- Webster JD, Goldoff B, Sintoni MF, Shimizu N, Vivo BD (2014) C–O–H–Cl–S–F volatile solubilities, partitioning, and mixing in phonolithic-trachytic melts and aqueous-carbonic vapor ± saline liquid at 200 MPa. *J Petrol* 55:2217–2248
- White WH, Bookstrom AA, Kamilli RJ, Ganster MW, Smith RP, Ranta DE, Steinger RC (1981) Character and origin of Climax-type molybdenum deposits. *Economic Geology 75th Anniversary Volume*: 270–316
- Williams-Jones AE, Heinrich CA (2005) Vapor transport of metals and the formation of magmatic-hydrothermal ore deposits. *Econ Geol* 100:1287–1312

- Wyman D, Kerrich R (1989) Archaean lamprophyre dykes of the Superior Province, Canada: distribution, petrology and geochemical characteristics. *J Geophys Res* 94:4667–4696
- Yang K, Bodnar RJ (1994) Magmatic-hydrothermal evolution in the “bottoms” of porphyry copper systems: evidence from silicate melt and aqueous fluid inclusions in granitoid intrusions in the Gyeongsang Basin, South Korea. *Int Geo Rev* 36:608–628
- Yang XM, Lentz DR (2005) Chemical composition of rock-forming minerals in gold-related granitoid intrusions, southwestern New Brunswick, Canada: implications for crystallization conditions, volatile exsolution, and fluorine-chlorine activity. *Contrib Miner Petrol* 150:287–305
- Zajacz Z, Seo JH, Candela PA, Piccoli PM, Heinrich CA, Guillong M (2010) Alkali metals control the release of gold from volatile-rich magmas. *Earth Planet Sci Lett* 297:50–56
- Zajacz Z, Candela PA, Piccoli PM, Wälle M, Sanchez-Valle C (2012) Gold and copper in volatile saturated mafic to intermediate magmas: solubilities, partitioning, and implications for ore deposit formation. *Geochimica Cosmochimica Acta* 91:140–159
- Zellmer GF, Edmonds M, Straub SM (2015) The role of volatiles in the genesis, evolution and eruption of arc magmas. *Geological Society Special Publication* vol 410, pp 292
- Zhang M, Suddaby P, Thompson RN, Thirlwall MF, Menzies MA (1995) Potassic volcanic rocks in NE China: geochemical constraints on mantle source and magma genesis. *J Petrol* 36:1275–1303

10.1 Introduction

Successful exploration for the next generation of major copper-gold deposits is likely to require a greater emphasis on covered terranes (Hronsky et al. 2012; Sillitoe, pers. comm., 2013). Hence, regional-scale target generation will become increasingly more important in mineral exploration in the next decade. However, such predictive targeting capability requires a generic, regional-scale understanding of copper and gold metallogeny and its controls (Hronsky et al. 2012). The definition of prospective igneous belts with a fertile geochemistry is an essential step in target generation (e.g. the well endowed Eocene-Oligocene igneous belt in northern Chile). The extension of these prospective belts can be delineated under cover by the interpolation of limited outcrops in deep cross-cutting valleys or in exploration drill holes.

Some of the data and interpretations discussed in previous chapters of this book can be used to define the most prospective igneous belts in regional-scale target generation and the exploration for world-class gold and copper-gold deposits, since many of these deposits are spatially associated with, or hosted by, potassic igneous rocks (Mutschler et al. 1985; Müller and Groves 1993; Müller 2002; Sillitoe 2002; Bi et al. 2004; Hu et al. 2004, 2015; Kouzmanov et al. 2009; Soloviev and Krivoschenkov 2011; Fornadel et al. 2012; Hronski et al. 2012; Lehmann et al. 2013; Lu et al. 2013a; Soloviev et al.

2013; Witt et al. 2014; Bissig and Cooke 2014; Chai et al. 2014; Maghsoudi et al. 2014; Soloviev 2014a, b, 2015; Xu et al. 2014, 2015; Zhao et al. 2014a, b; Heidari et al. 2015; Jamali and Mehrabi 2015; Shafaroudi et al. 2015). The points listed below may be particularly useful.

10.2 Target Generation

10.2.1 Composition of Host Rocks

Rocks of the alkaline suite are generally more prospective for giant and bonanza gold deposits than normal calc-alkaline andesites (Müller and Groves 1993; Sillitoe 1993, 1997, 2002). Specifically, four of the nine largest epithermal gold-silver deposits and four of the ten largest porphyry copper-gold deposits are associated with high-K calc-alkaline and shoshonitic rocks (Hedenquist, pers. comm., 1999; Sillitoe 1997, 2002). The high-K igneous rocks only comprise between 5 and 10 vol% of arc rocks, yet are associated with 40 % of the largest epithermal and porphyry deposits, clearly indicating their selective importance.

Epithermal gold and porphyry copper-gold deposits are abundant in convergent-plate margin settings, reflecting their direct genetic association with high-K calc-alkaline and shoshonitic magmatism (Clark 1993; Müller 2002; Soloviev 2014a). The occurrence of potassic igneous rocks clearly indicates a potentially high prospectivity

for epithermal gold and porphyry copper-gold deposits in that area (Müller and Groves 1993). These rocks are defined by high K_2O (>1 wt% at 50 wt% SiO_2), high Ce/Yb ratios (>15), high LILE and low HFSE (see Chaps. 2, and 3) contents. Fertile potassic igneous rocks also contain high contents of volatiles such as H_2O , Cl and F (see Chap. 9). Importantly, from a field exploration viewpoint, high volatile contents of the rocks can commonly be recognized in hand specimen by their porphyritic texture, with abundant hydrous phenocrysts of biotite, phlogopite, and/or amphibole (see Figs. 6.9, 6.14, 6.16, 6.18, 6.20, 6.29, and 6.31). Modern studies (Richards 2011; Chiaradia et al. 2012; Loucks 2014; Lu et al. 2015) suggest that high H_2O contents of igneous rocks are also reflected in high whole-rock Sr/Y ratios (>35). During fractional crystallization, Y behaves as a compatible element in hornblende phenocrysts and is depleted from the melt as hornblende and pyroxene accumulate at the bottom of the magma chamber, while Sr is incompatible and remains in the residual melt (Richards 2011; Loucks 2014; Lu et al. 2015), at least until the onset of plagioclase fractionation. In addition, due to their high volatile contents, ore-related potassic igneous rocks may be characterized by the occurrence of interconnected miarolitic cavities (Candela 1997; Ohtani 2001). The hypabyssal lamprophyre intrusions are typified by a lack of plagioclase phenocrysts, reflecting the relatively high water content of the magmas, which suppressed the crystallization of feldspar (Carmichael et al. 1996). However, extrusive high-K rocks can have plagioclase phenocrysts. Potassic igneous rocks are also characterized microscopically by apatite microphenocrysts and a groundmass that is dominated by potassic feldspar or leucite.

10.2.2 Tectonic Setting

The definition of the tectonic setting in which the high-K host rocks have been generated is essential, since known epithermal gold and/or porphyry copper-gold mineralization appears to

be restricted to the three subduction-related tectonic settings: continental, postcollisional, and late oceanic arcs. However, there is also evidence for an association between iron-oxide-Cu-Au (IOCG) mineralization and volatile-rich potassic igneous rocks in within-plate settings (e.g. Olympic Dam, South Australia: see Chap. 7).

The potassic igneous rocks themselves can be used to help discriminate the tectonic setting, as discussed in Chap. 3, via the use of hierarchical chemical discrimination diagrams (Figs. 3.9 and 3.10).

For target generation, the presence of caldera settings (e.g. Emperor), deep-seated structural lineaments (e.g. Porgera) or their intersections (e.g. Olympic Dam) is favourable, as they represent potential *loci* of mineralization. Such lithosphere-scale structures are vital to allow the focused transport of fertile magmas and/or fluids to the upper crust (Hronsky et al. 2012; Korschv and Doublier 2015). Hence, it may be no coincidence that numerous significant copper and gold deposits are spatially associated with crustal- to lithosphere-scale lineaments and the intersection of orogen-parallel structures of this style with transfer structures at a high-angle to the orogen trend (O'Driscoll 1983; Richards et al. 2001). Such structural intersections are likely to provide a highly permeable pipe-like connection between the mantle and the upper crust (Hronsky et al. 2012).

In continental and oceanic arc-settings, additional prospective exploration criteria are subducted seamounts that commonly result in kinks or flexures of the subducting oceanic slab, and a resulting change of the subduction angle along both sides of the flexure (e.g. the “flat-slab zone” in the central Andes; Kay et al. 1987, 2005). Progressive subduction of kinks or flexures in the downgoing plate might eventually lead to tearing of the oceanic slab (Kerrick et al. 2000; Garwin 2002; Müller et al. 2002a), thus promoting the uprise of deep asthenospheric mantle melts that are normally blocked off by the downgoing slab (Müller 2003; Logan and Mihalynuk 2014; Sigoyer et al. 2014; Sect. 6.4.1). Hence, slab

tears may play a dominant role in the formation of porphyry copper-gold deposits globally (Logan and Mihalynuk 2014).

10.3 Prospect Evaluation

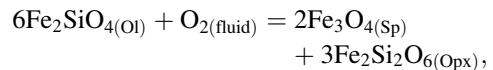
10.3.1 Favourable Tectonic Elements on the Prospect Scale

There is considerable evidence that many epithermal gold and porphyry copper-gold deposits which have been generated in late oceanic arcs are located either within, or at the margin of, collapsed caldera structures (cf. Soeria-Atmadja et al. 1998). Examples are the Emperor gold deposit and the Dinkidi and Northparkes (Goonumbla) copper-gold deposits (Müller and Groves 1993). In addition, the intersections of major structures may be favourable tectonic elements on the prospect scale, as, for example, at Emperor (Setterfield 1991). Other major structures which favour mineralization (Sillitoe 1993) are high-angle reverse faults (e.g. El Indio), strike-slip faults (e.g. epithermal gold deposit at Baguio, Philippines), and reactivated collisional sutures (e.g. Porgera). The mineralization in Upper Eocene to Lower Oligocene porphyry-copper deposits in northern Chile (e.g. Chuquicamata, El Salvador, La Escondida, Zaldivar) appears to be controlled by a major dextral transpressive structure (Domeyko Fault; Clark 1993; Arriagada et al. 2000; Palacios et al. 2007). Field studies by Arriagada et al. (2000) emphasize the importance of extensional structures caused by clockwise tectonic rotations for mineral exploration in the north Chilean Andes. Thus, both synvolcanic structures and post- to late-volcanic structures may control mineralization in prospective environments.

10.3.2 High Oxygen Fugacities (fO_2) of the Magmas

Oxygen fugacity is defined as the activity (or partial pressure) of O_2 within a system (Frost 1991) and represents a fundamental variable,

such as pressure and temperature, that provides a measure of the systems redox potential at equilibrium (Lee et al. 2005). The fO_2 is commonly determined indirectly, by O_2 thermobarometry, wherein the activities of the different valence states of a redox-sensitive element in minerals (or glasses) are measured (Lee et al. 2005). In homogeneous, single-phase, systems (e.g. magma) experimentally calibrated relationships between fO_2 and the activities of Fe^{3+} and Fe^{2+} in a glass are typically used to obtain the fO_2 of a magma just prior to quenching (Kress and Carmichael 1991). In a heterogeneous, multi-phase, system, the fO_2 of last equilibration is recorded by the distribution of Fe^{3+} in different system phases (Lee et al. 2005) according to the reaction:



where fayalite, magnetite, and ferrosilite occur in solid solution with olivine, spinel, and orthopyroxene, respectively (e.g. Ballhaus et al. 1991). During this reaction, initially a free SiO_2 phase is formed, which is instable under mantle conditions, and hence, reacts to orthopyroxene (Franz, pers. comm., 2001).

This barometric method of inferring fO_2 has been widely applied to mantle xenoliths (e.g. Franz et al. 2002; Franz and Romer 2010), lavas and intrusions (e.g. Müller et al. 2001, 2003). As the oxygen geobarometer of Ballhaus et al. (1991) is restricted to spinels with TiO_2 contents of <1 wt% (Ballhaus, pers. comm., 2000), the oxygen fugacity of titanomagnetite-bearing intrusive rocks should be determined using the QUILF program of Lindsley and Frost (1992) version of Andersen et al. (1993).

An alternative method to estimate the fO_2 of igneous rocks is promoted by Ballard et al. (2002) because the conventional use of quantitative oxygen barometers based on Fe–Ti oxides can be limited by the overprint of hydrothermal alteration. The authors suggest instead the use of laser ablation ICP-MS facilities, permitting the calculation of Ce^{4+}/Ce^{3+} ratios of zircons using a lattice-strain model for mineral-melt partitioning

of Ce^{4+} and Ce^{3+} , respectively. As zircon occurs in most calc-alkaline and shoshonitic intrusions and is resistant to subsolidus alteration, zircon $\text{Ce}^{4+}/\text{Ce}^{3+}$ ratios provide a useful tool to estimate the $f\text{O}_2$ of igneous rocks (Ballard et al. 2002). Their pilot study on zircons from composite intrusions hosting the El Abra porphyry copper deposit in Chile reveal that the oxygen fugacities of intrusive complexes increase with progressing fractionation from older, basic, to younger, felsic, units. Within this sequence (Ballard et al. 2002), porphyry copper mineralization is genetically associated with intrusions with high zircon $\text{Ce}^{4+}/\text{Ce}^{3+}$ ratios (>300). More recent work (Burnham and Berry 2012) confirms that the partition coefficient of Ce in zircon varies systematically with $f\text{O}_2$ and that porphyry copper mineralization is preferentially hosted by intrusions with high $\text{Ce}^{4+}/\text{Ce}^{3+}$ ratios (Xu et al. 2015).

The oxidation state of the lithospheric upper mantle is heterogeneous, with a variation in the oxygen fugacity ($f\text{O}_2$) of at least four log units (Ballhaus et al. 1990; Ballhaus 1993). Lithosphere above subduction zones is commonly more oxidized than other mantle regimes either because of its infiltration by slab-derived fluids generated from dehydration and decarbonation reactions (Arculus 1985; Haggerty 1990; Lange and Carmichael 1990; Mungall 2002; Sun et al. 2004; Richards 2011; Chen et al. 2015) or due to the effect of later crustal processes, including protracted fractionation and degassing of volatile-rich magmas (Humphreys et al. 2015). Recent studies on oxygen isotopes of zircons from shoshonitic intrusions collected in western Yunnan, China, reveal much higher $\delta^{18}\text{O}$ values (6.26–7.05 ‰) than normal mantle material, suggesting some ^{18}O enrichment during earlier subduction-related metasomatism of their lithospheric mantle source (Lu et al. 2013b). High $f\text{O}_2$ in potassic igneous rocks are also suggested by experimental studies (e.g. Li and Audetat 2013). Phlogopite phenocrysts from subduction-related potassic igneous rocks have the highest $\text{Fe}^{3+}/\text{Fe}^{\text{T}}$ ratios (0.77–0.87), which is consistent with the high magmatic $f\text{O}_2$ inferred for these magmas (Feldstein et al. 1996). The dissociation of H_2O and the release of H should enrich the system in oxygen at an early

stage before the onset of partial melting (Abdel-Rahman 1994). However, experimental studies by Moore et al. (1995) indicate that dissolved water does not measurably affect the redox state of iron in natural melts. Therefore, the high oxygen fugacities, which are commonly recorded in H_2O -rich magmas (e.g. Lange and Carmichael 1990), are probably a record of other processes that have imposed a high $f\text{O}_2$ upon the melt, and are not a reflection of the amount of dissolved water (Moore et al. 1995). For example, studies by Dixon et al. (1997) show that the lowest degree partial melts have the highest relative $f\text{O}_2$ and this decreases with increasing extent of melting. The most oxidized basaltic melts are potassic lamprophyres such as minettes from mature continental arcs (Ballhaus 1993) and primitive trachybasalts from oceanic arcs (Frost and Lindsley 1992; Müller et al. 2001). While the $f\text{O}_2$ of low-K tholeiites (MORB) ranges between -2.0 and $+0.7$ log units from the FMQ buffer (Lee et al. 2005; Rowe et al. 2009), high-K oceanic arc basalts typically have high $f\text{O}_2$ ranging from $+0.3$ to $+6.0$ log units ΔFMQ (Lee et al. 2005). High $f\text{O}_2$ ($+1.4$ to $+4.8$ log units ΔFMQ) are also recorded for potassic igneous rocks from a late oceanic arc setting at Lihir Island (Müller et al. 2001), and Conical Seamount ($+0.7$ to $+2.5$ log units ΔFMQ), Papua New Guinea (Müller et al. 2003). Most authors agree that oxidation of the upper mantle above subduction zones is related to the metasomatic addition of oxidized fluids carrying sulphates and/or sediments derived from dehydration of the subducting slab (Carmichael 1991; Schmidt and Poli 1998; Stern 2002; Hou et al. 2015; Richards 2015). In fact, most metasomatizing processes are likely to be oxidizing (McGuire et al. 1991; McCammon et al. 2001). Some authors (e.g. Holloway 2004) hypothesized that rapidly crystallized magmas may undergo an auto-oxidation process in which ferrous iron is oxidized by water to generate magnetite and H_2 , the latter of which is free to leave the system as a fluid or by de-gassing. The loss of H_2 will then result in an increase in the ferric iron content (Holloway 2004).

There is also a positive correlation between the average volatile content in basalts and their calculated $f\text{O}_2$. Thus, those basalts from oceanic arcs

which are most oxidized also have the highest abundances of volatile phases such as magmatic water (Ballhaus 1993), and Cl and F (Müller et al. 2001, 2003). More recent studies (Rowe et al. 2009) reveal that oxygen fugacity is positively correlated with fluid-mobile trace element and LREE contents in basalts. Moreover, melt inclusions from shoshonitic lavas show increasing fO_2 and trace element abundances closer to the subduction trench (Rowe et al. 2009). Studies by Lee et al. (2005) suggest a positive correlation between fO_2 and V/Sc ratios. Hence, elevated oxygen fugacities of arc lavas exceeding +1.0 log unit ΔFMQ are reflected in high whole-rock V/Sc ratios (>12; Lee et al. 2005). However, the interpretation of V/Sc ratios is not straightforward as high V/Sc ratios could also be caused by residual garnet in the upper mantle sources of these magmas (Lee et al. 2005).

At magmatic temperatures, fO_2 is a major factor controlling element partitioning (e.g. Ballhaus 1995; Blevin and Chappell 1996; Lee et al. 2005; Rowe et al. 2009). At high values of fO_2 , iron is partially transformed into Fe^{3+} and oxide minerals such as magnetite crystallize in preference to Fe^{2+} -bearing silicate minerals (Haggerty 1990). The high alkali content of potassic melts increases their Fe^{3+}/Fe^{2+} ratios, thus resulting in a higher oxygen fugacity (Wyborn 1994). A high fO_2 of the magmas, as indicated by significant concentrations of primary magnetite (>5 vol.%) in their crystallized products, favours precipitation of large quantities of gold (Sillitoe 1979). So it is no coincidence that the potassic host rocks of many epithermal gold and porphyry copper-gold deposits are characterized by appreciable magnetite. Examples are the high-K rocks hosting the porphyry copper-gold deposits at Bajo de la Alumbrera, Argentina (Stults 1985), Northparkes (Goonumbla), New South Wales, Australia (Müller et al. 1994), Grasberg, Indonesia (Kavaliaris, pers. comm., 1996), Ladolam, Lihir Island, Papua New Guinea (Müller et al. 2001, 2002b), and Marian, Philippines (Sillitoe 1979), which all contain up to 5 vol.% magnetite. These magnetite-rich igneous rocks result in a high magnetic susceptibility, generating magnetic responses of up to 4500 gammas, and may,

therefore, be identified in airborne magnetic surveys. However, in areas where the rocks are strongly affected by hydrothermal alteration, the effects of supergene martitization (i.e. alteration of magnetite to haematite) can minimize this effect in the vicinity of mineralization.

At constant temperatures, as fO_2 increases, the concentration of dissolved sulphide (S^{2-}) in the melt decreases, whereas the dissolved sulphate (SO_4^{2-}) increases as sulphur is oxidized (Carmichael and Ghiorso 1986; Campbell et al. 1998; Ballard et al. 2002; Richards 2009, 2011). Thus, the potential for precious metal segregation into magmatic sulphide phases is reduced (Candela 1992; Sun et al. 2004; Richards 2009; Sect. 5.2). At high fO_2 , sulphate phases have a much higher solubility in silicate melts than sulphides (Carroll and Rutherford 1985; Ballard et al. 2002). The transition between sulphide-dominant and sulphate-dominant melt compositions is quite abrupt, occurring over about one log unit of oxygen fugacity (Matthews et al. 1999). If the sulphide concentration in the melt is reduced, gold and copper will be concentrated in the volatile-enriched top part of the magma chamber (Müller et al. 2002a). Once volatile saturation occurs during secondary boiling, the magma chamber releases pulses of metal- and volatile-enriched melts capable of forming porphyry copper-gold mineralization in the upper crust (Richards 1995; Müller et al. 2002a). In agreement with this, Kesler (1997) and, more recently, Tang et al. (2010) have pointed out that alkaline magmas also can dissolve more sulphate, thus making it unlikely for the magma to become saturated with metal sulphides. Alkali-rich, basic magmas, particularly potassic melts, may contain sulphate minerals (e.g. anhydrite) and are, therefore apparently considerably more oxidized than, for example, tholeiites (Haggerty 1990; Tang et al. 2010; Hou et al. 2015). The abundance of late anhydrite veins in the host rocks at Ladolam (Sect. 6.3.1), Grasberg (Sect. 6.5.1), and Porgera (Standing, pers. comm., 1993; Sect. 6.5.3) gold deposits may be consistent with a high fO_2 for these potassic intrusions, and the occurrence of anhydrite may be a further guide to mineralization at the prospect scale.

10.3.3 Elevated Halogen Contents of the Magmas

The important role of halogens, such as Cl and F, for the transport of metals in ore deposits related to igneous intrusions is discussed in Chap. 9. Experimental studies of Cl partitioning in granitic systems suggest that the strongest enrichment of magmatic-hydrothermal fluids in Cl and ore metals complexed with Cl will most likely be in fluids exsolved from magmas that are relatively enriched in K₂O (Webster 1992; Chevychelov et al. 2008; Melluso et al. 2012; Webster et al. 2014; Chen et al. 2015). The halogen contents of mica phenocrysts from high-K igneous suites may be used as a measure of gold-copper mineralization potential in continental, postcollisional, and late oceanic arcs. In exploration target generation, those potassic igneous rocks whose mica phenocrysts have Cl contents >0.04 wt% and F contents >0.5 wt% can be regarded as prospective (Müller and Groves 1993; Müller et al. 2001; Kroll et al. 2002; Yang and Lentz 2005; Sarjoughian et al. 2015). However, caution must be used in universal application of the halogen contents of high-K rocks as a tool in mineral exploration because such rocks analyzed to date from within-plate settings also have high halogen contents, although no direct genetic relationships to epithermal gold and porphyry copper-gold deposits have yet been established (Müller and Groves 1993). An exception might be iron-oxide copper-gold (IOCG) deposits derived in within-plate tectonic settings (e.g. Olympic Dam; Sect. 7.2.2).

References

- Abdel-Rahman AM (1994) Nature of biotites from alkaline, calc-alkaline and peraluminous magmas. *J Petrol* 35:525–541
- Andersen DJ, Lindsley DH, Davidson PM (1993) QUILF: a Pascal program to assess equilibria among Fe–Mg–Mn–Ti oxides, pyroxenes, olivine, and quartz. *Comput Geosci* 19:1333–1350
- Arculus RJ (1985) Oxidation status of the mantle: past and present. *Ann Rev Earth Planet Sci* 13:75–95
- Arriagada C, Roperch P, Mpodozis C (2000) Clockwise block rotations along the eastern border of the Cordillera de Domeyko, northern Chile (22°45′–23°30′S). *Tectonophysics* 326:153–171
- Ballard JR, Palin JM, Campbell IH (2002) Relative oxidation states of magmas inferred from Ce(IV)/Ce(III) in zircon: application to porphyry copper deposits of northern Chile. *Contrib Miner Petrol* 144:347–364
- Ballhaus C (1993) Redox states of lithospheric and asthenospheric upper mantle. *Contrib Miner Petrol* 114:331–348
- Ballhaus C (1995) Is the upper mantle metal-saturated? *Earth Planet Sci Lett* 132:75–86
- Ballhaus C, Berry RF, Green DH (1990) Oxygen fugacity controls in the Earth's upper mantle. *Nature* 348:437–440
- Ballhaus C, Berry RF, Green DH (1991) High pressure experimental calibration of the olivine-orthopyroxene-spinel oxygen geobarometer: implications for the oxidation state of the upper mantle. *Contrib Miner Petrol* 107:27–40
- Bi X, Hu R, Cornell DH (2004) The alkaline porphyry associated Yao'an gold deposit, Yunnan, China: rare earth element and stable isotope evidence for magmatic-hydrothermal ore formation. *Mineral Depos* 39:21–30
- Bissig T, Cooke DR (2014) Introduction to the special issue devoted to alkali porphyry Cu–Au and epithermal Au deposits. *Econ Geol* 109:819–825
- Blevin PL, Chappell BW (1996) Controls on the distribution and character of the intrusive-metallogenic provinces of Eastern Australia. *Geol Soc Austr* 41:42 Abstracts
- Burnham AD, Berry AJ (2012) An experimental study of trace element partitioning between zircon and melt as a function of oxygen fugacity. *Geochim Cosmochim Acta* 95:196–212
- Campbell IH, Compston DM, Richards JP, Johnson JP, Kent AJR (1998) Review of the application of isotopic studies to the genesis of Cu–Au mineralization at Olympic Dam and Au mineralization at Porgera, the Tennant Creek district and Yilgarn Craton. *Aust J Earth Sci* 45:201–218
- Candela PA (1992) Controls on ore metal ratios in granite-related ore systems: an experimental and computational approach. *Trans Royal Soc Edinburgh, Earth Sci* 83:317–326
- Candela PA (1997) A review of shallow, ore-related granites: textures, volatiles, and ore metals. *J Petrol* 38:1619–1633
- Carmichael ISE (1991) The redox states of basic and silicic magmas: a reflection of their source regions? *Contrib Mineral Petrol* 106:129–141

- Carmichael ISE, Ghiorso MS (1986) Oxidation-reduction relations in basic magma: a case for homogeneous equilibria. *Earth Planet Sci Lett* 78:200–210
- Carmichael ISE, Lange RA, Luhr JF (1996) Quaternary minettes and associated volcanic rocks of Mascota, western Mexico: a consequence of plate extension above a subduction modified mantle wedge. *Contrib Miner Petrol* 124:302–333
- Carroll MR, Rutherford MJ (1985) Sulphide and sulphate saturation in hydrous silicate melts. In: Proceedings of the 15th lunar and planetary science conference, Part 2. *Journal of Geophysical Research Supplement* vol 90, pp C601–C612
- Chai P, Sun JG, Xing SW, Men LJ, Han JL (2014) Early Cretaceous arc magmatism and high-sulphidation epithermal Au and porphyry Cu–Au mineralization in Yanbian area, Northeast China: the Duhuangling example. *International Geology Review*. doi:10.1080/00206814.2014.960013
- Chen JL, Xu JF, Wang BD, Yang ZM, Ren JB, Yu HX, Liu H, Feng Y (2015) Geochemical differences between subduction- and collision-related copper-bearing porphyries and implications for metallogenesis. *Ore Geol Rev* 70:424–437
- Chevychelov VY, Botcharnikov RE, Holtz F (2008) Partitioning of Cl and F between fluid and hydrous phonolitic melt of Mt. Vesuvius at 850–1000 °C and 200 MPa. *Chem Geol* 256:172–184
- Chiaradia M, Ulianov A, Kouzmanov K, Beate B (2012) Why large porphyry Cu deposits like high Sr/Y magmas? *Nature Scientific Reports* 2:685. doi:10.1038/srep00685
- Clark AH (1993) Are outsize porphyry copper deposits either anatomically or environmentally distinctive? In: Whiting BH, Hodgson CJ, Mason R (eds) *Giant Ore Deposits*. *Econ Geol Spec Publ* 2:213–283
- Dixon JE, Clague DA, Wallace P, Poreda R (1997) Volatiles in alkali basalts from the North Arch volcanic field, Hawaii: extensive degassing of deep submarine-erupted alkali series lavas. *J Petrol* 38:911–939
- Feldstein SN, Lange RA, Vennemann T, O'Neil JR (1996) Ferric-ferrous ratios, H₂O contents and D/H ratios of phlogopite and biotite from lavas of different tectonic regimes. *Contrib Miner Petrol* 126:51–66
- Fornadel AP, Voudouris PC, Spry PG, Melfos V (2012) Mineralogical, stable isotope, and fluid inclusion studies of spatially related porphyry Cu and epithermal Au–Te mineralization, Fakos Peninsula, Limnos Island, Greece. *Mineral Petrol* 105:85–111
- Franz L, Romer RL (2010) Different styles of metasomatic veining in ultramafic xenoliths from the TUBAF seamount (Bismarck microplate, Papua New Guinea). *Lithos* 114:30–53
- Franz L, Becker KP, Kramer W, Herzig PM (2002) Metasomatic mantle xenoliths from the Bismarck Microplate (Papua New Guinea)—Thermal evolution, geochemistry and extent of slab-induced metasomatism. *J Petrol* 43:315–343
- Frost BR (1991) Introduction to oxygen fugacity and its petrologic importance. In: Lindsley DH (ed) *Oxide minerals: petrologic and magnetic significance*. Mineralogical Society of America, *Reviews in Mineralogy* vol 25, pp 1–9
- Garwin S (2002) The geologic setting of intrusion-related hydrothermal systems near the Batu Hijau porphyry copper-gold deposit, Sumbawa, Indonesia. *Econ Geol Spec Publ* 9:333–366
- Haggerty SE (1990) Redox state of the continental lithosphere. In: Menzies MA (ed) *Continental Mantle*. Clarendon Press, Oxford, pp 87–109
- Heidari SM, Daliran F, Paquette J-L, Gasquet D (2015) Geology, timing, and genesis of the high sulphidation Au (–Cu) deposit of Touzlar, NW Iran. *Ore Geol Rev* 65:460–486
- Holloway JR (2004) Redox reactions in seafloor basalts: possible insights into silicic hydrothermal systems. *Chem Geol* 210:225–230
- Hou Z, Yang Z, Lu Y, Kemp A, Zheng Y, Li Q, Tang J, Yang Z, Duan L (2015) A genetic linkage between subduction- and collision-related porphyry Cu deposits in continental collision zones. *Geology* 43:247–250
- Hronsky JMA, Groves DI, Loucks RR, Begg GC (2012) A unified model for gold mineralization in accretionary orogens and implications for regional-scale exploration targeting methods. *Mineral Depos* 47:339–358
- Hu RZ, Burnard PG, Bi XW, Zhou MF, Pen JT, Su WC, Wu KX (2004) Helium and argon isotope geochemistry of alkaline intrusion-associated gold and copper deposits along the Red River–Jinshajiang fault belt, SW China. *Chem Geol* 203:305–317
- Hu YB, Liu JQ, Ling MX, Ding W, Liu Y, Zartman RE, Ma XF, Liu DY, Zhang CC, Sun SJ, Zhang LP, Wu K, Sun WD (2015) The formation of Qulong adakites and their relationship with porphyry copper deposit: geochemical constraints. *Lithos* 223:60–80
- Humphreys MCS, Brooker RA, Fraser DG, Burgisser A, Mangan MT, McCammon C (2015) Coupled interactions between volatile activity and Fe oxidation state during arc crustal processes. *J Petrol* 56:795–814
- Jamali H, Mehrabi B (2015) Relationships between arc maturity and Cu–Mo–Au porphyry and related epithermal mineralization at the Cenozoic Arasbaran magmatic belt. *Ore Geol Rev* 65:487–501
- Kay SM, Maksiyev V, Moscoso R, Mpodozis C, Nasi C (1987) Probing the evolving Andean lithosphere: mid-late Tertiary magmatism in Chile (29°–30°30'S) over the modern zone of subhorizontal subduction. *J Geophys Res* 92:6173–6189
- Kay SM, Godoy E, Kurtz A (2005) Episodic arc migration, crustal thickening, subduction erosion, and magmatism in the south-central Andes. *Geol Soc Am Bull* 117:67–88
- Kerrick R, Goldfarb R, Groves DI, Garwin S (2000) The geodynamics of world-class gold deposits: characteristics, space-time distribution, and origins. *Econ Geol Rev* 13:501–551

- Kessler SE (1997) Metallogenic evolution of convergent margins: selected ore deposit models. *Ore Geol Rev* 12:153–171
- Korschv RJ, Doublier MP (2015) Major crustal boundaries of Australia, and their significance in mineral systems targeting. *Ore Geol Rev* (in press)
- Kouzmanov K, Moritz R, von Quadt A, Chiaradia M, Peytcheva I, Fontignie D, Ramboz C, Bogdanov K (2009) Late Cretaceous porphyry Cu and epithermal Au–Cu association in the southern Panagyurishte District, Bulgaria: the paired Vlaykov Vruh and Elshitsa deposits. *Mineral Depos* 44:611–646
- Kress VC, Carmichael ISE (1991) The compressibility of silicate liquids containing Fe_2O_3 and the effect of composition, temperature, oxygen fugacity and pressure on their redox states. *Contrib Miner Petrol* 108:82–92
- Kroll T, Müller D, Seifert T, Herzig PM, Schneider A (2002) Petrology and geochemistry of the shoshonite-hosted Skouries porphyry Cu–Au deposit, Chalkidiki, Greece. *Mineral Depos* 37:137–144
- Lange RA, Carmichael ISE (1990) Hydrous basaltic andesites associated with minette and related lavas in Western Mexico. *J Petrol* 31:1225–1259
- Lee CTA, Leeman WP, Canil D, Li ZX (2005) Similar V/Sc systematic in MORB and arc basalts: implications for the oxygen fugacities of their mantle source regions. *J Petrol* 46:2313–2336
- Lehmann ST, Barcikowski J, von Quadt A, Gallhofer D, Peytcheva I, Heinrich CA, Serafimovski T (2013) Geochronology, geochemistry and isotope tracing of the Oligocene magmatism of the Buchim-Damjan-Borov Dol ore district: implications for timing, duration and source of the magmatism. *Lithos* 181:216–233
- Li Y, Audetat A (2013) Gold solubility and partitioning between sulfide liquid, monosulfide solid solution and hydrous mantle melts: implications for the formation of Au-rich magmas and crust-mantle differentiation. *Geochimica Cosmochimica Acta* 118:247–262
- Lindsley DH, Frost BR (1992) Equilibria among Fe–Ti oxides, pyroxenes, olivine, and quartz: part I. theory. *Am Mineral* 77:987–1003
- Logan JM, Mihalynuk MG (2014) Tectonic controls on early Mesozoic paired alkaline porphyry deposit belts (Cu–Au \pm Ag–Pt–Pd–Mo) within the Canadian Cordillera. *Econ Geol* 109:827–858
- Loucks RR (2014) Distinctive composition of copper-ore-forming arc magmas. *Aust J Earth Sci* 61:5–16
- Lu YJ, Kerrich R, Kemp AIS, McCuaig TC, Hou ZQ, Hart CJR, Li ZX, Cawood PA, Bagas L, Yang ZM, Cliff J, Belousova EA, Jourdan F, Evans NJ (2013a) Intracontinental Eocene–Oligocene porphyry Cu mineral systems of Yunnan, western Yangtze Craton, China: compositional characteristics, sources, and implications for continental collision metallogeny. *Econ Geol* 108:1541–1576
- Lu YJ, Kerrich R, McCuaig TC, Li ZX, Hart CJR, Cawood PA, Hou ZQ, Bagas L, Cliff J, Belousova EA, Tang S (2013b) Geochemical, Sr–Nd–Pb, and zircon Hf–O isotopic compositions of Eocene–Oligocene shoshonitic and potassic adakite-like felsic intrusions in western Yunnan, SW China: petrogenesis and tectonic implications. *J Petrol* 54:1309–1348
- Lu YJ, Loucks RR, Fiorentini ML, Yang ZM, Hou ZQ (2015) Fluid flux melting generated postcollisional high Sr/Y copper ore-forming water-rich magmas in Tibet. *Geology* 43:583–586
- Maghsoudi A, Yazdi M, Mehrpartou M, Vosoughi M, Younesi S (2014) Porphyry Cu–Au mineralization in the Mirkuh Ali Mirza magmatic complex, NW Iran. *J Asian Earth Sci* 79:932–941
- Matthews SJ, Moncrieff DHS, Carroll MR (1999) Empirical calibration of the sulphur valence oxygen barometer from natural and experimental glasses: method and applications. *Miner Mag* 63:421–431
- McCammion CA, Griffin WL, Hee SH, O'Neill HSC (2001) Oxidation during metasomatism in ultramafic xenoliths from the Wesselton kimberlite, South Africa: implications for the survival of diamond. *Contrib Miner Petrol* 141:287–296
- McGuire AV, Dyar MD, Nielson JE (1991) Metasomatic oxidation of upper mantle peridotite. *Contrib Miner Petrol* 109:252–264
- Melluso L, de Gennaro R, Fedele L, Franciosi L, Morra V (2012) Evidence of crystallization in residual, Cl–F-rich, agpaite, trachyphonolitic magmas and primitive Mg-rich basalt-trachyphonolite interaction in the lava domes of the Phlegrean Fields (Italy). *Geol Mag* 149:532–550
- Moore G, Righter K, Carmichael ISE (1995) The effect of dissolved water on the oxidation state of iron in natural silicate liquids. *Contrib Miner Petrol* 120:170–179
- Müller D (2002) Preface—Gold-copper mineralization in alkaline rocks. *Mineral Depos* 37:1–3
- Müller D (2003) Geochemical variations of alkaline rocks as vector to epithermal gold mineralization at the giant Ladolam gold deposit, Lihir Island, Papua New Guinea. Unpl. Habilitation Thesis, TU Freiberg, Germany
- Müller D, Groves DI (1993) Direct and indirect associations between potassic igneous rocks, shoshonites and gold-copper deposits. *Ore Geol Rev* 8:383–406
- Müller D, Heithersay PS, Groves DI (1994) The shoshonite porphyry Cu–Au association in the Goonumbla district, N.S.W., Australia. *Miner Petrol* 51:299–321
- Müller D, Franz L, Herzig PM, Hunt S (2001) Potassic igneous rocks from the vicinity of epithermal gold mineralization, Lihir Island, Papua New Guinea. *Lithos* 57:163–186
- Müller D, Herzig PM, Scholten JC, Hunt S (2002a) Ladolam gold deposit, Lihir Island, Papua New Guinea: gold mineralization hosted by alkaline rocks. *Econ Geol Spec Publ* 9:367–382
- Müller D, Kaminski K, Uhlig S, Graupner T, Herzig PM, Hunt S (2002b) The transition from porphyry- to epithermal-style gold mineralization at Ladolam, Lihir Island, Papua New Guinea: a reconnaissance study. *Mineral Depos* 37:61–74

- Müller D, Franz L, Petersen S, Herzig PM, Hannington MD (2003) Comparison between magmatic activity and gold mineralization at Conical Seamount and Lihir Island, Papua New Guinea. *Mineral Petrol* 79:259–283
- Mungall JE (2002) Roasting the mantle: slab melting and the genesis of major Au and Au-rich Cu deposits. *Geology* 30:915–918
- Mutschler FE, Griffin ME, Scott-Stevens D, Shannon SS (1985) Precious-metal deposits related to alkaline rocks in the North American Cordillera—An interpretative view. *Trans Geol Soc S Afr* 88:355–377
- O'Driscoll EST (1983) Deep tectonic foundations of the Eromanga Basin. *Aust Petrol Explor Assess J* 23:5–17
- Ohtani T, Nakano T, Nakashima Y, Muraoka H (2001) Three-dimensional shape analysis of miarolitic cavities and enclaves in the Kakkonda granite by X-ray computed tomography. *J Struct Geol* 23:1741–1751
- Palacios C, Ramirez LE, Townley B, Solari M, Guerra N (2007) The role of the Antofagasta-Calama lineament in ore deposit deformation in the Andes of northern Chile. *Mineral Depos* 42:301–308
- Richards JP (1995) Alkalic-type epithermal gold deposits—A review. In: Thompson JFH (ed) *Magmas, Fluids, and Ore Deposits*. Mineralogical Association of Canada, Toronto, Short Course Handbook vol 23, pp 367–400
- Richards JP (2009) Postsubduction porphyry Cu–Au and epithermal Au deposits: products of remelting of subduction-modified lithosphere. *Geology* 37:247–250
- Richards JP (2011) High Sr/Y arc magmas and porphyry Cu ± Mo ± Au deposits: just add water. *Econ Geol* 106:1075–1081
- Richards JP (2015) The oxidation state, and sulphur and Cu contents of arc magmas: implications for metallogeny. *Lithos* (in press)
- Richards JP, Boyce AJ, Pringle MS (2001) Geologic evolution of the Escondida area, northern Chile: a model for spatial and temporal localization of porphyry Cu mineralization. *Econ Geol* 96:271–305
- Rowe MC, Kent AJR, Nielsen RL (2009) Subduction influence on oxygen fugacity and trace and volatile elements in basalts across the Cascade volcanic arc. *J Petrol* 50:61–91
- Sarjoughian F, Kananian A, Ahmadian J, Murata M (2015) Chemical composition of biotite from the Kuh-e Dom pluton, Central Iran: implications for granitoid magmatism and related Cu–Au mineralization. *Arab J Geosci* 8:1521–1533
- Schmidt MW, Poli S (1998) Experimentally based water budgets for dehydrating slabs and consequences for arc magma generation. *Earth Planet Sci Lett* 163:361–379
- Setterfield TN (1991) Evolution of the Tavua caldera and associated hydrothermal systems, Fiji. Unpl. PhD Thesis, University of Cambridge, Cambridge
- Shafaroudi AM, Karimpour MH, Stern CR (2015) The Khopik porphyry copper prospect, Lut Block, Eastern Iran: geology, alteration and mineralization, fluid inclusion, and oxygen isotope studies. *Ore Geol Rev* 65:522–544
- Sigoyer J, Vanderhaeghe O, Duchêne S, Billerot A (2014) Generation and emplacement of Triassic granitoids within the Songpan Ganze accretionary-oro-genic wedge in a context of slab retreat accommodated by tear faulting, Eastern Tibetan plateau, China. *J Asian Earth Sci* 88:192–216
- Sillitoe RH (1979) Some thoughts on gold-rich porphyry copper deposits. *Mineral Depos* 14:161–174
- Sillitoe RH (1993) Giant and bonanza gold deposits in the epithermal environment: assessment of potential genetic factors. In: Whiting BH, Hodgson CJ, Mason R (eds) *Giant Ore Deposits*. *Econ Geol Spec Publ* 2:125–156
- Sillitoe RH (1997) Characteristics and controls of the largest porphyry copper-gold and epithermal gold deposits in the circum-Pacific region. *Aust J Earth Sci* 44:373–388
- Sillitoe RH (2002) Some metallogenic features of gold and copper deposits related to alkaline rocks and consequences for exploration. *Mineral Depos* 37:4–13
- Soeria-Atmadja R, Sunarya Y, Sutanto Hendaryono S (1998) Epithermal gold-copper mineralization associated with late Neogene-magmatism and crustal extension in the Sunda-Banda arc. *Geol Soc Malays Bull* 42:257–268
- Soloviev SG (2014a) The metallogeny of shoshonitic magmatism (Volume I). Scientific World Publications, Moscow: 1–528 pp (in Russian)
- Soloviev SG (2014b) The metallogeny of shoshonitic magmatism (Volume II). Scientific World Publications, Moscow: 1–472 pp (in Russian)
- Soloviev SG (2015) Geology, mineralization, and fluid inclusion characteristics of the Kumbel oxidized W–Cu–Mo skarn and Au–W stockwork deposit in Kyrgyzstan, Tien Shan. *Mineral Depos* 50:187–220
- Soloviev SG, Krivoschekov NN (2011) Petrochemistry of rocks in the Chorukh-Dairon monzonite-syenite-granite pluton, northern Tajikistan. *Geochem Int* 49:691–710
- Soloviev SG, Kryazhev SG, Dvurechenskaya SS (2013) Geology, mineralization, stable isotope geochemistry, and fluid inclusion characteristics of the Novogodnee-Monto oxidized Au-(Cu) skarn and porphyry deposit, Polar Ural, Russia. *Mineral Depos* 48:603–627
- Stern RJ (2002) Subduction zones. *Rev Geophys* 40:1012. doi:10.1029/2001RG000108
- Stults A (1985) Geology of the Bajo de la Alumbrera porphyry copper-gold prospect, Catamarca Province, Argentina. Unpl. MSc Thesis, The University of Arizona, Tucson
- Sun W, Arculus RJ, Kamenetsky VS, Binns RA (2004) Release of gold-bearing fluids in convergent margin magmas prompted by magnetite crystallization. *Nature* 431:975–978
- Tang J, Li F, Li Z, Zhang L, Deng Q, Lang X, Huang Y, Yao X, Wang Y (2010) Time limit for formation of main geological bodies in Xiongcu copper-gold

- deposit, Xietongmen County, Tibet: evidence from zircon U–Pb ages and Re–Os age of molybdenite. *Miner Depos* 29:461–475 (in Chinese)
- Webster JD (1992) Water solubility and chlorine partitioning in Cl-rich granitic systems: effects of melt composition at 2 kbar and 800 °C. *Geochim Cosmochim Acta* 56:679–687
- Webster JD, Goldoff B, Sintoni MF, Shimizu N, Vivo BD (2014) C–O–H–Cl–S–F volatile solubilities, partitioning, and mixing in phonolithic–trachytic melts and aqueous-carbonic vapor ± saline liquid at 200 MPa. *J Petrol* 55:2217–2248
- Witt WK, Hagemann SG, Villanes C (2014) Geochemistry and geology of spatially and temporally associated calc-alkaline (I-type) and K-rich (A-type) magmatism in a Carboniferous continental arc setting, Pataz gold-mining district, northern Peru. *Aust J Earth Sci* 61:17–42
- Wyborn D (1994) Mantle magmatism and large gold-copper deposits. In: *Ore Deposit Studies and Exploration Models: Porphyry Copper-Gold Deposits, Short-Course Manual*. CODES, University of Tasmania, Hobart: 5.1–5.4
- Xu L, Bi X, Hu R, Tang Y, Jiang G, Qi Y (2014) Origin of the ore-forming fluids of the Tongchang porphyry Cu–Mo deposit in the Jinshajiang-Red River alkaline igneous belt, SW China: constraints from He, Ar, and S isotopes. *J Asian Earth Sci* 79:884–894
- Xu L, Bi X, Hu R, Qi Y, Tang Y, Wang X, Zhu J (2015) Redox states and genesis of magmas associated with intra-continental porphyry Cu–Au mineralization within the Jinshajiang-Red River alkaline igneous belt, SW China. *Ore Geol Rev* (in press)
- Yang XM, Lentz DR (2005) Chemical composition of rock-forming minerals in gold-related granitoid intrusions, southwestern New Brunswick, Canada: implications for crystallization conditions, volatile exsolution, and fluorine-chlorine activity. *Contrib Miner Petrol* 150:287–305
- Zhao X, Xue C, Symons DTA, Zhang Z, Wang H (2014a) Microgranular enclaves in island-arc andesites: a possible link between known epithermal Au and potential porphyry Cu–Au deposits in the Tulasu ore cluster, western Tianshan, Xinjiang, China. *J Asian Earth Sci* 85:210–223
- Zhao X, Xue C, Chi G, Wang H, Qi T (2014b) Epithermal Au and polymetallic mineralization in the Tulasu Basin, western Tianshan, NW China: potential for the discovery of porphyry Cu–Au deposits. *Ore Geol Rev* 60:76–96

This chapter provides 32 Tables summarizing the characteristic features of global gold-copper deposits associated with potassic igneous rocks for which substantial information is available.

11.1 Abbreviations

Abbreviations for ore minerals: Apy, arsenopyrite; Bn, bornite; Cal, calaverite; Cc, chalcocite; Cinn, cinnabar; Cov, covellite; Cpy, chalcopyrite; Dig, digenite; En, enargite; Gn, galena; Mar, marcasite; Mol, molybdenite; Po, pyrrhotite; Py, pyrite; Sch, scheelite; Sl, sphalerite; Stib, stibnite; Tel, telluride; Ten, tennantite; Tet, tetrahedrite.

Abbreviations for silicate minerals: Af, potassic feldspar; An, analcite; Ap, apatite; Bio, biotite; Cpx, clinopyroxene; Foids, feldspathoid minerals; Hb, hornblende; Mt, magnetite; Ol, olivine; Opx, orthopyroxene; Phl, phlogopite; Pl, plagioclase; Qz, quartz; Ti, titanite.

11.2 Tables of Deposit Characteristics

The deposit tables are arranged alphabetically for ease of use but the following lists indicate their tectonic settings.

Continental arcs: Andacollo, Bajo de la Alumbrera, Bingham, Buchim, Choquelimpie, Cripple Creek (transitional), El Indio, Maricunga Belt Mining District, Skouries, Summitville, Twin Buttes.

Postcollisional arcs: Axi, Grasberg, Guilaizhuang, Kirkland Lake Mining District, Misima, Mount Kare, Mount Morgans, Ok Tedi, Porgera, Qulong, Touzlar, Wiluna, Yao'an.

Late oceanic arcs: Cadia, Dinkidi, Emperor, Ladolam, Northparkes, Oyu Tolgoi, Peschanka, Woodlark Island.

Within-plate settings: Cripple Creek (transitional) (Tables [11.1](#), [11.2](#), [11.3](#), [11.4](#), [11.5](#), [11.6](#), [11.7](#), [11.8](#), [11.9](#), [11.10](#), [11.11](#), [11.12](#), [11.13](#), [11.14](#), [11.15](#), [11.16](#), [11.17](#), [11.18](#), [11.19](#), [11.20](#), [11.21](#), [11.22](#), [11.23](#), [11.24](#), [11.25](#), [11.26](#), [11.27](#), [11.28](#), [11.29](#), [11.30](#), [11.31](#) and [11.32](#)).

Table 11.1 Andacollo, Chile

Deposit	Andacollo
Mineralization	Porphyry copper-gold, highest grades associated with potassic alteration
Estimated reserves	About 300 Mt at 0.7 wt% Cu and 0.25 g/t Au (about 2.1 Mt of copper and 2.5 Moz of gold)
Location	Central Chile; 400 km north of Santiago
Host rocks	Andesite
Texture	Porphyritic
Structure	Fine to medium grained
Mineralogy	Phenocrysts: Pl-Hb-Bio±Af Groundmass: Pl-Af-Qz
Geochemistry	High-K calc-alkaline to shoshonitic, high LILE, moderate LREE, low HFSE
Ore minerals	Py±Cpy±S±Gn±Cinn
Alteration	Potassic and propylitic
Age	Host rocks: cretaceous (104 ± 3 to 98 ± 2 Ma) Mineralization: coeval with host rocks
Tectonic setting	Continental arc
Structural features	–
References	Reyes (1991)

Table 11.2 Axi, Xinjiang Province, China

Deposit	Axi
Mineralization	Epithermal gold
Estimated reserves	About 2.4 Moz of gold; high average grades of 5.57 g/t Au
Location	Central part of the Tulasu basin in the western Tianshan Orogen; about 30 km northwest of Yining City, Xinjiang Province, NW China
Host rocks	Quartz-monzonite
Texture	Porphyritic
Structure	Medium grained
Mineralogy	Phenocrysts: Pl-Qz-Bio±Ap Groundmass: Af-Pl-Qz
Geochemistry	High-K calc-alkaline, high LILE, moderate LREE, low HFSE, but elevated Nb (up to 10 ppm)
Ore minerals	Py-Mar-Apy±Cpy±native gold
Alteration	Silicification, phyllic, and propylitic
Age	Host rocks: carboniferous (346.7 ± 3.0 to 361.6 ± 3.9 Ma) Mineralization: coeval with host rocks
Tectonic setting	Postcollisional arc
Structural features	Circular diatreme with ring structures
References	Li et al. (1998), Yang et al. (2009), Chen et al. (2012), Zhao et al. (2014a, b)

Table 11.3 Bajo de la Alumbrera, Catamarca Province, Argentina

Deposit	Bajo de la Alumbrera
Mineralization	Porphyry copper-gold
Estimated reserves	About 806 Mt at 0.53 wt% Cu and 0.64 g/t Au
Location	Catamarca Province, Northwest Argentina; 100 km northeast of Belen and 300 km southwest of Tucuman
Host rocks	Dacite
Texture	Porphyritic
Structure	Fine to medium grained
Mineralogy	Phenocrysts: Pl-Qz-Bio±Hb±Ap Groundmass: Af-Pl-Qz
Geochemistry	High-K calc-alkaline to shoshonitic, high LILE, moderate LREE, low HFSE
Ore minerals	Py-Cpy±Bn
Alteration	Potassic, phyllic, and propylitic
Age	Host rocks: 7.9 Ma Mineralization: coeval with host rocks
Tectonic setting	Continental arc
Structural features	Mineralization is located within a tectonic depression and crosscut by late northwest-striking andesite dykes
References	Stults (1985), Müller and Forrestal (1998), D. Keough (written comm. 1998), Ulrich et al. (2001), Ulrich and Heinrich (2002), Profett (2003), Harris et al. (2004)

Table 11.4 Bingham, Utah, USA

Deposit	Bingham
Mineralization	Porphyry copper-molybdenum±gold, highest grades associated with potassic alteration
Estimated reserves	Up to 2004, Bingham yielded more than 17 Mt of copper, 23 Moz of gold, 190 Moz of silver, and 850 million pounds of molybdenum
Location	Bingham Canyon, Utah, USA
Host rocks	Quartz-monzonite
Texture	Porphyritic
Structure	Fine to medium grained
Mineralogy	Phenocrysts: Af-Qz-Pl-Bio Groundmass: Af-Pl-Qz±Ap
Geochemistry	High-K calc-alkaline, high LILE, moderate LREE, low HFSE
Ore minerals	Py-Cpy±Mol
Alteration	Potassic and propylitic
Age	Host rocks: Eocene (39.8 ± 0.4 to 38.8 ± 0.4 Ma) Mineralization: coeval with host rocks
Tectonic setting	Continental arc
Structural features	Mineralization and igneous intrusions are controlled by the intersection of northeast-trending faults with the Copperton anticline
References	Butler (1920), Lanier et al. (1978a, b), Warnaars et al. (1978), Einaudi (1982), Bowman et al. (1987), Keith et al. (1997), Waite et al. (1997), Maughan et al. (2002), Redmond et al. (2004), Gruen et al. (2010), Landtwing et al. (2010), Redmond and Einaudi (2010)

Table 11.5 Buchim, Macedonia

Deposit	Buchim
Mineralization	Porphyry copper-gold
Estimated reserves	Total pre-mining reserves of about 120 Mt at 0.34 wt% Cu and 0.35 g/t Au
Location	In the eastern part of Macedonia
Host rocks	Trachyandesite (hypabyssal)
Texture	Porphyritic
Structure	Medium grained
Mineralogy	Phenocrysts: Pl-Hb-Af-Bio±Ap Groundmass: Af-Pl-Hb
Geochemistry	High-K calc-alkaline, transitional to shoshonite, high LILE, moderate LREE, low HFSE
Ore minerals	Cpy-Py±Bn±native gold
Alteration	Potassic, phyllic, argillic, and propylitic
Age	Host rocks: Oligocene (27.5–24.9 Ma) Mineralization: Oligocene (24.5–24.0 Ma)
Tectonic setting	Continental arc
Structural features	The main structural trend is oriented northwest-southeast
References	Lehmann et al. (2013)

Table 11.6 Cadia, New South Wales, Australia

Deposit	Cadia
Mineralization	Porphyry copper-gold cluster
Estimated reserves	Pre-mine resources at Cadia were 2.3 Mt of copper and >19.5 Moz of gold
Location	New South Wales, Australia; 25 km south of Orange
Host rocks	Trachyandesite
Texture	Porphyritic
Structure	Medium grained
Mineralogy	Phenocrysts: Pl-Hb Groundmass: Af-Pl-Hb
Geochemistry	Shoshonitic, with high LILE, moderate LREE, low HFSE
Ore minerals	Py-Cpy-Bn±native gold
Alteration	Potassic, phyllic, and propylitic
Age	Host rocks: Two pulses during the Upper Ordovician: 1) 456 ± 6 Ma (Cadia-Ridgeway), and 2) 437 ± 4 Ma (Cadia-Quarry, Cadia-Hill, Cadia-East), respectively. Mineralization: coeval with host rocks
Tectonic setting	Late oceanic arc
Structural features	Deposits are crosscut by northeast-striking normal faults
References	Welsh (1975), Wood and Holliday (1995), Holliday et al. (1999, 2002), Harper (2000), Tedder et al. (2001), Blevin (2002), Wilson et al. (2003, 2007)

Quartz-monzonite
Porphyritic
Medium-grained
Phenocrysts: Pl-Qz-Bio±Ap
Groundmass: Af-Pl-Qz

Table 11.7 Choquelimpie, Chile

Deposit	Choquelimpie
Mineralization	Epithermal gold-silver
Estimated reserves	About 6.7 Mt at 2.23 g/t Au and 87 g/t Ag (about 0.5 Moz gold and 1.5 Moz silver)
Location	Northern Chile; about 115 km east of Arica
Host rocks	Andesite
Texture	Porphyritic
Structure	Fine to medium grained
Mineralogy	Phenocrysts: Pl-Hb-Bio±Af Groundmass: Pl-Af-Qz
Geochemistry	High-K calc-alkaline, high LILE, moderate LREE, low HFSE
Ore minerals	Py-Sl-Gn-Tet±Po±native silver
Alteration	Argillic and siliceous
Age	Host rocks: Miocene Mineralization: coeval with host rocks
Tectonic setting	Continental arc
Structural features	Magmatism controlled by northeast- and northwest-striking lineaments
References	Gröpper et al. (1991)

Table 11.8 Cripple Creek, Colorado, USA

Deposit	Cripple Creek		
Mineralization	Epithermal gold		
Estimated reserves	To date, the Cripple Creek district has produced about 23.5 Moz of gold		
Location	Teller County, Colorado, USA		
Host rocks	Syenite	Phonolite	Lamprophyre
Texture	Massive	Porphyritic	Porphyritic
Structure	Fine grained	Fine to medium-grained	Medium grained
Mineralogy	Af-Pl-Qz±Bio	Phenocrysts: Foids-Ol-Cpx Groundmass: Foids-Ol	Phenocrysts: Pl-Hl-Ol-Cpx Groundmass: Af-Hb ± Pl
Geochemistry	Alkaline, with high LILE and LREE, low HFSE, very high volatiles (e.g. CO ₂ , H ₂ O, Cl, F)		
Ore minerals	Cal±Py±Cpy±Tet±Tel		
Alteration	Potassic, propylitic and sericitic		
Age	Host rocks: 31.5–32.5 Ma Mineralization: coeval with host rocks		
Tectonic setting	Transitional between continental arc and within-plate setting		
Structural features	Diatreme vent		
References	Lindgren and Ransome (1906), Lindgren (1933), Loughlin and Koschmann (1935), Walker and Walker (1956), Mutschler et al. (1985), Thompson et al. (1985), Mutschler and Mooney (1993), Jensen and Barton (1997), Kelly et al. (1998), Kelley and Ludington (2002), Jensen (2003)		

Table 11.9 Dinkidi, Didipio, Philippines

Deposit	Dinkidi
Mineralization	Porphyry gold-copper
Estimated reserves	About 2.06 Moz of Au and 272.4 Kt of Cu
Location	Didipio Igneous Complex, North Luzon, Philippines
Host rocks	Monzodiorite
Texture	Massive
Structure	Medium grained
Mineralogy	Pl-Qz-Cpx-Bio-Hb Phenocrysts: Pl-Hb-Bio±Ap Groundmass: Af-Pl-Oz
Geochemistry	Shoshonitic, high LILE, moderate LREE, low HFSE
Ore minerals	Cpy±Bn
Alteration	Potassic, phyllic, and propylitic
Age	Host rocks: Early Miocene Mineralization: Early Miocene (23.2 ± 0.6 Ma), coeval with host rocks
Tectonic setting	Late oceanic arc
Structural features	Intersection of east-northeast-trending transfer structures with north-northwest-trending fractures parallel to the Philippine fault
References	Garrett (1996), Haggman (1997a, b), Corbett and Leach (1998), Wolfe et al. (1998), Kamenetsky et al. (1999), Wolfe (2001), McIntyre et al. (2010), Wolfe and Cooke (2011)

Table 11.10 El Indio, Chile

Deposit	El Indio
Mineralization	Epithermal gold-silver
Estimated reserves	About 5.5 Moz of gold and 24 Moz of silver
Location	Central Chile, near border with Argentina; about 500 km north of Santiago and 180 km east of La Serena
Host rocks	Dacite
Texture	Porphyritic
Structure	Medium grained
Mineralogy	Phenocrysts: Qz-Pl-Hb-Bio Groundmass: Af-Pl-Qz
Geochemistry	High-K calc-alkaline, high LILE, moderate LREE, low HFSE
Ore minerals	En-Ten-Py-native gold
Alteration	Advanced argillic and pervasive silicification
Age	Host rocks: 5.0–9.5 Ma Mineralization: 6.0–9.5 Ma
Tectonic setting	Continental arc
Structural features	Major north-south trending faults subparallel to the Andean trend; however, mineralized veins occur within a structural block, 150 by 500 m wide, and bounded by two northeast-striking principal faults
References	Walthier et al. (1985), Siddeley and Araneda (1986), Jannas et al. (1990), Bissig et al. (2001, 2002, 2003)

Table 11.11 Emperor, Viti Levu, Fiji

Deposit	Emperor
Mineralization	Epithermal gold
Estimated reserves	7 Moz of gold
Location	Viti Levu, Fiji
Host rocks	Monzonite
Texture	Equigranular
Structure	Medium grained
Mineralogy	Pl-Af-Cpx-Phl Phenocrysts: Pl-Cpx-Ol±Phl±Hb Groundmass: Pl-Af-Cpx
Geochemistry	Shoshonitic, with high LILE, moderate LREE, low HFSE
Ore minerals	Py-Tel-Mar±Apy
Alteration	Potassic and propylitic
Age	Host rocks: Pliocene Mineralization: 3.71 ± 0.13 Ma
Tectonic setting	Late oceanic arc
Structural features	Mineralization is hosted by flat-lying quartz-sericite±carbonate veins, steep faults, stockwork zones, and hydrothermal breccias, located within caldera
References	Ahmad (1979), Anderson and Eaton (1990), Setterfield (1991), Setterfield et al. (1991, 1992), R. Jones (pers. comm., 1993), Pals et al. (2003), Pals and Spry (2003), Scherbarth and Spry (2006), Smith et al. (2008)

Table 11.12 Northparkes (Goonumbla), New South Wales, Australia

Deposit	Northparkes (Goonumbla)
Mineralization	Porphyry copper-gold cluster
Estimated reserves	About 287.8 Mt at 0.57 wt% Cu and 0.26 g/t Au
Location	New South Wales, Australia; 28 km northwest of Parkes
Host rocks	Quartz-monzonite
Texture	Porphyritic
Structure	Medium grained
Mineralogy	Phenocrysts: Pl-Qz-Bio-Hb±Ap Groundmass: Af-Pl-Qz
Geochemistry	Shoshonitic, with high LILE, moderate LREE, low HFSE, high halogens (i.e. Cl, F)
Ore minerals	Cpy-Bn-Cc±Py±Sl
Alteration	Potassic, phyllic, and propylitic
Age	Host rocks: Ordovician (438 ± 3.5 Ma) Mineralization: Ordovician (439.2 ± 1.2 Ma), coeval with host rocks
Tectonic setting	Late oceanic arc
Structural features	Mineralization is located within caldera
References	Jones (1985), Heithersay et al. (1990), Perkins et al. (1990a, b), Müller et al. (1994), Heithersay and Walshe (1995), Blevin (2002), Lickfold et al. (2003), Butcher et al. (2011), Harris and Holcombe (2014)

Table 11.13 Grasberg, Indonesia

Deposit	Grasberg
Mineralization	Porphyry copper-gold
Estimated reserves	In 2002, total recoverable reserves were estimated as 51 billion pounds of copper, 62.4 Moz of gold, and 135.5 Moz of silver
Location	Irian Jaya Province, Indonesia
Host rocks	Monzodiorite
Texture	Porphyritic
Structure	Medium grained
Mineralogy	Phenocrysts: Pl-Hb-Bio±Ap Groundmass: Af-Pl-Qz-Bio
Geochemistry	High-K calc-alkaline, high LILE, moderate LREE, low HFSE, but relatively high Nb
Ore minerals	Cpy-Bn-Py±Cc±Djg±Cov
Alteration	Potassic, phyllic, and propylitic
Age	Host rocks: Pliocene (3.33–3.01 Ma) Mineralization: coeval with host rocks
Tectonic setting	Postcollisional arc
Structural features	Mineralization controlled by intersections of reverse faults and sinistral strike-slip faults
References	Hickson (1991), Van Nort et al. (1991), McMahon (1994), MacDonald and Arnold (1994), Pollard and Taylor (2002, 2005)

Table 11.14 Guilaizhuang, China

Deposit	Guilaizhuang
Mineralization	Epithermal gold
Estimated reserves	About 1.2 Moz of gold; high average grade of 8.1 g/t Au
Location	Luxi Block; eastern margin of the North China Craton, northern China
Host rocks	Quartz-monzodiorite
Texture	Porphyritic
Structure	Medium grained
Mineralogy	Phenocrysts: Pl-Qz-Hb-Bio Groundmass: Af-Pl±Hb
Geochemistry	Shoshonitic, with high LILE, moderate LREE, low HFSE
Ore minerals	Apy-Py±TeI
Alteration	Fluorite-carbonate alteration
Age	Host rocks: Jurassic (184.7–180.1 Ma) Mineralization: Coeval with host rocks
Tectonic setting	Postcollisional arc
Structural features	Hydrothermal breccias
References	Lan et al. (2012), Xu et al. (2015)

Table 11.15 Kirkland Lake Mining District, Superior Province, Canada

Deposit	Kirkland Lake Mining District (example of Canadian lode-gold deposit)
Mineralization	Orogenic gold
Estimated reserves	Not available (>24 Moz of gold)
Location	Superior Province, Ontario, Canada
Associated rocks	Syenite
Texture	Equigranular
Structure	Medium grained
Mineralogy	Af-Pl-Cpx-Bio-Mt±Ap Lamprophyre Porphyritic Medium grained Phenocrysts: Hb±Phl Groundmass: Pl-Af
Geochemistry	Shoshonitic, with high LILE, moderate LREE, low HFSE
Ore minerals	Cpy-Py
Alteration	Secondary carbonate
Age	Associated rocks: Archaean (2680 ± 1 Ma) Mineralization: Archaean (2680 ± 1 Ma)
Tectonic setting	Postcollisional arc
Structural features	Mineralization and lamprophyres occur along major, deep-seated, shear zones
References	Wyman and Kerrich (1989a, b), Wyman (1990), R. Kerrich (pers. comm., 1993), Rowins et al. (1993), Blichert-Toft et al. (1996)

Table 11.16 Ladolam, Lihir Island, Papua New Guinea

Deposit	Ladolam
Mineralization	Epithermal gold
Estimated reserves	Total resource of >46 Moz of gold; the ore contains an average grade of 2.52 g/t Au
Location	Lihir Island, New Ireland Province, Papua New Guinea
Host rocks	Monzoniorite
Texture	Porphyritic
Structure	Medium grained
Mineralogy	Phenocrysts: Pl-Hb-Phl Groundmass: Pl-Af
Geochemistry	High-K calc-alkaline, transitional to shoshonites, with high LILE, moderate LREE, low HFSE, high halogens (i.e. Cl, F)
Ore minerals	Py±Gn±Mar±Tet
Alteration	Potassic, propylitic and illite alteration
Age	Host rocks: Pleistocene (0.342–0.917 Ma) Mineralization: Pleistocene (0.10–0.35 Ma)
Tectonic setting	Late oceanic arc
Structural features	High-grade mineralization is controlled by north-trending structures. Volcanism and mineralization might be related to a north-striking flexure and related tear in the north-vergent subducting Solomon plate.
References	Wallace et al. (1983), Plimer et al. (1988), Moyle et al. (1990), Diemock et al. (1993), Hoogvliet (1993), Spooner (1993), Carman (1994, 2003), Corbett (1999), Corbett et al. (2001), Müller et al. (2001, 2002a, b, 2003), Simmons and Brown (2006), Blackwell et al. (2014)

Table 11.17 Maricunga Belt Mining District, Chile

Deposit	Maricunga Belt Mining District (e.g. Marte, Lobo)
Mineralization	Porphyry gold±copper±silver, highest grades associated with potassic alteration
Estimated reserves	About 14 Moz of gold and 467 Moz of silver
Location	Central Chile; between latitudes 26°00' and 28°00'
Host rocks	Andesite
Texture	Porphyritic
Structure	Fine to medium grained
Mineralogy	Phenocrysts: Pl-Hb-Bio±Af Groundmass: Pl-Af-Qz
Geochemistry	High-K calc-alkaline, high LILE, moderate LREE, low HFSE
Ore minerals	Py±Cpy±Bn±Mo±S±En±Ten
Alteration	Potassic, propylitic, and argillic
Age	Host rocks: Miocene (23–12.9 Ma) Mineralization: Miocene (20–13 Ma)
Tectonic setting	Continental arc
Structural features	–
References	Sillitoe (1991), Vila and Sillitoe (1991)

Table 11.18 Misima, Misima Island, Papua New Guinea

Deposit	Misima
Mineralization	Epithermal gold
Estimated reserves	About 2.5 Moz of gold and 39.5 Moz of silver
Location	Island in the Louisiade Archipelago, Papua New Guinea; about 240 km east-southeast of the mainland
Host rocks	Granodiorite
Texture	Porphyritic
Structure	Coarse to medium grained
Mineralogy	Phenocrysts: Pl-Qz-Bio-Hb Groundmass: Qz-Pl-Af
Geochemistry	High-K calc-alkaline
Ore minerals	Py-Sl-Gn±Cpy±native gold±native silver
Alteration	Phyllic and propylitic
Age	Host rocks: granodiorite Miocene (8.0 Ma); lamprophyres Pliocene (3.5 Ma) Mineralization: Pliocene (3.5 Ma)
Tectonic setting	Postcollisional arc
Structural features	Mineralization is controlled by major northwest-striking extensional fault
References	Keyser (1961), Clarke (1988), Clarke et al. (1990), Lewis and Wilson (1990), Appleby et al. (1995), A.K. Appleby (written comm. 1996), Fallon et al. (2002)

Table 11.19 Mount Kare, Enga Province, Papua New Guinea

Deposit	Mount Kare
Mineralization	Epithermal gold
Estimated reserves	About 2.0 Moz of gold
Location	Highlands of Papua New Guinea; about 18 km southwest of Porgera mine
Host rocks	Feldspar porphyry
Texture	Porphyritic
Structure	Coarse to medium grained
Mineralogy	Phenocrysts: Pl-Cpx±Hb±Ph±Ap Groundmass: Af-Pl-Ol
Geochemistry	High-K alkaline, with high LILE, moderate LREE, very high Nb (up to 122 ppm)
Ore minerals	Py-Sl-Gn-Tel±native gold
Alteration	No potassic alteration
Age	Host rocks: Miocene (6.0 ± 0.1 Ma) Mineralization: Miocene (5.5 ± 0.1 Ma)
Tectonic setting	Postcollisional arc
Structural features	Mineralization occurs along major transform fault
References	Brunker and Cairthness (1990), Richards and Ledlie (1993)

Table 11.20 Mount Morgans, Eastern Goldfields, Western Australia

Deposit	Mount Morgans		
Mineralization	Orogenic gold		
Estimated reserves	About 0.5 Moz of gold		
Location	Eastern Goldfields Province, Yilgarn Block, Western Australia; between Leonora and Laverton		
Associated rocks	Lamprophyre	Qz-Fsp porphyry	Banded iron formation
Texture	Porphyritic	Porphyritic	Layered
Structure	Medium grained	Medium grained	Fine grained
Mineralogy	Phenocrysts: Pl-Cpx±Ap Groundmass: Pl-Af	Phenocrysts: Qz-Pl-Hb Groundmass: Pl-Af	Mt-Qz
Geochemistry	Shoshonitic	High-K calc-alkaline	
Ore minerals	Py±native gold		
Alteration	Secondary carbonate		
Age	Associated rocks: Late Archaean (2649 ± 10 Ma) Mineralization: Late Archaean (probably 2650 ± 7 Ma)		
Tectonic setting	Postcollisional arc		
Structural features	Mineralization, lamprophyres, and porphyries are controlled by fold and fault systems		
References	Perring (1988), Groves and Ho (1990), Vielreicher et al. (1994, 2015), Salier et al. (2005)		

Table 11.21 Ok Tedi, Papua New Guinea

Deposit	Ok Tedi
Mineralization	Porphyry copper-gold
Estimated reserves	Pre-mining resource of about 4.8 Mt of copper and 16.3 Moz of gold
Location	Northwestern part of Western Province, highlands of Papua New Guinea, near border with Indonesia
Host rocks	Quartz-monzonite
Texture	Porphyritic
Structure	Fine to medium grained
Mineralogy	Phenocrysts: Pl-Af-Qz-Bio±Hb±Ap±Ti Groundmass: Af-Pl
Geochemistry	High-K calc-alkaline, with high LILE, moderate LREE, low HFSE
Ore minerals	Py-Cpy±Bn±Mol±native gold
Alteration	Potassic, argillic, and propylitic
Age	Host rocks: Pliocene (2.6 Ma) Mineralization: Pleistocene (1.2–1.1 Ma)
Tectonic setting	Postcollisional arc
Structural features	Quartz-monzonite intrusion is controlled by a series of steeply dipping north-northwest- and north-northeast-striking faults
References	Bamford (1972), Arnold and Griffin (1978), Rush and Seegers (1990), Hettler et al. (1997)

Table 11.22 Oyu Tolgoi, Mongolia

Deposit	Oyu Tolgoi
Mineralization	Porphyry copper-gold cluster
Estimated reserves	Total resource of >41.7 Mt of copper and 49.8 Moz of gold
Location	Southern Mongolia; 650 km south of Ulaanbaatar and about 80 km from the Chinese border
Host rocks	Quartz-monzodiorite
Texture	Porphyritic
Structure	Medium grained
Mineralogy	Phenocrysts: Pl-Qz-Hb-Bio±Ap Groundmass: Af-Pl
Geochemistry	High-K calc-alkaline, with high LILE, moderate LREE, low HFSE
Ore minerals	Bn-Cpy-Py-Mol±Cov±En
Alteration	Potassic, phyllic, argillic, and propylitic
Age	Host rocks: Late Devonian (quartz-monzodiorite at Hugo Dummett orebody: 369 ± 2 Ma) Mineralization: Late Devonian (molybdenite at Hugo Dummett orebody: 370 ± 1.2 Ma)
Tectonic setting	Late oceanic arc
Structural features	Controlled by regional northeast-striking lineament
References	Perello et al. (2001), Kavalieris and Wainwright (2005), Khashgerel et al. (2006, 2008, 2009), D. Crane (pers. comm. 2011), Wainwright et al. (2011), Crane and Kavalieris (2012), Dolgoplova et al. (2013)

Table 11.23 Peschanka, Russia

Deposit	Peschanka
Mineralization	Porphyry copper-gold cluster
Estimated reserves	About >8.3 Mt of copper, >200 kt of molybdenum, >14 Moz of gold, >116 Moz of silver; high exploration potential for additional orebodies remains
Location	Chukotka Autonomous Region, Siberia, Russia; about 250 km southwest of Bilibino
Host rocks	Quartz-monzonite
Texture	Porphyritic
Structure	Medium grained
Mineralogy	Phenocrysts: Pl-Af-Qz-Bio±Hb Groundmass: Af-Pl-Qz
Geochemistry	High-K calc-alkaline, with high LILE, moderate LREE, low HFSE
Ore minerals	Py-Cpy-Bn±Mol
Alteration	Potassic, phyllic, and propylitic
Age	Host rocks: Cretaceous (138–141 Ma) Mineralization: coeval with host rocks
Tectonic setting	Late oceanic arc
Structural features	High grade stockwork zones are related to north- and northeast-trending strike-slip faults, where the potassic alteration assemblages are overprinted by sericitic alteration
References	Volchkov et al. (1982), Maraeva et al. (1988), Sidorov and Eremin (1994), Volkov et al. (2006), Seltmann et al. (2010), Chitalin et al. (2012), Baksheev et al. (2010, 2012, 2013), Marushchenko (2013), Marushchenko et al. (2015), Nagomaya (2010), Nikolaev et al. (2013, 2014), Soloviev (2014a, b)

Table 11.24 Porgera, Enga Province, Papua New Guinea

Deposit	Porgera
Mineralization	Epithermal gold
Estimated reserves	Total resource of about 22.9 Moz of gold and >30 Moz of silver
Location	Enga Province in the highlands of Papua New Guinea, about 130 km to the west of Mount Hagen
Host rocks	Trachybasalt
Texture	Porphyritic
Structure	Medium grained
Mineralogy	Phenocrysts: Cpx-Pl-Ol-Phl±Ap Groundmass: Af-Pl-Cpx
Geochemistry	Alkaline, with high LILE, moderate LREE, low HFSE, but high Nb
Ore minerals	Py-Tel±Apy±native gold
Alteration	roscoelite alteration; no potassic alteration
Age	Host rocks: Miocene (5.99 ± 0.08 Ma) Mineralization: Miocene (5.98 ± 0.13 Ma)
Tectonic setting	Postcollisional arc
Structural features	High-grade mineralization is controlled by major transform fault; disruption of this fault probably altered hydrothermal fluid pressure and flow regimes, initiating gold precipitation
References	Fleming et al. (1986), Handley and Henry (1990), Richards (1990a, b, 1992), Richards et al. (1990, 1991), Wall et al. (1995), Cameron (1998), Ronacher et al. (2002, 2004), Peterson and Mavrogenes (2014)

Table 11.25 Qulong, Tibet Province, China

Deposit	Qulong
Mineralization	Porphyry copper-molybdenum
Estimated reserves	About 10.6 Mt of copper and 0.5 Mt of molybdenum
Location	Tibet Province, SW China
Host rocks	Granodiorite
Texture	Equigranular
Structure	Coarse to medium grained
Mineralogy	Pl-Af-Qz±Bio±Hb±Ap Monzogranite Porphyritic Coarse to medium grained Phenocrysts: Pl-Qz-Af Groundmass: Af-Pl-Qz±Bio
Geochemistry	High-K calc-alkaline, with low MgO (<2.0 wt%), high LILE, moderate LREE, low HFSE
Ore minerals	Py-Cpy ± Mol ± Bn ± Cc
Alteration	Potassic, phyllic, propylitic, and weak argillic
Age	Host rocks: Miocene (15.3 ± 0.6 Ma) Mineralization: coeval with host rocks
Tectonic setting	Postcollisional arc
Structural features	–
References	Xiao et al. (2012), Hu et al. (2015)

Table 11.26 Skouries, Chalkidiki Province, Greece

Deposit	Skouries
Mineralization	Porphyry gold-copper
Estimated reserves	About 5.4 Moz of gold and 1.2 Mt of copper
Location	Chalkidiki Peninsula of northeastern Greece; about 90 km southeast of Thessalonici
Host rocks	Monzonite
Texture	Porphyritic
Structure	Medium grained
Mineralogy	Phenocrysts: Pl-Af-Hb-Bio Groundmass: Af-Pl-Qz
Geochemistry	Shoshonitic, with high LILE, moderate LREE, low HFSE
Ore minerals	Cpy-Bn-Py
Alteration	Potassic, phyllic, and propylitic
Age	Host rocks: Miocene (19 Ma) Mineralization: coeval with host rocks
Tectonic setting	Continental arc
Structural features	Intrusions were emplaced along a deep-seated northwest-striking fault system
References	Frei (1992), Veranis (1994), Tobey et al. (1998), Kroll et al. (2002)

Table 11.27 Summitville, Colorado, USA

Deposit	Summitville
Mineralization	Epithermal gold
Estimated reserves	About 1 Moz of gold
Location	San Juan volcanic field, Colorado, USA; about 10 km northwest of Platoro
Host rocks	Quartz-lattice
Texture	Porphyritic
Structure	Medium grained
Mineralogy	Phenocrysts: Pl-Af-Qz-Bio-Hb±Af Groundmass: Af-Pl-Qz
Geochemistry	High-K calc-alkaline, with high LILE, moderate LREE, low HFSE
Ore minerals	En-Py±Cpy
Alteration	Advanced argillic
Age	Host rocks: Miocene (22.8 Ma) Mineralization: Miocene (22.4 Ma)
Tectonic setting	Continental arc
Structural features	Intrusions and mineralization are controlled by northwest-striking fault system and its intersection with a caldera ring
References	Mehnert et al. (1973), Stoffregen (1987), Gray and Coolbaugh (1994)

Table 11.28 Touzlar, Iran

Deposit	Touzlar
Mineralization	Epithermal gold
Estimated reserves	About 1.5 Mt of ore at 2.2 g/t Au and 0.3 wt% Cu
Location	In the Zanjan Province, NW Iran; about 440 km northwest of Tehran
Host rocks	Trachyandesite
Texture	Porphyritic
Structure	Medium grained
Mineralogy	Phenocrysts: Pl-Cpx Groundmass: Af-Pl-Cpx
Geochemistry	Shoshonitic, with high LILE, moderate LREE, low HFSE, but elevated Nb (up to 13 ppm)
Ore minerals	Py-Cpy-Bn-Cc-Cov±En±Gn±Sl±Tet±Ten
Alteration	Phyllic, argillic, advanced argillic, and propylitic
Age	Host rocks: Trachyandesite lavas—Miocene (19.2 ± 0.2 Ma) Microdiorite intrusions—Miocene (19.4 ± 0.5 Ma)
Tectonic setting	Mineralization: coeval with host rocks Postcollisional arc
Structural features	The deposit is exposed in the root zone of an eroded stratovolcano; intrusions are emplaced along northwest-striking faults
References	Heidari et al. (2015)

Table 11.29 Twin Buttes, Arizona, USA

Deposit	Twin Buttes
Mineralization	Porphyry copper, highest grades associated with potassic alteration
Estimated reserves	About 8.0 Mt of copper
Location	Pima County, Arizona, USA
Host rocks	Quartz-monzonite
Texture	Porphyritic
Structure	Coarse to medium grained
Mineralogy	Phenocrysts: Af-Pl-Bio±Af Groundmass: Af-Pl-Qz
Geochemistry	High-K calc-alkaline, high LILE, moderate LREE, low HFSE
Ore minerals	Cpy-Py
Alteration	Potassic, phyllic, and propylitic
Age	Host rocks: Paleocene (57.1 ± 2.1 Ma) Mineralization: coeval with host rocks
Tectonic setting	Continental arc
Structural features	Mineralization and intrusions are controlled by northeast-trending faults
References	Salek (1976), Kelly (1977), Barter and Kelly (1982)

Table 11.30 Wiluna, Eastern Goldfields, Western Australia

Deposit	Wiluna
Mineralization	Orogenic gold
Estimated reserves	About 3.5 Moz of gold
Location	Northern part of the Eastern Goldfields Province, Yilgam Block, Western Australia
Associated rocks	Lamprophyre
Texture	Porphyritic
Structure	Coarse grained
Mineralogy	Phenocrysts: Hb±Ap Groundmass: Pl-Af
Geochemistry	Lamprophyres are shoshonitic, with high LILE, moderate LREE, low HFSE
Ore minerals	Py-Apy-Stib±Cpy±Sch±native gold
Alteration	Secondary carbonate
Age	Associated rocks: Archaean (2640 Ma) Mineralization: Archaean (2632 ± 12 Ma)
Tectonic setting	Postcollisional arc
Structural features	Mineralization and lamprophyres are controlled by dextral strike-slip fault system
References	Hagemann et al. (1992), Hagemann (1993), Kent and Hagemann (1996), Vielreicher et al. (2015)

Table 11.31 Woodlark Island, Papua New Guinea

Deposit	Woodlark Island
Mineralization	Epithermal gold
Estimated reserves	About 0.3 Moz of gold
Location	In the Solomon Sea, Papua New Guinea; about 600 km east of Port Moresby and 160 km north of Misima Island
Host rocks	Monzonite
Texture	Porphyritic
Structure	Medium grained
Mineralogy	Phenocrysts: Pl-Bio Groundmass: Af-Pl
Geochemistry	Shoshonitic
Ore minerals	Py±Gn±S±Cpy±Tet
Alteration	Phyllic and propylitic
Age	Host rocks: Miocene (16.5–13.0 Ma) Mineralization: Miocene (12.3 Ma)
Tectonic setting	Late oceanic arc
Structural features	Mineralization and alteration are controlled by northwest-striking faults and a phreatic explosion breccia
References	Russell and Finlayson (1987), Russell (1990), Corbett et al. (1994)

Table 11.32 Yao'an, Yunnan Province, China

Deposit	Yao'an
Mineralization	Porphyry gold
Estimated reserves	About 0.3 Moz of gold
Location	In the western Yunnan Province, China
Host rocks	Quartz-monzonite
Texture	Porphyritic
Structure	Medium grained
Mineralogy	Phenocrysts: Pl-Qz-Af-Bio Groundmass: Af-Pl
Geochemistry	Shoshonitic, with high LILE, moderate LREE, low HFSE, but high Nb (up to 26 ppm)
Ore minerals	Py-Cpy
Alteration	Potassic, phyllic, and propylitic
Age	Host rocks: Eocene to Oligocene (33.4 ± 1.6 Ma) Mineralization: Coeval with host rocks
Tectonic setting	Postcollisional arc
Structural features	The orebodies are located between two northwest-trending strike-slip faults, developed in the core of a northwest-trending anticline, and are controlled by east-striking secondary structures
References	Bi et al. (2004), Hu et al. (2004), Lu et al. (2013a, b)

References

- Ahmad M (1979) Fluid inclusion and geochemical studies at the Emperor gold mine, Fiji. Unpl. Ph.D. thesis, University of Tasmania, Hobart
- Anderson WB, Eaton PC (1990) Gold mineralization at the Emperor mine, Vatukoula, Fiji. In: Hedenquist JW, White NC, Siddeley G (eds) Epithermal gold mineralization of the circum-pacific; geology, geochemistry, origin and exploration, II; *J Geochem Explor* 36:267–296
- Appleby AK, Circosta G, Fanning M, Logan K (1995) A new model for controls on Au–Ag mineralization on Misima Island, Papua New Guinea. Proceedings of 101st annual Northwest Mining Association Convention. Northwest Mining Association, Spokane, pp 122–127
- Arnold GO, Griffin TJ (1978) Intrusions and porphyry copper prospects of the Star mountains, Papua New Guinea. *Econ Geol* 73:785–795
- Baksheev IA, Chitalin AF, Yapaskurt VO, Vigasina MF, Bryzgalov IA, Ustinov VI (2010) Tourmaline in the Vetka porphyry copper-molybdenum deposit of the Chukchi Peninsula of Russia. *Mosc Univ Geol Bull* 65:27–38
- Baksheev IA, Prokof'ev VY, Zaraisky GP, Chitalin AF, Yapaskurt VO, Nikolaev YN, Tikhomirov PL, Nagornaya EV, Rogacheva LI, Gorelikova NV, Kono-nov OV (2012) Tourmaline as a prospecting guide for porphyry-style deposits. *Eur J Mineral* 24:957–979
- Baksheev IA, Nikolaev YN, Prokof'ev VY, Nagornaya EV, Sidorina YN, Maruschenko LI, Kal'ko IA, Chitalin AF (2013) Porphyry-epithermal system of the Baimka Cu–Au trend, western Chukchi Peninsula, Russia. *SGA Newsletter* 2013, p A193
- Bamford RW (1972) The Mount Fubilan (Ok Tedi) porphyry copper deposit, territory of Papua and New Guinea. *Econ Geol* 67:1019–1033
- Barter CF, Kelly JL (1982) Geology of the Twin Buttes mineral deposit, Pima mining district, Pima County, Arizona. In: Titley SR (ed) *Advances in geology of the porphyry copper deposits, Southwestern North America*. University of Arizona Press, Tucson, Arizona, pp 407–432
- Bi X, Hu R, Cornell DH (2004) The alkaline porphyry associated Yao'an gold deposit, Yunnan, China: rare earth element and stable isotope evidence for magmatic-hydrothermal ore formation. *Mineral Deposita* 39:21–30
- Bissig T, Lee JKW, Clark AH, Heather KB (2001) The Cenozoic history of volcanism and hydrothermal alteration in the Central Andean flat-slab region: new ^{40}Ar – ^{39}Ar constraints from the El Indio-Pascua Au (–Ag, Cu) Belt, 29°20'–30°30' S. *Int Geol Rev* 43:312–340
- Bissig T, Clark AH, Lee JKW, Hodgson CJ (2002) Miocene landscape evolution and geomorphologic controls on epithermal processes in the El Indio-Pascua Au–Ag–Cu belt, Chile and Argentina. *Econ Geol* 97:971–996
- Bissig T, Clark AH, Lee JKW, von Quadt A (2003) Petrogenetic and metallogenetic responses to Miocene slab flattening: new constraints from the El Indio-Pascua Au–Ag–Cu belt, Chile/Argentina. *Mineral Deposita* 38:844–862
- Blackwell JL, Cooke DR, McPhie J, Simpson KA (2014) Lithofacies associations and evolution of the volcanic host succession to the Minifie ore zone: Ladolam gold deposit, Lihir Island, Papua New Guinea. *Econ Geol* 109:1137–1160
- Blevin PL (2002) The petrographic and compositional character of variably K-enriched magmatic suites associated with Ordovician porphyry Cu–Au mineralization in the Lachlan Fold Belt, Australia. *Mineral Deposita* 37:87–99
- Blichert-Toft J, Arndt NT, Ludden JN (1996) Precambrian alkaline magmatism. *Lithos* 37:97–111
- Bowman JR, Parry WT, Kropp WP, Kruer SA (1987) Chemical and isotopic evolution of hydrothermal solutions at Bingham, Utah. *Econ Geol* 82:395–428
- Brunker RL, Caithness SJ, (1990) Mount Kare gold deposit. In: Hughes FE (ed) *Geology of the mineral resources of Australia and Papua New Guinea*. The Australasian institute of mining and metallurgy, Parkville, Australasian Institute of Mining and Metallurgy Monograph, vol 14, pp 1755–1758
- Butcher A, Cunningham R, Edwards K, Lye A, Simmons J, Stegman C, Wyllie A (2011) Northparkes mines. In: *Australasian mining and metallurgical operating practices*. AusIMM Monograph, vol 28, pp 861–878
- Butler BS (1920) Oquirrh range. In: *The ore deposits of Utah*. US geological survey professional paper, vol 111, pp 335–362
- Cameron GH (1998) The hydrothermal evolution and genesis of the Porgera gold deposit, Papua New Guinea. Unpl. Ph.D. thesis, Australian National University, Canberra, 137 p
- Carman GD (1994) Genesis of the Ladolam gold deposit, Lihir Island, Papua New Guinea. Unpl. Ph.D. thesis, Monash University, Melbourne
- Carman GD (2003) Geology, mineralization and hydrothermal evolution of the Ladolam gold deposit, Lihir Island, Papua New Guinea. *Econ Geol Spec Publ* 10:247–284
- Chen YJ, Pirajno F, Wu G, Qi JP, Xiong XL (2012) Epithermal deposits in North Xinjiang, NW China. *Int J Earth Sci* 101:889–917
- Chitalin AF, Fomichev E, Usenko V, Agapitov D, Shtengelov A (2012) Structural model of the Peschanka porphyry Cu–Au–Mo deposit, western Chukotka, Russia. In: Vearncombe J (ed) *Structural geology and resources—2012*. Australian Institute of Geosciences Symposium, Kalgoorlie, 26–28 Sept 2012, pp 21–27
- Clark DS (1988) Lateral zonation within epithermal gold mineralization, Misima Island, Papua New Guinea. *Australas Inst Min Metall Bull Proc* 293:63–66

- Clark DS, Lewis RW, Waldron HM (1990) Geology and trace-element geochemistry of the Umuna gold-silver deposit, Misima Island, Papua New Guinea. *J Geochem Explor* 36:201–223
- Corbett GJ (1999) Comments on the structural controls and styles of gold mineralization in the Minifie pit, Lihir Island. Unpl Report to Lihir Management Company, Port Moresby, p 23
- Corbett GJ, Leach TM (1998) Southwest Pacific rim and gold-copper systems: structure, alteration, and mineralization. *Econ Geol Spec Publ* 6:1–236
- Corbett GJ, Leach TM, Shatwell DO, Hayward SB (1994) Gold mineralization on Woodlark Island, Papua New Guinea. In: Rogerson R (ed) *Geology, Exploration and Mining Conference*, June 1994, Lae, Papua New Guinea, Proceedings. Australasian Institute of Mining and Metallurgy, Parkville, pp 92–100
- Corbett GJ, Hunt S, Cook A, Tamaduk P, Leach T (2001) Geology of the Ladolam gold deposit, Lihir Island, from exposures in the Minifie open pit. PNG *Geology, exploration and mining conference*, June 2001, Port Moresby, pp 69–77
- Crane D, Kavalieris I (2012) Geologic overview of the Oyu Tolgoi porphyry Cu-Au-Mo deposits, Mongolia. *Econ Geol Spec Publ* 16:187–213
- Dimock RR, Carter CJ, Forth JR, Hoogvliet H, Jacobsen WL, Ketcham VJ, Probert TI, Thiel KF, Watson DL, Zavodni ZM (1993) Proposed gold ore mining and treatment operations at the Lihir Island Project, New Ireland Province, Papua New Guinea. *Australas Inst Min Metall Monogr* 19:913–922
- Dolgoplova A, Seltmann R, Armstrong R, Belousova E, Pankhurst RJ, Kavalieris I (2013) Sr-Nd-Pb-Hf isotope systematic of the Hugo Dummett Cu-Au porphyry deposit (Oyu Tolgoi, Mongolia). *Lithos* 167:47–64
- Einaudi MT (1982) Description of skarns associated with porphyry copper plutons. In: Titley SR (ed) *Advances in geology of the porphyry copper deposits, Southwestern North America*. University of Arizona Press, Tucson, pp 139–183
- Fallon SJ, White JC, McCulloch MT (2002) Porite corals as recorders of mining and environmental impacts: Misima Island, Papua New Guinea. *Geochim Cosmochim Acta* 66:45–62
- Fleming AW, Handley GA, Williams KL, Hills AL, Corbett GJ (1986) The Porgera gold deposit, Papua New Guinea. *Econ Geol* 81:660–680
- Frei R (1992) Isotope (Pb-Rb-Sr-S-O-C-U-Pb) geochemical investigations on tertiary intrusions and related mineralizations in the Serbo-Macedonian (Pb-Zn, Sb +Cu-Mo metallogenic) Province in northern Greece. Unpl. Ph.D. thesis, ETH Zürich, Switzerland
- Garrett S (1996) The geology and mineralization of the Dinkidi porphyry-related Au-Cu deposit. In: *Porphyry-related copper and gold deposits of the Asia Pacific region*. Australian Mineral Foundation, Cairns, pp 6.0–6.15
- Gray JE, Coolbaugh MF (1994) *Geology and geochemistry of Summitville, Colorado: an epithermal acid sulphate deposit in a volcanic dome*. *Econ Geol* 89:1906–1923
- Gröpper H, Calvo M, Crespo H, Bisso CR, Cuadra WA, Dunkerley PM, Aguirre E (1991) The epithermal gold-silver deposit of Choquelimpie, Northern Chile. *Econ Geol* 86:1206–1221
- Groves DI, Ho SE (1990) A short review of gold in the Yilgarn Block. In: Hughes FE (ed) *Geology of the mineral resources of Australia and Papua New Guinea*. Australas Inst Min Metall Monogr 14:539–553
- Gruen G, Heinrich CA, Schroeder K (2010) The Bingham Canyon porphyry Cu-Mo-Au deposit. II. Vein geometry and ore shell formation by pressure-driven rock extension. *Econ Geol* 105:69–90
- Hagemann SG (1993) *The Wiluna lode-gold deposits, Western Australia: a case study of a high crustal level Archaean lode-gold system*. Unpl. Ph.D. thesis, The University of Western Australia, Perth
- Hagemann SG, Groves DI, Ridley JR, Vearncombe JR (1992) The Archaean lode gold deposits at Wiluna, Western Australia: high-level brittle-style mineralization in a strike-slip regime. *Econ Geol* 87:1022–1053
- Haggman JA (1997a) Philippines exploration: discovery of the Dinkidi gold-copper porphyry. *Min Eng* 49:34–39
- Haggman (1997b) The discovery, exploration and future development of the Didipio Project. In: *World gold '97 conference*. Australasian institute of mining and metallurgy publication series, vol 2, no 97, pp 183–188
- Handley GA, Henry DD (1990) Porgera gold deposit. In: Hughes FE (ed.) *Geology of the mineral deposits of Australia and Papua New Guinea*, vol 14. Australasian Institute of Mining and Metallurgy, Parkville, Monograph, pp 1717–1724
- Harper BL (2000) Hydrothermal alteration at the Ridge-way porphyry gold-copper deposit, NSW. Unpl. Honours thesis, University of Tasmania, Hobart
- Harris AC, Holcombe RJ (2014) Quartz vein emplacement at the E26 porphyry Cu–Au deposit, New South Wales. *Econ Geol* 109:1035–1050
- Harris AC, Kamenetsky VS, White NC, Steele DA (2004) Volatile phase separation in silicic magmas at Bajo de la Alumbrera porphyry Cu-Au deposit, NW Argentina. *Res Geol* 54:341–356
- Heidari SM, Daliran F, Paquette JL, Gasquet D (2015) Geology, timing, and genesis of the high sulphidation Au (-Cu) deposit of Touzlar, NW Iran. *Ore Geol Rev* 65:460–486
- Heithersay PS, Walshe JL (1995) Endeavour 26 North: a porphyry copper-gold deposit in the Late Ordovician shoshonitic Goonumbra volcanic complex, New South Wales, Australia. *Econ Geol* 90:1506–1532
- Heithersay PS, O'Neill WJ, van der Helder P, Moore CR, Harbon PG (1990) Goonumbra porphyry copper district—Endeavour 26 North, Endeavour 22 and Endeavour 27 copper-gold deposits. In: Hughes FE (ed) *Geology of the mineral resources of Australia and Papua New Guinea*, vol 14. Australasian Institute of Mining and Metallurgy, Parkville, Monograph, pp 1385–1398

- Hettler J, Irion G, Lehmann B (1997) Environmental impact of mining waste disposal on a tropical lowland river system: a case study on the Ok Tedi mine, Papua New Guinea. *Mineral Deposita* 32:280–291
- Hickson RJ (1991) Grasberg open-pit: Ertsberg's big brother comes onstream in Indonesia. *Min Eng* 43:385–391
- Holliday JR, McMillan C, Tedder I (1999) Discovery of the Cadia Ridgeway gold-copper deposit. New generation gold mines—case histories of discovery. Australian Mineral Foundation, Perth, pp 101–107
- Holliday JR, Wilson AJ, Blevin PL, Tedder IJ, Dunham PD, Pfitzner M (2002) Porphyry gold-copper mineralization in the Cadia district, eastern Lachlan Fold Belt, New South Wales, and its relationship to shoshonitic magmatism. *Mineral Deposita* 37:100–116
- Hoogvliet H (1993) The Ladolam gold deposit—at least two major events. *Aust J Min* 20
- Hu RZ, Burnard PG, Bi XW, Zhou MF, Pen JT, Su WC, Wu KX (2004) Helium and argon isotope geochemistry of alkaline intrusion-associated gold and copper deposits along the Red River-Jinshajiang fault belt, SW China. *Chem Geol* 203:305–317
- Hu YB, Liu JQ, Ling MX, Ding W, Liu Y, Zartman RE, Ma XF, Liu DY, Zhang CC, Sun SJ, Zhang LP, Wu K, Sun WD (2015) The formation of Qulong adakites and their relationship with porphyry copper deposit: geochemical constraints. *Lithos* 223:60–80
- Jannas RR, Beane RE, Ahler BA, Brosnahan DR (1990) Gold and copper mineralization at the El Indio deposit, Chile. *J Geochem Explor* 36:233–266
- Jensen EP (2003) Magmatic and hydrothermal evolution of the Cripple Creek gold deposit, Colorado, and comparisons with regional and global magmatic-hydrothermal systems associated with alkaline magmatism. Unpl. Ph.D. thesis, The University of Arizona, Tucson
- Jensen EP, Barton MD (1997) Types of potassium silicate alteration and related base metal mineralization in the Cripple Creek district, Colorado. *Geol Soc Am Abstr Programs* 29:207
- Jones GJ (1985) The Goonumbla porphyry copper deposits, N.S.W. *Econ Geol* 80:591–613
- Kamenetsky VS, Wolfe RC, Eggins SM, Mernagh TP, Bastrakov E (1999) Volatile exsolution at the Dinkidi Cu-Au porphyry deposit, Philippines: a melt-inclusion record of the initial ore-forming process. *Geology* 27:691–694
- Kashgerel BE, Rye RO, Hedenquist JW, Kavalieris I (2006) Geology and reconnaissance stable isotope study of the Oyu Tolgoi porphyry Cu-Au system, South Gobi, Mongolia. *Econ Geol* 101:503–522
- Kashgerel BE, Kavalieris I, Hayashi KI (2008) Mineralogy, textures, and whole-rock geochemistry of advanced argillic alteration: Hugo Dummett porphyry Cu-Au deposit, Oyu Tolgoi mineral district, Mongolia. *Miner Deposita* 43:913–932
- Kashgerel BE, Rye RO, Kavalieris I, Hayashi KI (2009) The sericitic to advanced argillic transition: stable isotope and mineralogical characteristics from the Hugo Dummett porphyry Cu–Au deposit, Oyu Tolgoi District, Mongolia. *Econ Geol* 104:1087–1110
- Kavalieris I, Wainwright A (2005) Whole-rock geochemistry of Late-Devonian island arc and intrusive suites from Oyu Tolgoi, South Gobi, Mongolia. In: Seltmann R, Gerel O, Kirwin D (eds) *Geodynamics and Metallogeny of Mongolia with a special emphasis on copper and gold deposits*, vol 11. IAGOD Guidebook Series, pp 169–174
- Keith JD, Whitney JA, Hattori K, Ballantyne GH, Christiansen EH, Barr DL, Cannan TM, Hook CJ (1997) The role of magmatic sulphides and mafic alkaline magmas in the Bingham and Tintic mining districts, Utah. *J Petrol* 38:1679–1690
- Kelley KD, Ludington S (2002) Cripple Creek and other alkaline-related gold deposits in the southern Rocky Mountains, USA: influence of regional tectonics. *Mineral Deposita* 37:38–60
- Kelly JL (1977) Geology of the Twin Buttes copper deposit, Pima County, Arizona. *SME-AIME Trans* 262:110–116
- Kelley KD, Romberger SB, Beaty DW, Pontius JA, Snee LW, Stein HJ, Thompson TB (1998) Geochemical and geochronological constraints on the genesis of Au-Te deposits at Cripple Creek, Colorado. *Econ Geol* 93:981–1012
- Kent AJR, Hagemann SG (1996) Constraints on the timing of lode-gold mineralization in the Wiluna greenstone belt, Yilgarn Craton, Western Australia. *Aust J Earth Sci* 43:573–588
- Keyser F (1961) Misima Island—geology and gold mineralization. *Bur Mineral Res Aust BMR Rep* 57:1–36
- Kroll T, Müller D, Seifert T, Herzig PM, Schneider A (2002) Petrology and geochemistry of the shoshonite-hosted Skouries porphyry Cu–Au deposit, Chalkidiki, Greece. *Mineral Deposita* 37:137–144
- Lan TG, Fan HR, Santosh M, Hu FF, Yang KF, Yang YH (2012) Early Jurassic high-K calc-alkaline and shoshonitic rocks from the Tongshi intrusive complex, eastern North China Craton: implication for crust-mantle interaction and post-collisional magmatism. *Lithos* 140:183–199
- Landtwing MR, Furrer C, Pettke T, Guillong M, Heinrich CA (2010) The Bingham Canyon porphyry Cu-Mo-Au deposit: III. Zoned copper-gold ore deposition by magmatic vapor expansion. *Econ Geol* 105:91–118
- Lanier G, John EC, Swensen AJ, Reid J, Bard CE, Cadday SW, Wilson JC (1978a) General geology of the Bingham mine, Bingham Canyon, Utah. *Econ Geol* 73:1228–1241
- Lanier G, Raab WJ, Folsom RB, Cone S (1978b) Alteration of equigranular monzonite, Bingham mining district, Utah. *Econ Geol* 73:1270–1286

- Lewis RW, Wilson GI (1990) Misima gold deposit. In: Hughes FE (ed) *Geology of the mineral resources of Australia and Papua New Guinea*, vol 14. Australasian Institute of Mining and Metallurgy, Parkville, Monograph, pp 1741–1745
- Li HQ, Xie CF, Chang HL, Cai H, Zhu JP, Zhou S (1998) Study on metallogenetic chronology of nonferrous and precious metallic ore deposits in North Xinjiang, China. Geological Publishing House, Beijing, 264 p (in Chinese)
- Lickfold V, Cooke DR, Smith SG, Ullrich TD (2003) Endeavour Cu–Au porphyry deposits, Northparkes, NSW: intrusive history and fluid evolution. *Econ Geol* 98:1607–1636
- Lindgren W (1933) *Mineral deposits*, 4th edn. McGraw-Hill Book Company, New York, p 797
- Lindgren W, Ransome FL (1906) *Geology and gold deposits of the Cripple Creek district, Colorado*. US Geol Surv Prof Pap 54:1–516
- Loughlin GF, Koschmann AH (1935) *Geology and ore of the Cripple Creek District, Colorado*. Proc Colorado Sci Soc 13:217–435
- Lu YJ, Kerrich R, McCuaig TC, Li ZX, Hart CJR, Cawood PA, Hou ZQ, Bagas L, Cliff J, Belousova EA, Tang S (2013a) Geochemical, Sr–Nd–Pb, and zircon Hf–O isotopic compositions of Eocene–Oligocene shoshonitic and potassic adakite-like felsic intrusions in western Yunnan, SW China: petrogenesis and tectonic implications. *J Petrol* 54:1309–1348
- Lu YJ, Kerrich R, Kemp AIS, McCuaig TC, Hou ZQ, Hart CJR, Li ZX, Cawood PA, Bagas L, Yang ZM, Cliff J, Belousova EA, Jourdan F, Evans NJ (2013b) Intracontinental Eocene–Oligocene porphyry Cu mineral systems of Yunnan, western Yangtze Craton, China: compositional characteristics, sources, and implications for continental collision metallogeny. *Econ Geol* 108:1541–1576
- MacDonald GD, Arnold LC (1994) Geological and geochemical zoning of the Grasberg igneous complex, Irian Jaya, Indonesia. *J Geochem Explor* 50:143–178
- Maraeva RN, Migachev IF, Sapozhnikov VG, Shishakov VB (1988) Geological settings of copper-porphyry mineralization in the western Chukotka. In: Migachev IF (ed) *Mineralization of porphyry type in the far east of Russia*. Far East Branch of the USSR Academy of Science Publishing, pp 94–105
- Marushchenko LI (2013) The mineralogy of propylites of the large Peschanka porphyry copper deposit (West Chukotka). *Moscow Univ Geol Bull* 68:79–88
- Marushchenko LI, Bakshiev IA, Nagornaya EV, Chitalin AF, Nikolaev YN, Kalko IA, Prokofiev VY (2015) Quartz-sericite and argillic alterations at the Peschanka Cu–Mo–Au deposit, Chukchi Peninsula, Russia. *Geol Ore Dep* 57:213–225
- Maughan DT, Keith JD, Christiansen EH, Pulsipher T, Hattori K, Evans NJ (2002) Contributions from mafic alkaline magmas to the Bingham porphyry Cu–Au–Mo deposit, Utah, USA. *Mineral Deposita* 37:14–37
- McIntyre J, Moore J, Wyche J (2010) Technical report for the Didipio gold-copper project, Luzon, Philippines. Unpl. OceanaGold company report, 29th Oct 2010, 171 p
- McMahon T (1994) Pliocene intrusions in the Gunung Bijih (Ertsberg) mining District, Irian Jaya, Indonesia: major and trace element chemistry. *Int Geol Rev* 36:925–946
- Mehnert HH, Lipman PW, Steven TA (1973) Age of mineralization at Summitville, Colorado, as indicated by K–Ar dating of alunite. *Econ Geol* 68:399–401
- Moyle AJ, Doyle BJ, Hoogvliet H, Ware AR (1990) Ladolam gold deposit, Lihir Island. In: Hughes FE (ed) *Geology of the mineral resources of Australia and Papua New Guinea*, vol 14. Australasian Institute of Mining and Metallurgy, Parkville, Monograph, pp 1793–1805
- Müller D, Forrestal P (1998) The shoshonite porphyry Cu–Au association at Bajo de la Alumbrera, Catamarca Province, Argentina. *Mineral Petrol* 64:47–64
- Müller D, Heithersay PS, Groves DI (1994) The shoshonite porphyry Cu–Au association in the Goonumbla district, N.S.W., Australia. *Mineral Petrol* 51:299–321
- Müller D, Franz L, Herzig PM, Hunt S (2001) Potassic igneous rocks from the vicinity of epithermal gold mineralization, Lihir Island, Papua New Guinea. *Lithos* 57:163–186
- Müller D, Kaminski K, Uhlig S, Graupner T, Herzig PM, Hunt S (2002a) The transition from porphyry- to epithermal-style gold mineralization at Ladolam, Lihir Island, Papua New Guinea: a reconnaissance study. *Mineral Deposita* 37:61–74
- Müller D, Herzig PM, Scholten JC, Hunt S (2002b) Ladolam gold deposit, Lihir Island, Papua New Guinea: gold mineralization hosted by alkaline rocks. *Econ Geol Spec Publ* 9:367–382
- Müller D, Franz L, Petersen S, Herzig PM, Hannington MD (2003) Comparison between magmatic activity and gold mineralization at Conical Seamound and Lihir Island, Papua New Guinea. *Mineral Petrol* 79:259–283
- Mutschler FE, Mooney TC (1993) Precious metal deposits related to alkaline igneous rocks—provisional classification, grade-tonnage data, and exploration frontiers. In: Kirkham RV, Sinclair WD, Thorpe RI, Duke JM (eds) *Mineral deposit modeling*, vol 40. Geol Assoc Canada Spec Pap, pp 479–520
- Mutschler FE, Griffin ME, Scott-Stevens D, Shannon SS (1985) Precious-metal deposits related to alkaline rocks in the North American Cordillera—an interpretative view. *Trans Geol Soc S Afr* 88:355–377
- Nagornaya EV (2010) Wall-rock alteration at the porphyry copper-molybdenum deposits of the Baimka ore cluster, Chukchi Peninsula. In: *International conference on geochemistry of alkaline rocks*, 12–16 Sept 2010, Moscow, p 12
- Nikolaev YN, Prokof'ev VY, Apletalin AV, Vlasov EA, Bakshiev IA, Kal'ko IA, Komarova YS (2013)

- Gold-telluride mineralization of the western Chukchi Peninsula, Russia: mineralogy, geochemistry, and formation conditions. *Geol Ore Deposits* 55:96–124
- Nikolaev YN, Prokof'ev VY, Baksheev IA, Chitalin AF, Marushchenko LI, Kal'ko IA (2014) The first data on the zoned distribution of fluid inclusions in the ore-forming system of the Peschanka gold-copper porphyry deposit (Northeast Russia). *Dokl Earth Sci* 459:1615–1618
- Pals DW, Spry PG (2003) Telluride mineralogy of the low-sulfidation epithermal Emperor gold deposit, Vatukoula, Fiji. *Mineral Petrol* 79:285–307
- Pals DW, Spry PG, Chryssoulis S (2003) Invisible gold and tellurium in arsenic-rich pyrite from the Emperor gold deposit, Fiji: implications for gold distribution and deposition. *Econ Geol* 98:479–493
- Perello J, Cox D, Garamjav D, Sanjdorj S, Diakov S, Schissel D, Munkhbat TO, Oyun G (2001) *Econ Geol* 96:1407–1428
- Perkins C, McDougall I, Clauè-Long J, Heithersay PS (1990a) $^{40}\text{Ar}/^{39}\text{Ar}$ and U-Pb geochronology of the Goonumbla porphyry Cu-Au deposits, N.S.W., Australia. *Econ Geol* 85:1808–1824
- Perkins C, McDougall I, Clauè-Long J (1990b) Dating of ore deposits with high precision: examples from the Lachlan Fold Belt, N.S.W., Australia. In: *Proceedings of Pacific Rim congress 90*. Australasian Institute of Mining and Metallurgy, Parkville, pp 105–112
- Perring CS (1988) Petrogenesis of the lamprophyre-“porphyry” suite from Kambalda, Western Australia. In: Ho SE, Groves DI (eds) *Advances in understanding precambrian gold deposits volume II*, vol 12. Geology Department & University Extension, The University of Western Australia, Perth, Publication, pp 277–294
- Peterson EC, Mavrogenes JA (2014) Linking high-grade gold mineralization to earthquake-induced fault-valve processes in the Porgera gold deposit, Papua New Guinea. *Geology* 42:383–386
- Plimer IR, Andrew AS, Jenkins R, Lottermoser BG (1988) The geology and geochemistry of the Lihir gold deposit, Papua New Guinea. *Geol Soc Austr Abstr* 22:139–143
- Pollard PJ, Taylor RG (2002) Paragenesis of the Grasberg Cu-Au deposit, Irian Jaya, Indonesia: results from logging section 13. *Mineral Deposita* 37:117–136
- Pollard PJ, Taylor RG, Peters L (2005) Ages of intrusion, alteration, and mineralization at the Grasberg Cu-Au deposit, Papua, Indonesia. *Econ Geol* 100:1005–1020
- Proffett JM (2003) Geology of the Bajo de la Alumbrera porphyry copper-gold deposit, Argentina. *Econ Geol* 98:1535–1574
- Redmond PB, Einaudi MT (2010) The Bingham canyon porphyry Cu-Mo-Au deposit: I. sequence of intrusion, vein formation, and sulfide deposition. *Econ Geol* 105:43–68
- Redmond PB, Einaudi MT, Inan EE, Landtwing MR, Heinrich CA (2004) Copper deposition by fluid cooling in intrusion-centered systems: new insights from the Bingham porphyry ore deposit, Utah. *Geology* 32:217–220
- Reyes M (1991) The Andacollo strata-bound gold deposit, Chile, and its position in a porphyry copper-gold system. *Econ Geol* 86:1301–1316
- Richards JP (1990a) The Porgera gold deposit, Papua New Guinea: geology, geochemistry and geochronology. Unpl. Ph.D. thesis, The Australian National University, Canberra
- Richards JP (1990b) Petrology and geochemistry of alkaline intrusive at the Porgera gold deposit, Papua New Guinea. *J Geochem Explor* 35:141–199
- Richards JP (1992) Magmatic-epithermal transitions in alkali systems: porgera gold deposit, Papua New Guinea. *Geology* 20:547–550
- Richards JP, Ledlie I (1993) Alkalic intrusive rocks associated with the Mount Kare gold deposit, Papua New Guinea: comparison with the Porgera intrusive complex. *Econ Geol* 88:755–781
- Richards JP, Chappell BW, McCulloch MT (1990) Intraplate-type magmatism in a continent-island-arc collision zone: Porgera intrusive complex, Papua New Guinea. *Geology* 18:958–961
- Richards JP, McCulloch MT, Chappell BW, Kerrich R (1991) Sources of metals in the Porgera gold deposit, Papua New Guinea: evidence from alteration, isotope, and noble metal geochemistry. *Geochim Cosmochim Acta* 55:565–580
- Ronacher E, Richards JP, Villeneuve ME, Johnston MD (2002) Short life-span of the ore-forming system at the Porgera gold deposit, Papua New Guinea: laser $^{40}\text{Ar}/^{39}\text{Ar}$ dates for roselite, biotite, and hornblende. *Mineral Deposita* 37:75–86
- Ronacher E, Richards JP, Reed MH, Bray CJ, Spooner ETC, Adams PD (2004) Characteristics and evolution of the hydrothermal fluid in the North Zone high-grade area, Porgera gold deposit, Papua New Guinea. *Econ Geol* 99:843–867
- Rowins SM, Cameron EM, Lalonde AE, Ernst RE (1993) Petrogenesis of the late Archaean syenitic Murdoch Creek pluton, Kirkland Lake, Ontario: evidence for an extensional tectonic setting. *Can Mineral* 31:219–244
- Rush PM, Seegers HJ (1990) Ok Tedi copper-gold deposit. In: Hughes FE (ed) *Geology of the mineral deposits of Australia and Papua New Guinea*, vol 14. Australasian Institute of Mining and Metallurgy, Parkville, Monograph, pp 1747–1754
- Russell PJ (1990) Woodlark Island gold deposits. In: Hughes FE (Ed.), *Geology of the mineral deposits of Australia and Papua New Guinea*, vol 14. Australasian Institute of Mining and Metallurgy, Parkville, Monograph, pp 1735–1739
- Russell PJ, Finlayson EJ (1987) Volcanic-hosted epithermal mineralization on Woodlark Island, Papua New Guinea. In: *Pacific Rim Congress 87, Gold Coast, Queensland*. Australasian Institute of Mining and Metallurgy, Parkville, PACRIM 87 Proceedings, 26–29 Aug 1987, pp 381–385

- Salek H (1976) The silver occurrence study of a sample from the Twin Buttes project, Pima County, Arizona. Unpublished. Anaconda Company Report, 1976
- Salier BS, Groves DI, McNaughton NJ, Fletcher IR (2005) Geochronological and stable isotope evidence for widespread orogenic gold mineralization from deep seated fluid source at ca. 2.65 Ga in the Laverton Gold Province, Western Australia. *Economic Geology* 100:1363–1388
- Scherbarth NL, Spry PG (2006) Mineralogical, petrological, stable isotope, and fluid inclusion characteristics of the Tuvatu gold-silver telluride deposit, Fiji: comparisons with the Emperor deposit. *Econ Geol* 101:135–158
- Seltmann R, Solovieva R, Shatov V, Pirajno F, Naumov E, Cherkasov S (2010) Metallogeny of Siberia: tectonic, geologic and metallogenic settings of selected significant deposits. *Aust J Earth Sci* 57:655–706
- Setterfield TN (1991) Evolution of the Tavua caldera and associated hydrothermal systems, Fiji. Unpl. Ph.D. thesis, University of Cambridge, Cambridge
- Setterfield TN, Eaton PC, Rose WJ, Sparks RSJ (1991) The Tavua caldera, Fiji: a complex shoshonitic caldera formed by concurrent faulting and downsagging. *Journal of the Geological Society* 148:115–127
- Setterfield TN, Mussett AE, Oglethorpe RDJ (1992) Magmatism and associated hydrothermal activity during the evolution of the Tavua caldera: ^{40}Ar - ^{39}Ar dating on the volcanic, intrusive and hydrothermal events. *Econ Geol* 87:1130–1140
- Siddeley G, Araneda R (1986) The El Indio—Tambo gold deposits, Chile. In: Macdonald AJ (ed) *Proceedings of Gold '86 international symposium on the geology of gold deposits*, Toronto, pp 445–456
- Sidorov AA, Eremin RA (1994) Metallogeny and gold lode deposits of northeastern Russia. In: ICAM-94 *Proceedings*, pp 247–256
- Sillitoe RH (1991) Gold metallogeny of Chile—an introduction. *Econ Geol* 86:1187–1205
- Simmons SF, Brown KL (2006) Gold in magmatic hydrothermal solutions and rapid formation of a giant ore deposit. *Science* 314:288–291
- Smith B, Smith C, Wilson EW (2008) The Emperor mine, Vatukoula, Viti Levu, Fiji. *Mineral Rec* 39:397–301
- Soloviev SG (2014a) The metallogeny of shoshonitic magmatism, vol I. Scientific World Publications, Moscow, pp 1–528 (in Russian)
- Soloviev SG (2014b) The metallogeny of shoshonitic magmatism, vol II. Scientific World Publications, Moscow, pp 1–472 (in Russian)
- Spooner ETC (1993) Magmatic sulphide/volatile interaction as a mechanism for producing chalcophile element-enriched, Archaean Au-quartz hydrothermal ore fluids. *Ore Geol Rev* 7:359–379
- Lehmann St, Barcikowski J, von Quadt A, Gallhofer D, Peytcheva I, Heinrich CA, Serafimovski T (2013) Geochronology, geochemistry and isotope tracing of the Oligocene magmatism of the Buchim-Damjan-Borov Dol ore district: implications for timing, duration and source of the magmatism. *Lithos* 181:216–233
- Stoffregen R (1987) Genesis of acid-sulphate alteration and Au-Cu-Ag mineralization at Summitville, Colorado. *Econ Geol* 82:1575–1591
- Stults A (1985) Geology of the Bajo de la Alumbrera porphyry copper-gold prospect, Catamarca Province, Argentina. Unpl. M.Sc. thesis, The University of Arizona, Tucson
- Tedder IJ, Holliday JR, Hayward S (2001) Discovery and evaluation drilling of the Cadia Far East gold-copper deposit. *NewGen Gold 2001*, Australian Mineral Foundation, Perth, pp 212–216
- Thompson TB, Trippel AD, Dwelley PC (1985) Mineralized veins and breccias of the Cripple Creek district, Colorado. *Econ Geol* 80:1669–1688
- Tobey E, Schneider A, Alegria A, Olcay L, Perantonis G, Quiroga J (1998) Skouries porphyry copper-gold deposit, Chalkidiki, Greece. In: Porter TM (ed) *Porphyry and hydrothermal Cu-Au deposits. A global perspective*. Australian mineral foundation conference proceedings, Glenside, South Australia, pp 159–168
- Ulrich T, Heinrich CA (2002) Geology and alteration geochemistry of the porphyry Cu-Au deposit at Bajo de la Alumbrera, Argentina. *Econ Geol* 97:1865–1888
- Ulrich T, Günther D, Heinrich CA (2001) The evolution of a porphyry Cu-Au deposit, based on LA-ICP-MS analysis of fluid inclusions: Bajo de la Alumbrera, Argentina. *Econ Geol* 96:1743–1774
- Van Nort SD, Atwood GW, Collinson TB, Potter DR (1991) The geology and mineralization of the Grasberg porphyry copper-gold deposit, Irian Jaya, Indonesia. *Min Eng* 43:300–303
- Veranis N (1994) Geological structure and primary raw materials in the Chalkidiki Peninsula. IGME Report, Athens (in Greek)
- Vielreicher RW, Groves DI, Ridley JR, McNaughton NJ (1994) A replacement origin for the BIF-hosted gold deposit at Mt. Morgans, Yilgarn block, Western Australia. *Ore Geol Rev* 9:325–347
- Vielreicher N, Groves DI, McNaughton N, Fletcher I (2015) The timing of gold mineralization across the eastern Yilgarn craton using U-Pb geochronology of hydrothermal phosphate minerals. *Mineral Deposita* 50:391–428
- Vila T, Sillitoe RH (1991) Gold-rich porphyry systems in the Maricunga Belt, Northern Chile. *Econ Geol* 86:1238–1260
- Volchkov AG, Sokirkin GI, Shishakov VB (1982) Geological setting and ore composition of the Anyiskoe copper-porphyry deposit. *Geol Ore Deposits* 4:89–94
- Volkov AV, Savva NE, Sidorov AA, Egorov VN, Shapovalov VS, Prokof'ev VY, Kolova EE (2006) Spatial distribution and formation conditions of Au-bearing porphyry Cu-Mo deposits in the northeast of Russia. *Geol Ore Deposits* 48:448–472
- Wainwright AJ, Tosdal RM, Wooden JL, Mazdab FK, Friedman RM (2011) U-Pb (zircon) and geochemical constraints on the age, origin, and evolution of

- Paleozoic arc magmas in the Oyu Tolgoi porphyry Cu-Au district, southern Mongolia. *Gondwana Res* 19:764–787
- Waite KA, Keith JD, Christiansen EH, Whitney JA, Hattori K, Tingey DG, Hook CJ (1997) Petrogenesis of the volcanic and intrusive rocks associated with the Bingham Canyon porphyry Cu-Au-Mo deposit, Utah. In: John DA, Ballantyne GH (eds) *Geology and ore deposits of the Oquirrh and Wasatch mountains, Utah*, vol 29. *Economic Geology Guidebook Series*, pp 69–90
- Walker RT, Walker WJ (1956) The origin and nature of ore deposits. Walker Associates, Colorado Springs, unpaginated
- Wall VJ, Munroe SM, Cameron GH, Heinrich CA, Cox SF, Walshe JL (1995) Porgera: plumbing and processes of gold mineralization. In: Clark AH (ed) *Giant Ore Deposits—II. Proceedings of the second giant ore deposits workshop*, Queen's University, Kingston, Ontario, pp 649–667
- Wallace DA, Johnson RW, Chappell BW, Arculus RJ, Perfit MR, Crick IH (1983) Cainozoic volcanism of the Tabar, Lihir, Tanga, and Feni islands, Papua New Guinea: geology, whole-rock analyses, and rock-forming mineral compositions. *Bur Mineral Res Aust BMR Rep* 243:1–138
- Walthier TN, Sirvas E, Araneda R (1985) The El Indio gold, silver, copper deposit. *Eng Min J* 186:38–42
- Warnaars FW, Smith WH, Bray RE, Lanier G, Shafiqullah M (1978) Geochronology of igneous intrusions and porphyry copper mineralization at Bingham, Utah. *Econ Geol* 73:1242–1249
- Welsh TC (1975) Cadia copper-gold deposits. In: Knight CL (ed) *Economic geology of Australia and Papua New Guinea*, vol 5. Australasian Institute of Mining and Metallurgy, Parkville, Monograph, pp 711–716
- Wilson AJ, Cooke DR, Harper BL (2003) The Ridgeway gold-copper deposit: a high-grade alkali porphyry deposit in the Lachlan Fold Belt, New South Wales, Australia. *Econ Geol* 98:1637–1666
- Wilson AJ, Cooke DR, Stein HJ, Fanning CM, Holliday JR, Tedder IJ (2007) U-Pb and Re-Os geochronologic evidence for two alkali porphyry ore-forming events in the Cadia District, New South Wales, Australia. *Econ Geol* 102:3–26
- Wolfe RC (2001) Geology of the Didipio region and paragenesis of the Dinkidi Cu-Au porphyry deposit. Unpl. Ph.D. thesis, University of Tasmania, Hobart
- Wolfe RC, Cooke DR (2011) Geology of the Didipio region and genesis of the Dinkidi alkali porphyry Cu-Au deposit and related pegmatites, Northern Luzon, Philippines. *Econ Geol* 106:1279–1315
- Wolfe RC, Cooke DR, Joyce P (1998) The Dinkidi Au-Cu porphyry – an alkaline porphyry deposit from North Luzon, Philippines. *Geol Soc Aust Abstr* 49:131
- Wood D, Holliday JR (1995) Discovery of the Cadia gold/copper deposit. In: *New South Wales: new generation gold mines—case histories of discovery*. Australian Mineral Foundation, Perth, pp 11.1–11.10
- Wyman D (1990) *Archaeon shoshonitic lamprophyres of the Superior Province, Canada: petrogenesis, geodynamic setting, and implications for lode gold deposits*. Unpl. Ph.D. thesis, University of Saskatchewan, Saskatoon
- Wyman D, Kerrich R (1989a) *Archaeon shoshonitic lamprophyres associated with Superior Province gold deposits: distribution, tectonic setting, noble metal abundances and significance for gold mineralization*. In: Keays RR, Ramsay WRH, Groves DI (eds) *The geology of gold deposits: the perspective in 1988*, vol 6. *Economic Geology Monograph*, pp 651–667
- Wyman D, Kerrich R (1989b) *Archaeon lamprophyre dykes of the Superior Province, Canada: distribution, petrology and geochemical characteristics*. *J Geophys Res* 94:4667–4696
- Xiao B, Qin K, Li G, Li J, Xia D, Chen L, Zhao J (2012) Highly oxidized magma and fluid evolution of Miocene Qulong giant porphyry Cu-Mo deposit, southern Tibet, China. *Resource Geology* 62:4–18
- Xu WG, Fan HR, Hu FF, Santosh M, Yang KF, Lan TG, Wen BJ (2015) Geochronology of the Guilaizhuang gold deposit, Luxi Block, eastern North China Craton: constraints from zircon U-Pb and fluorite-calcite Sm-Nd dating. *Ore Geol Rev* 65:390–399
- Yang F, Mao J, Bierlein FP, Pirajno F, Zhao C, Ye H, Liu F (2009) A review of the geological characteristics and geodynamic mechanisms of late paleozoic epithermal gold deposits in North Xinjiang, China. *Ore Geol Rev* 35:217–234
- Zhao X, Xue C, Symons DTA, Zhang Z, Wang H (2014a) Microgranular enclaves in island-arc andesites: a possible link between known epithermal Au and potential porphyry Cu-Au deposits in the Tulasu ore cluster, western Tianshan, Xinjiang, China. *J Asian Earth Sci* 85:210–223
- Zhao X, Xue C, Chi G, Wang H, Qi T (2014b) Epithermal Au and polymetallic mineralization in the Tulasu Basin, western Tianshan, NW China: potential for the discovery of porphyry Cu-Au deposits. *Ore Geol Rev* 60:76–96

Index

- A**
Absarokite, 31
Accumulation, 29, 36
Accuracy, 31
Adakites, 39
 adakititic, 40
Adiabatically, 9
Africa, 12
 Bufumbira, 71
 Democratic Republic of the Congo, 70
 East African rift, 23, 70
 Karagwe-Ankolean System, 71
 Karisimbi, 71
 Kibaran Orogeny, 71
 Nyiragongo, 71
 Rwanda, 70
 South Africa, 78
 Frank Smith, 78
 Limpopo Belt, 213
 Wessleton, 78
 Toro-Ankole, 12
 Uganda, 70
 Virunga, 70
 Zimbabwe, 213
 Limpopo Belt, 213
Age, 57
 ^{40}Ar - ^{39}Ar dating, 115
 $^{40}\text{Ar}/^{39}\text{Ar}$ age, 223
 $^{40}\text{Ar}/^{39}\text{Ar}$ step-heating, 125
 Ar laser step-heating plateau ages, 154
 K-Ar, 172
 K-Ar ages, 83
 K/Ar mica cooling ages, 57
 Pb–Pb isochron, 204, 212
 U–Pb in zircon, 211, 219
 U/Pb zircon ages, 138
 Uranium–Pb zircon dating, 121
Alaska, 197
 Chatanika Terrane, 198
 Fairbanks, 197
 Fish Creek, 197
 Tintina gold province, 198
 Yukon–Tanana Terrane, 198
Alkali basalt, 11
Alkalic, 10
Alkaline, 10, 247, 251
Alteration, 193, 250
 adularia alteration, 159
 advanced argillic, 134
 albite-actinolite alteration, 193
 albitic, 199
 alkali, 193
 alteration selvages, 199
 argillic, 110, 155
 biotite-magnetite-anhydrite, 145
 biotite-magnetite, 134
 carbonaceous, 129
 carbonate, 277
 chlorite-magnetite, 119
 chloritization, 207
 clay-carbonate-muscovite-silica-sericite, 118
 clay-silica, 110
 diopside-actinolite-orthoclase, 118
 Fluorite-carbonate, 271
 hematite-dusting, 15, 129
 hematite-phyllsilicate, 195
 hematite-sericite, 15, 123
 hydrothermal, 36
 hydrothermal alteration, 199
 hydrothermal orthoclase flooding, 125
 hydrous, 87, 136
 illite-adularia, 109
 leached cap, 169
 martitization, 195
 pervasive sericite, 125
 phyllitic, 169, 199
 Potassic, 129
 potassic alteration, 165
 biotite-magnetite, 165
 hydrothermal biotite, 165
 hydrothermal orthoclase, 165
 propylitic, 109, 115
 Propylitic, 129
 roscoelite, 281
 saussuritization, 84, 125
 saussuritized, 59, 62
 selvages, 129
 sericite, 134
 sericite-clay-carbonate, 118
 sericite-hematite, 195

- sericitic halos, 164
- sericitization, 205, 207
- silicification, 129, 193
- sodic-calcic, 134, 193
- America, 22
 - California, 23
 - Crater Lake, 23
 - Navajo Province, 23
 - Sierra Nevada, 23, 33
 - Colorado, 23, 158
 - Colorado Mineral belt, 158
 - Colorado Springs, 158
 - Crater Lake, 23
 - Laramide orogeny, 158
 - Navajo Province, 23
 - Oquirrh Mountains, 146
 - Rio Grande rift, 158
 - Rocky Mountains, 158
 - Salt Lake City, 146
 - Sierra Nevada, 23, 33
 - New Mexico, 23, 158
 - Colorado Mineral belt, 158
 - Crater Lake, 23
 - Navajo Province, 23
 - Rio Grande rift, 158
 - Sierra Nevada, 23, 33
 - North American Cordillera, 23, 142
 - North Dakota, 23
 - Oregon, 23
 - Crater Lake, 23
 - South American Andes, 142
 - Utah, 146
 - Colorado Mineral belt, 158
 - Crater Lake, 23
 - Navajo Province, 23
 - Oquirrh Mountains, 146
 - Rio Grande rift, 158
 - Salt Lake City, 146
 - Sierra Nevada, 23, 33
 - Wyoming, 23, 33, 42
- Amphibolite-facies, 198
- Analytical methods, 31
 - atomic-absorption spectroscopy (AAS), 31, 90
 - cathodoluminescence, 169
 - detection limit, 90
 - flame photometer, 31
 - fluid inclusions, 79
 - fluid inclusion studies, 115
 - ICP-MS, 31
 - INAA, 31
 - isotopic $\delta^{34}\text{S}$ values, 115
 - melt inclusions, 79
 - Metallurgical studies, 145
 - Pb-fire-assay, 90
 - SARM-7 standard, 90
 - stable isotope, 115
 - Sulphur isotopic compositions, 141
 - XRF, 31
- Andes, 248
- Anhydrite seal, 110
- (TNT) Anomalies, 25
- Antarctica, 12
 - Gaussberg, 12
- Apophyses, 194
- Arborescent, 216
- Argentina, 143
 - Cordillera Oriental, 143
 - Farallon Negro Formation, 142
 - Puna, 143
 - Sierra de Aconquija, 146
 - Sierra de Quilmes, 146
 - Sierras Pampeanas, 143
- Ascent, 42
- Aseismic ridge, 19
- Ash flow, 149
- Assimilation, 9, 92, 142, 191
 - crustal assimilation, 42, 73, 90
- Asthenosphere, 42
- Asthenospheric, 248
- Australia, 68, 191
 - Argyle, 12
 - Australian plate, 67, 109
 - Curnamona province, 195
 - Ellendale Field, 78
 - Gawler Craton, 194
 - Karinya Syncline, 203, 209
 - Kimberley craton, 191
 - Leonora-Laverton, 203
 - New Celebration-Kambalda, 203
 - New South Wales, 14
 - Bogan Gate, 121
 - Cadia Intrusive Complex, 129
 - Hillgrove district, 223
 - Kosciusko Terrane, 121
 - Lachlan Fold Belt, 104
 - Litchfield domain, 204
 - Nimbuwah domain, 204
 - Orange, 127
 - Parkes, 121
 - Sydney, 127
 - Wagga Metamorphic Belt, 121
 - Northern Territory, 203
 - Darwin, 204
 - Katherine, 204
 - Litchfield domain, 204
 - Mount Bundey, 204
 - Nimbuwah domain, 204
 - Pine Creek Geosyncline, 203
 - Rum Jungle, 204
 - Tennant Creek, 223
 - Top End Orogeny, 204
 - Pilbara, 191
 - Pine Creek Inlier, 204
 - Roxby Downs, 195
 - Roxby Downs station, 194
 - South Australia, 80
 - Adelaide Geosyncline, 80
 - Frankton, 80

- Kanmantoo Trough, 81
- Karinya Syncline, 80
- Murchison, 214
- Nimbuwah domain, 204
- Robertstown, 83
- Truro, 80
- Stuart Shelf, 194
- West Kimberley, 83
- Yilgarn Block, 203
- Yilgarn Craton, 203
 - Eastern Goldfields, 214
 - Golden Mile, 215
 - Kalgoorlie, 215
 - Murchison, 214
 - Norseman-Wiluna Belt, 215
 - Southern Cross, 214
 - Western Gneiss Terrain, 214, 215
- Austria, 56
 - Adriatic plate, 57
 - Austro-Alpine, 56
 - Calcareous Alps, 56
 - Drau Valley, 56
 - Eastern Alps, 56
 - Insubric Line, 56
 - Iselsberg, 56
 - Kreuzeck Mountains, 56
 - Möllbrücke, 56
 - Möll Valley, 56
 - Penninic, 56
 - Periadriatic Lineament, 56
 - Polinik Unit, 57
 - Strieden Unit, 57
 - Tauern Window, 57
- Auto-oxidation, 250

- B**
- Ba, 191
- Back-arc, 20
- Barometric, 249
- Barren, 228
- Basaltic andesite, 31
- Basalts, 250
- Basanite, 11
- Basement, 56, 204
- Base metals, 43
- Basic, 191, 250
- Batholith, 146
- Benioff Zone, 2, 10, 19
- Bimodal, 198
- Birefringence, 84
- Bonanza, 247
- Boninites, 14
- Brazil, 203
 - Bahia province, 203
 - São Francisco Craton, 203
- Breccias, 193
 - explosion breccia, 11
 - heterolithic, 110, 196
 - hydraulic, 108
 - hydrothermal breccia, 110
 - matrix-poor, 196
 - matrix-supported, 195, 196
 - phreatic, 108
 - phreatic explosion breccia, 288
 - rock flour, 134
 - talus breccia, 108
 - volcanic breccias, 107
- Brines, 193
- by-product, 194

- C**
- Calc-alkaline, 10, 247
- Calculation, 249
- Caldera, 249
- Calibrated, 249
- Canada, 203
 - Abitibi Belt, 218
 - Churchill Province, 216
 - Grenville Province, 216
 - Hemlo region, 218
 - Hollinger-McIntyre, 203
 - interior plains, 216
 - Kerr Addison-Chesterville, 203
 - Kirkland Lake, 218
 - Moose river basin, 216
 - Red Lake, 218
 - Southern Province, 216
 - Superior Province, 203, 216
- Carbonatitic, 11
- Chemical, 248
- Chemistry, 228
 - CO₂, 71
 - Eu anomalies, 136
 - geochemistry, 207
 - HFSE, 41, 65
 - LILE, 41
 - LREE, 41
 - mineral, 228
 - REE, 41, 136
 - stable isotope, 58, 73
- Chile, 104, 109
 - Andes, 104
 - Chilean Andes, 153
 - Juan-Fernandez Ridge, 143
 - La Serena, 153
 - Main Cordillera, 153
 - Maricunga, 154
 - Maricunga belt, 109, 156
 - Nazca plate, 154
 - Santiago, 153
- Chilean Andes, 249
- China, 19, 133, 203, 250
 - Inner Mongolia Province, 133
 - Sulu Orogen, 203
 - Tibet, 19
 - Yunnan, 250

- Yunnan Province, 19, 203
- Chlorophile, 227
- Chondritic, 193, 195
- Cl, 248
- Classification scheme, 10
- Clast, 195
- Co, 191
- Cogenetic, 195
- CO₂-rich, 197
- Collapsed, 249
- Collision, 2, 19
 - continent-continent collision, 57
 - plate collision, 56
- Collisional sutures, 249
- Compatible, 9
 - mantle-compatible, 12
- Complexed, 252
- Complexes, 228
 - bisulphide, 230
 - chloride, 230
 - Cl-bearing, 228
 - HS-bearing, 228
 - hydrosulphide, 228
- Composite intrusion, 199
- Concentration, 251
- Conduit, 212
- Conical Seamount, 250
- Copper, 251
- Core, 11
- Costa Rica, 33
- Craton, 192
 - Gawler craton, 195
 - North American craton, 191, 197
- Craton margins, 191, 197
- Cratonic margins, 191
- Crustal contamination, 162
- Crustal processes, 250
 - crustal thickening, 19
 - tectonic uplift, 19
 - volcanism, 19
- Crystallization, 229, 248
 - core, 59
 - rim, 59
 - zoning, 59
- Crystallize, 251
- Crystal mush, 11
- Cumulates, 77
- D**
- Dacite, 30
- Database, 28
 - GOLD1, 104, 105
 - IGBA, 29
 - LAMPDA, 29
 - PETCHEM, 29
 - SHOSH1, 30
 - SHOSH2, 30, 103
- Decarbonation, 250
- Deformation, 210
- Degassing, 79, 250
- Dehydration, 25, 250
- Depressurization, 109
- Devolatilization, 230
- Diatreme, 83, 159
- Diatreme-maar, 195
- Differentiation, 29
- Diffusion, 79
- Discrimination diagrams, 27, 105, 248
 - discriminants, 30
- Dispersed, 10
- Disproportionation, 230
- Dissociation, 250
- Dissolved, 250
- Distribution coefficients, 80
- Dome, 67
- Domeyko Fault, 249
- Dyke, 11–13, 194, 195, 198
 - dyke swarm, 58, 207, 213
 - ring dyke, 122
- E**
- Earthquake, 108, 177
- Eclogite, 39, 41
- Electrum, 212
- Element partitioning, 251
- Elements, 227
 - chalcophile, 209, 211, 216, 218, 222
 - compatible, 69, 78, 231
 - gold pathfinder, 22
 - immobile, 24, 33
 - incompatible, 231
 - major, 28, 30
 - mobile, 24
 - mobility, 24
 - mobilization, 207
 - pathfinder, 209
 - trace, 24, 30
 - trace-element, 59
- Emplacement, 56, 90, 196
- Epithermal gold, 1, 2
- Equilibration, 249
- Equilibrium, 249
- Eroded, 115
- Erosion, 145
- Eu anomalies, 40
- Evolved, 9, 11
- Expert-system, 27
- Exploration, 247
 - aeromagnetic anomaly, 118
 - demagnetized, 107
 - diamond drilling, 117
 - drill hole, 194, 205, 247
 - endowed, 116, 247
 - exploration criteria, 248
 - exploration guides, 228
 - exploration program, 194

- fertile, 80, 247, 248
 - field exploration, 248
 - geological mapping, 117, 159
 - geophysical modeling, 204
 - gravity anomalies, 145
 - interpolation, 247
 - IP survey, 117
 - joint venture, 197
 - mineralization potential, 252
 - panning, 197
 - predictive targeting, 247
 - prospecting tool, 228
 - prospective, 247, 248, 252
 - prospectivity, 83, 247
 - resource, 118
 - resource base, 121
 - soil sampling, 118, 136, 197
 - target generation, 247, 248, 252
 - trenching, 197
 - Exploration models, 2
 - chalcocite blankets, 132
 - Exsolution, 193
 - Extrusive, 14
- F**
- F, 248
 - Feldspathoids, 10
 - Felsic, 14, 56, 191, 195, 250
 - Ferric iron, 250
 - Ferromagnesian, 12, 83, 135
 - Ferrous iron, 250
 - Fertile, 191
 - First boiling, 229
 - Flat-slab zone, 248
 - Flexure, 248
 - Fluid inclusion, 193, 230, 231
 - Fluids, 250, 252
 - alkali-chloride, 77
 - aqueous, 41, 227, 228
 - auriferous, 212
 - boiling, 156
 - CO₂-rich, 209
 - conduit, 215
 - crustal, 77
 - fluid migration, 191
 - hydrosaline, 230
 - hydrothermal fluids, 191, 197
 - hypersaline, 177
 - low salinity, 230
 - magmatic, 77, 115
 - mantle, 77
 - metamorphic, 77
 - metasomatic, 26
 - metasomatizing, 39
 - meteoric, 115
 - mixing, 156
 - ore fluid, 58, 191
 - oxidized fluids, 250
 - residual, 26
 - saline, 115, 227
 - solubility, 77, 227
 - sulfate-chloride brine, 110
 - thiosulphate, 77
 - FMQ buffer, 250
 - Fore-arc, 20, 23
 - Foreland, 143
 - Fractional crystallization, 64, 219, 248
 - Fractionation, 36, 248, 250
 - fractionation trend, 111, 113
 - gravitational fractionation, 80
 - open-system fractionation, 79
 - plagioclase fractionation, 40
- G**
- Geobarometer, 249
 - Geochemistry, 14, 191
 - Geological cross-section, 199
 - Geothermal, 110
 - Geotherms, 39
 - Germany, 203
 - Erzgebirge, 203
 - Glasses, 249
 - Globular structures, 11
 - Glomero-phenocrysts, 199
 - Gold, 211, 251
 - bonanza gold, 177
 - electrum, 119
 - Native gold, 119
 - solubility, 77, 228
 - Gold mineralization, 232
 - epithermal, 232
 - porphyry copper-gold, 203, 232
 - Gough Island, 64
 - Granite, 195
 - Granitic, 252
 - Granodiorite, 198
 - Gravity anomalies, 194
 - Greece, 162
 - Athens, 162
 - Chalkidiki peninsula, 162
 - Kassandra mining district, 162
 - Lavrion mining district, 162
 - Serbomacedonian Massif, 162
 - Groundmass, 11, 14, 62, 248
 - feldspathic groundmass, 218
- H**
- H₂O, 248
 - H₂O-rich, 250
 - Halogens, 227, 252
 - chlorine, 227
 - Cl, 252
 - F, 252
 - Fluorine, 231
 - Hand specimen, 12, 248

Harzburgite, 12
 HFSE, 248
 High-K, 247
 High-K igneous rocks, 3
 High-K magmatism, 3
 Hot-spot, 22
 HREE, 191
 Hybrid, 191, 197
 Hydraulic fracturing, 229
 Hydrogen, 26, 79
 Hydrology, 110
 Hydrothermal, 191
 Hydrothermal alteration, 249
 Hydrous, 10, 194, 248
 Hydroxyl, 26
 Hydroxyl site, 227
 Hypabyssal, 10, 11, 14, 111
 Hypogene, 134, 169

I

Igneous rocks, 249
 Immiscibility, 193
 Immiscible, 79
 Impregnate, 135
 Incompatible, 191, 248
 Indonesia, 64
 Irian Jaya, 166
 Batu Tara, 64
 Grasberg Igneous Complex, 169
 Merapi Volcano, 79
 Sunda Arc, 64
 Batu Tara, 64
 Infiltration, 250
 Instable, 249
 Intrusion, 58, 249
 Intrusive complexes, 250
 Intrusive contact, 200
 IOCG, 2
 Iran, 203
 IRGD, 2
 Iron, 250
 Italy, 13
 Aeolian Islands, 19
 Alban Hills, 53
 Amiata, 53
 Apennine Fold belt, 53
 Balearic Basin, 58
 Calabrian Arc, 53
 Cupaello, 13
 Elba, 53
 Phlegrean Fields, 53
 Roccamonfina, 53
 Roccastrada, 53
 Roman Magmatic Province, 13
 Roman Province, 13, 24, 53
 Sabatini, 24, 33, 53
 San Venanzo, 13
 San Vincenzo, 53

Sardinia, 58
 Vesuvius, 53
 Vico, 53
 Vulcini, 53
 Vulsinian district, 53
 Vulture, 53

J

Juvenile clasts, 109

K

Kamafugites, 10, 12
 kamafugitic, 10
 Katungite, 13
 Kimberlite, 9, 11, 13
 Group I, 13
 Group II, 13
 Kinks, 248

L

Lamproites, 11, 12
 Lamprophyres, 198, 248, 250
 alkaline lamprophyres, 11, 12, 59, 65
 calc-alkaline lamprophyres, 59
 kersantite, 11, 12, 216, 218
 minette, 11, 12, 149, 218
 shoshonitic, 62, 204, 232
 shoshonitic lamprophyres, 62, 65
 spessartite, 11, 216
 ultramafic lamprophyres, 11, 159
 vogesite, 11, 218
 Laser ablation ICP-MS, 249
 Laths, 195
 Latite, 284
 Lattice, 11
 Lattice-strain model, 249
 Lava, 13, 249
 lava flow, 53
 pillow lavas, 69
 Leucitite, 14
 Leucocratic, 12
 Lihir island, 250
 LILE, 248
 Lithosphere, 42, 191, 250
 Lithospheric, 250
 Lithostatic unloading, 108
 LOI, 30
 LREE, 191, 251

M

Mafic, 14, 56, 195
 Mafurite, 13
 Magma, 249
 magma chamber, 79
 magma mixing, 149

- mixing, 79
 - parent magmas, 197
- Magma chamber, 111, 248, 251
- Magma composition, 62
 - alkaline, 62, 77, 80, 84, 98
 - Dupal-type, 64
 - EM2-type, 64
 - evolved, 62
 - potassic, 64
 - primary, 64
 - primitive, 62, 71, 80, 89, 207, 208, 212, 216, 231
 - shoshonitic, 56, 203, 232
- Magmas, 250
- Magmatic belt, 198
- Magmatic-hydrothermal, 252
- Magmatic-hydrothermal transition, 227, 229
- Magmatic water, 251
- Magnetic surveys, 251
- Mantle, 250
 - asthenospheric, 70
 - compatible, 69, 78, 231
 - lithospheric, 70
 - lithospheric mantle, 197
 - mantle residue, 80
 - metasomatized, 231
 - primitive, 62, 80, 87, 89, 207, 208, 209, 216, 218
- Mantle conditions, 249
- Mantle melts, 248
- Mantle regimes, 250
- Mantle wedge, 26, 39, 42
- Marble, 198
- Martitization, 251
- MASH, 40
- Matrix, 196
- Mature, 250
- Mediterranean Series, 9
- Megacrysts, 199
- Melanocratic, 11
- Melt, 251
 - adakitic, 39, 40
 - alkalic, 216
 - alkaline, 56, 77, 88, 111
 - basic, 80, 236
 - boninitic, 20
 - calc-alkaline, 90
 - conduits, 223
 - felsic, 209, 215
 - fertile, 80, 247
 - fractionated, 207
 - hydrous, 87, 136
 - interstitial, 130, 195
 - lamprophyric, 212
 - melt fractions, 119
 - melt increments, 9, 79, 231
 - parental, 111, 119
 - peralkaline, 87
 - phonolitic, 230
 - primitive, 30, 62, 71, 80, 87, 207–209, 216, 231
 - residual, 26, 79
 - residual melt, 230
 - shoshonitic, 56, 207, 232
 - silica-deficient, 71
 - silicate, 227
 - sulphide, 227
 - syenitic, 212
 - tholeiitic, 20, 215
 - ultrabasic, 77
 - undersaturated, 78
- Melt inclusions, 231, 251
- Melting, 250
 - adiabatic decompression, 109
 - dehydration, 22, 35
 - dehydration melting, 66
 - melt increments, 9, 79, 231
 - partial melting, 9, 12, 26
- Metal, 251
- Metal deposits, 1
 - Agua Rica, 146
 - Andacollo, 156
 - Axa, 1
 - Baguio, 1, 249
 - Bajo de la Alumbreira, 1, 15, 142, 251
 - Batu Hijau, 109
 - Bingham, 1, 15, 146, 193, 203
 - Brewery Creek, 198
 - Cadia, 1, 14, 104, 127
 - Cadia East, 127
 - Cadia Far East, 127
 - Cadia Hill, 127
 - Cadia Quarry, 127
 - Cadia Ridgeway, 127
 - Candelaria, 193
 - Carlin, 2
 - Carlin deposits, 193
 - Carlin province, 193
 - Carrapateena, 195
 - Choquelimpie, 151
 - Chuquicamata, 249
 - Cripple Creek, 1, 158
 - Dinkidi, 116, 249
 - Donlin Creek, 197, 198
 - Dublin Gulch, 198
 - Dvoynoi, 138
 - El Abra, 250
 - El Hueso, 151
 - El Indio, 151, 249
 - El Salvador, 144, 249
 - El Teniente, 180, 203
 - Emperor, 1, 114, 248, 249
 - Ertsberg, 166
 - Fort Knox, 2, 191, 197
 - Glendale, 125
 - gold deposits, 2
 - Goodall, 203
 - Goonumbla, 104, 251
 - Grasberg, 1, 166, 232, 251
 - Hamilton, 83
 - Hillgrove, 92

- Jinjushan, 2
 Kambalda, 215
 Kanmantoo, 82
 Kapunda, 82
 Khopik, 2
 Kidston, 197
 Kiruna, 191
 Kori Kollo, 197
 Kupol, 138
 La Coipa, 151
 Ladolam, 1, 105, 232, 251
 La Escondida, 249
 Lamaque stockwork, 2
 Marian, 251
 Mirkuh Ali Mirza, 2
 Misima, 171
 Moppa, 83
 Morila, 197
 Mount Morgan, 215
 Northparkes, 1, 15, 121, 232, 249, 251
 E22, 121
 E26 North, 121
 E27, 121
 E48, 121
 Goonumbla, 121
 Oblaga, 133
 Olympic Dam, 2, 82, 191, 193, 248, 252
 Oyu Tolgoi, 1, 130
 Central Oyu, 130
 Heruga, 132
 Hugo Dummett, 130
 Southwest Oyu, 132
 Turquoise Hill, 132
 Pascua-Llama, 151
 Peschanka, 1, 15, 136
 Pogo, 197, 198
 Porgera, 1, 105, 174, 232, 248, 251
 Prominent Hill, 195
 Prospector Mountain, 2
 Puren, 151
 Salobo, 191, 193
 Scheelite Dome, 200
 Sheahan-Grants, 125
 Shotgun, 198
 Skouries, 1, 15, 162
 Tambo, 151
 Telfer, 191, 197
 Tom's Gully, 203
 Tuvatu, 115
 Vasilkovsky, 197
 Veladero, 151
 Vetka, 138
 Wiluna, 215
 Woolwonga, 204
 Yao'an, 1, 203
 Zaldivar, 249
 Metamorphism, 36
 amphibolites-facies, 143, 146
 granulite facies, 204, 215
 greenschist-amphibolite, 215
 greenschist facies, 56, 204
 greenstone belt, 214
 greenstone terrains, 213
 metamorphic recrystallization, 220
 polymetamorphic, 56
 Metasomatic, 250
 Metasomatized, 191
 Metasomatizing processes, 250
 Mexico, 203
 Mica schists, 198
 Microdiorite, 285
 Microphenocrysts, 248
 Microplate, 56
 Microscopically, 248
 Mineralization, 65, 251
 alluvial gold, 117
 banded iron-formations, 215
 base-metal, 14, 80, 88
 disseminated, 109, 170, 205
 epigenetic, 58, 205
 epithermal, 204
 epithermal gold-silver, 154
 gold-tellurium, 115
 lode-gold, 215
 low-sulphidation epithermal, 110
 massive sulphides, 90, 115
 mine, 58
 molybdenum mineralization, 180
 ore, 77
 ore-shoot, 211
 orogenic copper-gold-bismuth, 223
 orogenic gold, 205, 219
 PGE deposits, 77
 polymetallic, 110
 porphyry copper-gold, 209
 precious metal, 77, 89
 precious-metal budget, 77
 prospect, 58
 quartz reef, 211
 skarn, 133
 stratiform, 164
 stratiform gold, 204
 submarine-exhalative, 58
 sulphide mineralization, 205
 VMS, 115, 180
 VMS deposits, 215
 Mineralized, 228
 Mineralogy, 9, 14
 Minerals, 249
 actinolite, 150, 198
 adularia, 110
 albite, 196
 allanite, 166
 alunite, 156
 amphibole, 10, 248
 analcime, 160
 anhydrite, 108, 142, 251
 apatite, 10, 13, 83, 248

- armalcolite, 12
 - asbestos, 83
 - augite, 69, 115, 136
 - azurite, 125
 - barite, 83, 196
 - bastnaesite, 195
 - biotite, 10, 199, 248
 - primary, 231
 - secondary, 231
 - britholite, 195
 - calcite, 13
 - carbonates, 9, 11, 204
 - chalcedony, 110
 - chlorite, 59, 195
 - chromite, 71
 - clinopyroxene, 10, 13
 - cummingtonite, 83
 - diamond, 12
 - dickite, 156
 - diopside, 12, 13, 71
 - epidote, 11, 84
 - fayalite, 249
 - feldspar, 248
 - ferrosilite, 249
 - florencite, 195
 - fluorapatite, 151
 - fluorite, 11, 195, 196
 - forsterite, 78
 - garnet, 129, 163
 - graphite, 198
 - gypsum, 142
 - haematite, 251
 - hornblende, 199, 248
 - hypersthene, 69
 - illite, 110
 - ilmenite, 13, 26
 - jarosite, 156
 - jepeite, 12
 - K-feldspar, 10, 199
 - kaersutite, 59
 - kalsilite, 12–14
 - kaolinite, 156
 - labradorite, 125
 - leucite, 10, 12–14, 248
 - libethenite, 125
 - magnetite, 249, 250
 - malachite, 123
 - melilite, 12–14
 - monazite, 195
 - montmorillonite, 156
 - muscovite, 163
 - nepheline, 10, 12, 69
 - olivine, 10, 249
 - orthoclase, 199, 212
 - orthopyroxene, 67, 249
 - perovskite, 13, 14
 - phlogopite, 10, 13, 248
 - pitchblende, 196
 - plagioclase, 10, 12, 248
 - potassic feldspar, 248
 - prehnite, 141
 - priderite, 12, 14
 - pyrophyllite, 156
 - pyroxene, 248
 - richterite, 12, 14
 - riebeckite, 12, 83
 - roscoelite, 115
 - rutile, 26, 141
 - salite, 71
 - sanidine, 11–13, 54
 - sapphire, 149
 - serpentine, 13
 - shcherbakovite, 12
 - siderite, 195, 196
 - sillimanite, 57
 - silver sulphosalts, 58
 - spinel, 13, 249
 - spinel, 84
 - staurolite, 163
 - sulphates, 11
 - talc, 83
 - thorite, 166
 - titanaugite, 72
 - titanian phlogopite, 12
 - titanite, 12, 26, 83, 216
 - titanomagnetite, 71, 115, 249
 - tourmaline, 83, 163
 - tschermakite, 59
 - vanadium mica, 115
 - wadeite, 12
 - xenotime, 195
 - zeolites, 11
 - zircon, 30, 215, 249
 - zircon, 249
 - Minettes, 250
 - Mixing, 193
 - Modal, 71
 - Model, 57
 - MOHO, 191
 - Molecular, 11
 - Mongolia, 130
 - Altaid Tectonic Belt, 132
 - Gobi desert, 130
 - Tuva Mongol arc, 132
 - Ulaanbaatar, 130
 - Monzodiorite, 14
 - Monzogabbro, 276
 - Monzogranite, 196, 199
 - Monzogranites, 195
 - Monzonite, 283
 - Monzonite, 14
 - Mélanges, 81
- N**
- Native gold, 197
 - Nevada, 2

- Ni, 191
 Normalizing, 36
 normalized, 209
 normalizing factors, 218
 Normative, 59, 64
- O**
 Oceanic slab, 248
 Octahedral site, 227
 OIB, 231
 Oman, 203
 Open pit, 205
 Ophiolites, 81
 Ore metal, 227
 Orebody, 196
 Orenditic, 10
 Orogenic, 10, 12
 Oxidation, 195, 250
 Oxidation state, 79, 227, 250
 Oxidized, 228, 250
 Oxygen, 249, 250
 Oxygen fugacities, 77, 249, 251
 Oxygen isotopes, 250
- P**
 Pacific, 2, 22
 Bismarck microplate, 109
 Fiji, 22, 113
 Ambrym, 67
 Anneityum, 67
 Aoba, 67
 Borneo, 20
 Central Island Province, 65
 Erromango, 67
 Feni, 106
 Gaua, 67
 Guam, 65
 Huniho, 107
 Java, 23
 Kinami, 107
 Lihir Island, 22, 105, 107
 Londolovit, 107
 Luise, 107
 Minami Iwo Jima, 65
 Nakaudavadra Mountains, 113
 New Ireland, 105
 New Ireland Province, 105
 Nishino Shima, 65
 Northern Seamount Province, 65
 Sarigan, 66
 Southern Seamount Pr, 65
 Tabar, 106
 Tanga, 106
 Tanna, 106
 Tavua, 115
 Uracas, 65
 Viti Levu, 113
 Wurtol, 107
 Indonesia, 23
 Borneo, 25
 Java, 23
 Sumatra, 23
 Sumbawa Island, 109
 Sunda Arc, 23
 Kilinaillau trench, 108
 Manus basin, 109
 Mariana Arc, 20, 65
 Central Island Province, 65
 Guam, 65
 Minami Iwo Jima, 65
 Nishino Shima, 65
 Northern Seamount Province, 65
 Sarigan, 66
 Southern Seamount Province, 65
 Uracas, 65
 Melanesian Arc, 67
 Melanesian trench, 108
 New Britain arc, 107
 New Britain trench, 109
 New Hebrides, 22, 67
 Ontong-Java plateau, 108
 Pacific plate, 65, 108
 Papua New Guinea, 22, 65
 Enga Province, 174
 Feni, 106
 Huniho, 107
 Kinami, 107
 Lihir Island, 22, 105, 107
 Londolovit, 107
 Louiadiade Archipelago, 171
 Luise, 107
 Misima Island, 171
 Mount Hagen, 174
 New Ireland, 108
 New Ireland Province, 105
 Porgera Intrusive Complex, 177
 Port Moresby, 174
 Tabar, 106
 Tanga, 106
 Tanna, 106
 Tavua, 67
 Wurtol, 107
 Philippine Sea plate, 65
 Philippines, 116
 Cagayan Valley, 118
 Didipio, 116
 Didipio Igneous Complex, 118
 Luzon, 117
 Luzon Trench, 118
 Nakaudavadra Mountains, 113
 Nueva Vizcaya Province, 117
 Sierra Madre Mountains, 116
 Tonga-Kermadec Trench, 114
 Vanuatu, 67
 Ambrym, 67
 Anneityum, 67

- Aoba, 67
 - Erromango, 67
 - Gaua, 67
 - Guam, 65
 - Minami Iwo Jima, 65
 - Nishino Shima, 65
 - Northern Seamount Province, 65
 - Sarigan, 66
 - Southern Seamount Province, 65
 - Tanna, 67
 - Uracas, 65
 - Vanuatu Trench, 114
 - Paragenesis, 200
 - Paragenetically, 195
 - Partial melting, 250
 - Partial melts, 250
 - Partition coefficient, 250
 - Partitioning, 227, 249, 252
 - Pegmatite, 118, 199
 - Peralkaline, 10, 12
 - Peridotite, 9, 10
 - Petrogenesis, 9
 - PGE, 227
 - Phase, 231, 249, 251
 - insoluble, 41
 - refractory, 26
 - solid, 231
 - vapour, 231
 - Phenocrysts, 248, 250
 - microphenocrysts, 10, 212, 232
 - Pillow, 108
 - Pilot study, 250
 - Pipe, 12
 - Placer deposits, 197
 - Plate boundaries, 19
 - Plug, 11, 128
 - Plumbing system, 191
 - Plume, 2, 191
 - asthenospheric plumes, 191
 - magma plumes, 42
 - mantle plumes, 9, 42, 178, 191
 - Pluton, 58, 197, 219
 - aureole, 211
 - Plutonic, 10, 14
 - Porphyry copper-gold, 3
 - Post-mineral, 195
 - Potassic, 14
 - Potassic igneous rocks, 2
 - Potassic intrusions, 251
 - Precious metal, 251
 - Precipitation, 230, 251
 - Precision, 31
 - Pressure, 77, 249
 - Primary, 251
 - Primitive, 250
 - Production, 121
 - block-caving, 121
 - open pit, 121, 132
 - Protolith, 57
 - Pseudomorph, 178
 - Pulses, 251
 - Pumice, 149
 - Pyroclastic rocks, 54
 - ignimbrites, 54
 - tuffs, 54
- Q**
- Quantitative, 249
 - Quartzites, 198
 - Quenching, 249
- R**
- Radiogenic isotope data, 198
 - ratios, 36, 248
 - Spitz ratios, 87
 - reaction, 249
 - recycled, 64
 - redox conditions, 228
 - redox potential, 249
 - redox state, 250
 - reduced, 251
 - reducing, 79
 - reducing conditions, 12
 - residual, 251
 - resources, 194
 - indicated, 194
 - rhyolite, 198
 - rift, 10
 - rim, 11
 - rocks, 54
 - agglomerates, 145
 - amphibolites, 57
 - Andesite, 66
 - andesites, 65
 - augite-basalt, 132
 - augite-olivine cumulates, 111
 - basalt, 64
 - basalts, 65
 - basanite, 71
 - blueschist, 81
 - carbonates, 204
 - conglomerate, 204
 - conglomerates, 138
 - cumulates, 79
 - diabase, 213
 - diorite, 118, 213
 - dolomite, 169
 - eclogite, 57
 - epiclastic, 123
 - epiclastic rocks, 107
 - felsic, 218
 - gabbro, 127
 - gneiss, 57, 216
 - granite, 212
 - graphitic pelites, 212
 - greenstones, 127

- greywackes, 205
- kimberlites, 78
- komatiite, 215
- lamproites, 78
- lamprophyres, 216
- latite, 54, 71, 107
- leucitite, 54
- lherzolite, 71
- limestone, 121
- mafic, 218
- marble, 163
- melilitite, 71
- monzodiorite, 107, 170
- monzogabbro, 138
- monzonite, 107
- mudstones, 138
- mugearite, 71, 72
- nephelinite, 71
- olivine-clinopyroxene cumulate, 111
- paragneisses, 143
- phonolite, 54, 111, 159
- pyroclastic, 107
- rhyolite, 134
- sandstones, 138, 204
- sedimentary, 218
- shale, 204, 205
- siltstones, 138, 204
- syenite, 134, 212
- syenogranite, 130
- tephrite, 54, 159
- trachyandesite, 107, 213
- trachybasalt, 67, 107
- trachyte, 54, 71, 123
- turbidites, 127
- ultramafic, 218
- ultramafics, 215
- root zones, 191
- Russia, 136, 280
 - Chukotka Autonomous Region, 280
 - Siberia, 136, 280
 - Baimka ore district, 136
 - Bilibino, 136
 - Chukotka Autonomous Region, 136
 - Nakhodka area, 138
 - Okhotsk-Chukotka volcanic belt, 138
 - Pevek, 136
 - Siberian Craton, 138
- S**
- Saline, 193
- Saturated, 251
- Schist, 198
- Scoria, 108
- Seamount, 19, 39
- Seamounts, 248
 - Conical, 107
 - Edison, 107
 - TUBAF, 107
- Second boiling, 229
- Secondary boiling, 251
- Sediments, 40, 250
 - metapelites, 57
 - schist, 57
 - volcanosedimentary, 56
- Segregation, 11, 79, 230, 251
- Shallow seismicity, 109
- Shield volcano, 71
- Shield volcano, 67
- Shoshonites, 1, 10
- Shoshonitic, 247
- Silica-deficient, 10
- Silica-saturated, 10, 54
- Silica-undersaturated, 54
- Sill, 11
- Slab, 248
- Slab tears, 248
- Solid solution, 249
- Solubility, 26, 193, 251
 - gold solubility, 228
- Spidergram, 25, 40, 87
- Stable isotope, 193
- Statistical method, 33
 - canonical coefficients, 36
 - data-matrix, 33
 - discriminant functions, 33
 - multigroup linear discriminant analysis, 33
- Stock, 11, 198
- Structures, 249
 - caldera, 71
 - chevron folding, 108, 114, 118, 172, 178
 - collage, 116, 132
 - crenulation fabrics, 172
 - deep-seated, 77
 - detachment fault, 172
 - dextral, 138, 249
 - dilational, 173
 - dilational structure, 128
 - dip, 58, 121
 - dipping, 195
 - discordantly, 58
 - extensional, 58, 249
 - fault zone, 143, 209
 - faults, 222
 - fissure, 108
 - flexure, 109, 144
 - fold, 198, 205
 - fold axial planes, 205
 - foliation, 172
 - fractured, 195
 - fractures, 58, 118
 - graben, 71
 - high-angle, 198, 249
 - inclination, 67
 - intersections, 249
 - joint planes, 83
 - kink, 83, 109, 144
 - left-lateral strike slip, 199

- lineament, 56, 82, 114
 - listric fault, 108
 - low-angle, 198
 - nappe, 56
 - pinches and swells, 211
 - plunging, 172
 - reactivated, 249
 - reverse faults, 249
 - Riedel structures, 141
 - rift, 71
 - shatter zones, 115
 - shear zone, 198, 199, 214, 222
 - sheeted, 58, 127
 - slab tear, 109
 - strike, 58, 83
 - strike-slip, 132, 198
 - strike-slip faults, 249
 - structural corridor, 129
 - structural trend, 198
 - suture, 56, 57, 191
 - transfer structures, 118
 - transpressive, 56, 218, 249
 - wrench shearing, 211
 - Sub-alkaline, 191
 - Subaerially, 65
 - Subduction, 2
 - convergence rate, 19, 68
 - oblique, 23
 - orthogonal, 23
 - paleo-subduction, 191
 - Subduction angle, 248
 - flat-slab zone, 143
 - flat subduction, 19
 - shallow subduction, 143
 - steep subduction, 20
 - Subduction trench, 251
 - Subduction zones, 250
 - Submarine, 65, 67
 - Subsolidus, 231, 250
 - Subvolcanic, 228
 - Sulphate, 79, 250, 251
 - Sulphides, 193, 251
 - arsenian pyrite, 110
 - arsenopyrite, 205, 211
 - bismite, 199
 - bismuthinite, 197, 199
 - bornite, 125, 193
 - chalcocite, 123, 193
 - chalcopyrite, 193, 205
 - covellite, 129, 169
 - digenite, 169
 - enargite, 134, 156
 - galena, 110, 139
 - loellingite, 211
 - maldonite, 199
 - marcasite, 110
 - molybdenite, 138, 150
 - pyrite, 193, 205
 - sphalerite, 123, 139
 - tennantite, 139, 156
 - tetradymite, 199
 - tetrahedrite, 110
 - Sulphur, 251
 - Sulphur saturation, 79
 - Sulphur-undersaturated, 79
 - Supergene, 141, 251
 - Supracrustal, 213
 - Susceptibility, 251
 - magnetic susceptibilities, 200
 - Suture, 2
 - Switzerland, 56
 - Central Alps, 56
 - Western Alps, 58
 - Syenite, 289
 - Synvolcanic, 249
 - System, 249
- T**
- Tearing, 248
 - Tectonic rotations, 249
 - Tectonics, 58
 - accretion, 132
 - accretionary events, 218
 - accretionary processes, 127
 - amalgamation, 138
 - anticline, 148
 - anticlinorial, 121
 - back-arc spreading, 58
 - collage, 116, 132, 216
 - collision, 132, 221
 - compression, 58
 - compressional deformation, 143
 - deformation, 58
 - extensional, 58, 249
 - intramontane basin, 143
 - microcontinental block, 132
 - mobile belts, 132
 - oblique compression, 215
 - Orogeny, 81
 - shortening, 158
 - syncline, 148
 - synclinorial, 121
 - transpressive, 56, 218, 249
 - underthrusting, 218
 - uplift, 81, 158
 - Tectonic setting, 1, 3, 19, 248
 - arc-related, 103
 - back-arc rifting, 66
 - back arc basin, 118
 - continental, 248
 - continental-arc, 19, 54
 - convergent-plate margin, 247
 - craton margins, 14
 - intra-cratonic, 204
 - island arc, 65
 - late oceanic arcs, 248
 - oceanic arc, 20, 250

- initial oceanic arc, 20, 31
 - late oceanic arc, 22, 43
 - postcollisional, 248
 - postcollisional arc, 19, 62
 - rift, 14
 - within-plate, 13, 23, 42, 248
 - Temperature, 77, 249
 - Terranes, 2
 - Texture, 248
 - accumulate, 248
 - angular, 109
 - aphanitic, 135
 - banded, 156
 - battlement, 11
 - battlemented, 216
 - brain rock, 199
 - cherty, 156
 - chilled margins, 83, 133, 212
 - coarse-grained, 196
 - cockade, 58
 - cognate, 205
 - colloform, 58, 156
 - composite intrusions, 250
 - corroded, 195
 - crackle, 196
 - crenulated, 199
 - cryptocrystalline, 84, 156
 - dendritic, 199
 - disseminated, 195
 - dog-tooth, 110
 - drusy, 156
 - equigranular, 14, 119, 125
 - euhedral, 83, 195, 216
 - extrusive, 248
 - fibrous, 84
 - fine-grained, 195, 199
 - flow textures, 83, 84
 - glassy, 11, 69
 - globular structures, 84
 - glomeroporphyritic, 71
 - granular, 123
 - heterolithic, 110, 196
 - holocrystalline, 14
 - interstitial, 130, 195
 - jigsaw, 196
 - lamellae, 115
 - massive, 196
 - matrix-supported, 195, 196
 - medium-grained, 199
 - miarolitic cavities, 146, 178, 248
 - microcrystalline, 59
 - monolithic, 110
 - mosaic, 119
 - mylonitic, 57
 - ocelli, 84, 160, 216
 - perthitic, 119
 - phyric, 58, 67
 - poorly sorted, 110
 - porphyritic, 10, 67, 248
 - rapakivi, 196
 - recrystallization, 65
 - resorbed, 199
 - reworked, 196
 - saccharoidal, 146
 - seriate, 130
 - subangular, 109
 - unfoliated, 58
 - vesicles, 111, 178
 - vesicular, 108
 - vug, 11
 - vughy, 119
 - zonation, 59, 71
 - Thermobarometry, 249
 - Tholeiites, 14, 251
 - TNT anomalies, 25
 - Trace element, 251
 - Trachyandesite, 10, 31, 285
 - Trachybasalt, 9, 10, 250
 - Trachyte, 10, 30
 - Trench, 10, 20, 33
 - Turkey, 203
 - Twinning, 216
 - Type locality, 9
- U**
- U, 191
 - Ugandite, 13
 - Ultrabasic, 13, 191
 - Ultramafic, 195
 - Ultrapotassic, 1, 10, 53
 - leucitites, 1
 - Unconformably, 210
 - Underplating, 40, 193
 - Upper mantle, 250
 - Uprise, 11, 80, 92, 248
 - Upwelling, 42
- V**
- Valence states, 249
 - Veins, 251
 - A-type, 125
 - B-type, 140

- D-type, 141
 - gangue material, 156
 - quartz veins, 193
 - S-type, 125, 170
 - sheeted, 127, 140
 - stockwork veining, 205
 - stockwork veins, 199
 - stringer, 139
 - vein density, 199
 - veinlets, 118, 199
 - Vent, 11, 12, 71
 - Volatile content, 250
 - Volatile phases, 251
 - Volatile-rich, 248
 - Volatiles, 248
 - magmatic volatiles, 177
 - volatile exsolution, 79
 - Volatile saturation, 79, 251
 - Volcanic, 10, 14
 - Volcanic arc, 191
 - Volcanoes, 71, 107
 - caldera, 108, 114, 121
 - collapse amphitheatre, 108
 - crater, 107
 - sector collapse, 109
 - shield volcano, 114
 - stratovolcano, 107
 - unroofing, 109
 - volcanic edifice, 106
 - volcanic slope failure, 108
- W**
- Water, 248, 250
 - Weathering, 29
 - Whole-rock, 200, 251
 - Within-plate, 2
 - Wyoming, 9
 - Yellowstone Park, 9
- X**
- Xenocryst, 59, 71
 - Xenoliths, 9, 78, 249
- Y**
- Yugoslavia, 56
- Z**
- Zoned, 11